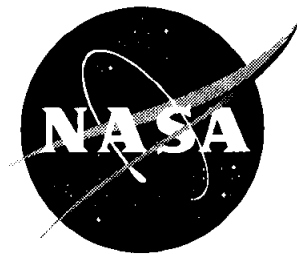


NASA/CP-1999-209549



National Educators' Workshop: Update 98

Standard Experiments in Engineering, Materials Science, and Technology

Compiled by

*Ginger L. F. Arrington and James E. Gardner
Langley Research Center, Hampton, Virginia*

James A. Jacobs

Norfolk State University, Norfolk, Virginia

Karl J. Swyler

Brookhaven National Laboratory, Upton, New York

Leonard W. Fine

Columbia University, New York, New York

October 1999

The NASA STI Program Office . . . in Profile

Since its founding, NASA has been dedicated to the advancement of aeronautics and space science. The NASA Scientific and Technical Information (STI) Program Office plays a key part in helping NASA maintain this important role.

The NASA STI Program Office is operated by Langley Research Center, the lead center for NASA's scientific and technical information. The NASA STI Program Office provides access to the NASA STI Database, the largest collection of aeronautical and space science STI in the world. The Program Office is also NASA's institutional mechanism for disseminating the results of its research and development activities. These results are published by NASA in the NASA STI Report Series, which includes the following report types:

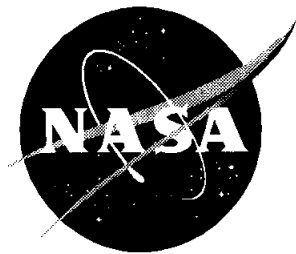
- **TECHNICAL PUBLICATION.** Reports of completed research or a major significant phase of research that present the results of NASA programs and include extensive data or theoretical analysis. Includes compilations of significant scientific and technical data and information deemed to be of continuing reference value. NASA counterpart or peer-reviewed formal professional papers, but having less stringent limitations on manuscript length and extent of graphic presentations.
- **TECHNICAL MEMORANDUM.** Scientific and technical findings that are preliminary or of specialized interest, e.g., quick release reports, working papers, and bibliographies that contain minimal annotation. Does not contain extensive analysis.
- **CONTRACTOR REPORT.** Scientific and technical findings by NASA-sponsored contractors and grantees.
- **CONFERENCE PUBLICATION.** Collected papers from scientific and technical conferences, symposia, seminars, or other meetings sponsored or co-sponsored by NASA.
- **SPECIAL PUBLICATION.** Scientific, technical, or historical information from NASA programs, projects, and missions, often concerned with subjects having substantial public interest.
- **TECHNICAL TRANSLATION.** English-language translations of foreign scientific and technical material pertinent to NASA's mission.

Specialized services that complement the STI Program Office's diverse offerings include creating custom thesauri, building customized databases, organizing and publishing research results . . . even providing videos.

For more information about the NASA STI Program Office, see the following:

- Access the NASA STI Program Home Page at <http://www.sti.nasa.gov>
- Email your question via the Internet to help@sti.nasa.gov
- Fax your question to the NASA STI Help Desk at (301) 621-0134
- Telephone the NASA STI Help Desk at (301) 621-0390
- Write to:
NASA STI Help Desk
NASA Center for Aerospace Information
7121 Standard Drive
Hanover, MD 21076-1320

NASA/CP-1999-209549



National Educators' Workshop: Update 98

Standard Experiments in Engineering, Materials Science, and Technology

*Compiled by
Ginger L. F. Arrington and James E. Gardner
Langley Research Center, Hampton, Virginia*

*James A. Jacobs
Norfolk State University, Norfolk, Virginia*

*Karl J. Swyler
Brookhaven National Laboratory, Upton, New York*

*Leonard W. Fine
Columbia University, New York, New York*

Proceedings of a workshop sponsored jointly by the National Aeronautics and Space Administration, Washington, DC; Norfolk State University, Norfolk, Virginia; the National Institute of Standards and Technology, Gaithersburg, Maryland; Brookhaven National Laboratory, Upton, New York; the International Council for Materials Education, Columbia University, New York, New York; and Gateway Coalition, State University of New York at Stony Brook, New York

and held in
Upton, New York
November 1-4, 1998

National Aeronautics and
Space Administration

Langley Research Center
Hampton, Virginia 23681-2199

October 1999

The use of trademarks or names of manufacturers in this report is for accurate reporting and does not constitute an official endorsement, either expressed or implied, of such products or manufacturers by the National Aeronautics and Space Administration.

Available from the following:

NASA Center for Aerospace Information (CASI)
7121 Standard Drive
Hanover, MD 21076-1320
(301) 621-0390

National Technical Information Service (NTIS)
5285 Port Royal Road
Springfield, VA 22161-2171
(703) 487-4650

PREFACE

NEW:Update 98, hosted by Brookhaven National Laboratory, Columbia University and the University of Stony Brook in New York, was held on November 1 - 4, 1998.

The 13th Annual NEW:Update built on themes, activities and presentations based on extensive evaluations from participants of previous workshops as we continued efforts to strengthening materials education. About 100 participants witnessed demonstrations of experiments, discussed issues of materials science and engineering (MS&E) with people from education, industry, government, and technical societies, heard about new MS&E developments, and chose from nine, three-hour mini workshops in state-of-the-art laboratories. Faculty in attendance represented high schools, community colleges, smaller colleges, and major universities. Undergraduate and graduate students also attended and presented.

As in past years we were fortunate to have excellent support from our hosts. Karl Swyler, Leonard Fine, and Chris Berndt helped to coordinate the many scientist, engineers, professors and other staff, by providing funding, opening their facilities, developing presentations and activities.

NEW:Update 98 participants saw the demonstration of about forty experiments and aided in evaluating them. We also heard updating information relating to materials science, engineering and technology presented at mini plenary sessions.

The experiments in this publication can serve as a valuable guide to faculty who are interested in useful activities for their students. The material was the result of years of research aimed at better methods of teaching materials science, engineering and technology. The experiments developed by faculty, scientists, and engineers throughout the United States and abroad add to the collection from past workshops. There is a blend of experiments on new materials and traditional materials.

Experiments underwent an extensive peer review process. After submission of abstracts, selected authors were notified of their acceptance and given the format for submission of experiments. Experiments were reviewed by a panel of specialists through the cooperation of the International Council for Materials Education (ICME). Comments from workshop participants provided additional feedback which authors used to make final revisions, which were then submitted to the NASA editorial group for this publication.

The ICME encourages authors of experiments to make submissions for use in the Journal of Materials Education (JME). The JME offers valuable teaching and curriculum aids including instructional modules on emerging materials technology, experiments, book reviews, and editorials to materials educators.

As with previous NEW:Updates, critiques were made of the workshop to provide continuing improvement of this activity. The evaluations and recommendations made by participants provide valuable feedback for the planning of subsequent NEW:Updates.

NEW:Update 98 and the series of workshops that go back to 1986 are, to our knowledge, the only national workshops or gatherings for materials educators that have a focus on the full range of issues on strategies for better teaching about the full complement of materials. NEW:Update 98, with its diversity of faculty, industry, and government MSE participants, served as a forum for

both formal and informal issues facing MSE education that ranged from the challenges of keeping faculty and students abreast of new technology to ideas to ensure that materials scientists, engineers, and technicians maintain the proper respect for the environment in the pursuit of their objectives.

We demonstrated the Experiments in Materials Science, Engineering & Technology, (EMSET) CD-ROM with all 213 experiments from the first decade of NEW:Updates. This CD-ROM is another example of cooperative efforts to support materials education. The primary contributions came from the many authors of the demo and experiments for NEW:Updates. Funding for the CD came from both private industry and federal agencies. Please see the attached information for obtaining the CD.

We express our appreciation to all those who helped to keep this series of workshops viable. Special thanks goes to those on our national organizing committee, management team, hosts, sponsors, and especially those of you have developed and shared your ideas for experiments, demonstrations, and novel approaches to learning. All of us who participated in the workshop appreciated the excellent coordination of activities by Jim Gardner, Diana LaClaire, and Ginger Arrington.

We hope that the experiments presented in this publication will assist you in teaching about materials science, engineering and technology. We would like to have your comments on their value and means of improving them. Please send comments to Jim Jacobs, School of Science and Technology, Norfolk State University, Norfolk, Virginia 23504.

The use of trademarks or manufacturers' names in this publication does not constitute endorsement, either expressed or implied, by the National Aeronautics and Space Administration.

MANAGEMENT TEAM

Workshop Co-Directors

James A. Jacobs
Workshop Co-chairperson
Norfolk State University

Karl J. Swyler
Workshop Co-chairperson
Brookhaven National Laboratory

Leonard W. Fine
Workshop Co-chairperson
Department of Chemistry
Columbia University

NASA LaRC Coordinators

James E. Gardner and Ginger L. F. Arrington
National Aeronautics and Space Administration
Langley Research Center

Assistant Director

Diana P. LaClaire
Norfolk State University

Committee Members

Christopher C. Berndt
Dept. of Materials Science and Engineering
State University of NY - Stony Brook

Robert Berrettini
International Council for Materials Education

Paul W. Brown
International Council for Materials Education

S. Raj Chaudhury
Norfolk State University

James A. Clum
State University of NY - Binghamton

Morton B. Friedman
School of Engineering
Columbia University

Kenneth L. Jewett
National Institute of Standards & Technology

Thomas F. Kilduff
Thomas Nelson Community College

Socky Lugo
Columbia University

James V. Masi
Western New England College

Alfred E. McKenney
IBM Corporation, Retired

Heidi Ries
Norfolk State University

Thomas G. Stoebe
University of Washington

Laura L. Sullivan
American Society for Engineering Education

Acknowledgments

We greatly appreciate the support provided by these organizations:

The American Society for Engineering Education

The ASM Foundation

The International Council for Materials Education

CONTENTS

PREFACE	iii
MANAGEMENT TEAM	v
ACKNOWLEDGMENTS	vi
REVIEWERS OF EXPERIMENTS	xi
LISTINGS OF EXPERIMENTS FROM NEW:UPDATES	xiii
ORDERING INFORMATION FOR ADDITIONAL RESOURCES	xxix
PARTICIPANTS	xxxiii
MATERIALS SCIENCE WITH PHOTONS AND NEUTRONS	1
Denis McWhan - Brookhaven National Laboratory	
MAGNETO-RHEOLOGICAL FLUID TECHNOLOGY	29
John A. Marshall - University of Southern Maine	
X-RAY EXCITED EMISSION OF Mn²⁺ IONS IN Mn: YAIO₃	35
M. A. Noginov, M. Warren, G. B. Loutts - Norfolk State University	
AN INEXPENSIVE 2732°F MINIATURE ELECTRIC FURNACE FOR TEACHING MATERIALS SCIENCE	43
Luke Ferguson and Thomas Stoebe - University of Washington	
TEACHING STATISTICAL QUALITY CONTROL AND PROCESS ANALYSIS IN MATERIALS LABORATORY	65
Neda S. Fabris - California State University	
SYSTEM UPGRADE OF ATOMIC OXYGEN GENERATOR FOR SPACE MATERIALS RESEARCH	73
Kyo D. Song - Norfolk State University, Bruce Budde (LARSS) student - New Mexico State University and Carolyn Hamilton (LARSS) student - University of New Mexico	
INVESTIGATION OF THERMAL BLEACHING IN MANGANESE DOPED ORTHOALUMINATE SINGLE CRYSTALS	95
George B. Loutts, Mikhail A. Noginov, Rosalind Wynne, Kai T. Ross and Talia Grandy - Norfolk State University	
THE MATERIALS SCIENCE OF SUPERCONDUCTING MAGNETS	105
David Welch - Brookhaven National Laboratory	
THE COLORFUL CHARACTER OF MATERIALS	137
Edward L. Widener - Purdue University	

LABORATORY MEASUREMENT OF J-INTEGRAL	143
Yulian Kin, Harvey Abramowitz, Toma Hentea, Jim Higley, and Jason Richards - Purdue University - Calumet	
USE OF A FOUR-POINT BEND APPARATUS TO DETERMINE THE MODULUS OF ELASTICITY	153
Richard B. Griffin, L. Roy Cornwell, Carlos Yapura, Sivasubramaniam Krishnan and John Hallford - Texas A&M University	
MICROCHEMISTRY AND THE NEW SCANNING ELECTRON MICROSCOPES	165
Matthew J. Kasdan - Coto de Casa, and Stephen K. Kennedy - RJ Lee Group, Inc.	
DETERMINATION OF THE CURIE TEMPERATURE IN FERRO AND FERRIMAGNETS	173
R. Valenzuela and E. Amano - National University of Mexico	
EDUCATIONAL AND PUBLIC OUTREACH FOR THE MARS SAMPLE RETURN PROJECT	183
S. Raj Chaudhury and Gae Golembiewski - Norfolk State University	
GALVANOSTATIC POLARIZATION CURVES FOR TEACHING PURPOSES	187
Carlos E. Umana - University of Costa Rica	
THE UNDERLYING STRUCTURE OF ENGINEERING MATERIALS	207
Mike L. Meier and Karl Ewald - University of California, Davis	
RENDERING ASBESTOS INTO A NON-REGULATED MATERIAL	217
Leon Petrakis - Brookhaven National Laboratory	
EDUCATIONAL PROGRAMS AT BNL AND OTHER DOE LABS	249
Karl Swyler - Brookhaven National Laboratory	
LIQUID CRYSTAL p-AZOXYANISOLE IN MICROWAVE FIELD	267
Jai N. Dahiya - Southeast Missouri State University	
ARTIFICIAL MICROSTRUCTURES	277
Mike L. Meier - University of California, Davis	
CRYSTAL GROWTH	289
Merrill Rudes - Energy Concepts, Inc.	
SIMULATING OPTICAL CORRELATION ON A PC	295
B. F. Draayer - Southeast Missouri State University	
TRENDS FOR AUTOMOTIVE MATERIALS	311
John E. Fillion - DaimlerChrysler Corporation	
DENDRITIC POLYMER PROPERTIES AND MACROMOLECULAR ARCHITECTURE	337
Donald A. Tomalia - Michigan Molecular Institute in Midland	
TUTORIALS FOR INTRODUCTION TO MATERIALS ENGINEERING	351
Charles J. McMahon, Jr. - University of Pennsylvania	

ROOM TEMPERATURE CREEP OF SOLDER	365
Robert G. Stang - University of Washington	
USE OF PIEZOELECTRIC CRYSTALS FOR VOICE RECOGNITION	379
Harvey Abramowitz - Purdue University - Calumet	
CONCURRENT ENGINEERING	393
James B. Higley, Yulian B. Kin, Bernard W. Parsons II, and Christopher M. Prochnow - Purdue University Calumet	
STRETCHY "ELASTIC" BANDS II	429
Alan K. Karplus - Western New England College	
PRODUCING PDF FILES USING ADOBE ACROBAT CAPTURE V2.01	445
Alfred E. McKenney - Williamsburg, Virginia	
CAST IRON, WROUGHT IRON & STEEL (HISTORICAL PERSPECTIVE OF PROPERTIES OF FERROUS MATERIAL)	455
Archie M. Cooke - Carson City, Nevada	

REVIEWERS FOR NEW:Update 98

Paul W. Brown
Professor Ceramics Science and Engineering
The Pennsylvania State University

Else Breval
Senior Research Associate
Materials Research Laboratory
The Pennsylvania State University

William Callister
Adjunct Professor of Metallurgy
University of Utah

James A. Clum
University of Detroit - Mercy

Technical notebooks and announcements of the workshop were provided by
NASA LANGLEY RESEARCH CENTER

LISTING OF EXPERIMENTS FROM NEW:UPDATES

EXPERIMENTS & DEMONSTRATIONS IN STRUCTURES, TESTING, AND EVALUATION

NEW:Update 88

NASA Conference Publication 3060

Sastri, Sankar. "Fluorescent Penetrant Inspection"

Sastri, Sankar. "Magnetic Particle Inspection"

Sastri, Sankar. "Radiographic Inspection"

NEW:Update 89

NASA Conference Publication 3074

Chowdhury, Mostafiz R. and Chowdhury, Farida. "Experimental Determination of Material Damping Using Vibration Analyzer"

Chung, Wenchiang R. "The Assessment of Metal Fiber Reinforced Polymeric Composites"

Stibolt, Kenneth A. "Tensile and Shear Strength of Adhesives"

NEW:Update 90

NIST Special Publication 822

Azzara, Drew C. "ASTM: The Development and Application of Standards"

Bates, Seth P. "Charpy V-Notch Impact Testing of Hot Rolled 1020 Steel to Explore Temperature Impact Strength Relationships"

Chowdhury, Mostafiz R. "A Nondestructive Testing Method to Detect Defects in Structural Members"

Cornwell, L. R., Griffin, R. B., and Massarweh, W. A. "Effect of Strain Rate on Tensile Properties of Plastics"

Gray, Stephanie L., Kern, Kristen T., Harries, Wynford L., and Long, Sheila Ann T.

"Improved Technique for Measuring Coefficients of Thermal Extension for Polymer Films"

Halperin, Kopl. "Design Project for the Materials Course: To Pick the Best Material for a Cooking Pot"

Kundu, Nikhil. "Environmental Stress Cracking of Recycled Thermoplastics"

Panchula, Larry and Patterson, John W. "Demonstration of a Simple Screening Strategy for Multifactor Experiments in Engineering"

Taylor, Jenifer A. T. "How Does Change in Temperature Affect Resistance?"

Wickman, Jerry L. and Corbin, Scott M. "Determining the Impact of Adjusting Temperature Profiles on Photodegradability of LDPE/Starch Blown Film"

Widener, Edward L. "It's Hard to Test Hardness"

Widener, Edward L. "Unconventional Impact-Toughness Experiments"

NEW:Update 91

NASA Conference Publication 3151

Bunnell, L. Roy. "Tempered Glass and Thermal Shock of Ceramic Materials"

Lundeen, Calvin D. "Impact Testing of Welded Samples"

Gorman, Thomas M. "Designing, Engineering, and Testing Wood Structures"

Strehlow, Richard R. "ASTM - Terminology for Experiments and Testing"

Karplus, Alan K. "Determining Significant Material Properties, A Discovery Approach"

Spiegel, F. Xavier and Weigman, Bernard J. "An Automated System for Creep Testing"

Denton, Nancy L. and Hillsman, Vernon S. "Isotropic Thin-Walled Pressure Vessel Experiment"

Allen, David J. "Stress-Strain Characteristics of Rubber-Like Materials: Experiment and Analysis"

Dahl, Charles C. "Computer Integrated Lab Testing"

Cornwell, L. R. "Mechanical Properties of Brittle Material"

NEW:Update 92**NASA Conference Publication 3201**

- Bunnell, L. Roy. "Temperature-Dependent Electrical Conductivity of Soda-Lime Glass and Construction and Testing of Simple Airfoils to Demonstrate Structural Design, Materials Choice, and Composite Concepts"
- Marpet, Mark I. "Walkway Friction: Experiment and Analysis"
- Martin, Donald H. "Application of Hardness Testing in Foundry Processing Operations: A University and Industry Partnership"
- Masi, James V. "Experiments in Corrosion for Younger Students By and For Older Students"
- Needham, David. "Micropipet Manipulation of Lipid Membranes: Direct Measurement of the Material Properties of a Cohesive Structure That is Only Two Molecules Thick"
- Perkins, Steven W. "Direct Tension Experiments on Compacted Granular Materials"
- Shih, Hui-Ru. "Development of an Experimental Method to Determine the Axial Rigidity of a Strut-Node Joint"
- Spiegel, F. Xavier. "An Automated Data Collection System For a Charpy Impact Tester"
- Tipton, Steven M. "A Miniature Fatigue Test Machine"
- Widener, Edward L. "Tool Grinding and Spark Testing"

NEW:Update 93**NASA Conference Publication 3259**

- Borst, Mark A. "Design and Construction of a Tensile Tester for the Testing of Simple Composites"
- Clum, James A. "Developing Modules on Experimental Design and Process Characterization for Manufacturing/Materials Processes Laboratories"
- Diller, T. E. and A. L. Wicks, "Measurement of Surface Heat Flux and Temperature"
- Denton, Nancy and Vernon S. Hillsman, "An Introduction to Strength of Materials for Middle School and Beyond"
- Fisher, Jonathan H. "Bridgman Solidification and Experiment to Assess Boundaries and Interface Shape"
- Gray, Jennifer "Symmetry and Structure Through Optical Diffraction"
- Karplus, Alan K. "Knotty Knots"
- Kohne, Glenn S. "An Automated Digital Data Collection and Analysis System for the Charpy Impact Tester"
- Olesak, Patricia J. "Scleroscope Hardness Testing"
- Speigel, F. Xavier, "Inexpensive Materials Science Demonstrations"
- Wickman, J. L. "Plastic Part Design Analysis Using Polarized Filters and Birefringence"
- Widener, Edward L. "Testing Rigidity by Torque Wrench"

NEW:Update 94**NASA Conference Publication 3304**

- Bruzan, Raymond and Baker, Douglas, "Density by Titration"
Dahiya, Jai N., "Precision Measurements of the Microwave Dielectric Constants of Polyvinyl Stearate and Polyvinylidene Fluoride as a Function of Frequency and Temperature"
Daufenbach, JoDee and Griffin, Alair, "Impact of Flaws"
Fine, Leonard W., "Concrete Repair Applications and Polymerization of Butadiene by an "Alfin" Catalyst"
Hillsman, Vernon S., "Stress Concentration: Computer Finite Element Analysis vs. Photoelasticity"
Hutchinson, Ben, Giglio, Kim, Bowling, John, and Green, David, "Photocatalytic Destruction of an Organic Dye Using TiO₂"
Jenkins, Thomas J., Comtois, John H., and Bright, Victor M., "Micromachining of Suspended Structures in Silicon and Bulk Etching of Silicon for Micromachining"
Jacobs, James A. and Jenkins, Thomas J., "Mathematics for Engineering Materials Technology Experiments and Problem Solving"
Karplus, Alan K., "Paper Clip Fatigue Bend Test"
Kohne, Glenn S., "Fluids With Magnetic Personalities"
Liu, Ping and Waskom, Tommy L., "Ultrasonic Welding of Recycled High Density Polyethylene (HDPE)"
Martin, Donald H., Schwan, Hermann, Diehm, Michael, "Testing Sand Quality in the Foundry (A Basic University-Industry Partnership)"
Shull, Robert D., "Nanostructured Materials"
Werstler, David E., "Introduction to Nondestructive Testing"
White, Charles V., "Glass Fracture Experiment for Failure Analysis"
Wickman, Jerry L. and Kundu, Nikhil K., "Failure Analysis of Injection Molded Plastic Engineered Parts"
Widener, Edward L., "Dimensionless Fun With Foam"

NEW:Update 95**NASA Conference Publication 3330**

- Brown, Scott, "Crystalline Hors d'oeuvres"
Karplus, Alan K., "Craft Stick Beams"
Kern, Kristen, "ION Beam Analysis of Materials"
Kozma, Michael, "A Revisit to the Helicopter Factorial Design Experiment"
Pond, Robert B., Sr., "Recrystallization Art Sketching"
Roy, Rustum, "CVD Diamond Synthesis and Characterization: A Video Walk-Through"
Saha, Hrishikesh, "Virtual Reality Lab Assistant"
Spiegel, F. Xavier, "A Novel Approach to Hardness Testing"
Spiegel, F. Xavier, "There are Good Vibrations and Not So Good Vibrations"
Tognarelli, David, "Computerized Materials Testing"
Wickman, Jerry L., "Cost Effective Prototyping"

NEW:Update 96**NASA Conference Publication 3354**

- Chao, Julie, Currotto, Selene, Anderson, Cameron, Selvaduray, Guna, "The Effect of Surface Finish on Tensile Strength"
Fabris, Neda S., "From Rugs to Demonstrations in Engineering Materials Class"
Ferguson, Luke, Stoebe, Thomas, "Hysteresis Loops and Barkhausen Effects in Magnetic Materials"
Karplus, Alan K., "Holy Holes or Holes Can Make Tensile Struts Stronger"
Koon, Daniel W., "Relaxation and Resistance Measurements"
Liu, Ping, Waskom, Tommy L., "Composite of Glass Fiber with Epoxy Matrix"
Song, Kyo D., Ries, Heidi R., Scotti, Stephen J., Choi, Sang H., "Transpiration Cooling Experiment"
South, Joe, Keilson, Suzanne, Keefer, Don, "In-Vivo Testing of Biomaterials"
Thorogood, Michael G., "Tensile Test Experiments With Plastics"
Widener, Edward L., "Brinelling the Malay Snail"

NEW:Update 97**NASA Conference Publication 208726**

- Banerjee, Gautam, Miller, Albert E. "Understanding Galvanic Corrosion Tricks to Prevent Some Expensive Failures"
- Cadwell, John and Eric, Piippo, Steven. "Strength Testing of Composite Materials"
- Diez, C. Ray. "Case Hardening: An Activity to Demonstrate Brinnell Hardness"
- Draayer, B. F., Dahiya, J. N. "A Computerized Microwave Spectrometer for Dielectric Relaxation Studies"
- Erickson, Glen C., Chung, W. Richard. "Effectiveness of Ultrasonic Testing Method in Detecting Delamination Effects in Thick Composites"
- Fabris, Neda S. "Learning More From Tensile Test Experiment"
- Ferguson, Luke, Stoebe, Thomas. "Properties of Magnetic Ferrites With a Simple Fabrication Method"
- Fine, Leonard W. "Demonstrating the Critical Properties of Carbon Dioxide"
- Goranson, Ulf. "Jet Transport Structures Performance Monitoring"
- Gorman, Thomas M. "Relationship Between Moisture Changes and Dimensional Change in Wood"
- Griffin, R. B., Cornwell, L. R. "Measurement of the Modulus of Elasticity Using a Three-Point Bend Test"
- Homidany, Mtrook Al, Weick, Brian L. "A Device for Measuring the Elastic Modules of Spherical Materials"
- Hudson, John B., Svanes, Torkel, Bryson, Daniel, Sawyer, W. Gregory, "An Interactive Molecular Dynamics Simulation of Atomic Behavior"
- Karplus, Alan K. "Stretchy "Elastic" Bands"
- Liu, Paul Cheng-Hsin, Moore, Kenneth, Ogu, Chris. "Rapid Prototyping Processes and Procedures"
- Loutts, George B. "Crystal Growth of Mixed Optical Materials With the Automatic Czochralski Puller"
- Lund, David W. "High Speed Civil Transport - Design Challenges"
- Masi, James V. "Experiments in Diffusion: Gases, Liquids, and Solids For Under Five Dollars"
- McCoy, Robert A. "How a Heat Pack Works"
- Nydam, Andrew. "Low Dollar Tensile (Torsion) Tester"
- Song, Kyo D. "Design of Hypervelocity Flow Generator and Its Flow Visualizations"
- Spiegel, F. Xavier. "Medicine, Magic, Materials, and Mankind"
- Umaña, Carlos E. "The Combined Effect of Thermal Conductivity and Thermal Expansion in a PMMA Plastic Heated by Thermal Radiation"
- Vanasupa, Linda, Braun, David. "The Human Half-Adder: Understanding the Big Picture of Digital Logic"
- Warren, Matthew E., Loutts, George. "Optical Experiments With Manganese Doped Yttrium Orthoaluminate, A Potential Material For Holographic Recording and Data Storage"
- Werstler, David. "Case Studies in Metal Failure and Selection"
- Whang, Kyumin and Hsu, Matthew. "Evaluating the Strength and Biodegradation of a Gelatine-Based Material"
- Williams, John R. "Corrosion Demonstration Utilizing Low Cost Materials"

NEW:Update 98**NASA Conference Publication**

- Griffin, Richard B., Cornwell, L. Roy, Yapura, Carlos, Krishnan, Sivasubramaniam, Hallford, John. "Use of a Four-Point Bend Apparatus to Determine the Modulus of Elasticity"
- Karplus, Alan K. "Stretchy "Elastic" Bands II"
- McWhan, Denis. "Materials Science With Photons and Neutrons"
- Meier, Mike L., Ewald, Karl. "The Underlying Structure of Engineering Materials"
- Meier, Mike L., "Artificial Microstructures"
- Rudes, Merrill. "Crystal Growth"
- Song, Kyo D., Budde, Bruce, Hamilton, Carolyn. "System Upgrade of Atomic Oxygen Generator for Space Materials Research"
- Stang, Robert G. "Room Temperature Creep of Solder"
- Umaña, Carlos E. "Galvanostatic Polarization Curves for Teaching Purposes"

EXPERIMENTS & DEMONSTRATIONS IN METALS

NEW:Update 88

NASA Conference Publication 3060

- Nagy, James P. "Sensitization of Stainless Steel"
Neville, J. P. "Crystal Growing"
Pond, Robert B. "A Demonstration of Chill Block Melt Spinning of Metal"
Shull, Robert D. "Low Carbon Steel: Metallurgical Structure vs. Mechanical Properties"

NEW:Update 89

NASA Conference Publication 3074

- Balsamel, Richard. "The Magnetization Process - Hysteresis"
Beardmore, Peter. "Future Automotive Materials - Evolution or Revolution"
Bunnell, L. Roy. "Hands-On Thermal Conductivity and Work-Hardening and Annealing in Metals"
Kazem, Sayyed M. "Thermal Conductivity of Metals"
Nagy, James P. "Austempering"

NEW:Update 90

NIST Special Publication 822

- Bates, Seth P. "Charpy V-Notch Impact Testing of Hot Rolled 1020 Steel to Explore Temperature Impact Strength Relationships"
Chung, Wenchiang R. and Morse, Margery L. "Effect of Heat Treatment on a Metal Alloy"
Rastani, Mansur. "Post Heat Treatment in Liquid Phase Sintered Tungsten-Nickel-Iron Alloys"
Spiegel, F. Xavier. "Crystal Models for the Beginning Student"
Yang, Y. Y. and Stang, R. G. "Measurement of Strain Rate Sensitivity in Metals"

NEW:Update 91

NASA Conference Publication 3151

- Cowan, Richard L. "Be-Cu Precipitation Hardening Experiment"
Kazem, Sayyed M. "Elementary Metallography"
Krepiski, Richard P. "Experiments with the Low Melting Indium-Bismuth Alloy System"
Lundeen, Calvin D. "Impact Testing of Welded Samples"
McCoy, Robert A. "Cu-Zn Binary Phase Diagram and Diffusion Couples"
Patterson, John W. "Demonstration of Magnetic Domain Boundary Movement Using an Easily Assembled Videocam-Microscope System"
Widener, Edward L. "Heat-Treating of Materials"

NEW:Update 92

NASA Conference Publication 3201

- Dahiya, Jai N. "Phase Transition Studies in Barium and Strontium Titanates at Microwave Frequencies"
Rastani, Mansur. "Improved Measurement of Thermal Effects on Microstructure"
Walsh, Daniel W. "Visualizing Weld Metal Solidification Using Organic Analogs"

NEW:Update 93

NASA Conference Publication 3259

- Guichelaar, Philip J. "The Anisotropy of Toughness in Hot-Rolled Mild Steel"
Martin, Donald H. "From Sand Casting TO Finished Product (A Basic University-Industry Partnership)"
Petit, Jocelyn I. "New Developments in Aluminum for Aircraft and Automobiles"
Smith, R. Carlisle "Crater Cracking in Aluminum Welds"

NEW:Update 94

NASA Conference Publication 3304

- Gabrykewicz, Ted, "Water Drop Test for Silver Migration"
Kavikondala, Kishen and Gambrell, Jr., S. C., "Studying Macroscopic Yielding in Welded Aluminum Joints Using Photostress"
Krepiski, Richard P., "Exploring the Crystal Structure of Metals"
McClelland, H. Thomas, "Effect of Risers on Cast Aluminum Plates"
Weigman, Bernard J. and Courpas, Stamos, "Measuring Energy Loss Between Colliding Metal Objects"

NEW:Update 95**NASA Conference Publication 3330**

Callister, William, "Unknown Determination of a Steel Specimen"

Elban, Wayne L., "Metallographic Preparation and Examination of Polymer-Matrix Composites"

Shih, Hui-Ru, "Some Experimental Results in the Rolling of Ni₃Al Alloy"**NEW:Update 96****NASA Conference Publication 3354**

Callister, Jr., William D., "Identification of an Unknown Steel Specimen"

Elban, Wayne L., "Metallurgical Evaluation of Historic Wrought Iron to Provide Insights into Metal-Forming Operations and Resultant Microstructure"

Griffin, R. B., Cornwell, L. R., Ridings, Holly E., "The Application of Computers to the Determination of Corrosion Rates for Metals in Aqueous Solutions"

Hilden, J., Lewis, K., Meararipous, Selvaduray, Guna, "Measurement of Springback Angle in Sheet Bending"

Moss, T. S., Dye, R. C., "Experimental Investigation of Hydrogen Transport Through Metals"

Olesak, Patricia J., "2nd Steel Heat Treatment Lab: Austempering"

Spiegel, F. Xavier, "A Magnetic Dilemma: A Case Study"

Werstler, David E., "Lost Foam Casting"

NEW:Update 97**NASA Conference Publication 208726**

Dalton, William K., Olesak, Patricia J. "Making a Phase Diagram"

Hartwig, K. T., Haouaoui, M., Cornwell, L. R. "Alloy Composition Determinations"

Kin, Yulian, Abramowitz, Harvey, Hentea, Toma, Xu, Ying. "Life Estimate Based on Fatigue Crack Propagation"

NEW:Update 98**NASA Conference Publication**

Biancanello, Frank S., Jiggetts, Rodney D., Ridder, Stephen D. "Characterization of High Nitrogen Stainless Steel (HNSS) Produced via Inert Gas Atomization and Hip Consolidation"

Cooke, Archie M. "Cast Iron, Wrought Iron & Steel (Historical Perspective of Properties of Ferrous Material"

Kin, Yulian, Abramowitz, Harvey, Hentea, Toma, Higley, Jim, Richards, Jason. "Laboratory Measurement of J-Integral"

Experiments & Demonstrations in Polymers

NEW:Update 89

NASA Conference Publication 3074

- Chung, Wenchiang R. "The Assessment of Metal Fiber Reinforced Polymeric Composites"
Greet, Richard and Cobaugh, Robert. "Rubberlike Elasticity Experiment"
Kern, Kristen T., Harries, Wynford L., and Long, Sheila Ann T. "Dynamic Mechanical Analysis of Polymeric Materials"
Kundu, Nikhil K. and Kundu, Malay. "Piezoelectric and Pyroelectric Effects of a Crystalline Polymer"
Kundu, Nikhil K. "The Effect of Thermal Damage on the Mechanical Properties of Polymer Regrinds"
Stibolt, Kenneth A. "Tensile and Shear Strength of Adhesives"
Widener, Edward L. "Industrial Plastics Waste: Identification and Segregation"
Widener, Edward L. "Recycling Waste-Paper"

NEW:Update 90

NIST Special Publication 822

- Brostow, Witold and Kozak, Michael R. "Instruction in Processing as a Part of a Course in Polymer Science and Engineering"
Cornwell, L. R., Griffin, R. B., and Massarweh, W. A. "Effect of Strain Rate on Tensile Properties of Plastics"
Gray, Stephanie L., Kern, Kristen T., Harries, Wynford L., and Long, Sheila Ann T. "Improved Technique for Measuring Coefficients of Thermal Extension for Polymer Films"
Humble, Jeffrey S. "Biodegradable Plastics: An Informative Laboratory Approach"
Kundu, Nikhil. "Environmental Stress Cracking of Recycled Thermoplastics"
Wickman, Jerry L. and Corbin, Scott M. "Determining the Impact of Adjusting Temperature Profiles on Photodegradability of LDPE/Starch Blown Film"

NEW:Update 91

NASA Conference Publication 3151

- Allen, David J. "Stress-Strain Characteristics of Rubber-Like Materials: Experiment and Analysis"
Chowdhury, Mostafiz R. "An Experiment on the Use of Disposable Plastics as a Reinforcement in Concrete Beams"
Gorman, Thomas M. "Designing, Engineering, and Testing Wood Structures"
Lloyd, Isabel K., Kolos, Kimberly R., Menegaux, Edmond C., Luo, Huy, McCuen, Richard H., and Regan, Thomas M. "Structure, Processing and Properties of Potatoes"
McClelland, H. T. "Laboratory Experiments from the Toy Store"
Sorensen, Carl D. "Measuring the Surface Tension of Soap Bubbles"
Wickman, Jerry L. and Plocinski, David. "A Senior Manufacturing Laboratory for Determining Injection Molding Process Capability"

NEW:Update 92

NASA Conference Publication 3201

- Kundu, Nikhil K. "Performance of Thermal Adhesives in Forced Convection"
Liu, Ping. "Solving Product Safety Problem on Recycled High Density Polyethylene Container"
Wickman, Jerry L. "Thermoforming From a Systems Viewpoint"

NEW:Update 93

NASA Conference Publication 3259

- Csernica, Jeffrey "Mechanical Properties of Crosslinked Polymer Coatings"
Edblom, Elizabeth "Testing Adhesive Strength" & "Adhesives The State of the Industry"
Elban, Wayne L. "Three-Point Bend Testing of Poly (Methyl Methacrylate) and Balsa Wood"
Labana, S. S. "Recycling of Automobiles an Overview"
Liu, Ping and Tommy L. Waskom, "Application of Materials Database (MAT.DB>) to Materials Education and Laminated Thermoplastic Composite Material"
Marshall, John A. "Liquids That Take Only Milliseconds to Turn into Solids"
Quaal, Karen S. "Incorporating Polymeric Materials Topics into the Undergraduate Chemistry Cor Curriculum: NSF-Polyed Scholars Project: Microscale Synthesis and Characterization of Polystyrene"

NEW:Update 94**NASA Conference Publication 3304**

Fine, Leonard W., "Concrete Repair Applications and Polymerization of Butadiene by an "Alfin" Catalyst"
Halperin, Kopl, Eccles, Charles, and Latimer, Brett, "Inexpensive Experiments in Creep and Relaxation of Polymers"

Kern, Kristen and Ries, Heidi R., "Dielectric Analysis of Polymer Processing

Kundu, Mukul and Kundu, Nikhil K., "Optimizing Wing Design by Using a Piezoelectric Polymer"

Kundu, Nikhil K. and Wickman, Jerry L., "An Affordable Materials Testing Device"

Stienstra, David, "In-Class Experiments: Piano Wire & Polymers"

NEW:Update 95**NASA Conference Publication 3330**

Fine, Leonard W., "Polybutadiene (Jumping Rubber)"

Liu, Ping, and Waskom, Tommy L., "Plastic Recycling Experiments in Materials Education"

Liu, Ping, and Waskom, Tommy L., "Compression Molding of Composite of Recycled HDPE and Recycled Tire Chips"

Masi, James V., "Experiments in Natural and Synthetic Dental Materials: A Mouthful of Experiments"

NEW:Update 96**NASA Conference Publication 3354**

Brindos, Richard, Selvaduray, Guna, "Effect of Temperature on Wetting Angle"

Liu, Ping, Waskom, Tommy L., "Making Products Using Post Consumer Recycled High Density Polyethylene: A Series of Recycling Experiments"

Spiegel, F. Xavier, "Elasticity, Plasticity and Anelasticity: Demonstrations"

NEW:Update 97**NASA Conference Publication 208726**

Liu, Ping, Waskom, Tom L. "Study of Rheological Behavior of Polymers"

Sullivan, Laura L. "Correlation of Birefringent Patterns to Retained Orientation in Injection Molded Polystyrene Tensile Bars"

NEW:Update 98**NASA Conference Publication**

Tomalia, Donald A. Dendritic Polymer Properties and Macromolecular Architecture"

EXPERIMENTS & DEMONSTRATIONS IN CERAMICS

NEW:Update 88

NASA Conference Publication 3060

Nelson, James A. "Glasses and Ceramics: Making and Testing Superconductors"
Schull, Robert D. "High T_c Superconductors: Are They Magnetic?"

NEW:Update 89

NASA Conference Publication 3074

Beardmore, Peter. "Future Automotive Materials - Evolution or Revolution"
Bunnell, L. Roy. "Hands-On Thermal Conductivity and Work-Hardening and Annealing in Metals"
Link, Bruce. "Ceramic Fibers"
Nagy, James P. "Austempering"
Ries, Heidi R. "Dielectric Determination of the Glass Transition Temperature"

NEW:Update 90

NIST Special Publication 822

Dahiya, J. N. "Dielectric Behavior of Superconductors at Microwave Frequencies"
Jordan, Gail W. "Adapting Archimedes' Method for Determining Densities and Porosities of Small Ceramic Samples"
Snail, Keith A., Hanssen, Leonard M., Oakes, David B., and Butler, James E. "Diamond Synthesis with a Commercial Oxygen-Acetylene Torch"

NEW:Update 91

NASA Conference Publication 3151

Bunnell, L. Roy. "Tempered Glass and Thermal Shock of Ceramic Materials"
Craig, Douglas F. "Structural Ceramics"
Dahiya, J. N. "Dielectric Behavior of Semiconductors at Microwave Frequencies"
Weiser, Martin W., Lauben, David N., and Madrid, Philip. "Ceramic Processing: Experimental Design and Optimization"

NEW:Update 92

NASA Conference Publication 3201

Bunnell, L. Roy. "Temperature-Dependent Electrical Conductivity of Soda-Lime Glass"
Henshaw, John M. "Fracture of Glass"
Stephan, Patrick M. "High Thermal Conductivity of Diamond"
Vanasupa, Linda S. "A \$.69 Look at Thermoplastic Softening"

NEW:Update 93

NASA Conference Publication 3259

Bunnell, L. Roy and Stephen Piippo, "Property Changes During Firing of a Typical Porcelain Ceramic"
Burchell, Timothy D. "Developments in Carbon Materials"
Dahiya, J.N., "Dielectric Measurements of Selected Ceramics at Microwave Frequencies"
Ketrion, L.A. "Preparation of Simple Plaster Mold for Slip Casting and Slip Casting"
Masi, James V. "Experiments in Diamond Film Fabrication in Table Top Plasma Apparatus"
Werstler, David E. "Microwave Sintering of Machining Inserts"

NEW:Update 94

NASA Conference Publication 3304

Bunnell, L. Roy and Piippo, Steven, "The Development of Mechanical Strength in a Ceramic Material During Firing"
Long, William G., "Introduction to Continuous Fiber Ceramic Composites"
Reifsnider, Kenneth L., "Designing with Continuous Fiber Ceramic Composites"
West, Harvey A. & Spiegel, F. Xavier, "Crystal Models for the Beginning Student: An Extension to Diamond Cubic"

NEW:Update 95

NASA Conference Publication 3330

Louden, Richard A., "Testing and Characterizing of Continuous Fiber Ceramic Composites"

NEW:Update 96

NASA Conference Publication 3354

Bunnell, L. Roy, Piippo, Steven W., "Evaluation of Chemically Tempered Soda-Lime-Silica Glass by Bend Testing"

Dahiya, J. N., "Microwave Measurements of the Dielectric Relaxation in Different Grain Size Crystals of BaTiO₃"

Masi, James V., "Experiments in Sol-Gel: Hydroxyapatite and YBCO"

Stang, Robert G., "The Effect of Surface Treatment on the Strength of Glass"

Thomas, Shad, Hasenkamp, Erin, Selvaduray, Guna, "Determination of Oxygen Diffusion in Ionic Solids"

NEW:Update 98

NASA Conference Publication

Ferguson, Luke, Stoebe, Thomas. An Inexpensive 1600°C (2912°F) Miniature Electric Furnace for Teaching Materials Science.

Welch, David. "Superconducting Magnets and Applications"

EXPERIMENTS & DEMONSTRATIONS IN COMPOSITES

NEW:Update 88 **NASA Conference Publication 3060**
Nelson, James A. "Composites: Fiberglass Hand Laminating Process"

NEW:Update 89 **NASA Conference Publication 3074**
Beardmore, Peter. "Future Automotive Materials - Evolution or Revolution"
Chung, Wenchiang R. "The Assessment of Metal Fiber Reinforced Polymeric Composites"
Coleman, J. Mario. "Using Template/Hotwire Cutting to Demonstrate Moldless Composite Fabrication"

NEW:Update 90 **NIST Special Publication 822**
Bunnell, L. R. "Simple Stressed-Skin Composites Using Paper Reinforcement"
Schmenk, Myron J. "Fabrication and Evaluation of a Simple Composite Structural Beam"
West, Harvey A. and Sprecher, A. F. "Fiber Reinforced Composite Materials"

NEW:Update 91 **NASA Conference Publication 3151**
Greet, Richard J. "Composite Column of Common Materials"

NEW:Update 92 **NASA Conference Publication 3201**
Thornton, H. Richard. "Mechanical Properties of Composite Materials"

NEW:Update 93 **NASA Conference Publication 3259**
Masters, John "ASTM Methods for Composite Characterization and Evaluation"
Webber, M. D. and Harvey A. West. "Continuous Unidirectional Fiber Reinforced Composites:
Fabrication and Testing"

NEW:Update 95 **NASA Conference Publication 3330**
Craig, Douglas F., "Role of Processing in Total Materials"
Wilkerson, Amy Laurie, "Computerized Testing of Woven Composite Materials"

NEW:Update 97 **NASA Conference Publication 208726**
Gardea, Luis, Weick, Brian L. "A Method for Measuring the Shear Strength of Polymers and
Composites"

EXPERIMENTS & DEMONSTRATIONS IN ELECTRONIC AND OPTICAL MATERIALS

NEW:Update 88

NASA Conference Publication 3060

Sastri, Sankar. "Magnetic Particle Inspection"

NEW:Update 89

NASA Conference Publication 3074

Kundu, Nikhil K. and Kundu, Malay. "Piezoelectric and Pyroelectric Effects of a Crystalline Polymer"

Molton, Peter M. and Clarke, Clayton. "Anode Materials for Electrochemical Waste Destruction"

Ries, Heidi R. "Dielectric Determination of the Glass Transition Temperature"

NEW:Update 90

NIST Special Publication 822

Dahiya, J. N. "Dielectric Behavior of Superconductors at Microwave Frequencies"

NEW:Update 91

NASA Conference Publication 3151

Dahiya, J. N. "Dielectric Behavior of Semiconductors at Microwave Frequencies"

Patterson, John W. "Demonstration of Magnetic Domain Boundary Movement Using an Easily Assembled Videocam-Microscope System"

NEW:Update 92

NASA Conference Publication 3201

Bunnell, L. Roy. "Temperature-Dependent Electrical Conductivity of Soda-Lime Glass"

Dahiya, Jai N. "Phase Transition Studies in Barium and Strontium Titanates at Microwave Frequencies"

NEW:Update 94

NASA Conference Publication 3304

Elban, Wayne L., "Stereographic Projection Analysis of Fracture Plane Traces in Polished Silicon Wafers for Integrated Circuits"

Parmar, Devendra S. and Singh, J. J., "Measurement of the Electro-Optic Switching Response in Ferroelectric Liquid Crystals"

NEW:Update 95

NASA Conference Publication 3330

Dahiya, Jai N., "Temperature Dependence of the Microwave Dielectric Behavior of Selected Materials"

Marshall, John, "Application Advancements Using Electrorheological Fluids"

Ono, Kanji, "Piezoelectric Sensing and Acoustic Emission"

Ries, Heidi R., "An Integrated Approach to Laser Crystal Development"

NEW:Update 96

NASA Conference Publication 3354

Jain, H., "Learning About Electric Dipoles From a Kitchen Microwave Oven"

NEW:Update 97

NASA Conference Publication 208726

Marshall, John A. "Magneto-Rheological Fluid Technology"

Umana, Carlos E. "How to Compute the Atomic Magnetic Dipole Moment of An Element: An Engineering Approach"

NEW:Update 98

NASA Conference Publication

Abramowitz, Harvey. "Use of Piezoelectric Crystals for Voice Recognition"

Dahiya, J. N. "Liquid Crystal p-Azoxyanisole in Microwave Field"

Draayer, Bret. "Simulating Optical Correlation on a PC"

Kasdan, Matthew, Kennedy, Stephen K. "Microchemistry and the New Scanning Electron Microscopes"

Loutts, George B., Noginov, Mikhail A., Wynne, Rosalind, Ross, Kai T., Grandy, Talia. "Investigation of thermal Bleaching in Manganese Doped Orghoaluminate Single Crystals"

Marshall, John A. "Magneto-Rheological Fluid Technology"

Noginov, M. A., Warren, M., Loutts, G. B. "X-ray Excited Emission of Mn^{2+} ions in Mn: $YAlO_3$

Valenquela, R., Amano, E. "Determination of the Curie Temperature in Ferro and Ferrimagnets"

EXPERIMENTS & DEMONSTRATIONS IN MATERIALS SYSTEMS

NEW:Update 96

NASA Conference Publication 3354

Aceves, Salvador M., Smith, J. Ray, Johnson, Norman L., "Computer Modeling in the Design and Evaluation of Electric and Hybrid Vehicles"

Benjamin, Robert F., "Experiments Showing Dynamics of Materials Interfaces"

Daugherty, Mark A., "Electrolytic Production of Hydrogen Utilizing Photovoltaic Cells"

Fine, Leonard W., "The Incandescent Light Bulb"

MacKenzie, James J., "Hydrogen -- The Energy Carrier of the Future"

NEW:Update 97

NASA Conference Publication 208726

Bunnell, L. Roy. "Weakening of Latex Rubber by Environmental Effects"

Chadwick, Margaret. "Automotive Materials For the Next Millennium"

NEW:Update 98

NASA Conference Publication

Fabris, Neda S. "Teaching Statistical Quality Control and Process Analysis in Materials Laboratory"

Widener, Edward L. "The Colorful Character of Materials"

EXPERIMENTS & TOPICS IN MATERIALS CURRICULUM

NEW:Update 93

NASA Conference Publication 3259

Bright, Victor M. "Simulation of Materials Processing: Fantasy or Reality?"

Diwan, Ravinder M. "Manufacturing Processes Laboratory Projects in Mechanical Engineering Curriculum"

Kundu, Nikhil K. "Graphing Techniques for Materials Laboratory Using Excel"

McClelland, H. T. "Process Capability Determination of New and Existing Equipment and Introduction to Usable Statistical Methods"

Passek, Thomas "University Outreach Focused Discussion: What Do Educators Want From ASM International"

NEW:Update 94

NASA Conference Publication 3304

Brimacombe, J. K., "Transferring Knowledge to the Shop Floor"

Burte, Harris M., "Emerging Materials Technology"

Constant, Kristen P. and Vedula, Krishna, "Development of Course Modules for Materials Experiments"

Coyne, Jr., Paul J., Kohne, Glenn S., Elban, and Wayne L., "PC Laser Printer-Generated Cubic Stereographic Projections with Accompanying Student Exercise"

Masi, James V., "Bubble Rafts, Crystal Structures, and Computer Animation"

McKenney, Alfred E., Evelyn D., and Berrettini, Robert, "CD-ROM Technology to Strengthen Materials Education"

Olesak, Patricia J., "Understanding Phase Diagrams"

Scheer, Robert J., "Incorporating "Intelligent" Materials into Science Education"

Schwartz, Lyle H., "Technology Transfer of NIST Research"

Spiegel, F. Xavier, "Demonstrations in Materials Science From the Candy Shop"

Uhl, Robert, "ASM Educational Tools Now and Into the Future"

NEW:Update 95

NASA Conference Publication 3330

Belanger, Brian C., "NIST Advanced Technology Programs"

Berrettini, Robert, "The VTLA System of Course Delivery and Faculty in Materials Education"

Kohne, Glenn S., "An Autograding (Student) Problem Management System for the Compeuwtr Ilittur8"

Russ, John, "Self-Paced Interactive CD-ROMS"

NEW:Update 96

NASA Conference Publication 3354

Chaudhury, S. Raj, Escalada, Larry, Zollman, Dean, "Visual Quantum Mechanics - A Materials Approach"

Gulden, Terry D., Winter, Patricia, "Explorations in Materials Science"

McKelvy, Michael J., Birk, James P., Ramakrishna, B. L., "Bringing Advanced Experimental Technology Into Education"

McMahon, Jr., Charles J., "Labs on Videotape for Materials Science and Engineering"

Parkin, Don M., "Los Alamos - The Challenging World of Nuclear Materials Science"

Pendleton, Stuart E., "Next Generation Multimedia Distributed Data Base Systems"

Russ, John C., "Impact of Multimedia and Network Services on an Introductory Level Course"

Spiegel, F. Xavier, "NEW:Update, The Experience of One College"

Wilkerson, Amy, Self, Donna, Rodriquez, Waldo J., Ries, Heidi R., "A "Problem Based Learning" Approach to Reflection and Refraction"

Winter, Patricia S., "Business Involvement in Science Education"

NEW:Update 97**NASA Conference Publication 208726**

Chaudhury, S. Raj. "The National Educators' Workshop WEB"

Hudson, John B., Shadler, Linda S., Palmer, Mark A., Moore, James A. "Integration of Laboratory Experiences Into An Interactive Chemistry/Materials Course"

Jacobs, James A., McKenney, Alfred E. "213 Experiments on CD-ROM From 10 Years of NEW:Updates"

Kayser, Jack R. "Structural Laboratory Manual"

Russ, John C. "Impact of Multimedia and Network Services on an Introductory Level Course"

Sawyer, W. Gregory, Bryson, Daniel, Svanes, Torkel, and Hudson, John B. "Effective Learning Through Interactive Computer Simulation and Experimentation."

Shackelford, James F., Meier, Michael. "Computer Applications For The Materials Laboratory/Classroom: Illustrating Structure and Diffraction"

Swyler, Karl J., Fine, Leonard W. "Preview of NEW:Update 98"

Winter, John M. Jr., Lipetzky, Kirsten G. "X-Ray Radiographic Exercises for an Undergraduate Materials Lab"

NEW:Update 98**NASA Conference Publication**

Berndt, C. C. "Internet Research and the Undergraduate Learning Experience"

Chaudhury, S. Raj, Golembiewski, Gae. "Educational and Public Outreach for the Mars Sample Return Project"

Halada, Gary. "Earthquake Resistant Engineering Design"

Halada, Gary. "Teaching Through Engineering Disaster"

Higley, James B. "Concurrent Engineering"

McKenney, Alfred E. "Producing PDF Files Using Adobe Acrobat Capture V2.01"

McMahon, Charles J., Jr. "Tutorials for Introduction to Materials Engineering"

Petrakis, Leon. "Rendering Asbestos Harmless"

Swyler, Karl. "Educational Programs at BNL and Other DOE Labs"

EMSET CD ROM
EXPERIMENTS IN MATERIALS SCIENCE, ENGINEERING & TECHNOLOGY
 ISBN: 0-13-648486-7
James A. Jacobs

A Multimedia Tool of Laboratory Experiments and Classroom Demonstrations

FEATURES:

- Over 200 laboratory experiments and classroom demonstrations which you can modify to suit your teaching objectives, environment, and students' needs.
- Access to instructional aids developed by hundreds of materials educators and industry specialists in the field of materials science, engineering and technology.
- Provides students with "hands-on" activities that cover the full range of materials science and technology: topics such as woods, metals, and emerging technologies including processing and structures of advanced composites and sol-gel ceramics.
- Flexibility: emphasis is placed on low-cost, multi-concept exercises in recognition of the many settings in which materials education occurs.
- The CD-ROM allows you to read, navigate, search for other experiments/documents, print, and edit.

CATEGORIES OF EXPERIMENTS:

TESTING & EVALUATION, POLYMERS, METALS, CERAMICS, COMPOSITES, ELECTRONIC MATERIALS & MATERIALS CURRICULUM

A BONUS CD OF VIDEO CLIPS:

A bonus CD provides video segments on selected concepts.
STM & AFM MICROSCOPY, POLYMERS, CERAMICS, AND COMPOSITES

PLATFORMS SUPPORTED:

This CD-ROM can be used on Windows and Macintosh platforms. Acrobat Reader and QuickTime software is included on the disk for Windows 3x, Windows 95 and Macintosh. The disk may be used on other platforms provided the appropriate software is installed.

TO ORDER A COPY	
Call: 1 (800) 947-7700 OR Visit our web site: www.prenhall.com	
OR simply fill out and mail this to:	
Prentice Hall, Order Processing Dept. 200 Old Tappan Road, Old Tappan, NJ 07675	
Date _____	Tax Exempt Cert. No. _____
P.O. Number _____	
<u>BILL TO:</u>	<u>SHIP TO:</u>
Account No. _____	Cust. Key No. _____
Name _____	Name _____
Dept. _____	Dept. _____
School/Org. _____	School/Org. _____
Address _____	Address _____
City _____	City _____
State, Zip _____	State, Zip _____
<i>CD-ROM Price: \$150.00</i>	

ORDERING INFORMATION FOR ADDITIONAL RESOURCES

Twenty copies of the NATIONAL EDUCATORS' WORKSHOP PUBLICATIONS (NASA-CPs from 1988 - 1997) are available on a first come, first served basis from

Dr. James A. Jacobs
Department of Technology
Norfolk State University
2401 Corprew Avenue
Norfolk, VA 23504

NASA publications may be ordered from

National Technical Information Center (NTIC)
Attention: Document Sales
5285 Port Royal Road
Springfield, VA 22161

or

National Center for Aerospace Information (CASI)
P. O. Box 8757
Baltimore, MD 21240-0757

BOB POND'S "FUN IN METALS" TAPE - AVAILABLE FROM

Johns Hopkins University
Maryland Hall 210
3400 N. Charles Street
Baltimore, MD 21218

Cost = \$30.00

JOURNAL OF MATERIALS EDUCATION SUBSCRIPTIONS:

JME has two categories of subscription: Institutional and Secondary. The institutional subscription -- for university departments, libraries, government laboratories, industrial, or other multiple-reader agencies is \$269.00 (US\$) per year. Institutional two-year subscriptions are \$438.00 (US\$). When the institution is already a subscriber, secondary subscriptions for individuals and subdivisions are \$45.00 (US\$). (Secondary subscriptions may be advantageous where it is the desire to preserve one copy for reference and cut up the second copy for ease of duplication.) Two-year subscriptions for secondary for individual or subdivision are \$75.00 (US\$). Back issues of JME are \$100 per year prior to 1996 (US\$).

Other Materials Education Council Publications available :

Classic Crystals: A Book of Models - Hands-on Morphology. Twenty-Four Common Crystal models to assemble and study. Aids in learning symmetry and Miller indices. \$19.00.

A Set of Four Hardbound Volumes of Wood Modules - The Clark C. Heritage Memorial Series. Published by MEC in cooperation with the U.S. Forest Products Laboratory, Madison, Wisconsin. A compilation of nine modules entitled Wood: Its Structure and Properties (I), edited by Frederick F. Wangaard. A compilation of eight modules especially developed for architects and civil engineers entitled Wood As A Structural Material (II). Also, Adhesive Bonding of Wood and Other Structural Materials III and Wood: Engineering Design Concepts (IV). Each of the first three wood volumes costs \$31.00; the fourth volume costs \$41.00. The entire four-volume set is only \$ 126.00 plus \$4.50 shipping (\$7.00 overseas).

The Crystallography Course - MEC's popular nine-unit course on crystallography. \$39.00.

Instructional Modules in Cement Science - Five units prepared for civil engineering and ceramic materials science students and professionals. \$19.00.

Laboratory Experiments in Polymer Synthesis and Characterization - A collection of fifteen peer-reviewed, student-tested, competency-based modules. \$25.00. Topics include: bulk polycondensation and end-group analysis, interfacial polycondensation, gel permeation chromatography, x-ray diffraction and others.

Metallographic Atlas - Royal Swedish Institute of Technology. \$33.00. A brief introduction to the microstructures of metallic materials - how they appear and how they can be modified.

Please add \$3.00 per book shipping charge.
Checks payable to The Pennsylvania State University

Managing Editor, JME
110 Materials Research Laboratory
The Pennsylvania State University
University Park, PA 16802

PARTICIPANTS



1998 NATIONAL EDUCATORS' WORKSHOP

Row 1: W. Li, O. Elkassir, E. Widener, R. Valenzuela, T. Allen, J. Li, J. Cheung, D. LaClaire, S. R. Chaudhury, R. Lopez, Joan Raitano. Row 2: C. R. Diez, K. Song, N. Fabris, J. Jacobs, L. Aldridge, K. Cordero, A. McKenney, B. Ross, C. Alderman. Row 3: R. Griffin, M. Meier, A. Karplus, S. Kennedy, D. Freeman, R. LaClaire, T. Roberts, R. Jiggetts, P. Lippel. Row 4: Y. Wei, B. Kim, J. Stantley, E. Helmer, B. Stang, T. Kilduff, J. Fillion, K. Swyler. Row 5. C. Umana, P. Brown, R. Berrettini, J. Higley, M. Rudes.

NATIONAL EDUCATORS' WORKSHOP 1998

PARTICIPANTS

Enrique Abola
Biology Department
Brookhaven National Laboratory

Harvey Abramowitz
Department of Engineering
Purdue University - Calumet
2200 169th Street
Hammond, IN 46323
219-989-2473
e-mail harveya@calumet.purdue.edu

Cheryl Alderman
North Carolina State University at UNCA
CPO 2360
One University Heights
Asheville, NC 28804-8511
828-251-6943
e-mail alderman@eos.ncsu.edu

Lori Aldridge
Northwestern High School
2503 W. Main Street
Rockhill, SC 29732
803-547-0969
e-mail LL1516@aol.com

Peter Allen
Columbia University in the
City of New York

Tatiana Allen
Department of Physics, Geology
and Astronomy
University of Tennessee at Chattanooga
15 McCallie Avenue
Chattanooga, TN 37403
423-755-4520
e-mail Tatiana-Allen@ute.edu

Ginger L. F. Arrington
NASA Langley Research Center
MS 211
Hampton, VA 23681-0001
757-864-9696
e-mail g.l.freeman@larc.nasa.gov

Gerard Ateshian
Columbia University in the
City of New York

Empress A. Arthur
Center for Materials Research
Norfolk State University
2401 Corprew Avenue
Norfolk, VA 23504
757-823-0953
e-mail earthur@vger.nsu.edu

Christopher C. Berndt
SUNY at Stony Brook
Department of Materials Science
and Engineering
306 Old Engineering
Stony Brook, NY 11794-2275
516-632-8507
e-mail cberndt@ccmail.sunysb.edu

Robert Berrettini
1019 Amelia Avenue
State College, PA 16802-4242
814-237-0301
rbb3@psu.edu

Kendra Brown
Center for Materials Research
Norfolk State University
2401 Corprew Avenue
Norfolk, VA 23504
757-547-8329

Paul W. Brown
International Council for Materials Education
Pennsylvania State University
110 Materials Research Laboratory
University Park, PA 16802
814-865-5352
e-mail etx@psu.edu

C. Raj Chaudhury
Norfolk State University
2401 Corprew Avenue
Norfolk, VA 23504
757-823-2241
e-mail schaudhury@vger.nsu.edu

Michelle Churma
Prentice-Hall, Inc.
445 Hutchinson Avenue 4th floor
Columbus, OH 43235
e-mail michele_churma@prenhall.com

David Crew
Materials Science Division
Brookhaven National Laboratory

Carl Czajkowski
Department of Advanced Technology
Brookhaven National Laboratory

Jai N. Dahiya
Physics Department
Southeast Missouri State University
One University Plaza
MS 6600
Cape Girardeau, MO 63701
573-651-2390
e-mail dahiya@physics.semo.edu

C. Ray Diez
Industrial Technology
University of North Dakota
Box 7118
Grand Forks, ND 58202-7118
701-777-2198

Bret Draayer
Southeast Missouri State University
Physics Department
One University Plaza
Cape Girardeau, MO 63701
573-651-2391
e-mail draayer@physics.semo.edu

Chris Durning
Columbia University in the
City of New York

Sonja Ebron
Norfolk State University
2401 Corprew Avenue
Norfolk, VA 23504
757-823-8771
e-mail SEbron@vger.nsu.edu

Andy Eng
IT Associates
Columbia University
505 Havermeyer
Chemistry Dept.
300 Broadway
New York, NY 10027
212-854-8575
e-mail aeng@chem.columbia.edu

Neda S. Fabris
Mechanical Engineering
California State University, Los Angeles
5151 State University
Los Angeles, CA 90032
213-343-5218
e-mail nfabris@calstatela.edu

Huan Feng
Department of Applied Science
Brookhaven National Laboratory

Luke Ferguson
University of Washington, MSE
1521 95th Street, NE
Seattle, WA 98115
206-525-4249
e-mail lukef@u.washington.edu

John E. Fillion
Manager of Body Materials Engineering
CIMS: 482-00-11
DaimlerChrysler Corporation
800 Chrysler Drive
Auburn Hills, MI 48326-2757
248-576-7472
e-mail jef2@chrysler.com

Leonard W. Fine
Department of Chemistry
Columbia University in the
City of New York
Havemeyer Hall
New York, NY 10027
212-854-2017
e-mail fine@chem.columbia.edu

Shanee' S. Frazier
Center for Materials Research
Norfolk State University
2401 Corprew Avenue
Norfolk, VA 23504
757-626-3020
e-mail sfrazier@vger.nsu.edu

Morton Friedman
Columbia University
School of Engineering and Applied Science
500 West 120th Street
Room 510 Mudd
New York, NY 10027
212-854-2986
e-mail friedman@columbia.edu

Janis Fulgham
Center for Materials Research
Norfolk State University
2401 Corprew Avenue
Norfolk, VA 23504
757-626-2994

James E. Gardner
Technical Staff Assistant
NASA Langley Research Center
Building 1219, Room 217
MS 118
Hampton, VA 23681-0001
757-864-6003
j.e.gardner@larc.nasa.gov

Dave Garza
Prentice-Hall, Inc.
One Lake Street
Upper Saddle River, NJ 07458

Edward S. Gillman
Norfolk State University
2401 Corprew Avenue
Norfolk, VA 23504
757-823-2632
gillman@jlab.org

Richard B. Griffin
Department of Mechanical Engineering
Texas A&M
College Station, TX 77843
409-845-9779
e-mail rgriffin@mengr.tamu.edu

Gary Halada
SUNY at Stony Brook
308 Old Engineering
Stony Brook, NY 11794-2275
e-mail ghalada@ccmail.sunysb.edu

James H. Haliburton
Center for Materials Research
Norfolk State University
2401 Corprew Avenue
Norfolk, VA 23504
757-626-2631

Gar Harbottle
Chemistry Department
Brookhaven National Laboratory

Brian Keith Harris
Norfolk State University
2401 Corprew Avenue
Norfolk, VA 23504
757-626-2665

Charmagne D. Harris
Center for Materials Research
Norfolk State University
2401 Corprew Avenue
Norfolk, VA 23504
757-855-9121
e-mail chharris@vger.nsu.edu

Corinta Harris
Center for Materials Research
Norfolk State University
2401 Corprew Avenue
Norfolk, VA 23504
757-823-2381

John Heiser
Department of Advanced Technology
Brookhaven National Laboratory

Eric Helmer
Ocean Lakes High School
885 Schumann Drive
Virginia Beach, VA 2345
757-721-4110

Laura Henderson-Lewis
Materials Science Division
Brookhaven National Laboratory

Lael Herbert
Norfolk State University
2401 Corprew Avenue
Norfolk, VA 23504
757-626-2665
e-mail lherbert@vger.nsu.edu

Herbert Herman
Director
The Center for Thermal Spray Research
Brookhaven National Laboratory

Irving Herman
Columbia University in the
City of New York

James B. Higley
Purdue University Calumet
METS Department
Hammond, IN 46323
219-989-2584
e-mail higley@calumet.purdue.edu

Holli D. Horton
Center for Materials Research
Norfolk State University
2401 Corprew Avenue
Norfolk, VA 23504
757-855-8432
e-mail hhorton@vger.nsu.edu

James A. Jacobs
Norfolk State University
Department of Technology
2401 Corprew Avenue
Norfolk, VA 23504
757-823-8109
e-mail j_jacobs@vger.nsu.edu

Rodney D. Jiggetts
Physical Scientist
National Institute of Standards
and Technology
Bldg. 223, Room B 122
Gaithersburg, MD 20899
301-975-5122

Erik Johnson
NSLS Department
Brookhaven National Laboratory

David Jones
Center for Materials Research
Norfolk State University
2401 Corprew Avenue
Norfolk, VA 23504
757-245-2063
e-mail djones@vger.nsu.edu

Paul Kalb
Department of Advanced Technology
Brookhaven National Laboratory

Alan K. Karplus
Department of Mechanical Engineering
Western New England College
Springfield, MA 01119-2684
413-782-1220
e-mail akarplus@wnec.edu

Matthew Kasdan
31932 Violeta Lane
Coto de Casa, CA 92679
949-858-1165

Stephen K. Kennedy
RJ Lee Group, Inc.350 Hochberg Road
Monroeville, PA 15146
724-325-1776
e-mail skennedy.rjlg.com

Thomas F. Kilduff
504 Brafferton Circle
Hampton, VA 23663
757-857-0272
e-mail tkilduff@whro.net

Yulian Kin
Purdue University Calumet
2200 169th Street
Hammond, IN 46323
219-989-2684
e-mail kin@nwi.calumet.purdue.edu

Diana P. LaClaire
Norfolk State University
Department of Technology
2401 Corprew Avenue
Norfolk, VA 23504
757-823-9072
e-mail d_laclaire@vger.nsu.edu

Jackie Li
The Cooper Union for the Advancement
of Science and Art
51 Astor Place
New York, NY 10003
201-353-4042
e-mail jli@cooper.edu

Philip Lippel
L-Cubed Consulting
61 Boston Street
Somerville, MA 02143
617-628-3704

George Loutts
Norfolk State University
2401 Corprew Avenue
Norfolk, VA 23504
757-823-2031
e-mail g_loutts@vger.nsu.edu

Socky Lugo
Columbia University in the
City of New York
212-854-2163

Nancy Manning
Biology Department
Brookhaven National Laboratory

John Marshall
University of Southern Maine
John Mitchell Center
Gorham, ME 04038
207-780-5447
e-mail jmarshall@usm.maine.edu

Alfred E. McKenney
516 Fairfax Way
Williamsburg, VA 23185-8200
757-221-0476
e-mail hdjc41@prodigy.com

Charles McMahon
University of Pennsylvania
Department of MSE
3231 Walnut Street
Philadelphia, PA 19104
215-898-7979
e-mail cmcmahon@crsm.upenn.edu

Denis McWhan
Associate Director for
Basic Energy Sciences
Brookhaven National Laboratory
P. O. Box 5000
Upton, NY 11973-5000
516-344-3927
e-mail mcwhan1@bnl.gov

Mike Meier
University of California Davis
Department Chemical Engineering &
Materials Science
Davis, CA 95616
530-752-5166
e-mail mlmeier@ucdavis.edu

Ashanti Mitchell
Center for Materials Research
Norfolk State University
2401 Corprew Avenue
Norfolk, VA 23504
757-527-5331
amitchell@vger.nsu.edu

Arnie Moodenbaugh
Brookhaven National Laboratory

Stephen Murray
Columbia University in the
City of New York

Shree Nayar
Columbia University in the
City of New York

Mikhail A. Noginov
Norfolk State University
2401 Corprew Avenue
Norfolk, VA 23504
757-823-2204
e-mail mnoginov@vger.nsu.edu

Catherine Osiecki
Brookhaven National Laboratory
516-344-7171

Leon Petrakis
Energy Efficiency and Conservation Division
Department of Applied Science
Brookhaven National Laboratory
P. O. Box 5000
Upton, NY 11973-5000
516-344-3037
e-mail petrakis@bnl.gov

Michelle Ramotowski
NSLS Department
Brookhaven National Laboratory

Anthony Renshaw
Columbia University in the
City of New York

Lester Richardson
Norfolk State University
2401 Corprew Avenue
Norfolk, VA 23504
757-588-2188
e-mail lrichardson@vger.nsu.edu

Thomas E. Roberts
Milwaukee Area Technical College
700 W. State Street
Milwaukee, WI 53210
414-297-7280
e-mail srobe@execpc.com

Bill Ross
Muskegon Community College
221 S. Quarterline Road
Muskegon, MI 49442
616-777-0367
e-mail rossb@muskegon.cc.mi.us

Merrill Rudes
Energy Concepts, Inc.
595 Bond Street
Lincolnshire, IL 60069
847-821-1900 ext. 312
e-mail ecieng1@aol.com

James Schafer
Ivory Entrprises, Inc.
1625 Pine View Drive, NW
Issaquah, WA 98027

Carlos Smith
Norfolk State University
2401 Corprew Avenue
Norfolk, VA 23504
757-423-0053
e-mail vdamone@hotmail.com

Kyo D. Song
Norfolk State University
2401 Corprew Avenue
Norfolk, VA 23504
757-823-8105
e-mail kdsong@vger.nsu.edu

Peter Soo
Department of Advanced Technology
Brookhaven National Laboratory

Robert G. Stang
Department of Materials Science
and Engineering
University of Washington
Box 352120
Seattle, WA 98195-2120
206-543-2623
e-mail stang@u.washington.edu

James T. Stanley, II
Arizona State University
College of Engineering and Applied Sciences
Chemistry Biological & Materials
Engineering
P. O. Box 876006
Tempe, AZ 85287-6006
602-727-6309
e-mail jtsii@imap3.asu.edu

Toshi Sugama
Department of Applied Science
Brookhaven National Laboratory

Karl J. Swyler
Office of Educational Programs
Science Education Center
Brookhaven National Laboratory
Associated Universities, Inc.
P. O. Box 5000
Upton, NY 11973-5000
516-344-7171
e-mail swyler @bni.gov

Neda Tafreshi
P. O. Box 2059
Garden City, NY 11531
516-746-1590
e-mail gazanak@idt.net

Sturks Taylor, Jr.
Norfolk State University
2401 Corprew Avenue
Norfolk, VA 23504
757-623-3170
e-mail staylor@vger.nsu.edu

Jim Thomas
Columbia University in the
City of New York

Donald A. Tomalia
Michigan Molecular Institute in Midland
1910 West Saint Andrews Road
Midland, MI 48640
517-832-5555 ext. 601
e-mail tomalia@mimi.org

Carlos E. Umana
School of Mechanical Engineering
University of Costa Rica
San Pedro, Costa Rica
506-207-4548
e-mail cumana@pacuare.eie.ucr.ac.cr

Raul Valenzuela
Institute for Materials Research
National University of Mexico
P. O. Box 70-360
Mexico 04510 Mexico
525-622-46 53
e-mail monjaras@servidor.unam.mx

David Welch
Head - Materials Science Division
Department of Applied Science
Brookhaven National Laboratory
P. O. Box 5000
Upton, NY 11973-5000
516-344-3517
e-mail welch@sun2.bnl.gov

Charles V. White
Kettering University
1700 W. Third Avenue
Flint, MI 48504-4898

Edward L. Widener
Purdue University
Knob Hall 119
West Lafayette, IN 47907-1317
765-494-7521
e-mail elwidener@tech.purdue.edu

Amy Wilkerson
Center for Materials Research
Norfolk State University
2401 Corprew Avenue
Norfolk, VA 23504
757-823-2096
e-mail awilkerson@vger.nsu.edu

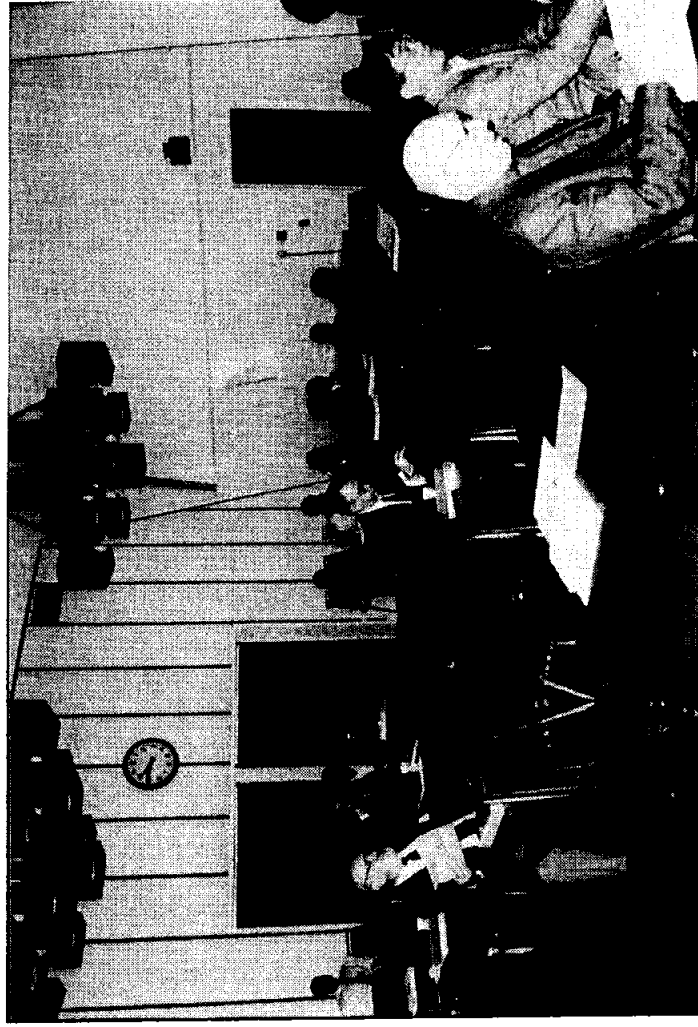
Eyad Youssef
Norfolk State University
2401 Corprew Avenue
Norfolk, VA 23504
757-823-8831
eyad@vger.nsu.edu

Bo Yu
Instrumentation Division
Brookhaven National Laboratory

Vladimir Zajic
Brookhaven National Laboratory

Mike Zarcone
Brookhaven National Laboratory

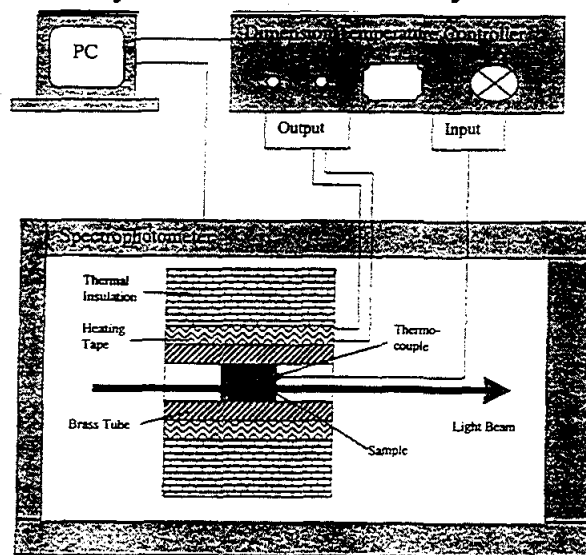
PARTICIPANTS



NATIONAL EDUCATORS' WORKSHOP

Update 98: Standard Experiments in Engineering Materials, Science, and Technology

November 1 - 4, 1998 - Brookhaven National Laboratory
Columbia University and Gateway Coalition
Stony Brook State University of New York



Sponsored by



National Aeronautics & Space
Administration
Langley Research Center



Norfolk State University
School of Science and
Technology

Brookhaven National Laboratory



Columbia University and Gateway Coalition
School of Engineering and Applied Science



**STONY
BROOK**
STATE UNIVERSITY OF NEW YORK

NIST

National Institute of Standards & Technology
Materials Science & Engineering Laboratories

with the support of

American Society for Engineering Education
American Society for Testing and Materials
ASM International
Boeing Commercial Airplane Company
Los Alamos National Laboratory
Council for Materials Education
Oak Ridge National Laboratory

WELCOME



Karl Swyler



Jim Jacobs

CONTRIBUTIONS



Jim Gardner



Diana LaClaire

CONTRIBUTIONS (Continued)



Donald Tomalia and Len Fine



Chris Berndt

REGISTRATION



Diana La Claire, Ginger Arrington, and Karl Swyler



Ginger Arrington

**MINI WORKSHOPS
AT
BROOKHAVEN NATIONAL LABORATORY
AND
SUNY AT STONY BROOK**

BNL MINI-WORKSHOPS
TUESDAY, NOVEMBER 3, 1998

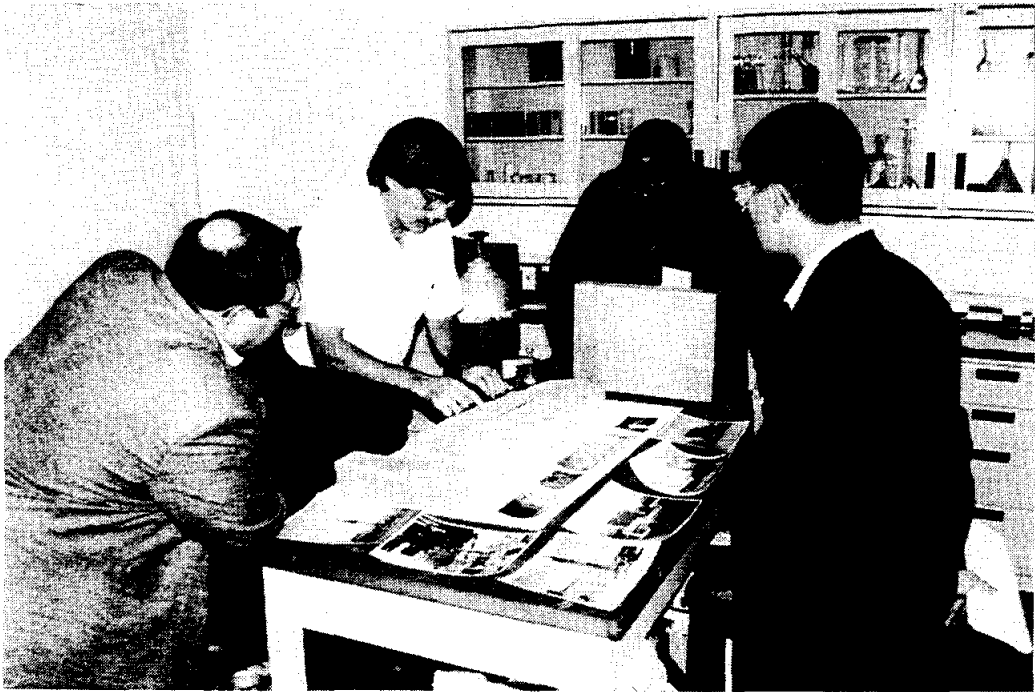
- 1. Accelerators in Materials Processing** - Mr. Chuck Carlson, Physics Department - Application of BNL'S Van De Graaff to testing electronic materials and fabricating microstructures.
- 2. Advanced Magnet Development** - Dr. Laura Henderson-Lewis, Materials Science Division - Studies in development of superconducting accelerator magnets and 'hard' magnets for energy-efficient motors.
- 3. Coating Technology** - Dr. Toshi Sugama, Department of Applied Science - Explore and evaluate the use of low-cost organic coatings to provide corrosion resistance.
- 4. Electronic Detector Technology** - Dr. Velko Radeka, et. al., Instrumentation Division - Investigate development of state-of-the-art systems for detecting high-energy particles and photons.
- 5. Failure Analysis** - Dr. Carl Czajkowski, Department of Advanced Technology - Apply techniques and methods of identifying metallurgical failure modes in nuclear reactor applications.
- 6. Hard X-ray Micromachining** - Dr. Erik Johnson, NSLS Department - Use of synchrotron radiation in the production of microstructures and characterizing the product.
- 7. High Tc Superconductors** - Dr. Arnie Moodenbaugh - Explore the properties of Hi Tc materials and possibilities for their practical application.
- 8. Materials Science at Large Facilities** - Dr. John Larese, et. al. Chemistry Department - Review principles of techniques used to characterize materials with synchrotron radiation and neutrons.
- 9. Nuclear Chemistry: Art and Archeology** - Dr. Gar Harbottle, chemistry Department - Investigate basic concepts of nuclear chemistry and review their application to studies in art and archaeology.
- 10: Oxidation and Degradation of Organic Martials** - Dr. Peter Soo, Department of Advanced Technology - Review/explore techniques used to study and assess the impact of oxidation on cable insulation.
- 11. Protein Crystallography** - Dr. Enrique Abola, Biology Department - Investigate the fundamentals of structural analysis by diffraction and educational applications of BNL's protein data bank.
- 12. Trace Element Analysis** - Dr. Keith Jones, Department of Applied Science - Detection of trace elements by X-ray fluorescence, and applications to materials science and engineering.
- 13. Wasteform, Container and Barrier Materials** - Dr. Paul Kalb, Department of Advanced Technology - Review/explore properties of materials relevant to hazardous waste management.
- 14. X-Ray Microtomography** - Dr. Betsy Dowd, National Synchrotron Light Source - Use of X-rays and advanced computational techniques to permit 3-d visualization of internal microstructure.

**SUNY AT STONY BROOK WORKSHOPS
TUESDAY, NOVEMBER 3, 1998**

- 1. Workshop on Material Properties of Biomedical Materials**
- 2. Tour and Demonstration of Facilities: Coatings and Manufacturing Technology**
- 3. Workshop on the Fracture Probability and Statistics of Glass**

Christopher C. Berndt
Department of Materials Science and Engineering
SUNY at Stony Brook

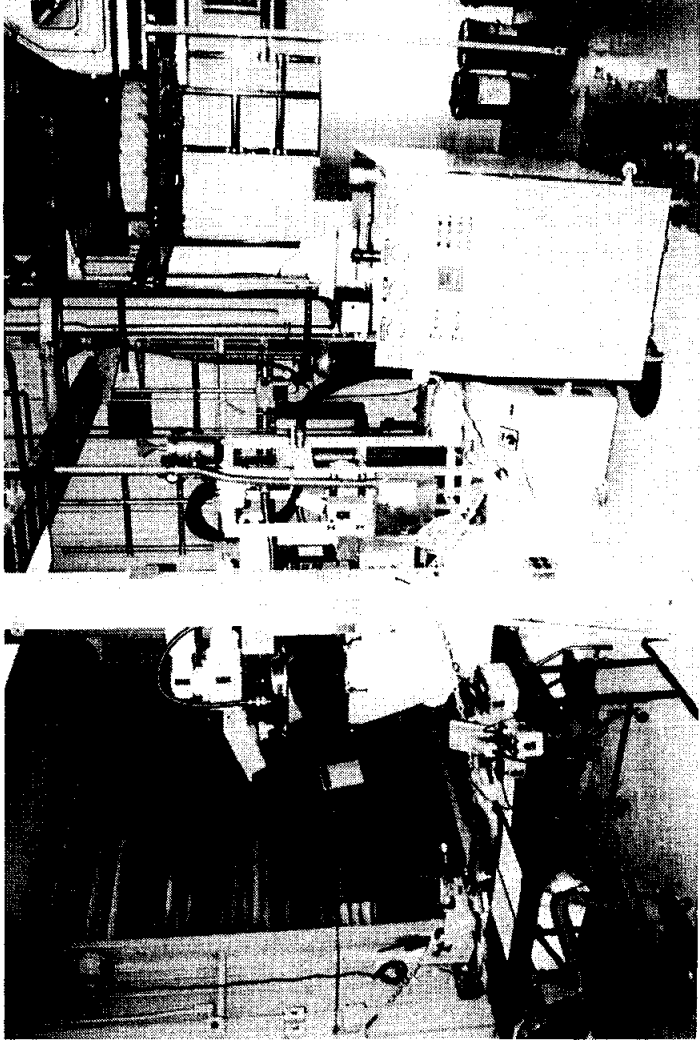
MINI WORKSHOPS



MINI WORKSHOPS (Continued)



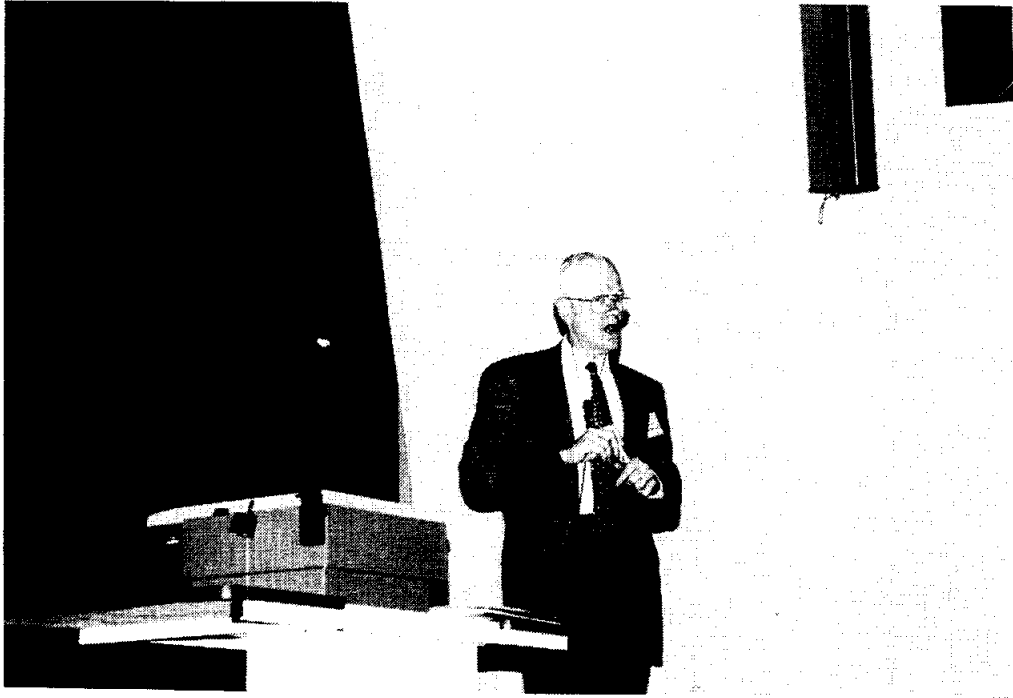
MINI WORKSHOPS (Concluded)



MATERIALS SCIENCE WITH PHOTONS AND NEUTRONS

Denis McWhan

Associate Director
for Basic Energy Sciences
Brookhaven National Laboratory
P. O. Box 5000
Upton, New York 11973-5000
516-344-3927
e-mail mcwhan1@bni.gov



Denis McWhan

Materials Science with Photons and Neutrons

OUTLINE

- DOE User Facilities
- Brookhaven User Facilities
 - National Synchrotron Light Source
 - High Flux Beam Reactor
- Imaging Techniques
 - Infrared Microspectroscopy
 - X-Ray Microtomography
 - Scanning Transmission X-Ray Microscope
- Scattering and Spectroscopy
 - High Temperature Superconductivity



DOE Science and Technology

Top Five Government Research Organizations for*:

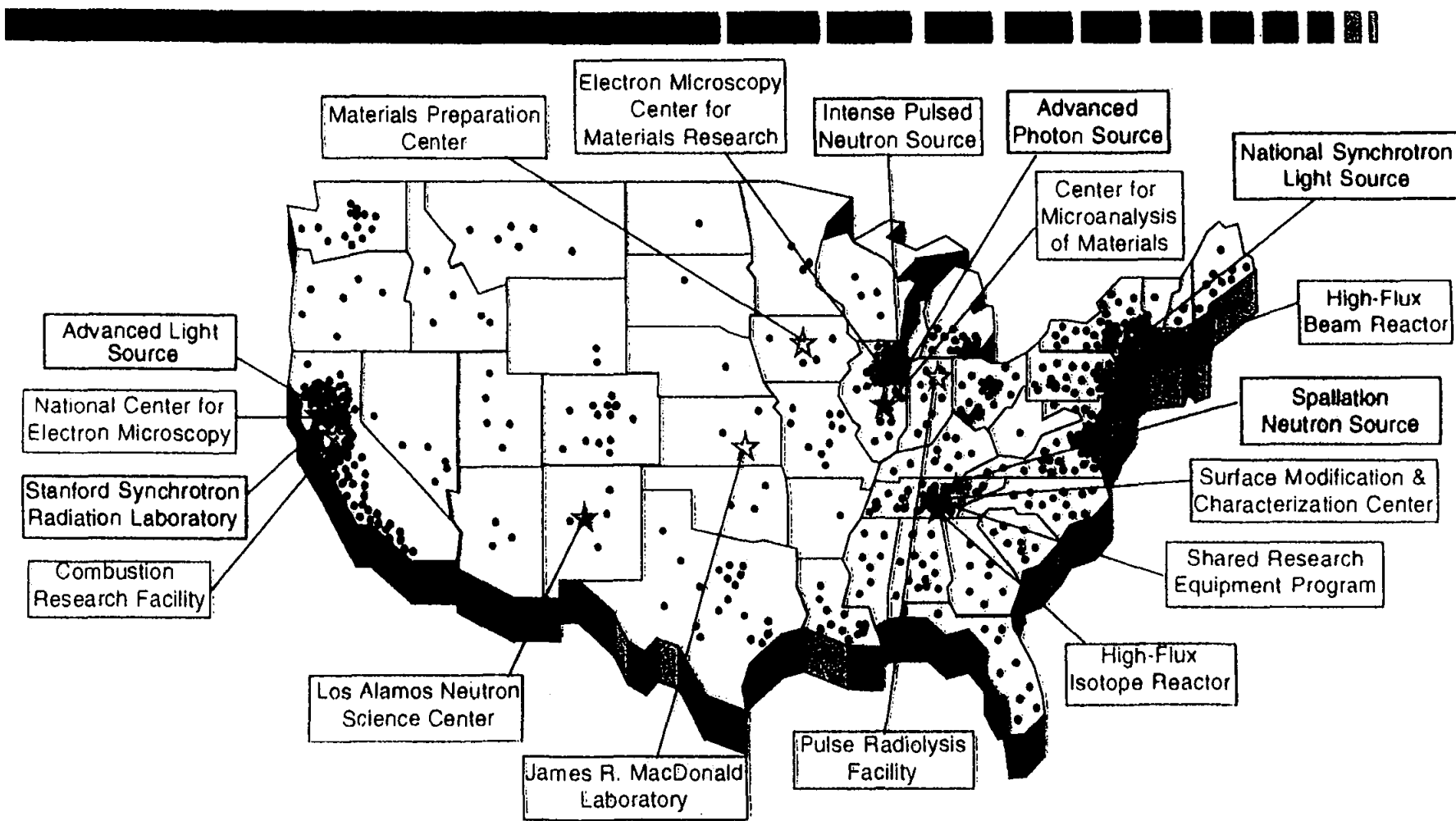
Physical Sciences	Environmental Sciences	Mathematics & Computing	Engineering
1. Energy (1,919)	1. NASA (974)	1. DOD (703)	1. DOD (1,979)
2. NASA (1,003)	2. NSF (459)	2. NSF (344)	2. NASA (1,690)
3. NSF (478)	3. Energy (399)	3. Energy (330)	3. Energy (586)
4. DOD (380)	4. DOD (385)	4. HHS (100)	4. NSF (464)
5. HHS (164)	5. DOC (264)	5. NASA (79)	5. DOC (179)

** Numbers are FY 97 Dollars in Millions - Source: NSF
Basic & applied research only - does not include development or construction*



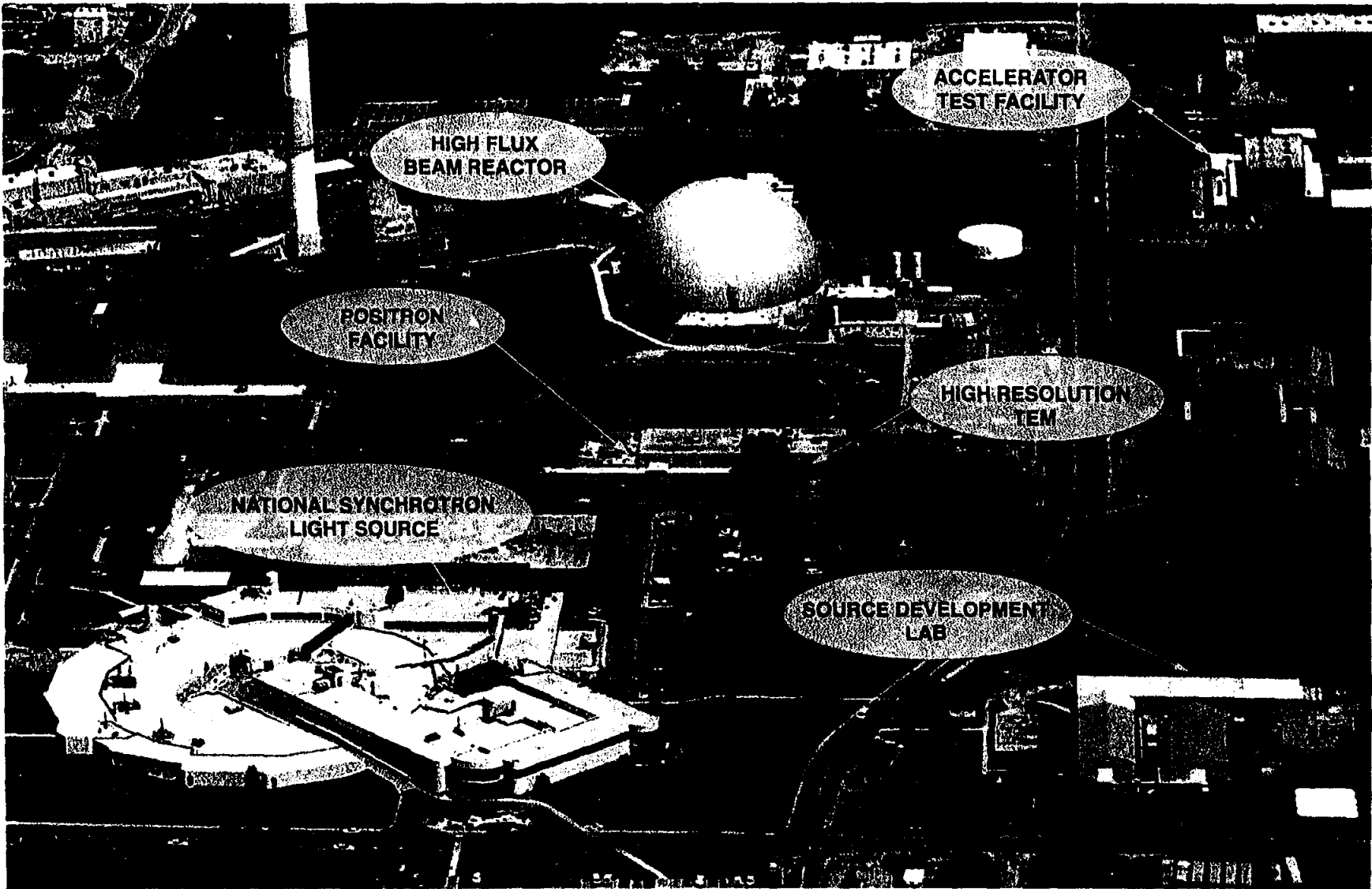
Office of Basic Energy Sciences

18 Scientific User Facilities (☆) and 1,400 Research Projects at 200 Institutions (•)



- 4 Synchrotron Radiation Light Sources
- 5 High-Flux Neutron Sources
- 4 Electron Beam Microcharacterization Centers

BROOKHAVEN NATIONAL LABORATORY



High Flux Beam Reactor

- One of 3 high flux research reactors in the world
- 15 instruments
- Presently shutdown awaiting decision to restart or decommission - to be made by Sec. Of Energy after completion of environmental impact statement

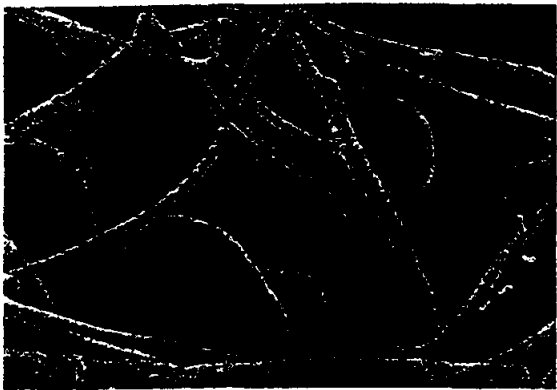
High Flux Beam Reactor

- Biology: membranes, protein crystallography
- Crystallography: organometallics, molecular crystals
- Condensed Matter Physics: magnetism, lattice dynamics, phase transformations
- Solid State Chemistry: physisorption, catalysis
- Powder Diffraction: zeolites, residual stress
- Reflectometer: polymer coatings, liquid-surfactant coatings
- Nuclear Physics: neutron capture in complex nuclei

Understanding Molecular Biology

Neutron beams from the HFBR are used by biologists to discover the molecular structure of proteins, nucleic acids, and other cellular components. Determining these structures is a critical step in understanding the functioning of muscle, ribosomes, chromatin, enzymes and many other biomolecules. Medical applications may result directly from this research, but more often indirectly, by providing a roadmap for the design of specific drugs. Recent research at the HFBR provides insights into:

- Activation of plasminogen in blood clotting
- Packaging of DNA in chromatin
- Structure of the immunosuppressant cyclosporin
- Location of anesthetics and anti-viral drugs in the cell membrane

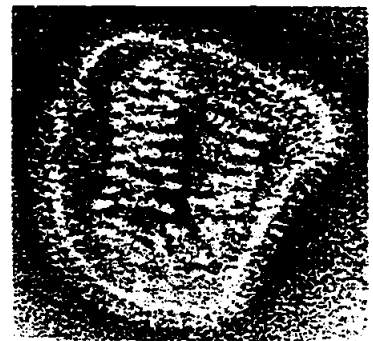
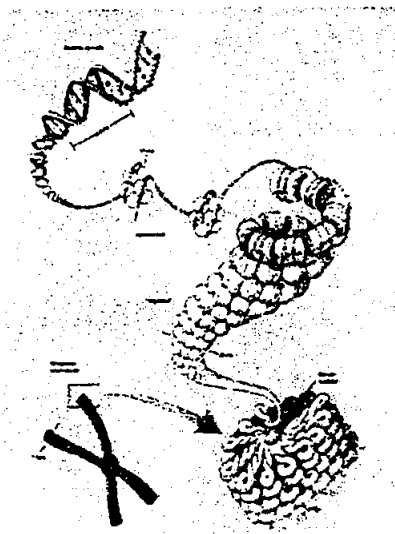


Dissolving Blood Clots

Neutrons are uniquely suited to probe the shape and changes in shape of biomolecules. Studies at the HFBR have shown that the inactive form of plasminogen circulating in the bloodstream is a compact molecule. When activated in a blood clot, it unfolds to expose a potent enzyme that dissolves the network of filaments that entangle blood cells. The action of a new drug, Tissue Plasminogen Activator (TPA), can be understood with this unfolding mechanism, and ways to increase its effectiveness in treating victims of heart attacks and strokes are being pursued.

DNA Packaging

X-ray experiments by J. Watson and F. Crick established the famous double-helix structure of DNA (top left), which holds the blueprint of life. Recent neutron studies at the HFBR revealed the structure of a higher order of its packaging (center right) – consisting of about 2 meters of DNA (blue) and protein cores (red) – which subsequently fold into chromosomes (bottom left). These studies are crucial to the understanding of cellular function, the expression of selected proteins, DNA repair and reproduction.



Membrane Bound Drugs

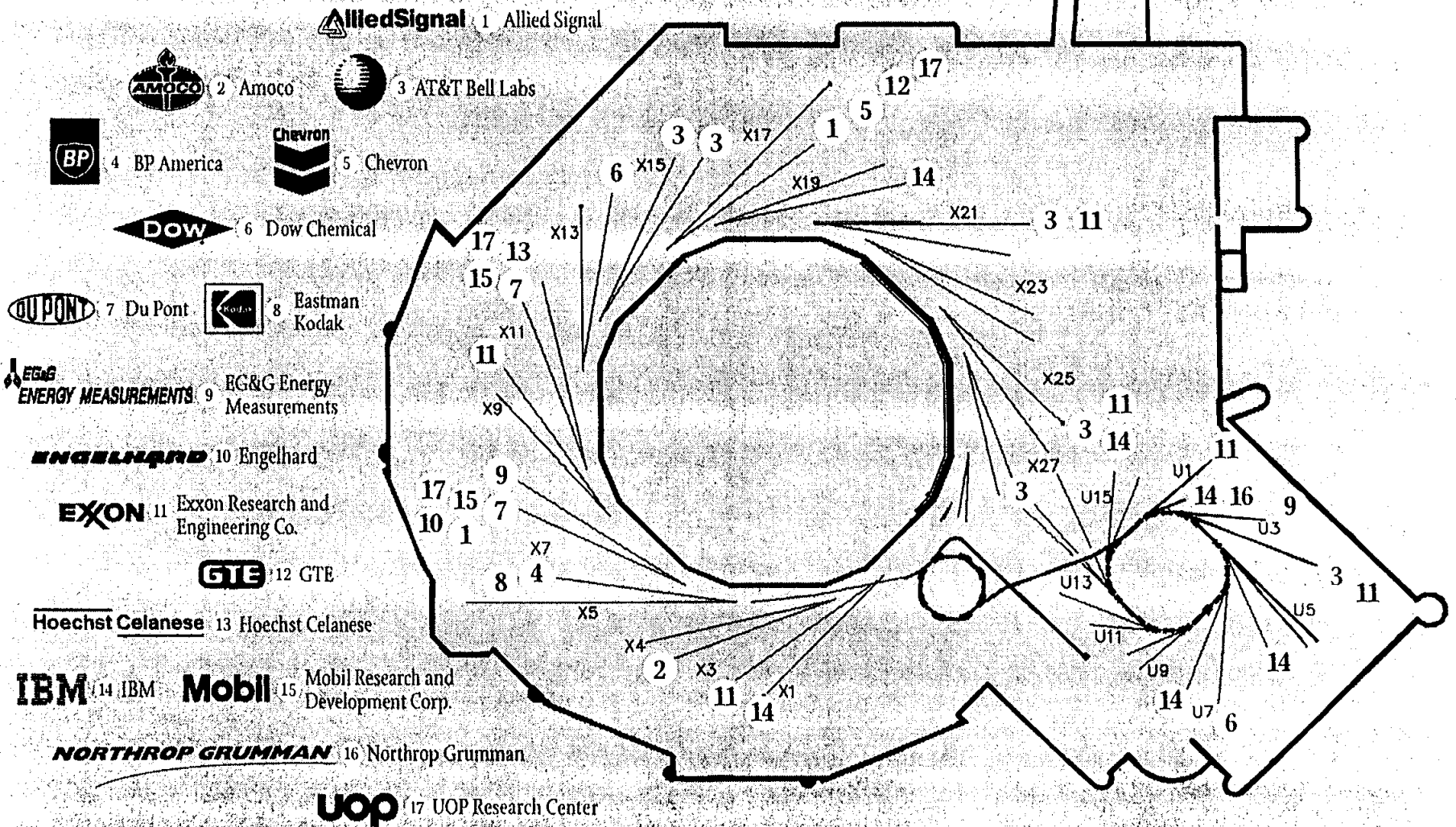
Lipid membranes enclose all cells, providing containment, anchoring protein channels, and aiding in defense mechanisms. These intrinsic membrane functional groups are uniquely recognizable using neutron diffraction. A small anti-viral drug, amantadine, was recently located deeply buried in the fatty layer of the membrane. This surprising result suggests that the drug prevents infection by the common cold virus (shown) by blocking its penetration of the membrane. Similarly constructed drugs may prove effective against other virus attacks.

National Synchrotron Light Source

- Two storage rings provide about 5000 hrs of beamtime at 80 experimental stations each year
- Photon energies from 0.1meV [12 mm] to 300MeV [4 fm] are used in experiments at NSLS
- Each year NSLS has 2200 Users in:
 - Chemical Sciences
 - Materials Sciences
 - Life Sciences and Medicine
 - Geosciences and Ecology
 - Applied Science and Engineering
 - Optical/Nuclear & General Physics

Corporations that contributed to PRTs at Brookhaven National Laboratory's National Synchrotron Light Source

11



Access to User Facilities

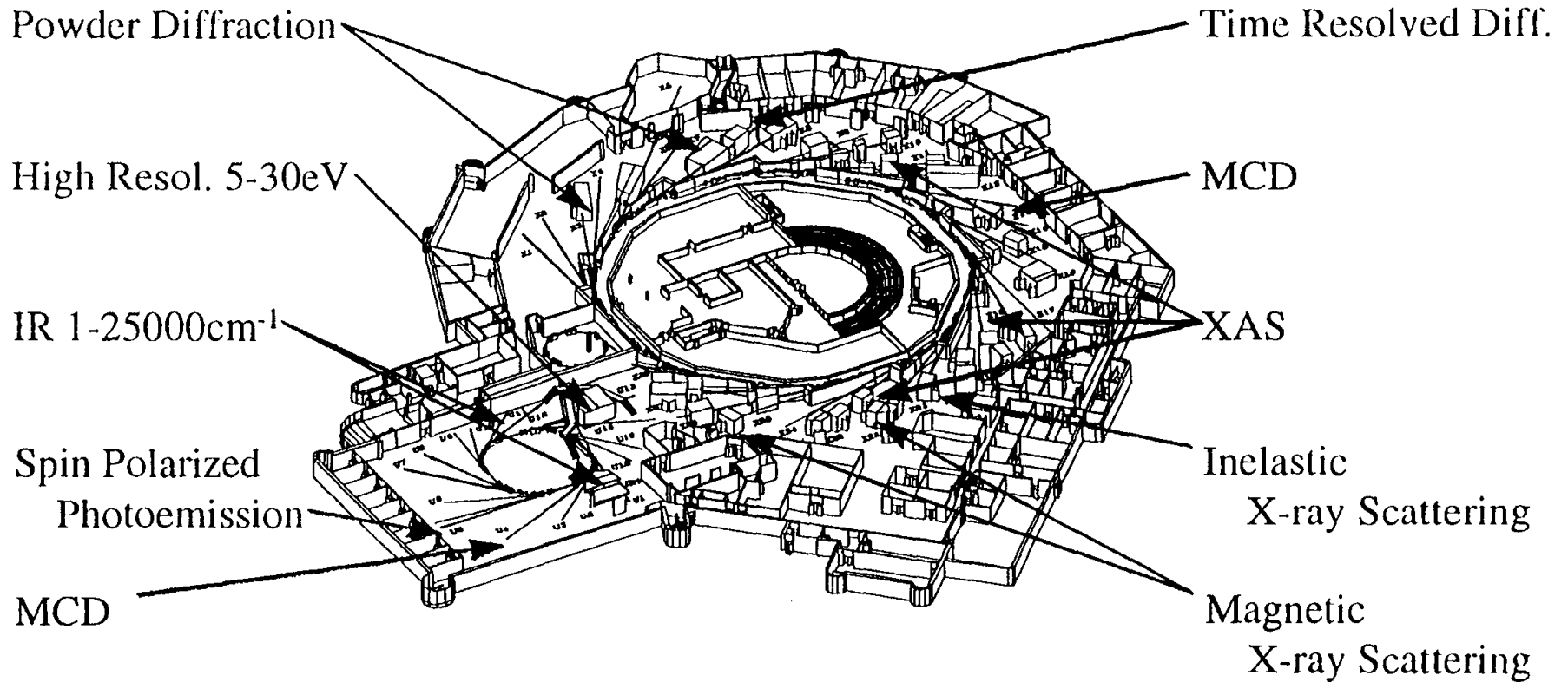
- HFBR and NSLS have Participating Research Teams, PRTs, that build and operate the beam lines.
- PRTs composed of researchers from industrial, university, and government laboratories and the NSLS.
- PRTs get between 75% and 25% of the beamtime depending on the degree of involvement of the NSLS.
- The remaining time is available for peer reviewed general user proposals.
- Full cost recovery is paid for beamtime for proprietary research. Beamtime is free for basic research.



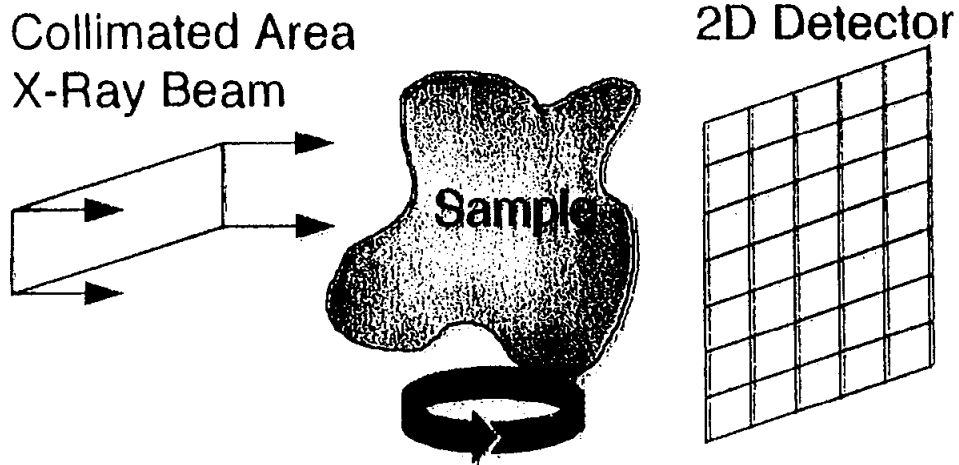
Oxide Studies at the NSLS



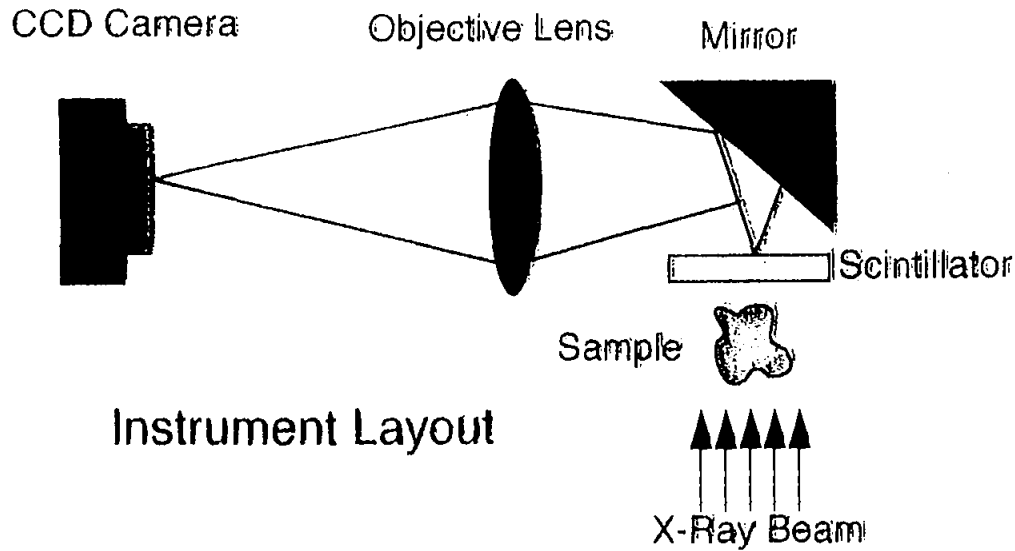
13



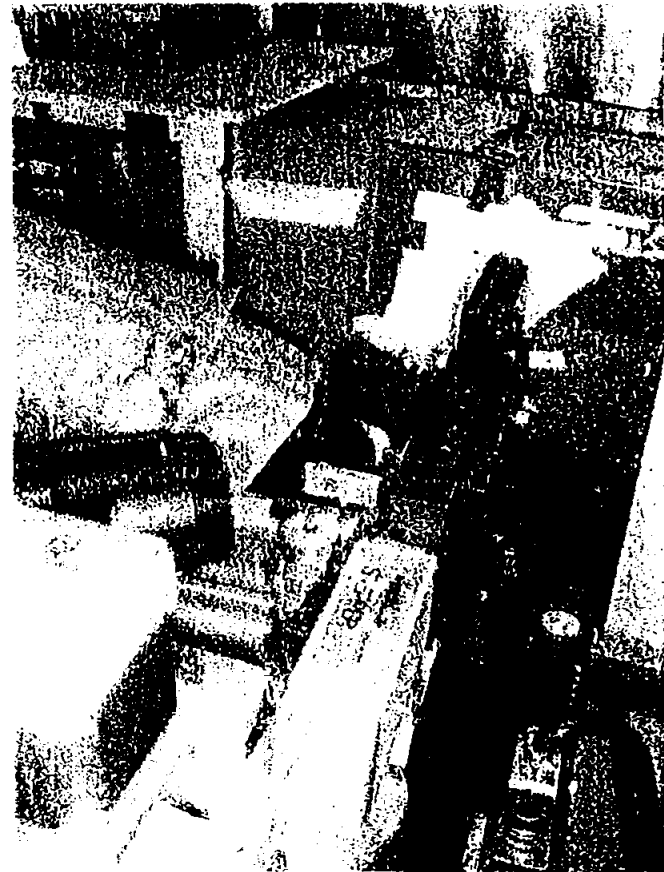
Synchrotron X-ray Computed Microtomography (XCMT)



Parallel-Beam Geometry Used for XCMT

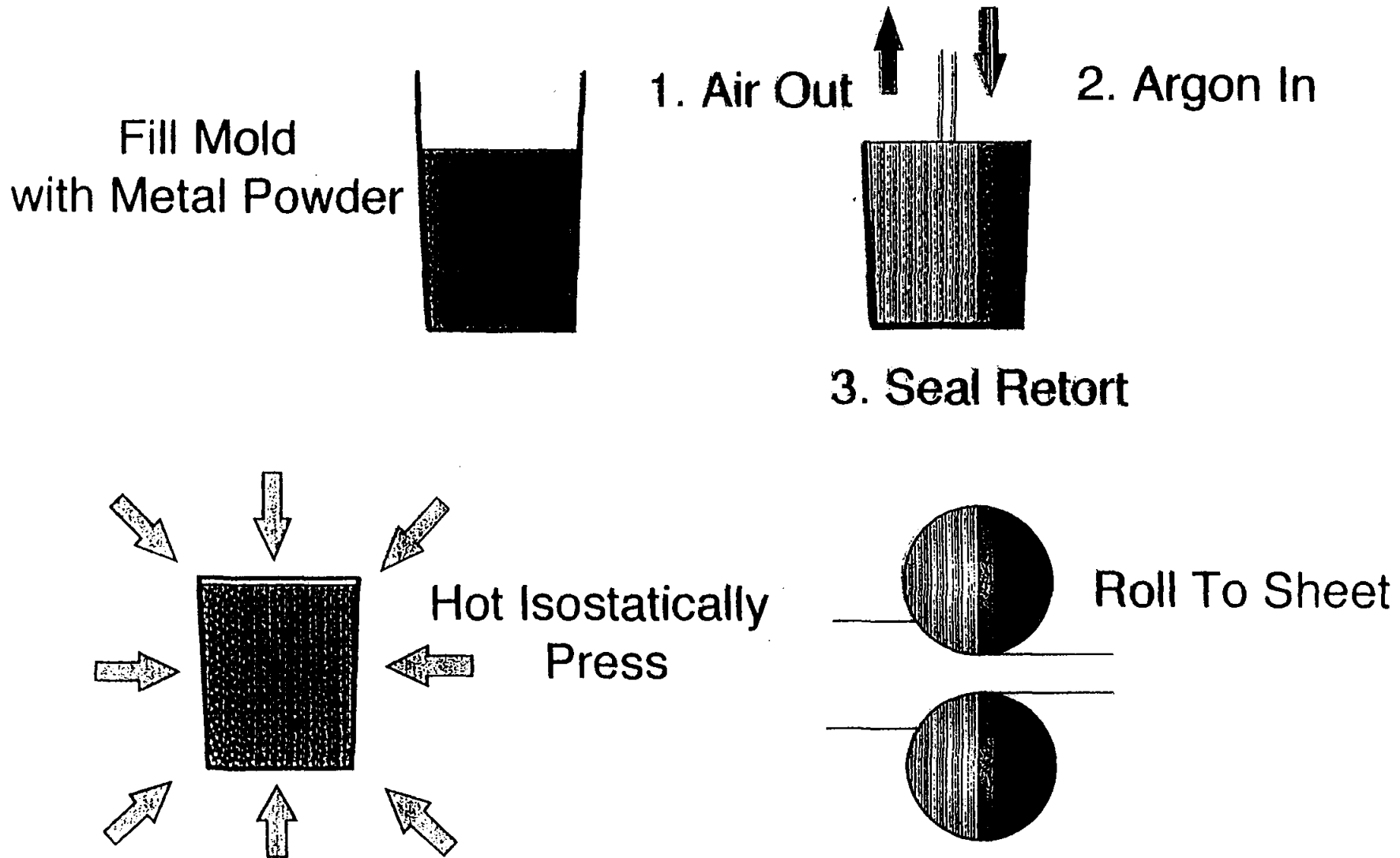


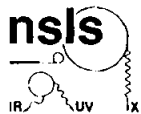
Instrument Layout



NSLS Beamline X27A

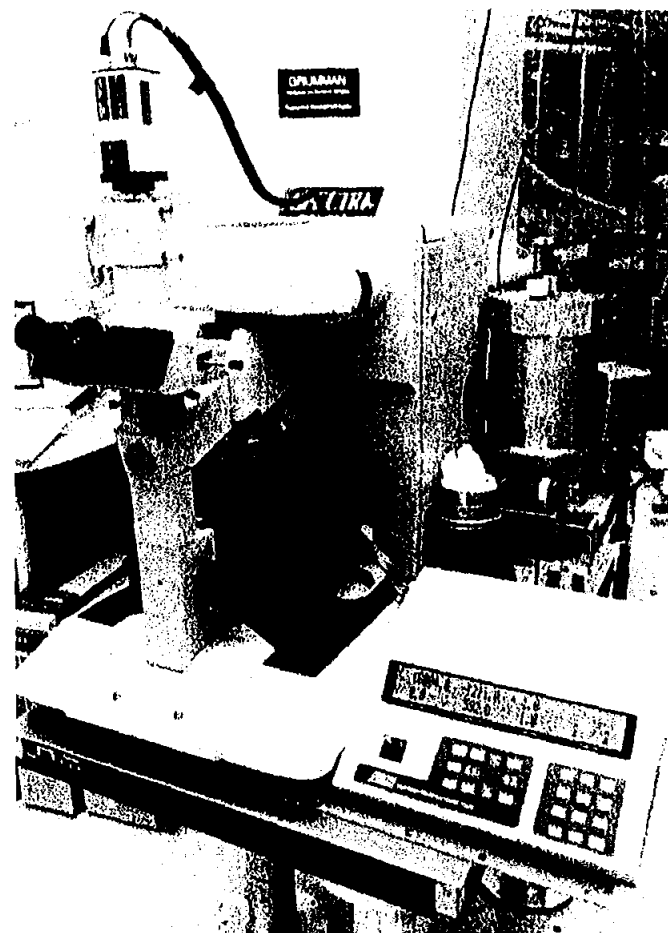
Boeing Low Density Core (LDC) Manufacturing Process

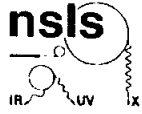




1st NSLS infrared microspectroscopy facility

- NSLS/ATDC CRADA.
- High brightness synchrotron IR source.
- Color CCD camera with image capture.
- All reflecting optics; $<2\mu\text{m} < \lambda < 25\mu\text{m}$.
- $\sim 1\ \mu\text{m}$ spatial resolution automated XY mapping stage for sample scanning.
- Shown with 4.2K Ge:Cu detector (also internal MCT).

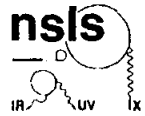




Infrared spectroscopy

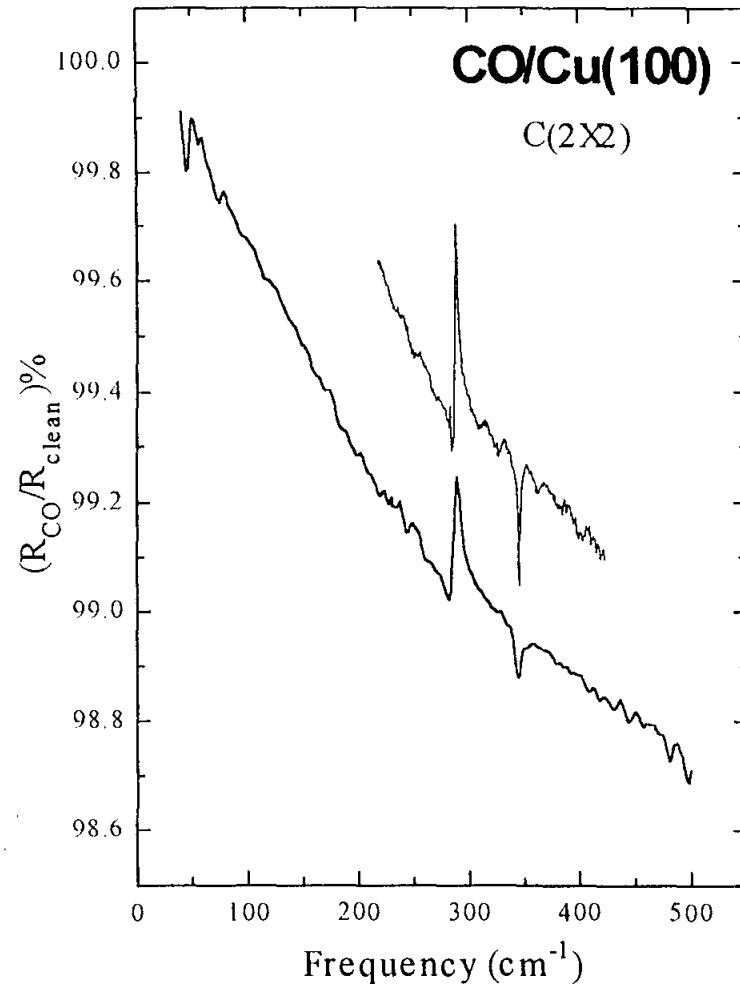
$$1\text{mm} > \lambda > 0.7\mu\text{m} \quad 1\text{ meV} < h\nu < 1\text{ eV} \quad 10\text{ cm}^{-1} < \bar{\nu} < 15,000\text{ cm}^{-1}$$

- vibrational / rotational modes of molecules and molecular units
- semiconductor bandgap transitions
- impurities (electronic states, vibrations)
- mobile carriers (electrons, holes)
- superconductivity (pair breaking, condensate dynamics)
- charge dynamics in “complex” metals (oxides, doped polymers, organics, C₆₀,...)



U4IR Beamline

- 90 mrad by 90 mrad port on VUV ring
 - $\theta_{nat} \sim 1.6(\rho v)^{-1/3}$
 \Rightarrow 100% collection down to 30 cm^{-1} .
 - Nicolet vacuum interferometer (20 cm^{-1} to 3,000 cm^{-1}).
- Operations begun in ~1987
- Surface science (*NSLS, AT&T, Exxon*)
 - adsorbates on metal crystals.
 - electrochemical interfaces (*NRL, ANL*)



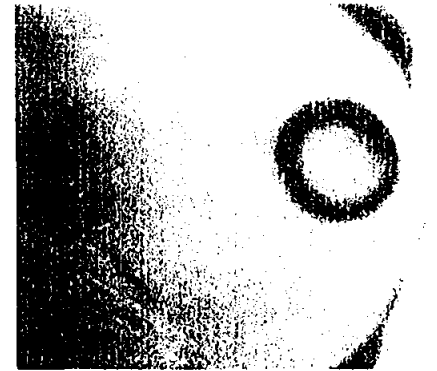
Fluid inclusions in minerals

N. Guilhaumou (*ENS*)
P. Dumas (*LURE*)

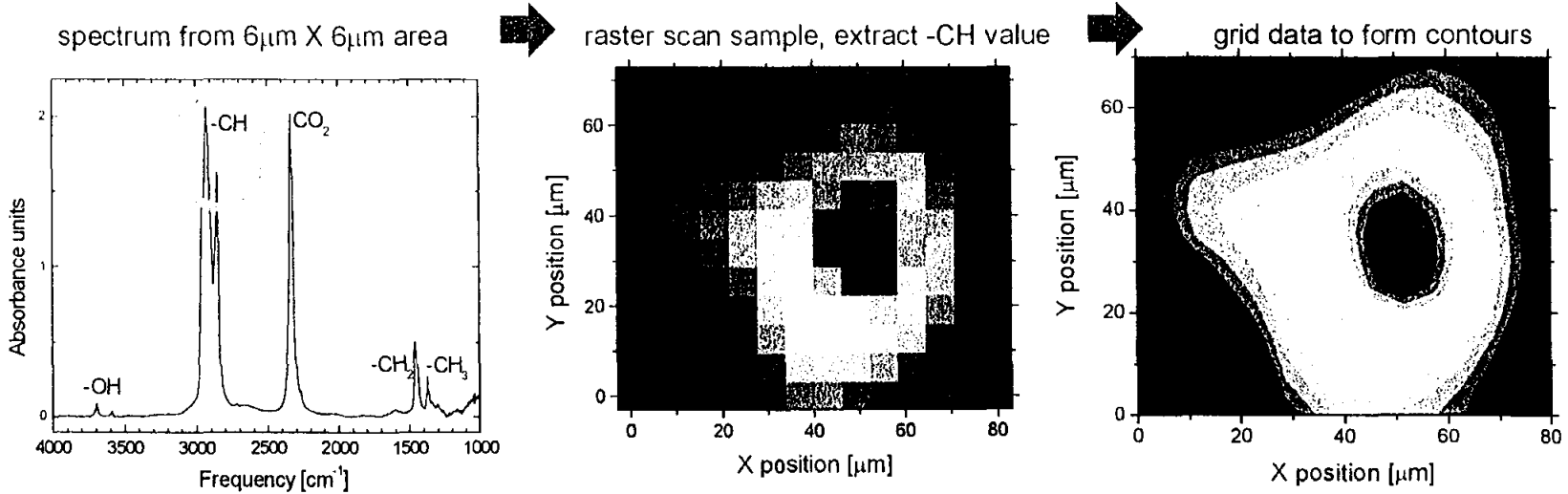
Fluid inclusion and gas bubble within fluorite

Transmission IR microspectroscopy study to determine composition of fluid and gas

visible image



19

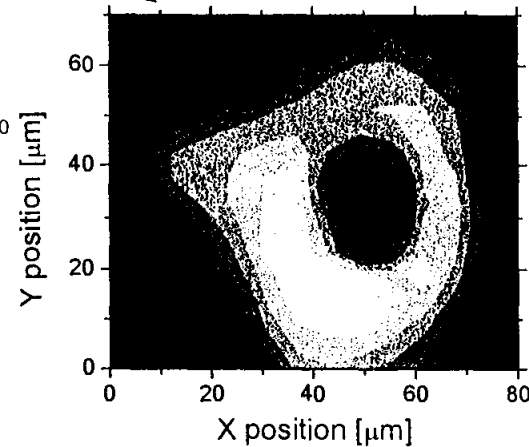
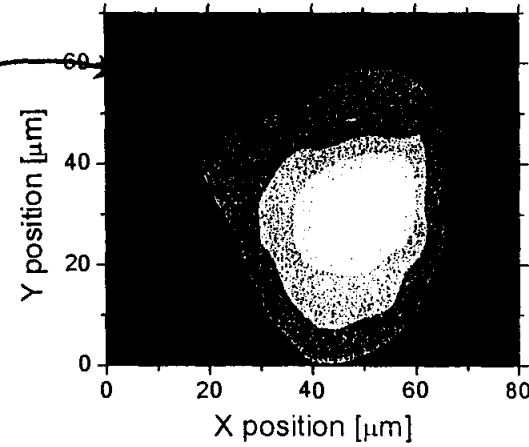
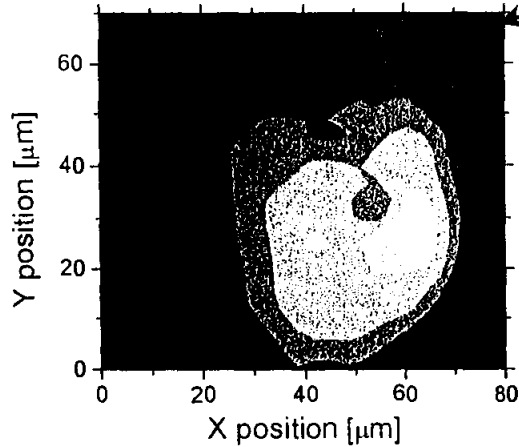
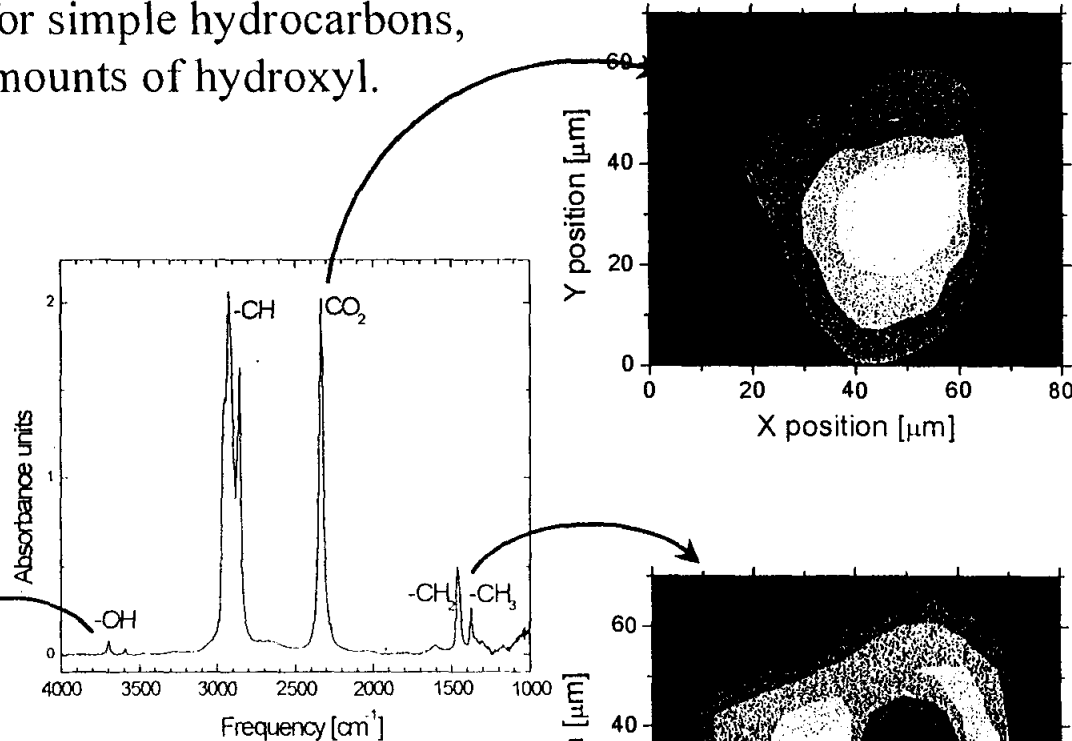


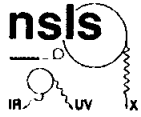
Fluid inclusions in minerals

IR spectra shows evidence for simple hydrocarbons, carbon dioxide, and small amounts of hydroxyl.

IR maps indicate:

- 1) hydrocarbon fluid (oil).
- 2) CO₂ bubble (plus dissolved in the oil).
- 3) hydroxyl groups likely at fluid/solid interface.



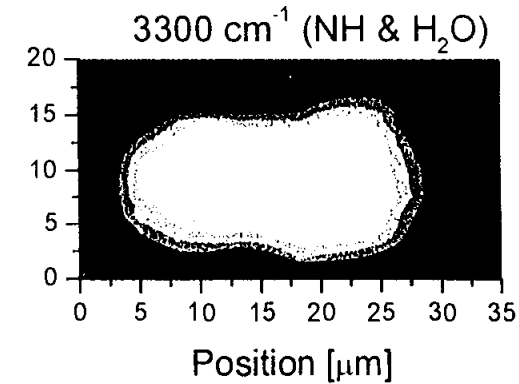
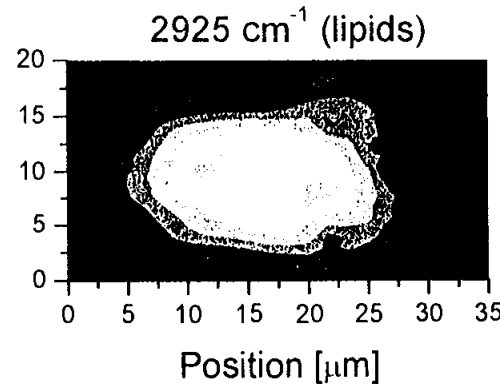
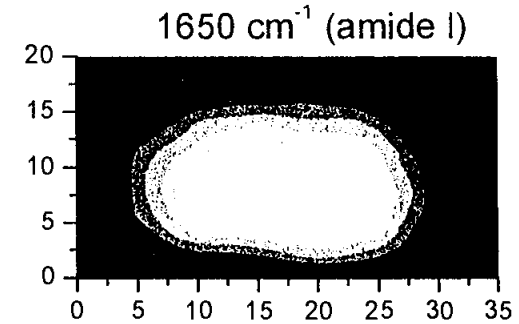
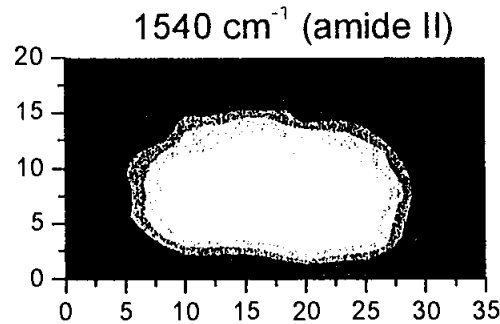


Infrared microspectroscopy of living cells

IR spectroscopic maps of various molecular functional groups of cells during mitosis (division).

21

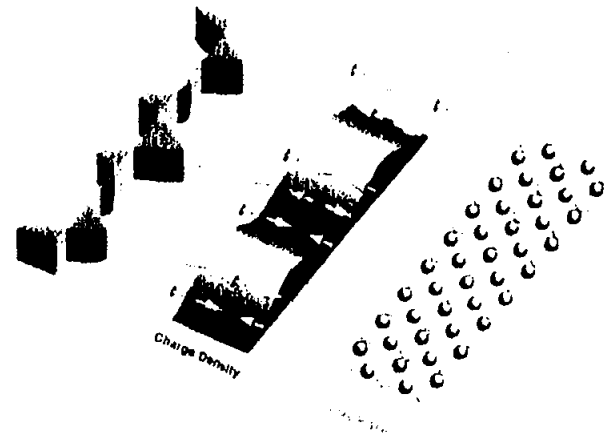
optical image
→



N. Jamin	CEA-DIEP Saclay
J.L. Teillaud	Institut Curie-Paris
P. Dumas	LURE- Orsay
G.L. Carr	NSLS-Brookhaven
G.P. Williams	NSLS-Brookhaven

Rivers of Charge: Stripes and Superconductivity

John Tranquada
Physics Department



Brookhaven
Science Associates

U.S. Department of Energy
Brookhaven National Laboratory

Introduction

- **Superconductors: definition**
 - **Materials which conduct electrical current without loss**
- **Applications**
 - **Electromagnets (MRI, RHIC, etc.)**
 - **Microwave filters for cellular phones**
- **High-temperature superconductors**
 - **Copper-oxide compounds**
 - **Require much less cooling than conventional superconductors**
 - **Mechanism of superconductivity is still a mystery**

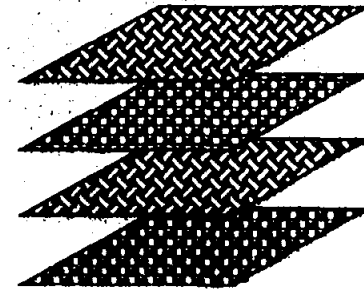
Background

- **Copper-oxide superconductors**

- **Layered compounds**

- **CuO₂ planes**

Many structures determined at
NSLS and HFBR

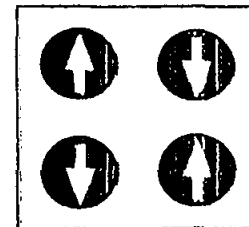


- **Parent compounds**

- **Electronic insulators**

- **Antiferromagnetic order
in CuO₂ planes**

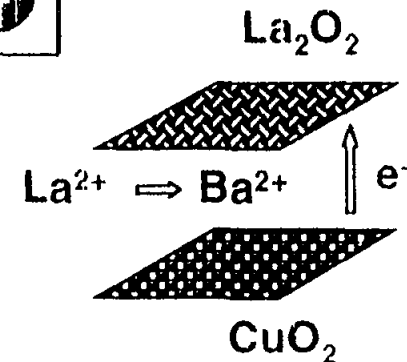
Discovered at HFBR



- **Charge carriers**

- **Introduced into CuO₂ planes
by chemical substitution**

Characterized at NSLS



Problem

- **Local antiferromagnetism coexists with superconductivity**
 - Antiferromagnetism tied to insulating behavior
 - Superconductivity requires mobile charge carriers

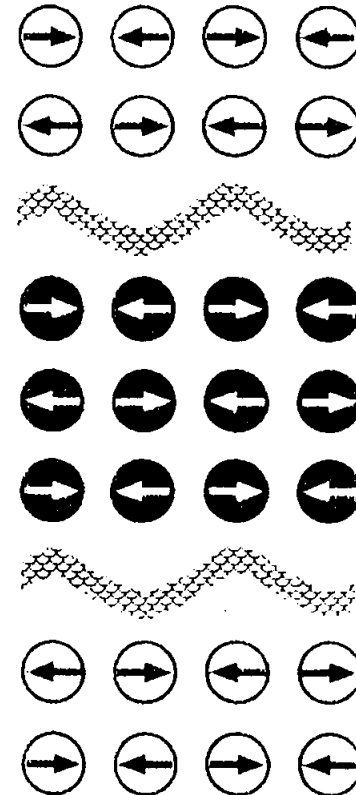
- **Conventional theories assume:**
 - Electronic homogeneity
 - Spatial uniformity

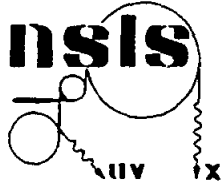
- **How can conflicting properties coexist?**

Solution

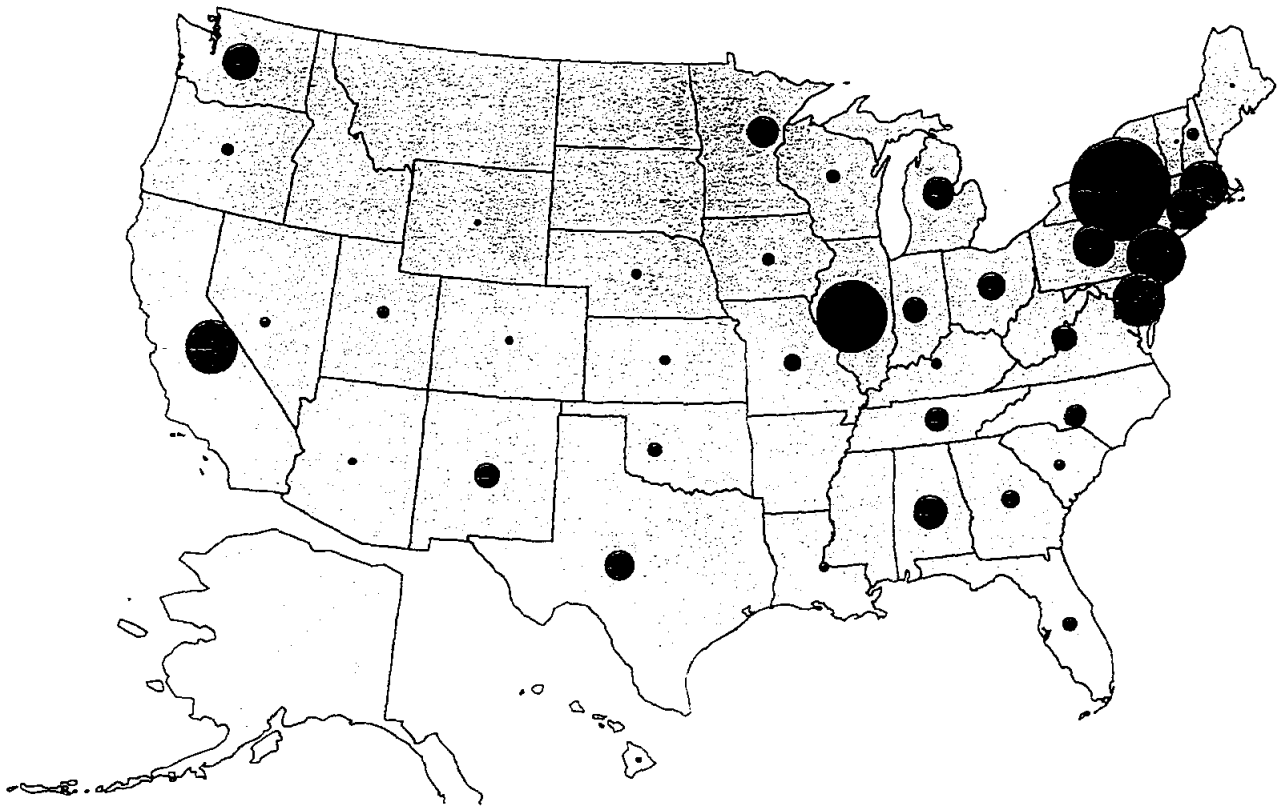
- **Spatial inhomogeneity**
 - "Rivers of charge between antiferromagnetic islands"
 - or Stripes

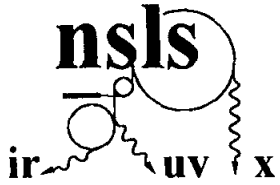
- **Driven by competing interactions**
 - Kinetic energy of charges
 - Magnetic exchange energy
 - Coulomb repulsion



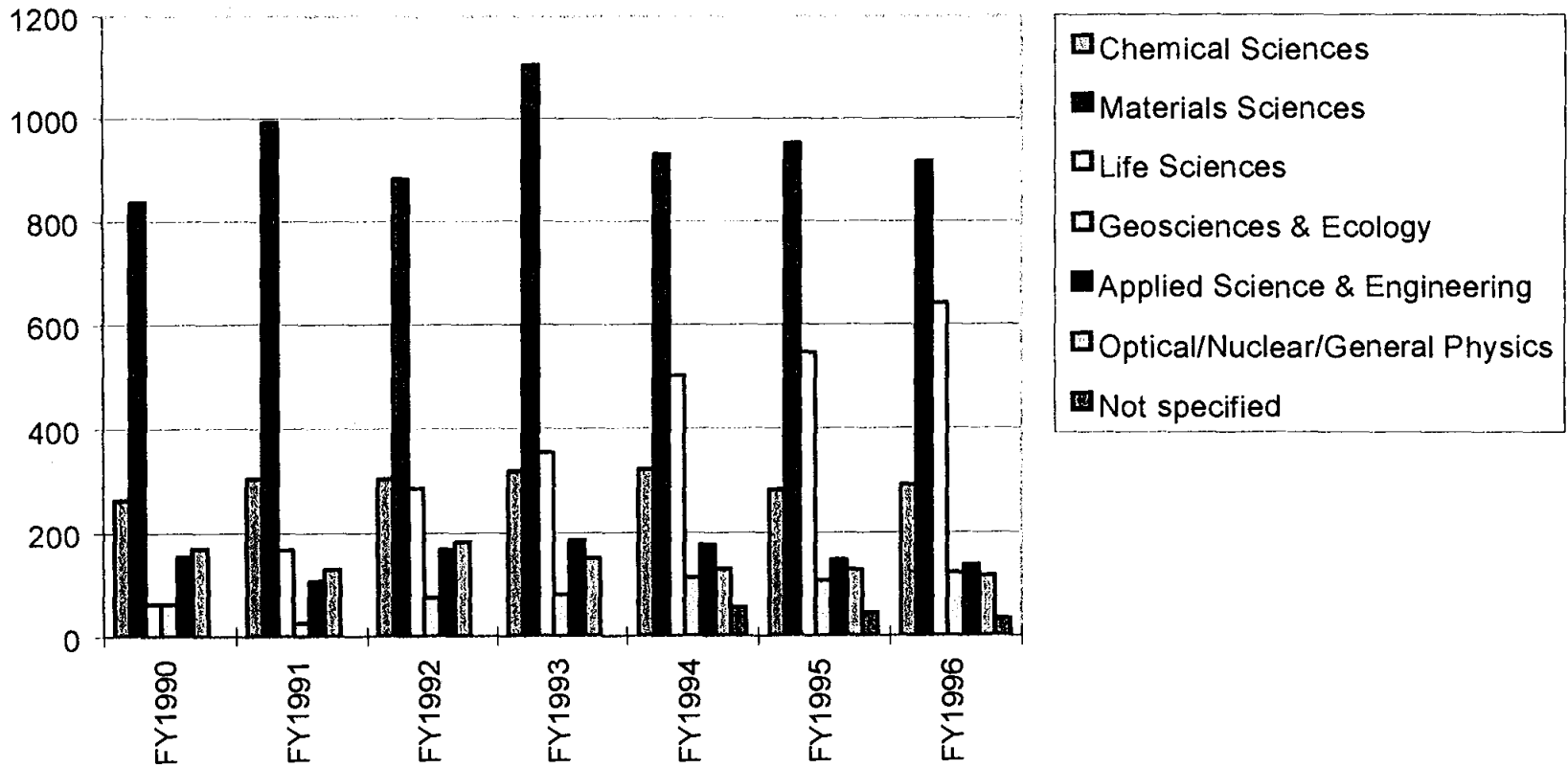


NSLS Active User Appointments





NSLS Users in various disciplines

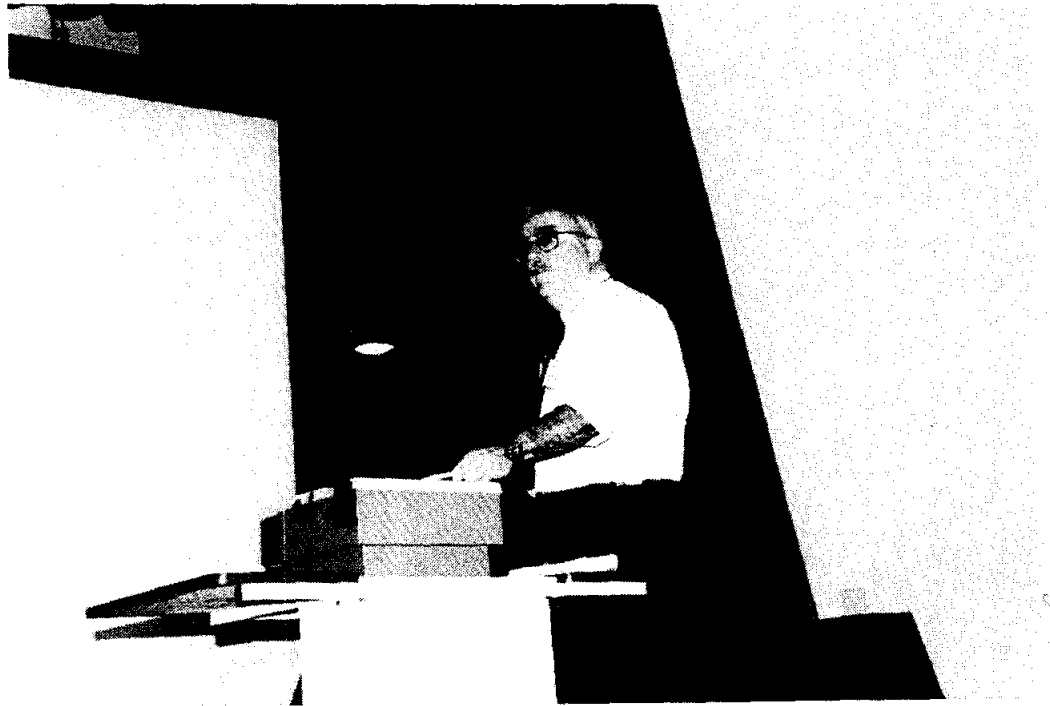


MAGNETO-RHEOLOGICAL FLUID TECHNOLOGY

John Marshall

University of Southern Maine
John Mitchell Center
Gorham, Maine 04038

Telephone 207-780-5447
e-mail jmarshal@usm.maine.edu



John Marshall

Magneto-Rheological Fluid Technology

**John A. Marshall, PHD
University of Southern Maine**

Key Words:

Hydraulics, mechanical power transmission, and rheology.

Perquisite Knowledge:

Elementary concepts of power transmission.

Objective:

To observe the tunable characteristics of magneto-rheological fluids.
To understand the potential power transmission advantages of these fluids.

Equipment and Supplies:

Magneto-rheological clutch assembly and power supply.

Introduction:

Magneto-rheological fluids change their flow characteristics when subjected to an electrical field. Response, which takes only milliseconds, is in the form of a progressive gelling that is proportional to field strength. With no field present, the fluid flows as freely as hydraulic oil (Korane, 1991).

Magneto-rheological fluids represent a technology that has the potential to widen the performance range of automated electromechanical and electrohydraulic equipment. Research and ongoing developments are refining this technology and experts predict an important future for these fluids.

Importance of Magneto-rheological Fluids:

Current automation capabilities are not advanced enough to build a robot that could play tennis. Even though cameras and computers could direct the robot towards a ball, robot's move in an awkward, lumbering fashion because conventional hydraulic valves cannot keep pace with the commands of the computerized controllers.

With magneto-rheological fluid technology, this type of response time is possible. This technology will allow devices that can operate instantly and without mechanical valves. Increased productivity and better product quality through more dependable and responsive automated equipment is just a small part of what this maturing technology can deliver.

How Magneto-rheological Fluid Functions:

Magneto-rheological fluids are composed of two primary components. They are the carrier fluid and the suspended particles. The carrier fluid needs to be a good insulator, compatible with the materials they contact. Typical particle materials include polymers, minerals, and ceramics (Scott, 1984).

When an magnetic field is applied to the fluid, positive and negative charges on the particles respond by separating, so each particle then has a positive end and a negative end. Particles of the magneto-rheological fluid then link together in the same manner that the north pole of one magnet is attracted to the south pole of another magnet (Duclos, 1988).

Potential Applications:

Magneto-rheological fluids can change from solids to liquids so fast, they will work well with fast-acting computers. These characteristics suggest a number of unusual engineering applications such as fluid clutches and vibration isolators (Duclos, 1988).

According to Hans Conrad, professor of materials science and engineering at North Carolina State University, magneto-rheological fluids will lead to a whole new generation of brakes, automatic transmissions, actuator devices, hydraulic valves, pump parts, and motors (Conrad, 1992).

Procedure:

Safety Considerations:

1. Protective eye wear is mandatory for all those in the lab area.
2. Read the operating instructions that accompany the magneto-rheological clutch assembly and power supply.
3. Obtain a "Material Data Safety Sheet" on the fluid from the supplier. Read the sheet completely and ask questions to any information you do not understand.

Observing the tunable clutch assembly:

1. With the power supply off, notice how easily the shafts can be rotated by hand.
2. Increase the power output through the range of 4, 8, 16, 32, 60, and 80 % and record your findings on the data sheet.
3. Vary the cycling frequency through the range of 4, 8, 16, and 32 Hz and notice the pulsating sensation while rotating the shafts. Record your findings on the data sheet.

Sample Data Sheet:

Record below the characteristics of the clutch when varying the power output.

Record below the characteristics of the clutch when varying the cycling frequency.

Instructor Notes:

1. The power being transmitted through the clutch increases proportionally when the power output is increased.
2. The impulses of power transmission increase as the cycling frequency is increased.

References:

Korane, K.: Putting ER Fluids To Work. Machine Design, May 9,1991, pp. 52-57.

Scott, D.: Amazing Hardening Fluids Open a New World of Hydraulic Drives. Popular Science, April 1984, pp. 42-46.

Duclos, T.G.: Electrorheological Fluids and Devices. Automotive Engineering, December 1988, pp.45-48.

Conrad, H.: The Impact of ER Fluids. Compressed Air Magazine, March 1992, pp.14-17.

“Procedure Demonstration Power Supply Controller” directions which accompany the tunable clutch.

Source of Supplies:

Internet resource to supplies and additional information:

<http://www.rmit.edu.au/departments/ch/rmpc/>

Biographical Information:

Dr. JOHN ALLEN MARSHALL taught senior high school prior to receiving his Ph.D. from Texas A&M University. He has seventeen years of university teaching experience, and is currently the Director of the Power and Energy curriculum and laboratories as well as the Internship Coordinator for the University of Southern Maine’s Department of Technology.

**X-RAY EXCITED EMISSION OF
Mn²⁺ IONS IN Mn:YAIO₃**

M. A. Noginov

M. Warren

and

G. B. Loutts

Center for Materials Research
Norfolk State University
2401 Corprew Avenue
Norfolk, Virginia 23504

Telephone: 757-683-2204
e-mail mnoginov@vger.nsu.edu



M. A. Noginov

X-ray excited emission of Mn²⁺ ions in Mn:YAlO₃

M. A. Noginov, M. Warren, G. B. Loutts
*Center for Materials Research,
Norfolk State University, Norfolk, VA*

Keywords:

Luminescence, Transition-metal ions in solids, Scintillators, Optical measurements

Prerequisite knowledge:

The student

1. should have basic understanding of different types of electromagnetic radiation (X rays, visible light)
2. should have basic knowledge of the materials science and/or solid-state physics and/or optical spectroscopy

Objectives:

The objectives of this experiment are:

- to demonstrate to the student the possibility of the X ray-to-visible energy conversion in solid states,
- to teach the student the basics of operation of X ray sources and conducting optical spectroscopic measurements,
- to demonstrate to the student the example of the analysis of the material parameters on the basis of the results of the spectroscopic measurements.

Equipment and supplies:

- The X-ray diffractometer Rigaku D/Max-2200 TB, Cu K_{α1} radiation, λ=0.154 nm. [Any standard source of X ray radiation can be used instead].
- The Mn:YAlO₃ crystal. [The experiment can also be conducted using many different scintillator crystals. The interpretation of the observed visible emission in each particular case will depend on the nature of the luminescent ion.]
- Model SR541 optical light chopper and model SR540 chopper controller from Stanford Research Systems, Inc. [Any similar chopper and controller can be used].
- 1m long and 8 mm in diameter optical bundle. We used the bundle from the light source model 1-150 from CUDA products corp. [Other similar bundles can be used as well.]
- Model H20 monochromator from ISA John Yvon, SPEX.. (Any similar monochromator can be used.)
- Any photomultiplier tube (PMT) with the maximum sensitivity in the visible range of the spectrum.
- Tektronix TDC 774 color four channel digitizing oscilloscope. [Any digitizing oscilloscope with the storage function can be used].

- The high voltage power supply for PMT (0-1500V). We used FLUKE high voltage power supply model 405B from FLUKE Mfg. Co. Inc. [Any power supply with similar characteristic can be used.]
- Electrical cables.

Background introduction:

In Ref. [1], Mn doped YAlO₃ was shown to be a promising material for holographic recording and optical data storage. The detailed characterization of Mn:YAlO₃ requires the spectroscopic study of all Mn valence states in the crystal. However, the ground state level in Mn²⁺ (⁶A₁) is the only sextet level in the system and all ground state transitions in Mn²⁺ are spin-forbidden and weak [2]. This makes optical excitation of Mn²⁺ luminescence very difficult, especially in the presence in the crystal of other Mn valence states.

In scintillator crystals the conversion of X-ray excitation into visible emission occurs in three common stages: conversion, transfer, and luminescence [3, 4]. In the first stage the radiation produces primary very hot electrons which in turn produce a cloud of secondary hot electrons thermalizing to electron hole pairs of low energy. In the second stage electron hole pairs very likely form excitonic centers of many forms in the scintillation centers. At this stage we have the process of energy transfer from these centers to the scintillation centers. In the third stage the scintillation centers (Mn²⁺ in our case) radiate the energy (visible light).

Experiment:

We found that Mn doped YAlO₃ crystals, single doped and co-doped with Ce, emit greenish light when excited with X-rays in the X-ray diffractometer (Rigaku D/Max-2200 TB, Cu K_{α1} radiation, λ=0.154 nm). We collected luminescence in the chamber of the diffractometer using the optical fiber bundle, sent light to the input slit of a small monochromator that we attached to the X-ray set up, and detected the signal with a photomultiplier tube. The schematic of the experiment is shown in Figure 1.

To increase the signal-to-noise ratio, we chopped the X-ray beam in the chamber with a regular chopper used in optical spectroscopy. The obtained emission spectrum (collected point by point using the averaging oscilloscope) is shown in Figure 2. It consists of the relatively broad emission line peaking at 0.53 μm and more narrow band centered at ≈0.71 μm.

We attribute the 0.71 μm emission band to Mn⁴⁺ ions (see Refs. [1,5,6]) and the 0.53 μm emission to Mn²⁺ ions. (In Ref. [7] the luminescence of Mn²⁺ ions in YAlO₃ was reported to be centered at 560 nm. However, many spectroscopic properties of Mn ions (in different valence states) reported in Ref. [7] were different from those in our crystals. As it was discussed in Ref. [3], possible reasons for this discrepancy are the different crystal growth technique (optical floating zone) and the post-growth annealing of the crystals used in work [7].) Using the analogy with the literature, we assign the 0.53 μm luminescence to the transition ⁴T₁→⁶A₁ in Mn²⁺.

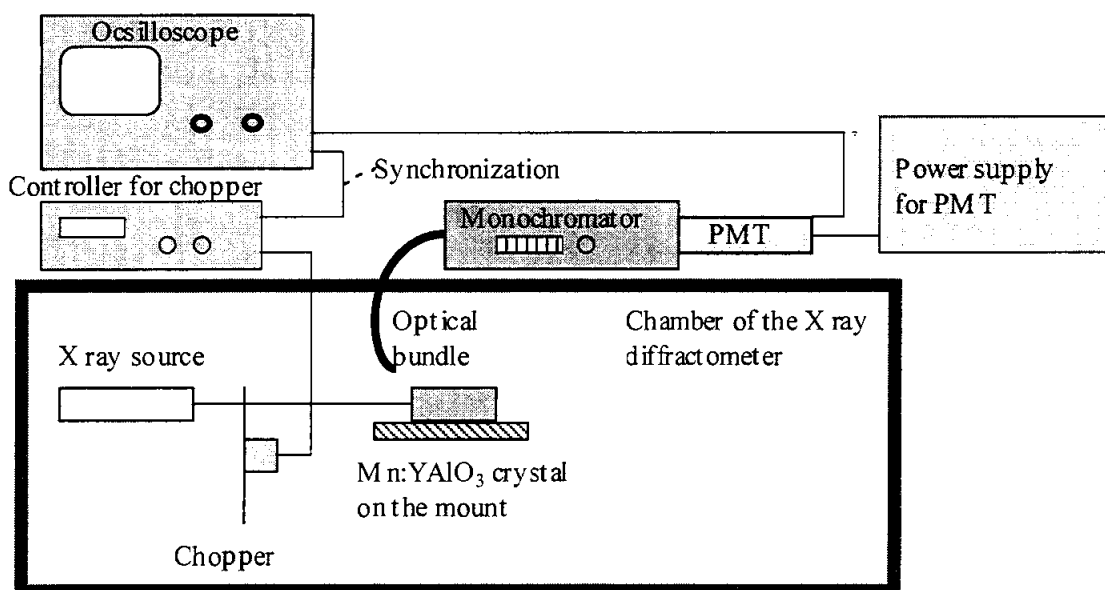


Figure 1. Experimental set up.

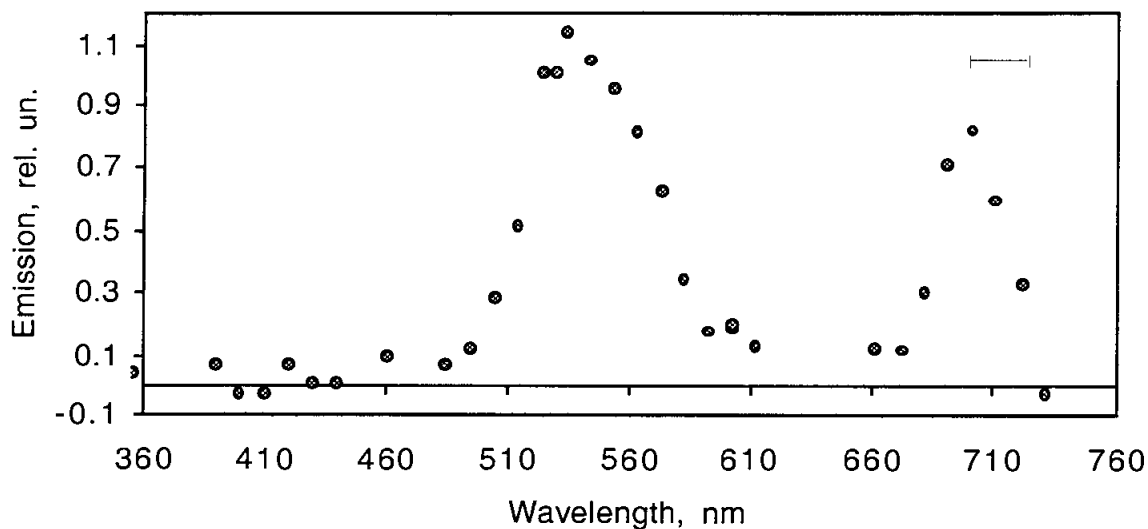


Figure 2. Visible emission excited in Mn(0.5%):YAlO₃ with X-ray beam ($\lambda=0.154$ nm). The horizontal bar in the figure shows the spectral resolution.

The Tanabe-Sugano diagram (showing the energies of different electronic states in transition metal ions as a function of the crystal field Dq) for a $3d^5$ electron configuration, calculated in Ref. [8] for the ratio of the Racah parameters $C/B=5.55$, is shown in Figure 3.

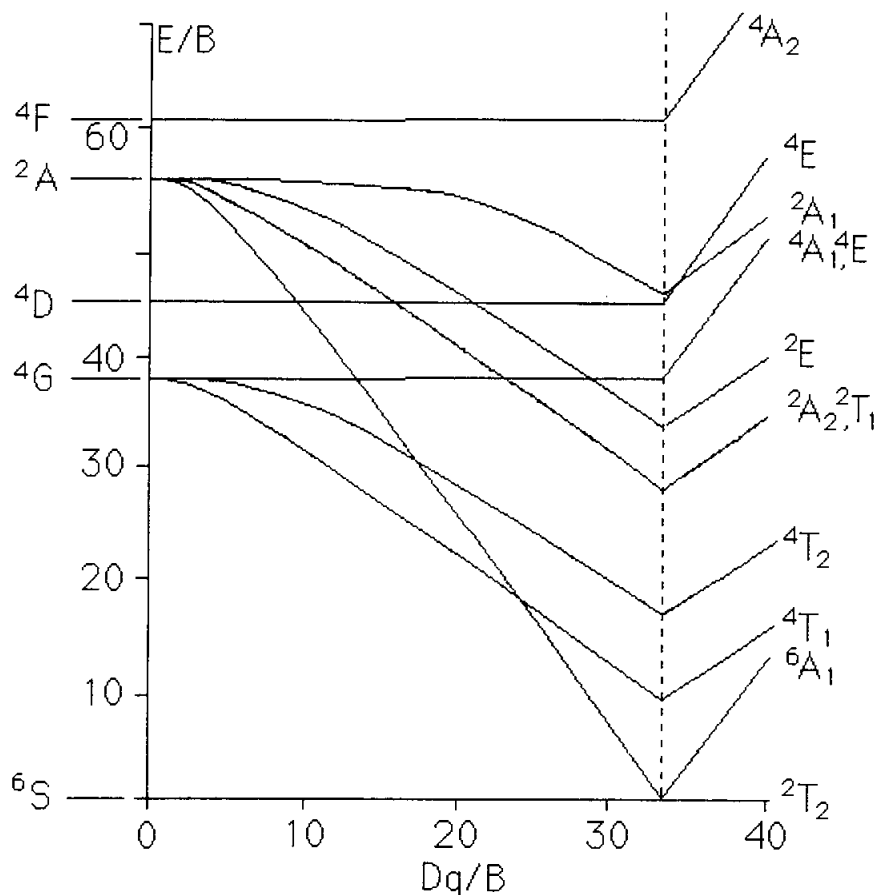


Figure 3. The Tanabe-Sugano energy level diagram of a $3d^5$ system (calculated in Ref. [8] for $C/B=5.55$).

As it follows from Figure 8, the energy gap between the levels $6A_1$ and $4T_1$ is strongly dependent on the crystal field Dq , being larger at small Dq and smaller at large Dq . Since the crystal field splitting is larger in octahedral sites than in dodecahedral or tetrahedral sites ($Dq_o:Dq_d:Dq_t=1:-1/2:-4/9$, where the negative signs indicate that d_z^2 and $d_{x^2-y^2}$ become the more stable set relative to the other three d orbitals [2]), the type of the site occupancy of Mn^{2+} ion can be determined, in a first approximation, by the color of Mn^{2+} luminescence. As follows from Table 1 summarizing data on Mn^{2+} emission in various crystals, green color of Mn^{2+} luminescence observed in our experiment is the evidence that Mn^{2+} ions occupy in $YAlO_3$ dodecahedral (Y^{3+}) but not octahedral (Al^{3+}) sites. This consideration confirms our initial assumption based on the ion sizes and the decrease in the lattice parameters.

Crystal	Site coordination	Wavelength of the maximum luminescence, nm	Color of luminescence	Temperature, K	Reference
<i>YAlO₃</i>	<i>Dodecahedral</i>	<i>530</i>	<i>green</i>	<i>300</i>	<i>This work</i>
ZnAl ₂ O ₄	Tetrahedral	509	green	4.2	[9]
LaAlO ₃	Dodecahedral	518	green	4.2	[9]
MgAl ₂ O ₄	Tetrahedral (low Mn concentration)	530	green	300 (?)	[21]
Y ₃ Sc ₂ Ga ₃ O ₁₂	Dodecahedral	573	yellow	12	[11]
Y ₃ Al ₅ O ₁₂	Dodecahedral	585	yellow-orange	12	[11]
Y ₃ Al ₅ O ₁₂	Dodecahedral	609	orange	300	[8]
Al ₂ O ₃	Octahedral	600	orange	4.2	[9]
Ca ₃ Ga ₂ Ge ₄ O ₁₄	Octahedral	625	red		[10]
Mg ₂ SiO ₄	Strongly distorted octaheder	650	red	300	[22]

Table 1. Site symmetry and luminescence wavelength of Mn²⁺ ions in different hosts

Acknowledgments:

The work was partially supported by the AFOSR/BMDO grant #F49620-98-1-0101 and DOE grant #DE-FG01-94EW11493. The authors thank C. E. Bonner, N. Noginova, and C. Jackson for the help with experiments.

References:

1. G. B. Louts, M. Warren, L. Taylor, R. R. Rakhimov, H. R. Ries, G. Miller III, M. A. Noginov, M. Curley, N. Noginova, N. Kukhtarev, J. C. Caulfield, P. Venkateswarlu, "Manganese-doped yttrium orthoaluminate: A potential material for holographic recording and data storage", *Phys. Rev. B*, **57**, pp. 3706-3709 (1998).
2. R. G. Burns, "Mineralogical applications of crystal field theory", Second Edition, Cambridge University Press, Cambridge, 1993, 551 pp.
3. A. Lempicki, A. J. Wojtowicz, E. Berman, "Fundamental limits of scintillator performance", *Nuclear Instruments and Methods in Physics Research A*, **333**, pp. 304-311 (1993).
4. J. Anderson, P. Dorenbos, C. W. E. van Eijk, "Calculation of energy levels of cerium in inorganic scintillator crystals", *Materials Research Society Symposium Proceedings*, Vol. **348**, pp., 355-365 (1994).

5. M. A. Noginov, N. Noginova, M. Curley, N. Kukhtarev, H. J. Caulfield, P. Venkateswarlu, G. B. Loutts “Optical characterization of Mn:YAlO₃, material for holographic recording and data storage”, JOSA B, **15**, pp. 1463-1468 (1998).
6. M. A. Noginov, G. B. Loutts, “Spectroscopic studies of Mn⁴⁺ ions in yttrium orthoaluminate”, submitted to JOSA B.
7. V. A. Antonov, P. A. Arsenev, Sh. A. Vakhidov, E. M. Ibragimova, “Colour centers in yttrium aluminate crystals activated with transition metal ions”, phys. stat. sol. (a), **22**, pp. 391-399 (1974).
8. B. Henderson, G. F. Imbusch, “Optical spectroscopy of inorganic solids”, Clarendon Press, Oxford, 1989, 645 p.

**AN INEXPENSIVE 2732°F
MINIATURE ELECTRIC FURNACE FOR
TEACHING MATERIALS SCIENCE**

Luke Ferguson

and

Thomas Stoebe

Department of Materials Science and Engineering
University of Washington
Box 352120
Seattle, Washington 98195-2120

Telephone 206-543-7090
e-mail lukef@u.washington.edu
stoebe@u.washington.edu



Luke Ferguson

An Inexpensive 2732°F Miniature Electric Furnace for Teaching Materials Science

Luke Ferguson and Thomas Stoebe

*The Department of Materials Science and Engineering
University of Washington, Box 352120
Seattle, WA 98195-2120*

Key Words

High temperature electric furnace, high temperature refractory materials, furnace design, thermal conductivity, heat transfer, silicon carbide heating element, materials compatibility, ceramic materials, insulation and energy efficiency, energy balance, alumina and zirconia fibrous refractory board, alumina cement, moldable refractory materials, thermal stress and thermal shock resistance, thermal expansion, platinum thermocouples, thermometry.

Prerequisite Knowledge

Basic laboratory safety skills are required, and supervision by qualified personnel is also required. College level chemistry, physics or materials science, basic electronics, and basic construction skills such as using cements or mortars and insulating materials are recommended for those involved in this work. Experience in the operation of a standard pottery kiln or furnace would definitely be helpful. Some basic knowledge about refractory ceramics and metals and their compatibility issues is strongly recommended.

Abstract

This experiment teaches principles of high-temperature electric furnace design, energy efficiency, and thermal properties of materials. The furnace described in this experiment is constructed with commercially available refractory materials, and is built on a small scale to minimize construction cost. The furnace is capable of reaching temperatures far above those of a standard pottery kiln, and may be used for many interesting experiments involving technical ceramics and metallurgy. Some of the experiments that may be performed using the miniature furnace include high temperature solid-state diffusion experiments, the sintering of technical ceramics such as alumina, magnesia, zirconia or magnetic ceramics [see reference #1], the alloying of high temperature metals and glasses, high temperature annealing and heat treating of materials, crystal growth, thermo-power measurements, and the fabrication of superconductors or electro-ceramics such as barium titanate or PZT.

Safety Precautions

High temperature furnaces are easily destroyed by misuse, and an explosion or fire hazard exists if incompatible materials are used. Always follow safety guidelines. If you're not sure about the safety or compatibility of any materials then DO NOT use them to insulate the furnace or put them in the furnace!

KEEP all furnaces away from anything that is flammable such as wood tabletops, paper, cloth, or plastic, and never leave the furnace unsupervised. Be sure the area around the furnace is well ventilated. ALWAYS put the furnace on a bare concrete floor or other high temperature resistant surface when in operation. Have proper fire extinguisher equipment nearby and ready to use.

DO NOT open the furnace or lift the furnace when it is operating at high temperatures. Be sure the core of the furnace has cooled down to below 75°C before opening or transporting the furnace. AVOID touching heater elements with anything at all times.

DO NOT put any materials in the furnace that produce flammable or toxic gasses, including alcohol, methanol, acetone, or any flammable solvents. DO NOT operate the furnace in the presence of combustible gasses such as carbon monoxide, hydrogen, or fuel oil. Avoid using metal-chlorides, methyl chloride, any sulfides, phosphates, or strong alkalis in the furnace, or other compounds that can produce toxic and corrosive or explosive fumes. Even finely ground organic materials such as carbon, coal dust, or wood, and many metals are explosive in high temperature air atmospheres. A listing of hazardous mixtures defined by Group can be found in National Fire Protection Association document NFPA 497 M.

USE the recommended high temperature electrical hook-up wire to connect heater elements and be sure that all electrical connections are properly insulated and mechanically secure before operating the furnace. This experimental furnace operates at line voltages, and reasonable precautions against the danger of electrical shock must be observed.

USE high temperature gloves, safety glasses, and other protective clothing when working around furnaces and other high temperature experiments. As with nearly all refractory ceramic materials, keep any fibers or dust off hands and face, and avoid breathing any fibers or dust.

The high temperature furnace described in this paper is for teaching purposes only, and should not be used for any other purpose. The authors of this paper make a diligent effort to insure the safety of the furnace design and its safe operation. However, due to the experimental nature of the furnace, the authors cannot be held responsible for any use or misuse that actually occurs.

Equipment and Supplies

1. "Insboard 2600" ceramic fiberboard available from A. P. Green Industries, Inc., Mexico, Missouri, USA. The ceramic fiberboard is about \$6.69 per square foot and may be purchased in 2' by 3' by 1" sections. A superior high-density version, "Insboard 2600HD" is also available. The maximum recommended temperature is about 1425°C and the thermal coefficient is 0.17 W/m°C @ 1095°C.
2. "ECO" Alumina Insulating Board type ECO-20AA, or Premium Grade Alumina Insulating Board type SALI available from ZIRCAR Products, Inc., Florida, N.Y.

Standard samples of ½” by 2” by 3” boards were obtained from ZIRCAR for the construction of this furnace. Other required materials include sample amounts of ZIRCAR Alumina Papers types APA-1, APA-2, or APA-3 Insulation, Alumina Insulation type SALI Moldable, and at least 1 pint of ZIRCAR Alumina Cement (C4001 AL-CEM), at a cost of \$56.50 per pint. Phone (914)-651-448, Home Page www.zircar.com, e-mail sales@zircar.com.

3. A thermal fuse or thermal cutoff (TCO). The maximum temperature for opening should be about 220°F. Suppliers include NTE Electronics, Inc., Bloomfield, NJ, phone 973-748-5089, www.nteinc.com, and Elmwood Sensors Inc., Pawtucket, RI, phone 800-356-9663, www.devicelink.com. Cotronics Corporation, Brooklyn N.Y., phone (718)-646-7996, also offers high-temperature safety products including gloves, clothing, and emergency fire blankets.
4. A 4-amp slow-blow electrical fuse and inline fuse holder.
5. Silicon carbide heating elements. For this experiment, two “Norton Crystar Igniter” elements were used, model 271R with 4” ceramic block and 450°C temperature wire. These model 271R Crystar Igniters were obtained from Norton Igniter Products, Powers Street, Milford, New Hampshire. The cost is about \$21 per igniter element.
6. Thermocouple element. A “type B” (Pt-30% Rh, Pt-6% Rh) thermocouple wire is recommended for temperature sensing inside the furnace. Type “B” platinum thermocouples with alumina insulators are available in 12” lengths of AWG wire size 30 for about \$50.00 (part number XDH-30-B-12) from Omega Engineering, Inc., Stamford CT, phone (203)-359-1660, FAX (203) 359-7700. Omega Engineering, Inc., supplies a free “Temperature Handbook” with a great deal of useful information concerning temperature measurement, and tables for converting thermocouple voltages to temperatures.
7. A portable voltmeter, such as the Fluke 87 Multimeter, can be used to read the output voltage from the “type B” thermocouple if the voltmeter has a sensitivity of 0.1 milli-Volts. The voltage can be converted to a corresponding temperature using tables such as the ones in the “Temperature Handbook” available from Omega Engineering, Inc. Handheld thermometers for use with thermocouples are also available from various sources such as Omega.
8. High temperature heater hookup wire. Teflon-Glass and Silicone Rubber Insulated Heater Hookup Wire are available from Omega Engineering, Inc., in 25’ spools of plated copper strand. Teflon-Glass 16 gauge or larger wire is recommended. This 16 gauge wire has a temperature rating of 250°C, and has an electrical current carrying capacity of about 10 amps at 200°C including a temperature correction factor of 0.49 (the cost is about \$45.00 for 25 feet). Useful information about heater hookup wire and thermal data for materials can be found in the “Supplement” or “Heaters” handbooks that may be obtained free from Omega Engineering, Inc. A line cord capable of safely carrying at least 7 amps is recommended.
9. A commercially available 120 volt (60Hz), 10 amp, 1.4kVA variable autotransformer or “Variac” is used to adjust the electrical power supplied to the furnace.
10. Simple hand tools including sandpaper, paint brushes, sponges, small spatula, a ruler, a hacksaw, a scroll saw blade, wire cutters and strippers, tin snips, files, mixing containers and measuring cups, and a chemical balance should be available.
11. Miscellaneous items include disposable rubber gloves, flexible metal electrical conduit, sheet metal and materials for building frame for furnace, electrical tape and duct tape, fire bricks, apron or lab jacket, eye protection, paper towels, plastic bags, a permanent ink marker, and disposable dust mask.

Introduction and Background

One of the most important tools for the materials scientist or engineer is the high temperature furnace. Many modern engineering materials require temperatures of 1400°C or greater for processing, and the cost of even a small commercial furnace that is capable of reaching these temperatures can be \$9000.00 or more. In this exercise, a method is presented for building a simple experimental furnace that is capable of operating at 1400°C (and intermittently at 1500°C), for a minimal construction cost of about \$200. (The actual cost will depend somewhat on the resourcefulness of the experimenter.) The cost of the experimental furnace is held at a minimum by building the furnace on a small scale, and by not using programmable or automatic temperature controllers (except for an over-temperature indicator or thermal fuse).

Miniaturization of the furnace often may allow the builder to obtain some of the construction materials on a free sample basis from a generous manufacturer or supplier. The small scale should also make it easier to operate the furnace safely, provided that good overall safety precautions are observed.

This miniature furnace can be constructed almost entirely using technical ceramic materials. The heating elements used for the high temperature furnace are made primarily out of silicon carbide, an electrically conducting ceramic material. In general, ceramic materials have very low electrical and thermal conductivity, and this is one of the reasons they are frequently used as insulators. The silicon carbide ceramic heating elements, however, achieve a remarkably high electrical and thermal conductivity because of natural impurities or dopants that are added during the manufacturing process. Given an adequate amount suitable insulation, the upper temperature limit that can be attained in the cavity of a typical furnace is set by the heating element that is used, and the size of the inner cavity. Metal-alloy heating elements have a maximum operating temperature in dry air of about 1200°C. A layer of chromium oxide forms on the outer surface of

nickel-chrome heater wires and protects them from oxidation until rapid deterioration takes place at the high temperature limit. A typical pottery kiln will use ni-chrome wire heating elements and will have a useful temperature limit of about 1150°C. Non-metal elements such as silicon carbide are used to achieve higher temperatures. Silicon carbide elements form a protective layer of silicon dioxide on the outer surface that allows them to achieve temperatures of a little over 1600°C in air atmospheres before rapid deterioration begins. One disadvantage with silicon carbide elements is the process known as aging whereby the electrical resistance of the elements increases with continued high temperature use. Higher temperatures cause the aging to take place more rapidly, decreasing the usefulness of the element.

Energy production needs are strongly dependent on the efficient use of power that is delivered on a giant scale such as the global production of heating and light, and on a much smaller level such as the energy “budget” for the miniature furnace described here. Insulating materials play a critical role in the efficient use of energy. Characteristics of superior high-temperature insulating materials include low specific heat and thermal conductivity, high resistance to thermal shock, excellent corrosion resistance, high resistance to oxidizing and reducing atmospheres, high temperature stability, high mechanical strength and resiliency, and low health hazard or environmental impact. There appears to be no existing insulating material that can satisfy all these requirements completely. The best available materials for high temperature furnace insulation tend to be technical ceramic compositions of aluminum oxide, silica, magnesium oxide, and stabilized zirconium oxide. These principle ceramic oxides are fabricated in fibrous “blanket” forms or stiff boards composed of bonded fibers. Fiber-based insulators, or very porous ceramics, tend to have high resistance to thermal shock or mechanical failure due to the ability of the small diameter fibers to expand or flex when subjected to severe thermal gradients. Large-scale crack propagation through the fibrous material is suppressed because the fibers absorb the stress created by differential thermal expansion resulting from steep thermal gradients.

Some disadvantages connected with fibrous insulators are high cost, health hazards due to respiratory size fibers or dust, and a lack of machinability.

Some of the experiments that may be performed using the miniature furnace include high temperature solid-state diffusion experiments, the sintering of technical ceramics such as alumina, magnesia, zirconia or magnetic ceramics [see reference #1], the alloying of high temperature metals and glasses, high temperature annealing and heat treating of materials, crystal growth, thermo-power measurements, and the fabrication of superconductors or electro-ceramics such as barium titanate or PZT.

Design Theory

Silicon carbide heating elements are not sized to a specific wattage output the way many common metal-alloy wire elements are. The amount of energy that a silicon carbide element is capable of converting from its electrical power source to heat energy is dependent on the operating temperature of the furnace and the atmosphere in the furnace. Silicon carbide elements can operate at higher temperatures in air atmosphere as opposed to reducing atmospheres.

The silicon carbide elements used in this furnace design have a relatively small total radiating surface area of about 2 square inches. If an ambient furnace temperature of 1400°C is chosen in an air atmosphere, the "Maximum Recommended Watt Loading" is about 49 Watts per square inch according to data from I Squared R Element Co., Inc. If the Maximum Recommended Watt Loading is exceeded, the useful service life of the element becomes increasingly shorter as the power input is increased. In any case, temperatures above 1500°C should not be exceeded because this is the operating limit of the insulating materials and the SiC elements before rapid thermal breakdown occurs. The radiating surface of each of these elements can therefore supply about 100 watts to heat the furnace cavity at an operating temperature of 1400°C. If two elements are used then a total of about 200 W is available (two household incandescent 100W light bulbs require about the same amount of power). This is not much power to drive up the temperature of the furnace, so the insulation must be very effective!

If the SiC element were in a vacuum, with no energy losses by conduction or convection, where it could only lose energy by radiative processes (photons or electromagnetic radiation), its steady-state temperature could be determined from Planck's Law and an energy balance equation. Given that the SiC element is a close approximation to a "blackbody" or ideal radiator, then

Electrical Power In = Radiated Power Out

$$200 \text{ W} = (\text{Surface Area})\sigma T^4 = (12.9 \times 10^{-4} \text{ m}^2)(5.67 \times 10^{-8} \text{ W}/(\text{m}^2 \text{K}^4))T^4$$

Solving for the equilibrium temperature of the element gives $T = 1010^\circ\text{C}$. This is the approximate steady state temperature that a SiC element would reach when radiating freely into open space with no heat transfer by convection or conduction. It is possible to achieve much higher steady state temperatures by surrounding the SiC elements with ceramic insulation, as will be shown next, and heat conduction through the insulation and inner cavity size will be shown to be the limiting factors.

Problems involving heat transfer, such as the flow of heat through the insulating walls of a furnace, often have close analogies with simple electronic circuits and may be analyzed using equations similar to Ohm's Law. The transfer of energy between adjacent parts of matter due to a temperature difference is called heat conduction. A wall of insulating material with cross sectional area A and thickness L whose faces are kept at different temperatures will experience a flow of heat, Q , perpendicular to the faces in a time t . The temperature difference between the faces of the wall corresponds to the potential difference across an electrical resistance, and the heat flow, $H = dQ/dT$, corresponds to the flow of charge through an electrical resistance. The thermal conductivity, k , of the insulation wall corresponds to the inverse of electrical resistance. The fundamental law of heat conduction is $H = -kAdT/dL$, where H is measured in Watts/ $^\circ\text{K}/\text{m}$ if SI units are being used.

Insulating materials are most critical in the core of the furnace. The goal in this design was intermittent operation at 1500°C and extended operation at 1400°C . Most importantly, the inner insulation walls must have sufficient chemical and thermal stability to withstand temperatures of

at least 1600°C, and after this condition is met, the thermal conductivity of the material should be as low as possible. A practical compromise between cost and performance appears to be “ECO-20AA Alumina Insulation Board” manufactured by Zircar Products, Incorporated. “ECO-20AA” refractory board is made with high purity alumina fibers and contains alumina powders that act as a cost reducing filler material.

The graphs of thermal conductivity as a function of temperature shown for “ECO-20AA” high temperature insulation in Figure 1, and “Insboard 2600” back-up insulation (A. P. Green Industries, Inc.) in Figure 2, were generated by fitting curves to some data obtained from the manufacturers at specific operating temperatures. The thermal conductivity of a material tends to increase in a non-linear way with increasing temperature, and this phenomenon can make heat flow calculations significantly more complicated. It so happens that the thermal conductivity of the insulating materials selected in this particular design increase in a very linear way with temperature over the operating range, as shown in Figures 1 and 2. The thermal conductivity of ECO-20AA can be described very well by the linear equation $k_1(T) = \alpha_1 + \beta_1 T$, where $\alpha_1 = 0.03$ and $\beta_1 = 1.5 \times 10^{-4}$. In a similar way, the thermal conductivity of “Insboard 2600” is described by $k_2(T) = \alpha_2 + \beta_2 T$, where $\alpha_2 = 0.04$ and $\beta_2 = 1.17 \times 10^{-4}$.

An estimate for the heat flow through the walls of a cubical container (or furnace), and the resulting equilibrium temperature within the inner cavity, was derived by noting that the surface area of a cube is $6(2L)^2$ (where $2L$ is the length of one side of the cube), and then integrating with respect to the heat flow equation. The result is

$$H_1 = (\alpha_1(T_1 - T_2) + \beta_1(T_1^2 - T_2^2) / 2) / R_1$$

where T_1 is the temperature on the inner wall surface and T_2 is the temperature on the outer wall surface of an insulation layer with thermal conductivity, $k_1(T) = \alpha_1 + \beta_1 T$. R_1 is the “thermal resistance” of the insulation layer and is given by

$$R_1 = (L_2 - L_1) / (24L_1L_2)$$

Where L_1 is the distance from the *center* of the cubical furnace to the inner surface of the first insulation layer, and L_2 is the distance from the center of the furnace to the outer surface of the first insulation layer.

It is cost effective to construct the inner insulation layer with the high temperature “ECO-20AA” material, and to use an outer back-up layer of the less expensive “Insboard 2600” insulating board. The total thermal resistance is given by $R_1 + R_2$, where R_2 follows from the relation for R_1 in a logical way, $R_2 = (L_3 - L_2)/(24L_2L_3)$. The heat flow through the inner insulation layer is therefore $H_1 = (\alpha_1(T_1 - T_2) + \beta_1(T_1^2 - T_2^2) / 2) / R_1$, and the heat flow through the outer backup layer is $H_2 = (\alpha_2(T_2 - T_3) + \beta_2(T_2^2 - T_3^2) / 2) / R_2$ where T_3 is the temperature of the outermost surface and T_2 is the temperature at the interface of the inner insulation layer and the back-up insulation layer. Given steady state heat conduction, the heat flow will be constant across each layer of insulation and $H_1 = H_2 = H$ or

$$H = (\alpha_1(T_1 - T_2) + \beta_1(T_1^2 - T_2^2) / 2) / R_1 = (\alpha_2(T_2 - T_3) + \beta_2(T_2^2 - T_3^2) / 2) / R_2$$

An iterative, or “trial and error”, technique was used to solve this system of equations using some practical values based on the available stock material sizes and the design goals. The size of the inner cavity was chosen to be a 2 inch cube with an inner cavity temperature of 1500°C and the temperature at the surface of the outermost insulation layer was set at 41°C, (a value near room temperature.) The thickness of the inner “ECO-20AA” insulation wall was fixed at ½” and the thickness of the outer “Insboard 2600” layer was fixed at 2”. This gives $T_1 = 1500^\circ\text{C}$, $T_3 = 41^\circ\text{C}$, $L_1 = 1.0$ inch, $L_2 = 1.5$ inches, and $L_3 = 3.5$ inches. It was found that these design goals were satisfied when only 175 Watts of input power from the SiC heating elements was available. The temperature was $T_2 = 1072^\circ\text{C}$ at the interface between the “ECO-20AA” and the “Insboard 2600” insulation layers, and $k_{1\text{avg}} = 0.2362$ W/°C/m for the “ECO-20AA” insulation and $k_{2\text{avg}} = 0.1106$ for the “Insboard 2600” layer. The temperature at the interface, $T_2 = 1072^\circ\text{C}$, is safely below the 1425°C maximum service temperature of the outer “Insboard 2600” material, and the

total input power of 175 Watts is close to the Maximum Recommended Watt Loading for two SiC heating elements. In actual practice, 175 Watts of input power will probably not be enough to produce an inner cavity temperature of 1500°C due to significant heat losses that are not accounted for (such as the flow of heat out through the dense ceramic blocks and electrical leads that are connected to the SiC heating elements.)

Construction Details

Figures 3 and 4 give approximate dimensions of the insulation layers and placement of components for the experimental furnace. The walls of the inner cavity are first constructed out of Zircar “ECO-20AA” or “SALI” type fibrous insulating board. The walls of the inner cavity should be completely lined with at least ½” thickness of one of these high service temperature, high purity alumina insulating boards. The high temperature insulation board can easily be cut by hand with a hacksaw blade and joined using Zircar Alumina Cement (C4001 AL-CM) to form a hollow cube with a 2” inner dimension and a 3” outer dimension. The total volume of the inner high temperature cavity will be about 8 cubic inches for firing samples. Be sure to wear a dust mask and protective clothing when cutting or shaping any of the insulation materials in this experiment. The Zircar Alumina Cement is applied to the surfaces to be joined, and the joined parts must be allowed to dry for about 1 day before moving or placing into service. Zircar Bulletin #ZPI-306 for Alumina Cement gives important application instructions, and should be read before beginning construction. The top section of the inner insulating cube is cemented to the furnace “Lid” as shown in figures 3 and 4, and NOT to the rest of the inner cube, so that the “Lid” can be removed to insert or remove the sample to be fired. The inner surface of the insulating cube is lined with Zircar Alumina Paper type APA-1, 2, or 3 to create a protective barrier. One side of the APA-1, 2 or 3 Alumina paper is given a brush-coat with Alumina Cement and then

pressed onto the inner cavity surface. Narrow 1/8" vertical slots are cut in opposing walls of the 1/2" thick high temperature insulation so that the black silicon carbide elements of Norton 271R "hot surface igniters" can be inserted into the inner cavity (see figures). The silicon carbide element should be about 1/8" away from the closest parallel insulation wall, and approximately centered vertically in the cavity (see figures 5 and 6).

The inner high-temperature insulating cube is enclosed with 3 layers of 1" thick "Insboard 2600" back-up insulation. All 90-degree joints between insulating boards are brush-coated and joined with Alumina Cement, and all edges including cross-cut surfaces of the insulating boards are also brush-coated with Alumina Cement. The Alumina Cement should be used to strengthen all edges because they are subject to crumbling, and the cement greatly reduces the amount of fiber or particles that can be given off by the insulation materials. Avoid completely coating the faces of the insulating boards in order to reduce the amount of Alumina Cement that is required, and so that the thermal conductivity of the insulating boards is not increased by the relatively low thermal resistance path created by the cement. Two exceptions are the inner surfaces of the furnace "Lid", and upper surfaces of the furnace that are in contact with the "Lid", where a solid coat of Alumina Cement should be applied. Holes for the 4" long ceramic block part of the Norton 271R heating element may be cut in the "Insboard 2600" insulation using a drill bit and a scroll saw blade. Cut a thermal gasket out of the high-purity alumina insulation paper that is about 1/2 inch by 3/4" with a slot in the middle that is big enough to push through the SiC meander element. Push the alumina paper gasket down the SiC meander until it covers the face of the ceramic insulating block. Gently insert the Norton 271 Elements with the alumina paper gasket in place until the alumina paper

gasket is compressed between the ceramic block and the outer wall of the innermost (high temperature) insulation layer. The SiC meander should protrude through the narrow 1/8" slot in the inner insulation wall into the open furnace cavity as depicted in figures. Any open insulation gaps that occur around the Norton 271R heating elements or at other joints should be filled or repaired with Zircar "SALI" Type Moldable Alumina Insulation. Use a light coat of Alumina Cement between the outer insulation wall and the Norton 271R heating element to hold the element securely in place. Too much Alumina Cement will make it difficult to remove and replace a damaged heating element. The "type B" platinum thermocouple is inserted with a solid alumina insulator down through the middle of the "Lid" and the bare thermocouple should extend slightly down into the inner cavity. The Norton 271R heating elements are connected in parallel (using 16 AWG high-temperature heater hook-up wire) to the output of an auto-transformer or "Variac". The output voltage of the auto-transformer is adjusted manually by the operator to control the electrical current through the silicon carbide heating elements, and thereby the temperature of the furnace. Be sure to electrically and thermally insulate all connections well, and the line cords must be able to carry at least 7 amps safely. *Place a 4-amp slow-blow electrical fuse and fuse holder in the electrical line between the output of the auto-transformer and the parallel connection to the heater elements. The 4-amp fuse should limit the total current flow to both heater elements so that the cavity temperature remains less than about 1500 C.* Temperatures greater than about 1500 C may cause the ceramic insulating block that holds the SiC heater element to melt and decompose the surrounding insulation! Place a thermal fuse or thermal cut-off (TCO) in contact with the outside center of the furnace insulation floor to be used as an over-

temperature sensor in the event of a malfunction. The case of the TCO can be pressed between the outside insulation floor of the furnace and another layer of suitable soft insulation such as left over sections of the 2' by 3' sheet of "Insboard 2600" insulation. The TCO is a non-resettable fuse, and if the outer temperature of the furnace becomes too high because of melting or decomposition of the inner furnace insulation, the TCO should open and stop the flow of electrical current to the heating elements. The TCO must be electrically connected in series with both the Norton 271R heating elements. Thermal cutoffs are commonly used for protection in appliances such as hot plates, or irons, and they are available from many sources such as Elmwood sensors, Inc., and NTE Electronics, Inc., (see the equipment and supplies section.) The maximum temperature for opening for the TCO should be around 220°F, and the walls of the furnace should stay below this temperature, except for the area around where the ceramic blocks of the heating elements protrude from the furnace sidewalls. Consult with the manufacturers applications engineer for the exact TCO model type and current prices before ordering.

It is highly recommended that the furnace be enclosed in an electrically conductive metal case before operation. The metal case can be made using sheet-metal aluminum or steel joined at the edges with bolts or fastened to a rigid metal frame. Standard electrical conduit hardware can be used to cover the terminals of the heater elements, and connecting wires should be well insulated and fed through flexible metal conduit between the heater elements (see Figure 6). Electrical line going into any metal case should be properly strain-relieved at the entry point. Standard safety practice requires that a secure electrical ground connection be made to the metal case.

Testing and Operation of the Experimental Furnace

Place the furnace on a non-conducting fire-resistant surface, such as a concrete building floor. Increase the power to the heating elements slowly while monitoring the cavity temperature with a sensitive voltmeter and the "type B" thermocouple. It should not be necessary to apply more than about 70 volts (or more than about 4 amps) to the heating elements in order to reach steady state temperatures well above 1400°C in the furnace cavity. The outer surface of the furnace should be below 220°F at all times during operation (the ceramic heater element blocks and the area surrounding them will run at higher temperatures because of the relatively high thermal conductivity of the dense ceramic blocks. The insulation used to construct this furnace contains organic binders that will smoke or out-gas during "burn-out" when the furnace is operated the first time or two at high temperatures. When a voltage of about 57.5 volts was applied across both heater elements, a current of about 1.54 amps flowed in each element (total of 3.08 amps), and our experimental furnace reached a steady state temperature of about 1400°C, (a voltage of about 8.7 millivolts across the type B thermocouple.) This is a total input power around 177 watts. This value appears to be higher than our theoretical prediction, probably due in large part to heat losses through the ceramic blocks of the silicon carbide heating elements and the relatively high thermal conductivity of the Alumina Cement that was used to construct the furnace.

Acknowledgements

The authors wish to acknowledge the partial support of the National Science Foundation's Advanced Technology Education Grant No. DUE:ATE 9602360, The Materials Aspects of Manufacturing Technology Institute Program.

REFERENCES

1. "Properties of Magnetic Ferrite's With a Simple Fabrication Method", by Luke Ferguson and Thomas Stoebe, National Educators' Workshop Update 97, November 2-5, 1997. NASA Conference Publication NASA/CP-1998-208726.

Figure Captions.

Figure 1. Thermal Conductivity of Zircar "ECO-20AA" Alumina Insulation Board.

Figure 2. Thermal Conductivity of A. P. Green Industries "Insboard 2600" Insulation.

Figure 3. Top View of the Experimental Furnace and Furnace "Lid".

Figure 4. Side View of the Experimental Furnace and Furnace "Lid".

Figure 5. Experimental Furnace with "Lid" removed to show Norton 271R silicon carbide element inside Furnace cavity (metal case not shown).

Figure 6. Auto-transformer, voltmeter, Norton 271R silicon carbide heating element, and Experimental Furnace with "Lid" in place for operation.

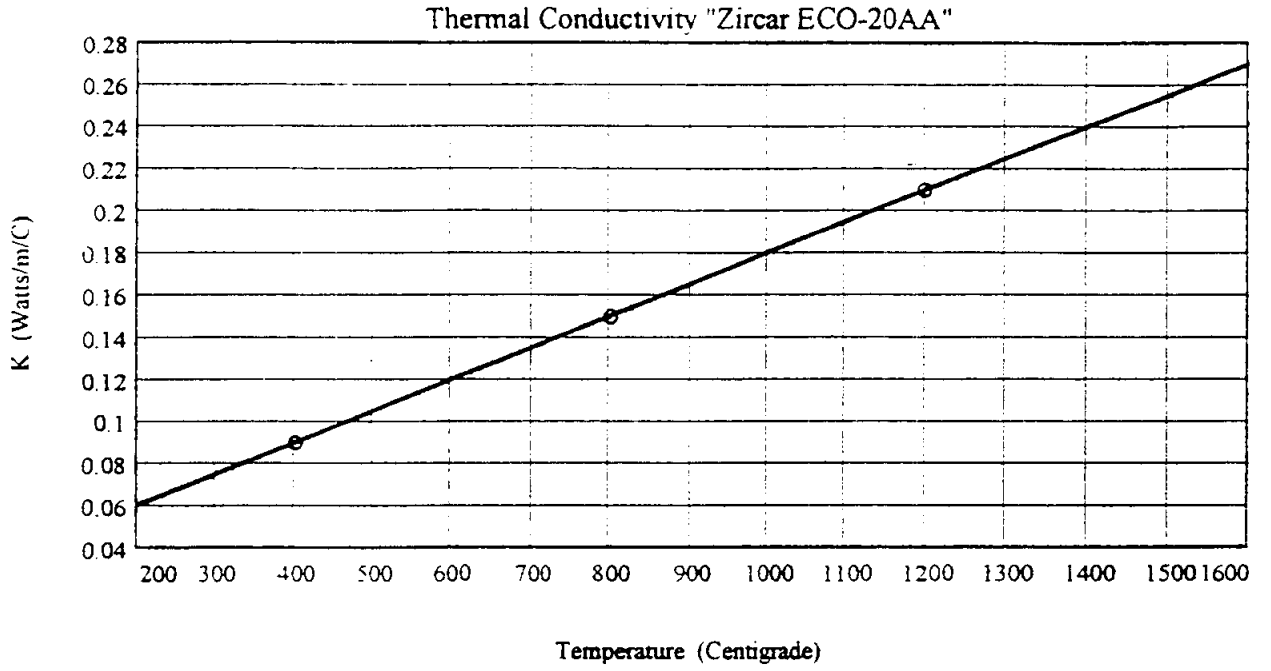


Figure 1. Thermal Conductivity of Zircar "ECO-20AA" Alumina Insulation Board.

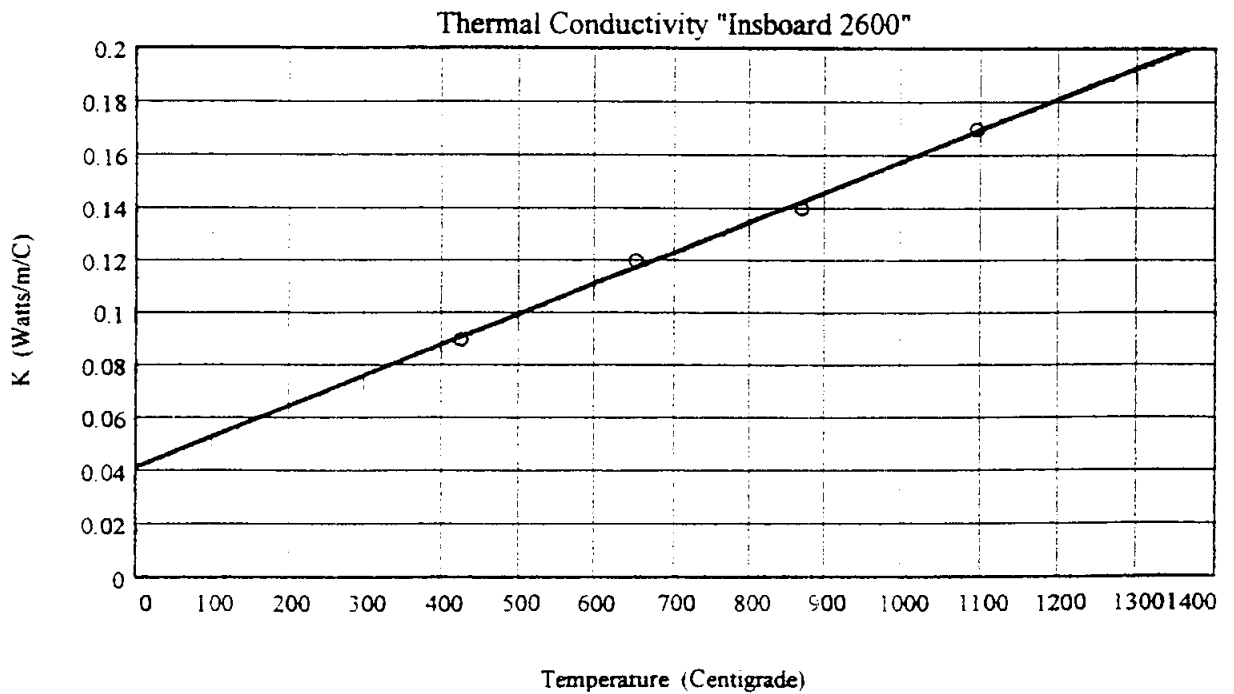


Figure 2. Thermal Conductivity of A. P. Green Industries "Insboard 2600" Insulation.

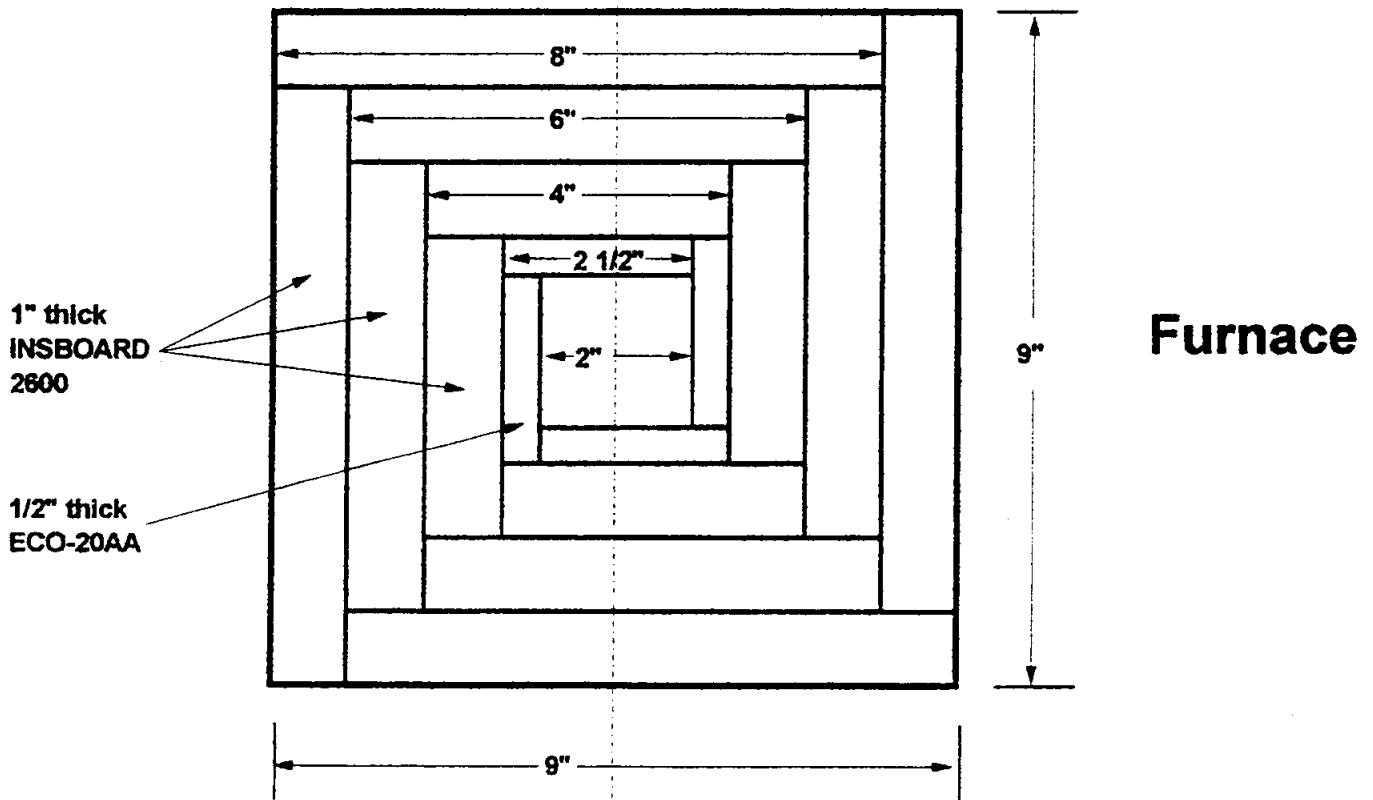
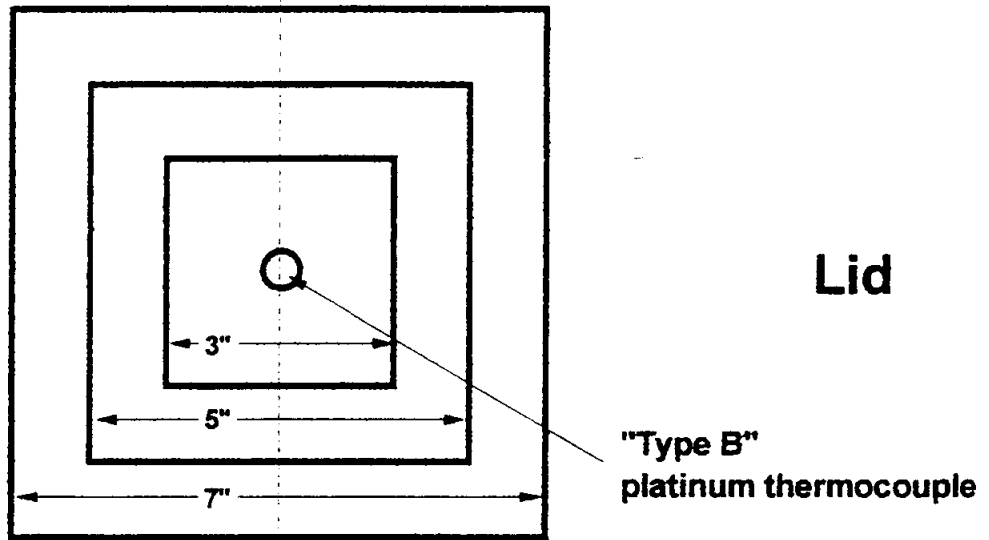


Figure 3. Top View

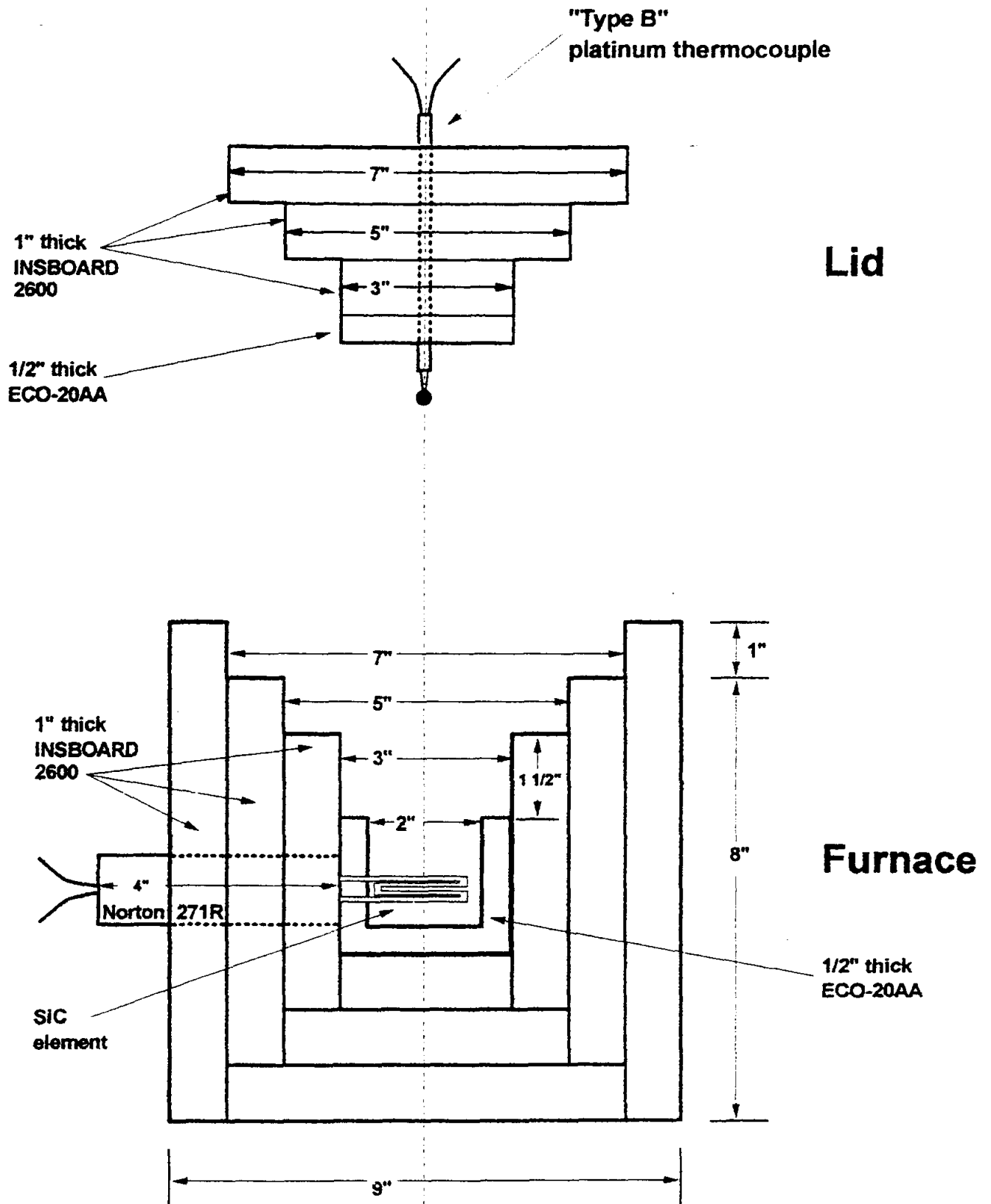


Figure 4. Side View

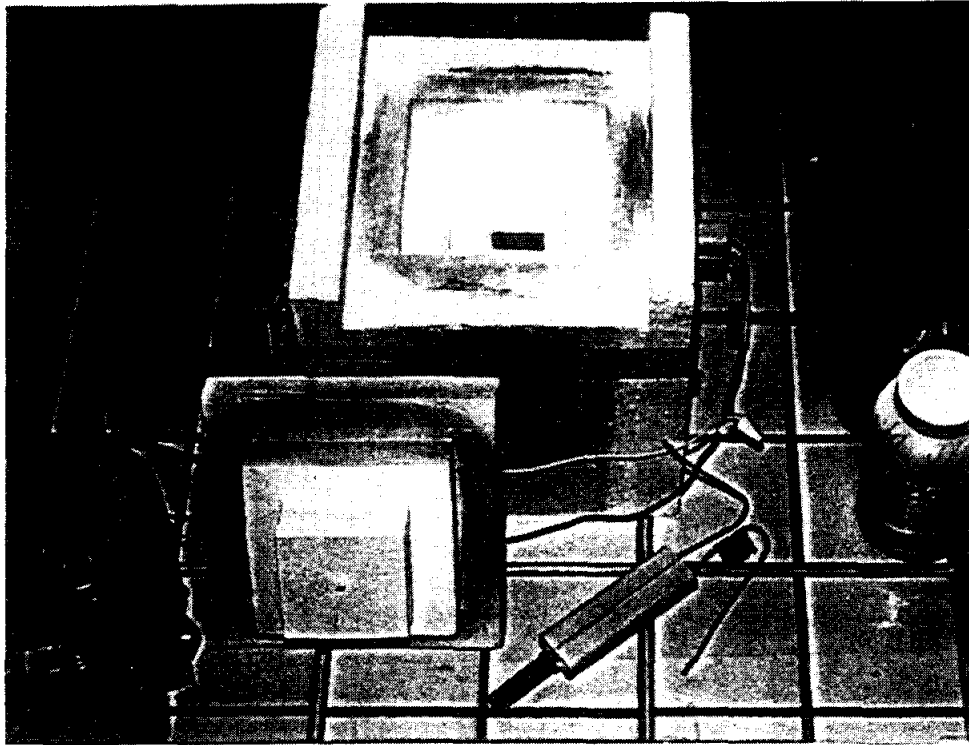


Figure 5. Experimental Furnace with "Lid" removed to show Norton 271R silicon carbide element inside Furnace cavity (metal case not shown).

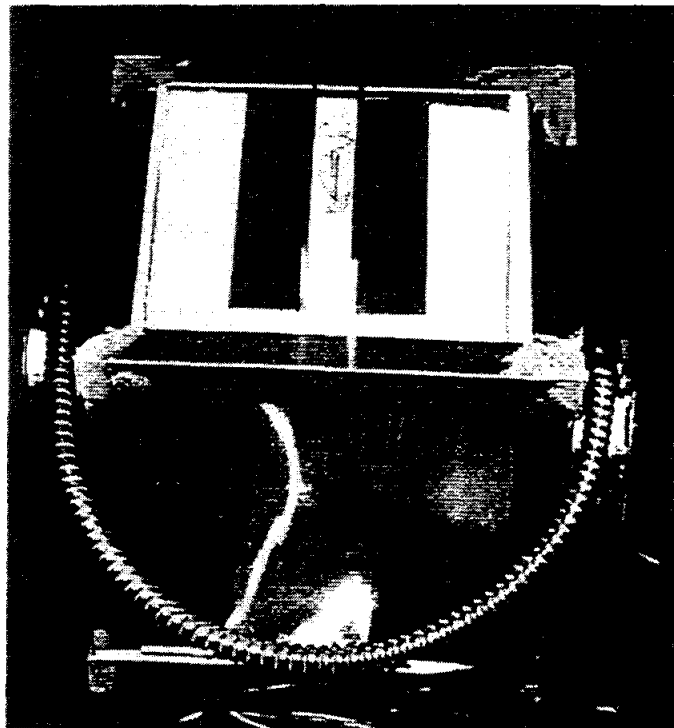


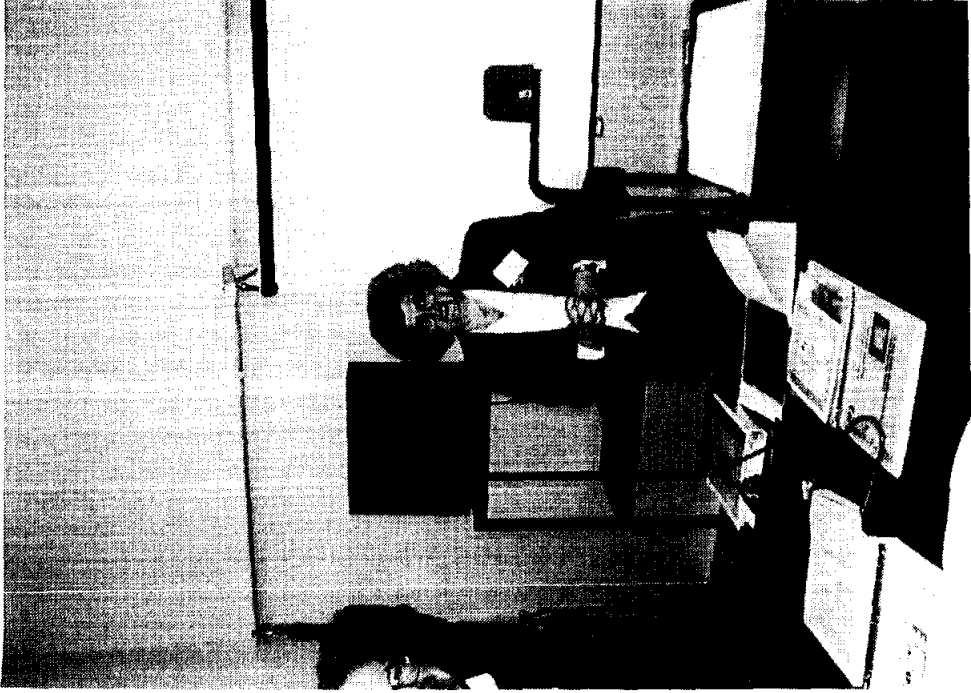
Figure 6. Auto-transformer, voltmeter, Norton 271R silicon carbide heating element, and Experimental Furnace with "Lid" in place for operation.

**TEACHING STATISTICAL QUALITY CONTROL
AND PROCESS ANALYSIS IN
MATERIALS LABORATORY**

Neda S. Fabris

Mechanical Engineering Department
California State University, Los Angeles
5151 State University
Los Angeles, California 90032

Telephone 213-343-5218
e-mail nfabris@calstatela.edu



Neda S. Fabris

TEACHING STATISTICAL QUALITY CONTROL AND PROCESS ANALYSIS IN MATERIALS LABORATORY

Neda S. Fabris, Ph.D.

**Professor, Mechanical Engineering California State University,
Los Angeles, California**

Key Words: Statistical Process Control, Standard Deviation, Machine Capability, Process Capability, Natural Tolerance Limits ($\pm 3\sigma$) and Six-Sigma Productions.

Prerequisite Knowledge: basic graphing, use of micrometer, basic algebra,
Desirable Knowledge: a) understanding of manufacturing processes, b) normal distribution, c) standard deviation

Objective: To introduce engineering students to Statistical Quality Control, Statistical Process Control, Machine Capability Indices: Cp and Cpk

Equipment:

1. micrometer for each student or group of students,
2. 20-30 tensile test specimens (or any other machined round bars)
3. graph paper
4. calculator

INTRODUCTION:

Today's modern industry, in its quest for improved quality and customer satisfaction, expects engineers to understand and implement statistical process control charts and methods in every step of their activities, from material selection to the design and manufacturing of new products.

On the other hand, most engineering students are not introduced to practical applications of statistics even if they have a class in probability and statistics. This class is usually taught by professors from the mathematics department and focuses on the probability and fundamentals of statistics. Even if it is taught by engineering professors, the majority of them are not familiar with the difference between statistical quality control and statistical process analysis. In order to introduce students to the practical application of the statistics and to prepare them for the modern industrial environment, I have developed a laboratory exercise, described below. This lab is part of the first experiment in the Engineering Measurement Laboratory, a required course for all juniors. In addition to this concept students are introduced to measurement techniques and the general characteristics of the measurement instruments.

In order to help students learn new materials the definitions of the new concepts are given in the hand-outs.

METROLOGY LABORATORY, STUDENT HAND-OUT

1. BACKGROUND MATERIAL

Definition of Quality and Statistical Tools.

Quality assurance is the total effort of the manufacturer to ensure that its product conforms to a detailed set of specifications and standards.

These standards cover several parameters, such as dimensions, surface finish, tolerances, color, mechanical, chemical and physical properties [1]*.

Today's companies work on the premise that *quality cannot be inspected in the product but must be built into the product*. This means you have to build quality products from the first step, not just separate good product from bad at the end of the cycle, using some measurement and inspection method. This approach requires that particular quantities are measured and inspected after each operation (for example, diameter of the part) and then if necessary, machine adjusted to produce a satisfactory part.

However, one hundred percent inspection in mass production is too costly and time consuming, so industry relies on *statistical quality control*, i.e. the measurement of the given quantity of the *sample of products* to determine the quality of the total production.

After the measurement of the given property the following charts are drawn [2] to *analyze the process (or machine)*:

- *\bar{X} chart*. Average measured value, or *mean*, of a certain quality (or quantity) for each of a series of samples taken from the production process. It indicates how the process mean varies over time.
- *R chart*. In this chart, the range of each sample is plotted. For example, the difference between the diameter of the smallest and a larger part in the sample of parts with the same nominal diameter.
- *p chart*. This chart is used to plot the percentage of defective parts in the sample (this includes parts whose sizes are outside the tolerance limits). If the percent of defective parts suddenly increases the process is *outside of statistical control*.
- *c chart*. Here the number or count of defects in the sample are plotted as a function of time.

Dimensional Tolerances is defined as a permissible or acceptable variation in the dimensions of the part.

* Number in [] represent references on the end of the article.

Standard deviation or σ [3] for the sample is given by equation (1):

$$\sigma = \sqrt{\frac{(x_1 - \bar{x})^2}{N} + \frac{(x_2 - \bar{x})^2}{N} + \dots + \frac{(x_N - \bar{x})^2}{N}} \quad (1)$$

Where
$$\bar{x} = \frac{(x_1 + x_2 + \dots + x_N)}{N} \quad (2)$$

Natural Tolerance Limits

To be successful in today's competitive environment, companies have to produce parts whose defect rate is minimal, i.e., at least \pm THREE SIGMA of the products have to be defect-free. In case of dimensions, this means that SIX-SIGMA of the products have sizes between UPPER SPECIFICATION LIMIT (USL) or upper tolerance and LOWER SPECIFICATION LIMIT (LSL) or lower tolerance. In that case, *machine capability potential index*, $C_p = 1$; where C_p is defined as

$$C_p = \frac{[(UPPER SPECIFICATION LIMIT) - (LOWER SPECIFICATION limit)]}{(MACHINE CAPABILITY)} = \frac{(USL - LSL)}{\pm 3\sigma} \quad (3)$$

If C_p is equal to 1, the process centered on the mean on the machine has the potential to consistently manufacture a conforming product, provided that the process does not drift, or there is no increase in the machine's inherent variability due to wear and tear. Value of $\pm 3\sigma$ are called *natural tolerance limits* for the given machine. This is shown in Figure 1.

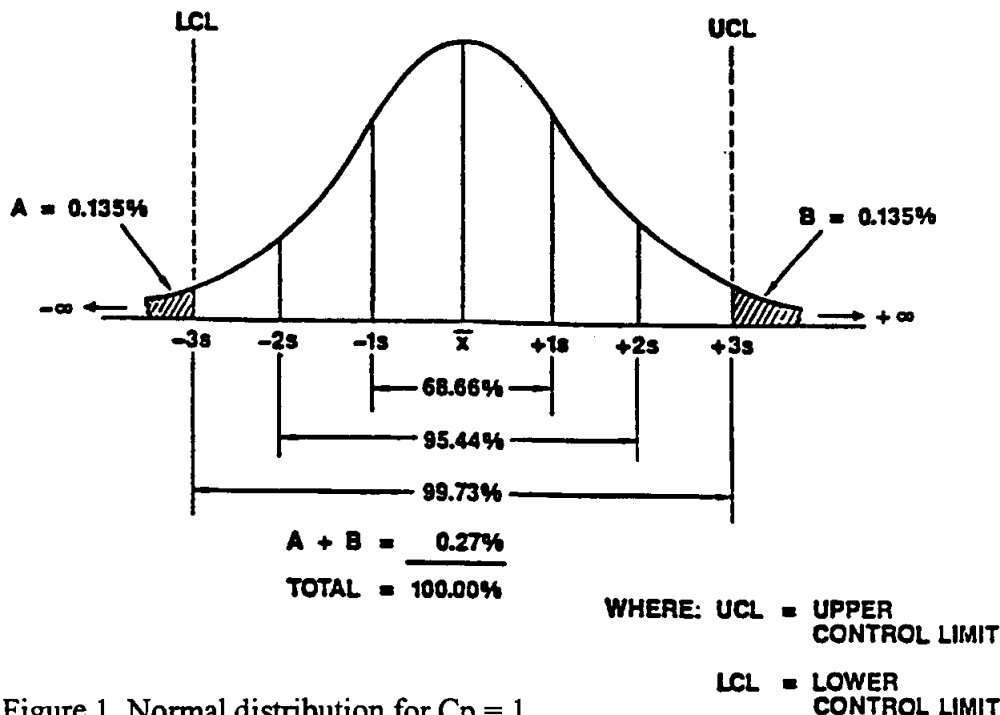


Figure 1. Normal distribution for $C_p = 1$

To compensate for the equipment wear and tear, quality conscientious companies today have even stricter requirements, i. e., they want the C_p to be 1.33, which means $\pm 4\sigma$ of products have to be defect-free or have dimensions between the given tolerance limits.

If a company has achieved $C_p = 2$, it is called a Six-Sigma quality program [4]. This means that $\pm 6\sigma$, (or totally 12σ of products) are defect-free or lie between USL and LSL. For example, Motorola, Inc., is a Six-Sigma company, and for its quality accomplishments it received in 1989 the very prestigious Malcolm Baldrige National Quality Award.

Students can appreciate the 6σ quality on the following example:

Quality of “ 3σ ” (or $C_p = 1$), process means:

2,700 defects per million parts, or

1.94 hours duration of power outages per month or,

1.35 misspelled words per page.

Quality of “ 4σ ”, (or $C_p = 1.33$) process means:

63 defects per million parts, or

2.72 minutes duration of power outages per month or,

1 misspelled word per 31 pages.

On the other hand “ 6σ ”, or ($C_p = 2$) process means:

0.002 defective parts per million or,

0.005 seconds of power outages per month or,

one misspelled word per small library!

Machine Capability and Machine Performance

Often the project is approached in a different way: the capability of the particular machine or process is determined by,

- measuring the dimensions, defect-free output, or some other characteristics of all the parts or a representative sample of the parts produced.
- Using these values, the $\pm 3\sigma$ of the production is computed and, in the case of dimensional measurements, *the tolerance limits* are determined. In a machine these limits represent *machine capability*. In a process, tolerance limits are determined for all parts produced in the shop on similar machines, (for example, a lathe) and they determine the so called *process capability*.
- Using $C_p = 1$ (or $C_p = 1.33$) the USL-LSL is computed. These limits are then called *natural tolerances of the machine (or process)*. **If the difference between upper and lower tolerance assigned to the part in the design process is equal or larger than USL-LSL, this machine (or process) can be used to produce the product.** For example, if USL-LSL for the given machine is 0.005 in., you can produce satisfactorily the parts with tolerances

equal or larger than that value. If in this case, the design requires the difference between the upper and lower value (i.e., tolerance range) of the part dimensions to be 0.001 in, you should look for the more accurate machine, or choose a different process (for instance grinding instead turning)! Otherwise you will have too many defective parts, whose sizes are too small or too large.

If the process is not symmetrical with respect to the nominal value, instead of C_p , C_{pk} is used where C_{pk} is the machine performance index, and is defined as the smallest value of two Z 's, i.e., Z_{min} , where Z_1 and Z_2 are defined as:

$$Z_1 = (\text{Mean value} - \text{LSL}) / 3\sigma \quad (4)$$

$$Z_2 = (\text{USL} - \text{Mean value}) / 3\sigma \quad (5)$$

Mean value is defined as the algebraic sum of all measured values divided by the number of specimens.

C_p and C_{pk} are equal if the process is centered on the nominal value of the part. The relationship between C_p and C_{pk} is given in Fig. 2.

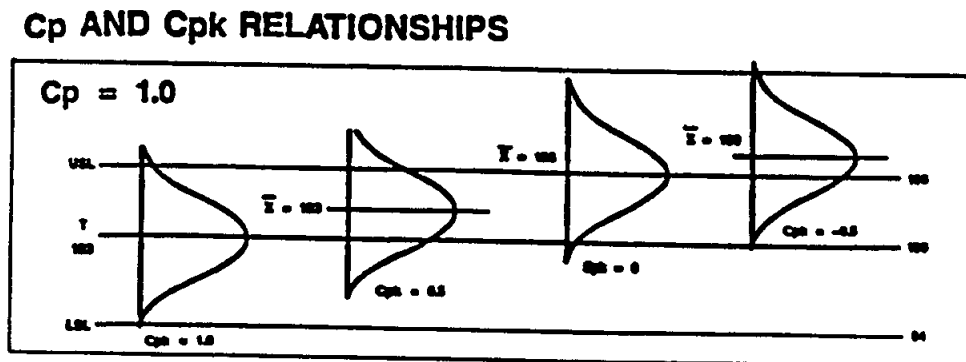


Figure 2. Normal Distribution for $C_p = 1$ and different C_{pk} '.

2. DATA SHEET

1. Using the given micrometer, measure the diameter of the given specimens in at least three positions (diameter can be different in the middle cross-section than on the end, due to the bending of the part during the cutting process). Find the average measurement for each part. Measure all other dimensions.

2. Sketch your specimen with all dimensions.

3. Draw the statistical distribution of the whole batch (all given parts), i.e., the *frequency of the occurrence of each measured diameter*.

3. REPORT

1. Compute the standard deviation (σ) for the given sample of parts.
2. Using C_p or (C_{pk} , if applicable) determine the NATURAL TOLERANCES OF THE MACHINE (assume all parts are machined on the same machine).
3. Determine the maximum part tolerances that can be machined on that machine so that the quality of the production is Six-Sigma.
4. Compare these tolerances with ones computed using 3σ quality production.
5. Assume that each day only two specimens are machined at the same machine. Take two specimens from the batch given. Draw \bar{X} and R charts for this production.
6. Explain the steps involved in manufacturing of the specimen: the machines and processes used.
7. Explain what is the reason for the variability of the sizes of the product, i.e., the difference in the measured diameters, and what can be done to decrease natural tolerance limits of the given machine.
8. Imagine that you have two machines: one is producing parts whose mean is equal to the given nominal value but the natural tolerances are large, other is producing parts whose mean value is different then nominal but natural tolerances are small. Which one, in your opinion is better machine? Explain your reasoning.

REFERENCES:

1. Johnson R.A., "*Miller & Freund's Probability & Statistics for Engineers*", Fifth Edition, Prentice-Hall, Inc. 1994
2. Groover M.P., "*Automation, Production Systems, and Computer-Integrated Manufacturing*", Prentice-Hall, Inc. 1987
3. Grant L.E., "*Statistical Quality Control*", Sixth Ed., Mc.Graw Hill, Inc. 1988
4. McFadden F.R., "*Six-Sigma Quality Program*" Quality Progress, June 1993

Neda Fabris, is Professor of Mechanical Engineering Department at California State University Los Angeles (CSULA). She has B.S. Degree from University of Sarajevo, Bosnia and Herzegovina, and M.S. and Ph.D. from Illinois Institute of Technology in Chicago Ill. She was a Member of Technical Staff at Bell Telephone Laboratory, Member of Research Staff at Technical University in Aachen, Germany, and has taught at the University of Sarajevo, at University of Illinois, and at CSULA (from 1979 till present). She served as a Chair of Mechanical Engineering Department from 1989-1993. Her research is in manufacturing material and pedagogy of teaching.

SYSTEM UPGRADE OF ATOMIC OXYGEN GENERATOR FOR SPACE MATERIALS RESEARCH

Kyo D. Song

Department of Technology
Norfolk State University
2401 Corprew Avenue
Norfolk, Virginia 23504

Telephone: 757-683-8105
e-mail kdsong@vger.nsu.edu

Bruce Budde

LARSS Student
New Mexico State University

and

Carolyn Hamilton

LARSS student
University of New Mexico



Kyo D. Song

System Upgrade of Atomic Oxygen Generator for Space Materials Research

Kyo D. Song, Professor, Department of Technology, Norfolk State University
Bruce Budde (LARSS) student, New Mexico State University
Carolyn Hamilton (LARSS) student, University of New Mexico

Keywords:

Atomic Oxygen, Space Materials, Erosion, Kapton, RF Generator

Objective:

This experiment provides a simulation capability for materials erosion of spacecraft in natural space environment (NSE) at low earth orbit (LEO).

The student will learn from the experiment to:

1. Understand significant composition of gas species in the LEO.
2. Understand interaction mechanism of atomic oxygen (AO) with space materials, such as Kapton and Mylar films.
3. Setup a mass spectrometer into the AO system.
4. Conduct experiment and monitoring the AO system with a mass spectrometer.
5. Find the fractional dissociation of molecular oxygen from the system.
6. How can the AO system be upgraded in terms of AO flux density and energy?

Abstract

An effort to upgrade an Atomic Oxygen (AO) system, that has a flux level of $3.5 \times 10^{15} / \text{cm}^2 \text{s}$ at 0.04 eV energy at NASA Langley Research Center was made to increase the level of flux and energy by at least one order of magnitude. The upgrade includes a new installation of an erosion monitoring system. The present capability of the AO system was not fitted to simulate the conditions of a lower orbit environment where the energy level of AO is 4 eV. The flux density increment is favorable for a short exposure time. In order to improve the physical parameters such as the AO flux density and the energy, input power of the RF generator, flow-rate and pressure have been changed. As result, AO flux density is increased to 19 times ($5.01 \times 10^{16} / \text{cm}^2 / \text{sec}$) and the energy has been increased to 25 times (1 eV) at 1.0 SCCM flow-rate. The higher efficiency operation of the system, however, was obtained at 0.4 SCCM of the flow-rate. At 1.6 SCCM flow-rate, however, there were no dissociation or glow observed.

The upgraded system has a capability to provide real-time mass information such as impurity, vacuum status, and erosion rate of space materials. LARSS (Langley Aerospace Research Summer Scholars) students have collected the detail experimental data in 1997 and 1998.

I. Introduction

Atmospheric composition

The composition and number of density of the atmosphere are function of altitude, local time, sunspot activity, solar flux, magnetic index. Neutral species present at Low Earth Orbit (LEO) include O, N₂, O₂, He, Ar, and H. Molecular nitrogen is the dominant below 200 km, whereas atomic oxygen dominates above 200 km. As one would expect, the number densities of neutral species decrease with increasing altitude [1].

The atomic oxygen density at 300 km is the $10^9/\text{cm}^3$ corresponds to the density of residual gas in a room temperature vacuum chamber at 10^{-7} torr as tabulated in Table 1. However, the high velocity of spacecraft in the altitude causes the atomic flux density on an exposed spacecraft material to be quite high as $10^{15}/\text{cm}^2/\text{sec}$. Assuming a spacecraft in orbit at 300 km with a velocity of 8 km/sec is subjected to oxygen atoms that are condensed upon the surface, a monolayer would form every second [1]. The kinetic energies of 8 km/sec for N₂, O and He particles are approximately 9.3, 5.3, and 1.3 eV, respectively. The physical parameters at the 300 km altitude is tabulated in Table 2.

Background

The previous AO system has been relayed on material erosion test by measuring of Kapton loss. This measurement did not provide any information of the causes for the material erosion. The previous system consisted of a RF generator, an UV lamp, and a test chamber. A RF generator with associated tuning circuits provided up to 100 W of power at 13.5 MHz. The chamber pressure was controlled by the internal vacuum pump in the range of 20 – 100 mtorr. The flow controller was set by 0.16 SCCM at the 13 psi gage pressure. From the previous parameters for the AO system, 0.04 eV of the atomic oxygen energy, $3 \times 10^{15} / \text{cm}^2 \text{ sec}$ of the flux density, $1 \times 10^{15} / \text{cm}^3$ of the density, 0.11 W/cm³ of the power density, and 1.1×10^{-6} W/molecule were obtained as described in Table 3. At the 20 mtorr of the chamber pressure, the average spacing between atoms is 0.1 μm, and the mean free path is to be 1.64 mm. The natural frequency of collision per molecule is calculated to be 0.3 MHz that should be much smaller than the applied frequency used (13.5 MHz) to have more collision.

To increase AO flux density and the energy, available parameters such as input power of the RF generator, flow-rate and pressure need to be changed. The following section will be described the experimental details for the upgrade of the AO system.

II. Experimental Setup

The experimental system consists of a Lockheed Oxygen Plasma apparatus (OPA) and the Dycor Quadrupole Mass Spectrometer (QMS) as shown in Fig. 1. The mass spectrometer is connected to a PC computer using the Dycor System 1000 interface card (DyCard) with associated software (presently state of the art).

The OPA contains a RF generator and an ultraviolet light (UV) to test materials exposing to atomic oxygen (AO) and/or the UV as shown in Fig. 2. The RF chamber is a 5 cm ID x 15 cm long quartz chamber with a 1.27 cm aperture at one end opening to the UV and sample chamber, which is a 7.62 cm ID x 17.8 cm long quartz chamber. The sample is placed in the chamber at 30 degrees to the oxygen plasma flow. The maximum allowable size for specimens is 2.5 in wide x 4 in. long.

The oxygen supply in the original configuration was furnished through a manual leak valve that was set by 10 std. cc/hr (0.167 SCCM) at 10 psi gauge pressure. This system has been modified so that the flow-rate and supply pressure can be adjusted to provide the desired test parameters in the range 10 –100 cc/hr and 36 psi gage pressure respectively. By altering the oxygen flow-rate and RF power the maximum atomic oxygen flux density and the energy can be found as well as optimum conditions of the dissociation of atomic oxygen.

It has been discovered through testing that only research grade oxygen of 99.999% purity or above should be used. Reducing impurity at the chamber is a critical factor based on the leak rate of the system and contamination of the system to get qualitative data during experiments. Typical signal/noise ratio which was generated from the impurity was 1,000 during the experiment.

R.F. power is generated up to 100 W at 13.56 MHz. The oscillator conservatively set at 50 watts forward power with minimal reflected power. To obtain a nominal flow-rate of 3×10^{15} AO/cm²/sec a Tesla wire is connected at the high potential electrode on the RF generator tube and attached to the exterior of the sample tube. No termination is necessary at the sample tube.

The OPA is connected to the Mass Spectrometer by means of interconnecting vacuum chambers. Separating the two vacuum chambers is a copper gasket with a center aperture of 0.0135 in. The OPA and test chamber maintains a vacuum of 10^{-3} torr while the chamber connected to the mass spectrometer maintains a very high vacuum of 10^{-7} .

The high vacuum section is constructed of stainless steel to minimize the effects of out gassing from the system. A gate valve separates the two vacuum chambers isolating the entire high vacuum section during sample insertion also permitting the chamber to retain vacuum pressure as shown in Fig. 1.

The analyzer head and vacuum chamber were baked up to maximum temperature of 350 °C before any experiments were run. The entire system was then allowed to run for two hours, allowing the AO and QMS to stabilize the mass signals before any data was collected.

The electrometer is connected directly to the analyzer head in order to obtain the best signal to noise ratio. The quadrupole control unit and computer are connected to the electrometer power supply and allowed to select a unit by means of an A/B switch. This allows for a backup of the system, control and data collection systems, if at any time the computer system should fail, as well as allowing for the calibration of the two control systems.

The advantage in using the computer over the Dycor control unit is that allow for more flexibility in the collecting of data. The data can be obtained in real-time and/or saved in a digital format as a computer file as well as having the ability to set a schedule for determining just when data is saved during the experiment.

The computer software also provides for the use of macro commands to automate the collection of data as well as setup of different modes of operation and configurations for viewing the data. This includes such modes as Analog, Bar Trend, Meter, Annunciator, Tabular, Library, and a custom mode which includes either a single mode display window or multiple mode display windows as well as display the parameters.

The software schedule option allows for the control of the scanning operations in either continuous or discrete modes and triggers the running of macro files (which allows for the automation of a series of commands) within the selected time intervals.

The Macro commands allow by the software include: saving data, turning the filament on/off, turning the scan on/off, loading of system files, renaming of files, transferring files, print commands, message text and error messages.

A glass rack was used to allow samples to be mounted inside the test chamber. Samples (Du Pont Kapton) used were cut into 1.5 cm by 4.0 cm, weighed prior to being placed in the chamber. To compare with the results from mass spectrum and Kapton weight-loss measurement the samples exposed to the AO plasma. After exposed the samples for two hours the samples were removed from the test chamber and re-weighed to determine the net weight loss.

An AO fluence and flux density could then be determined as follows. The influence (F_1) is calculated as

$$F_1 = \frac{\Delta m(\text{gr.})}{A(\text{cm}^2)\rho(\text{gr} / \text{cm}^3)R(\text{cm}^3 / \text{atom})} \quad (1)$$

where, Δm denotes the mass loss, A is the area of the material ρ denotes the sample density and R is the reactivity ($3 \times 10^{-24} \text{ cm}^3/\text{atom}$). The atomic oxygen flux (F_2) is shown equation (2) as

$$F_2(AO/cm^2 \text{ sec}) = \frac{F_1(AO/cm^2)}{t(\text{sec.})} \quad (2)$$

where, t denotes the exposure time in seconds.

Preparation of Experiment

For a measurement of reliable data, pre-experiments were needed to verify the impurity level of the system, stability of mass spectrum and limitation of the system. A typical base spectrum was measured as shown in Fig. 3. As shown in the figure, the partial pressures of water vapor, He gas are approximately 10^{-9} torr level while others showed in the range of 10^{-10} torr. The partial pressure of oxygen as a dominant species is in the range of 10^{-6} torr that indicates the s/n ratio is about 1,000 as neglecting impurities contained in the oxygen bottle.

Dwell time determines the scanning speed and the degree of background noise. In order to find the optimum dwell time, a base mass spectrum is measured in function of dwell time. As the result, the mass spectrum of various gas species shows some loss of the information at the dwell time of 120 msec. Based on the observation, a reliable mass information can be found at the 500 msec dwell time.

With a Kapton specimen loaded at the test chamber a mass spectrum is also measured with 1.0 cc/hr. of the flow-rate at 50 W RF power as shown in Fig. 4. In the spectrum, ammonia, methane and carbon as a byproduct from the Kapton were significantly showed. This indicates there is a process for erosion of a Kapton material. There may be a correlation between the erosion rate and time integration of mass spectrum for some products.

III. Results and Discussion

In order to understand what physical and chemical effects may arise from atmospheric atomic oxygen etching on spacecraft materials, ground facility needs to simulate the condition as close as possible. Some of important physical parameters were

calculated based on the measurements. The most probable velocity, v_{mp} , of particles leaving the RF source is

$$v_{mp} = \left(\frac{3kT}{m} \right)^{\frac{1}{2}} \quad (3)$$

where, m is the particle mass, k is Boltzmann's constant, and T is the absolute temperature. In order to obtain atomic oxygen at 8 km/sec, such a source must operate at over 5.3 eV which corresponds to 40,000 K.

In study of atomic oxygen experiment, many researchers [3-7] used other gases such as He, Ne, N₂, Ar and their combination to generate more energetic atomic oxygen due to more collision between molecules. However, inclusion of other gases is not valid to study for effects of atomic oxygen on materials based on Batten [8]. Fig. 5 shows the inclusion of other gases compared with pure oxygen on Kapton weight loss was changed to 6 – 60 % based on their result [8]. With a 95% of He and 95% Ar in 5% of O₂, more erosion of Kapton was observed while inclusion of the other gases has shown in quenching. In order to find effects of AO on materials, inclusion of other gases is not appropriate and the purity of oxygen should be controlled.

The degree of dissociation of oxygen molecules to atoms in the RF discharge was determined by using the mass spectrometer. For the calculation of the degree of dissociation based on the measurement, the following assumptions have been made. First, the effects dependent on two successive collisions can be neglected. Secondly, the sensitivity of the filter section is identical for O⁺ ions assumed either from O or from dissociative ionization of O₂. Based on the assumptions made, the modulated signals I_o and I_{o_2} at the peak of the O⁺ and O₂⁺ were measured with the discharge on, and the ratio $y = n_o/n_{o_2}$ of the atom to molecular number of densities was calculated using the equation from Miller [9]:

$$y = P \left(\frac{\sigma_{o_2}}{\sigma_o} \right) \left(\frac{1}{\eta} \frac{I_o}{I_{o_2}} - 1 \right) \quad (4)$$

where P is 0.3, the probability of dissociative ionization of O₂, $\sigma_{o_2}/\sigma_o = 1.67$ is the ratio of ionization cross-sections for O₂ and O [10]. The η is defined as I_o/I_{o_2} is measured with the mass peak ratios with no discharge.

A second method of determining the degree of dissociation requires measurement of the modulated signal I_{O_2} at the O_2^+ mass peak. The modulated signal I_{O_2} is measured with the RF discharge on and a series of modulated signals measured after the discharge is switched off. The difference between these signals, then, represents the O_2 molecules which are dissociated by the discharge and degree of dissociation is given by

$$\alpha = 1 - \frac{I_{O_2}}{I_{O_2}^*} \quad (5)$$

where, $I_{O_2}^*$ is the extrapolation of these signals to the time at which the discharge off under the same conditions.

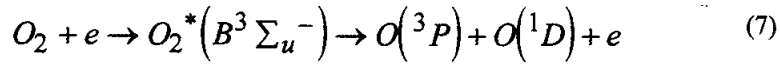
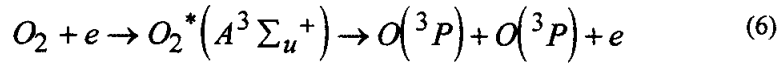
This method gives a degree of dissociation under several different running conditions in agreement with the method of equation (4). The degree of the dissociation was measured as function of power and flow-rate is shown in Fig. 6. The degree of dissociation was found to be as higher as 66 % under the lower pressure condition (~ 11 mtorr at 0.16 SCCM of flow-rate) in the figure. As the flow-rate increased the degree of dissociation decreased to 5 percentage. As each of the curves shows the extent of dissociation first increases as the flow-rate increases at the lower flow-rates and then levels off. This effects is more pronounced at lower flow-rate where the power density per molecule is higher. Over the higher flow-rate the yield was found to be relatively insensitive to the RF power due to the lower power density per molecule.

However, the atomic oxygen flux density is increased as the flow-rate increased as shown in Fig. 7. In the figure, the previous AO flux was measured as 2.7×10^{15} AO/cm²/sec. As the flow-rate increases the AO flux density in increased at 50W RF power. At 1.0 SCCM of flow-rate, the AO flux density is obtained as 5.01×10^{16} AO/cm²/sec. To verify the flux density a Kapton weight loss was measured with 0.70 SCCM of flow-rate at the 50W RF power. Based on the experiment, the AO flux density is measured as 2.67×10^{16} AO/cm²/sec shown as a white circle in the figure.

Mechanism of dissociation of molecular oxygen

A question may arise what potential state of atomic oxygen generated at the near surface of space vehicle in LEO. The previous Table 1 does not show atomic oxygen with a certain energy level for the consideration of their reaction with space materials. In the range of 1 –10 eV that most space vehicles experience, vibrational and electronic excitation. This needs to be considered for reaction with materials.

In Fig. 8, there are five potential energy curves given for the oxygen molecule [10]. When dissociation of the molecule takes place from any of the four lowest electronic states by collision of electron it leads to two oxygen atoms in a 3P state where both atoms would be released in their ground states. If dissociation is produced in the $B^3\Sigma_u^-$ excited state, then one 3P state oxygen atom is produced and one in the excited 1D state expressed in equation 4. The ground state of the oxygen atom is a 3P . The first excited state is 1D lying at 1.97 eV above the ground state, while the second and third excited states lie 4.19 and 9.10 eV above the ground state. Therefore, the possible dissociation of molecular oxygen can occur by one of two processes involving excitation from the ground state to either the $A^3\Sigma_u^+$ or the $B^3\Sigma_u^-$ excited state by electron collision.



This reaction can be measured by emission spectra between 200 and 900 nm.

Further Suggestions for a Upgrading Device

Atoms at thermal velocities have energies of a few tenths of an electron volt. In this application, however, the required atomic oxygen energy in the range from about 1 to 10 eV. Typical intensities of various continuous-flow molecular beam sources function of possible energy are shown in Fig. 9. For high energy AO system, an atomic oxygen generator using an Hollow Cathode discharge or a Corona discharge to produce metastable atoms of thermal energy may be suitable to generate up to 10 eV as shown in the figure. A higher energy of AO generator in combination of a RF and a Hollow cathode discharges will provide the energy level in the range of 10 eV. After generated AO through the RF discharge, the AO will be accelerated due to applied electrical potential (~ 1 kV) from two electrodes. Through the acceleration process most of atomic oxygen ion and electron will also be generated. After the Hollow cathode discharge a ground filter will help a recombination of ions and electrons to make neutral atomic oxygen. The operational condition of the Hollow cathode system will be approximately 1 kV with a few milli-ampere ranges.

For the further upgrade of the AO system, an OMA (Optical Multi-channel Analyzer) system is needed to study the ionization pattern and molecular physics for a detail study in erosion mechanism of materials.

Further recommendations for the AO system may include the followings:

1. Axial offset of the AO generator is needed to prevent line of sight ultraviolet irradiation of the sample. A proposed schematic for the recommendation is shown in Fig. 11.
2. Based on observation and the results from Batten's paper, the purity of oxygen is a critical factor to get qualitative data. Therefore, the purity level of oxygen should be held to research grade as 99.999% or above.
3. The Dwell time of the mass spectrometer is an important factor to get a correct data. It is recommended that dwell time be set to 500 msec.

IV. Conclusions

The previous AO flux was measured as 2.7×10^{15} AO/cm²/sec from the mass spectrometer. As the flow-rate increases the AO flux density is increased at 50W RF power. At 1.0 SCCM of flow-rate, the AO flux density is obtained as 5.01×10^{16} AO/cm²/sec which is 19 times greater than the previous set-up. To verify the flux density a Kapton weight loss was measured with 0.70 SCCM of flow-rate at the 50W RF power.

Based on the experiment, the AO flux density is measured as 2.67×10^{16} AO/cm²/sec that is fitted with the result from the mass spectrometer within 5 %. The degree of the dissociation was measured as function of power and flow-rate. Result shows the extent of dissociation first increases as the flow-rate increases at the lower flow-rates and then levels off. This effects is more pronounced at lower flow-rate where the power density per molecule is higher. Over the higher flow-rate the yield was found to be relatively insensitive to the RF power due to the lower power density per molecule.

References

- [1] Daniel R. Peplinski, Graham S. Arnold, and Eugene N. Borson, "Simulation of Upper Atmosphere Oxygen Satellite Exposure to Atomic Oxygen in Low Earth Orbit," NASA Conference Publication 2340, 1984.
- [2] G. S. Arnold, R. R. Herm, and D. R. Peplinski, "Atmospheric Effects in Low Earth Orbit and the DMSP ESA Offset Anomaly," Air Force Report SD-TR-82-31, 1982.
- [3] P. A. Gory and R. Grice, "Microwave Discharge source for the Production of Supersonic Atom and Free Radical Beams," J. Phys. E: Sci. Instrum., Vol. 12, 1979.
- [4] W. C. Neely, T. C. Yang, J. P. Wey, E. J. clothiaux, and S. D. Worley, "Production of Ground State Atomic Oxygen in a Multifactor Stress Environment," <http://hyperoptic.spi.auburn.edu/neely/groundao.htm>, 1997.
- [5] D. R. Miller and D. F. Patch, "Design and Analysis of a High-intensity Fast Oxygen Atom source," Rev. Sci. Instrum, Vol. 40, 1566-1569, 1969.
- [6] P. A. Gorry, C. V. Nowikow and R. Grice, "Rescattering of a Neon seeded Oxygen Atom Beam," Chem. Phys. Lett., Vol. 55, No. 1, 1978.
- [7] P. A. Gorry, C. V. Nowikow and R. Grice, "Reactive Scattering of a Helium-seeded Oxygen Atom Beam," Chem. Phys. Lett., Vol. 49, pp 116-120, 1977.
- [8] Carmen E. Batten, Kenneth G. Brown, and Beverly W. Lewis, "A Spectral Study of a Radio-frequency Plasma-Generated Flux of Atomic Oxygen," NASA Technical Mem 4612, 1994
- [9] D. R. Miller and D. F. Patch, "Design and Analysis of a High-intensity Fast Oxygen Atom source," Rev. Sci. Instrum, Vol. 40, 1566-1569, 1969.
- [10] Rapp D., Englander-Golden P and Briglia D., "Cross-sections for dissociative ionization of molecules by electron impact," J. Chem. Phys., vol. 42, pp3240-50, 1965.
- [10] John W. Bond, Jr., Kenneth M. Watson, and Jasper A. Welch, Jr., "Atomic Theory of Gas Dynamics," Addison-Wesley, p 144, 1965.
- [11] John R. Hollahan and Alexis T. Bell, "Techniques and Applications of Plasma Chemistry," p30, John Wiley & Sons, 1974
- [12] H. G. Kuhn, "Atomic Spectra," Academic Press, New York and London, p391, 1969.
- [13] Giacinto Scoles, "Atomic and Molecular Beam Methods," Vol.1, p142, 1988.
- [14] Robert F. Bacher and Samuel Goudsmit, "Atomic Energy States," Greenwood Press, p333-348, 1968.

Impinging Velocity:	~ 8 km/sec
Atomic Oxygen Density:	~ 10^9 /cm ³
Pressure:	~ 10^{-7} torr
Atom Oxygen Flux:	~ 10^{15} /cm ² sec
Ambient Temperature:	~1000-1500 K
Required Energy:	
8 km/sec (= 510 kJ/mole, 5.3 eV, 8.5×10^{-12} erg 122 kcal/mol)	
Equivalent temperature ~ 6.15×10^4 K	

Table 1. Physical Parameters at 300 km altitude

1. Energy:	0.04 eV (far short for 5 eV)
2. Atomic Oxygen Flux:	~ 3×10^{15} /cm ² sec
3. Atomic Oxygen density	: ~ 10^{15} /cm ³
4. Power Density:	0.11 W/cm ³
5. Power/molecule:	1.1×10^{-16} W/molecule
6. Pressure:	20 - 80 mtorr
At 20 mtorr, average spacing between atoms: ~ 0.1 μ m mean free path: 1.64 mm frequency of collision per molecules: 0.3 MHz	

Table 2. Status of the previous AO system

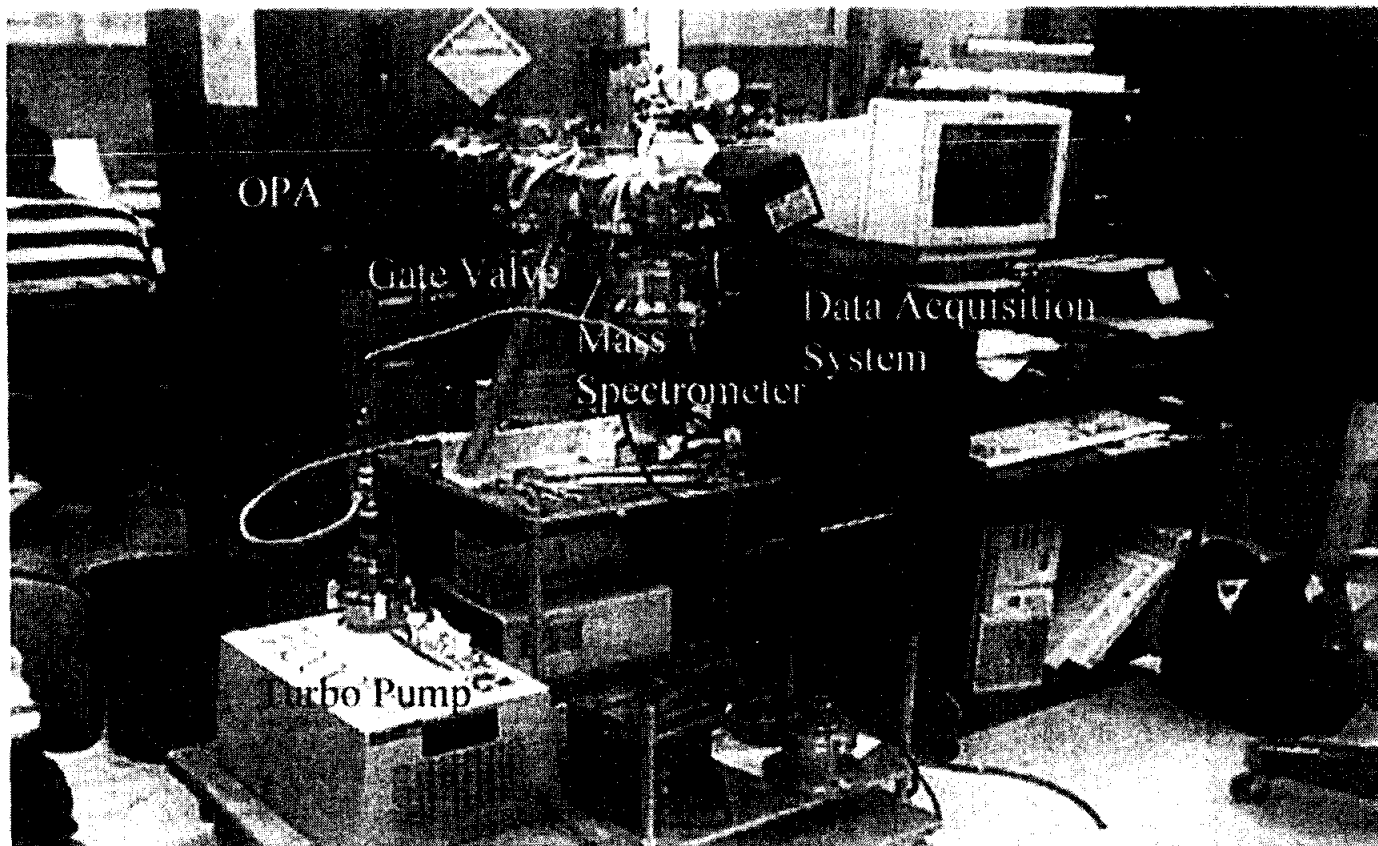


Fig. 1. Experimental setup for Atomic Oxygen System

Space Materials Characterization Lab.

LOCKHEED
OXYGEN
PLASMA
APPARATUS

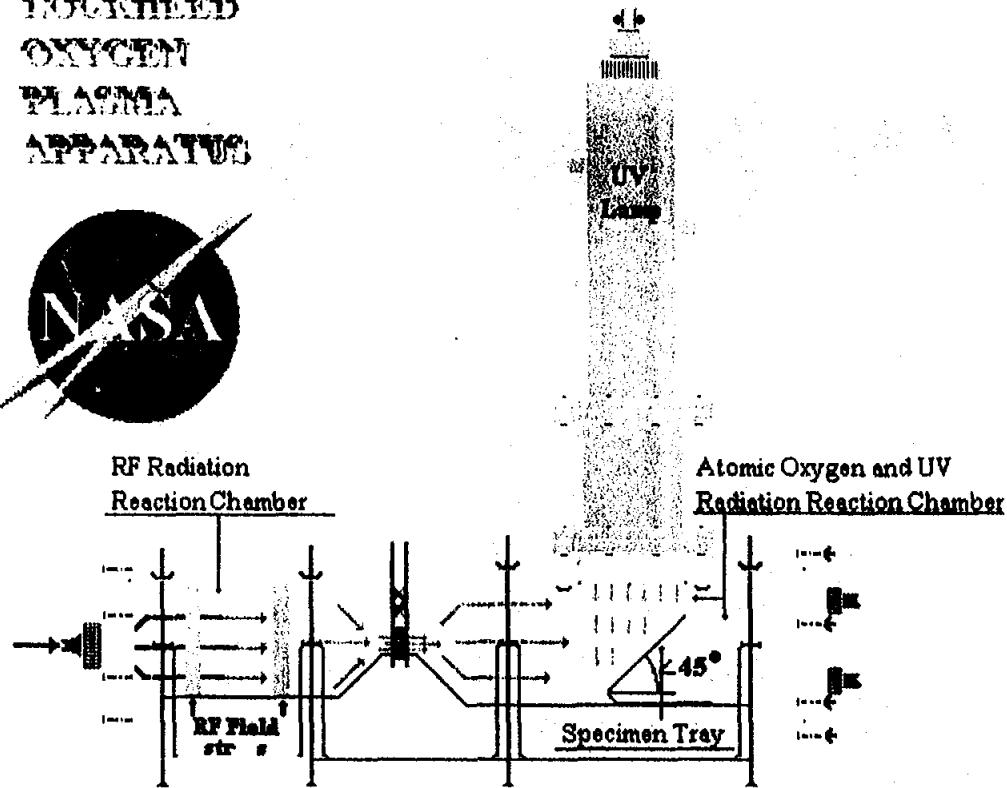


Fig. 2 Configuration of Oxygen Plasma Apparatus (OPA)

ANALOG 01

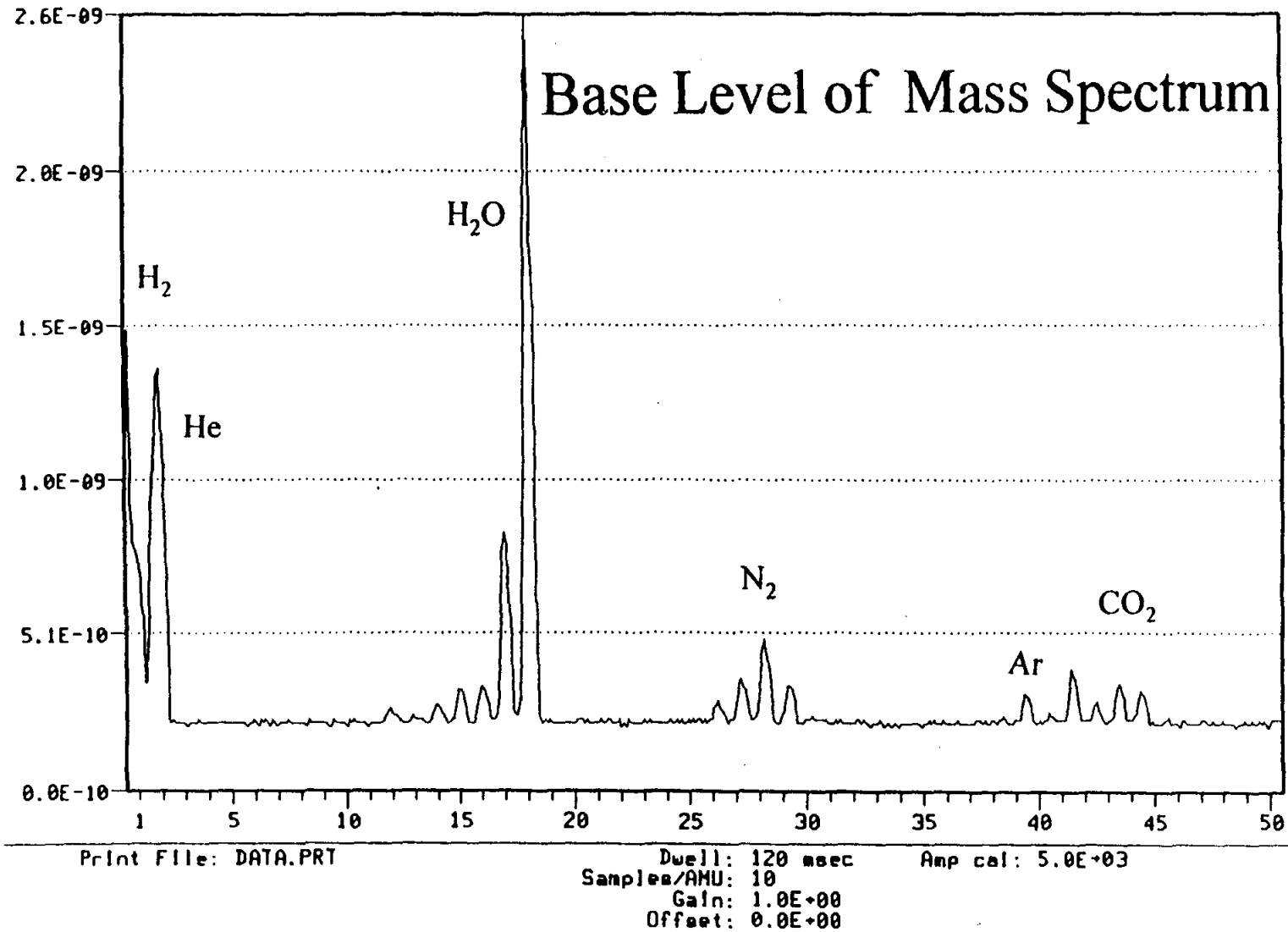


Figure 3. Typical Base Level of Mass Spectrum without Oxygen Flow

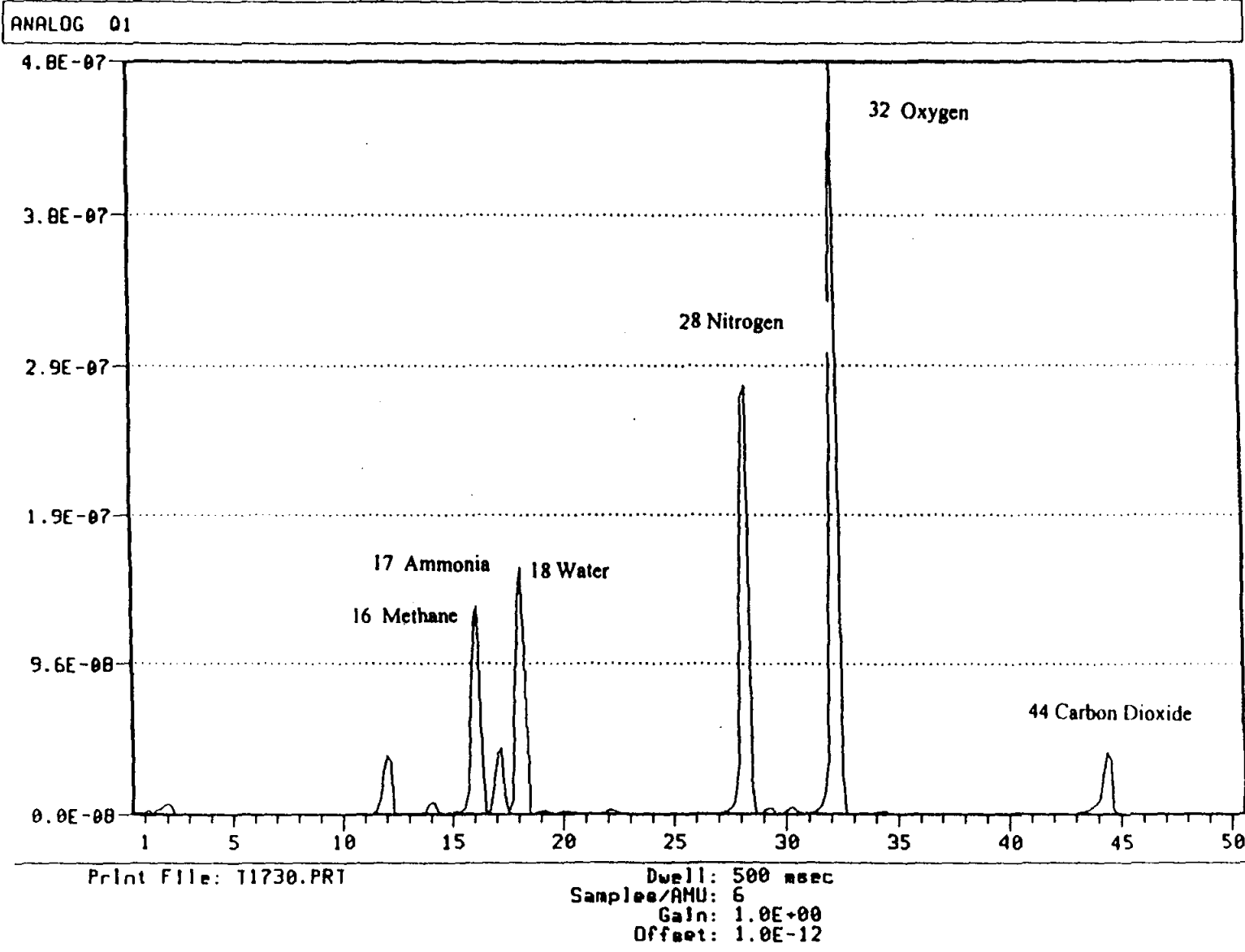


Figure 4. Typical Mass Spectrum of a Kapton Erosion at 0.7 SCCM and 50 W RF Power

68

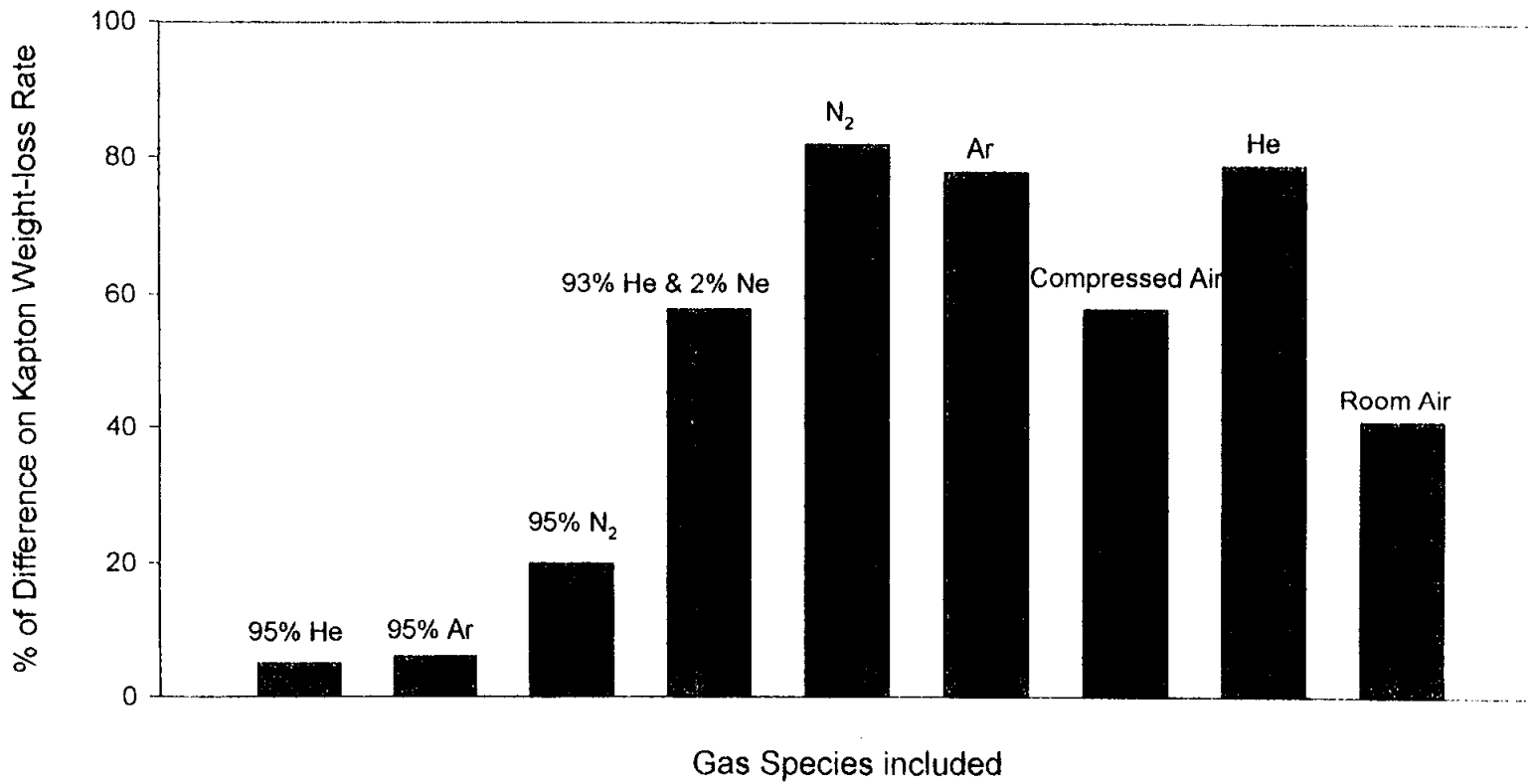


Figure 5. Effects of Inclusion of Various Gas Species on Kapton Weight-loss Rate based on Pure Oxygen [8]

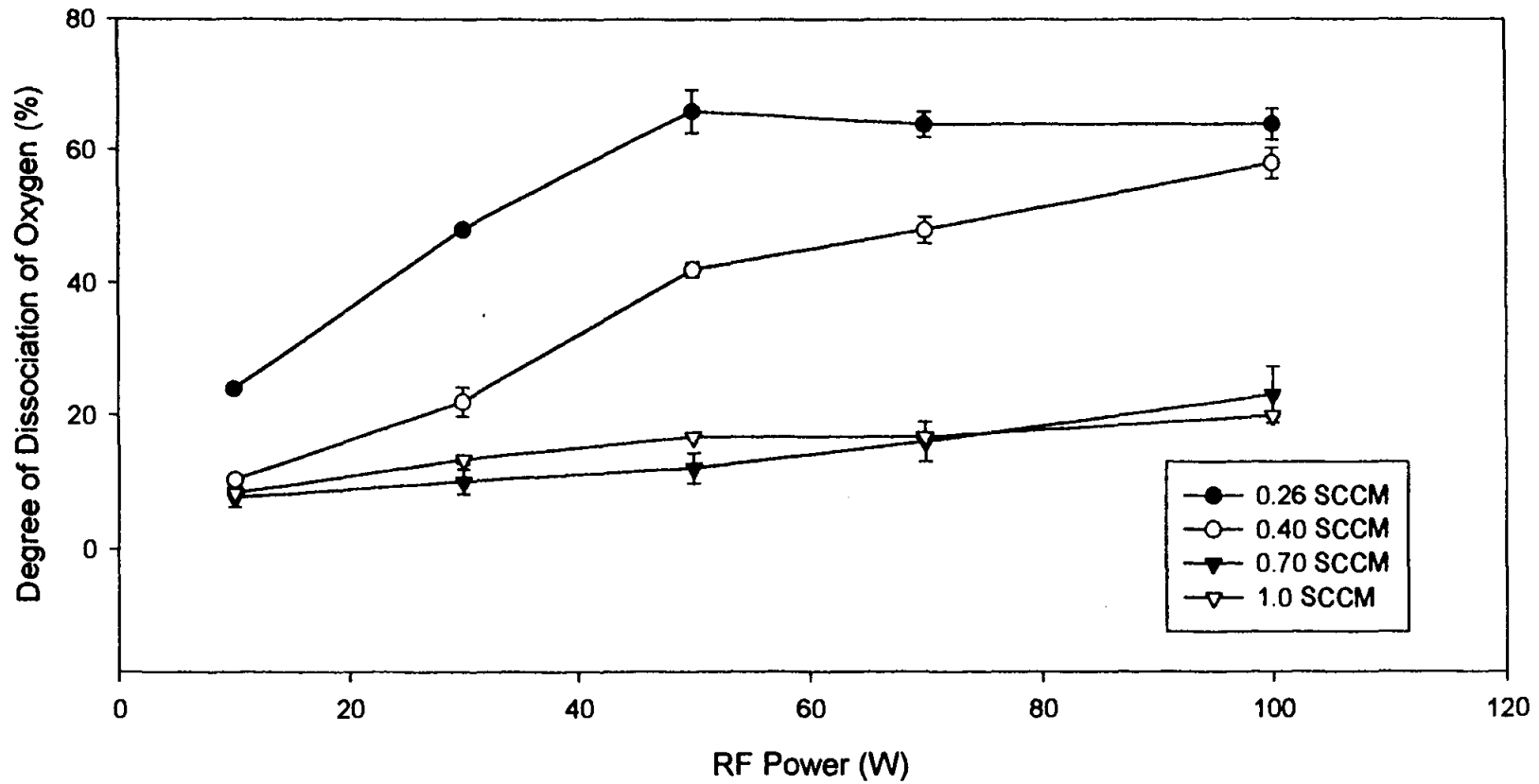


Figure 6. Degree of Dissociation of Oxygen v. RF Power

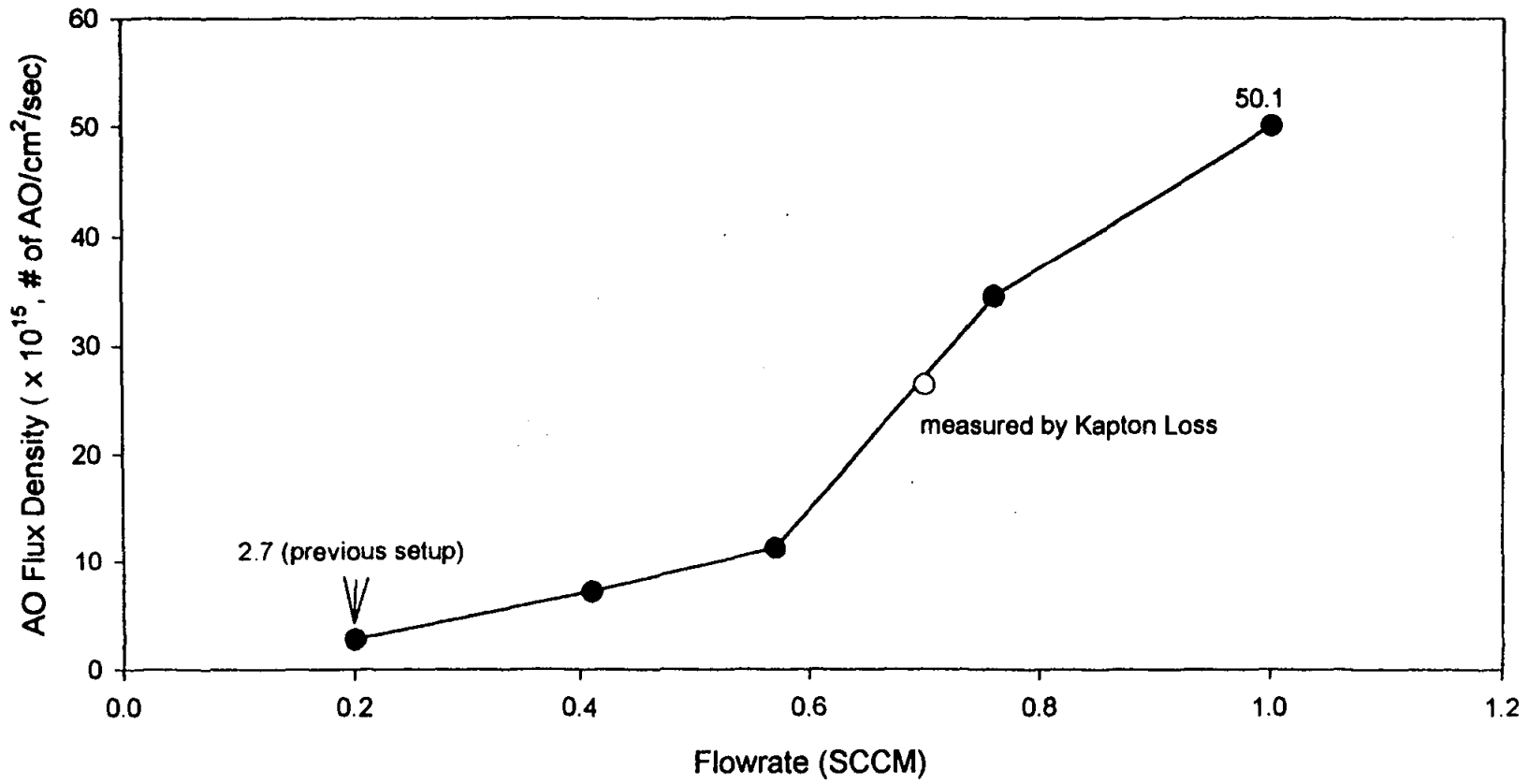


Figure 7. AO Flux Density vs. Flowrate

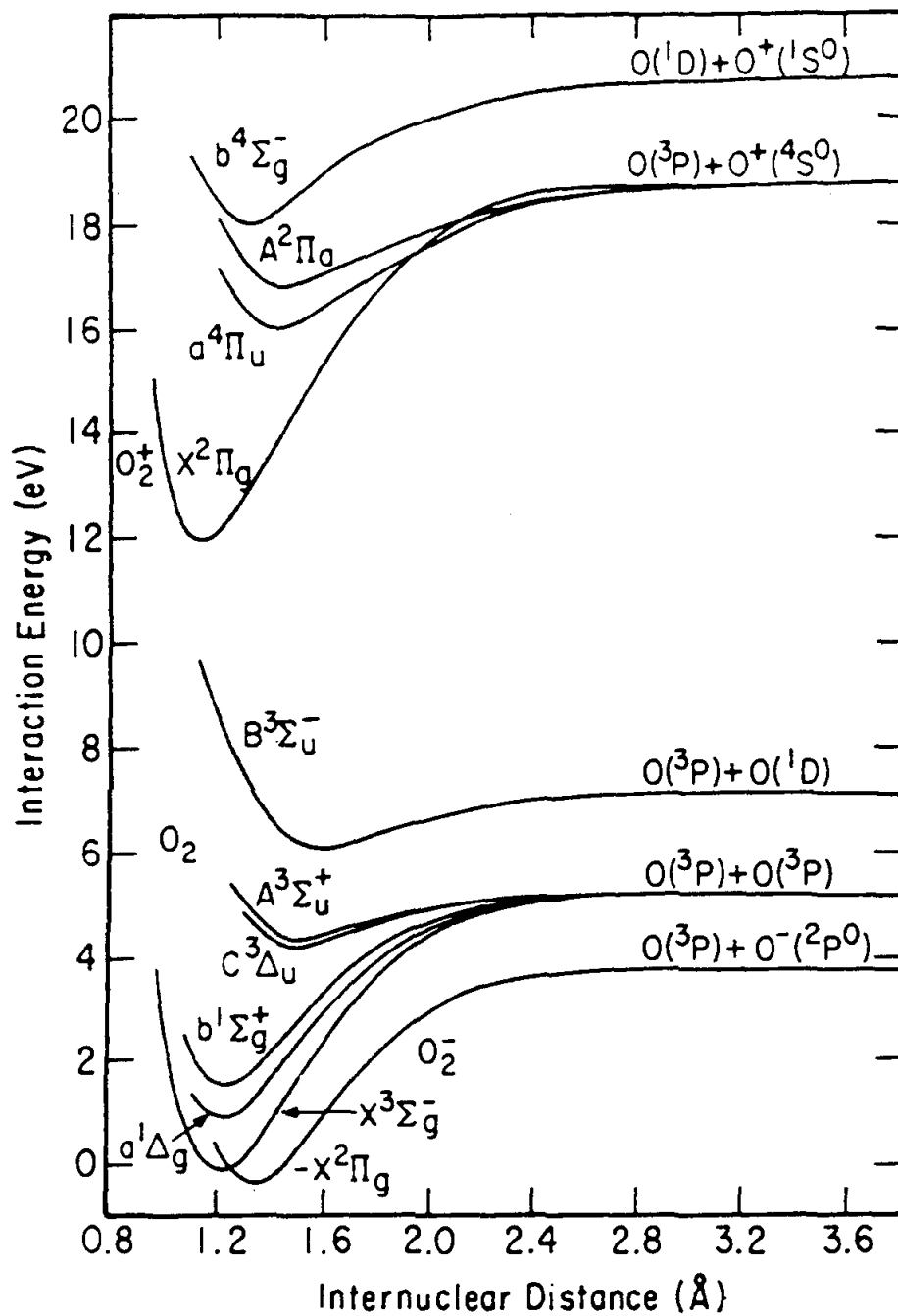


Figure 8. Potential Energy Curves for Some States of O_2 and Its Ions [11]

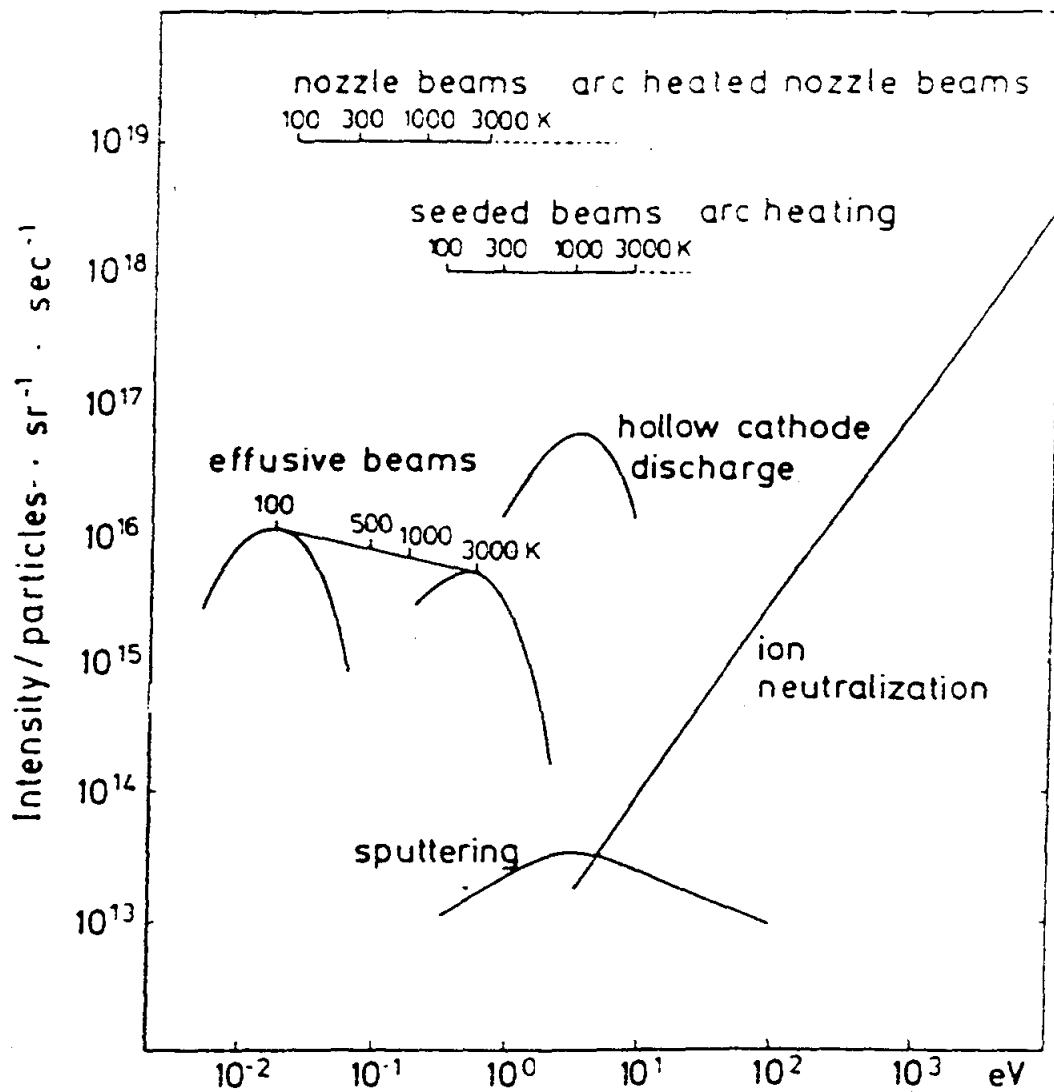


Figure 9. Typical Intensities of Various Continuous-flow Molecular Beam Source [13]

INVESTIGATION OF THERMAL BLEACHING IN MANGANESE DOPED ORTHOALUMINATE SINGLE CRYSTALS

George Loutts

Mikhail A. Noginov

Rosalind Wynne

Kai T. Ross

and

Talia Grandy

Center for Materials Research
Norfolk State University
2401 Corprew Avenue
Norfolk, Virginia 23504

Telephone: 757-683-2031
e-mail: g_loutts@vger.nsu.edu

Investigation of Thermal Bleaching in Manganese Doped Orthoaluminate Single Crystals

George B. Loutts, Mikhail A. Noginov, Rosalind Wynne, Kai T. Ross and Talia Grandy

Center for Materials Research
Norfolk State University
Norfolk, Virginia

Key Words

Materials for Optical Storage, Thermal Bleaching, Optical Absorption

Prerequisite Knowledge

It is useful to have basic knowledge of physics, chemistry, and spectroscopy.

Objectives

To study the kinetics of thermal bleaching in manganese doped orthoaluminate crystals at different temperatures using a custom-built temperature attachment to a Cary 5 spectrophotometer.

Equipment and Materials

- Mn-doped samples of YAlO_3 , YbAlO_3 and GdAlO_3 crystals, 4-10 mm thick
- Brass tube, around 3/8" I.D.
- Ceramic tube, 1" I.D.
- Heating tape
- Thermocouple, type K
- Temperature controller
- Cary 5 UV/Vis/IR spectrophotometer from Varian with Cary WinUV software (or any other visible spectrophotometer with the software for kinetics measurements)
- Microcal Origin or Microsoft Excell software

Introduction

Single crystalline manganese-doped yttrium orthoaluminate (Mn:YAlO_3) is a promising material for holographic recording and optical storage [1,2]. A broad-band coloration accompanied with a strong change in index of refraction can be photoinduced in the crystals with a laser light of 550 nm wavelength or shorter wavelength. The coloration is associated with the photoionization of Mn^{4+} ions to Mn^{5+} ions residing in the

aluminum octahedral sites. The coloration and optical data recorded in the material are stable for more than one year at room temperature. However, they can be erased within minutes at a temperature above 250°C due to the reverse reaction $\text{Mn}^{5+} + e \rightarrow \text{Mn}^{4+}$. The goal of this experiment is to study the kinetics of coloration bleaching at different temperatures and to compare thermal bleaching in Mn-doped orthoaluminates of yttrium, ytterbium and gadolinium (Mn:YAlO₃, Mn:YbAlO₃ and Mn:GdAlO₃). A custom-built temperature attachment to Cary 5G spectrophotometer has been developed for the experiment. The attachment allows measuring optical absorption of samples in the temperature range from room temperature to 800°C.

Mn-doped Crystal Samples

Orthoaluminates of yttrium, ytterbium and gadolinium have a distorted perovskite structure that belongs to the orthorhombic system, space group Pbnm [3]. Manganese enters the structure in the form of Mn²⁺ ions substituting Y³⁺ ions in the dodecahedral lattice sites [4] and Mn⁴⁺ ions substituting Al³⁺ ions in the octahedral lattice sites [5].

Manganese-doped single crystals of YAlO₃, YbAlO₃, and GdAlO₃ were grown by the Czochralski technique in iridium crucibles under nitrogen atmosphere with 0.2% of oxygen. The charges were prepared with Al₂O₃ and Y₂O₃ of 99.999% purity; Yb₂O₃, and Gd₂O₃ of 99.99% purity. Manganese was introduced in the charge as MnO₂ of 99.9% purity in the concentration of 0.5 at.% with respect to Al. The YAlO₃ crystals were grown on a seed, oriented along the “b” direction of the orthorhombic unit cell. Other orthoaluminates were nucleated on iridium wires. They became single crystalline after several millimeters of pulling and the final orientation of their boules was close to the crystallographic “c” axis. During growth, the pull rate was maintained at 1.5 mm/h and the rotation rate at 15 rpm.

Experimental samples were cut from the boules in the form of tetragonal prisms with faces parallel to the crystallographic planes “a”, “b”, and “c” and lengths of 4-10 mm. Square faces of the prisms were “window” polished and their corners were rounded to fit a 3/8 inch diameter tube.

Experimental setup

Prior the experiments, samples were photocolored with a 1W argon laser beam for several minutes. During the exposure the color changed from yellow-amber to dark bluish-gray.

Optical absorption spectra of the samples were taken using the ultraviolet-visible-infrared spectrophotometer Cary 5G from Varian. In order to measure absorption at elevated temperatures, a small furnace that fits the sample compartment of the spectrophotometer has been designed. A sketch of the furnace is shown in Figure 1. It consists of a brass tube with 3/8 inch inside diameter and about 3 inch long. The tube is wrapped with a heating tape and inserted in a porous alumina tube, 1 inch I.D., which

serves as heat insulation. A K-type thermocouple is inserted in a pocket in the brass tube and connected to a temperature controller. (We used a Dimension controller from Research, Inc). The output from the controller is connected to a power supply, which is hooked to the heating tape. The Dimension controller and the spectrophotometer are interfaced to a PC so that both temperature reading and optical absorption data can be downloaded and processed.

Optical absorption measurements

Optical absorption of photocolored samples was measured in order to determine the wavelength of maximum in the absorption spectrum and then to record thermal bleaching curves at that wavelength. Absorption spectra of the three materials are shown in Figure 1. The maxima are located at about 650 nm in all the three materials. This wavelength has been selected for recording of thermal bleaching curves and decay kinetics curves at different temperatures

Thermal bleaching curves

In order to record thermal bleaching, each photocolored sample was placed in the built furnace. The furnace was mounted inside the spectrophotometer so that the primary light beam passed through the sample and reached the detector. The temperature controller was programmed to raise the temperature from 25°C to 400°C linearly over one hour. During this time, both absorption at 650 nm wavelength and temperature was recorded simultaneously. The resulting graph is shown in Figure 3. It indicates a sharp drop in optical absorption at temperatures specific for each manganese-doped material. This implies that optical data recorded in the samples can be erased by heating them to about 250°C in case of Mn:GdAlO₃, 300°C in case of Mn:YAlO₃ and 350°C in case of Mn:YbAlO₃.

Kinetics of discoloration

Kinetics of discoloration in Mn:YAlO₃, shown in Figure 4, was recorded similarly. The temperature was quickly raised to a specific value and then maintained constant for the rest of the experiment. It is clear that the discoloration rate strongly depends on the temperature. In order to estimate the storage time at room temperature, normalized absorption in Mn:YAlO₃ was plot against logarithm of time, Figure 5. After the initial period of 150 minutes, the experimental data can be approximated with a straight line. The total duration of experiment was 4000 minutes. Assuming the kinetics continues to further follow the straight line, one can estimate that the recorded pattern will lose 50% of its initial intensity after around 120 years. This implies that Mn:YAlO₃ is a promising material for permanent holographic recording.

Acknowledgments

The work was supported in part by the AFOSR/BMDO grant #F49620-98-1-0101 and DOE grant #DE-FG01-94EW11493.

References

1. G.B. Loutts, M. Warren, L. Taylor, R.R. Rakhimov, H.R. Ries, G. Miller III, M.A. Noginov, M. Curley, N. Noginova, N. Kukhtarev, H.J. Caulfield, and P. Venkateswarlu. Manganese doped yttrium orthoaluminate: a potential material for holographic recording and data storage. *Physical Review B*, **57**, 1998, 3706-3709.
2. M.A. Noginov, N. Noginova, M. Curley, N. Kukhtarev, H.J. Caulfield, P. Venkateswarlu, G.B. Loutts. Optical characterization of Mn:YAlO₃, material for holographic recording and data storage. *J. Optical Society of America B*, **15**, 1998, 1463-1468.
3. P.D. Dernier and R.G. Maines, "High pressure synthesis and crystal data of the rare earth orthoaluminates", *Mat. Res. Bull.*, **6**, pp. 433-440, 1971.
4. M.A. Noginov, G.B. Loutts, Spectroscopic studies of Mn⁴⁺ ions in yttrium orthoaluminate, Submitted to *Journal of Optical Society of America B*, 1998.
5. M.A. Noginov, G.B. Loutts, M. Warren, Spectroscopic studies of Mn³⁺ and Mn²⁺ ions in YAlO₃, Submitted to *Journal of Optical Society of America B*, 1998.

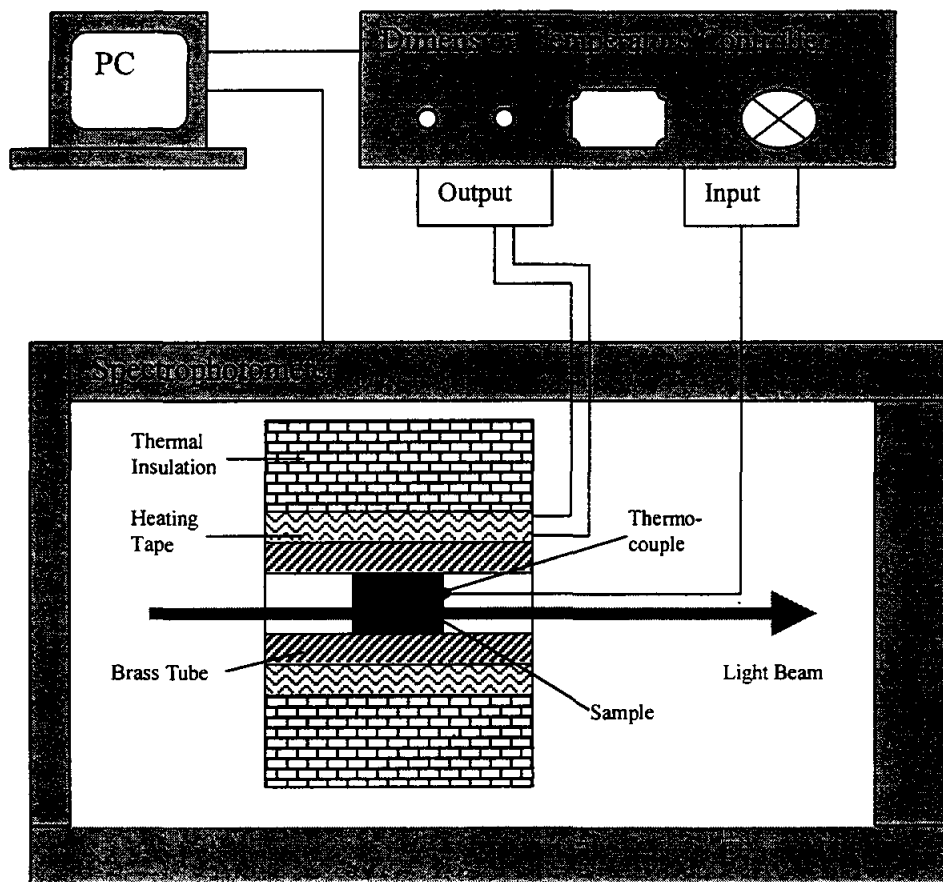


Figure 1. Schematic diagram of the temperature attachment.

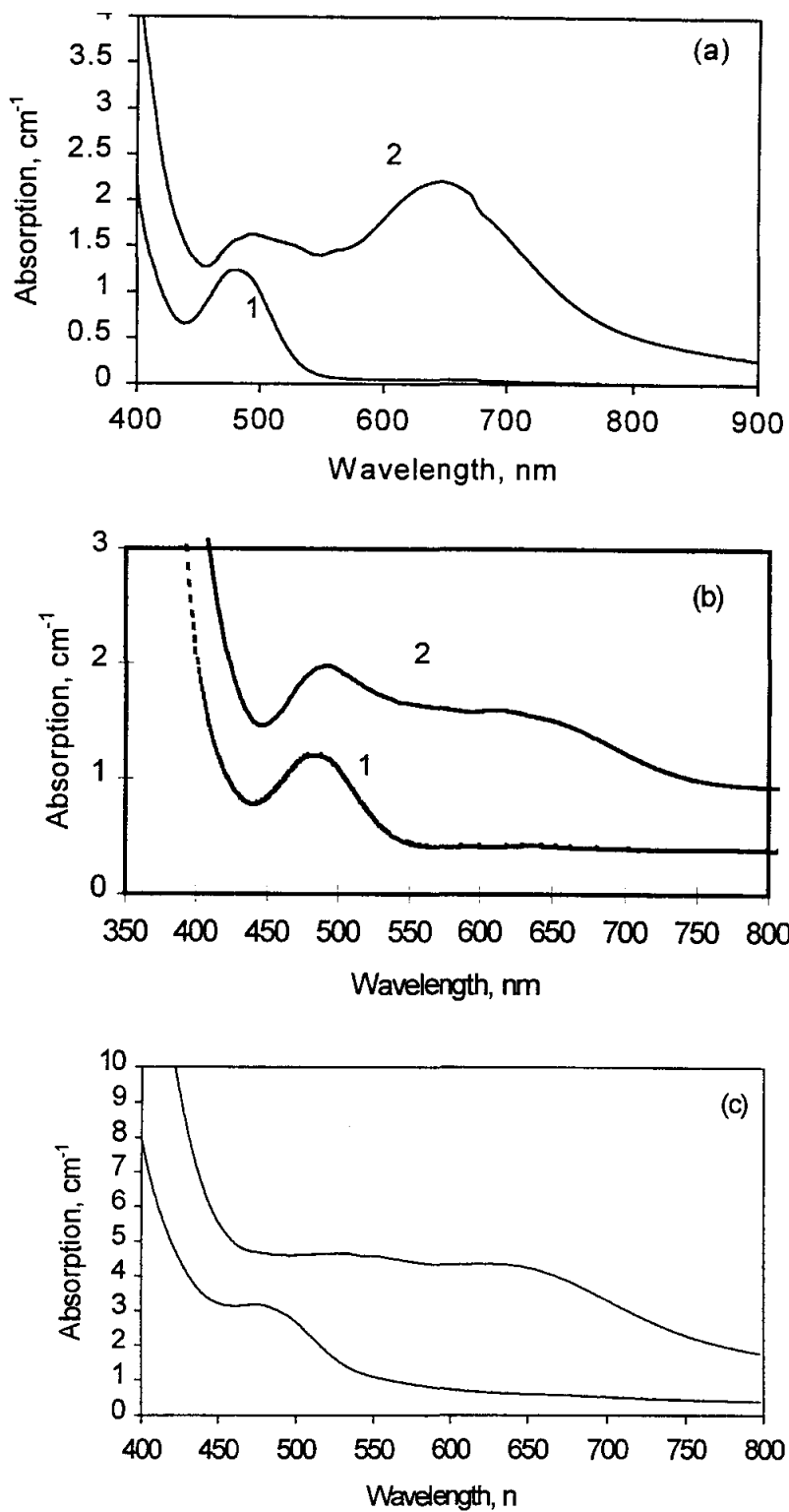


Figure 2. Room temperature absorption spectra of non-exposed (trace 1) and exposed (trace 2) samples of Mn:YAlO₃ (a), Mn:YbAlO₃ (b), and Mn:GdAlO₃ (c).

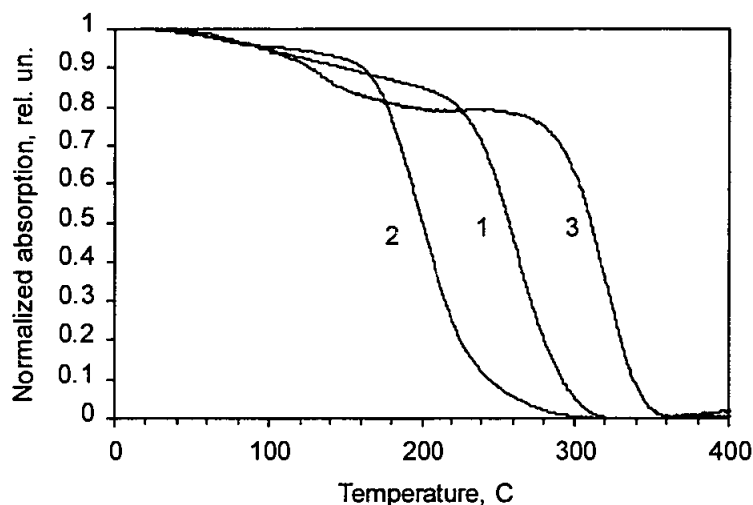


Figure 3. Thermal bleaching curves of Mn:YAlO₃ (1), Mn:GdAlO₃ (2), and Mn:YbAlO₃ (3) recorded at 620 nm.

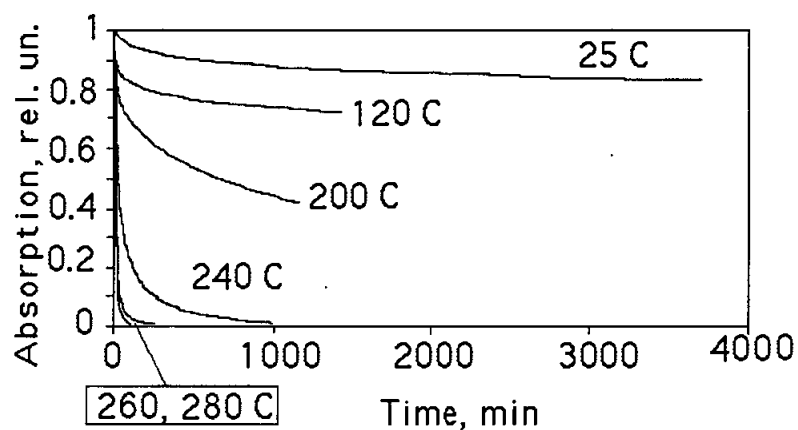


Figure 4. Kinetics of discoloration in Mn:YAlO₃ at different temperatures.

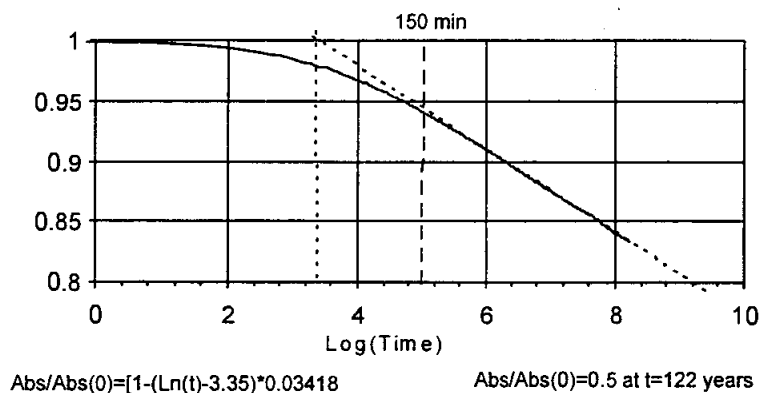


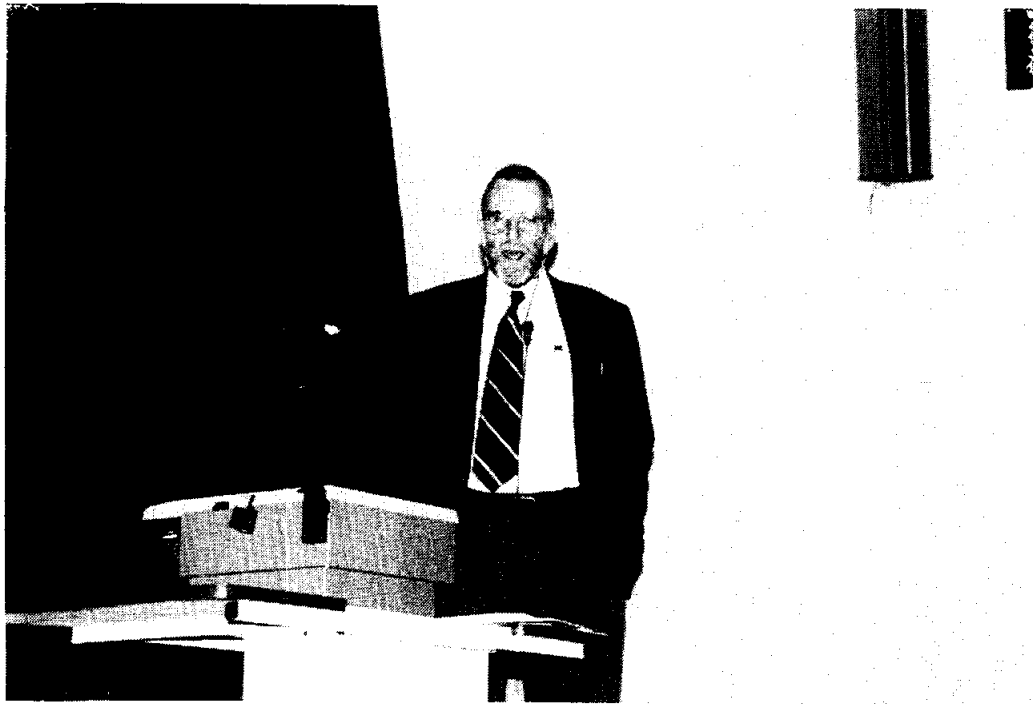
Figure 5. Kinetics of discoloration in Mn:YAlO₃ at room temperature approximated with a straight line.

THE MATERIALS SCIENCE OF SUPERCONDUCTING MAGNETS

David Welch

Head - Materials Science Division
Department of Applied Science
Brookhaven National Laboratory
P. O. Box 5000
Upton, New York 11973-5000

Telephone: 516-344-3517
e-mail welch@sun2.bnl.gov



David Welch

The Materials Science of Superconducting Magnets

David O. Welch

Materials Science Division
Department of Applied Science
Brookhaven National Laboratory

"Once molecules have learnt to compete and to create other molecules in their own image, elephants, and things resembling elephants, will in due course be found roaming through the countryside."

Ref. 1 Peter Atkins
The Creation
W. H. Freeman & Co. (1981)

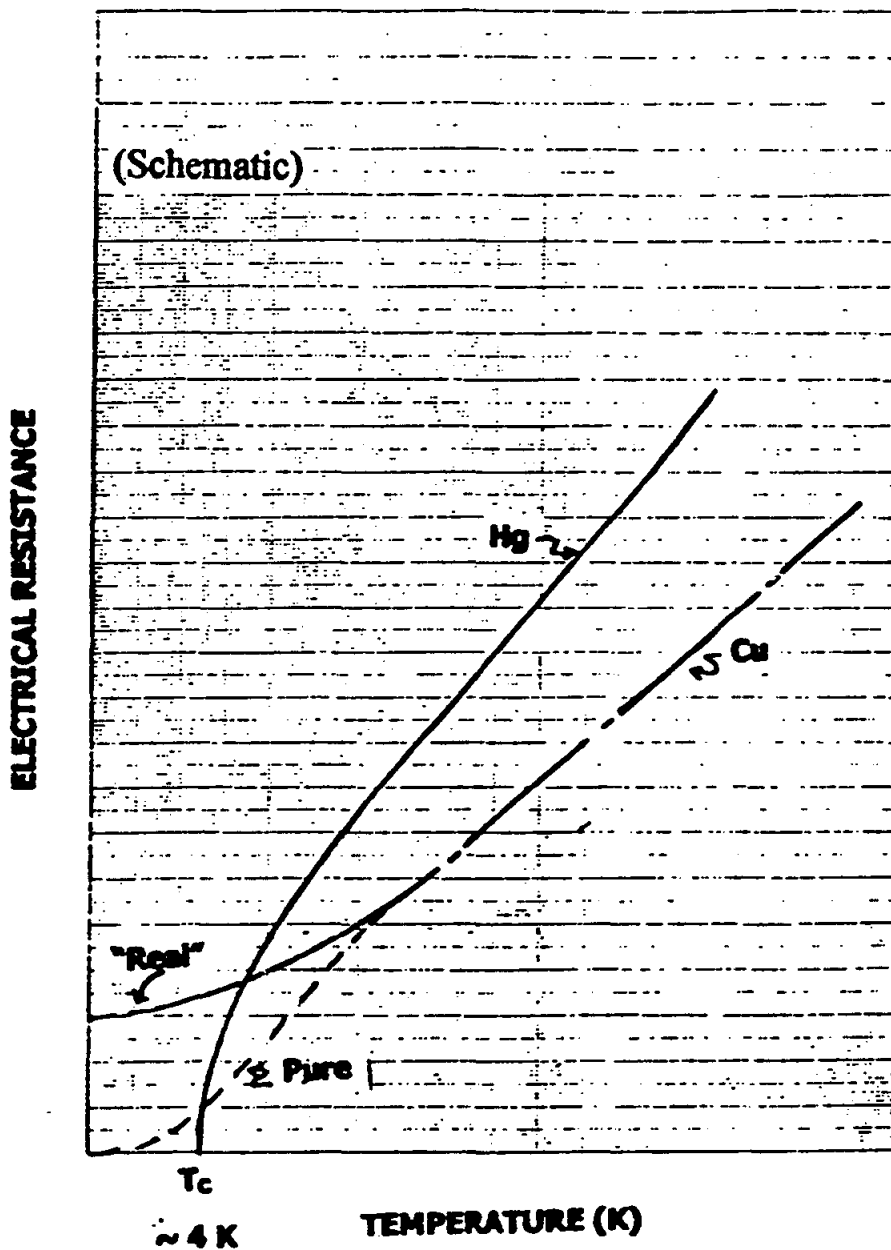
*In 1911 Mr. G. Holst, a graduate student, made a measurement with surprising results in the Cryogenic Laboratory of the Univ. of Leiden.

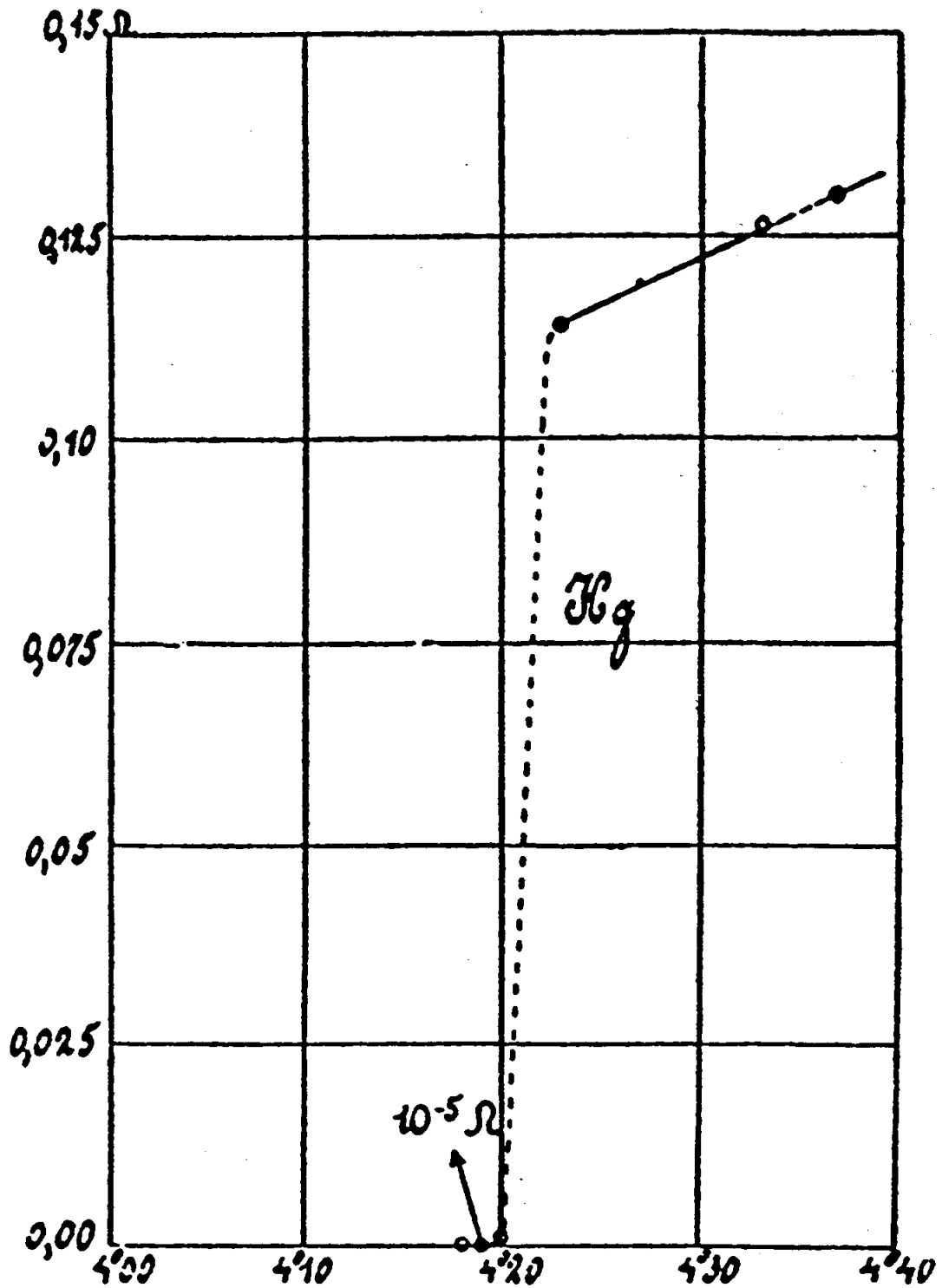
*In 1999 scientists at the Relativistic Heavy Ion Collider at BNL are expected to recreate conditions in the first microseconds of the universe.

WHAT IS THE CONNECTION?

SURPRISE !

Gilles Holst and Heike Kamerlingh Onnes discover that in some metals electrical resistance vanishes at a definite temperature (not zero), i.e., “superconductivity”. (1911)





HENDRIK CASIMIR

HAPHAZARD
REALITY

Half a Century of Science



HARPER COLOPHON BOOKS

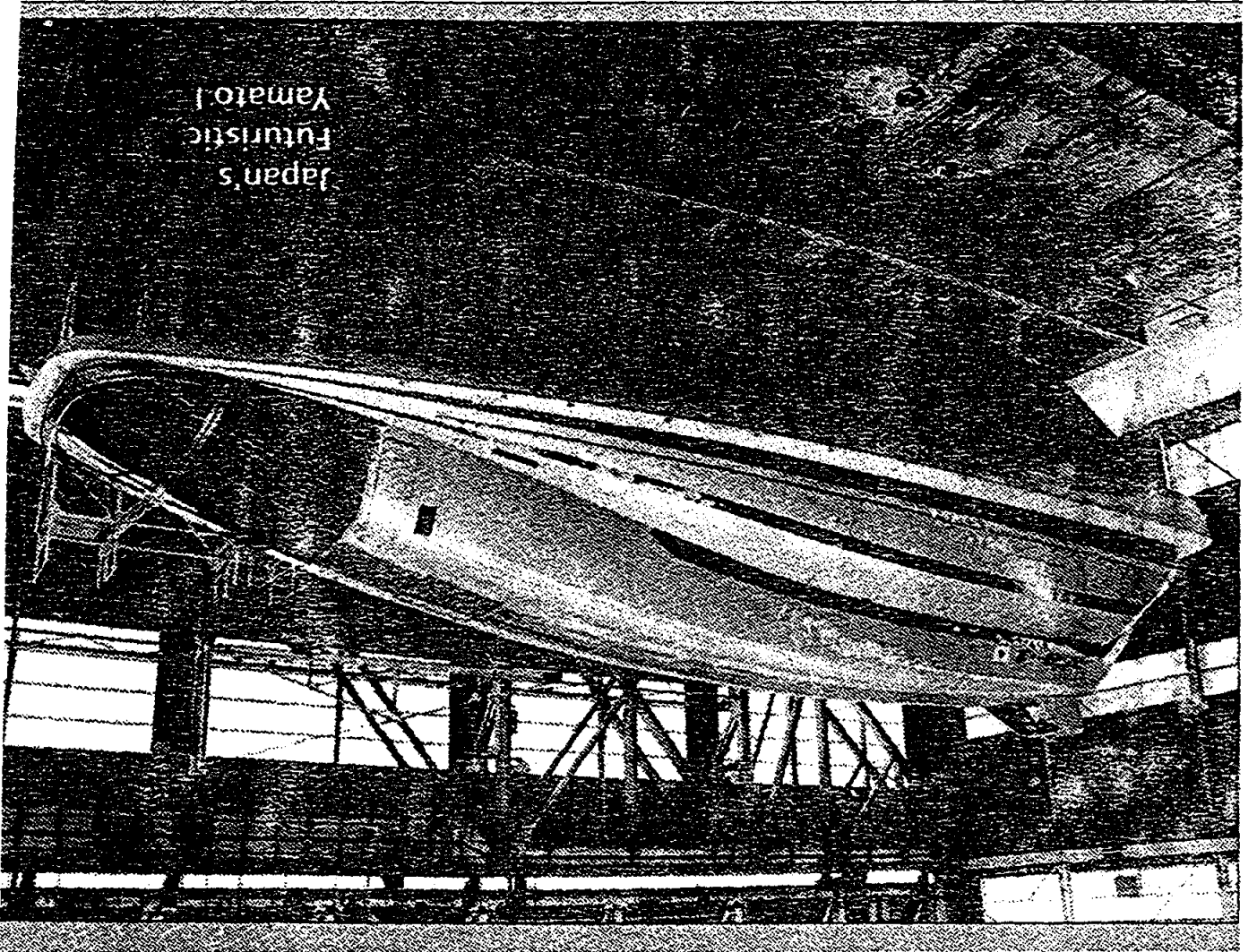
Harper & Row, Publishers

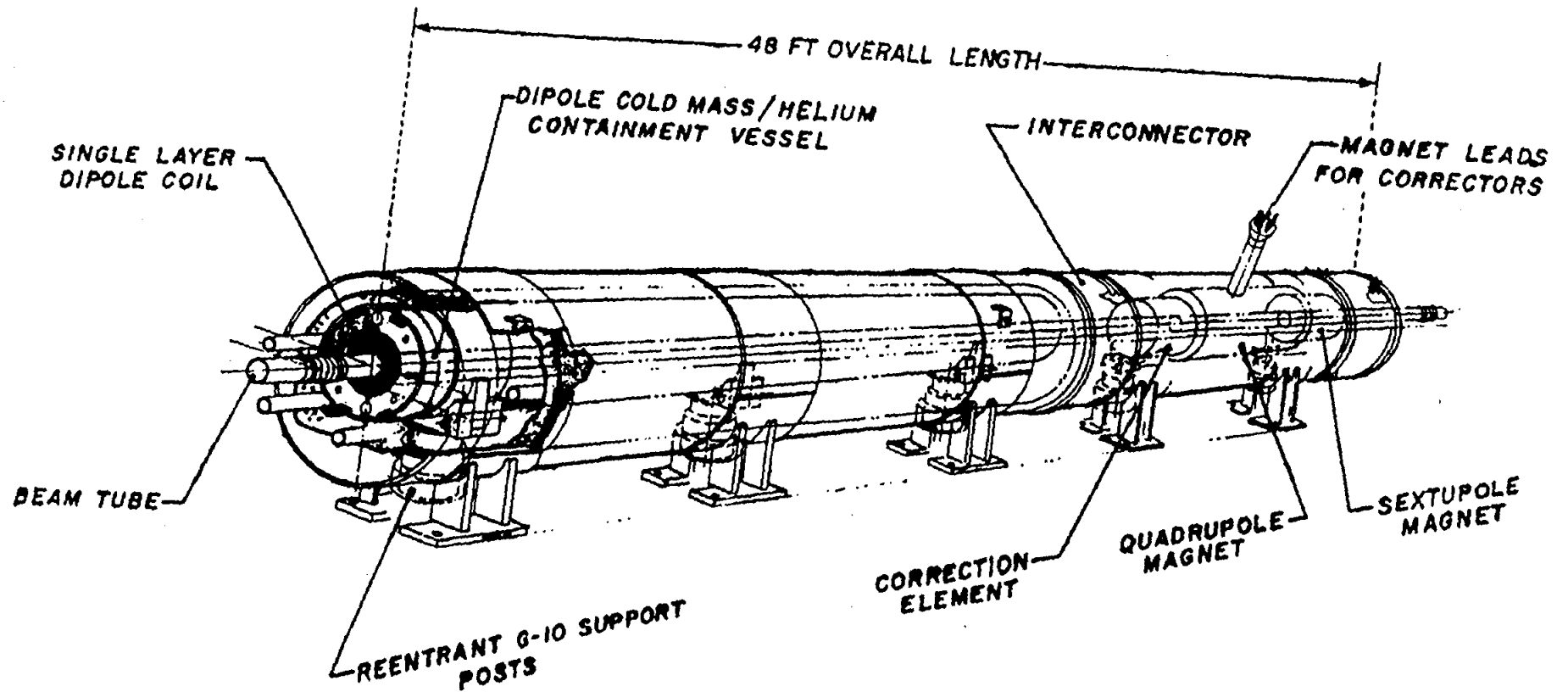
New York, Cambridge, Philadelphia, San Francisco,

London, Mexico City, São Paulo, Sydney

Reprinted with permission of David Welch and Hendrik Casimir

Fall 1990





RHIC MAGNET ASSEMBLY
(1000-2-2000)

*a superconducting
device*

October 26, 1998

SUPERCONDUCTOR WEEK **3**

RHIC Magnet Production Completed

Brookhaven National Lab (BNL) announced the end of magnet production for the Relativistic Heavy Ion Collider (RHIC). A total of 1,805 magnets, including 65 spares have been either manufactured at, or delivered to, BNL at a total cost of \$165 million. The *Brookhaven Bulletin* reported that magnet production required 929,500 tech-hours: 727,500 at BNL, 170,000 at Northrop Grumman, and 32,000 at Everson Electric Company. The magnets contain 21 million meters of superconducting wires.

BNL expects to complete mechanical assembly of the RHIC ring by the end of the year and begin subsystem testing in January. Injection of the gold beam will occur in March and detector installation is slated for April and May. RHIC's first run is scheduled for June or July of 1999. ○

Why Did It Take So Long For "Elephants" to Appear?

Because Materials Science and Engineering can take a very long time!

What Happened?

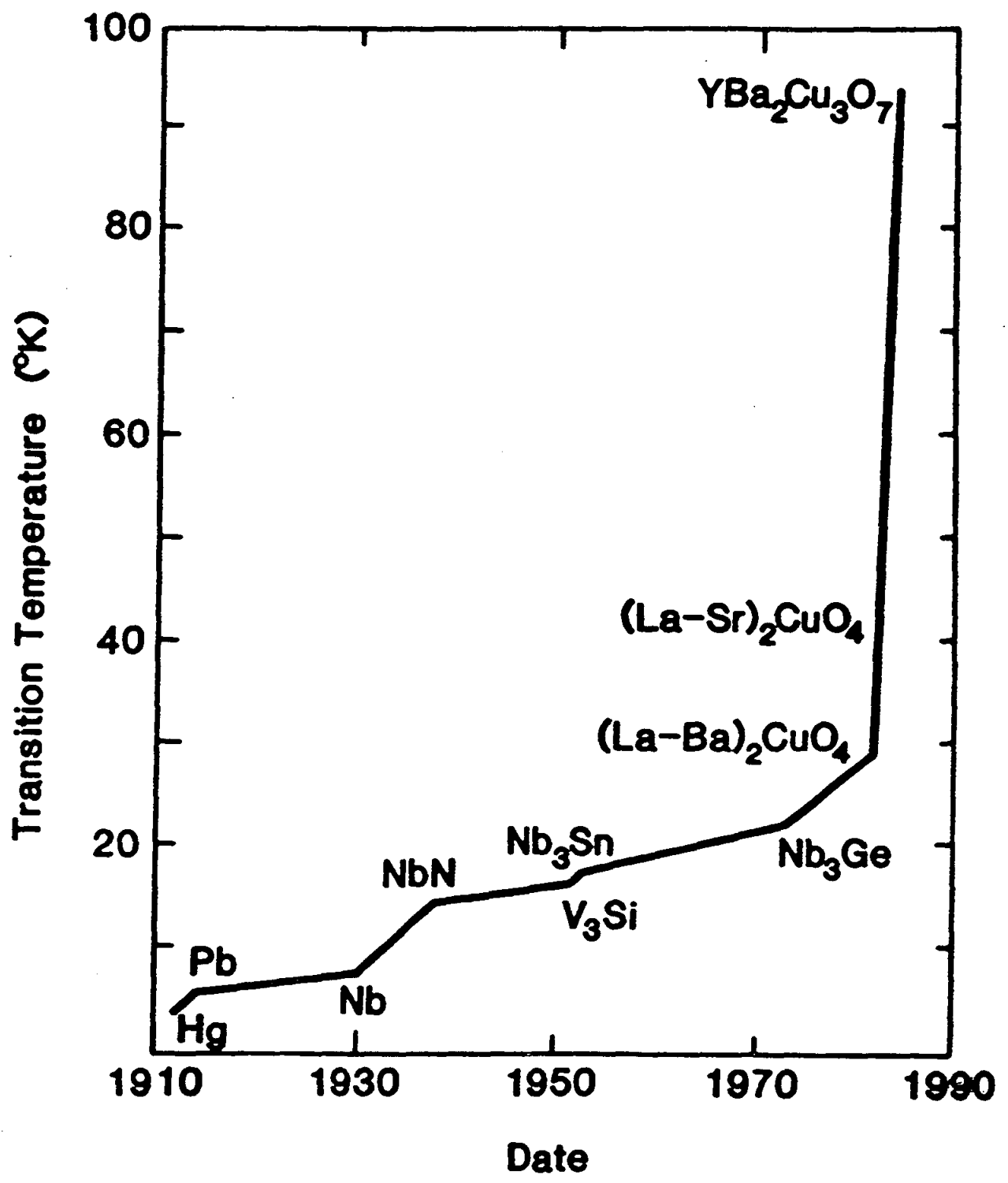
"The early workers in superconductivity soon discovered that there is an upper limit to the amount of current that can be passed along a piece of superconductor if it is to remain resistanceless. We call this the critical current of that particular piece. If the current exceeds this critical value, resistance appears."

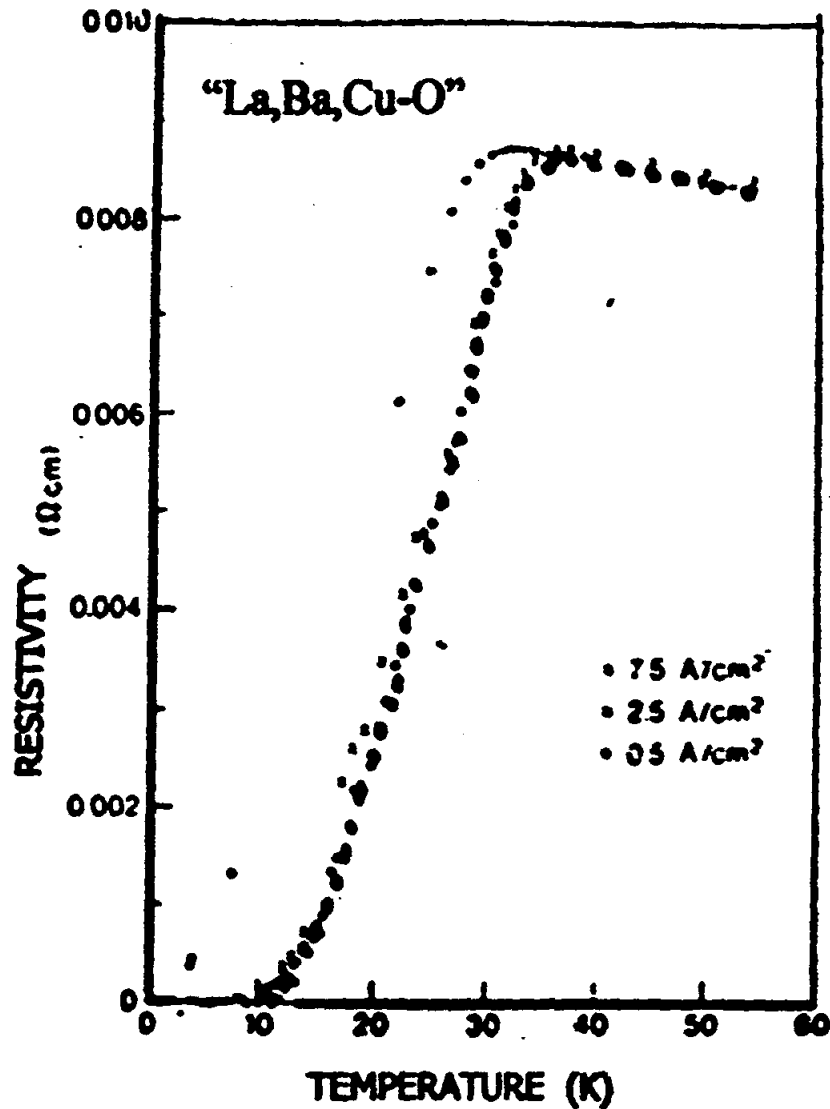
(A.C. Rose-Innes and E. H. Rhoderick, Introduction to Superconductivity)

Why Aren't The RHIC Magnets Made of "High-Temperature" Superconductors?

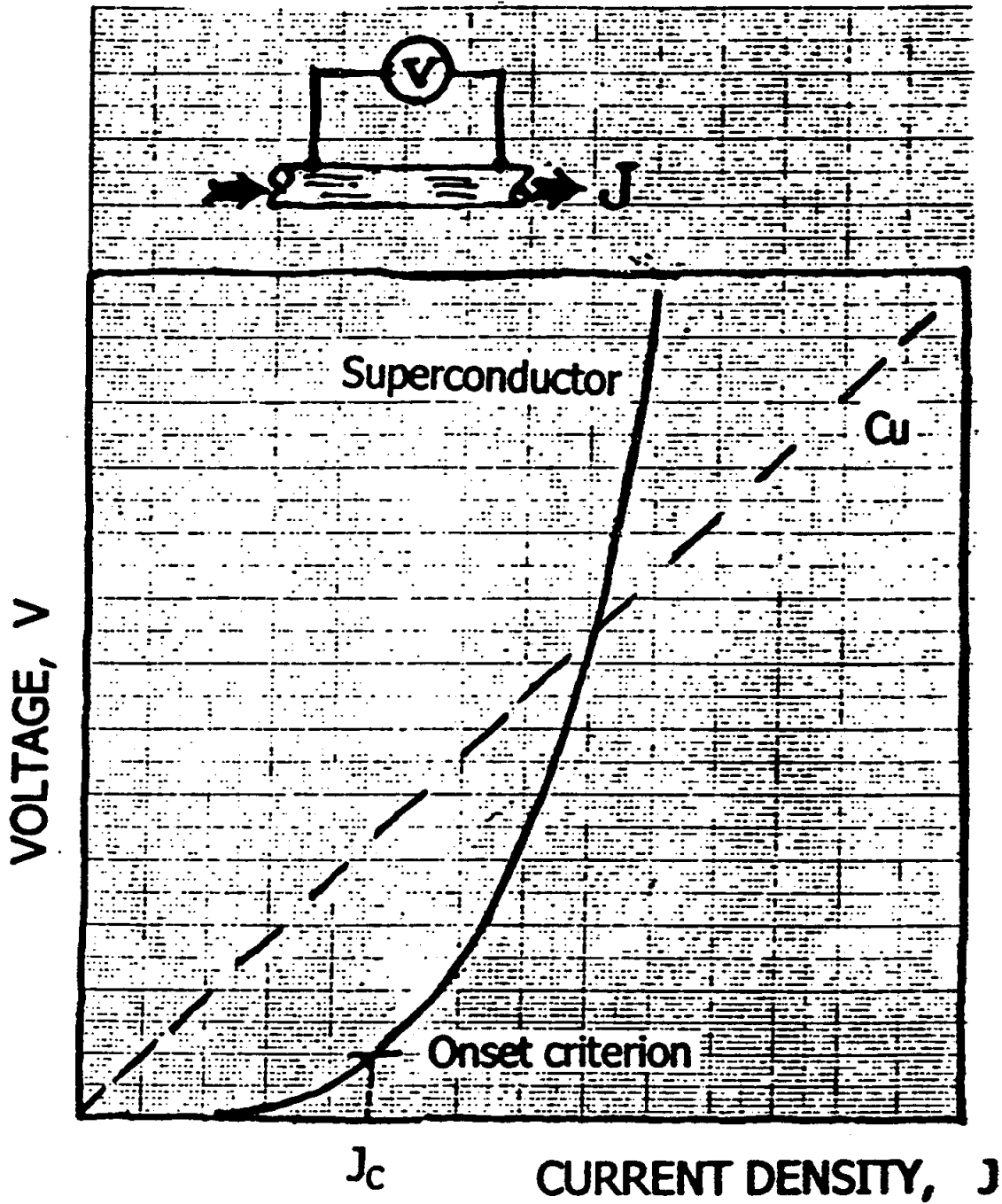
Because the critical current densities are too low without very sophisticated processing and because Materials Science and Engineering can take frustratingly long times!

Transition Temperature vs. Time

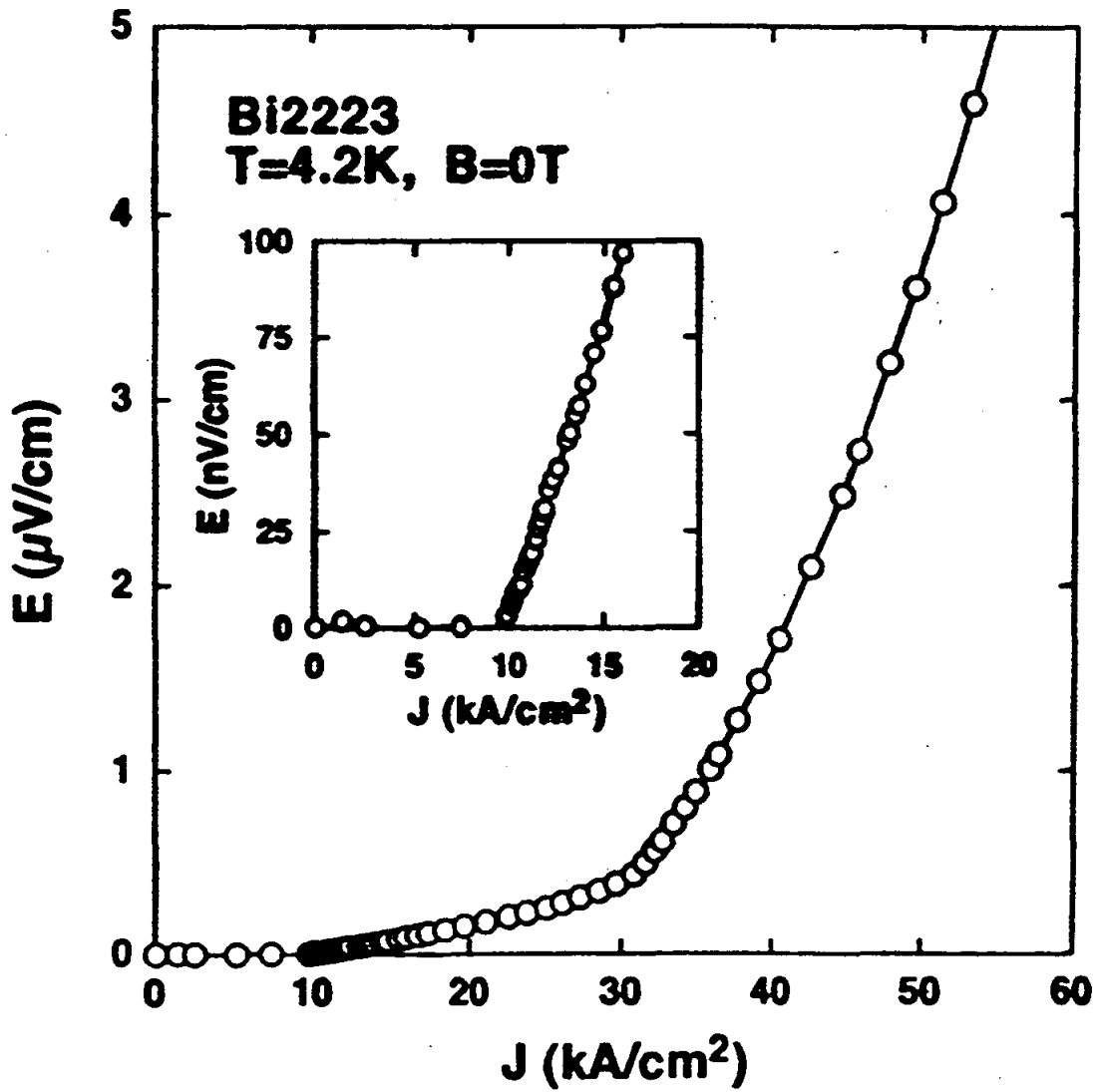


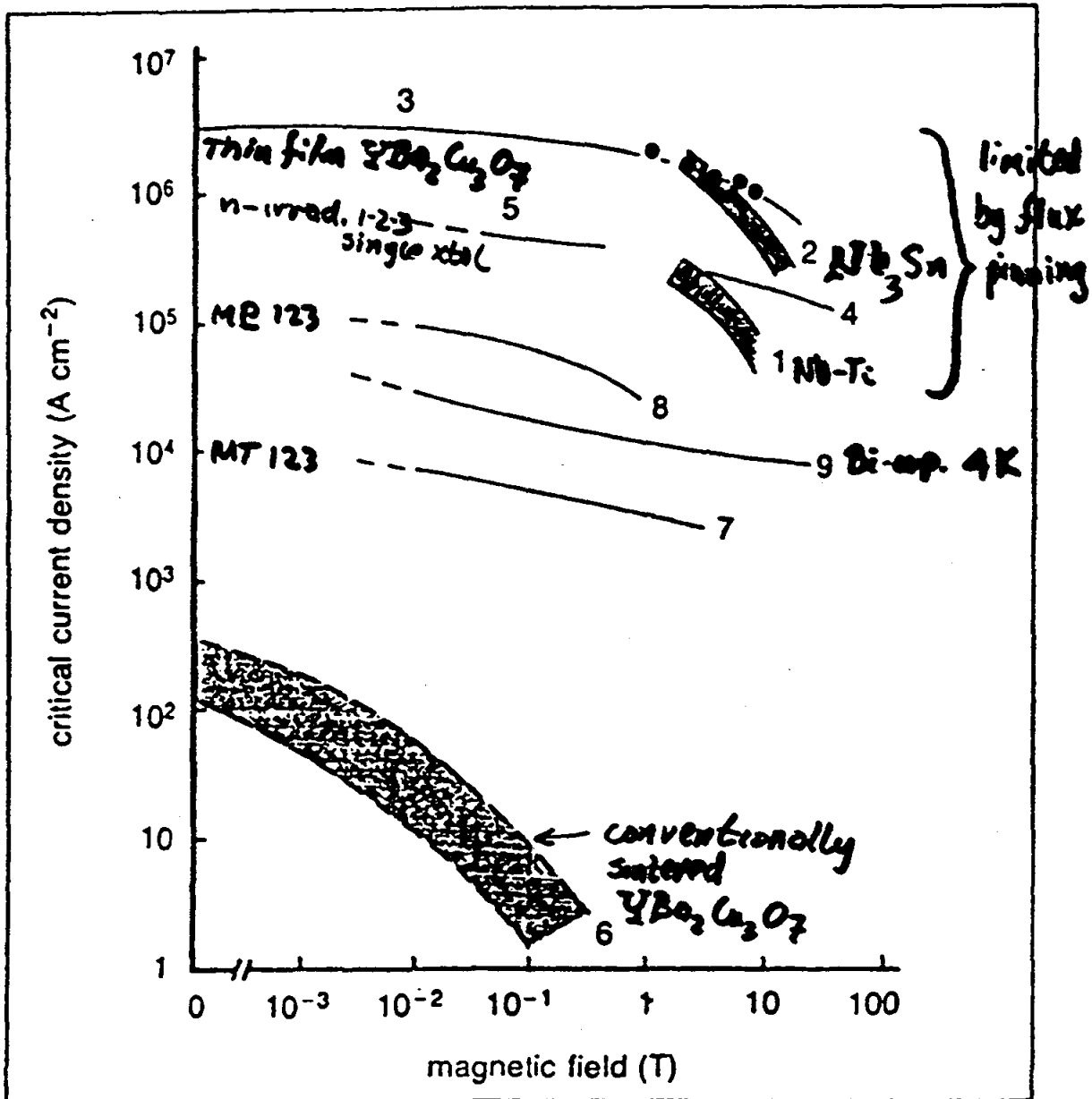


**The Era of “High-Temperature”
Superconductivity was ushered in by
J.G. Bednorz and K.A. Muller.
Z. Phys. B, October 1986 issue.**



OPERATIONAL DEFINITION OF CRITICAL CURRENT DENSITY

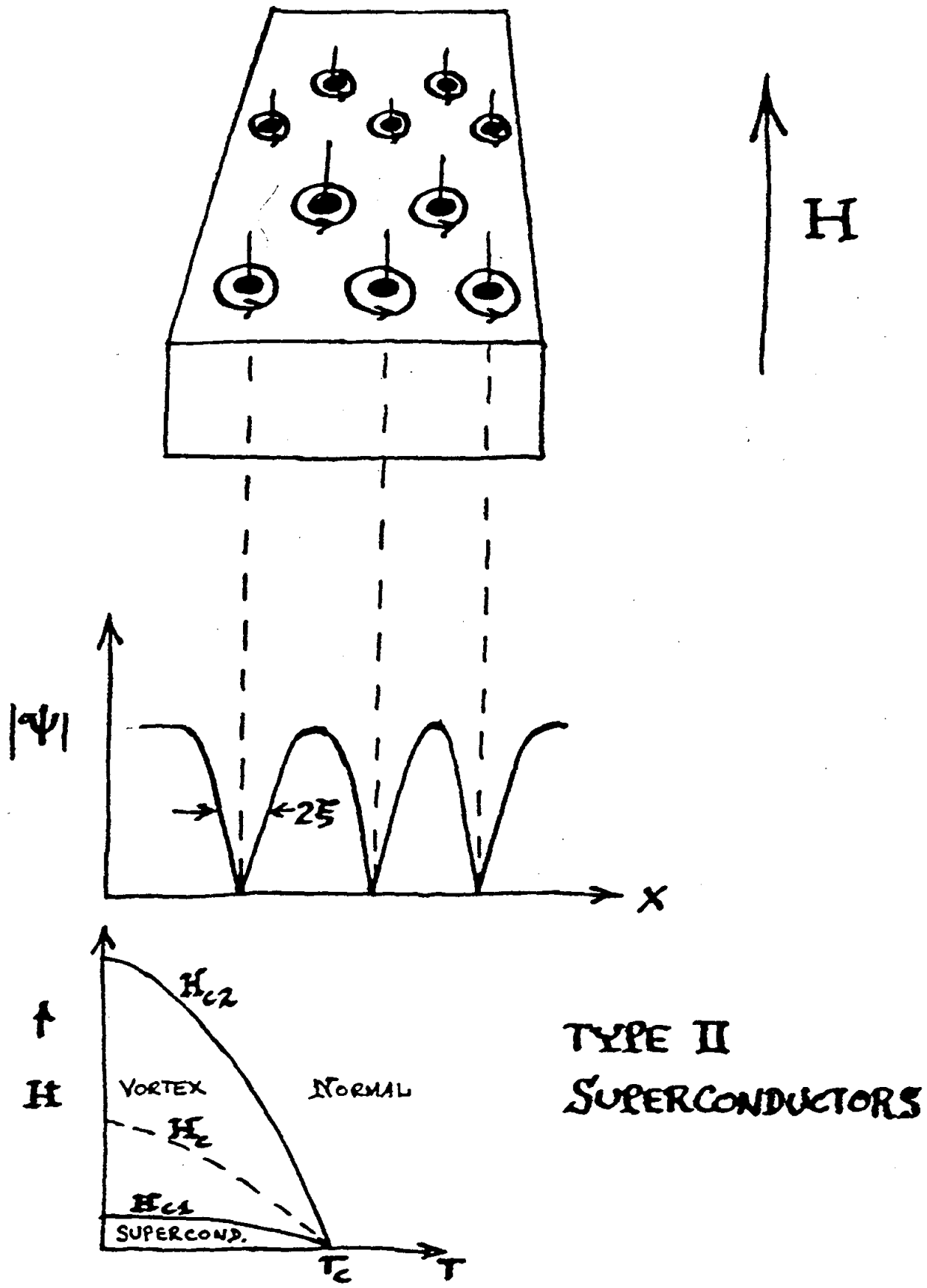




The variation of critical current density with magnetic field for different materials: 1 NbTi at 4 K; 2 Nb₃Sn at 4 K; 3 Y₁Ba₂Cu₃O₇, sputtered thin film at 77 K (Sumitomo); 4 Y₁Ba₂Cu₃O₇, MOCVD thin film at 77 K (Tohoku University); 5 Y₁Ba₂Cu₃O₇, neutron irradiated single crystal, critical current deduced from magnetisation at 77 K (AT&T Bell); 6 Typical values at 77 K for non-aligned polycrystalline Y₁Ba₂Cu₃O₇, bulk samples; 7 Y₁Ba₂Cu₃O₇, melt-textured wire at 77 K (AT&T Bell); 8 Y₁Ba₂Cu₃O₇, QMG processed sample at 77 K (Nippon Steel); 9 Bi₂Sr₂Ca₁Cu₂O_{8+x} wire at 4 K (Vacuumschmelze)

There are Two Major Issues in the Problem of the Critical Current Density in Superconductors:

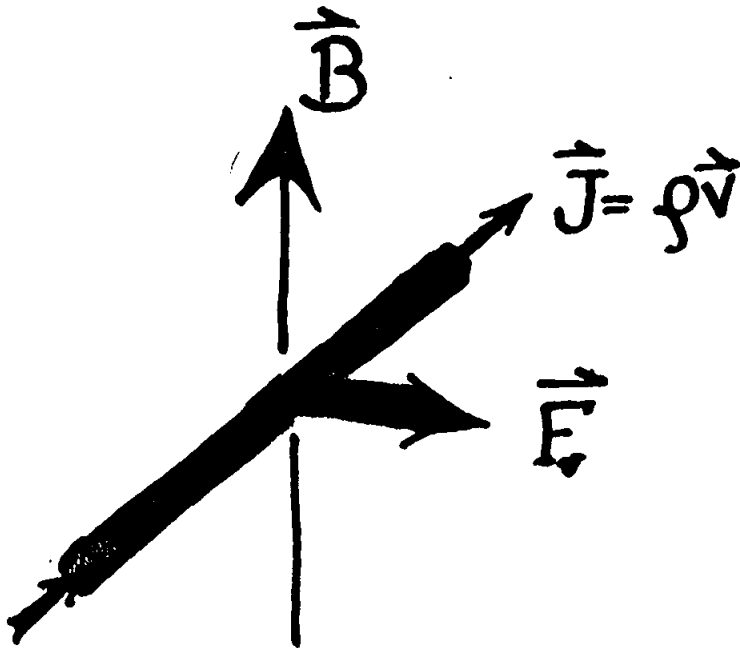
- **The Pinning of Magnetic Flux**
- **The Transmission of Supercurrent
Through the Grain Boundaries of
Polycrystalline Superconductors**



Also essential for consideration of charged particle motion is the Lorentz force equation,

$$\mathbf{F} = q\left(\mathbf{E} + \frac{\mathbf{v}}{c} \times \mathbf{B}\right) \quad (1.3)$$

that gives the force acting on a point charge q in the presence of electromagnetic fields.



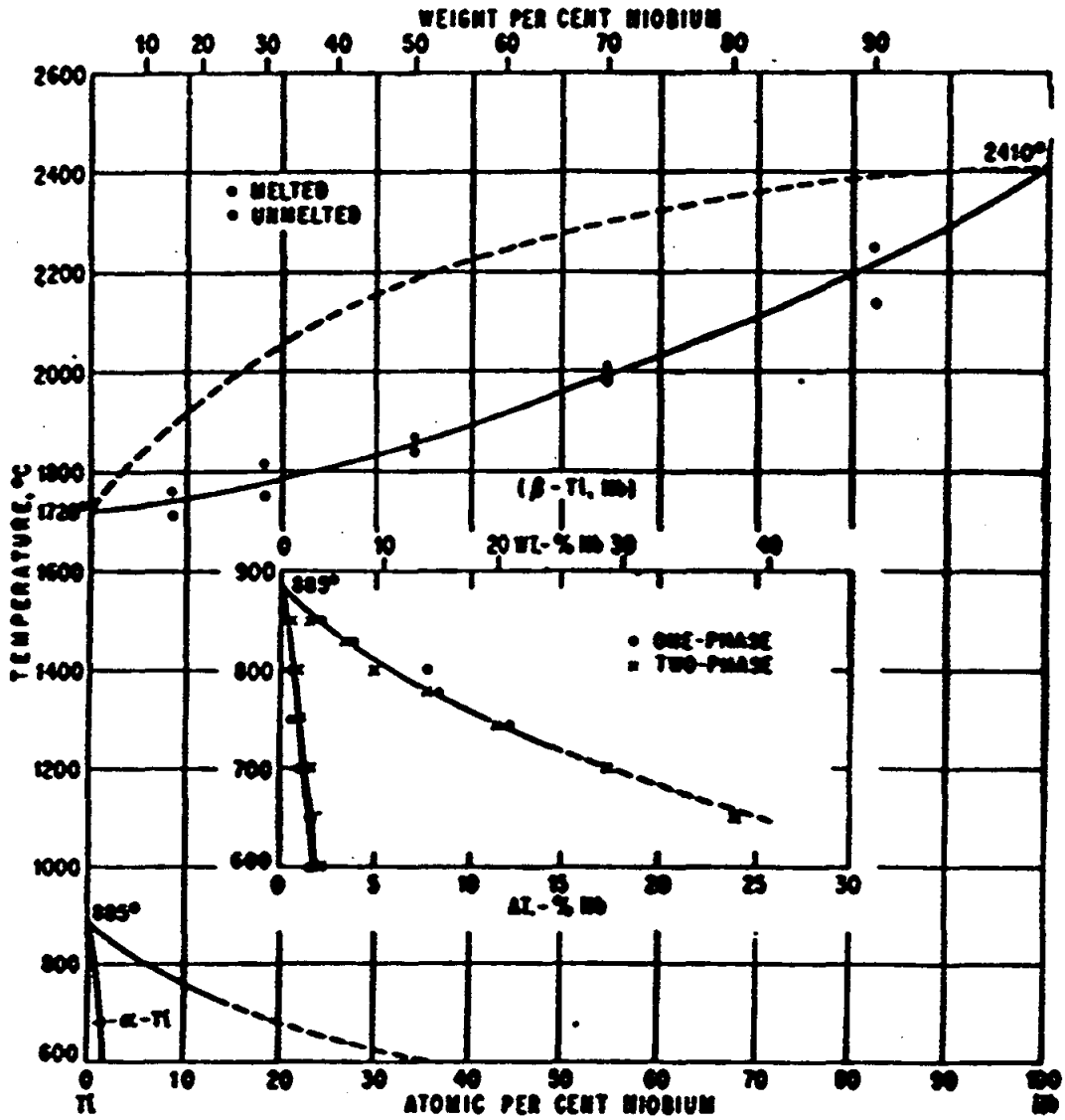
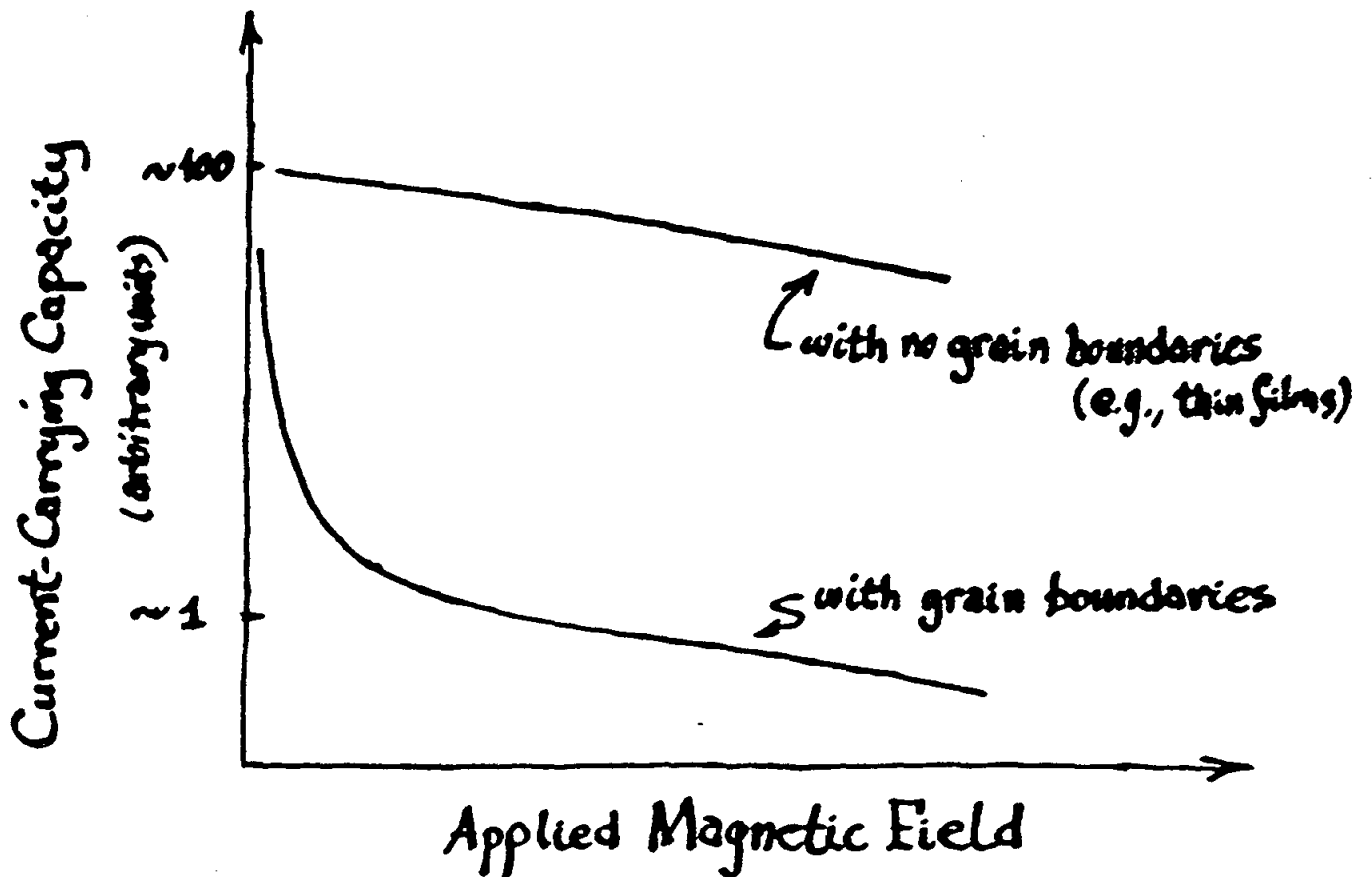


Fig. 560. Nb-Ti

Practical Bulk Superconductor



grain boundary
small crystallite, i.e. "grain"



WHY ??

Why Did It Take So Long For "Elephants" to Appear?

Because Materials Science and Engineering can take a very long time!

What Happened?

"The early workers in superconductivity soon discovered that there is an upper limit to the amount of current that can be passed along a piece of superconductor if it is to remain resistanceless. We call this the critical current of that particular piece. If the current exceeds this critical value, resistance appears."

(A.C. Rose-Innes and E. H. Rhoderick, Introduction to Superconductivity)

Why Aren't The RHIC Magnets Made of "High-Temperature" Superconductors?

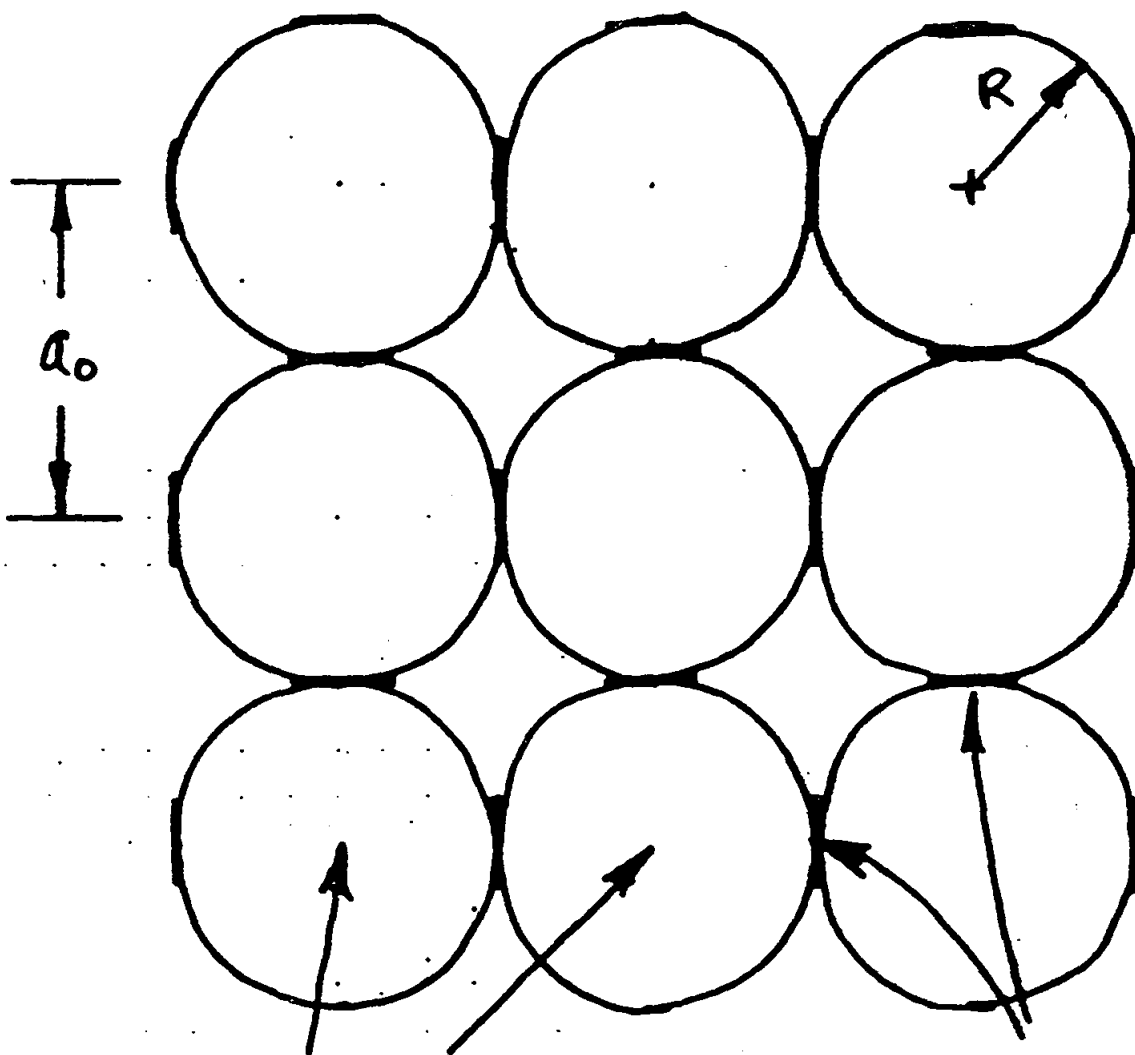
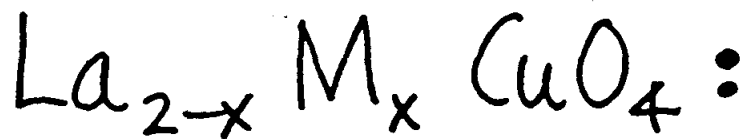
Because the critical current densities are too low without very sophisticated processing and because Materials Science and Engineering can take frustratingly long times!

Researchers at several of the DOE National Laboratories (e.g., Ames, Argonne, Brookhaven, Los Alamos, Oak Ridge, et al.), as well as DOE-funded researchers at several universities (e.g., Wisconsin, Houston, et al.) are making vital contributions to understanding and alleviating the problems of the critical current density of superconductors, both “high-temperature” and conventional.

The following are some examples of such research at Brookhaven (Qiang Li, Yimei Zhu, et al.) and Argonne (Ken Gray, Dean Miller, et al.) National Laboratories.

IDEALIZED THEORIST'S

PICTURE OF

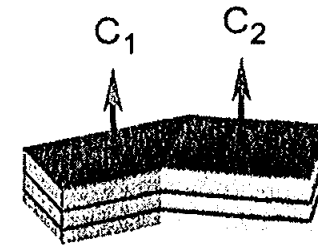
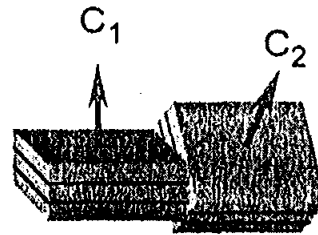
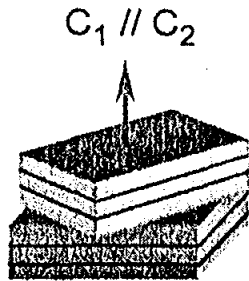


SUPERCONDUCTING
GRAINS

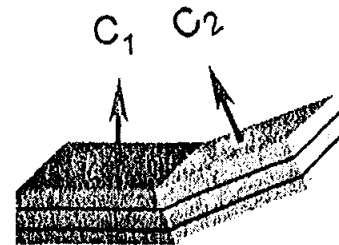
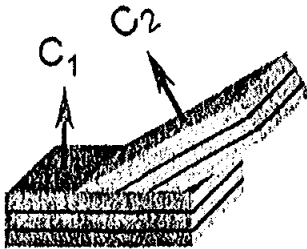
TUNNEL JUNCTIONS
BETWEEN GRAINS

Five basic types of grain-boundaries in Bi-2212:

- 1) basal-plane [001] twist 2) non-basal-plane twist 3) in-plane [001] tilt



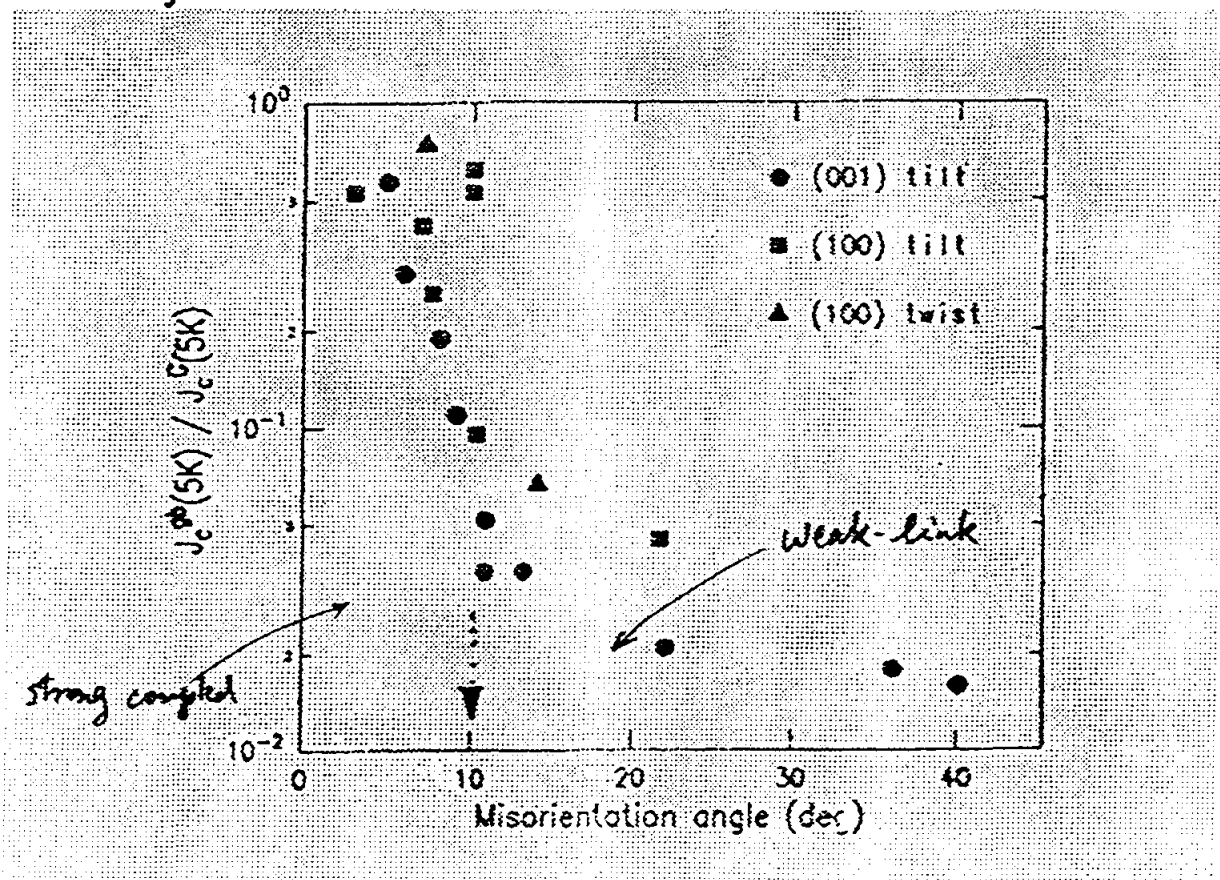
- 4) out-plane-tilt and basal-plane-faced 5) out-plane-tilt and non-basal-plane-faced



The two most important HTS:

- 1) $\text{YBa}_2\text{Cu}_3\text{O}_7$ (YBCO, 123)
- 2) $\text{Bi}_2\text{Sr}_2\text{CaCu}_2\text{O}_8$ and $\text{Bi}_2\text{Sr}_2\text{Ca}_2\text{Cu}_3\text{O}_{10}$ (Bi-based)

The previous studies of grain-boundary in HTS were primarily on YBCO

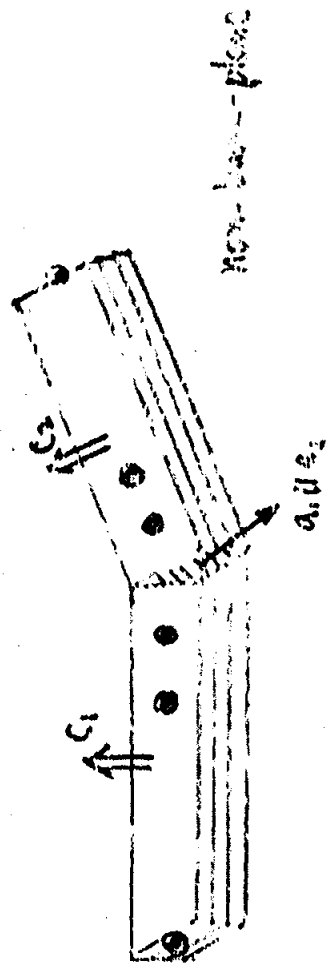
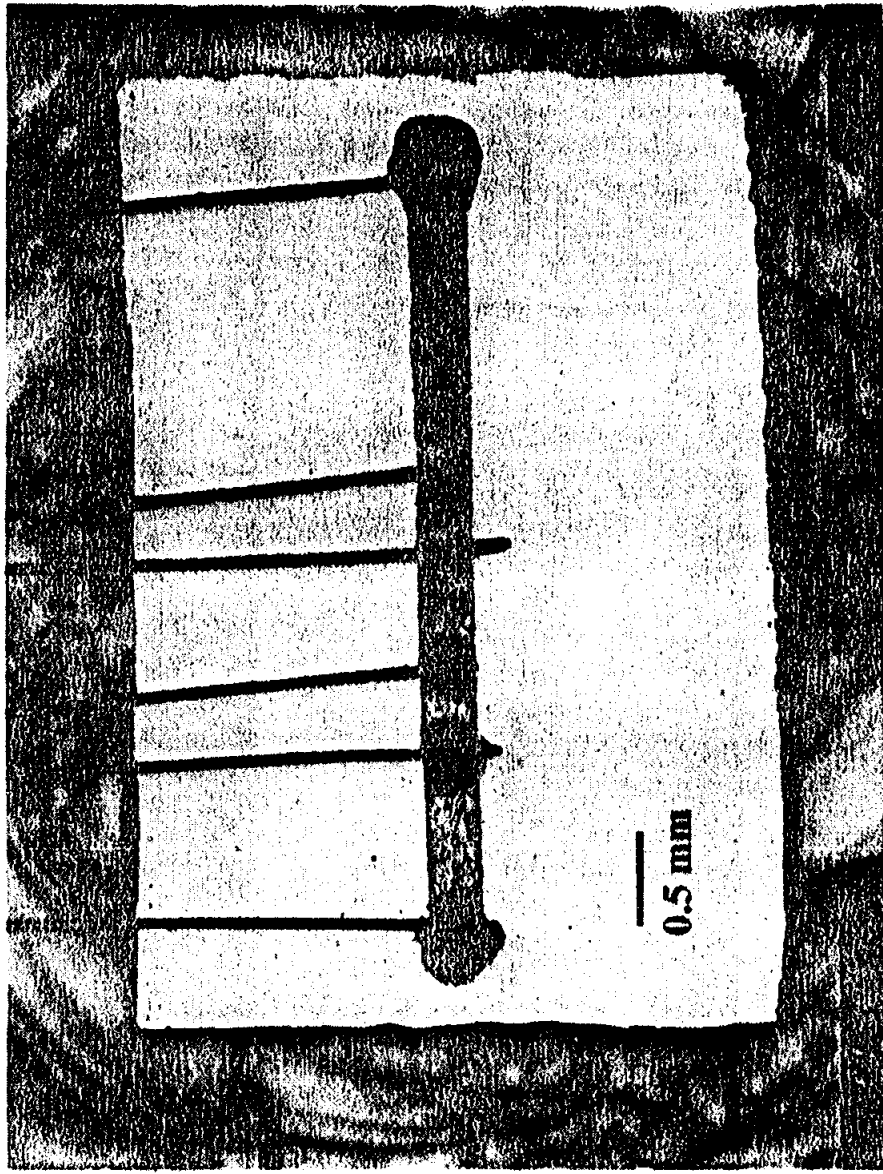


A Precipitous reduction of the transport critical current (J_c) in bicrystal thin film with high-angle ($\geq 10^\circ$) grain boundaries

"Magic angle"

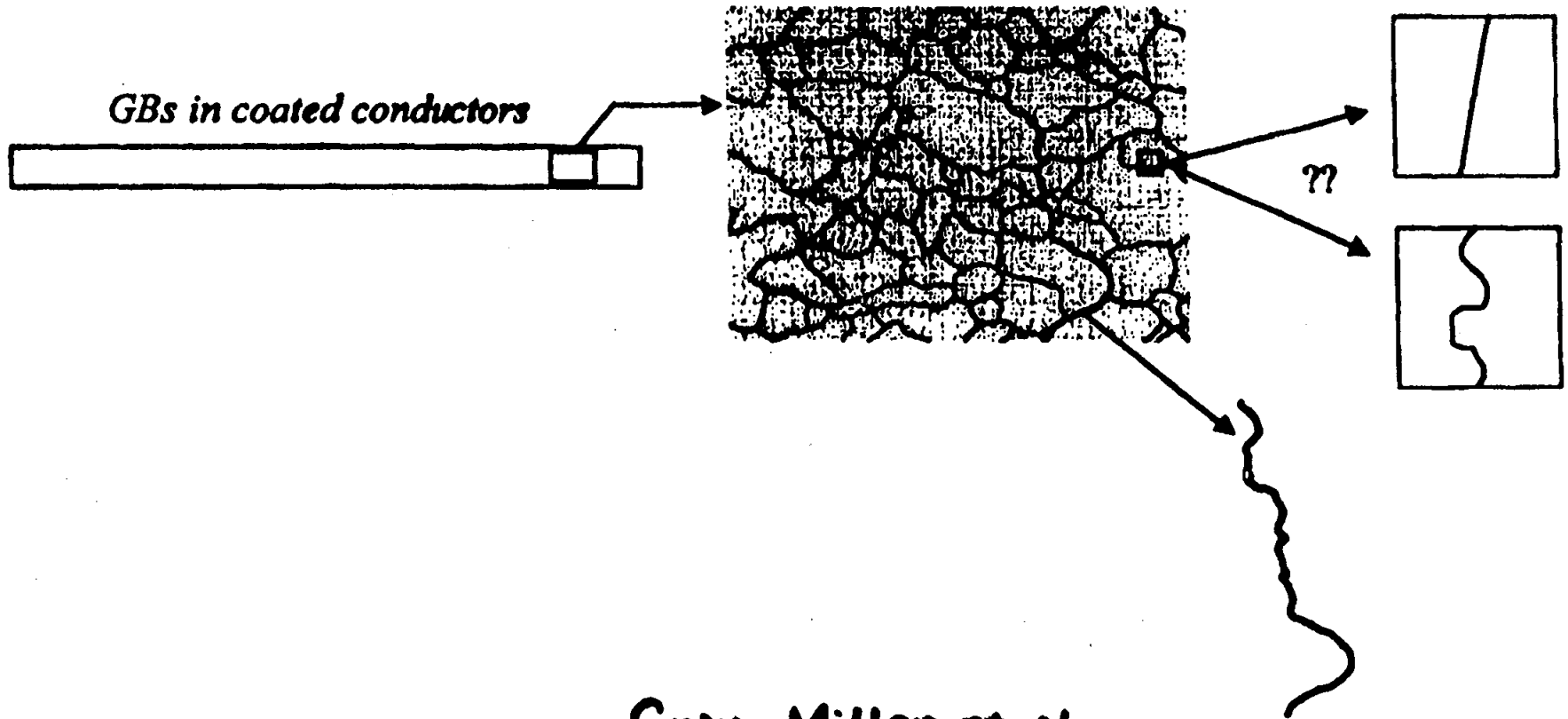
Out-plane-tilt, non-basal-plane-faceted.

7° [100] tilt



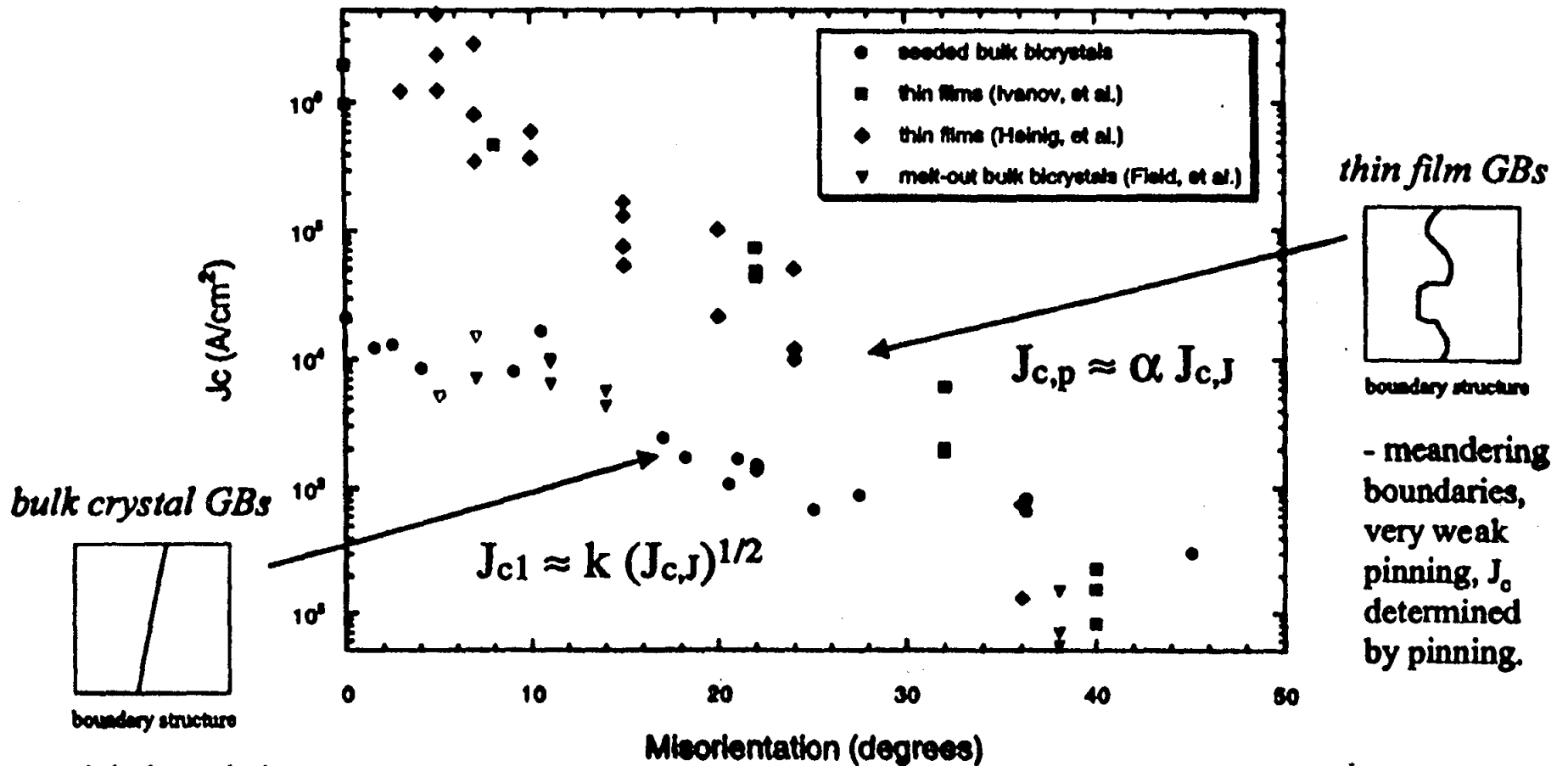
Measurements and modeling of transport across bicrystal boundaries suggests that pinning of both Abrikosov *and* Josephson vortices is important for optimum transport behavior in conductors:

133



Gray, Miller et al.

A model that considers pinning of Josephson vortices along a grain boundary can explain the significant differences in transport data across single grain boundaries in thin film and bulk bicrystal samples.



bulk crystal GBs

boundary structure

- straight boundaries, very weak pinning, J_c determined by flux penetration

thin film GBs

boundary structure

- meandering boundaries, very weak pinning, J_c determined by pinning.

Gray, Miller et al. (ANL)

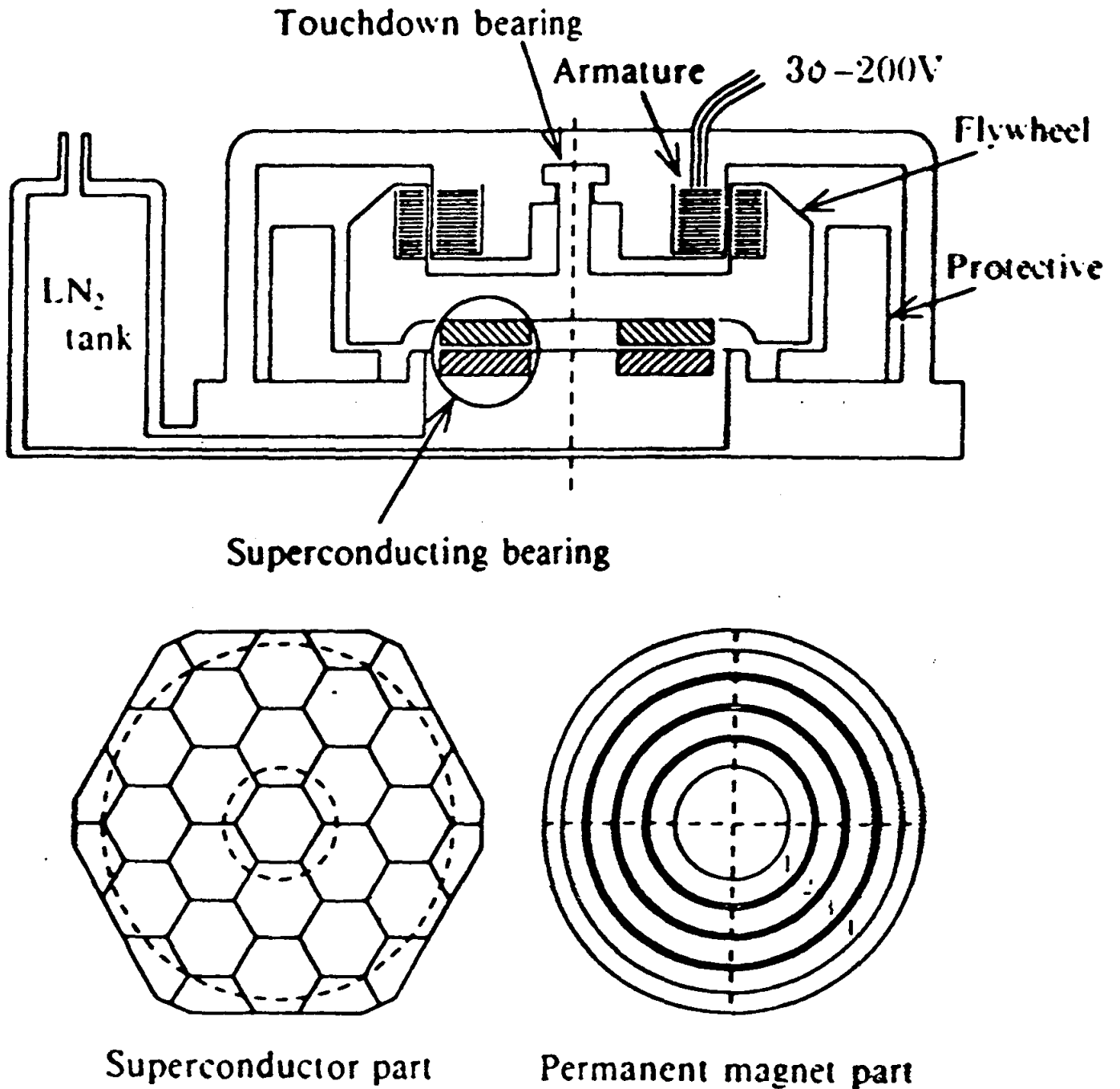


Fig. 1. Principle drawing.

CONCLUSIONS:

The large-scale applications of superconductivity, including superconducting magnets, will make important contributions to our society in the fields of electric power systems, transportation, medical imaging, scientific research, etc.

The role of Materials Science and Engineering in bringing the potential of “high-temperature” superconductivity to fruition is both vital and challenging!

THE COLORFUL CHARACTER OF MATERIALS

Edward L. Widener

School of Technology
Mechanical Engineering Technology
Purdue University
1417 Knoy Hall, Room 145
West Lafayette, Indiana 47907-1417

Telephone: 765-494-7521
e-mail elwidener@tech.purdue.edu



Edward L. Widener

THE COLORFUL CHARACTER OF MATERIALS

NEW:Update 98

Edward L. Widener – Purdue University

KEY WORDS: Brightness, Chroma, Coating, Colorant, Colorimetry, Illumination, Intensity, Tarnish

PRE-KNOWLEDGE: Primary & secondary hues. Metals-ceramics-polymers. Electro-chemical oxidation. Patina & tarnish. Painting & plating.

OBJECTIVES: To associate whiteness & purity. To appreciate the major influence of minor impurities. To understand the 3-dimensions of color. To describe colors accurately. To facilitate color-matching .

EQUIPMENT: 1. Small samples of commercial metals and alloys (steel, stainless steel, cast iron, aluminum, magnesium, titanium, copper, brass, bronze, tin, lead, pewter, solder, galvanized or chromed sheeting).

2. Small samples of plastics foams, films, and sheets (polyethene milk bottle, polyester pop bottle, polystyrene cup or packing, polypropene yogurt-cup or bottle-cap).
3. Small samples of ceramics (chalk, porcelain, drinking glass).
4. Magnifier, 5x – 10x.

BACKGROUND:

Everyone appreciates colorful scenes, jewels, textiles, photographs, movies, television - even comic strips. But a world of “pure materials” is essentially colorless. Do our Materials Labs reflect this cloudy-grey image of our pet topic? Are you neglecting the basics of Colorizing and Colorimetry by electing to focus on routine Structures and Properties?

The 3-dimensions of Color are: Chroma (hue), Intensity (strength), and Radiance (brightness). You can model these as a cylindrical tower, with circular floor-plans. Each floor is a level of Brightness, ranging from dark-basement to bright-penthouse. The Chroma-vector, like a horizontal compass-needle, points toward primary and secondary hues. Strength of hue is the vector’s radius.

Visible light is radiant energy, reflected from a material and seen by an eye. Combined wave-lengths make white-light; but crayons act like filters which absorb all but your desired color. Thus, mixing all crayons will make black. Abnormal eyes may see shades of grey, rather than spectral-colors. Closed eyes or shutoff lights make black.

Why are pure materials typically grey, white, cloudy, or clear (in various shades) except the gold, copper, and sulfur elements? What metals change color when heated? What colors persist, after cooldown? How do “rainbows” form on oil-slicks or soap bubbles? When do cold metals tarnish and turn into variegated hues?

Colorizing involves surface coating, painting, or plating; but liquid dyes and solid pigments may wholly permeate a product. Colorimetry depends on illumination, viewing angle, surface roughness, and color-fast standard samples. For side-by-side matching, the human eye is an excellent Color Comparator.

BLACK & WHITE:

Metals are usually dull-grey if rough, or bright-grey if polished. They reflect like silvered mirrors, being dense & opaque. Try looking through lightweight aluminum foil, when covering a lamp or flashlight. Most metals oxidize at room temperature and have a thin ceramic coating. Look for subtle oxide-tints, then clean each sample and judge each shade of grey. Steel oxides will range from pale yellow to light blue, if heated from 220 C – 340 C (say 430 – 640 F). Of course, “black-iron” or “hot-worked steel” was oxidized to Fe_3O_4 (red-hot at 900 C). And “damp-rust” is blood-red Fe_2O_3 . Thus we see iron-ores ranging from black (magnetite, loadstone) to red (hematite, taconite).

Non-metals (ceramics and polymers) are typically less dense than metals. They tend to be translucent (white, milky, cloudy) or even transparent (clear). Diamond is a cubic-crystal of pure carbon, and quartzite is a hexagonal-crystal of SiO_2 (silica); but the amorphous quartz-glass, known as “fine crystalware” is no crystal at all; so why isn’t it “cloudy”?

Plastics film also may be cloudy (polyethene milk-jug) or clear (polyester pop-bottle, polystyrene drinking-glass); foams and blocks are white, with polyethene duller than polyester. Several plastics have natural color, e.g. polyurethane (light orange), Nomex* Polyaramid (tan), and Kapton* Polyimide (deep

amber). Cellulosics (newsprint) will turn yellow in direct sunshine, being "tanned" by ultra-violet rays. And sulfate pulp (kraft) is found in semi-bleached (tan) or unbleached (brown) papers.

COLOR MODELING:

The scientific "tri-stimulus" model in 3-dimensions is a strange blob, bounded by the varying sensitivity of a normal human eye to visible light. However, a simplistic "Color Tower" may illustrate the 3-D aspects of color characterization. Start with a cylindrical mailing-tube, a paper-core, or a foot of plastic pipe; white vinyl-chloride or clear plexiglas-acrylic is good. When upright, the top of the tower is a bright-penthouse; whose center is white. the tower base is the dark cellar, whose center is black. In-between floors are shades of grey.

Each circular floor-plan is an horizontal compass, with N the Red-direction, ESE the Yellow, and WSW the Blue hue. Such Chroma are "primary colors", forming an equi-lateral triangle. Secondary colors make a smaller inscribed-triangle, with S the Green-direction, ENE the Orange, and WNW the Violet hue. Mixing two primary dyes (or pigments) gives a duller secondary color, as if moving to a lower floor. If blended dyes are 180-degrees apart, the result is much duller, even grey or black.

Thus, dull orange is called "brown". Weak solutions are called "pastel-hues"; so intensity (strength) is related to radial distance from the center of a room. A true dye, having innate secondary hue (orange, green, violet) may be brighter than a blend of primary dyes. A true black is "glossier" than a mixed-blend of opposing hues. Technically then, "platinum-blonde, gold, silver, copper, maize, and midnight" are misnomers to a colorist.

Amazingly, the blend of dots in a comic-strip or newspaper ads produces many hues, viewed by naked eye. However, when magnified 5-10 times, only the primary colors are usually seen. The dot-density corresponds to color intensity. Evidently, the brain integrates discrete dots to perceive another hue.

RAINBOWS:

Iridescent "spectra" are seen in oily-films (floating on water); on soap-bubbles (in sunshine); on walls (from glass-prisms); on CD-ROMs (from grooves); in color-photos of steel (pearlite lamina); in mother-of-pearl (abalone shells); in tarnished silver (spoons, coins); and in welded steel (hot oxides). When metals corrode, the ceramic coating will vary in thickness, depending on conditions. The hotter the steel, the thicker the translucent oxide, and the greater the diffraction of light. Thus different colors reach your eye, as with an oil-slick..

Similarly, as silver is exposed to sulfite (or sulfate) paper, the oxide-coating may vary in thickness and make a color-spectrum, at room temperature. Compare a plain-steel weld with a stainless-steel bead; see the narrow-rainbow in less-conductive stainless-steel. To exceed the "light-blue" temperature (about 340 F) is to produce rainbows of the second-order (or third); so, the oxide-color is related to temperature in only the "out-board" rainbow (farthest from the heat-source).

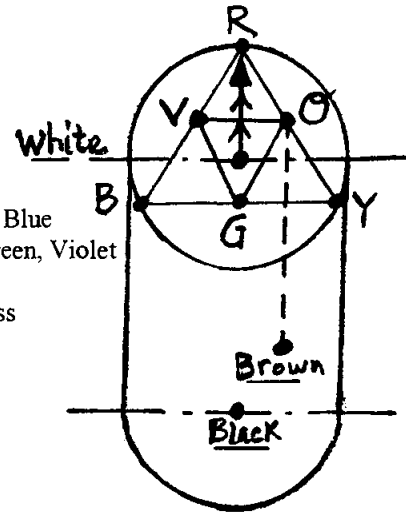
Observations of color have practical applications. We see a machine-tool with oxide-color, we suspect thermal over-heating, excessive grinder-pressure, or lack of coolant. The blacksmith "draws" a cold-chisel, by quenching and tempering to a light-blue oxide. Of course, contaminates may produce ugly corrosion, instead of "pretty toning"; then foreign materials or health hazards shall be explored.

REFERENCES:

1. Widener, E.L., "NEWmismatic Metallurgy", NEW:Update97 Proceedings, Seattle, WA (Coin Colors).
2. Bullens, D.K., "Steel & Its Heat Treatment - Vol.I", John Wiley, NY, 1948 (p.38, Drawing).
3. Parker, S.P., "McGraw-Hill Dictionary of Scientific & Technical Terms - 5th ed.", NY, 1994.

SKETCH:

THE COLOR TOWER - - - - Primary Hues = Red, Yellow, Blue
Secondary Hues = Orange, Green, Violet
Radius of Vector = Intensity
Elevation of Floor = Brightness



BIOGRAPHY:

E.L. Widener has taught mechanical technology (MET) at Purdue University (since 1978), concentrating on statics, hydraulics, materials labs, ecology, & technical writing. Member of ASME, ASEE, ASM, ISA, TAPPI. Registered P.E. in New York & Indiana. ABET visitor in from 1983 – 1990. BSME from Purdue U. & MSEM from U. Kansas. Taught evenings at IUPU-Indianapolis & Danville IL.

Development Engineer for Coria-collagen casings, with Teepak Div. of Continental Group in Danville (1976-78). Process Leader for Baker-McHenry-Welch in Indianapolis (1974-76). Project Leader for Creped-wadding & Secondary-fibers with Kimberly-Clark Co. in Memphis TN (1968-74). Process Engineer for Nomex-nylon with E.I.duPont Co. in Richmond VA (1963-68). Associate Engineer for Electro-furnace alloys with Union Carbide Co. in Niagara Falls NY (1952-60). Fuel Engineer with U.S.Steel in Gary IN (1951-52).

Ed was in Malaysia, from April 1995 – June 1996, teaching Metals Lab to future technology teachers.

LABORATORY MEASUREMENT OF J-INTEGRAL

Yulian Kin

Harvey Abramowitz

Toma Hentea

Jim Higley

and

Jason Richards

Department of Engineering
Purdue University Calumet
2200 169th Street
Hammond, Indiana 46323-2094

Telephone 219-989-2684
e-mail kin@nwi.calumet.purdue.edu



Yulian Kin

LABORATORY MEASUREMENT OF J-INTEGRAL

Yulian Kin
Harvey Abramowitz
Toma Hentea
Jim Higley
Jason Richards
Purdue University Calumet

Key Words: Fatigue, crack propagation, crack growth rate, stress intensity factor, and J-integral.

Prerequisite Knowledge: Knowledge of basic fracture mechanics concepts is helpful.

Objective: Observe crack propagation. Measure crack length and angular rotation of a cracked plate. Develop the following plots: moment versus angular displacement, energy versus crack length, J-integral versus crack extension. Determine critical J-integral value.

Equipment:

1. Fatigue machine with a control unit (MTS, for example).
2. Fixture system to provide loading of the specimen (flexure system in this experiment).
3. Specimens (0.5-inch polycarbonate).
4. Video camera.
5. Light sources.
6. Computer with a frame grabber.
7. Monitor, printer.
8. Software to observe crack image measurements ("Inspector" by Matrox in this experiment).
9. Video recorder.
10. 0.75-inch scotch tape for the specimen.

Introduction:

This experiment focused on the polycarbonate which is used as a structural component in the F-16 aircraft canopy. The canopy is often manufactured from a laminated composite material. Components of the composite are acrylic plies, a polycarbonate ply, interlayers and coatings. Design of the canopy allows unloading of the acrylic ply which is why the structural polycarbonate ply of the composite was the primary concern during fatigue investigation. One of the failures encountered frequently in the field is polycarbonate fracture. The nature of failures is not quite clear, but some evidence implies that transparency life is limited by fatigue of the polycarbonate ply [1]. Therefore, development of an inspection procedure which permits measurement of crack length and prediction of the part failure life is an important task.

At the 12th Annual National Educators' Workshop, the authors presented a paper [2] which was related to experimental determination of stress intensity factors and constant parameters in the Paris formulation. That experiment has been implemented in Machine Design and Material Science courses at Purdue University Calumet. This paper describes an additional fracture mechanics experiment for the course: Measurement of the J-integral. The experiment was conducted on the same MTS machine and on specimens of the same material.

Specimen:

The testing coupons were cut from 0.5-inch thick polycarbonate sheets. The sheets had been extruded, pressed and polished in accordance with the military specifications. The specimen configuration is shown in Figure 1.

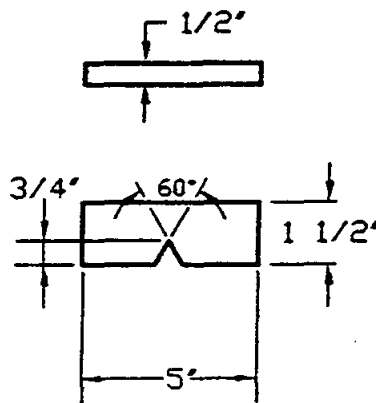


Figure 1: Specimen configuration.

Experimental Set-up:

Flexure tests were conducted on an MTS machine using a four-point loading technique to provide pure bending. The experimental set-up is shown in Figure 2.

The crack images were caught by an image grabber linked to the digital computer and video. An independent duplicate monitor connected to the video permitted constant observation of the crack development during command and calibration operations.

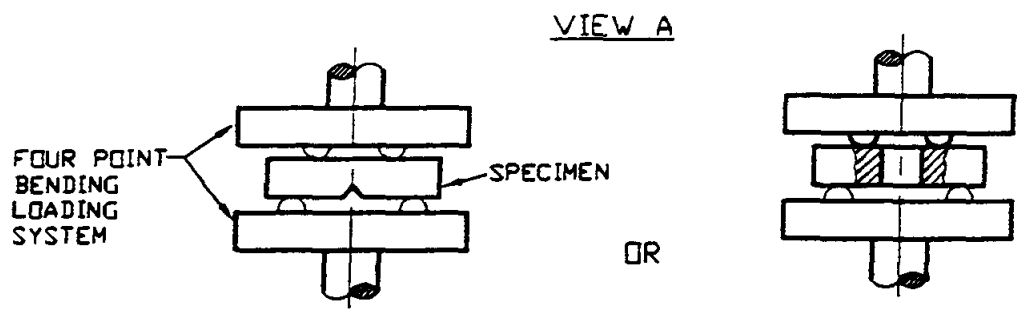
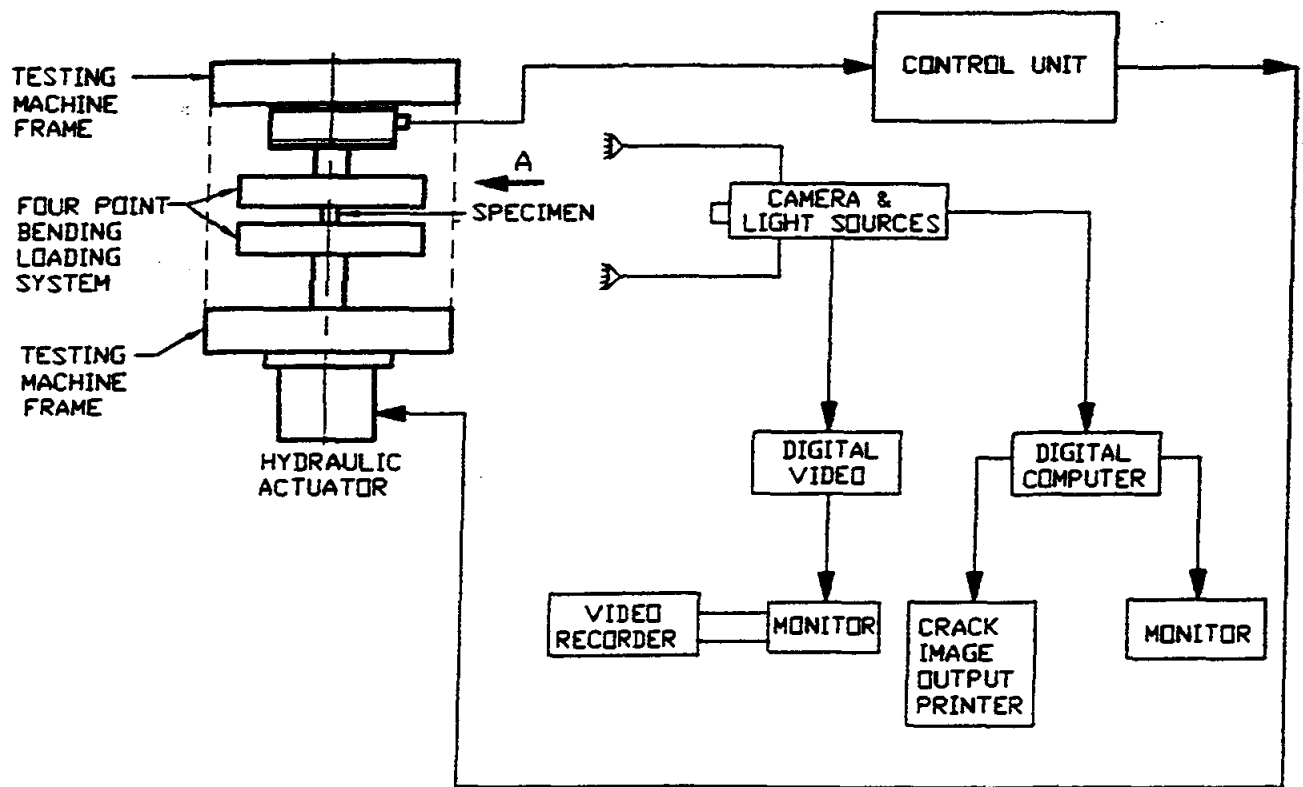


Figure 2: Experimental Set-Up

Observations:

Crack initiation and growth of the loaded PC specimen were constantly observed on the monitor screen. To verify that crack initiation had occurred, the camera periodically zoomed in on the specimen. During crack growth, the crack images were captured and stored by an image grabber after each 200-lb. force increment. During zooming and calibration, crack propagation was observed on the duplicate monitor.

Results:

Data is given in Table 1 and Table 2.

Table 1: Applied Load and Measured Deflection Data.

<u>Load P, N</u>	<u>Average Angular Deflection, Radians</u>	<u>Bending Moment M, N-mm</u>
890	0.006886	7242
1335	0.011097	10864
1779	0.012919	14477
2224	0.014113	18098
2669	0.016808	21719
3114	0.018267	25340
3559	0.020936	28961
4003	0.023151	32574
4448	0.025756	36197

From beam theory, the bending moment for the given geometry was calculated:

$$M = (P/2) * (1/2) * (94.46 - 61.91) \text{ N-mm} = (8.1375 * P) \text{ N-mm.}$$

The loading diagram is given in Appendix A. Angular deflection was determined from the displacement, which was measured from the image grabbed during the crack growth (see Appendix B).

Table 2: J-integral values calculated from the experimental data.

<u>Bending Moment M,</u> <u>N-mm</u>	<u>Area under Moment-</u> <u>Displacement Curve</u> <u>N-mm</u>	<u>Uncracked Ligament b,</u> <u>mm</u>	<u>J Value,</u> <u>J/mm²</u>	<u>Crack Length a, mm</u>
7242	18.5	19.05	0.306	.000
10864	64.8	19.024	1.072	.026
14477	93.2	18.996	1.546	.054
18098	114.4	18.982	1.898	.068
21719	170.3	18.997	2.824	.053
25340	205.1	19.000	3.400	.050
28961	277.1	18.984	4.600	.066
32574	344.9	18.943	5.734	.107
36197	434.1	18.907	7.232	.143

Values for the J-integral was calculated from the following equation:

$$J = 2 (h*U) / (B * b) \text{ mJ/mm}^2$$

where:

$h = 2$ for bending [3].

U - area under moment - angular displacement curve, N-mm

B - specimen thickness, mm

b - uncracked ligament, mm

The area under bending moment versus angular displacement curve was determined from:

$$U = \int (1,502,145 D - 2491) dD$$

The plots generated from the experimental data received are given in Figures 3, 4, and 5.

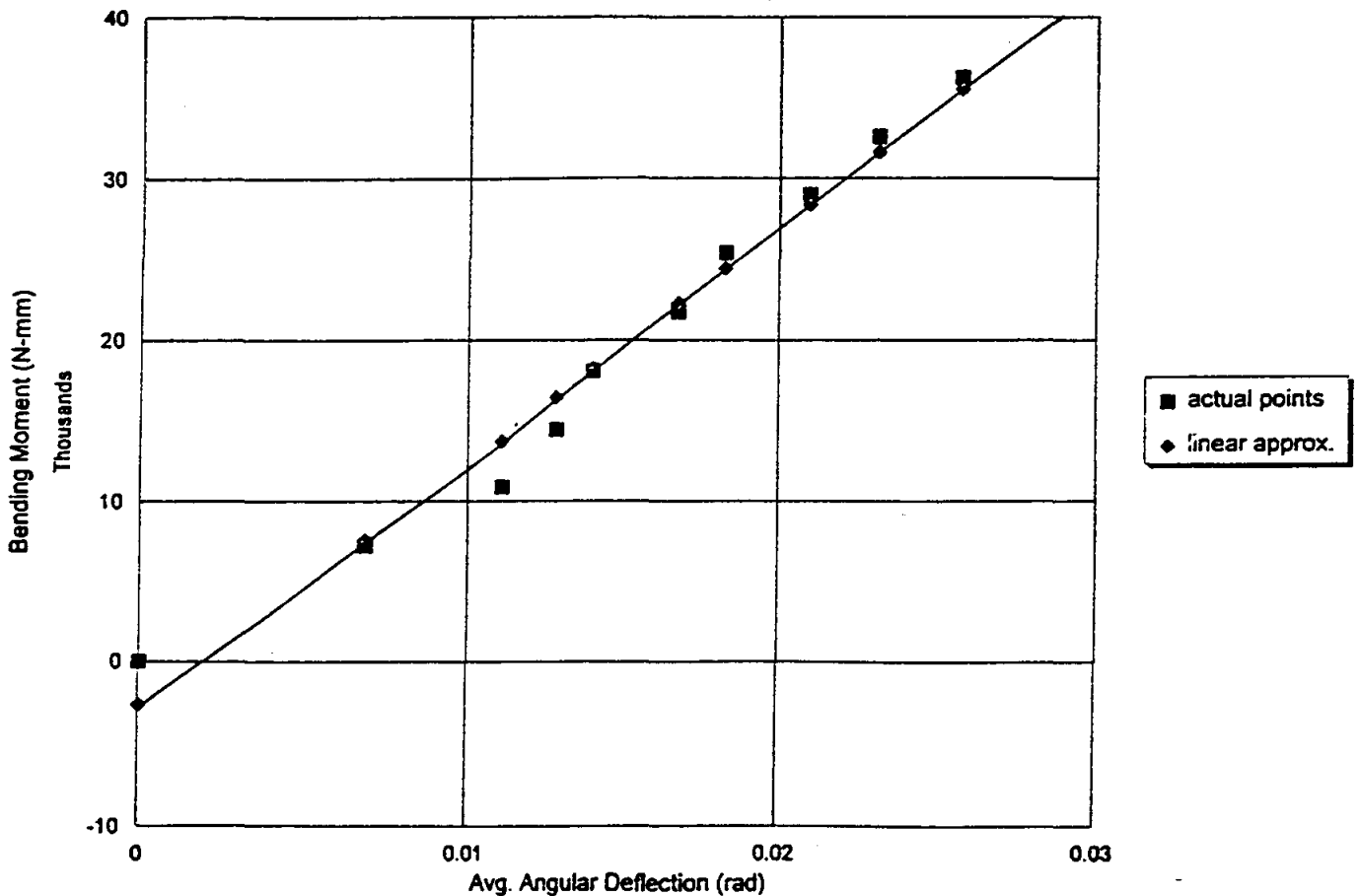


Figure 3: Moment Versus Angular Displacement.

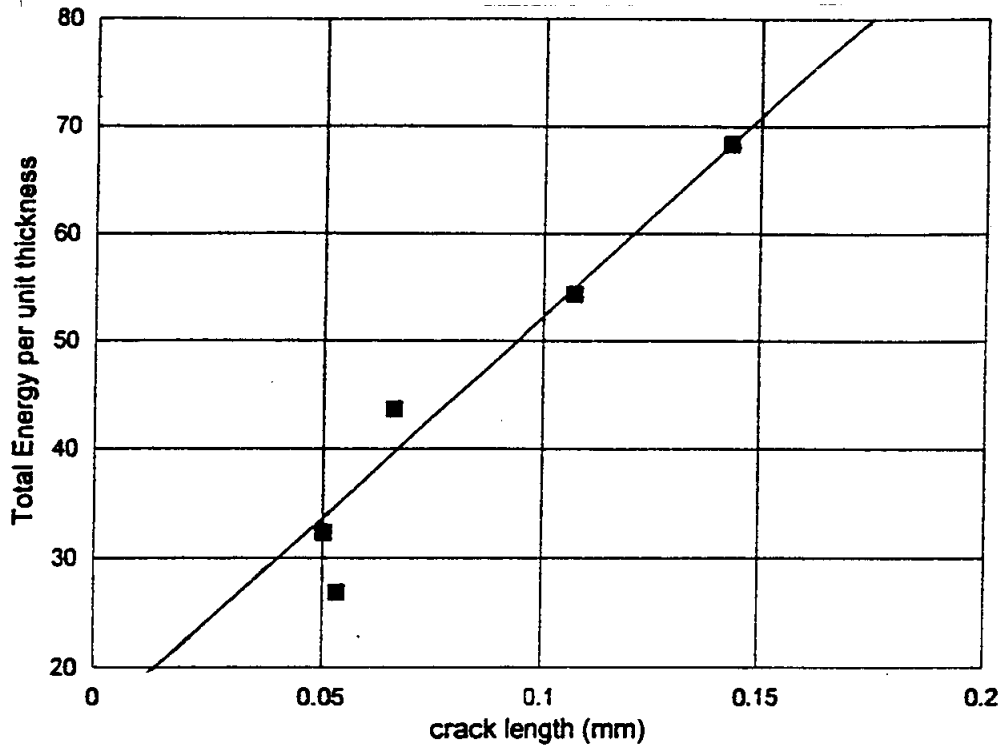


Figure 4: Total Energy per Unit Thickness Versus Crack Length.

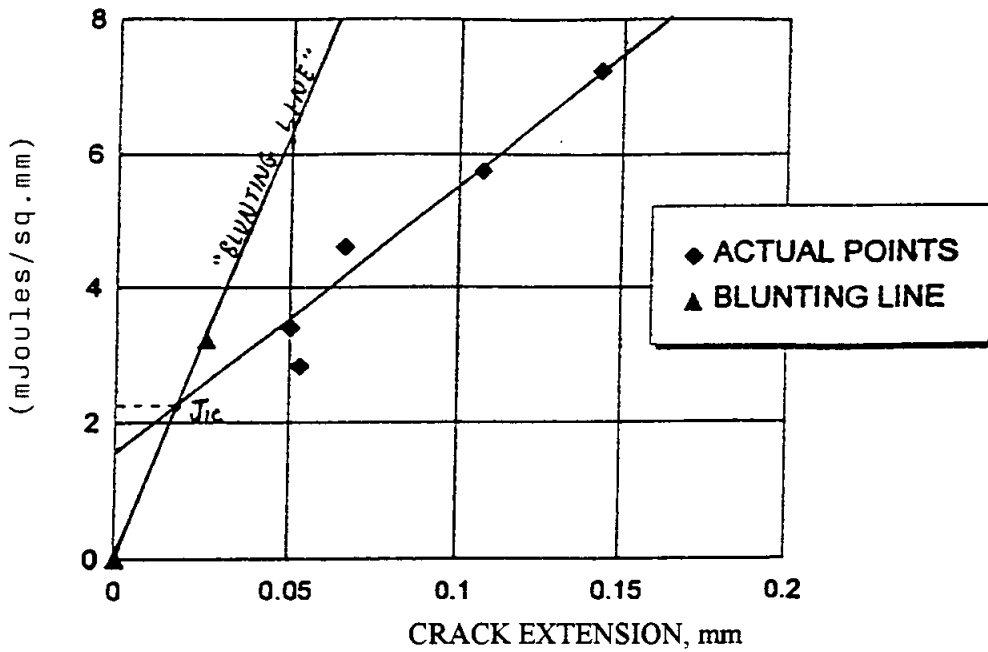


Figure 5: J-Integral Versus Crack Extension.

Note that the first four measurements (see Tables 1 and 2) were not included in plots Figures 4 and 5, because these measurements were made during crack initiation and considered suspicious.

Applications of J-integral for fracture control:

Application of J-integral intends to control elastic-plastic fracture [3]. Therefore, the critical J-integral value, J_c , for thick material permits one to determine the critical stress intensity factor, K_c , taking into account elastic-plastic behavior of the material around the notch:

$$K_c^2 = (J_c * E) / (1 - \nu^2),$$

where:

K_c = critical stress intensity factor for the mode I failure.

J_c = critical J-integral value for the mode I failure.

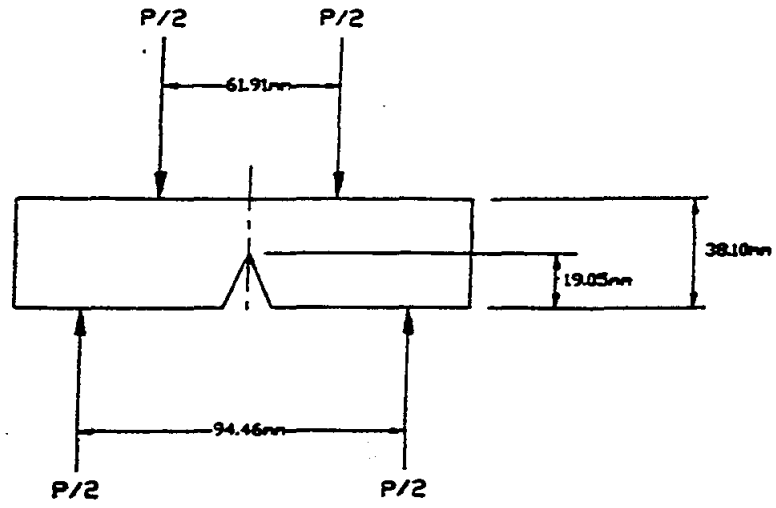
E = modulus of elasticity.

ν = Poisson's ratio.

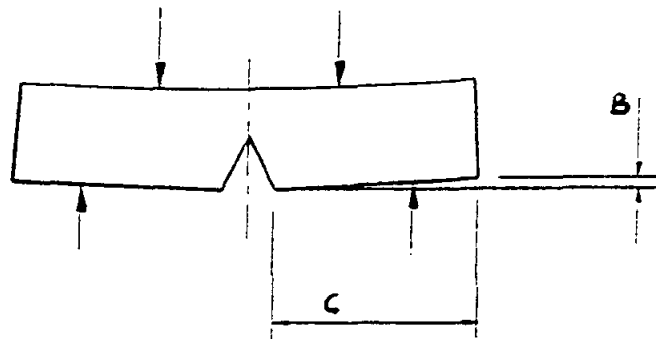
Now, using linear elastic calculations, we can determine the actual stress intensity factor, K, at certain stages of crack propagation and compare K and K_c determined earlier. For security purposes, it is also practical to calculate J at certain time intervals or after certain degrees of crack extension. Comparing J and J_c we can make a prognosis about the remaining resource of the part.

References:

1. H. Abramowitz, T. Hentea, Y. Kin, Y. Xu, "Fatigue Investigation of Polycarbonate Used for Aircraft Canopies", *Aging of Materials and Methods for the Assessment of Lifetimes of Engineering Plant - Proceedings of the 4th International Colloquium*, Cape Town, South Africa, April 21-25, 1997, Penny (ed.), Balkema, Rotterdam, Netherlands, ISBN 9054108746, 1997, pp. 309-317
2. Y. Kin, H. Abramowitz, T. Hentea, Y. Xu, "Life Estimate Based on Fatigue Crack Propagation", *12th Annual National Educators' Workshop Proceedings*, Boeing, Seattle, WA, 1997.
3. John M. Barsom, Stanley T. Roefe, *Fracture and Fatigue Control in Structures*. Prentice Hall, Englewood Cliffs, New Jersey, 1987.



Appendix A: Loading Diagram



Appendix B: Angular Displacement Calculation
 Angular Displacement = $\arctan (B/C)$

USE OF A FOUR-POINT BEND APPARATUS TO DETERMINE THE MODULUS OF ELASTICITY

Richard B. Griffin

L. Roy Cornwell

Carlos Yapura

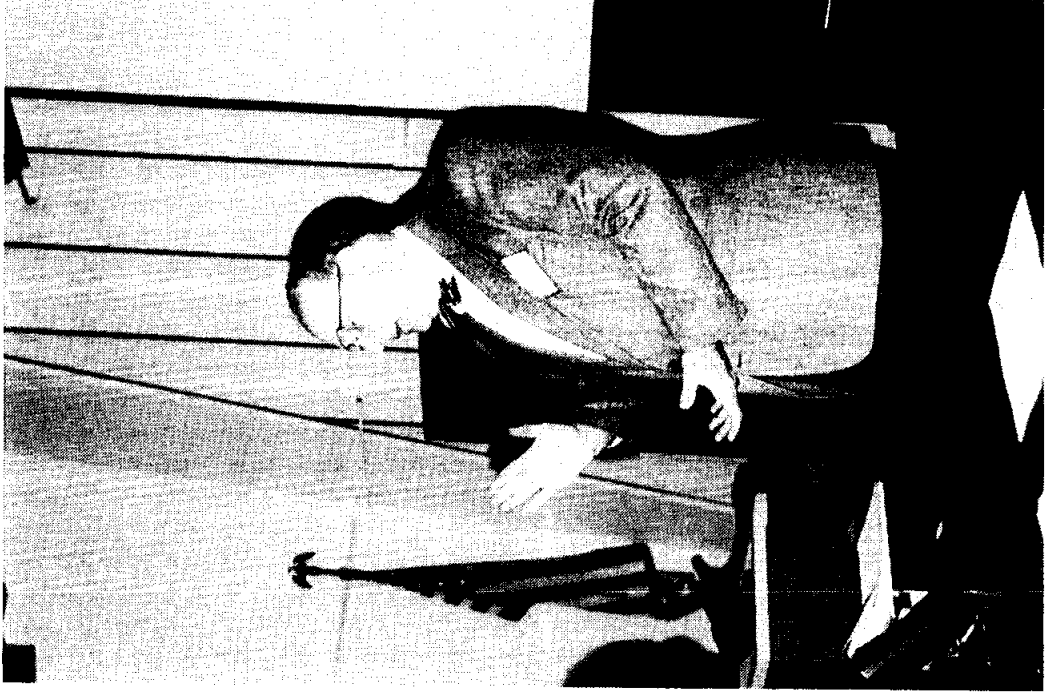
Sivasubramaniam Krishnan

and

John Hallford

Department of Mechanical Engineering
Texas A&M
College Station, Texas 77843-3123

Telephone: 409-845-9779
e-mail rgriffin@mengr.tamu.edu



Richard B. Griffin

Use of a Four-Point Bend Apparatus to Determine the Modulus of Elasticity

Richard B. Griffin*, L. Roy Cornwell*, Carlos Yapura⁺, Sivasubramaniam Krishnan⁺⁺, and John Hallford**

*Faculty, Mechanical Engineering, Texas A&M University

⁺Postdoctoral student, Aerospace Engineering, Texas A&M University

⁺⁺Graduate student in Mechanical Engineering, Texas A&M University

**Staff, Mechanical Engineering, Texas A&M University

ABSTRACT:

A four-point bend test has been developed for use in the classroom. The test is used to integrate fundamental knowledge in three courses: materials science, continuum mechanics, and electrical engineering. The students are given beams of approximately 1mm in thickness by 25mm wide by 150mm in length. The deflection is measured by placing masses on top of the beam. A dial indicator, supported on the underside of the beam, is used to measure the deflections. Since the dial indicator provides an upward force from the underside of the beam, the experiment provides an opportunity for the students' to apply the principle of superposition. The analysis for the deflection is not as simple as for the three-point bend test; however, using the four-point bend test eliminates concerns about bending moments. The coupling with electrical engineering results from the installation of strain gauges on the beams. The students' can see how strain gauges work and actually calibrate the gauges. The students may select from mild steel, 304 stainless steel, cartridge brass, and unidirectional graphite/epoxy beam materials. The results for determining the modulus of elasticity using a least squares approach are within 3% of tabulated values.

KEYWORDS: Bending, Modulus of Elasticity, Material Science, Four-point Bending, Continuum Mechanics, Laboratory Activity, Classroom Demonstration

PREREQUISTE KNOWLEDGE: Calculus, Mechanics, and Physics,

OBJECTIVES:

To measure the modulus of elasticity using a 4-point bend experiment.

To give students an opportunity to use equipment.

EQUIPMENT AND MATERIALS:

Table 1 lists the equipment required for the beam experiment and the estimated cost.

Table 1. Equipment needed for the 4-point bend test.

Components	Estimated cost
Bend Fixture, Stainless steel	\$50
Dial indicator, collet, and extension	\$53
Weights	\$25
Beams	Used available materials
Screws, bolts, and nuts	\$5
Vernier caliper	Available in laboratory
	\$133 Estimated cost per setup

SAFETY PRECAUTIONS: Proper laboratory procedures.

INTRODUCTION

Texas A&M University is a member of the Foundation Coalition, a National Science Foundation program for educational reform.¹ For the past five years, Texas A&M has been one of seven schools in the Foundation Coalition. During that time, a five-course sequence was developed for the sophomore year.^{2,3} Table 2 identifies the courses and topical areas, the semester taken, and the course number. The thrusts of the Foundation Coalition are teaming and active learning, integration, application of technology, and development of lifelong learning.⁴ The courses are based on the use of conservation principles in an effort to integrate subject areas.⁵

Table 2. Arrangement of courses.

Semester	Engineering Area	Course Numbers
Fall	Mechanics- Statics and Dynamics	ENGR 211
	Thermodynamics- plus some fluids	ENGR 212
Spring	Materials	ENGR 213
	Continuum Mechanics	ENGR 214
	Electrical Circuits and Electronics	ENGR 215

Currently, the majority of the departments take all of the courses. The courses are taught in lecture sections of about 80 students. The classrooms are equipped with desks where four students sit as a group with laptop computer(s) on the desks. The room is equipped with an instructor's computer, document camera, and VCR, all of which can be shown through the overhead projection system.

While these developments were very helpful, one area the faculty were concerned about was the hands-on aspect of engineering. The current generation of students has limited (in general) experience with building things, repairing equipment, or in performing experiments. In an effort to remedy this situation, faculty in several of the above sophomore courses have been developing activities, which can be performed in the classroom. The particular course the authors are involved with is a property of materials course, ENGR 213. The instructors have developed several in-class experiments; these include a tensile test, bend test, electrical component demonstration, and a thermal conductivity experiment.

Last year, we presented a three-point bend experiment for use in the classroom.⁶ As the results indicated, the experiment worked well and has been used. Unfortunately, the setup was not as robust as we had initially anticipated, and by the time 180 students got through with the tests, several items were either broken or not working. Subsequently, in an effort to upgrade the experiment, we decided to develop a four-point bend test experiment. The objective of this paper is to describe the development and implementation of the 4-point bend test.

The redesigned experimental setup is shown Figure 1. The drawings for the bend test apparatus are included in the appendix.



Figure 1. Photograph of the bend apparatus.

PROCEDURE

The students are asked to select two beam materials for testing. During fall 1998, which was the first time the new setup was used, it was requested that one of the beams be graphite epoxy. The other could be of their choice: 1018 steel, 304 stainless steel, or cartridge brass. The students measure the specimen's dimensions, and the distances on the bend fixture.

The model for the beam with its nomenclature is shown in Figure 2. The forces on the beam and the reactions are shown in Figure 3.

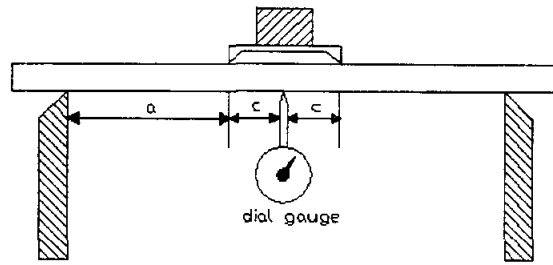


Figure 2. Schematic setup for the 4-point bend experiment.

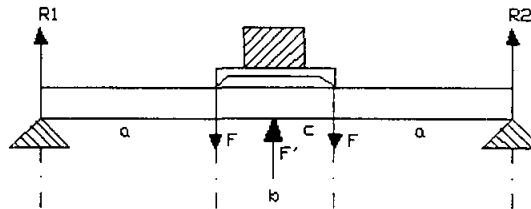


Figure 3. Forces and reactions for the 4-point beam experiment.

There are several methods for analyzing the 4-point bending beam experiment. The method of superposition is one method, and another is the double integration technique. Using the method of superposition, the following expression was derived, and the relationship for the measured deflection, δ , is given by the following expression.

$$\delta\left(\frac{L}{2}\right) = \frac{(3aL^2 - 4a^3)P}{(kL^3 + 48EI)} \quad \text{Equation 1}$$

If we rearrange this equation, we can solve for the modulus of elasticity, and the equation may be written as the following.

$$E = \frac{P(3aL^2 - 4a^3)}{48I\delta} - \frac{kL^3}{48I} \quad \text{Equation 2}$$

Where, P is the force, k is the spring constant (dial indicator), I is the moment of inertia, $L=2a+b$, a and b are defined in Figure 3, I is the moment of inertia.

Using the double integration method, the following expression can be arrived at for determining the modulus of elasticity. This expression explicitly contains the force

$$E = \frac{(F * C_1 + F' * C_2)}{I * \delta}$$

Equation 3

Where, $F = P/2$ (P is the load applied to the beam.)
 F' is force exerted by the dial gauge on the beam
 $C_1 = -a(8a^2 + 12ab + 3b^2)/24$ and $C_2 = (2a + b)^3/48$ are constants and for the geometry used in this setup $C_1 = -0.00007503$, and $C_2 = 0.00004671$
 I -moment of inertia = $wt^3/12$, w- width, t- thickness of the beam
 $I = 4.719 \times 10^{-12} \text{ m}^4$ (Graphite-Epoxy)
 δ - net displacement of the beam

of the spring from the dial gauge. The data obtained using the above expression are shown in Tables 4 and 5. For the beam tested, $a = 0.04004\text{m}$, $b = 0.0508\text{m}$, and $L = 0.1309\text{m}$ were the dimensions used.

Another way to look at this problem is to use the ASTM Standard Test Method, D 790-96a, Flexural Properties of Unreinforced and Reinforced Plastics and Electrical Insulating Materials. Two relationships are included in the standard for a load span of $1/2$ and $1/3$ of the support span. These relationships are:

$$E_b = 0.17L^3 \frac{m}{bd}$$

$$E_b = 0.21L^3 \frac{m}{bd}$$

Equation 4 for $1/2$ the support span.

Equation 5 for $1/3$ the support span.

L is defined earlier, b and d are specimen dimensions, and m is the slope of the load deflection curve.

These two equations do not consider any upward force associated with a dial indicator. The correction is relatively small, less than 5%, and therefore one could choose to ignore the correction. If one does, a question that could be asked of the students is how ignoring the upward force would affect the modulus that was determined. Of course, the measured modulus would appear to be higher or the material would appear to be stiffer when the force associated with the spring is ignored.

Determination of the spring constant

The dial indicator, shown in Figures 1 and 2, places a small upward force on the beam from the underside as shown in Figure 3, labeled F'. In order to measure the spring constant of the dial indicator, the extension on the dial indicator was removed, small masses were placed directly on the shaft, and the corresponding deflection was measured. An example of the determination of the spring constant is shown in Table 3.

Table 3. Determination of the spring constant for dial gauge No.1.

Load applied (N)	Deflection produced (m)	Spring constant (N/m)
0.07*9.81	0.00762	90.118
0.08*9.81	0.00965	81.309
0.09*9.81	0.01151	76.732
0.10*9.81	0.01344	73.090
0.11*9.81	0.01557	69.305
Average value =		78.0947

Determination of the modulus of elasticity

The students set the beam on the support, add masses, and measure the deflections. An example of the data obtained is shown in Tables 4 for cartridge brass, and Table 5 for graphite-epoxy beams.

Table 4. Data obtained for 70/30 or cartridge brass (C26000) beam.

Beam Material	Load (N)	Net Deflection of Beam (m)	Young's Modulus (GPa)
Brass 70/30	0.5 * 9.81	0.002794	104.0071
	0.6 * 9.81	0.0032766	104.1457
	0.7 * 9.81	0.0038273	102.4791
	0.8 * 9.81	0.0042672	103.7359
	0.9 * 9.81	0.0048006	102.8105

Table 5. Data obtained for unidirectional graphite epoxy beam.

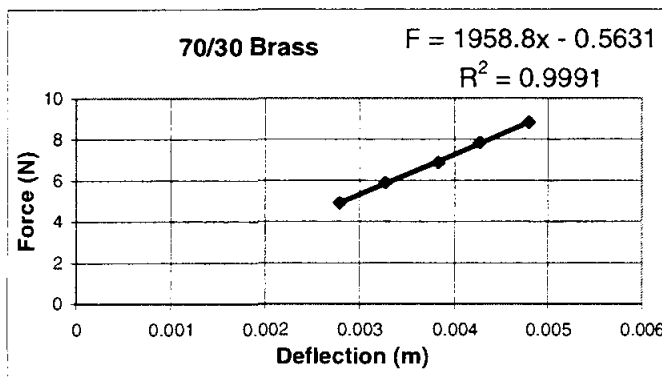
Beam Material	Load (N)	Net Deflection of Beam (m)	Young's Modulus (GPa)
Graphite Epoxy	-	-	-
	1.0 * 9.81	0.0003732	223.504
	1.2 * 9.81	0.0005002	197.9
	1.5 * 9.81	0.0006780	180.46
	1.7 * 9.81	0.00082296	176.905
	2.0 * 9.81	0.0009574	168.45
	2.2 * 9.81	0.001059	166.986

The data are plotted in Figures 3 and 4, and as can be observed they are linear. Certainly for the analysis that was done this is encouraging, and what is expected for an elastic analysis. Using the measured slopes, the modulus of elasticity has been determined. For cartridge brass, the average value was 103GPa which compares with 110GPa listed in the ASM Handbook.⁷ Unfortunately, the measured value for graphite

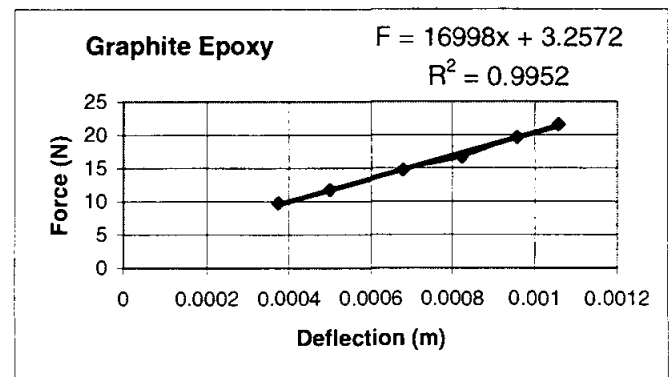
epoxy can not be compared to handbook values because the volume fraction of fibers and the type of graphite fibers in the epoxy are unknown. However, the number determined is reasonable.

CONCLUSION

We have developed 4-point bend test apparatus that can be used in a classroom setting. The test has been performed in a classroom containing more than 60 students. Currently, there are six setups available, and we are planning to increase the number to 20. The experiment couples with a sophomore level continuum mechanics course that the students may be taking concurrently. In the near future, several of the beams will be instrumented with strain gauges. The intent of this is to integrate with the electrical engineering course.



a.



b.

Figure 3a and 3b. Load deflection curves for brass and graphite-epoxy.

ACKNOWLEDGEMENTS

The authors would like to thank the Foundation Coalition and the NSF for their support of this project. A special note of thanks goes to Prof. Norris Stubbs for his help with the mechanics part of the project, and to the students in the classes who performed the tests.⁸

BIOGRAPHICAL INFORMATION

Richard Griffin has been at Texas A&M in Mechanical Engineering since 1977. His research area is aqueous corrosion and he has received a NACE Technical Achievement

Award in 1992. For the past four years, he has been a member of the Sophomore Team in the development of core engineering science courses for the Foundation Coalition.

L. Roy. Cornwell has been at Texas A&M since 1971. He has taught in the area of material science and manufacturing. His research interests are corrosion and deformation.

C. Yapura is a post-doctoral student from Aerospace Engineering. His interests are mechanics.

S. Krishnan is a first semester graduate student who is planning on studying mechanics.

J. Hallford is a technician in the materials area in Mechanical Engineering.

¹ Malave, C., "Teaming in the Integrated Curriculum of the Foundation Coalition at Texas A&M," ASEE National Conference, Washington, D.C., June 1996.

² Griffin, R. B., Everett, L. J., Keating, P., Lagoudas, D., Tebeaux, E., Parker, D., Bassichis, W. and Barrow, D., "Planning the Texas A&M University College of Engineering Sophomore Year Integrated Curriculum," Fourth World Conference on Engineering Education, Oct. 95, St Paul, MN, vol. 1 pp. 228-232.

³ Griffin, R. B., Everett, L., and Lagoudas, D., "Development of a Sophomore Year Engineering Program at Texas A&M University," FIE, Pittsburgh, PA, Nov. 1997.

⁴ Lagoudas, D., Griffin, R.B., Everett, L.J., Keating, P., and Parker, D., "The Implementation of a Sophomore Engineering Integrated Curriculum," ASEE Regional Conference, San Antonio, Texas, March 1996.

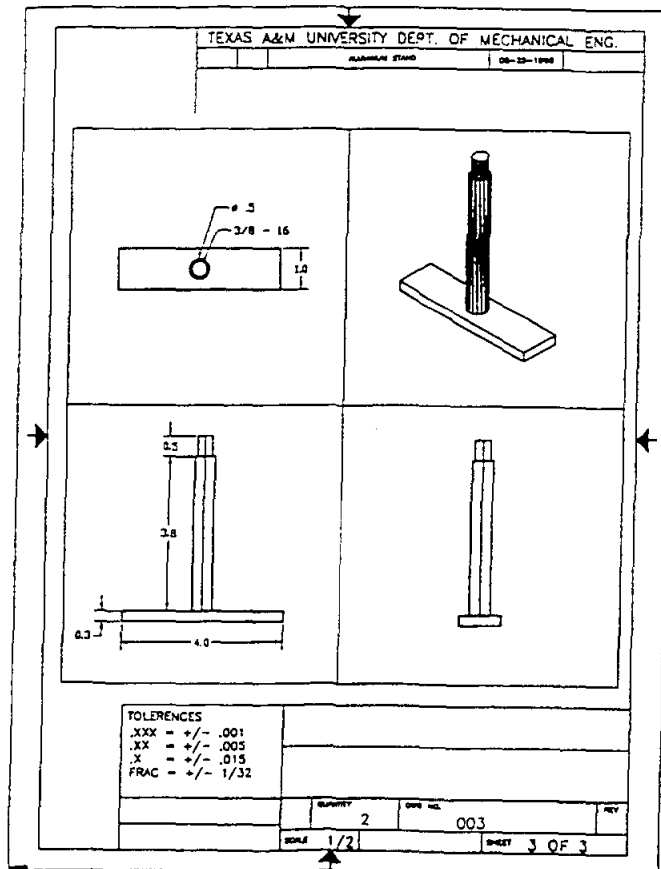
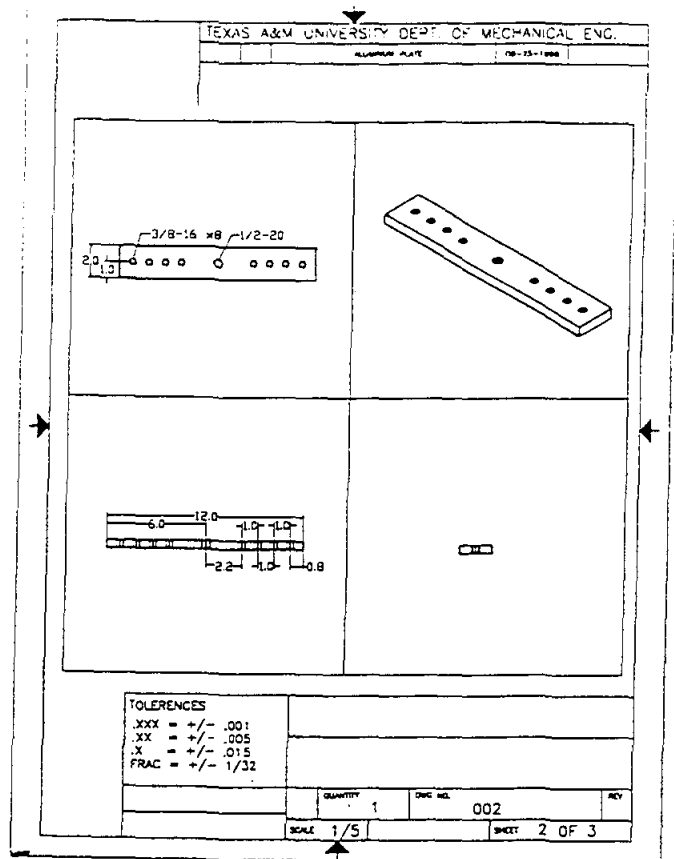
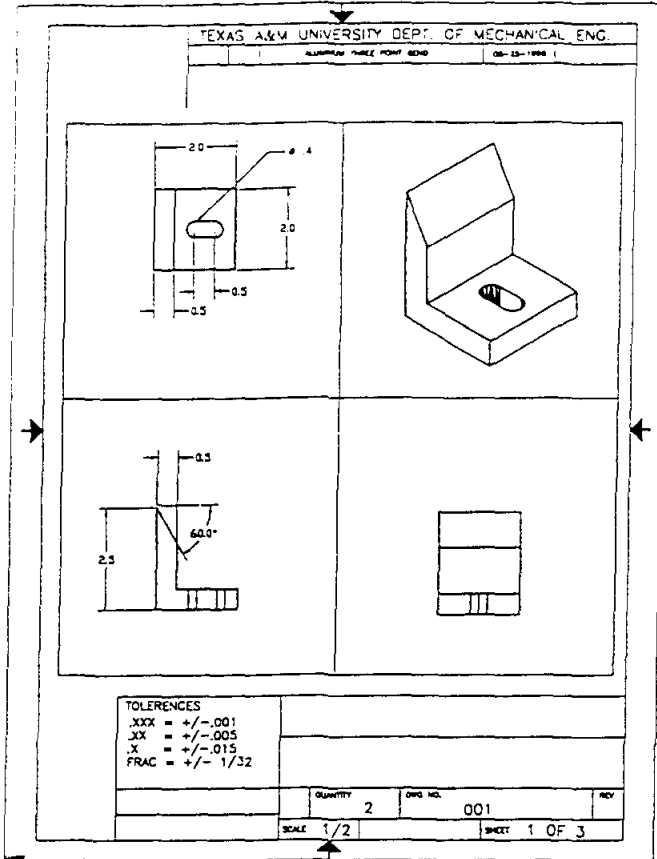
⁵ Glover, C., "Conservation Principles and the Structure of Engineering," McGraw-Hill, New York, NY, 1996.

⁶ R. B. Griffin and L. R. Cornwell, "Measurement Of the Modulus of Elasticity Using a Three-Point Bend Test," Conference, Seattle, WA, Oct. 1997.

⁷ Metals Handbook, vol. 2, Properties and Selection: Nonferrous Alloys and Pure Metals, ASM, Metals Park, OH, 1979.

⁸ College of Engineering Students in ENGR 213, Fall 1998.

Appendix



MICROCHEMISTRY AND THE NEW SCANNING ELECTRON MICROSCOPES

Matthew J. Kasdan

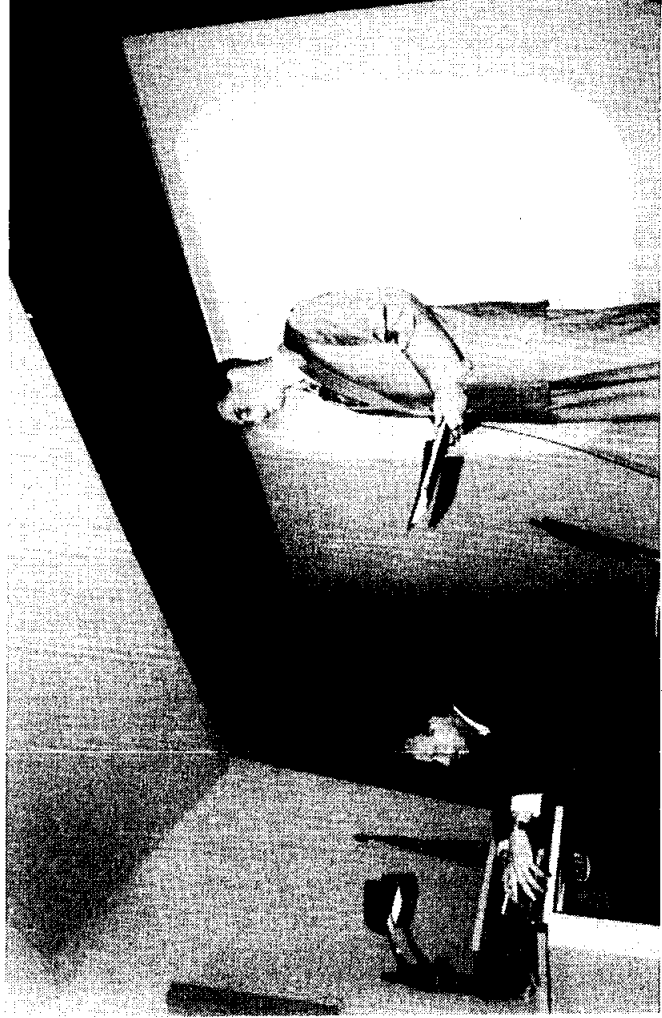
31932 Violeta Lane
Coto de Casa, California 92679

and

Stephen K. Kennedy

RJ Lee Group, Inc.
350 Hochberg Road
Monroeville, Pennsylvania 15146

Telephone: 724-325-1776
e-mail www.rjlg.com



Stephen K. Kennedy

Microchemistry and the New Scanning Electron Microscopes

Matthew J. Kasdan
31932 Violeta Lane
Coto de Casa, CA 92679

and

Stephen K. Kennedy, Ph.D., PG
RJ Lee Group, Inc.
350 Hochberg Road
Monroeville, PA 15146

Introduction:

Images produced by the scanning electron microscope (SEM) are becoming familiar to students of all ages. SEM images are presented in text books, but are also seen in print and TV advertisements for products such as hair treatments, wood finishes and insecticides. It is less well known that elemental chemistry is also obtained using the SEM, yet it the combination of imaging and microchemistry techniques that has lead to the widespread use of the SEM in research and industry. The same combination of capabilities make the SEM a potentially valuable tool in science education. The advances in modern SEM design with graphical user interfaces using the point and click method of input make the instrument available to students of all ages. However, even assuming that the SEM is an effective tool, it still remains that it is an expensive instrument that only one or two people can operate at a time. To get widespread use, the instrument needs to be a distributed resource. To this end, educational components can be constructed around computer based exercises or computer SEM simulator. The SEM generates an image (including the chemistry) that can be transferred over an intranet within a school building, through distance learning facilities at connected schools, and over the World Wide Web. Further, there are prototype systems developed by which instruments can be actually manipulated from remote locations. Using a mix of these strategies, the SEM will be a distributed and cost-effective resource.

Keywords:

Volcanism, Plate Tectonics, Earth's Crust, Scanning Electron Microscope, Microchemistry

Prerequisite Knowledge:

The student

1. should be familiar with the concept of plate tectonics
2. should know the classification of igneous rocks, including Bowen's reaction series

Objective:

The objective of this exercise is to help the student "discover" that there is a relationship between composition of volcanic materials and their plate tectonic setting, and to investigate the reason for this relationship. The student will learn to:

1. collect compositional data on the scanning electron microscope, or using a computer-based SEM program
2. determine average compositions for different types of volcanic materials
3. relate the compositions to their plate tectonic setting
4. use the information from Bowen's reaction series to explain the compositional differences.

Equipment and Supplies:

1. Map showing distribution of volcanic and earthquake activity on the earth's surface.
2. A diagram showing Bowen's reaction series in relation to the classification of igneous rocks.
3. A diagram showing the plate boundaries in cross section.
4. Scanning electron microscope with compositional analysis (energy dispersive spectrometer) capability.
5. Volcanic material from tectonic settings including continental margin, island arc, hot spot and/or ocean ridge.
6. Or stored digital images of 4 and 5 with display software.
7. Computer spread sheet if desired.

Test Activity:

This activity is to connect two concepts (volcanic activity in different plate tectonic settings and the classification of igneous rocks) to establish an hypothesis. This hypothesis is tested using data generated by an SEM. Implications resulting from these observations are discussed.

The first step is to review volcanic material (lava and magma) and how a volcano forms. Then, on a map showing the geographic distribution of volcanic activity, note that volcanic activity is not distributed randomly over the surface of the earth, but that it occurs at preferred locations. These locations mark plate boundaries which can be described as converging (colliding), diverging (spreading), or transform (slipping).

The second step is to review the classification of igneous rocks. In this step, the diagram showing the order of crystallization of the most common rock-forming silicate minerals (Bowen's reaction series) is emphasized. The first minerals to form (i.e., those formed at the highest temperature) are silicates that are rich in iron and magnesium. When these crystallize, they form igneous rocks that are referred to as ultramafic (ma for magnesium and fe for iron). Subsequent minerals to form are successively enriched in silicon and aluminum relative to decreasing amounts of iron and magnesium. When these crystallize, they form igneous rocks that are referred to as sialic.

Formation of Hypothesis One:

The students are asked to combine the information of the two concepts discussed above and to form an hypothesis regarding the composition of volcanic materials in various plate tectonic settings, starting from a diverging plate boundary (or hot spot). They are to predict in general terms such as most iron magnesium rich to most silicon aluminum rich or ultramafic, mafic and sialic. To assist them, the students will be given a diagram which is a cross section of the plate boundaries showing the volcanic activity.

The figure of a diverging boundary cross section shows that the volcanic material in this setting is derived from the asthenosphere which is composed of ultramafic material and is partially molten. The conceptual leap is for the students to predict the order in which silicate minerals will melt in a solid rock upon heating when the students have learned the order in which the minerals crystallize from a melt upon cooling. The students may recognize this by themselves, or the instructor may direct them to this approach through questions.

Once the hypothesis regarding the composition of volcanic material derived from a diverging plate boundary has been formed, the process is repeated for an island arc and ocean-continent converging margin setting. The island arc setting should follow directly from the logic employed in the diverging plate boundary. The ocean-continent converging margin is somewhat more complicated. The conceptual leap in this setting is to realize that sediment derived from the ocean floor and from the adjacent continent is subducted with the oceanic crust and partial melting of both materials occurs.

Formation of Hypothesis Two:

The student is asked to determine the general composition of ocean and continental sediment. We start again with Bowen's reaction series. The students know that the different silicate minerals crystallized at different temperatures. The problem is to relate the temperature of crystallization to stability at the temperature conditions at the earth's surface where sediment is formed from the decay of rocks.

Hypothesis Testing:

The hypothesis for the composition of volcanic material from each tectonic setting will be tested either by analyzing samples in the SEM, or by using a computer program which displays the SEM image and composition.

The material from divergent margins and hot spots is lava. Several locations on the specimen are examined for composition and the results for that specimen are averaged. The EDS spectrum is acquired and all elements are identified and their peaks labeled. This is illustrated in Figure 1. The relative proportion of each element is estimated as the area of the peak for each element. The general composition can be represented as the ratio of two groups of elements; magnesium plus iron (mafic), and silicon plus aluminum (sialic). The average composition of the four elements are determined (by hand or by using a spread sheet) and the ratio of iron plus magnesium to silicon plus aluminum is calculated. The higher the value of this ratio (closer to 1.0), the more mafic the composition and the lower the value the more sialic the composition.

The procedure is repeated for additional samples of the divergent margin setting and for multiple samples of volcanic material from the other plate tectonic settings as well. All data are presented in table form.

Results:

Results from the analysis of six samples from three tectonic settings are presented in Table I and in Figure 2. These results indicate that the composition of the volcanic material becomes increasingly sialic moving from hot spot to island arc to continental setting. A combination of partial melting and contribution of oceanic and continental sediment results in increasing the

silicon and aluminum content relative to iron and magnesium. The student writes a report in which the hypotheses are stated, and the results are summarized and interpreted.

Comments:

Extension of the concepts learned can form the basis of additional activities. The density of the mafic and sialic materials can be measured. This density can be related to the nature of the layered earth and the origin of ocean basins. First, it is because of density differences that the sialic material “floats” on the mafic material resulting in the layering of the earth’s crust. Second, because the sialic material is derived through the processes accompanying subduction at convergent plate boundaries it is a discontinuous layer of the earth’s surface. This results in the fact that there are two “preferred” elevations of the crust, one where approximately 45% of the earth’s surface elevation ranges between three and six kilometers below sea level, and approximately 29% ranges from minus one to plus one kilometer relative to sea level. Because the earth’s surface is covered with water, it is this distribution of elevation that results in defining continents of sialic crust and ocean basins of mafic crust.

Table I - Compositional Results

Setting	Location	Si	Al	Mg	Fe	Ratio
Hot Spot	Hawaii	32.7	18.4	4.1	10.2	
		36.7	10.2	13.3	14.3	
		43.9	17.4	2.0	8.2	
		43.4	18.2	3.0	8.1	
		39.2	8.3	16.5	14.4	
		<u>39.4</u>	<u>20.2</u>	<u>3.0</u>	<u>9.1</u>	
	Average	39.2	15.4	7.0	10.7	0.324
Island Arc	Mt Pinatubo	22.9	5.7	5.7	11.4	
		63.0	11.1	0.0	3.7	
		49.2	23.7	0.0	0.0	
		<u>52.6</u>	<u>21.1</u>	<u>0.0</u>	<u>0.0</u>	
	Average	46.9	15.4	1.4	3.8	0.084
Island Arc	Mt Pinatubo	47.4	10.5	0.0	1.8	
		55.7	9.8	0.0	1.6	
		48.4	15.6	0.0	0.0	
		26.7	20.0	3.3	3.3	
		32.0	12.0	8.0	4.0	
		41.4	20.7	3.5	6.9	
	<u>41.4</u>	<u>20.7</u>	<u>3.5</u>	<u>3.9</u>		
Average	41.9	15.6	2.6	3.5	0.106	
Continental	Mount St Helens	44.3	28.9	0.0	0.0	
		48.5	24.2	0.0	0.0	
		44.9	26.5	0.0	1.0	
		46.3	27.4	0.0	1.1	
		<u>64.3</u>	<u>13.3</u>	<u>0.0</u>	<u>2.0</u>	
	Average	49.7	24.1	0.0	0.8	0.011
Continental	Mt. Jemez	69.7	11.1	0.0	0.0	
		83.9	0.0	1.0	0.0	
		68.0	12.4	0.0	0.0	
		69.7	11.1	0.0	0.0	
		66.3	12.2	1.0	0.0	
		<u>69.1</u>	<u>12.4</u>	<u>0.0</u>	<u>0.0</u>	
	Average	71.1	9.9	0.3	0.0	0.004
Continental	Mt. Jemez	56.2	10.1	0.0	2.3	
		67.0	10.3	0.0	0.0	
		60.2	19.4	0.0	0.0	
		64.6	10.3	10.4	1.0	
		67.7	11.5	0.0	1.0	
		<u>71.9</u>	<u>12.5</u>	<u>0.0</u>	<u>1.0</u>	
	Average	64.6	12.3	1.7	0.9	0.011

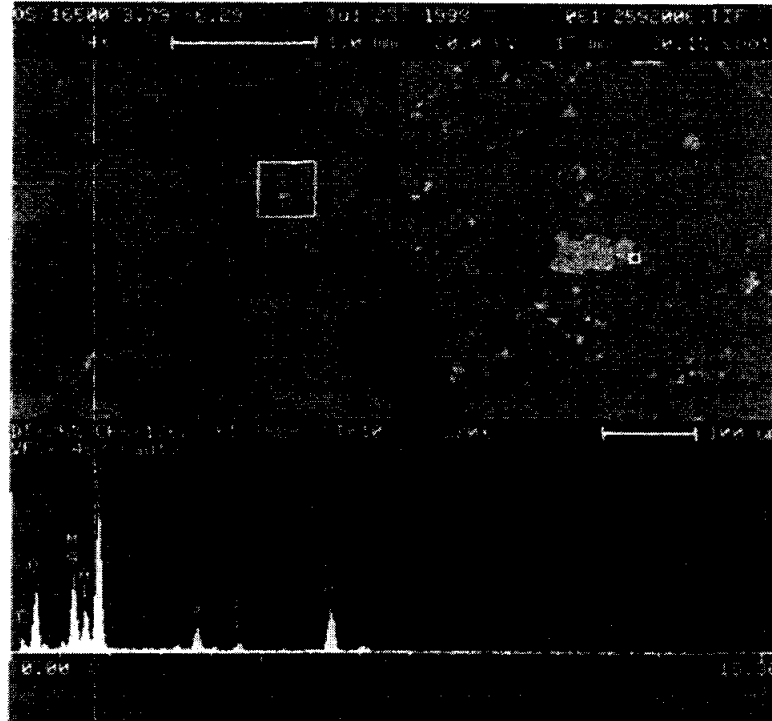


Figure 1 – SEM image and EDS chemistry of Hawaiian lava.

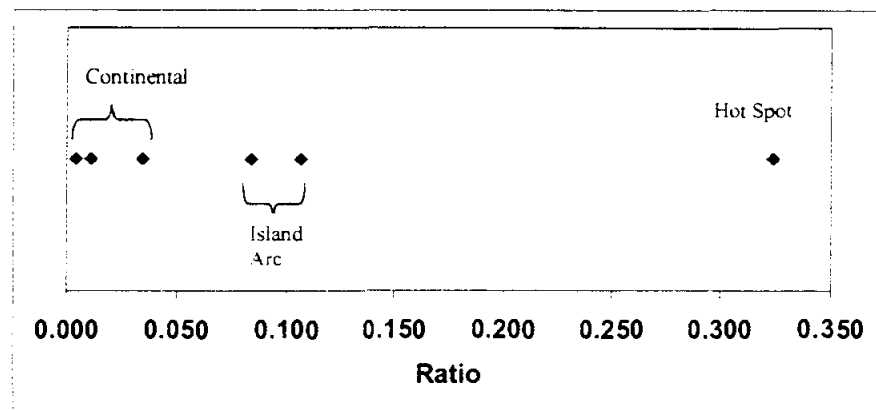


Figure 2 – Results showing increase in mafic composition from continental, to island arc, to hot spot plate tectonic setting.

DETERMINATION OF THE CURIE TEMPERATURE IN FERRO AND FERRIMAGNETS

R. Valenzuela

and

E. Amano

Institute for Materials Research
National University of Mexico
P. O. Box 70-360
Mexico 04510

Telephone: 525-622-4653
e-mail monjaras@servidor.unam.mx



R. Valenzuela

Determination of the Curie Temperature in Ferro and Ferrimagnets

R. Valenzuela and E. Amano
Institute for Materials Research
National University of Mexico, Mexico

Abstract

A system to measure the magnetic permeability as a function of temperature in a wide range of ferro and ferrimagnetic materials is presented. Since in most magnetic materials the permeability changes from a maximum in the magnetically ordered phase to a small value in the disordered paramagnetic phase, this system allows an accurate determination of the Curie temperature. The system is formed by relatively simple and inexpensive modules.

Key Words :

Ferromagnets, Ferrimagnets, Magnetic Transitions,

Prerequisite Knowledge :

The student

1. should know that some materials possess significant magnetic moments and show a spontaneous magnetic order,
2. should have a basic knowledge of magnetic structures such as magnetic domains and magnetic domain walls,
3. should be familiar with simple electrical circuits such as transformers, amplifiers, X-Y plotters, and rectifiers.

Objective :

The objective of this exercise is to provide a phenomenological experience that shows the effects of magnetic order on macroscopic properties such as magnetic permeability, how temperature affects it, and how the magnetic transition can provide information on the chemical composition and homogeneity.

The student will learn to:

1. Make the proper connections between the several modules in order to have an electrical circuit to measure permeability as a function of temperature,
2. Prepare primary and secondary coils on toroidal samples of ferri and ferromagnetic materials,
3. Test magnetic materials to determine their Curie temperature,
4. Analyze the results to understand the correlation between the thermal behavior of the magnetic permeability and the microstructure of the sample.

Equipment and Materials:

1. Signal generator in the 1-20 kHz frequency range (General Radio oscillator 1310-B); Amplifier-Rectifier with gain up to 40 dB (Philips PM 5171); X-Y Plotter with highest sensitivity about 1 mV/inch (HP 7035 B); bridge for measuring inductance (Philips RCL meter PM 6303); chromel-alumel thermocouple, with a length about 1 m; small Muffle Furnace (Thermolyne type 1500) for temperatures up to 500°C; two standard 50 Ω resistors
2. Copper wire for coiling (about 4 meters/sample)

3. X-Y plotter paper and pens
4. ferri and/or ferromagnetic samples, preferably with Curie temperature in the 50-300°C.
5. Support
6. Thermometer to measure room temperature and Vernier calliper to measure sample dimensions

Basis of the Measurement¹:

Ferro and ferrimagnetic are materials with a high content of transition-metal atoms (or ions), which leads to a non-zero magnetic moment. In addition, under certain circumstances of concentration and nearest-neighbor distance and arrangement, there exists a strong interaction, known as exchange, resulting in a spontaneous ordering of magnetic moments or spins. This is a ferromagnetic material. The magnetic ordering, capable of producing strong attraction and repulsion forces in a macroscopic scale, is perturbed by thermal agitation, and eventually it is destroyed at a well defined temperature, the Curie point, T_c . The determination of this transition temperature is therefore very important.

A ferromagnetic material at $T < T_c$ has a spontaneous ordering of spins, but due to the fact that producing magnetic flux outside the material requires energy, the material is instead divided into magnetic domains with different orientations in such a way that the magnetic flux closes within the sample. The domains are separated by domain walls, which are zones where spins rotate from the magnetic direction of one domain toward the direction of the neighboring domain. A simple case is a 180° wall, as the boundary between domains with opposite magnetization directions.

The application of an external field tends to produce a rotation of spins toward the direction of the field. An effective mechanism for these rotations when domain walls are present is the movements of these walls in such a way that domains with magnetization direction parallel to the applied field grow at the expense of domains with opposite orientation. This mechanism is very efficient since it requires fields significantly lower than the field required to produce a collective rotation of all individual spins. This can be evaluated by means of the magnetic permeability, μ , which is defined as the ratio between the magnetic induction, B , and the applied field, H : $\mu = B/H$.

In most ferromagnetic materials, permeability increases with temperature because thermal agitation makes easier to move domain walls as temperature increases. However, when the material reaches its Curie point, the exchange interaction is overcome by agitation, domain walls disappear and permeability decreases down to the value of a non-ordered material. This phenomenon is the basis of the measurement.

Some iron oxides, where magnetic ions are separated by oxygen can have “superexchange” interactions through the oxygen ions. Although these interactions usually lead to an antiparallel order, in some complex crystal structures there can exist several sublattices that produce a resulting magnetic moment; this is the case of “ferrites”. These oxides behave in a very similar way to ferromagnetic metals.

Test Activity Overview:

Circuit preparation:

The circuit layout appears in Fig. 1. The signal generator (SG) provides a small *ac* current to the primary coil (N_p); the magnetic field produced by this coil magnetizes the sample (S), and the magnetic flux produced by it is sensed by the secondary coil (N_s), as a voltage V_s .

This voltage is proportional² to the initial magnetic permeability, μ_i , of the sample. V_s is then amplified and rectified by the AR module. A *dc* voltage, V_r , proportional to the amplitude of V_s (and therefore to μ_i), is provided to the X-Y plotter, in the Y-axis.

The primary coil has typically a very small resistance; to limit the current amplitude and protect the signal generator from a virtual short-circuit operation, a 50 Ω resistor should be connected in series to the primary coil circuit.

Since the input impedance of the AR module is very high, the secondary coil voltage V_s is better detected by connecting a 50 Ω resistor in parallel and sensing this signal on the ends of this resistor. This allows the AR module to operate as a voltage amplifier, which is its normal operating mode.

Primary and secondary coils:

The use of toroidally shaped samples facilitates the measurements, since all the magnetic flux is inside the sample and demagnetization fields are absent. The number of primary and secondary coil turns depends on the size of the toroid, the magnetic softness and the initial permeability value of the particular sample. For most soft ferrites, however, values of N_p/N_s in the ranges (3-6)/(5-15) lead to a good signal-to-noise ratio.

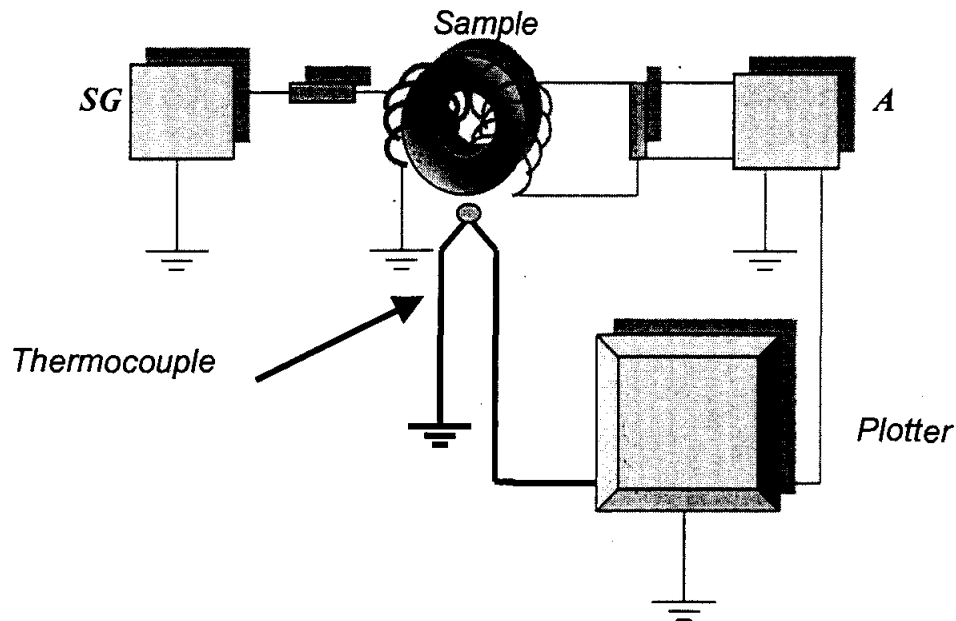


Figure 1. Layout of the measuring circuit.

Testing

Procedure:

Sample Preparation:

The first step is to measure sample dimensions, outer diameter (OD), inner diameter (ID), and height, h . A recommended procedure is to fabricate first the secondary coil, measure the sample inductance, L , and calculate the permeability. Since the secondary coil has more

turns than the primary one, it is easier to fabricate it first. Also, a larger value of inductance is obtained with more turns (the inductance value varies as N_s^2 , therefore reducing reading error. The relative (adimensional) permeability value is calculated as:

$$\mu = 50 (L) / [hN_s^2 \ln_e (OD/IN)] \quad (1)$$

where \ln_e is the e-based logarithms and h should be expressed in meters and L in μH (microHenrys). This value of permeability is used to set the Y-axis for final results.

The next step is to fabricate the primary coil. It is recommended to mark the ends of both coils with a bit of masking tape. These ends are connected and the sample is fixed to the thermocouple.

Calibration of plotter Y-level:

A convenient voltage, V_y , should be applied to the Y-axis of the plotter to obtain a proper $\mu(T)$ curve on the paper. The Y-voltage in the plotter depends on the following factors: permeability of the sample, μ , its dimensions, current level, i , and frequency, f , in the primary coil, N_p , N_s , gain in AR module and gain in the Y-axis itself. For a given sample, we can play (within certain limits, of course) with i , f , N_p , N_s , AR gain and Y-axis gain.

Increasing i leads to an increase in V_s . An excessive current amplitude can overcome the critical field which separates the initial permeability from hysteresis; under these conditions, the secondary voltage (V_s) is no longer a linear function of permeability. Fortunately, for most ferrites, the critical field (also known as propagation field) is relatively large, and a current amplitude of a few miliamps is safe enough to perform the experiment.

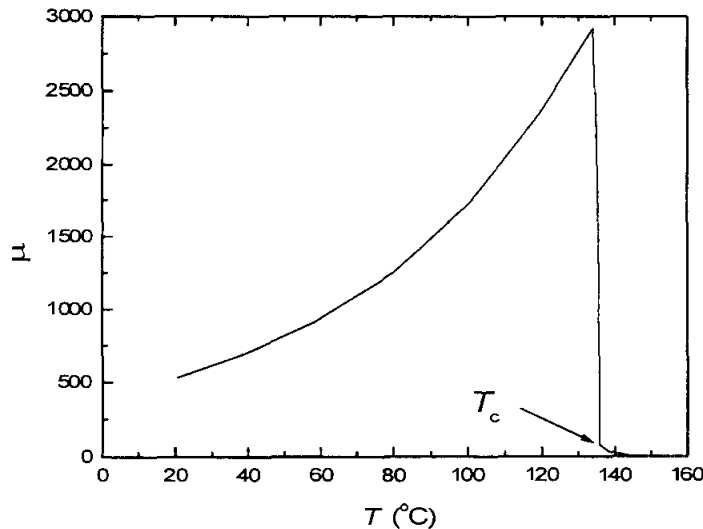


Figure 2. Typical thermal behavior of the permeability of an homogeneous MnZn ferrite, from Ref³.

The Y-axis response on the plotter can then be adjusted by combining AR and plotter gains. As a general practice, the Y-axis pen is initially positioned about the middle of the total available displacement, since most magnetic materials exhibit an increase in μ with temperature, Fig. 2.

Calibration of plotter X-level:

The thermocouple is connected to the X-axis of the plotter. The gain in the X-axis should be adapted to the expected Curie temperature of the sample, in order to have the maximum X displacement and therefore increases the measurement precision. In the plotter used, the highest sensitivity is 1 mV/in with a length of 10 in, therefore allowing measurements up to 246°C. For higher transition temperatures, a calibration of the X-axis can be done to some 2.5 mV/in which allows measurements up to 600°C, encompassing virtually all the known ferrites.

Testing

Once both X- and Y- plotter axis have been set, the sample is fixed to the thermocouple and introduced into the muffle. A slow heating rate is set (lower than 8 °C /min). In most magnetic materials, the initial permeability increases with temperature up to the transition point. At this temperature, a drop is observed indicating the phase change from an ordered magnetic structure (ferro or ferrimagnetic) toward a paramagnetic, disordered state, where the permeability has a very small value.

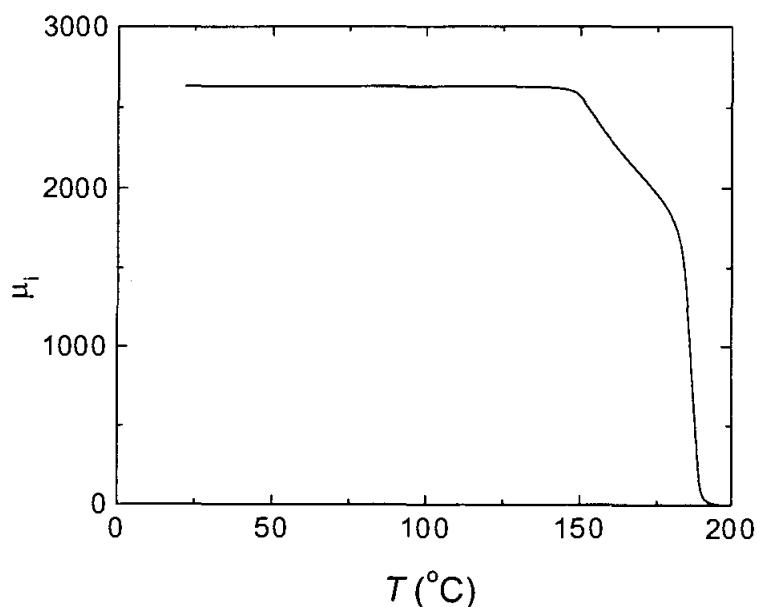


Figure 3. Example of an inhomogeneous NiZn ferrite, with a non-vertical drop at the Curie point. It is also indicated a method to evaluate T_c and inhomogeneity as ΔT (P. Gutiérrez-Amador, unpublished results)

Once this drop has occurred, the muffle is turned off, and the plotter pen is changed (a different color for cooling). It is always important to record the cooling process, since the transition is a reversible process.

In most cases, the permeability drop at the magnetic phase transition is not a perfect vertical. Since Curie point depends essentially of magnetic interactions, this implies that there is some degree of chemical inhomogeneity in the sample. To report the Curie temperature measurement, some convention has to be established. A simple one would be to report the temperature at the permeability half-height (in many cases the permeability value is maximum just before the drop), plus the temperature increase to reach the baseline, as shown in Fig. 3.

References

¹ R. Valenzuela. *Magnetic Ceramics*. Cambridge University Press, 1994

² E. Cedillo, J. Ocampo, V. Rivera and R. Valenzuela. An apparatus for the measurement of the initial magnetic permeability as a function of temperature. *J. Phys. E: Sci. Instr.*, Vol. 13, 1980, pp. 383-386

³ A. Peláiz-Barranco, M.P. Gutiérrez-Amador, A. Huanosta and R. Valenzuela. Phase transitions in ferrimagnetic and ferroelectric ceramics by *ac* measurements. *Appl. Phys. Lett.* Vol. 73, 1998, pp. 2039-41

Raul Valenzuela

Born April 28, 1946, at Mexico City, Mexico

Chemical Engineering from University of Mexico, 1969

Ceramic Engineering specialization from Ecole de Sevres, France, 1970

PhD on Materials Science from Universite de Paris VI, France, 1974

Full professor at Institute for Materials Research, National University of Mexico, Mexico

Head of the Metallic and Ceramic Materials Department

Author of the book *Magnetic Ceramics*, edited by Cambridge University Press, UK, 1994

Coauthor of some 80 research papers

Visiting professor (sabbatical) at the Department of Chemistry, University of Aberdeen, UK, 1991-1992.

Visiting professor (sabbatical) at Institute for Applied Magnetism, Universidad Complutense de Madrid, Spain, 1994-1995.

EDUCATIONAL AND PUBLIC OUTREACH FOR THE MARS SAMPLE RETURN PROJECT

S. Raj Chaudhury

and

Gae Golembiewski

BEST Lab
Center for Materials Research
Norfolk State University
2401 Corprew Avenue
Norfolk, Virginia 23504

Telephone: 757-683-2381
e-mail schaudhury@vger.nsu.edu
ggolem@vger.nsu.edu



S. Raj Chaudhury

Educational and Public Outreach for the Mars Sample Return Project

S. Raj Chaudhury and Gae Golembiewski
BEST Lab
Norfolk State University
2401 Corprew Avenue
Norfolk VA 23504

schaudhury@vger.nsu.edu
ggolem@vger.nsu.edu

NASA Langley Research Center will be responsible for the design, development, test, fabrication and integration of a Sample Return Capsule (re-entry vehicle) that will bring back to Earth several dozen samples of Martian soil and rocks. Within stringent cost and mass restrictions, appropriate materials must be selected for both the outer shell of the capsule itself as well as shock absorbent material designed to protect the cargo canister (sample holder).

Working with NASA Langley personnel, the BEST Lab team at NSU is embarking on an educational and public outreach effort to develop parallel laboratory activities for students in design, technology, engineering and physics. These will closely follow the actual concept implementation by the Langley group, who will rely solely on aerodynamics for deceleration and attitude control of the entry vehicle. Not using a parachute requires packaging the samples in a hardened container with sufficient energy-absorbing material to assure containment during ground impact.

Preliminary directions for the educational aspects of this project will be discussed.

--

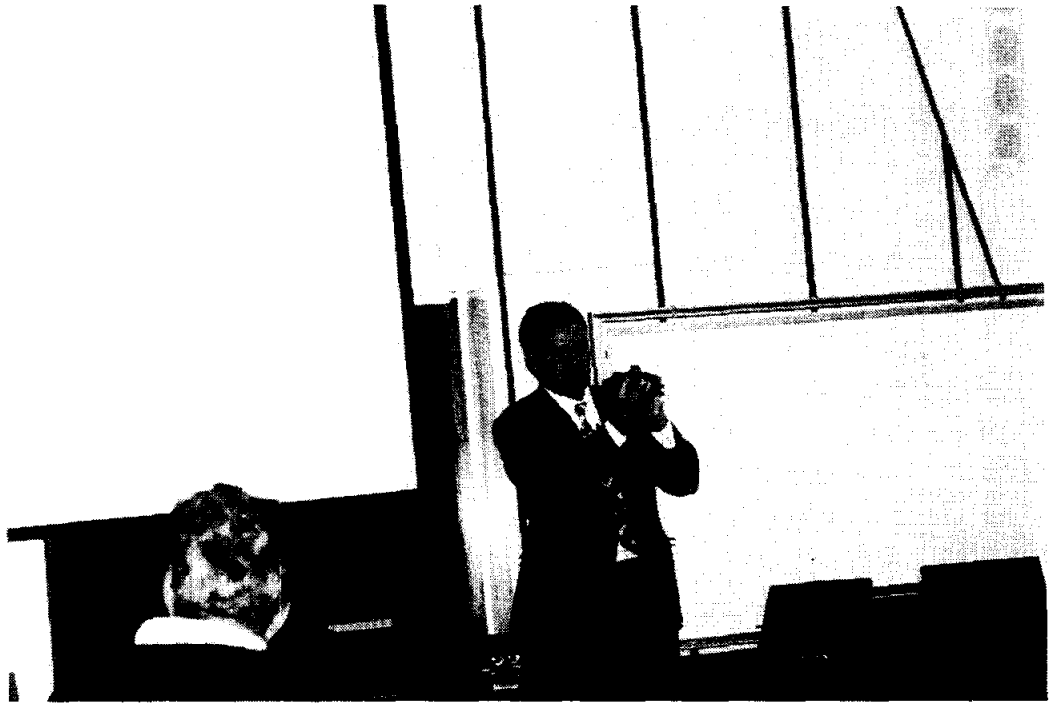
S. Raj Chaudhury Phone: (757) 683-2241
Norfolk State University Fax : (757) 683-9054
Center for Materials Research schaudhury@vger.nsu.edu
2401 Corprew Avenue raj@vigyan.nsu.edu
Norfolk VA 23504 http://vigyan.nsu.edu/

GALVANOSTATIC POLARIZATION CURVES FOR TEACHING PURPOSES

Carlos E. Umana

Department of Materials
School of Mechanical Engineering
University of Costa Rica
San Jose, Costa Rica

Telephone 506-235-6350
e-mail caruma@terraba.fing.ucr.ac.cr



Carlos E. Umana

GALVANOSTATIC POLARIZATION CURVES FOR TEACHING PURPOSES

Carlos E. Umaña
Departamento de Materiales
Escuela de Ingeniería Mecánica
Universidad de Costa Rica
San José, Costa Rica

KEY WORDS: Potentials and reference electrodes, current density, polarization, anodic and cathodic reactions, corrosion rate.

PREREQUISITE KNOWLEDGE: An understanding of the fundamentals of corrosion phenomena. This experiment can be done once the basic knowledge about polarization mechanisms has been taught.

OBJECTIVES:

1. To obtain polarization curves without having to use sophisticated equipment and without previous experience.
2. To bring hands on knowledge of the details involved in a polarization test.
3. To encourage students to explore the details of corrosion theory.

EQUIPMENT AND SUPPLIES:

1. Saturated calomel electrode (S.C.E.) 12 mm diameter x 110 mm length
2. Filtered DC power source (P.S.), output 0 to 40 v
3. Two digital high impedance multimeters. DC range: 0-2 v; 0-200 μ A and 0-2 mA
4. Three variable resistors 1M Ω (best known as potentiometers) and three graduated knobs for the variable resistors
5. Nitrogen tank and regulator
6. Balance (max. mass to weight \pm 12g), readability to 0.1 g
7. Hot plate
8. Stopwatch
9. Immersion thermometer \approx 0 - 50 $^{\circ}$ C
10. pH meter (optional)
11. One 600 ml beaker and two 250 ml beakers
12. A 300 x 120 x 5 mm PMMA plastic plate to build the electrode's supporting system
13. Aluminum bar (5/16" diameter x \approx 4") and angular shape (3/8" x 3/8" x \approx 2" length)
14. Two nylon cable ties (0.1" wide)
15. One mild steel bolt (1/4" diameter x 4.5")
16. 240-400-600 grid SiC paper
17. Caliper
18. Graphite bars from disposed size D dry cell batteries
19. Teflon[®] PTFE pipe thread sealer tape
20. 2 meters of polyethylene hose (1/8" inside diameter).
21. Two battery clips (10 amps size x 2" length) and three steel binder spring clips (3/4" wide)
22. Sodium Chloride (99 % pure or higher)
23. Distilled water (D.W.)

24. Piece of plastic spring binder to hold and control immersion depth of the S.C.E.
25. Glass tube of 1.5mm internal diameter x \approx 100 mm
26. Electric cables

INTRODUCTION:

Polarization curves have been used to study corrosion phenomena for many years (Ref. 1). They are a very important tool for researchers and engineers and are treated in almost all materials science and engineering texts available. However polarization curves involve some electrochemistry concepts which are difficult to assimilate.

It goes without saying that the most effective and easiest way to understand polarization curves is by measuring, plotting and analyzing them. These curves can be obtained by three experimental techniques (Ref.2): a. potentiodynamic, b. potentiostatic, and c. galvanostatic. The first two techniques require sophisticated equipment, usually not available in mechanical or materials engineering schools. The third technique has some limitations, but due to its simplicity offers a good alternative.

This experiment is based on the galvanostatic technique, which has been simplified in such a way that an instructor or professor can use it without the limitations of sophisticated equipment. Most of the materials and equipment required for the experiment are easily obtained.

After performing the experiment it is expected that students will have a better understanding of concepts such as reference electrodes, corrosion potential, corrosion current densities, cathodic and anodic over potentials, polarization, Tafel slopes, etc. It should be clear that even though the experiment described is only for teaching and not for research or professional purposes the basic principles are the same in all cases.

THEORETICAL BASIC CONCEPTS:

A corrosion system always consists of anodic and cathodic areas electrically connected and immersed in a common electrolyte. The most common form of corrosion is known as uniform or general overall corrosion (Ref.2). The external surface of any isolated piece of metal or alloy that undergoes uniform corrosion is always composed of multiple anodic and cathodic micro-areas as shown in Figure 1a. These micro-areas continuously change location as corrosion goes on. All anodic areas and all cathodic areas of the metal surface can be schematically represented as in Figure 1b. and usually it is assumed that both areas are equal (Ref.3). In this paper it is assumed that electron flow and current have the same direction.

If an external current is applied as occurs with a polarization test or an impressed current cathodic protection application, the system may be represented by the configuration of Figure 2. For a negative power source lead connection as shown in Figure 2, applied and internal currents converge at the cathodic area, which allows to establish the following current relation:

$$I_{c,tot} = I_{c,appl} + I_{c,int} \quad (1)$$

Where:

- $I_{c,tot}$ = Total cathodic current
- $I_{c,appl}$ = Applied cathodic current
- $I_{c,int}$ = Internal cathodic current

Normally relation (1) is divided by the total working electrode (W.E.) area to give the following current density relation:

$$i_{c,tot} = i_{c,appl} + i_{c,int} \quad (2)$$

Where:

$i_{c,tot}$ = Total cathodic current density
 $i_{c,appl}$ = Applied cathodic current density
 $i_{c,int}$ = Internal cathodic current density

For the W.E. connected to the positive lead, applied and internal current leave the anodic area giving as a result the following relations:

$$I_{a,tot} = I_{a,appl} + I_{a,int} \quad (3)$$

and

$$i_{a,tot} = i_{a,appl} + i_{a,int} \quad (4)$$

Where the suffix "a" stands for anodic. Also notice that $I_{c,int}$ and $i_{c,int}$ changes to $I_{a,int}$ and $i_{a,int}$ if the polarity is reversed.

Figure 3 shows a polarization diagram where E_{corr} is the open circuit corrosion potential and i_{corr} is the corrosion current density and these parameters are supposed to be constant for each metal or alloy in a specific electrolyte under controlled conditions. Overpotentials are measured using E_{corr} as reference potential, and for any potential it is deduced that $I_{c,int} = I_{a,int}$. Relations (2) and (4) are graphically represented in Figure 3.

Figure 4 shows how a polarization diagram is obtained from experimental polarization curves. These curves are plots of applied current density instead of total current density values, and for all cases $i_{appl} < i_{tot}$. This explains why experimental polarization curves deviate from a linear behavior for small overpotentials. Therefore it stands to reason that experimental polarization curves and polarization diagrams are not the same thing.

Average corrosion thickness loss rate is a function of the corrosion current density (i_{corr}) that results from the intersection of the cathodic extrapolation line with the E_{corr} line potential in a polarization diagram. This is possible using a form of the Faraday's equation which is as follows:

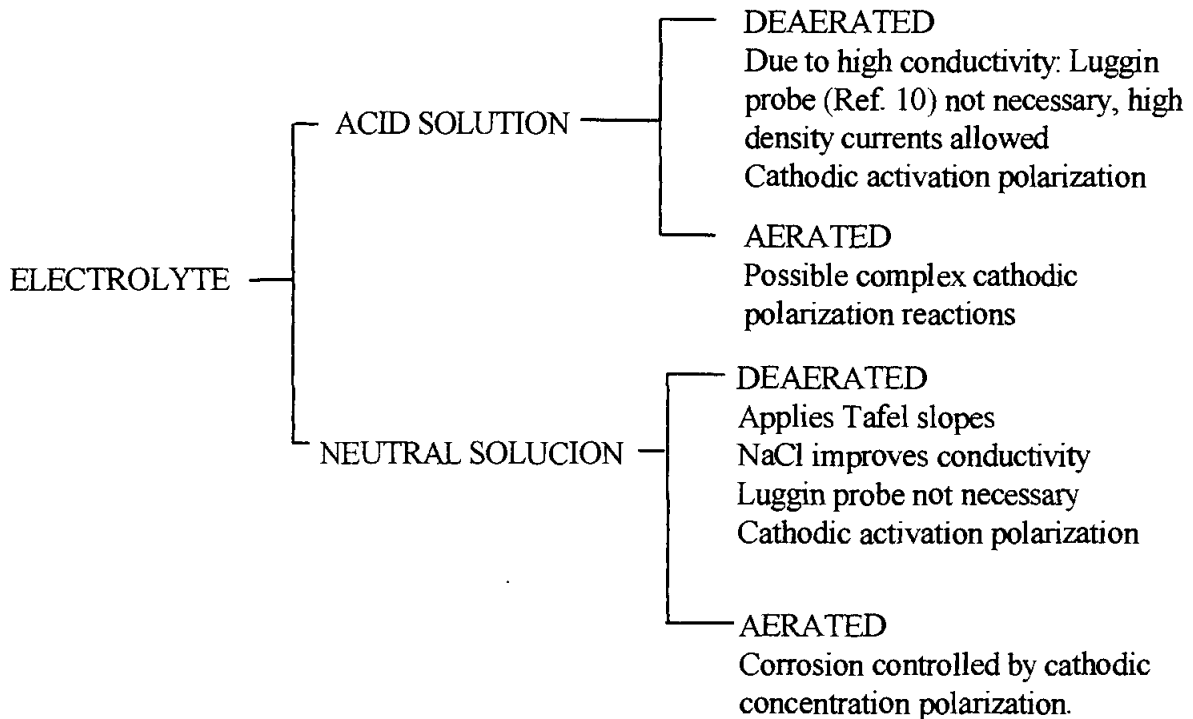
$$\frac{th}{t} = \frac{i \cdot A \cdot W.}{F \cdot n \cdot \rho} \quad (5)$$

Where:

th = Thickness (cm)
 t = Time (s)
 i = Current density (A/cm^2)
 $A.W.$ = 1 mol of the element (g)
 F = Faraday's constant: 96,500 (A.s)
 n = Element valence
 ρ = Density (g/cm^3)

The correct interpretation of the result of the equation 5 applied to a cylindrical surface means that the W.E. radius is decreasing at the rate given by this equation.
 As was mentioned before the anodic and cathodic micro-areas at the W.E. change location as corrosion goes on. For that reason the corrosion will affect the entire W.E. surface.

The type and nature of the electrolyte plays a very important role in corrosion behavior and according to the pH value and the oxygen content it is possible to have the following basic classification:



PROCEDURE:

1. Build the PMMA electrode's supporting system according to Figure 5.
 2. Open some discharged size D dry cell batteries and extract the central graphite bar. Wash and brush the graphite bars and immerse in distilled water for 24 hours. Choose the bars that do not show air bubbles adhered to the surface to minimize porosity. For the operation wear gloves and avoid skin contact. Dispose conveniently the residual material.
 3. Cut, degrease, wet grind with 240-400 and wet polish with 600 grid SiC paper the mild steel bolt, give emphasis on working area shown in Figure 6a. Rinse with distilled water and dry with an air blower.
 4. Cover the working electrode and the graphite auxiliary electrode with PTFE Teflon[®] pipe thread sealer tape according to Figure 6.
-
5. Fill the 600 ml beaker with distilled water.

6. Put the beaker on a hot plate, allow to heat up and let it boil for twenty minutes.
 7. Remove the beaker from the hot plate, cover it with a clean plastic bag and allow it to cool down to room temperature. This will take around 12 hours. Handle the beaker with care, do not shake it.
 8. Add pure sodium chloride to make up a solution equivalent to 20g of NaCl per 1 liter of D.W. Do not use mechanical stirring to dissolve the salt; instead bubble nitrogen to dissolve the salt to obtain an homogeneous solution.
 9. Fill a clean 250 ml beaker with 200 ml of the sample solution and save the rest of the solution. Pour the sample solution into the beaker slowly without air bubbling.
-
10. Set up the circuitry shown in Figure 7. Use an empty 250 ml spare beaker to hold the supporting plastic plate lid, install all the electrodes, except W.E., and connect them to the corresponding leads. Leave the common input ammeter-resistor connection open and the voltmeter common input connected to the S.C.E. The experimental arrangement is presented in Figure 8.
 11. Prepare the experimental data sheet of Table I and fill in the initial information, including the current values.
 12. Set the nitrogen flow in the 200 ml sample solution to about two bubbles per second and insert the glass nitrogen pipe in the lid.
 13. Make sure all the resistors are set to maximum resistance (0 reading on dials).
 14. Degrease the W.E. and install it in the supporting plastic plate lid and connect to the ammeter and to the voltmeter.
 15. Turn on and set the voltmeter to a 2-volt range.
 16. Place the plate lid on the sample solution beaker and measure the time from the moment of immersion.
 17. Record the open circuit potential ($E_{\text{corr}} \approx -520\text{mv}$) after 90 minutes for the cathodic test run. For the anodic test wait until the former E_{corr} is reached.
 18. Turn on and set the ammeter to the lowest current range, then turn on the power source (P.S.) and set it to around 2 volts (to avoid the reverse current due to the natural potential difference between mild steel and graphite).
 19. Insert into the ammeter the terminal from the resistors that closes the circuit, record the initial time and slowly increase the current by increasing the P.S. output voltage. From this moment it takes about 1 hour to complete the experiment for one curve, the average current rate is $5\mu\text{A}$ every 10 seconds.
 20. When $10\mu\text{A}$ is reached, wait 1 minute and then record the corresponding potential. Repeat this procedure for the different currents established in the polarization data sheet, corresponding to table I.

21. When P.S. maximum voltage is reached (around 42 V) increase the current by using resistor number 1 until resistor number 1 reaches zero resistance.
 22. Finally proceed as before but control the current by using alternatively resistors number 2 and number 3 until the maximum current is reached (the parallel connection makes it possible to control current at lower resistance values).
 23. Record the final time.
 24. Close the nitrogen supply and turn off the P.S., then turn off the amp and volt meters.
-
25. Move the supporting plastic plate lid to the spare 250 ml beaker.
 26. Dispose of the 200 ml solution, and fill again the 250 ml beaker with 200 ml of the original sample solution.
 27. Remove the Teflon[®] tape from the W.E. Wet grind with 240 grit SiC paper and wet polish with 600 grit SiC paper. Again cover the W.E. with Teflon according to Figure 6a.
 28. Reverse the P.S. (Anodic connection) and the ammeter connections (W.E. connected to common input , ammeter). Leave the ammeter-resistors connection open.
 29. Repeat steps 12 through 24 then go to step 30.
 30. Using the data of table I, plot the cathodic and anodic reaction curves on a 2-cycle semilogarithmic paper.

EXPERIMENTAL RESULTS:

Table I shows the values obtained in one polarization test and Figure 9 presents the cathodic and anodic reaction curves (This figure was obtained using MATLAB[®] with Simulink V4.0, The MathWorks, Inc.).

The average corrosion potential is $E_{\text{corr}} = -522$ mv and the cathodic and anodic curve extrapolation corresponding to Tafel behavior gives a corrosion current density of $i_{\text{corr}} = 32.3 \mu\text{A}/\text{cm}^2$. The cathodic Tafel slope is $\beta_c = -550$ mv / decade (1 cycle = decade) and the anodic Tafel slope is $\beta_a = 60$ mv / decade.

The average corrosion thickness loss rate is obtained by applying equation (5) as follows:

$$\frac{th}{t} = [32.3 \times 10^{-6} (\text{A}/\text{cm}^2) \cdot 55.85 (\text{g})] / [96,500 (\text{A}\cdot\text{s}) \cdot 2.7.86 (\text{g}/\text{cm}^3)] = 1.189 \times 10^{-9} (\text{cm} / \text{s})$$

$$\frac{th}{t} = 0.375 (\text{mm} / \text{year})$$

Table I. Polarization Data Sheet

POLARIZATION DATA SHEET TEST N° 24 DATE 10/27/98
 REFERENCE ELECTRODE S.C.E
 WORK ELECTRODE Mild Steel AREA 1 cm²
 AUXILIARY ELECTRODE Graphite AREA 2 cm²
 ELECTROLYTE 20 g NaCl / 1 liter D.W. pH _____ TEMP. 22.5 °C
 ELECTROLYTE TREATMENT Boiled for 20 minutes. Nitrogen bubbling

POLARIZATION MEASUREMENTS:

CATHODIC REACTION

CORROSION POTENTIAL: $E_{corr} = -520$ mv

Initial time: 5:23 pm Final time: 6:24 pm Notes 69 minutes to reach E_{corr}

	1	2	3	4	5	6	7	8	9	10
I μ A	10	15	20	25	30	35	40	50	60	70
E mv	-534	-543	-552	-561	-571	-583	-598	-630	-668	-714
	11	12	13	14	15	16	17	18	19	20
I μ A	80	90	100	125	150	175	200	250	300	350
E mv	-750	-776	-798	-837	-889	-936	-975	-1029	-1052	-1070
	21	22	23	24	25	26	27	28	29	30
I μ A	400	450	500	600	700	800	900	1000		
E mv	-1088	-1101	-1111	-1126	-1138	-1147	-1155	-1162		

ANODIC REACTION

CORROSION POTENTIAL: $E_{corr} = -524$ mv

Initial time: 7:40 pm Final time: 8:39 pm Notes 55 minutes to reach E_{corr}

	1	2	3	4	5	6	7	8	9	10
I μ A	10	15	20	25	30	35	40	50	60	70
E mv	-515	-514	-513	-508	-508	-508	-508	-505	-503	-503
	11	12	13	14	15	16	17	18	19	20
I μ A	80	90	100	125	150	175	200	250	300	350
E mv	-500	-500	-499	-493	-489	-485	-483	-478	-472	-468
	21	22	23	24	25	26	27	28	29	30
I μ A	400	450	500	600	700	800	900	1000		
E mv	-466	-464	-462	-457	-451	-451	-448	-447		

NOTES TO THE INSTRUCTOR:

1. Time plays a very important role in obtaining polarization curves.
2. Repeatability requires a perfect control of the parameters involved.
3. Strictly speaking experimental polarization curves never are truly cathodic or anodic curves, they are only applied current curves.
4. Due to the internal current effect corrosion takes place at the W.E. even under a cathodic applied current condition.
5. For the given conditions in this experiment, currents higher than 1000 μA are difficult to control due to the fact that external resistance should be much greater than cell resistance (Ref.2).
6. Going through this basic laboratory experiment will give an elementary but solid background in the field of corrosion testing. It is recommended before using sophisticated equipment.
7. In this project and for the sake of simplicity the salt bridge, the Luggin probe, the platinum electrode and the oxygen sensor were omitted. However each missing item was taken into account in the design of the experiment in such a way that the lack of each one can be justified.
8. Instructors can try another electrolyte-metal combinations. Be sure to use a different graphite bar for each different solution in order to avoid electrolyte contamination.

REFERENCES:

1. Mansfeld, F.: Don't Be Afraid of Electrochemical Techniques - But Use Them with Care!, Corrosion Vol. 44, N° 12, p. 856, NACE, Houston, Dec. 1988.
2. Jones, Denny A.: Principles and Prevention of Corrosion, Second edition, Prentice Hall, Inc., 1996.
3. Scully, J. C.: Fundamentos de la Corrosión, 1^{era} edición, Editorial Alambra, S.A., 1968.
4. Fontana, M. G.: Corrosion Engineering, 3rd edition, McGraw-Hill Book Company, New York, 1986.
5. Guichelaar, Philip J.; and Williams, Molly W.: A Simple Demonstration of Corrosion Cells, NASA Conference Publication 3074, National Educators' Workshop: Update 89, 1990.
6. Masi, James V.: Experiments in Corrosion for Younger Students by and for Older Students, NASA Conference Publication 3201, National Educators' Workshop: Update 92, 1993.
7. Masi, James V.: Experiments in Natural and Synthetic Dental Materials: A Mouthful of Experiments, NASA Conference Publication 3330, National Educators' Workshop: Update 95, 1996.
8. ASTM Designation G3, Annual Book of ASTM Standard, Philadelphia.
9. ASTM Designation G5, Annual Book of ASTM Standard, Philadelphia.
10. ASTM Designation G15, Annual Book of ASTM Standard, Philadelphia.

ACKNOWLEDGMENTS:

The author wishes to thank Prof. Glenn H. Dewey and Prof. Mark Bloomfield for reviewing the grammar and vocabulary of this paper and the Material's Department senior assistant Carlos Jiménez for helping in running the experiment and preparing this paper.

The author also wishes to thank the Universidad de Costa Rica (Vicerretoría de Investigación) and “La Fundación de la Universidad de Costa Rica para la Investigación” (FUNDEVI) for giving financial support to attend the NEW: Update 98.

SOURCES OF SUPPLIES:

1. Saturated Calomel Electrode
Corning Glass Works, Cat. N° 476002, Cole Parmer, Aldrich or any other scientific supply house.
2. Nitrogen Regulator
Air Products or Cole Parmer
3. Filtered DC Power Source
CPS 250 Tektronix
4. Variable Resistors and Knobs
Available from electronic parts stores
5. Sodium Chloride (99% pure or higher)
Sigma or any chemical compounds supplier

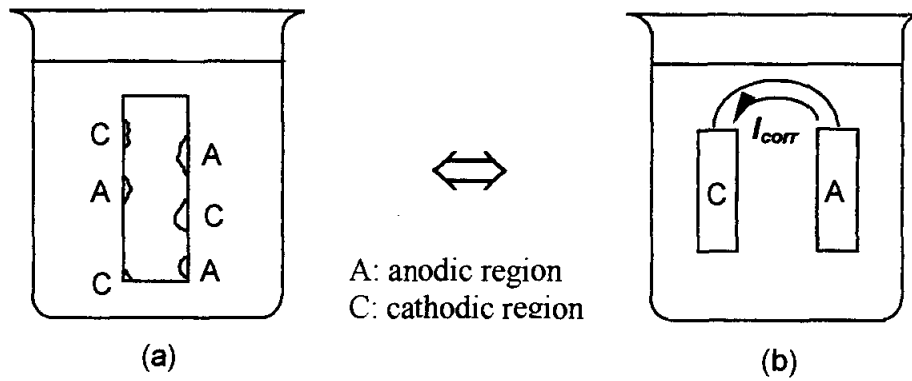


Figure 1. Representation of an isolated metal or alloy that undergoes uniform corrosion: a) Multiple anodic and cathodic micro-areas. b) Schematic representation of the corroding electrode.

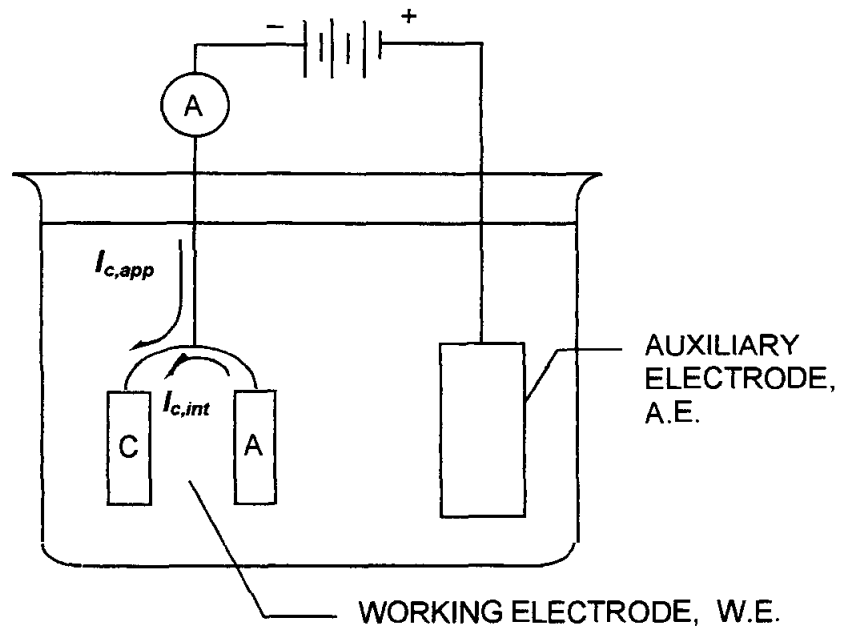


Figure 2. Schematic representation of a corrosion system with an external applied current.

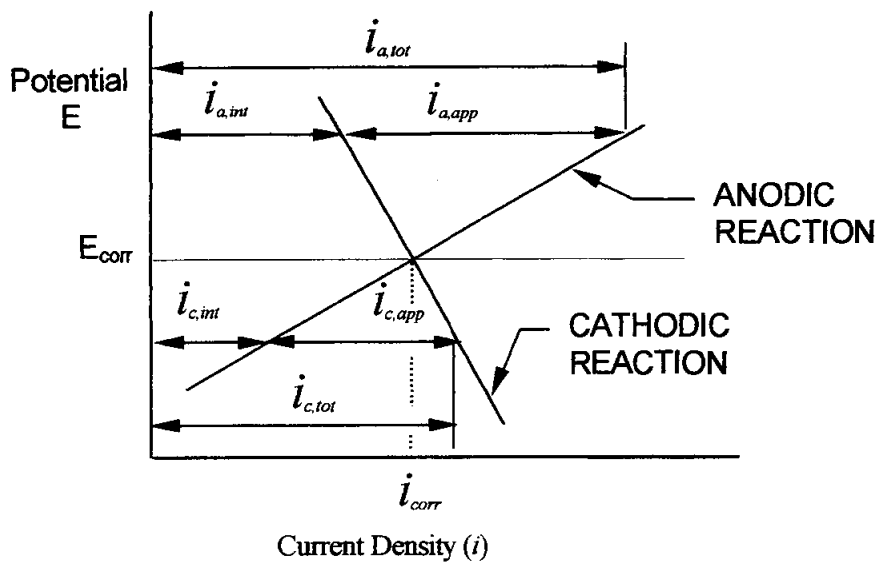


Figure 3. Schematic graphical representation of current density relations in a polarization diagram.

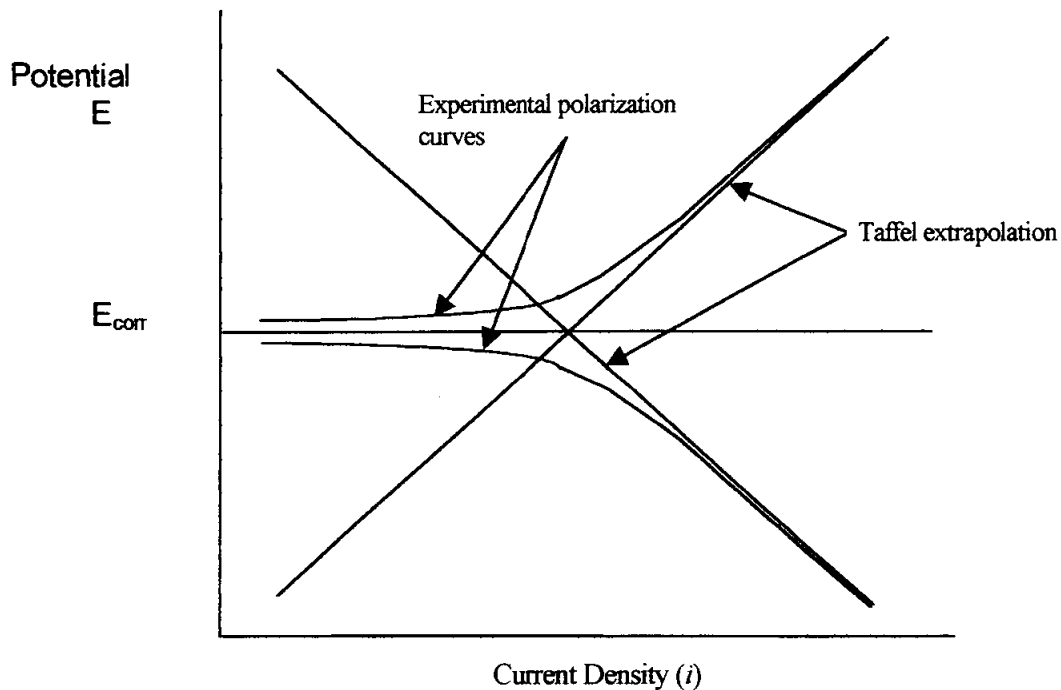
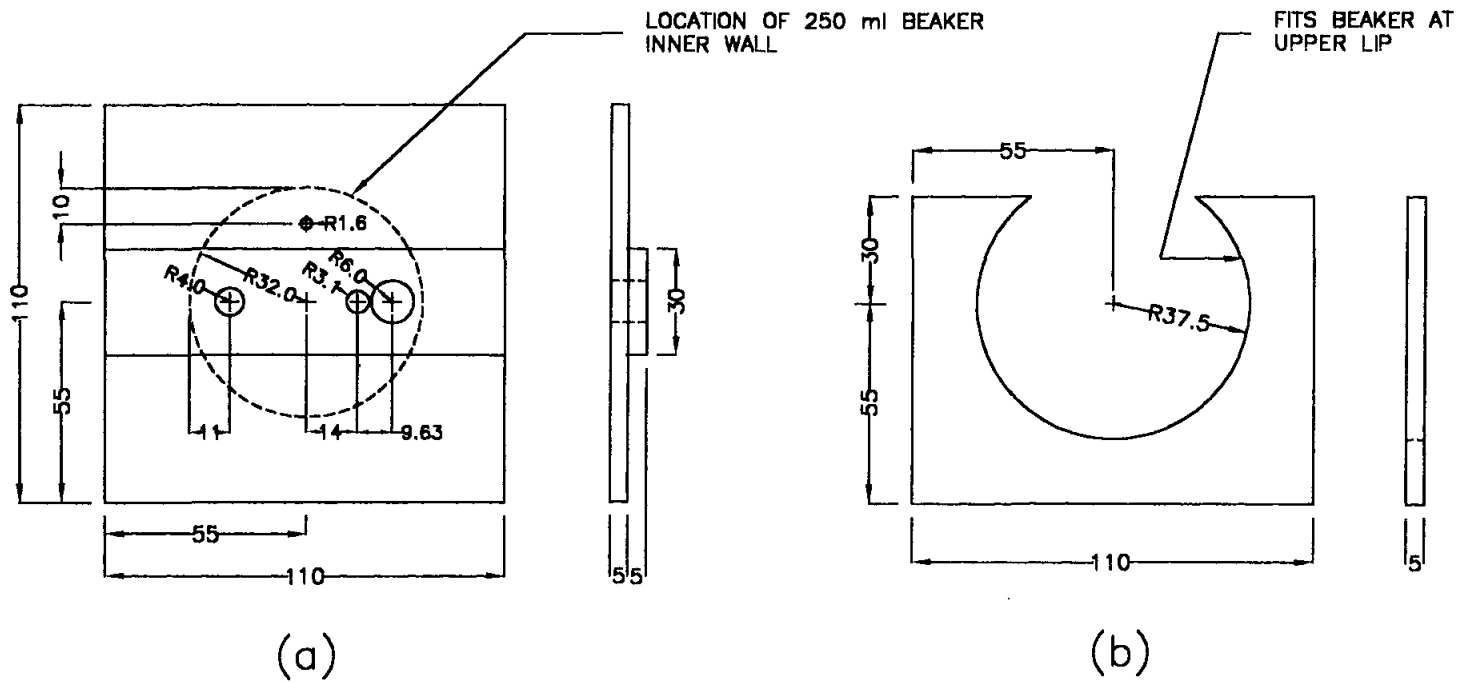


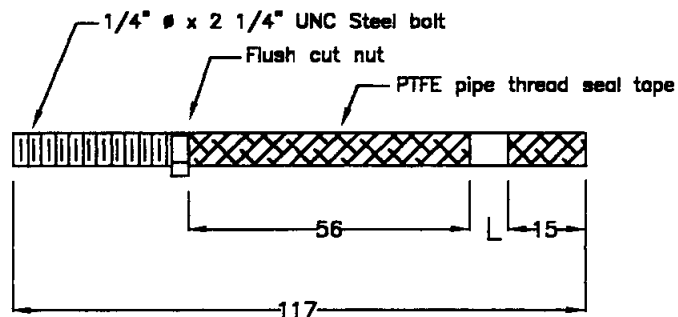
Figure 4. Schematic polarization diagram from Tafel extrapolation of experimental polarization curves.



DIMENSION: mm

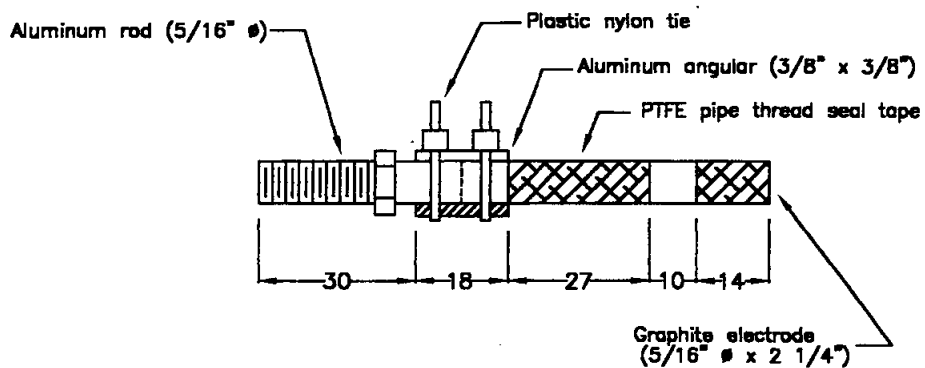
MATERIAL: PMMA

Figure 5. Electrodes supporting system to be used over a 250 ml beaker:
(a) Supporting lid plate (b) Guide plate



L as required for a 1 sq cm working area

(a)



(b)

DIMENSION: mm

Figure 6. Detail of working and auxiliary electrodes:
 (a) Working mild steel electrode
 (b) Auxiliary graphite electrode

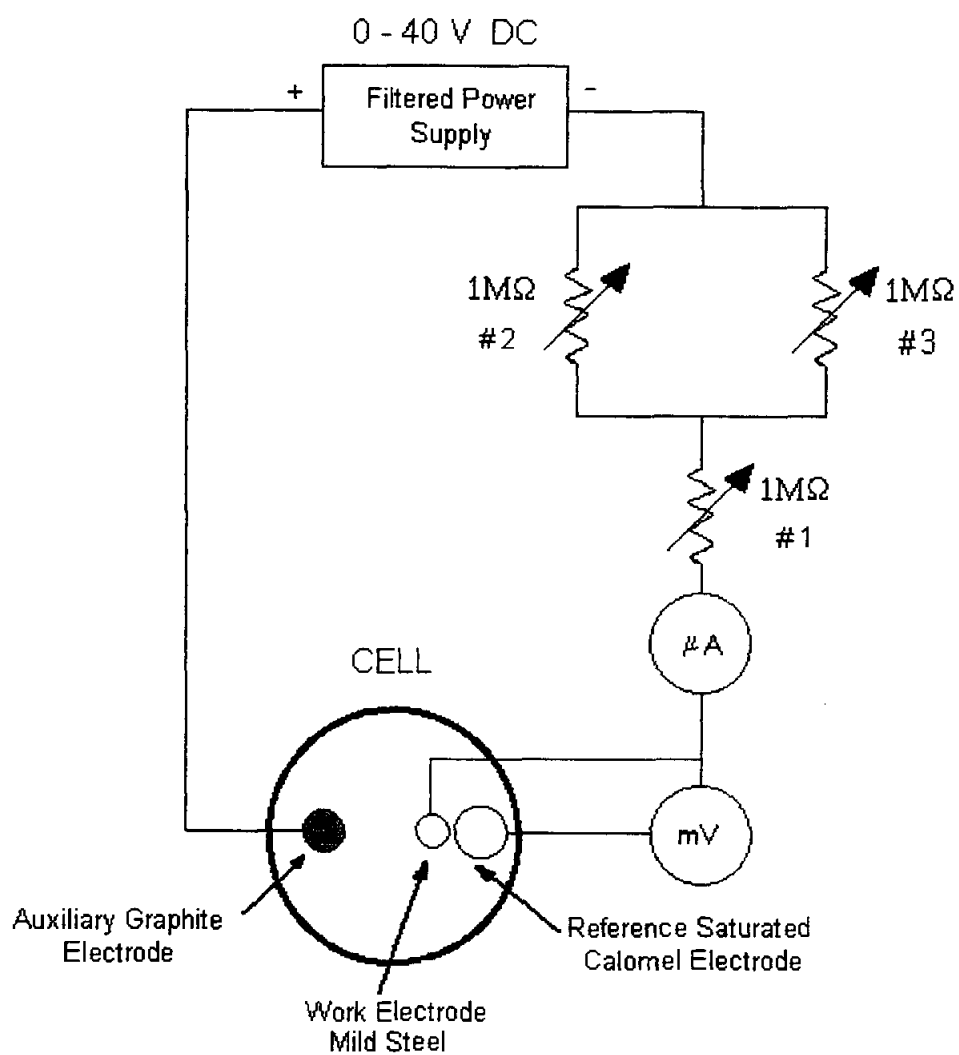


Figure 7. Schematic circuitry for cathodic polarization experiment.

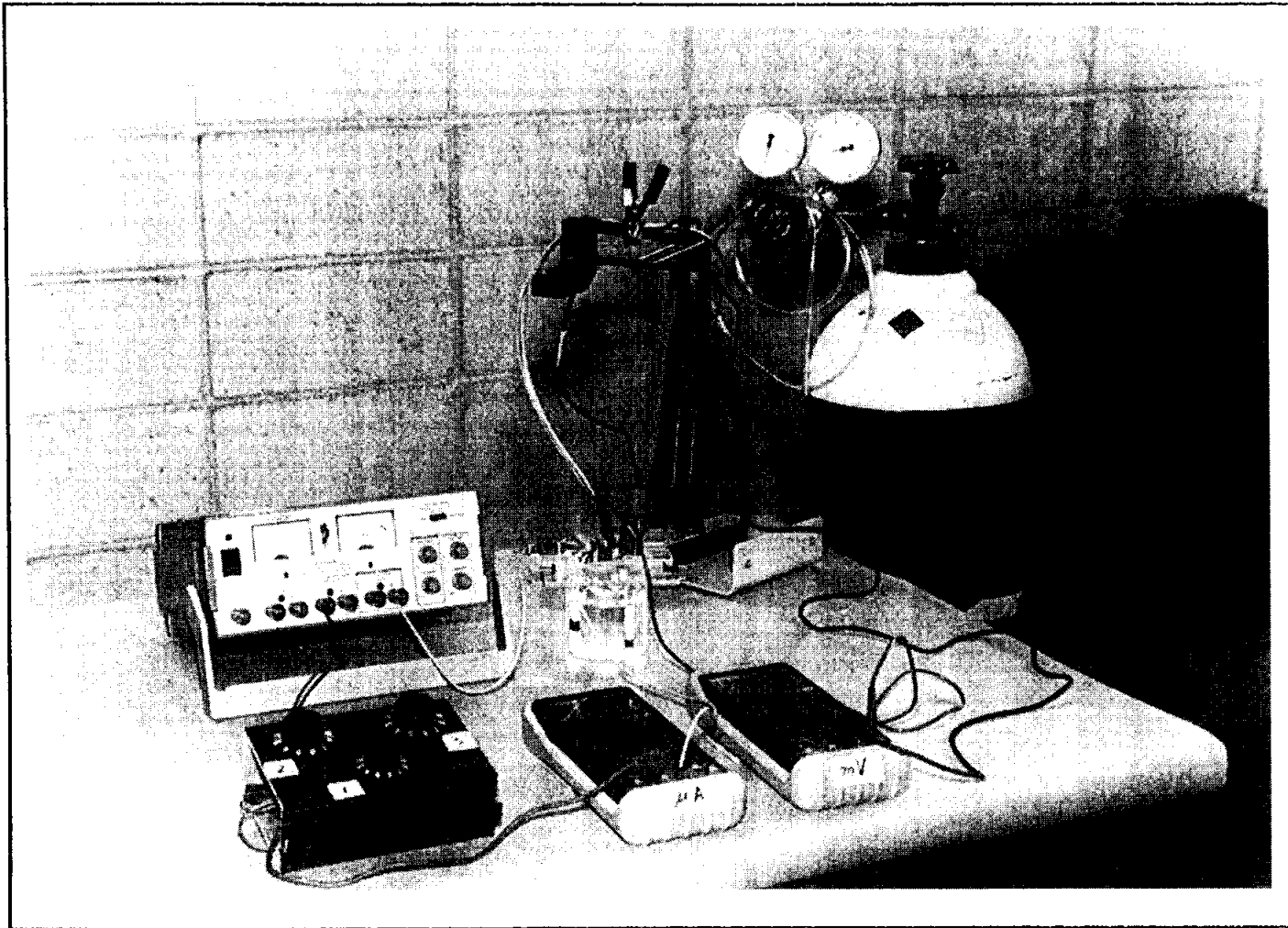


Figure 8. Experimental arrangement for galvanostatic polarization measurements.

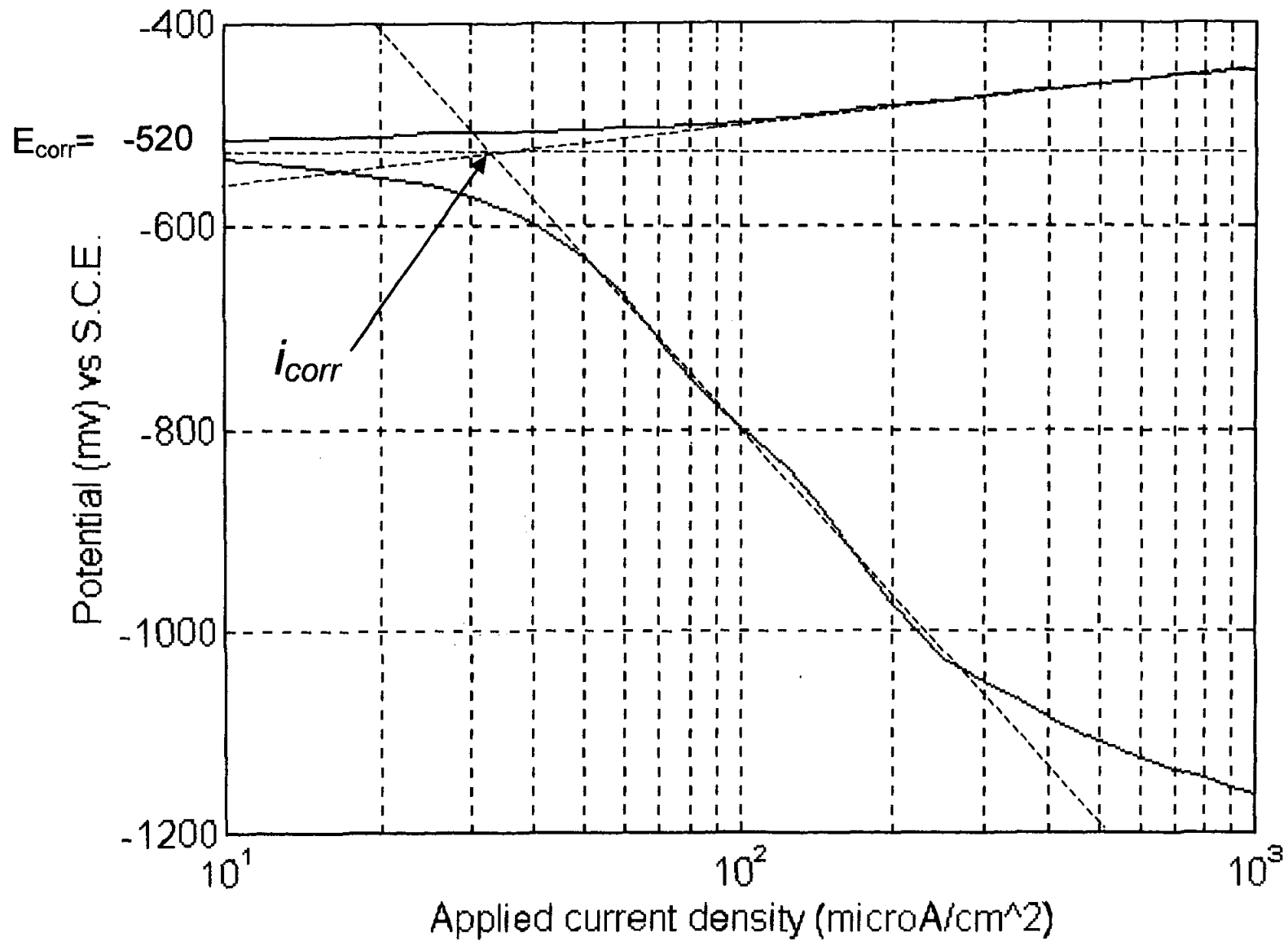


Figure 9. Experimental polarization curves for mild steel in a deaerated sodium chloride solution (20g/liter).

BIOGRAPHY

Carlos E. Umaña holds a Msc. in Metallurgy and Materials Science from Lehigh University (77) and a Mechanical Engineering degree from the Universidad de Costa Rica (72). He is an associate professor at the School of Mechanical Engineering of the Universidad de Costa Rica, where he has been in charge of courses in the fields of materials science, strength of materials and manufacturing.

He has worked in industry and has much experience in hard chromium electroplating. As a consulting engineer he has dealt with more than thirty cases on failure prevention, failure analysis and accident investigation.

In the field of materials science and engineering he is very interested in improving the teaching aids of basic concepts from a multidisciplinary point of view.

THE UNDERLYING STRUCTURE OF ENGINEERING MATERIALS

Mike L. Meier

and

Karl Ewald

Department of Chemical Engineering and Materials Science
University of California, Davis
Davis, California 95616

Telephone: 916-752-5166
e-mail mlmeier@ucdavis.edu

The Underlying Structure of Engineering Materials

Mike L. Meier, Karl Ewald
Department of Chemical Engineering and Materials Science
University of California, Davis
Davis, CA 95616

Abstract

This paper describes the procedure used to produce a short digital video and how it has been used in the classroom. The video is of a tensile test of a polished brass specimen as viewed through a stereo-zoom microscope. The subject is the relationship between structure and properties and the point being made is that the materials have an underlying structure that determines much of how they behave. The video has only been shown in class a couple of times and so far the results have been positive.

Keywords

Microstructure, microstructural evolution, tensile testing, digital video, deformation bands

Prerequisite Knowledge

The student should be familiar with the following:

1. Tensile testing
2. Crystal structure
3. Concepts of slip systems and critical resolved shear stress
4. The fact that many engineering materials are polycrystalline

Objectives

The objective of this paper is two-fold. The first is to offer a video to instructors that can be useful in the classroom. It was designed to impress students with the idea that the behavior of materials is dynamic, that materials themselves have their own characteristic structure, and that the two are intimately related. In this case a ductile metal is used to demonstrate the relationship between the crystalline structure and deformation processes. The second is to describe how this video was made. Digital video and video processing is relatively easy and inexpensive and can be done on most any desktop computer. Others may want to make their own videos of experiments that show the relationships between any number of materials behaviors (sintering, solidification, crystallization, grain growth, dislocations, others) and the microstructure of practically any material.

Equipment and Materials

The alloy used in this experiment was the C26000 alloy (70/30 brass, cartridge brass) which was received in the half-hard condition. Tensile specimens were machined from the 0.125 inch (3.175 mm) thick sheet. The gage length was 1.50 inches (38.1 mm) and the width was 0.50 inches (12.7 mm).

The equipment used to make the videos consisted of the following:

- Furnace - a box furnace capable of reaching 800°C
- Tensile testing system - in this case an Instron model 4204 (computer controlled, 50 kN capacity)

- Digital camera - a color CCD video camera with composite video output
- Video Capture - several AV Macs were available but they could not provide the desired frame rate for full size video capture. The computer used in this project was a 300 MHz Pentium II-based PC running Windows 95. It had 128 MB of SDRAM and a 9 GB UW-SCSI hard drive capable of 17 MB/sec sustained sequential data transfer rates (per Adaptec's SCSI Bench benchmark). The video capture board was capable of digitizing full motion video at 640x480x24 bits and 30 frames per second (fps).
- Video editing software - Adobe Premiere
- Microscope - the microscope used in this experiment was a stereo-zoom microscope capable of providing magnifications from 5 to 75X and a working distance of several inches
- Illumination - quartz lamp with two fiber optic light pipes

Safety Precautions

If one is making a video following a procedure like the one given here then the usual precautions taken in heat treating, metallography and tensile testing should be taken.

Introduction

Consider the “structure-properties-processing” principle that is the foundation of materials science. By the time our students graduate they will appreciate this principle and will have a good understanding of its many fundamental and practical aspects. But in an introductory course it may be difficult to make this point well, to impress the students that all materials have their own characteristic structure, that this structure is dynamic and that it has direct influence on phenomenon such as plastic deformation. This prompted the making of a short video that shows a brass specimen being tensile tested. Its purpose is to thoroughly convince the students that there is an underlying structure (in this case a microstructure), and not only can we see it but we can see it in action. This video can be played on most Windows-based PCs using the standard movie player program or one can use the program I wrote that plays the video and displays the test data simultaneously. The video, the data and the program are all available on a CD-ROM. This paper describes how the video was made and how it has been used in courses.

Procedure

Heat Treating

The tensile specimens were annealed in air at a temperature of 775°C for two hours. This produced grain sizes of several millimeters.

Polishing the Specimens

After heat treating the specimens were mounted in a specially designed holder and ground and polished using an automated polisher/grinder (8-inch wheels, 240-600 grit SiC, 6 μm diamond) with the final polishing being done using a vibratory polisher and a colloidal silica abrasive. The final results were a flat and nearly perfectly polished tensile testing specimen except for minor scalloping.

Tensile Testing

In the first video the specimen was tensile tested to failure using a crosshead speed of 6.00 mm per minute. In the second the crosshead was only 0.60 mm per minute and the test was stopped long before the specimen failed. In both tests the lower crosshead is stationary while the upper crosshead moves at the specified rate. During the test the load-elongation data was recorded and saved to disk.

Video Capture

The stereo-zoom microscope was mounted horizontally on a tripod and focused on the center of the specimen. The video camera was attached to the microscope's C-mount adapter and its output was connected to the PC, a VCR (in case the PC video capture failed) and to a color monitor. The light source was carefully adjusted so that it would illuminate the polished specimen but not reflect towards the microscope as a bright spot. This was accomplished by adjusting the aim of the light pipes and by placing a diffuser (a sheet of white paper) between them and the specimen. After making a few short test recordings the video capture system and the VCR were started and a few seconds later the tensile test was started. The video was recorded at the highest available resolution and frame rate (640x480x24-bits, 30 fps).

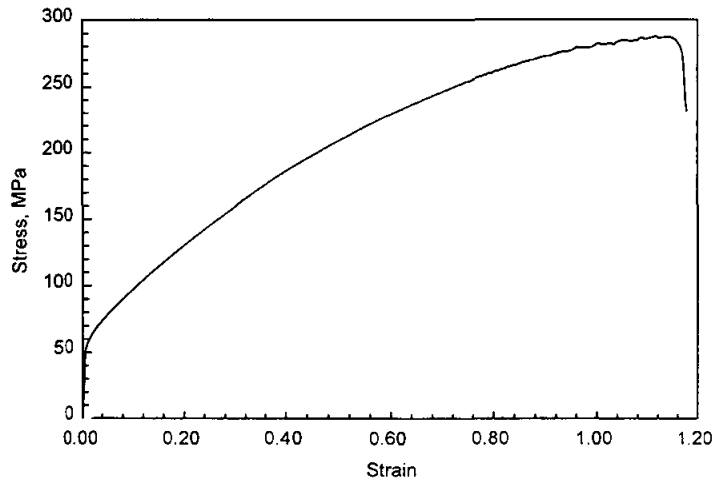


Figure 1 Stress-strain curve typical of all specimens tested during this project.

Video Processing

All video processing was done on the same PC that was used to perform the video capture. Adobe Premiere was used to create the title screens, transitions and micron bars, to cut and splice the video and to assemble the final video. Two versions of each video were produced, one at 320x240x24-bit and the other at 640x480x24-bit, both at a frame rate of 15 fps. These were also accelerated so that their runtimes would be less than five minutes.

CD-ROM

The videos, the data from the tensile tests, a Windows program that displays the video and the stress-strain data simultaneously and a few other files (drivers, readme, etc.) were written to a CD-ROM.

Results

Mechanical Properties

Figure 1 shows the typical stress-strain curve for the specimen tested in the first video. The stress-strain curve in the second video was similar up to a strain of 22% when the test was stopped. The yield strength was around 50 MPa, the UTS was 288 MPa and the strain to failure was 117%.

Video 1

The first video shows a polished brass specimen being tensile tested to failure. The magnification was set so that the specimen's width just filled the field of view and the microscope was focused on an area near the center of the specimen. After the title slides are shown one sees the smooth yellow brass metal. As soon as the tensile test starts the grains and twins appear and as the test continues the grains can be seen moving off the top of the screen. Meanwhile the surface of the specimen is becoming so rough and fibrous looking that it hardly looks like a metallic specimen at all. Finally the specimen fractures. This is

shown in the video as a sudden jerk of the specimen. The video ends a short clip showing the fractured region (figure 2).

Video 2

The second video is basically the same as the first except that the crosshead speed using in the tensile test was slower, the magnification was higher, and the test was not carried out to failure. This video clearly shows the formation of deformation bands (figure 3) and eventually the same grain boundary offsets as were shown in the first video.

Windows Program

A 32-bit Windows program was written so that one could show the stress-strain behavior and the microstructure simultaneously. This program displays three child forms in a main parent form (figure 4). The child forms show the stress-strain plot, the video and text that describes the test and the video. Standard VCR-type controls are used to start, stop and rewind the video. The plot of the stress-strain data tracks with the video.

Discussion

Some of our sophomore engineering students and visiting high school students are a little surprised to learn that most of our common engineering alloys are crystalline. In their world “common sense” says that crystals are rare, unusual, are somehow special and may even possess magical qualities that can influence our health and spiritual well-being. At very least they should be transparent, possibly colored and they are always brittle. It is a pleasure to be able introduce them to the “uncommon sense” of the scientific world, showing them that if one looks into the matter of crystals one may find them to be even more fascinating and also very ordinary. Even common metals are crystalline! Using these videos we can show them crystals in action in a way they had not imagined before and then we can go on to describe what they really are and how they influence many of the properties we take for granted.

In a more conventional series of lectures we might start with a discussion the space filling polyhedra (crystal systems) that defines and

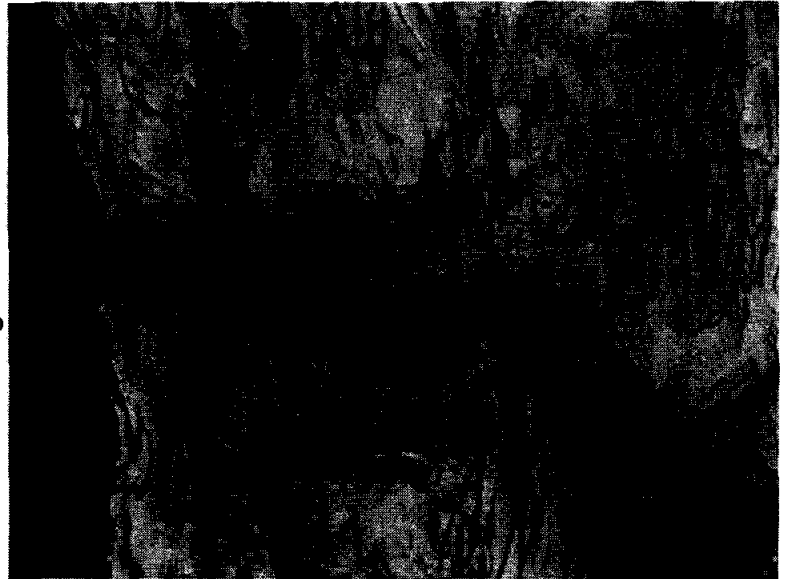


Figure 2 The region of final fracture. This is the final frame in the first video.

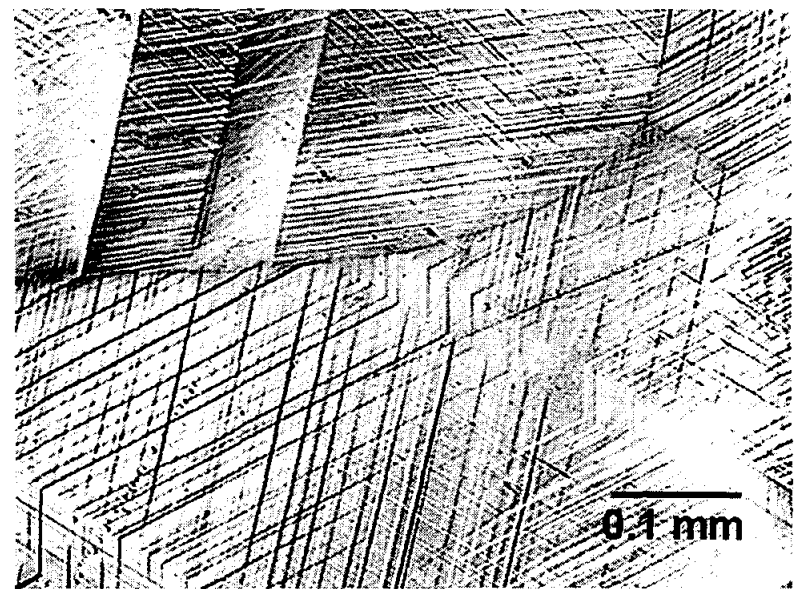


Figure 3 Deformation bands similar to those shown in the second video. This micrograph is from the grips section of the specimen in first video. A metallograph was used to take this digital photo.

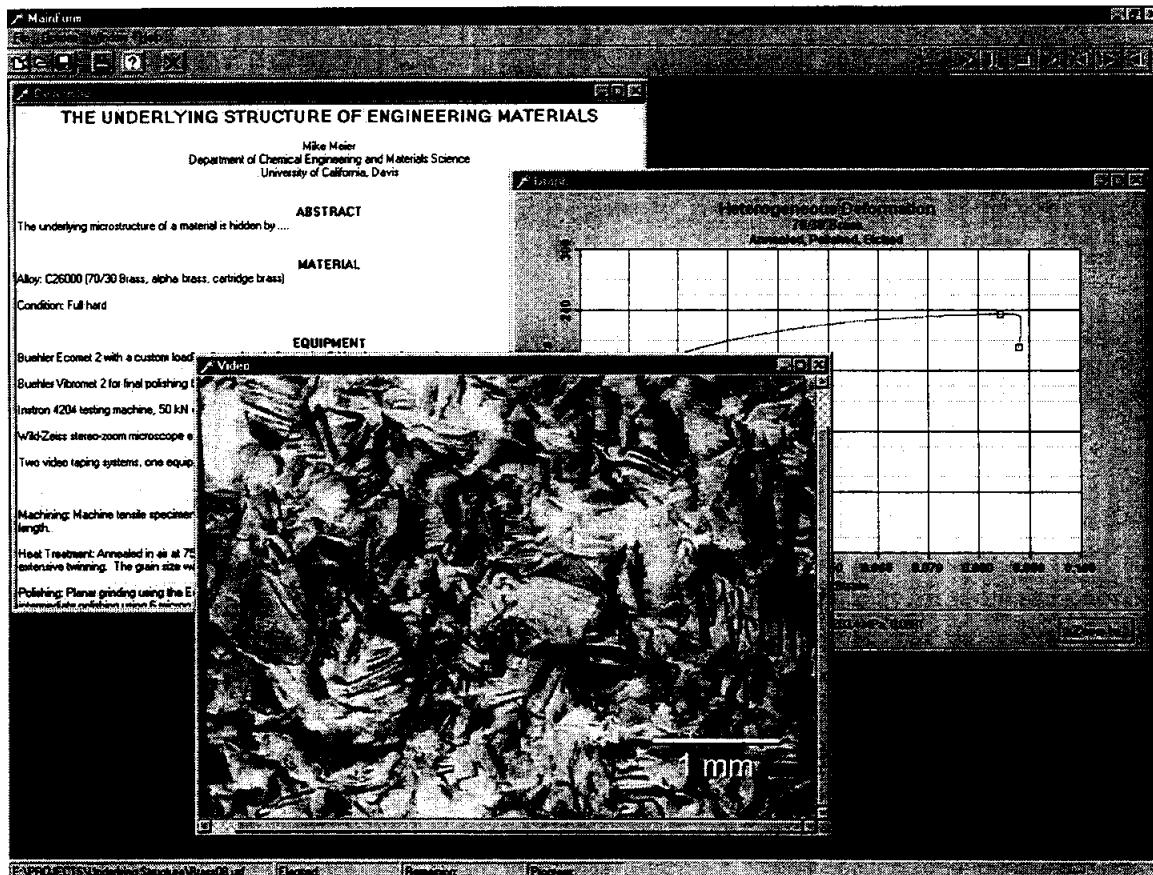


Figure 4 Screen image of the “Underlying Structures” program. (As you can see at the time of this writing the program is not quite finished.)

essential characteristic of crystalline materials, then the fourteen sets of points that repeat in space (Bravais lattices) and on to our systems for specifying the locations of lattice points, of directions in the lattice, the Miller indices of lattice planes, and eventually on to defects such as dislocations. Once the concept of the critical resolved shear stress is presented we must somehow relate this atomic-scale shear in the crystal to macroscopic stress and strain. At this point the student may or may not fully believe us so we show them Bragg’s bubble-raft video to convince them that dislocations really do glide, climb, etc. Next we can show them the videos described here so that they can see that while each grain deforms in a manner dictated its slip systems, orientation to the tensile axis and the confinement by neighboring grains and at the same time they can see how the aggregate behavior of these grains gives us the macroscopic mechanical properties we measure in the laboratory.

How We Have Used this Video

We have used this video in freshmen and sophomore introductory courses and we plan to try it out at the beginning of a junior level course on dislocation mechanics/mechanical properties. In the sophomore course our showing goes something like this:

- Show the students a shiny, polished piece of brass.
- Tell the students that it is crystalline but that they can’t see this without first etching the specimen.
- Show the students a picture of a polished and etched specimen or better yet show them a polished and

- etched metallography specimen. Describe the major features.
- Tell them that each grain has a different orientation and will slip in different directions with respect to the direction of loading, as if each grain were a randomly oriented stack of playing cards that will shear only in the plane of the cards.
 - Explain that deformation is isotropic on a microscopic scale, but because the grains are so small and so numerous it is, in the general case, macroscopically anisotropic.
 - Suggest that if the grains are large enough we should be able to see each one in action.
 - Describe what the video will show.
 - Show the video.
 - Discuss the video.

Showing the Video in Class

The two times we have shown these videos in class we ran them from the hard drive and projected it using an LCD projector. In both cases we showed the 640x480 format videos and the quality was very good.

The videos ran smoothly using the PC described above but if a slower PC is used and these videos do not run smoothly then one can use the 320x240 format videos. Also, since the CPU overhead required to operate the CD-ROM is about twice that of the hard drive we prefer to not run these videos from the CD-ROM.

Conclusion

Although these videos have been shown in only two classes the results have been positive. They have the gee-wiz element that helps make the subject interesting and it also gets the point(s) across.

These videos, data, programs and the still images can be downloaded from our web site at www.matsci.ucdavis.edu. Note that the 640x480 videos are 150+ MB files and the 320x240 videos are in the neighborhood of 40 MB. Download times may be impractical and besides you'll need to have a place to store these large files. If you would like to get a copy of these videos you can write or email the author to request copies of the CD-ROMs.

Acknowledgments

Funding for this project was provided by Teaching Resources Center and the Department of Chemical Engineering and Materials Science, both at the University of California, Davis, and by the authors.

Biographical Information

Michael L. Meier received his B.S. in Materials Engineering from North Carolina State University in 1979 and his M.S. (1986) and Ph.D. (1991) in Materials Science and Engineering from the University of California, Davis. After a two-year post-doctorate position at the Universität Erlangen-Nürnberg in Erlangen, Germany he returned to UC Davis where he has worked as a lecturer and as a manager for the department's teaching and research laboratories. One of his primary duties is developing and managing the materials science laboratory teaching program.

Karl H. Ewald received his B.S. in Mechanical Engineering/Materials Science and Engineering at UC Davis in 1990. He continued at UC Davis for his MS and PhD in Materials Science and Engineering in 1996 and 1998, respectively. He has been teaching various engineering and computer courses at Napa

Valley College since 1995 and spends his summers co-teaching computer arts courses for the California State Summer School for the Arts.

RENDERING ASBESTOS INTO A NON-REGULATED MATERIAL

Leon Petrakis

Energy Efficiency and Conservation Division
Department of Applied Science
Brookhaven National Laboratory
P. O. Box 5000
Upton, New York 11973-5000

Telephone: 516-344-3037
e-mail petrakis@bnl.gov



Leon Petrakis

Newsday

EDITORIALS

"Where there is no vision, the people perish."

RAYMOND A. JANSEN
Publisher, President and C.E.O.

ANTHONY MARRO, Editor
ROBERT F. BRANDT, Managing Editor
CHARLOTTE H. HALL, Managing Editor
HOWARD SCHNEIDER, Managing Editor

JAMES M. KLURFELD, Editor of the Editorial Page
CAROL R. RICHARDS, Deputy Editor of the Editorial Page

Brookhaven Breakthrough

By solving the asbestos disposal problem, the national lab proves again its value

Asbestos, once thought of as a wonder insulator, is also a deadly carcinogen, dangerous to disturb and costly to remove. That could change early in the new year as W.R. Grace & Co. moves a new product -- perfected at Long Island's Brookhaven National Laboratory -- to market. The breakthrough could not have come at a better time for the embattled federal facility. It adds new luster to the reputation of the laboratory, which -- despite recent attempts to transform it into a political football -- is a regional treasure.

The new product is a foam spray that leaches into asbestos and transforms it from dangerous dustiness into an inert, nonflammable, fireproof material. W.R. Grace researchers sought the collaboration with the national laboratory.

It's ironic: Sen. Alfonse D'Amato (R-N.Y.) and Rep. Michael Forbes (R-Quogue), demand closure of Brookhaven's nuclear reactor, contending it contaminates the environment. With this asbestos palliative, the lab has come up with the answer to one of the nation's

most serious environmental problems.

The controversy erupted last Jan when Suffolk health officials noted a plume of industrial solvents, not radioactive and necessarily from the laboratory, moving over an area of North Shirley. Faced with current charges of environmental laxity at the laboratory, the Department of Energy offered to pay to connect residents of the area to the public water system. When a plume of radioactive tritium was detected under the laboratory, Energy Secretary Federico Pena fired the laboratory's managers and later named a new management headed by physicist John Marburger, former president of the State University of New York at Stony Brook.

Sniffing demagogic opportunity, D'Amato and Forbes first demanded an investigation by the Energy Department's inspector general and then sought closure of the reactor.

Recently, addressing the reactor's future, Marburger said: "We need to convince ourselves we can run it without any more spills, accidents or danger to the environment." It should get the chance to do just that.

ETYMOLOGY

- ASBESTOS

- ἄσβεστος

- A = non

σβέννυμι = to extinguish

- "inextinguishable" (euphemistic)

- First mentioned by Aristotle's student Theophrastos in the text
ON STONES

ASBESTOS "MAGIC" MINERAL ARTICLES

- **Woven Articles** Cloaks, Tablecloths, Theater Curtains, Fireprotection Suits, Gloves, Shrouds
- **Insulation** Fireproofing of buildings and ships; thermal insulation of pipes
- **Automobiles** Brake and clutch linings
- **Filters** Cigarettes, Hospital ventilations, military gas masks, fruit juice & wine
- **Building materials** Roofing, Flooring (vinyl asbestos)
- **Military** Parachute flares, Bazooka shells and torpedos and surgical dressings
- **Miscellaneous** Buttons, telephones, toothpaste
- **"Asbestos Man"** Johns Mansville exhibit at the 1939 NY World's Fair

- **Peak Production** ~ 5×10^6 Metric tons/year

[90% Chrysotile]

- **Atmospheric Concentration**

- **10-100 ng/m³**
- **5×10^3 ng/m³ near factories**

- **Regulatory Agencies (EPA, OSHA)**

- **PEL 0.1 fiber/cc**
- **ACM ≥ 1 wt%**

AMPHIBOLES [SiO₄ Chain Structures]

- **AMOSITE**
 - **Brown Asbestos**
 - **Refractive Index 1.55 - 1.64**
 - **(Fe⁺² Mg)₇ Si₈ O₂₂ (OH)₂**

- **CROCIDOLITE**
 - **Blue Asbestos**
 - **Refractive Index 1.69 - 1.71**
 - **Na₂ Fe₂⁺³ (Fe⁺²Mg)₃ Si₈ O₂₂ (OH)₂**

SERPENTINES [Layered Silicate Structures]

- **CHRYSOTILE**
 - **White Asbestos**
 - **Refractive Index 1.50 - 1.57**
 - **Mg₃ (Si₂ O₅) (OH)₄**

	<u>SiO₂</u>	<u>FeO</u>	<u>MgO</u>
Chrysotile	39	~1	38
Amosite	49	41	7

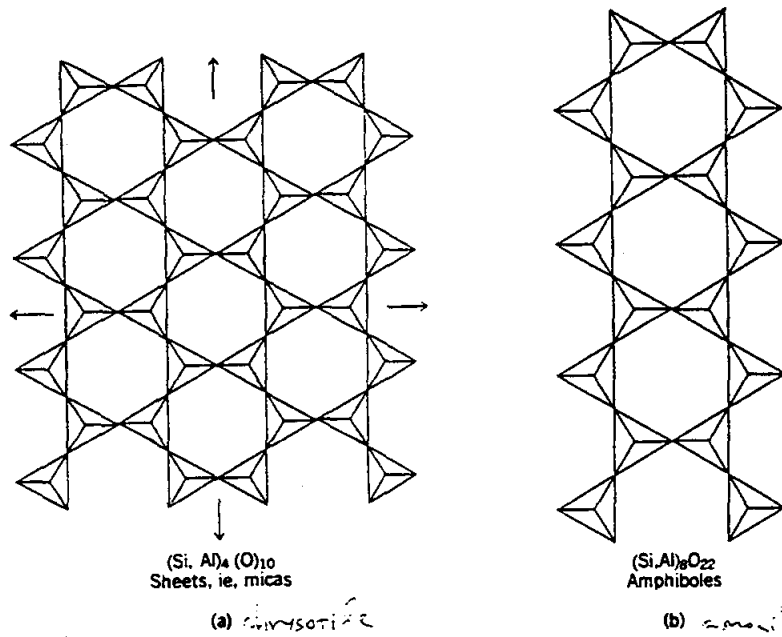


Fig. 3. Silicate backbones of chrysotile and amphiboles: (a) the sheet silicate structure of chrysotile, analogous to that of micas; (b) the double-chain silicate structure found in amphiboles (12). Courtesy of Oxford University Press.

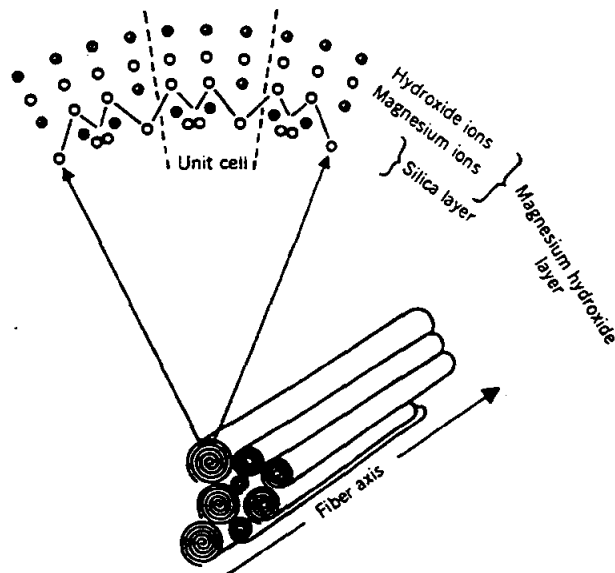
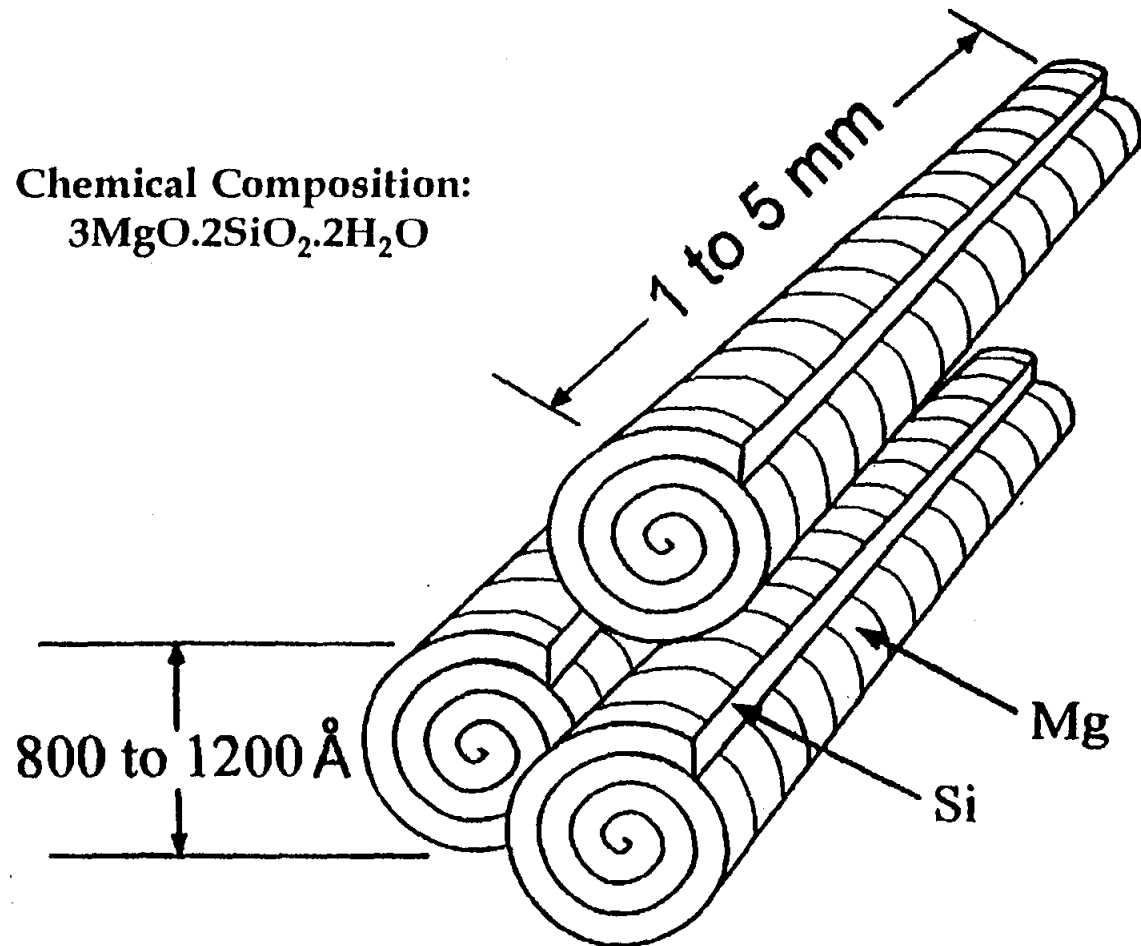


Fig. 4. Microscopic structure of chrysotile fibers (10). Reprinted with permission.

Kirk-Othmer

Asbestos Digestion Project

Chemical Composition:
 $3\text{MgO} \cdot 2\text{SiO}_2 \cdot 2\text{H}_2\text{O}$



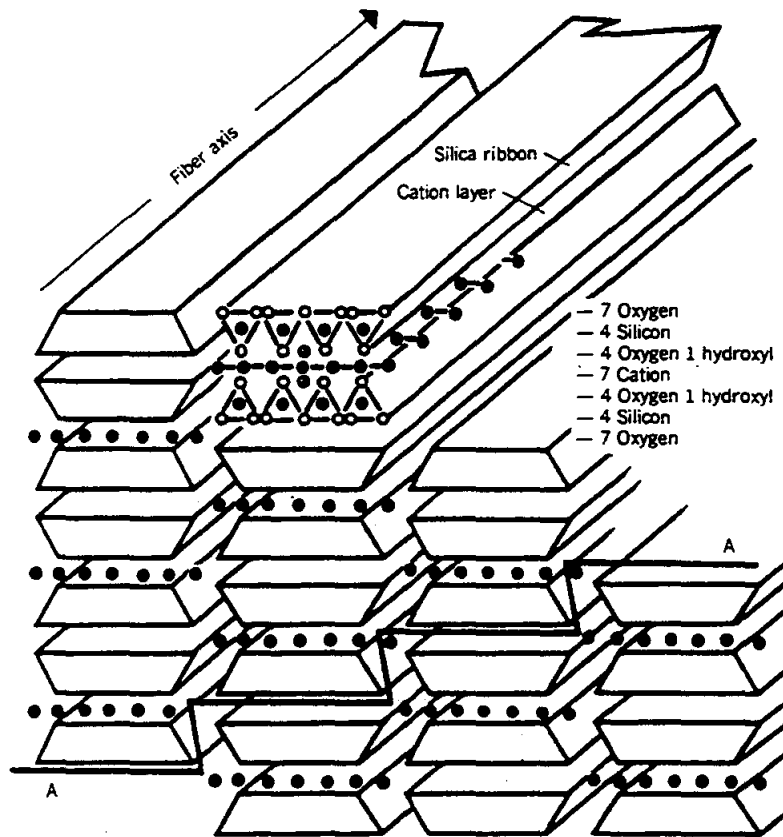


Fig. 5. Microscopic structure of amphibole fibers (10). Reprinted with permission.

Kirk-Othmer

HEALTH IMPLICATIONS

- 100 A.D. Pliny the Younger comments on diseases of asbestos workers
- 1890-1895 High death rates among French and English asbestos weaving/cording Asbestos workers
- 1927 Complete description of ASBESTOSIS (non-malignant scarring of lung tissue)
- 1936 Relationship between asbestos dust exposure and BRONCHIAL CARCINOMA.
- 1960 MESOTHELIOMA, exceptionally rare in the general public, mostly found among asbestos workers. Cancer of the linings of thoracic or more rarely of abdominal cavities (peritonium). Amphiboles seem to be implicated along with respirable (<1 nm diameter) fibers. Cigarette smoking synergism.
- A number of benign pleural changes (effusions, fibrosis)

SUPERACIDS

[Brönsted Acid + Fluorinated Lewis Acid]

[Acidity > 100% H_2SO_4]

<u>Acid</u>	<u>H_0</u>
H_2SO_4	-12 (Std)
$\text{H}_3\text{PO}_4 - \text{BF}_3$	-19
HSO_3F	
$\text{HSO}_3\text{F} - \text{SbF}_5$	
$\text{HF} - \text{SbF}_5$	

Patent 5,763,738 (6/9/98) (Sugama & Petrakis)

**Chemical Agents for Conversion of Chrysotile Asbestos
into Non-Hazardous Materials**

FSO₃H [Fluorosulfonic]

F P(O) (OH)₂ Fluorophosphoric

HBF₄ Fluoroboric

H₂Si F₆ Fluorosilicic

FCH₂CO OH Fluoroacidic

F C₆ H₄ CO OH Fluorobenzoic

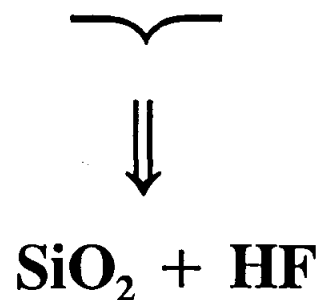
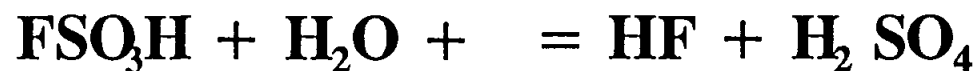
CF₃ SO₃ H

C₂ F₅ SO₃ H

C₅ F₁₁ SO₃ H

C₈ F₁₇ SO₃ H

CHRYSOTILE- FLUROSULFONIC ACID



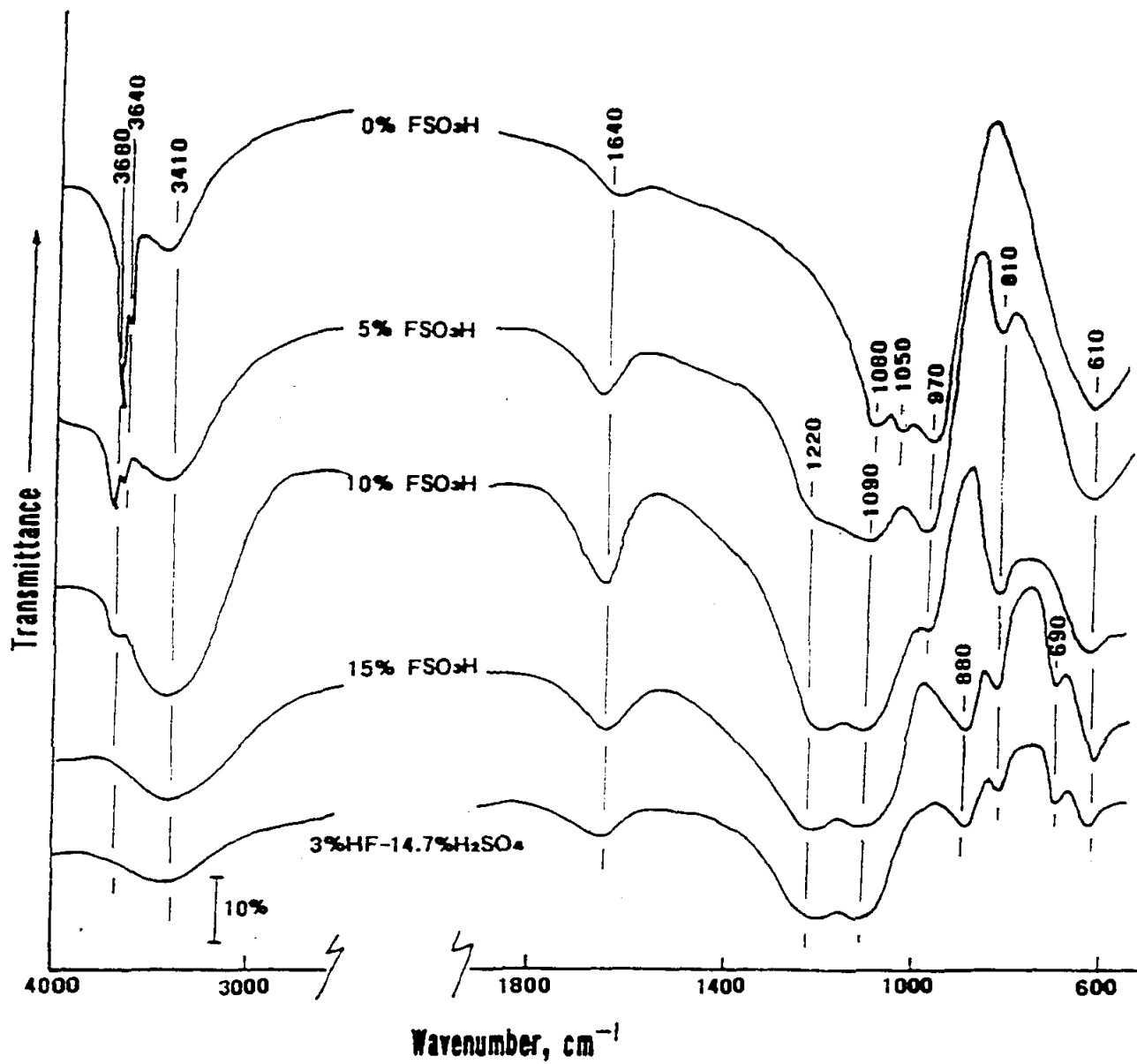


Figure 1. FT-IR absorption spectra for the 0, 5, 10, and 15 wt% FSO₃H-treated chrysotile asbestos samples, and the asbestos sample treated with a 3 wt% HF-14.7 wt% H₂SO₄ solution, corresponding to the equilibrium relation of 15 wt% FSO₃H in aqueous medium.

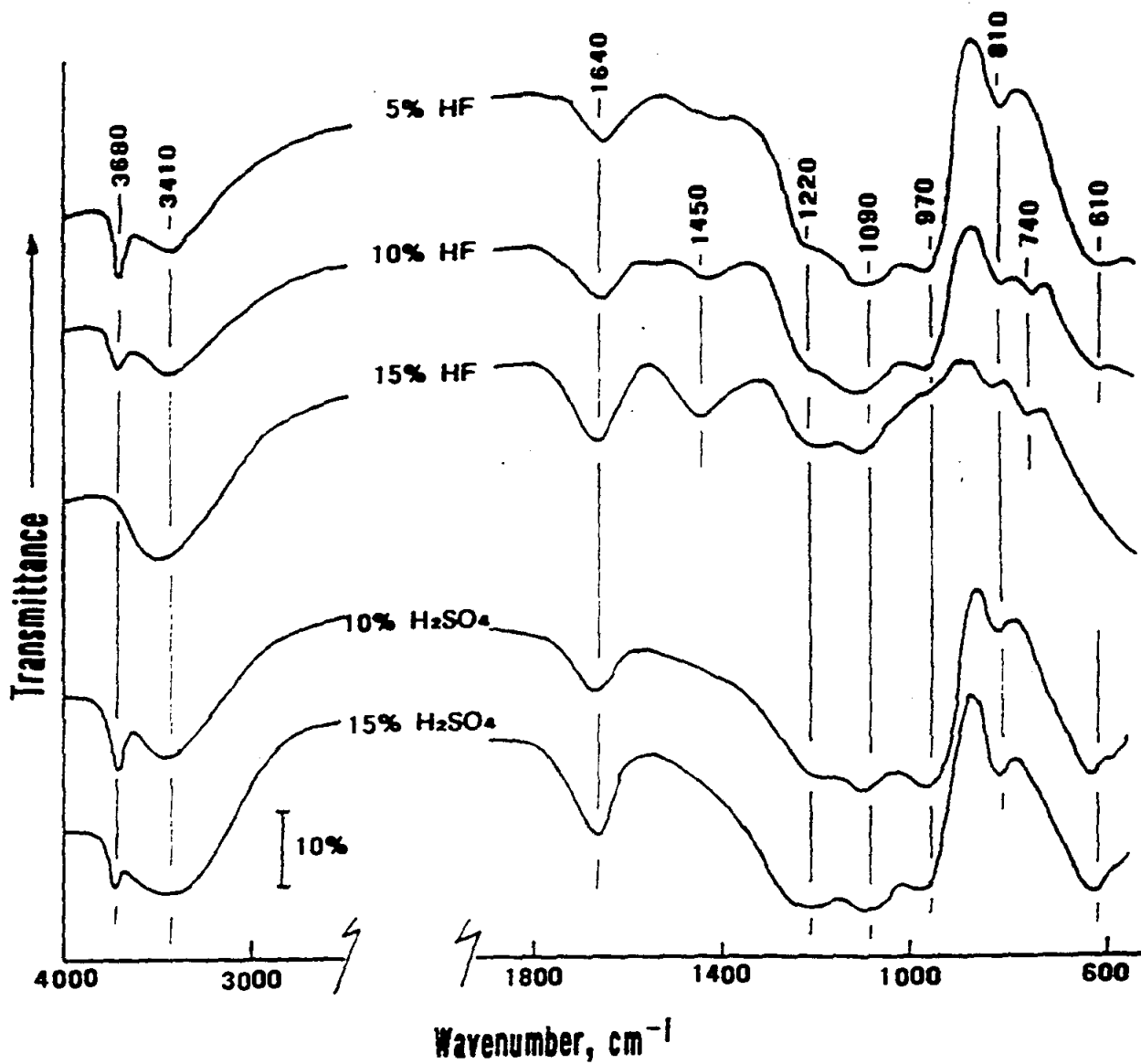


Figure 2. FT-IR spectra for 5, 10, and 15 wt% HF- and 10 and 15 wt% H₂SO₄-treated fibers.

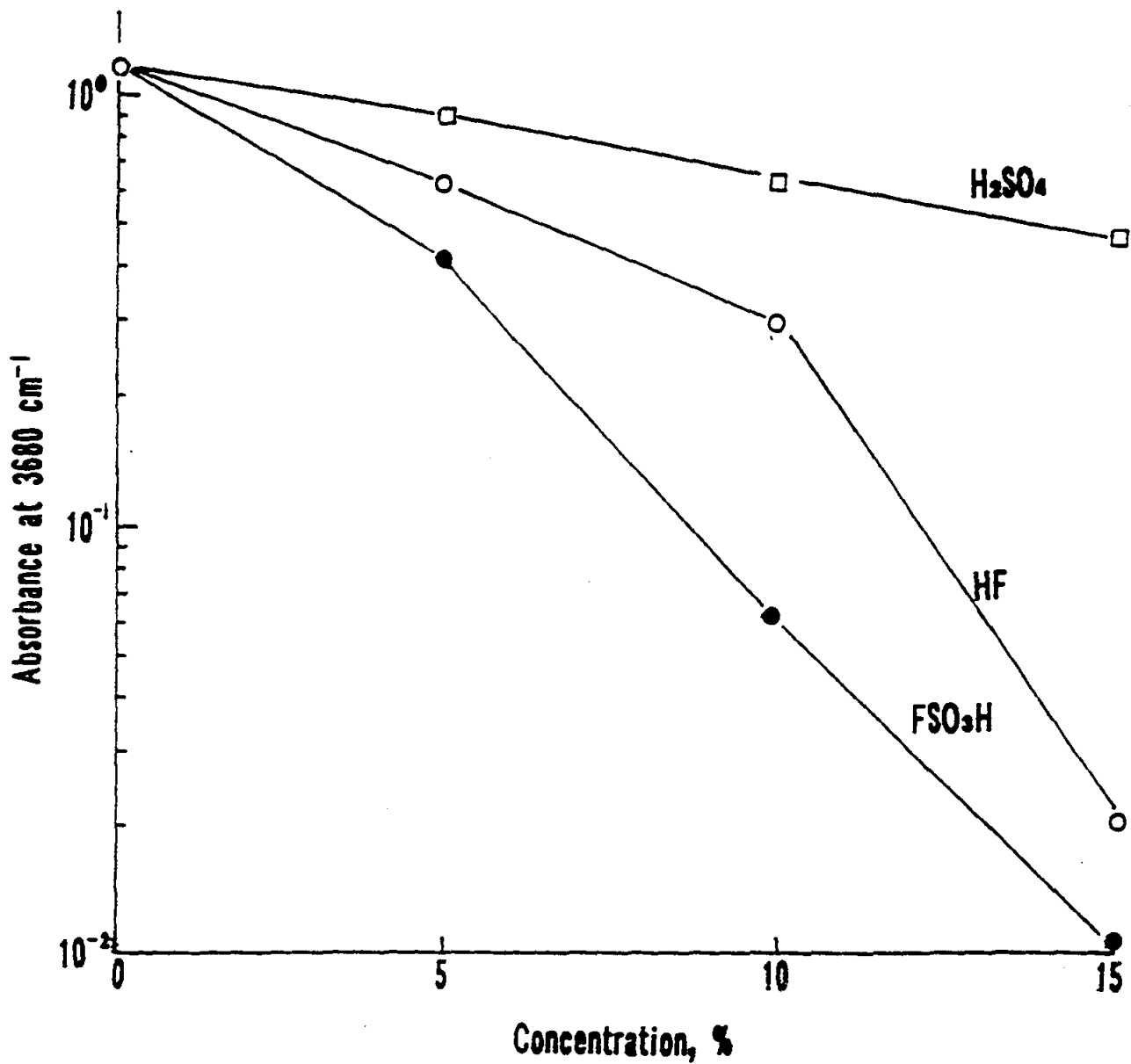


Figure 3. Changes in absorbance at 3680 cm^{-1} for the FSO_3H -, HF -, and H_2SO_4 -treated asbestos fibers as a function of concentration of chemical reagents.

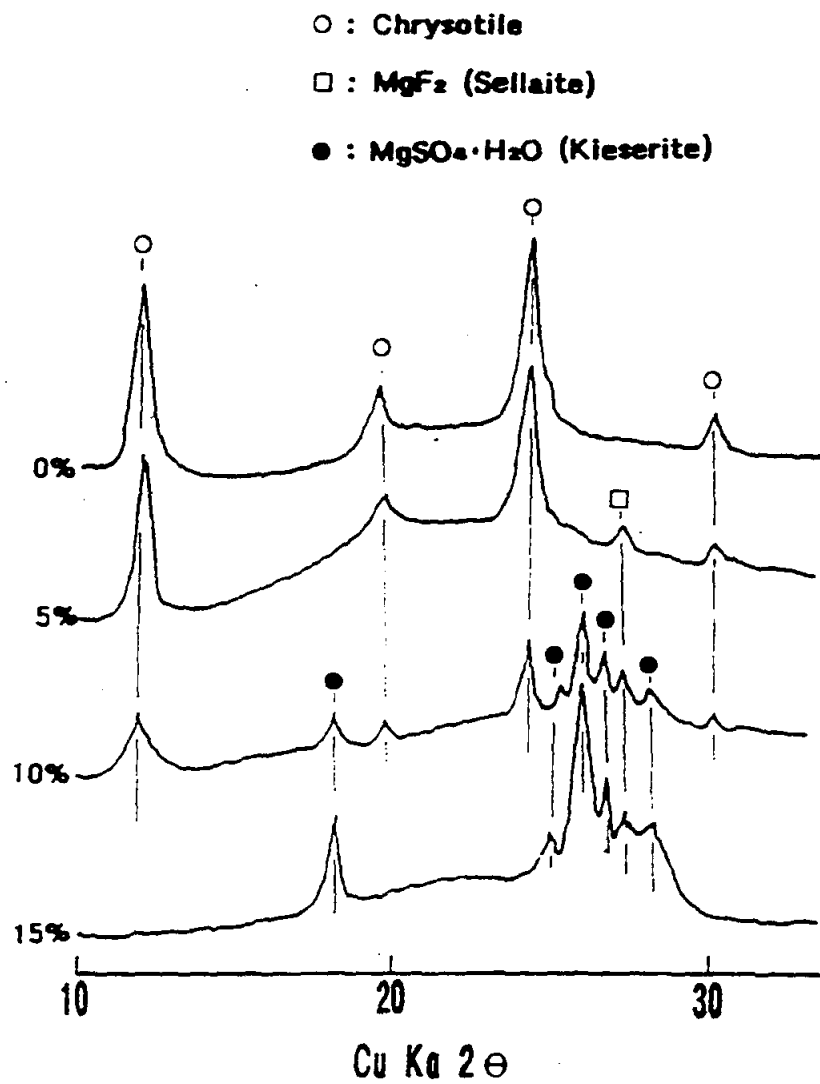


Figure 4. Comparison between XRD patterns for 0, 5, 10, and 15 wt% FSO₃H-treated chrysotile asbestos.

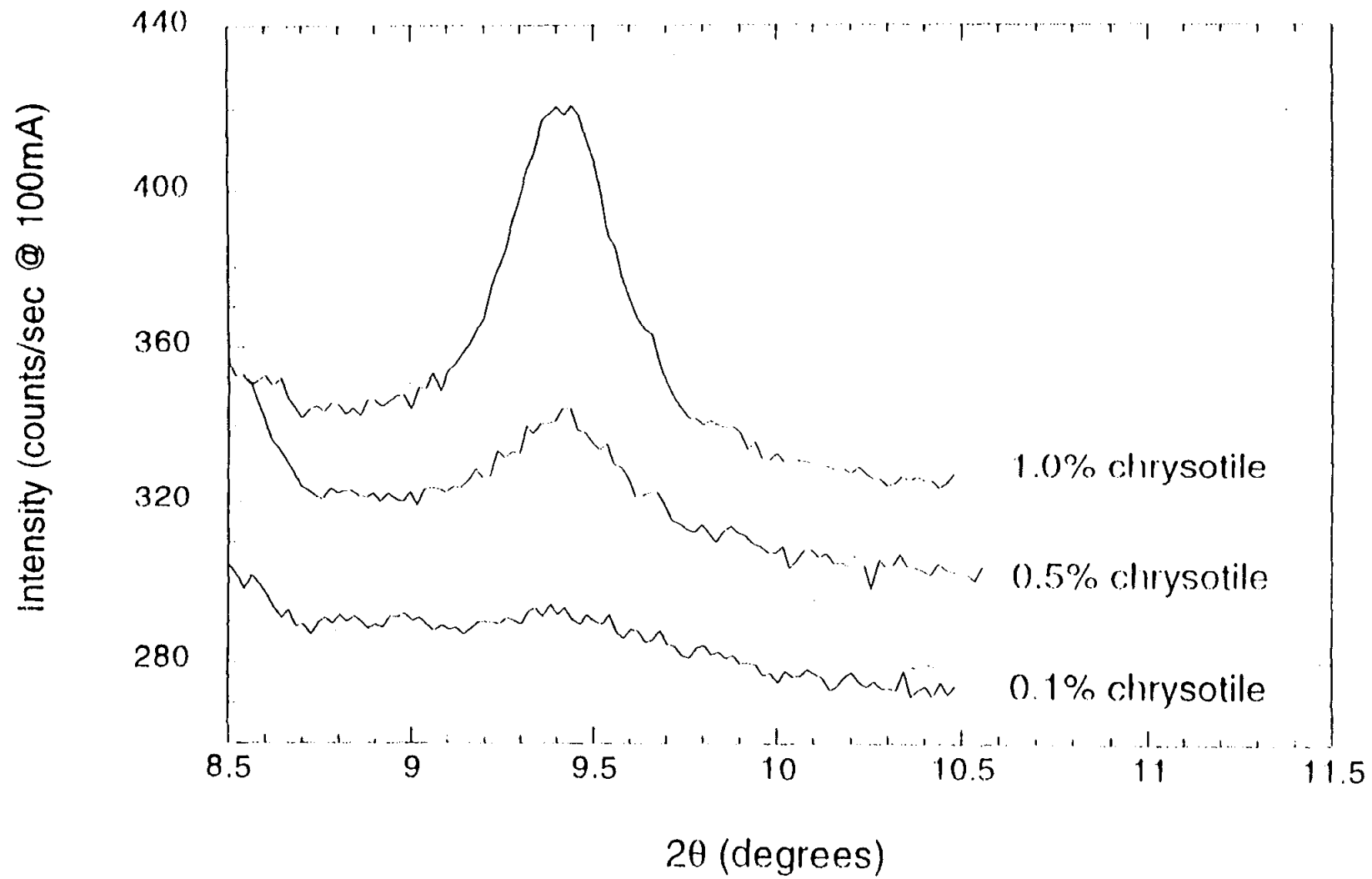


Figure 1.

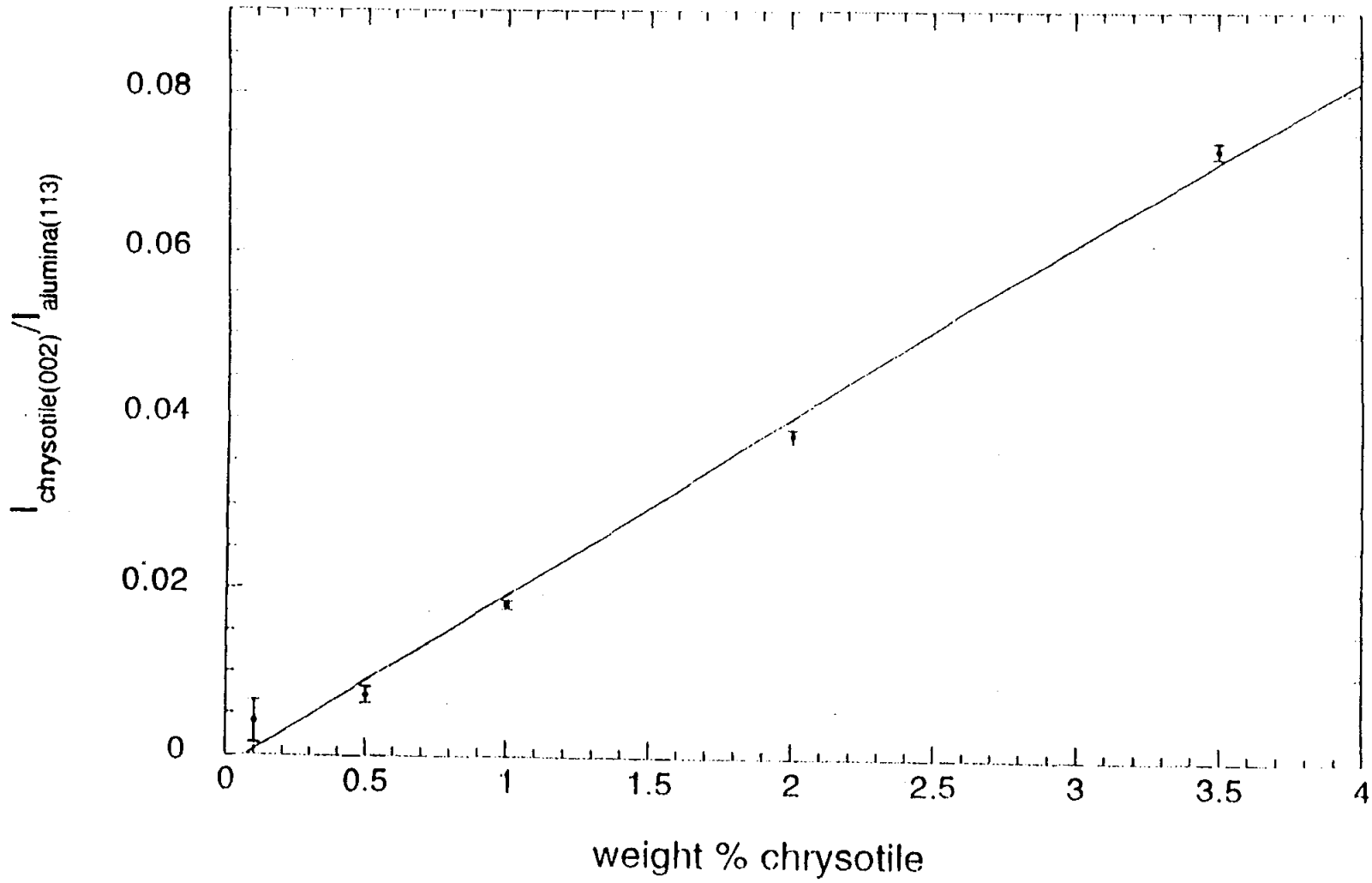


Figure 2.

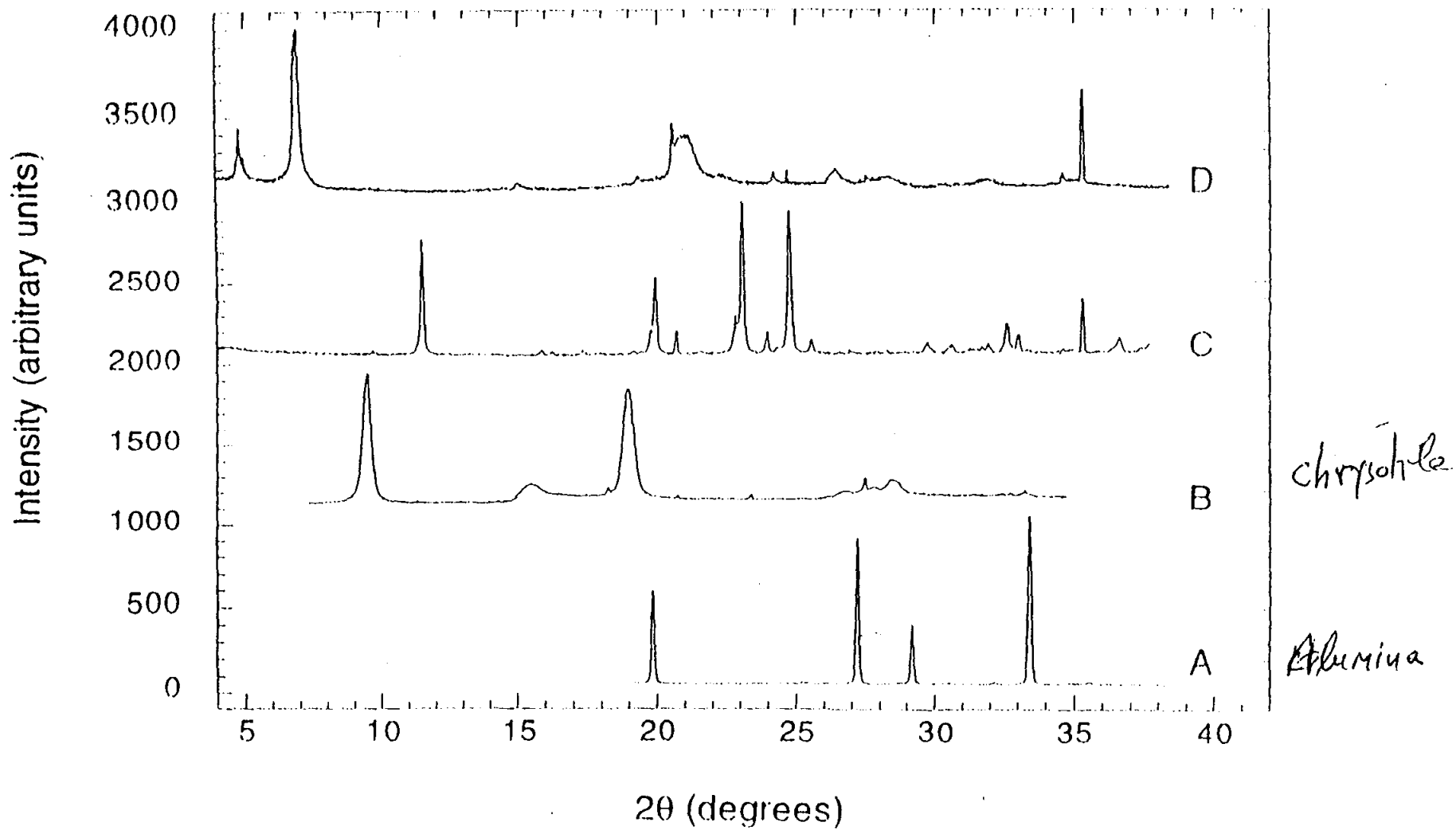
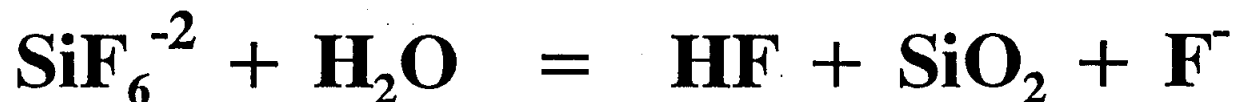
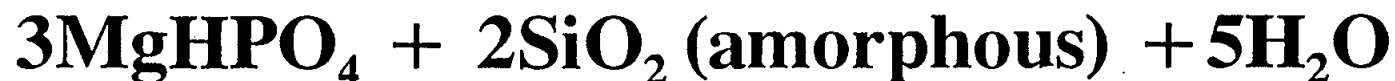


Figure 3.

DMA (H₃ PO₄ + Fluorosilicate)



PRODUCT COMPOSITION FOLLOWING APPLICATION OF DIGESTION AGENT

Component	Approximate wt. %
$\text{CaSO}_4 \cdot 2\text{H}_2\text{O}$ $\text{Ca}(\text{HPO}_4)_2 \cdot \text{H}_2\text{O}$ $\text{CaHPO}_4 \cdot 2\text{H}_2\text{O}$	55 - 65
$\text{MgHPO}_4 \cdot 7\text{H}_2\text{O}$	15 - 25
Vermiculite	10 - 20
$\text{CaF}_2, \text{AlPO}_4, \text{Fe}_2\text{O}_3$	< 5
Amorphous SiO_2	2 - 5
Chrysotile	< 1

The original product composition was approximately 63% Gypsum, 25% Vermiculite, and 12 % Chrysotile

AIR QUALITY MEASUREMENTS

	<u>TEST METHOD</u>	<u>OSHA PEL</u>	<u>ENGINEERING SCALE TESTS (ITE)</u>	<u>FIELD TEST</u>
Asbestos fibers released during digestion process	NIOSH 7400 (PCM)	0.1 f/cc	0-0.0052	0-0.035
	Impinger (PCM) FAM (PCM)		0.002-0.0078	
dry scraping of ACM	TEM N10SH 7402	0.1f/cc	0	
wet scraping of ACM	TEM N10SH 7402	0.1f/cc	0	
	N10SH 7400	0.1f/cc	0.0015-0.005	
	FAM	0.1f/cc	0.0002-0.0014	
Acid Droplets				
HF	N10SH 7903	3 ppm	<0.01-1.42	
H ₃ PO ₄	N10SH 7903	1 mg/m ³	<0.01-1.09	0-1.2
Acid Vapors				
HF	Diffusion Sensor	3 ppm	0.1-0.7	0-1.2
By-product Gases				
H ₂	Diffusion Sensor	LEL 4%	0-3% of LEL	
H ₂ S	Diffusion Sensor	10 ppm	0-0.7	

XRD ANALYSES OF ITF SAMPLES

- 34 PANELS AND BEAMS
- 9 CORES FROM EACH PANEL AND BEAM
- 3 SECTIONS (DEPTH) FROM EACH CORE
- DUPLICATE ANALYSES -BNL, WRGRACE
- LABORATORY XRD, PLM, NSLS

***ALL SAMPLES* FOR WHICH THE APPLICATION PROTOCOL WAS FOLLOWED SHOWED CHRYSOTILE AFTER TREATMENT TO BE < 1 WT % (VS. 12.7 % ORIGINALLY PRESENT)**

NOTE: REGULATORY AGENCIES CONSIDER ANYTHING BELOW 1% AS NON- ACM (ASBESTOS CONTAINING MATERIAL)

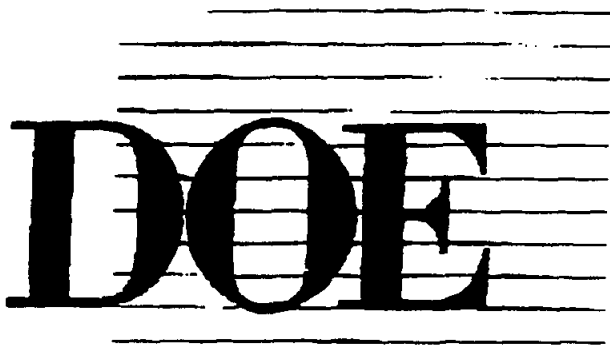
**ANOTHER LESSON LEARNED: CAREFULLY STRUCTURED
COLLABORATIONS DO WORK...**

- **PEER-REVIEWED PAPERS AND PRESENTATIONS**
- **TRAINING OF POST-DOCS**
- **UTILIZATION OF LARGE FACILITIES**
- **PATENTS**
- **SAFETY AND REGULATORY AGENCIES EARLY INPUTS A BIG PLUS**
- **COMMERCIAL PROCESS**
- **POSITIVE PUBLICITY**
- **.....**

STATUS

- ***Chrysotile (BNL, WRGRACE Patents)***
 - ***BNL Large Scale Demos in DOE and Federal Facilities***
 - ***WRGrace Commercialization in the Private Sector***

- ***Amosite (BNL Patents)***
 - ***US Navy, DOE, EPA, MarketSpan***



DOE

NEWS

NEWS MEDIA CONTACT:
Kara Villamil, 516/344-2345

FOR IMMEDIATE RELEASE
December 10, 1997

"Brookhaven Laboratory scientists have helped create an innovative, safe solution to a tough problem that affects people around the country. This is just one example of many achievements at Brookhaven, known for its contributions in medicine, basic research, energy and environmental science. Partnerships between Department of Energy laboratories and private industry consistently reap tangible rewards. In this case, we will make a difference in safely removing asbestos from schools, houses, offices and other buildings," said Secretary of Energy Federico Peña.

-DOE-

ACKNOWLEDGMENTS

Collaborators

Brookhaven National Laboratory

M. Allan
N. Carciello
D. Elling
C. Eylem
A. Goland
J. Hriljac
J. Hurst
L. Kukacka
K. Lynn
L. Petrakis
W. Reams
R. Sabatini
T. Sugama
R. Webster
Q. Zhu

W.R.Grace & Co

J. Block
D. Brewer
L. Ciesluk
L. Dolhert
M. Hager
L. Hegedus
N. Krupkin
R. Milton
H. Mirano
D. Myers
R. Hu

ACKNOWLEDGMENTS-SUPPORT

The Asbestos Project was a success due also to the wonderful cooperation with, and support from others than the researchers involved, inter alia, The BNL Directorate, Department of Applied Science, The Light Source, Physics, Medical, ES&H, Technology Transfer, DOE Brookhaven Office and Headquarters, EPA and OSHA.

- The Director (**Nick Samios**) personally and others in the Directorate (**Marty Blume, Peter Bond, Mike Bebon**) for general encouragement but also specific support that included key telephone calls, LDRD support, and the availability of the Inhalation Toxicology Facility in the Medical Department

-ES&H support and guidance with environmental and health issues and permits (**J. Williams, G. Adams, R. Selvey, P. Sullivan**); and the DAS Chairman (**J. Davenport**), safety personnel (**P. Carr, C.R. Krishna, J. Hurst**), Administrative staff, and the secretary to the project, **Gail Brown**.

- Plant Engineering, especially **R. Yadav**

-Technology Transfer Office (**P. Bogosian, M. Furey**)

-**D. Joel** (Medical Department); **D. Cox** (Physics) for X7A Beamline

-Public Relations (**Kara Villamil, Diane Greenberg**)

-DOE Brookhaven Area office staff; and at HQ's **A. Clafin** (ER), and **C. Frank, G. Boyd, J. Hyde** (EM)

- US EPA (**Tom Ripp**)

- US OSHA (**Dan Crane**)

EDUCATIONAL PROGRAMS AT BNL AND OTHER DOE LABS

Karl J. Swyler

Office of Educational Programs
Science Education Center
Brookhaven National Laboratory
Associated Universities, Inc.
P. O. Box 5000
Upton, New York 11973-5000

Telephone: 516-344-7171
e-mail swyler@bni.gov



Karl J. Swyler

EDUCATIONAL PROGRAMS AT BNL AND OTHER US DOE LABORATORIES



- *greater access to information than ever before*
- *more ways to use it than ever before*
- *which ways are best for education?*

Where will the new jobs be on LI, for example?

- *biotechnology/bioengineering*
- *emerging electronics*
- *graphic communications*
- *medical imaging/health information systems*
- *computer software*

WHAT WILL STUDENTS NEED TO KNOW?

1. Content

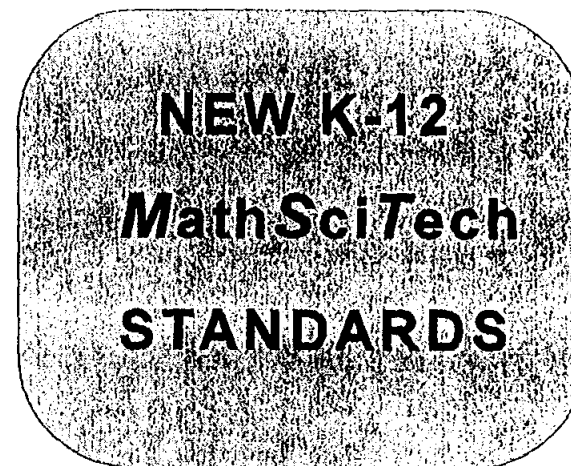
- *computer science*
- *life science and physical science*
- *engineering*

2. Process

- *how to think*
- *how to learn*
- *performance-based standards*

3. Motivation/Career Preparation

- *what's out there*
- *what's required to get there*



HOW CAN WE HELP THEM LEARN ALL THIS?

1. SHARE OUR INFORMATION RESOURCES: generate interest and support learning in state-of-the-art MST

2. ADD AN 'EXPERIENTIAL' DIMENSION to the learning process, reflecting actual practice.

3. SUPPORT CAREER 'PIPELINE' PROGRAMS, to help students identify & achieve career goals on LI

WHAT HAVE WE BEEN DOING?

1. Sharing Our Information Resources; Motivation

- **Nuclear Chemistry Summer School**
- **HS Teacher In-Service Course**
- **Introduction to Computers (5-6)**

- **BNL Science Museum Tour Programs**
- **Museum School Outreach Programs**
- **Museum Discovery Visits**

- ***Ad hoc* Internet-based efforts, mentoring**
- **School District Workshops**

2. Experiential Programs

- **Undergraduate Research Internships**
- **COMMUNITY COLLEGE TA PROGRAM (!)**

- **Teacher Research Associates (HS)**
- **NSF MSTe Program (elem. with USB, Hofstra)**

- **Community Summer Science HS Interns**
- **Minority HS Summer Apprenticeships**

- **National Model Bridge Contest**
- **Middle School MAGLEV Contest**
- **Elementary School Science Fair**

3. Support for Educational/Career Pipelines

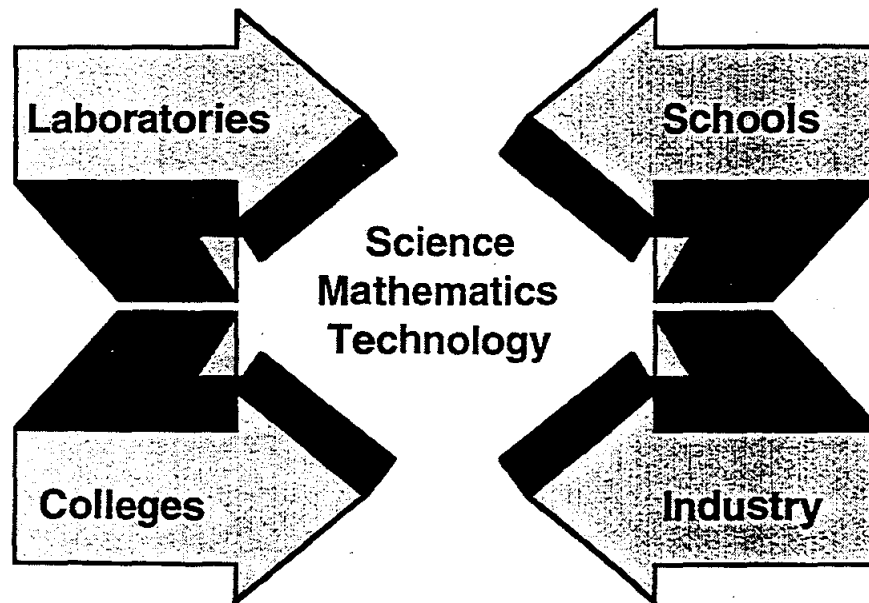
- **MST-1 Conference (Technology Education)**
- **LAB FOR USE Conference (Teacher Preparation)**

- **COLLABORATION IN NSF AMP PROGRAMS**
- **Internships/Traineeships through Diversity Office**

- **Brookhaven Women in Science (BWIS) Programs**
- **Collaboration in WISE Program**

- **Career Day Programs and Materials Development**
- **Collaboration in Project Vanguard.**

Local Alliance Building for Urban Science Education



 **Brookhaven National Laboratory, New York University** 
and Associated Universities, Inc.

MST I

PROCEEDINGS

**of a conference on the integration
of
Mathematics, Science and Technology
in
precollege education.**

**BROOKHAVEN NATIONAL LABORATORY
UPTON, NEW YORK
JUNE 5-6, 1995**

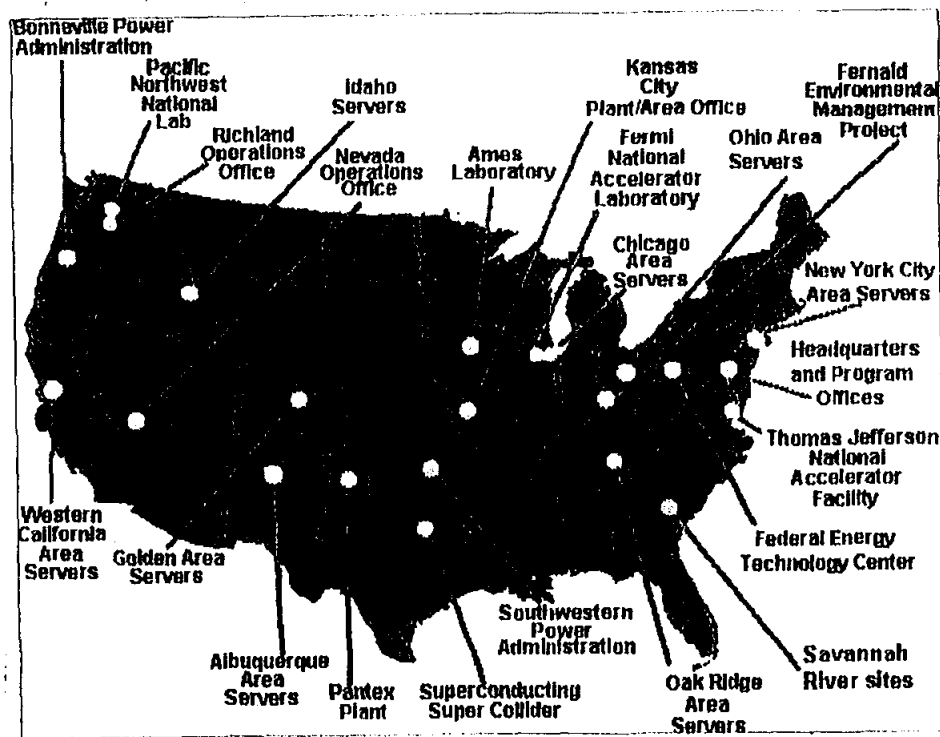
**SUPPORT FOR THIS CONFERENCE WAS PROVIDED BY
THE U. S. DEPARTMENT OF ENERGY, OFFICE OF SCIENCE EDUCATION,
AND BY ASSOCIATED UNIVERSITIES, INC.**

BNL Face-to-Face Community Involvement FY 1998

Program	Number of Participants
General Public	
Fairs & Festivals	5,513
Civic groups/community organizations (20/month, avg. 20 participants ea.)	4,800
Summer Sundays (8 weeks)	3,256
VIP Tours	245
Special Museum tours (adults)	420
College Level	
College Tours	1,236
Undergraduate Summer and Semester Students	76
Community College Semester and Mini-Semester	28
Nuclear Chemistry Summer School	12
High School Level	
High School Tours	547
Bridge Contest	250
Whiz-Bang Science Show (BOCES)	50
Community Summer Science/Academic Year Internships	34
Women in Science & Engineering	30
Minority Apprenticeships	29
Teacher Research Associates (summer)	2
Middle School Level	
Magnets to Go	7,014
Investigations in Science (Science Museum)	4,751
Maglev Contest	275
Whiz Bang Science Show	104
School Career Days	50
Elementary School Level	
Discovery Tours (Science Museum)	4,491
Discoveries to Go	821
Science Fair	760 students/ 1,240 visitors
Science Fair Workshops (parents/teachers)	100
Science Exploration Days	75
NSF Math, Science & Technology Program (teachers)	63
NSF National Teacher Enhancement Internships	6
Teachers - All Levels	
Misc. Teacher workshops and seminars	404
Mid-East Suffolk Teacher Center workshops	50
TOTAL	36,732

WHAT ARE OTHER DOE LABS DOING?

PROGRAMS SIMILAR TO THOSE DESCRIBED ARE CARRIED OUT ACROSS THE COUNTRY, as part of a coordinated national effort:



www.sandia.gov/ESTEEM/home.html

Brookhaven National Laboratory
Brookhaven Science Associates

ESTEEM

Education in Science, Technology, Energy, Engineering, and Math



"We have to do everything we can to make technology literacy a reality for every child in America"

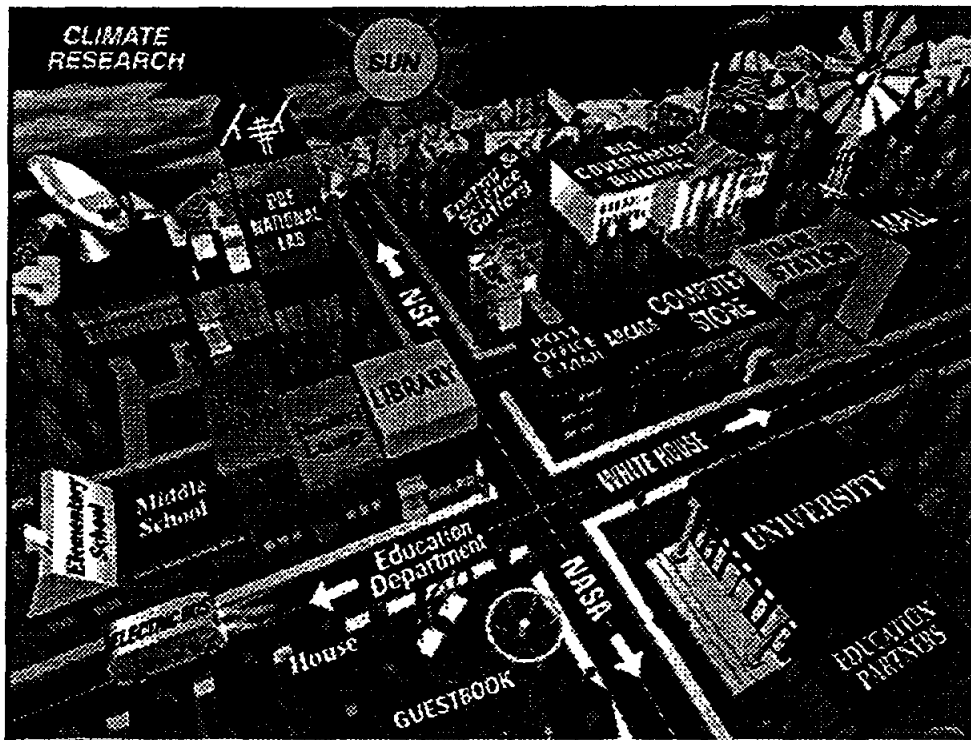
U.S. President, Bill Clinton



"...we must have a population that is able and learned in the new technologies and industries..."

DOE Secretary, Bill Richardson

The Energy Department's Education Community



<u>Arcade</u>	<u>Education Partners</u>	<u>High School</u>	<u>Post Office E-Mail</u>
<u>Climate Research</u>	<u>Electric Bus (Transportation)</u>	<u>House</u>	<u>Sun</u>
<u>Computer Store</u>	<u>Elementary School</u>	<u>Library</u>	<u>Teachers' Lounge</u>
<u>DOE Government Building</u>	<u>Energy & Science Gallery</u>	<u>Mall</u>	<u>University</u>
<u>DOE National Lab</u>	<u>Gas Station</u>	<u>Middle School</u>	<u>Windmill</u>

[| Back to top of page](#) | [| ESTEEM Contacts](#) | [| DOE Home Page](#) | [| Related Sites](#) |

Please visit and sign our GUESTBOOK.

Send comments to Feedback
Last modified: October 13, 1998

Brookhaven National Laboratory



Office of Educational Programs

- Educational Missions
- Educational Programs
- Calendar
- MSTe
- National Educator's Workshop
N E W: Update 98
- Science Ed Cen
- Undergraduate Research Oppor
(ERULF)
- Educator Resources
- Electronic HotLine

Bookmark this site NOW!!

Please Note: This site is very dynamic! Constant updates and revisions make this an interactive site that will be of tremendous value to you as an educator. Visit us often for lots of great stuff!

This site is designed and maintained by Eric Cohen from Wantagh High School Last update: 29 October 1998

EXAMPLE - THE ERULF PROGRAM

**ERULF - ENERGY RESEARCH UNDERGRADUATE
LABORATORY FELLOWSHIPS - NATIONAL PROGRAM.**

**ERULF UNDERGRADUATES PARTICIPATE IN RESEARCH
PROGRAMS AT ONE OF NINE DOE LABORATORIES.**

**TEN WEEK SUMMER OR SIXTEEN WEEK ACADEMIC
SEMESTER APPOINTMENTS. STIPEND AND TRAVEL AND
HOUSING ALLOWANCE PROVIDED.**

www.orau.gov/orise/edu/uggrad/srpdoe1.htm

*Brookhaven National Laboratory
Brookhaven Science Associate*

Energy Research Undergraduate Laboratory Fellowships

Administered by the Oak Ridge Institute for Science and Education

Program description: opportunities to participate in research relating to energy production, use, conservation, and societal implications

Disciplines: engineering, life sciences, mathematics, physical sciences, computer science

Eligibility/participants: undergraduate students; U.S. citizens or permanent residents

Location(s): Ames Laboratory (Ames, Iowa); Argonne National Laboratory (Argonne, Ill.); Brookhaven National Laboratory (Upton, N.Y.); Ernest Orlando Lawrence Berkeley National Laboratory (Berkeley, Calif.); Fermi National Accelerator Laboratory (Batavia, Ill.); National Renewable Energy Laboratory (Golden, Colo.); Oak Ridge National Laboratory (Oak Ridge, Tenn.); Pacific Northwest National Laboratory (Richland, Wash.); Princeton Plasma Physics Laboratory (Princeton, N.J.); Stanford Linear Accelerator Center (Stanford, Calif.); Thomas Jefferson National Accelerator Laboratory (Newport News, Va.)

Duration: 10-week summer appointments or 16-week semester appointments

Deadline(s): contact Program Manager Linda Holmes at 423-576-3192 or holmesl@ornl.gov

Awards made: number varies

Benefits: weekly stipend of \$300; limited travel reimbursement (round-trip transportation expenses between facility and home or campus)

Funding source(s): U.S. Department of Energy, Office of Energy Research

For more information and an on-line application, visit How to Apply (http://www.ornl.gov/doe_erulf/).



[How to Apply](#) || [Other Educational Opportunities](#) || [ORISE Home Page](#)



Copyright 1998, Oak Ridge Associated Universities

Updated 8/18/98

**1997 Fall Semester Student Research Presentations
Brookhaven National Laboratory
Science Education Center
December 4, 1997**

9:30 a.m.

Plasma Windows

Chris S. Castle

California Polytechnic Institute and
Biology Department, Brookhaven National Laboratory

10:00 a.m.

Specificity of Electron Donors for Plant Fatty Acid Desaturases

Alexis T. Ellicott

University of Illinois and
Biology Department, Brookhaven National Laboratory

10:30 a.m.

Inventory Data Base for Scientific Information Systems Group

David Olivares

State University of New York at Stony Brook and
Department of Applied Science, Brookhaven National Laboratory

11:00 a.m.

An Evaluation of Noise Reduction Filters for Image Processing

Alexandra G. Haines

University of San Francisco and
Computing and Communications Division, Brookhaven National Laboratory

LIQUID CRYSTAL p-AZOXYANISOLE IN MICROWAVE FIELD

J. N. Dahiya

Physics Department
Southeast Missouri State University
One University Plaza
MS 6600
Cape Girardeau, Missouri 63701

Telephone: 573-651-2390
e-mail dahiya@physics.semo.edu



J. N. Dahiya

Liquid Crystal p-Azoxyanisole in Microwave Field

Jai N. Dahiya
Physics Department
Southeast Missouri State University
Cape Girardeau, MO 63701
e-mail:dahiya@physics.semo.edu

Key Words

Liquid Crystals, Dielectric Relaxation, Frequency Shift, Q-Change, Microwave Resonant Cavity, Field Perturbation, Relaxation Times.

Summary

A cylindrical microwave resonant cavity in the TE_{011} mode is used to study the microwave dielectric response of liquid crystal p-azoxyanisole at microwave frequencies. The dielectric behavior of this liquid crystal is studied as a function of frequency from 8.0 GHz to 10.2 GHz. Several undergraduate students were involved in the design of the microwave spectrometer. This is a part of the undergraduate research courses that the students are required to take at the physics department at Southeast Missouri State University provided they maintain a certain GPA in their physics courses. Students were involved to design the amplifier, marker shaper circuit, the computer interface, and the heating and cooling circuit. The real and imaginary parts of the complex dielectric constant of this liquid crystal were calculated by using Slater's Perturbation Equations and the relaxation time was calculated using Debye's Equation for polar molecules.

Introduction

Liquid crystal materials generally have several common characteristics and one of the very important of these is in terms of having strong dipoles and/or easily polarizable. Another very important property of liquid crystals is the tendency of the molecules known mesogens to point along a common axis, called the director. This is opposite to the behavior of molecules in the liquid phase, which have no intrinsic order. But on the other hand, in the solid state the molecules are highly ordered and do not have much translational freedom. The liquid crystalline phase is between the liquid and the solid phase. It is a distinct phase that is observed between the crystalline and isotropic states. There are four different types of liquid crystal states: nematic, smectic, cholesteric, and columnar phases. These phases depend upon the amount of order in the material. The response of liquid crystals to an external electric field is the major characteristic of these materials that is used in their applications in industries. Because of the permanent dipoles, these materials align along an external field and this behavior is further affected by the frequency of the applied field. At lower frequencies the dipoles can follow the orientations of the applied field without any lagging behind. But at high frequencies such as microwaves, there is a time lag and only a certain fraction of these dipoles can follow the field and that basically determines the electrical characteristic of that material. Even if a molecule does not have permanent dipoles it can still be influenced by the applied field because of the induced electric dipoles. The main purpose of this

experiment is to study this behavior of liquid crystal p-azoxyanisole. This liquid crystal is of the nematic type and it is characterized by molecules that have no positional order but tend to point in the same direction.

Wave guide techniques were used in 1960's and 1970's to study the dielectric response of materials as a function of frequency and temperature. This technique was an approximate method to calculate the dielectric response because of nonuniform perturbation of the microwave field. It was also very difficult to maintain a certain temperature of the material under study. A microwave resonant cavity proves to be a very important tool for the dielectric relaxation studies. Complex electric permittivity as well as permeability can be studied by using such a cavity in the TE or TM modes. A similar cavity has been used by a number of investigators for dielectric relaxation studies of a number of materials (Ref 1-5). In this experiment a cylindrical microwave resonant cavity in the TE₀₁₁ mode is used as a probe to study the dielectric behavior of p-azoxyanisole. Dielectric response of this liquid crystal is studied as a function of frequency. A very effective thermal bath is used to control the temperature of the material under study. The main aim of this experiment is to establish a technique for the dielectric relaxation studies and to involve undergraduate students in different parts of the experiment.

Experimental Design and Results

A microwave spectrometer is designed by assembling a number of electronic components together as shown in Figure 1. A Varian klystron is powered by a HP power supply to produce frequencies between 8.0-12 GHz. The signal is transmitted through a waveguide to an attenuator that is used to adjust the microwave power. The signal then goes to the directional coupler that divides it in two parts, a part of which goes to the microwave resonant cavity and another part is mixed with a signal from a crystal oscillator to produce the markers using the technique of frequency multiplication. A radio receiver detects the difference of frequency between the signals coming from the klystron and the crystal oscillator and produces a series of marker signals. These markers are at a fixed frequency interval. The part of the signal that goes to the cavity is reflected and the differential display of this signal after modulation is in the form of a butterfly. This signal is detected by a microwave diode installed in to a detector. The signal is then amplified and displayed on an oscilloscope. A wavemeter is used to measure the exact frequency of the klystron. The markers are used to find the frequency shifts and the Q-changes of the microwave resonant signal coming out of the cavity. The field patterns of the microwave resonant cavity are shown in Figure 2. It can be seen from these patterns that as the sample under study is introduced in to the cavity it perturbs the electric field of the cavity and as a result of that resonant frequency shifts and the Q of the cavity changes.

The frequency shifts and the Q changes are related to the real and imaginary parts of the complex permittivity through Slater's Perturbation Equations # 1 and 2 as shown below (Ref. 6).

$$\frac{\Delta f}{f_0} = \frac{\epsilon' - 1}{2} \frac{\int \vec{E}_s \cdot \vec{E} dv}{\int \vec{E} \cdot \vec{E}_a dV} \quad (1)$$

$$\Delta \left(\frac{1}{Q} \right) = \epsilon'' \frac{\int \vec{E}_s \cdot \vec{E} dv}{\int \vec{E} \cdot \vec{E}_a dV} \quad (2)$$

Where E_a is the applied field, E_s is the field of the sample, and E is the total field of the system, Δf and $\Delta\left(\frac{1}{Q}\right)$ are the frequency shifts and the Q changes of the microwave resonant signal, ϵ' and ϵ'' are the real and imaginary parts of the complex permittivity.

The Q change is further related to the width of the signal as shown in Equation # 3 where square root of 3 is introduced because of the modulation correction. The value of the relaxation time is calculated using Debye's Equation # 4 (Ref. 7) where ϵ_s is the value of the static permittivity at room temperature, and τ is the relaxation time.

$$\Delta\left(\frac{1}{Q}\right) = \frac{\sqrt{3} \Delta W}{f_o} \quad (3)$$

$$\frac{\epsilon_s - \epsilon'}{\epsilon''} = \omega\tau \quad (4)$$

The sample under study is put in a capillary tube and this tube is introduced in to the resonant cavity through it's vertical axis. A fixed part of the sample is introduced to cause a certain amount of perturbation in the resonant signal as seen on the oscilloscope. The temperature of the sample is then allowed to change by flushing liquid nitrogen cooled air around the resonant cavity. The thermocouple is kept in direct contact with the sample to get it's exact temperature. A computer interface technique is used to monitor the temperature of the sample as it is going through a dielectric phase change. The thermal bath used in this experiment is very efficient to maintain a certain temperature at the phase change.

The frequency shifts vs frequency behavior of p-azoxyanisole is shown in Figure 3. As can be seen from Slater's equation # 1, the frequency shift corresponds to the real part of the complex permittivity of the material. There is a dramatic change in this behavior for this liquid crystal around a frequency of 9.6 GHz. The frequency shift drops from more than 7.0 MHz to less than 1.00 MHz at higher frequencies. The Q change that corresponds to the imaginary part of the dielectric constant peaks out at 9.6 GHz and drops to a very small value on both sides of this frequency as shown in Figure 4. This behavior is studied at a temperature of 125 °C. As suggested in the theory of nematic liquid crystals (Ref. 8), the applied field may cause disturbances in the anisotropic phase and that these disturbances tend to align the molecules parallel to the field. This behavior seems to be applicable to the results shown in Figures 3 and 4. Since the walls of the resonant cavity are effective in producing an alignment, even in the absence of an applied field there could be some disturbance present. This would tend to orientate the molecules with their long axes parallel to the walls. The applied frequencies seem to show a parallel alignment around 9.6 GHz. This indicates that at this frequency disturbances due to weak fields do not have much effect on the alignment that is already present due to the walls. It also indicates that the anisotropy in the dielectric constant is mainly responsible for the dielectric loss that is observed when the microwave field is applied to p-azoxyanisole. For this liquid crystal, the permanent dipole moment may consist of a part that belongs to the end groups of the molecule and can rotate freely, and the other part belongs to the central group of the molecule and is fixed in the molecule. The relaxation time for this molecule is of the order of 4.7×10^{-11} sec. The microwave resonant cavity is very successful in identifying the phase change for this liquid crystal.

REFERENCES:

1. Dahiya, J. N., "Temperature Dependence of the Microwave Dielectric Behavior of Selected Materials," *J. of Matr. Educ.*, 17 (3 & 4): 215 (1995).
2. Hong, K. H. and J. A. Roberts, "Microwave Properties of Liquids and Solids Using a Resonant Microwave Cavity as a Probe," *J. Appl. Phys.* 45(6): 2452 (1974).
3. Arlt, G., D. Hennings, and G. de With, "Dielectric Properties of Fine-grained Barium Titanate Ceramics," *J. Appl. Phys.* 58(4): 1619 (1985).
4. Poirier, M., G. Quirion, K. R. Poeppelmeier and J. P. Thiel, "Microwave Study of the High-Tc Superconductor $\text{La}_{1.8}\text{Sr}_{0.2}\text{CuO}_4$," *Phys. Rev. B* 36(7): 3906 (1987).
5. Pakulis, E. J. and T. Osada, "Microwave Absorption Studies of Y-Ba-Cu-O," *Phys. Rev. B.*, 37 (10): 5940 (1988).
6. Dahiya, J. N., S. K. Jani and J. A. Roberts, "Phase Transition Studies in Polar and Non-Polar Liquids at Microwave Frequencies," *J. Chem. Phys.* 74(6): 3609 (1981).
7. Debye, P., "Polar Molecules," *Chemical Catalog*, NY, Chap. V (1929).
8. Martin, Anna J., Gerhard Meier, and Alfred Saupe, "Extended Debye Theory of Dielectric Relaxations in Nematic Liquid Crystals," *Mol. Cryst.* 4 119 (1971).

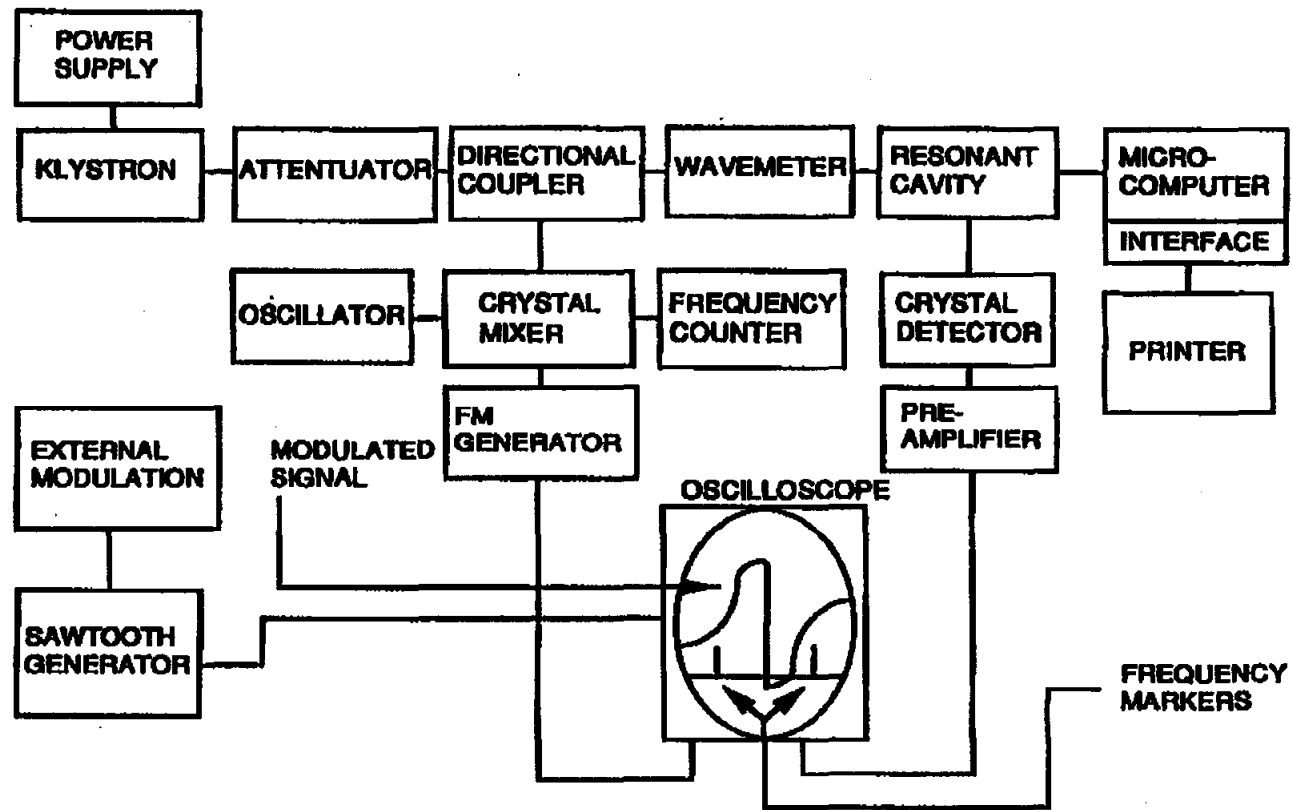


Figure 1. Block diagram of the microwave spectrometer used in this experiment.

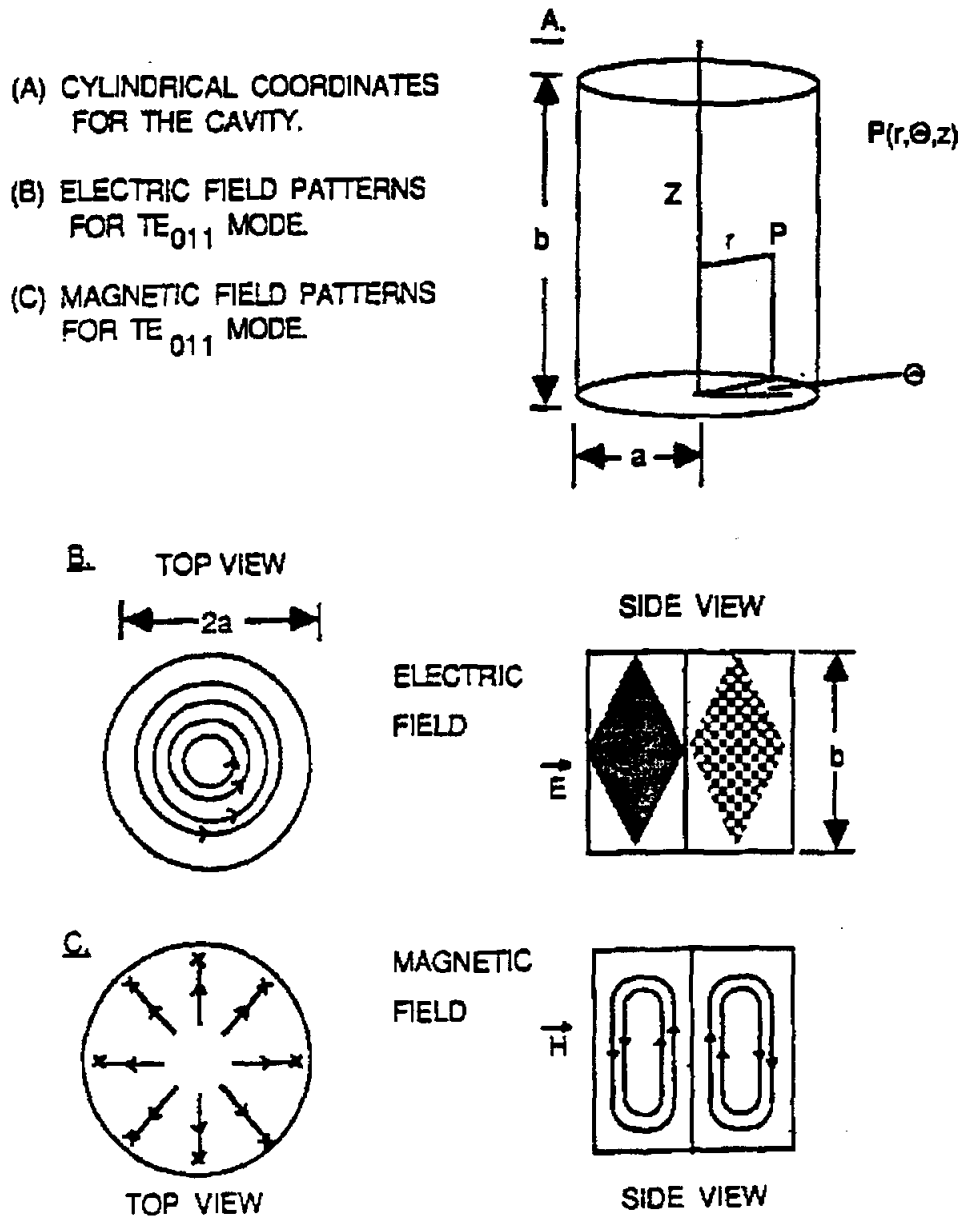


Figure 2. Electric and magnetic field patterns of a cylindrical cavity in TE_{011} mode used in this experiment.

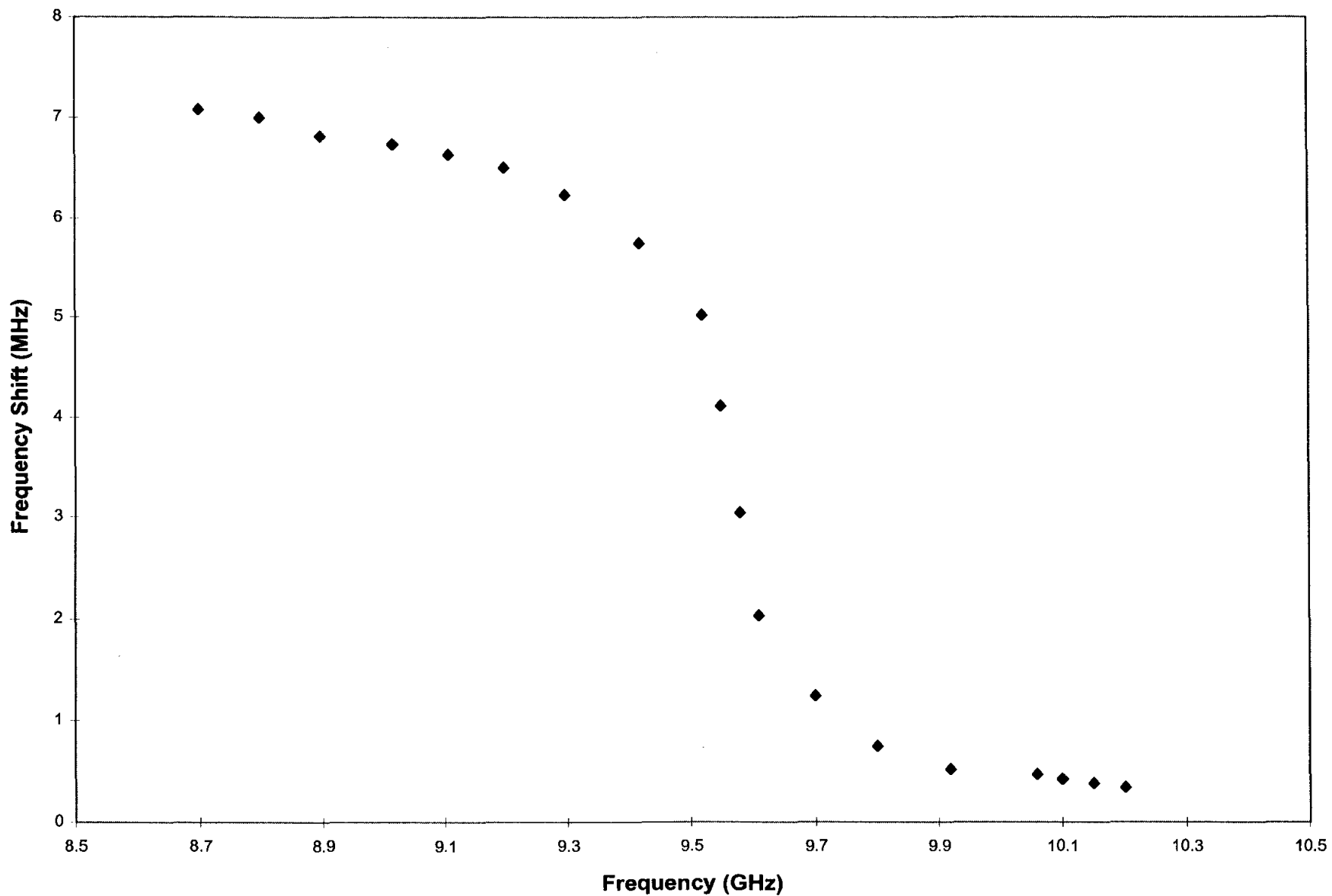


Figure 3: Frequency shift of a resonant microwave cavity as a function of the applied frequency for liquid crystal p-azoxyanisole.

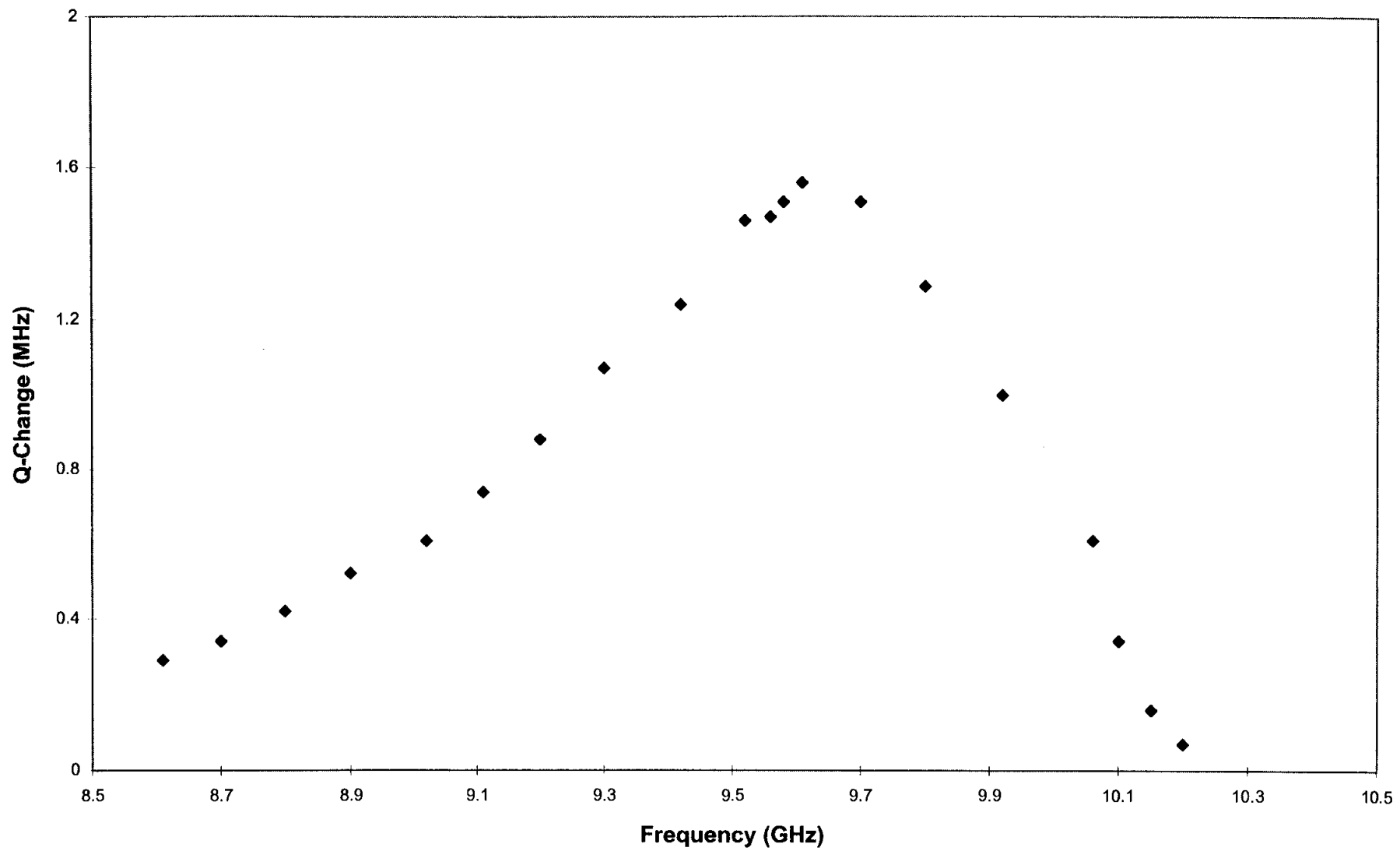


Figure 4: Q change of a resonant microwave cavity as a function of the applied frequency for liquid crystal p-azoxyanisole.

ARTIFICIAL MICROSTRUCTURES

Mike L. Meier

Department of Chemical Engineering and Materials Science
University of California, Davis
Davis, California 95616

Telephone: 916-752-5166
e-mail mlmeier@ucdavis.edu



Mike L. Meier

Artificial Microstructures

Mike L. Meier

Department of Chemical Engineering and Materials Science

University of California, Davis

Davis, CA 95616

Abstract

This paper describes simple methods for generating artificial, idealized micrographs which can be used in lessons on basic stereological techniques. The micrographs are artificial in that they were generated completely within Adobe Photoshop. They are idealized in the sense that all grain boundaries are clearly defined, all grains are clearly resolved, and distinction between different phases is easily made. These micrographs are suitable for exercises involving measuring grain size, grain aspect ratio, grain size and particle size distributions, volume fraction of phases, connectivity, etc. We have used them in classroom computer-based demonstrations using NIH Image and in home works and classroom exercises which give the students a chance to practice the above techniques before trying them on the more difficult, real microstructures.

Keywords

Metallography, microstructure, stereology, image analysis

Prerequisite Knowledge

The instructor should be familiar with the following:

1. Metallography and microstructure
2. Adobe Photoshop
3. Quantitative metallographic techniques such as Heyn's method (mean lineal intercept) and the point count method for measuring volume fraction of phases
4. NIH Image, ImagePC, UTHSCSA Image Tools or a similar image analysis program, optional.

Objectives

The objectives of this paper are:

1. To demonstrate how one can use programs such as Adobe Photoshop to generate images that are good likenesses of real microstructures
2. To offer suggestions on how one can use these artificial micrographs in classroom exercises.

Equipment and Materials

All that is needed in this exercise is a PC or Mac and Adobe Photoshop or a similar program.

Introduction

Laboratory experiments which investigate phenomena such as the Hall-Petch relationship, grain growth kinetics, heat treatments of steel and others require that qualitative and quantitative analyses of the microstructures be performed. A certain amount of knowledge and experience are required before one can even identify significant features and perform the qualitative analysis. Students usually do not have much trouble mastering this part of the analysis but considerably more experience is required when we proceed

with the quantitative analysis. Suddenly they find themselves making best guesses about the locations of unresolved grain boundaries, identifying the phase of the smallest grains, separating two particles which appear to be touching or when one is above the other as is often the case in TEM micrographs and, in general, trying to fit the features in our real micrographs into the neat and tidy terms defined in our text books and yet somehow keep our personal bias to a minimum. If this is disconcerting for the experienced metallographer imagine how students feels when we equip them with the stereological, mathematical and statistical tools necessary to be able to make reliable, unbiased measurements and then we start them off with difficult, real microstructures.

To build confidence in these measurement methods, one could start with simpler microstructures. Or one could forgo the time and expense of metallographic specimen preparation and instead simply sketch the microstructures. Unfortunately, sketching a 50x50 grain micrograph per the recommendations in Heyn's method (mean lineal intercept, ASTM Standard E 112-88) one would have to draw at least 2500 grains. Fortunately, the personal computer can do this for us plus it can add texture and distortion effects to make the artificial microstructure look more interesting and more realistic. All of this can be done using Adobe Photoshop or a similar program. No programing on our part is necessary.

Procedure

The following is the procedure for generating a basic microstructure for a single-phase material. This is followed by variations on this procedure which can be used to generate duplex, cold worked and recrystallized microstructures. All of the procedures described here take advantage of Adobe Photoshop's layering feature. Therefore Photoshop version 3.0 or higher is required. (We found layering in version 4.0 to be easier to use.) Version 4.0 was used to generate the micrographs in this paper so the procedures given here are for Photoshop version 4.0. The text in italics refers to specific menu items in Photoshop version 4.0.

Generate the Basic Microstructure

The procedure described here illustrates the basic method for generating artificial B/W micrographs. Figure 1 shows the image generated at each step.

Create a New Image Create a new image of appropriate size, type and resolution (*file: new*). One might want to generate grayscale images up to 8"x10" at 600 pixels per inch (ppi) for use by the students. Unfortunately, this image requires 28.8 MB of memory and disk storage as well as significant processing and printing time. Therefore we use smaller images, such as 4.5"x6" at 300 ppi (2.37 MB) to develop a new type of microstructure and then we repeat the procedure to generate the final, larger image.

Add Noise Use the noise filter (*filter: noise: add noise*) to darken the blank image. Note that this noise is being applied to the background layer of the new image. Optionally, you can render clouds (*filter: render: clouds*) to create dark and light areas.

Crystallize Duplicate the background layer and use the crystallize filter (*filter: pixelate: crystallize*) on this new layer to produce the grain-like image. You can specify grain size but not the shape. The grains will be equiaxed, fairly uniform in size and generally 5 or 6-sided polygons.

Note: for good statistics Heyn's method of measuring grain size the test line should intersect at least 50 grains.

Finally, adjust the gray levels (*image: adjust: levels*) to darken and lighten grains or *image: adjust: brightness/contrast* to achieve the desired effect.

Grain Boundaries Duplicate the crystallize layer and use the *find edges* filter (*filter: stylize: find edges*) to extract the grain boundaries. Adjust the brightness and contrast to achieve the desired effect.

DIC Effects Duplicate the crystallize layer again and use the emboss filter (*filter: stylize: emboss*) and the bas relief filter (*filter: stylize: bas relief*) to generate offsets at the grain boundaries and then use the *texturize* filter (*filter: texture: texturizer*) to give the grains a sandstone-like texture.

Blend Layers Adjust the opacity of each layer to achieve the desired effect. Also, experiment with the layering option: normal, multiply, difference, etc. and with the order, top to bottom, of the layers.

You will have to flatten this image before exporting it as a tiff file or any other type of bit mapped image.

The above procedure is not the only way to generate a crystallized structure. For instance, *filter: texture: stained glass* will also produce polygons with outlined grains. This filter will let you adjust the thickness of the grain boundaries.

Specific Types of Microstructures

The following procedures provide guidelines for generating specific types of microstructures.

Single Phase

The basic procedure described above produces images which look like single phase microstructures. Try readjusting the opacity of various layers and even turn off some of them to emphasize the grain boundaries, the tinting of each grain, etc. (figure 1)

Duplex Structures

Use the threshold feature (*image: adjust: threshold*) on a duplicate of the crystallized layer to convert it to black and white patches. Rename this layer the "Second Phase" layer. Duplicate the crystallized layer again and use the *find edges* filter to produce the grain boundaries. Make the crystallize layer invisible and blend the "Second Phase" and "Edges" layers to obtain the desired effects. (Figure 3)

Cold Worked and Recrystallized Microstructures

Once you have a crystallized image you can resize it to elongate and/or flatten the grains. Afterwards you can generate the grain boundaries and DIC layers as desired. To "recrystallize" this microstructure simply apply the crystallize filter again to the flattened grains layer but this time specify a smaller grain size. To represent a "grain growth anneal" you can use the crystallize filter again on the recrystallized image and specify larger grains. This technique can produce impressive

results: strings of dark and light equiaxed grains characteristic of a banded microstructure, even after extensive “annealing”. (Figure 4)

Super Alloys

You can use the *mosaic tiles* filter to create a superalloy-like microstructure. This will produce an array of squarish grains in a matrix phase. It may require some imagination to see this as a typical γ/γ' structure. One could use it as an example of a composite material.

Results

Figure 1 shows the individual layers and the final blended image described in the basic procedure. This would pass as a reasonable representation of aluminum, copper, austenitic stainless steel only without twins.

Two examples of two-phase microstructures are shown in figures 2 and 3. Figure 2 shows dark inclusions in an unetched matrix. The inclusions we produced using the *plaster* filter. Figure 3 shows a micro-duplex microstructure. It was produced by blending a *threshold* layer with a *find edges* layer, both derived from the same *crystallized* layer which in turn was based on an original *render clouds* layer. One can use these microstructures in exercises involving the measurement of grain size, particle size and volume fractions of phases, connectivity, contiguity in duplex microstructures.

Figure 4 shows a series of artificial microstructures starting with the as-received microstructure, followed by the cold worked microstructure, and then the subsequent microstructures produced by annealing at higher and higher temperatures. In this case the flattening of the grains was done by resizing the original image but one could also use a distortion filter instead to simulate the effect of bending on the microstructure.

Discussion

In our laboratory experiments we still use the manual methods for counting grain intercepts and point counts (volume fraction measurements) but we use spreadsheets and other programs to handle the math. The students try out these techniques using the artificial micrographs (figure 5 is one of the images we use) before they analyze the real microstructures. This type of rehearsal has been invaluable in the experiments where each student analyzes a couple of specimens and then shares their results with the whole class so that everyone can complete their investigations of the grain growth kinetics of C26000 brass, the Hall-Petch relationship for this same alloy, or to investigate the relationships between processing properties and microstructure for plain carbon steels.

Once the students are familiar with basic quantitative metallographic techniques one can demonstrate more advanced image enhancement and analysis techniques using commercial programs such as Image Analyzer Pro or the freeware program from NIH called Image. The artificial micrographs produced by the methods described here make good clean images which one can use to demonstrate image analysis procedures such as Fourier filtering, erosion and dilation, and thresholding. Next one can perform the analysis by measuring the mean grain size, obtaining histograms of the grain sizes, measuring the volume fraction of phases and even the particle size distributions using the Johnson-Saltykov method, analyzing the shapes and orientations of grains, and measuring the connectivity and contiguity in duplex structures.

In most cases the instructor will probably be the one who generates the microstructures (the fun part) that students analyze. Since these are not real microstructures the student will not learn about anything real materials but they can learn a number of valuable lessons beyond gaining proficiency with specified stereological techniques. A few of them are:

1. The nature of the measurement techniques: Stereology is a combination of the probability, the topological characteristics of the microstructural feature being measured, and the statistics related to our sampling techniques that yields a valid, unbiased and accurate measurement.
2. The value of validated, standardized techniques: The student should learn that only if employed correctly will everyone get the same result. From this point on in their work and their research they should be on the alert for indications that the methods other authors used were the proper techniques and that they were employed correctly.
3. Different techniques can be employed to measure the same thing: If the techniques are unbiased and if they are employed correctly they should give the same result. However, one should still pay careful attention to how the feature to be measured is defined.

Conclusion

The micrographs produced using the method described above are quite adequate for classroom exercises where the objective is to master the stereological techniques one will use in a real experiment. Photoshop's filters make it possible to go beyond making simple, flat sketches of grain outlines. The added degree of realism makes for more interesting micrographs and more credible exercises.

Biographical Information

Michael L. Meier received his B.S. in Materials Engineering from North Carolina State University in 1979 and his M.S. (1986) and Ph.D. (1991) in Materials Science and Engineering from the University of California, Davis. After a two-year post-doctorate position at the Universität Erlangen-Nürnberg in Erlangen, Germany he returned to UC Davis where he has worked as a lecturer and as a manager for the department's teaching and research laboratories. One of his primary duties is developing and managing the materials science laboratory teaching program.

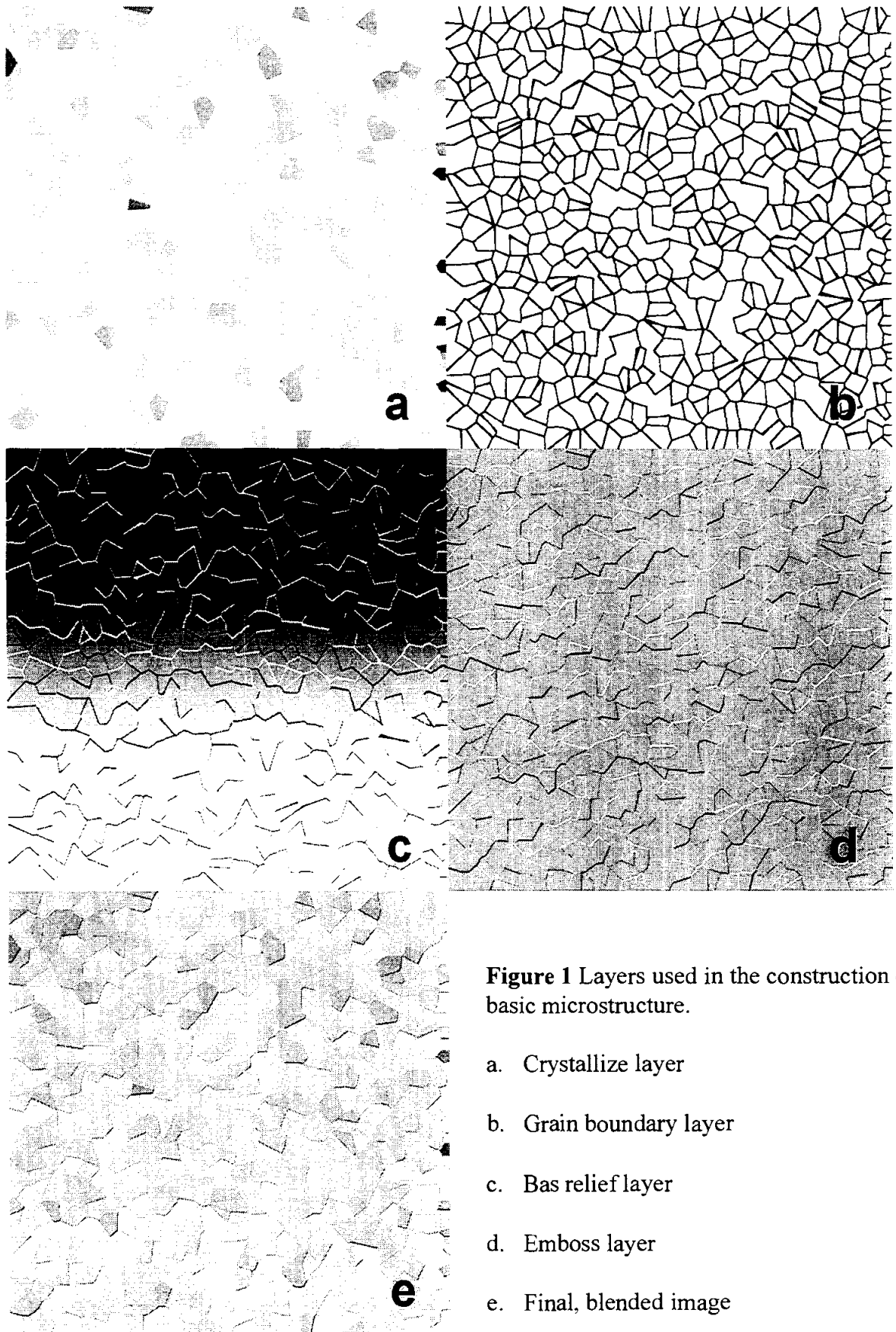


Figure 1 Layers used in the construction of the basic microstructure.

- a. Crystallize layer
- b. Grain boundary layer
- c. Bas relief layer
- d. Emboss layer
- e. Final, blended image



Figure 2 Artificial microstructure representing inclusions in an unetched matrix phase.

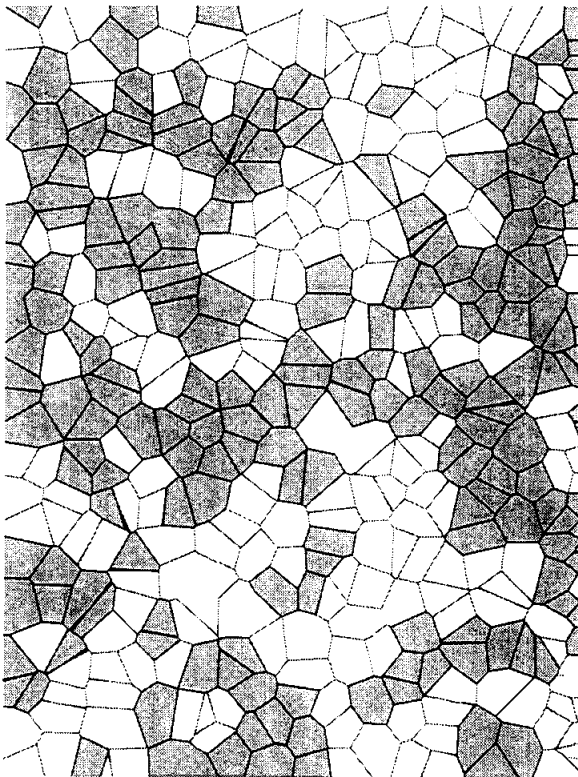


Figure 3 Artificial microstructure representing a duplex microstructure.

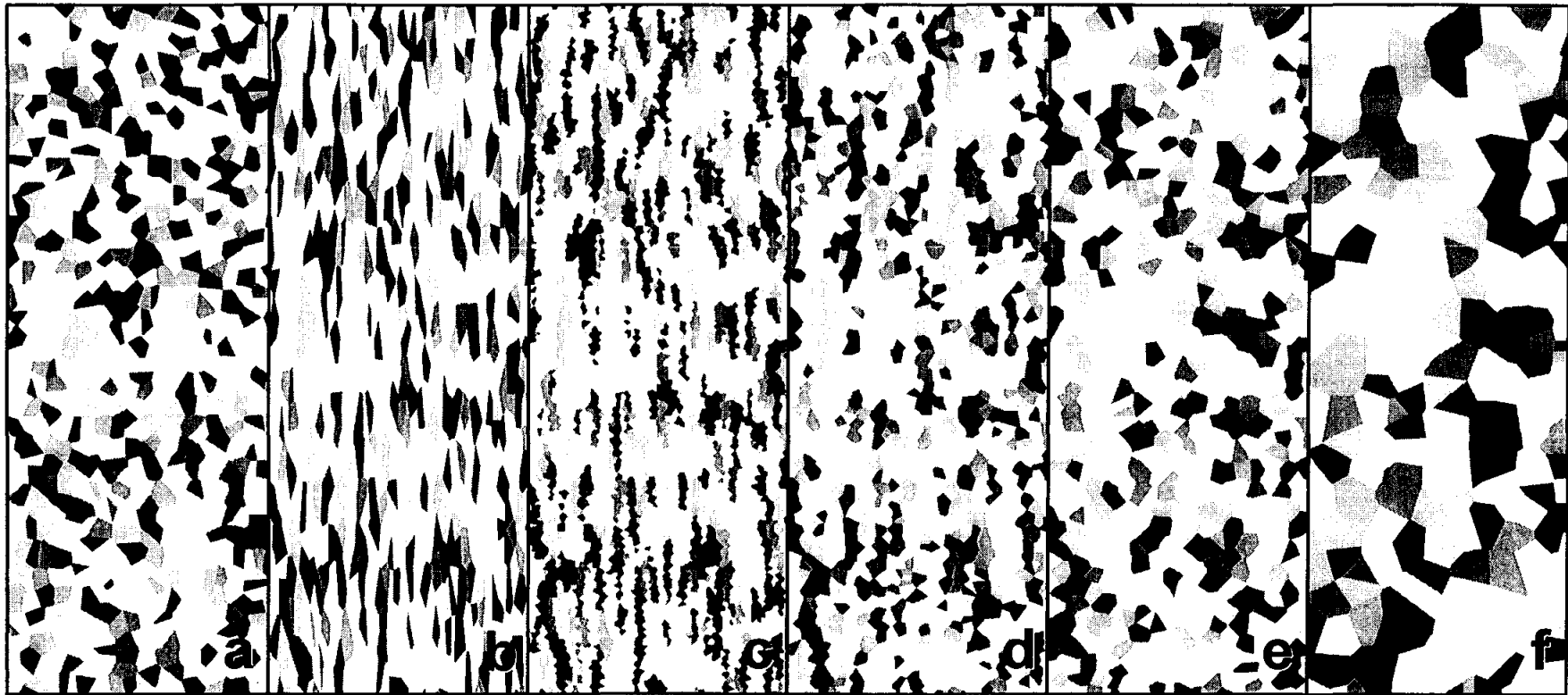


Figure 4 Artificial microstructure representing cold working, recrystallization and grain growth. Note the persistence of banding in the annealed microstructures.

- a. As-received condition, grain size = 75 pixels
- b. Cold worked 50%, grain size = 37×150 pixels
- c. Recrystallized, grain size = 25 pixels
- d. Grain growth, grain size = 50 pixels
- e. Grain growth, grain size = 75 pixels
- f. Grain growth, grain size = 150 pixels

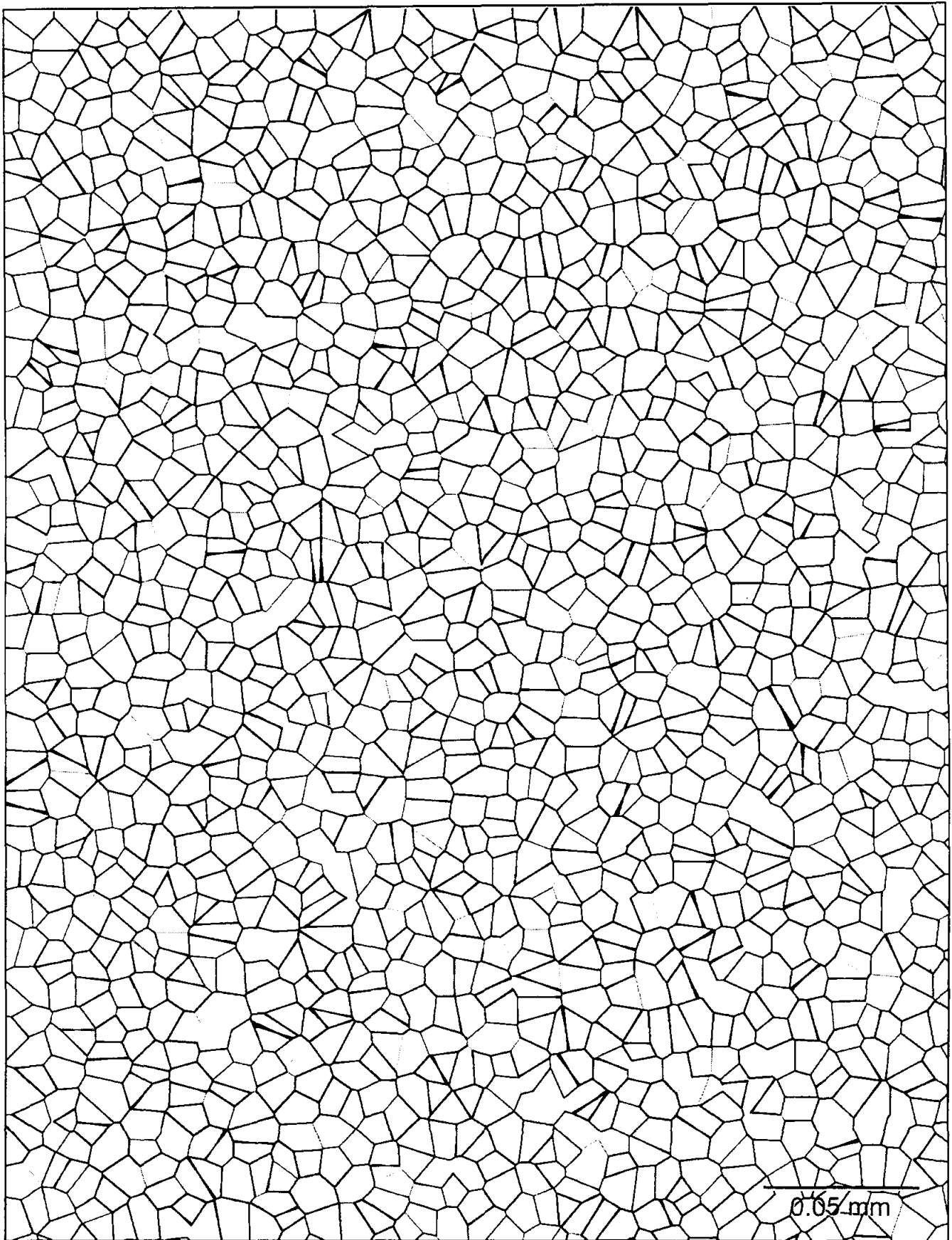


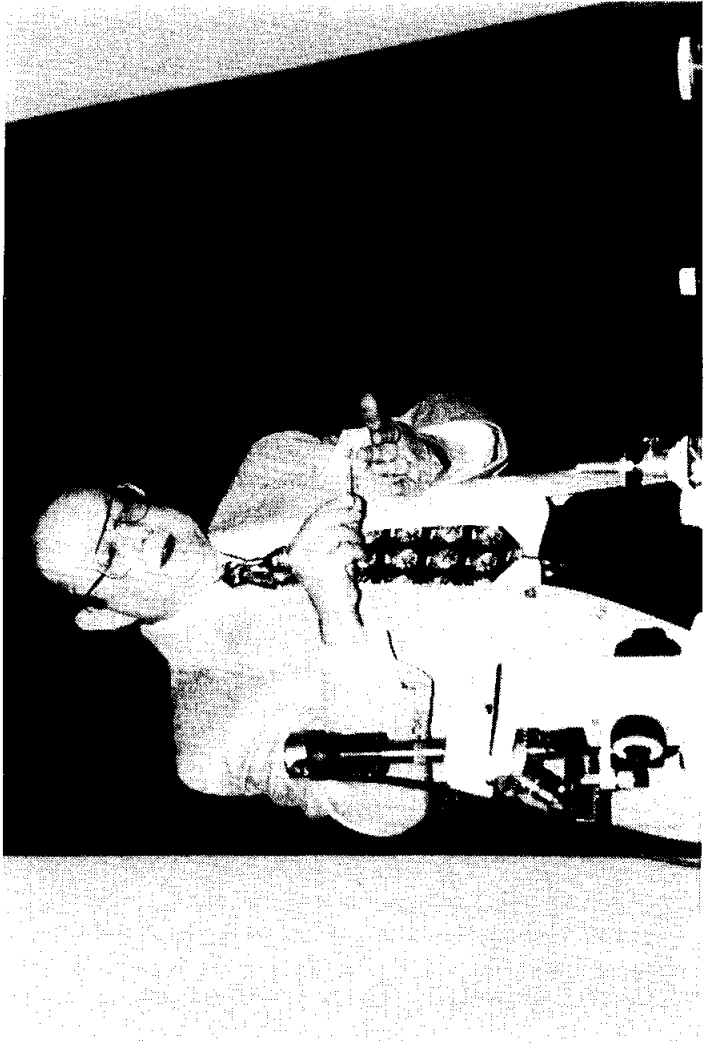
Figure 5 An artificial micrograph used in grain size measurement exercises.

CRYSTAL GROWTH

Merrill Rudes

Director of Product Development
Energy Concepts, Inc.
595 Bond Street
Lincolnshire, Illinois 60069

Telephone: 847-821-1900
e-mail ECIENG1@AOL.COM



Merrill Rudes

Crystal Growth

Merrill Rudes
Energy Concepts, Inc.
Lincolnshire, IL

Keywords:

Crystal, Chemical Reaction, Melt, Crystalline Solid, Amorphous Solid, Atoms, Molecules, Ions, Crystal Lattice

Prerequisite Knowledge:

The student:

1. should know that solids occur in the form of crystalline or amorphous structures.
2. should know that crystalline solids exhibit a repetitive, geometric arrangement of atoms, ions, or molecules.
3. should know that the crystalline structure is responsible in part for the properties and the appearance of many materials.

Objective:

The objective of this experiment is to demonstrate that crystals grow in a regular manner. The result of this growth is a solid with repetitive geometric structures. "A true crystalline solid possesses an ordered, three-dimensional, geometric arrangement that repeats itself." Jacobs and Kadoff (1), Engineering Material Science Technology. Two methods of growing crystals will be shown in this experiment.

The student will learn:

1. to grow crystals from a melt.
2. to grow crystals from a chemical reaction.
3. to observe the shape of different crystal structures.

Equipment and Supplies:

1. Copper Wire
2. Microprojector or Video Camera with Microscope Adapter (if done as demo)
3. Microscope
4. Microscope Slides
5. Phenyl Salicylate
6. Silver Nitrate, .01 M
7. Heat Source (i.e. Lighter, Match, Bunsen Burner)
8. Forceps
9. Bulb Pipette

Experiment/Demonstration Overview:

Many elements and compounds have crystalline structures. These crystal structures have particular properties associated with them that can be used to help identify them. These are size, shape, and unit cell type. The crystal of a particular material will always grow with the same angle and shapes.

“In the ideal crystal, the atoms or ions take on a definite ordered structure.” Booth (2), Material Science Technology, Solids. If the atoms did not take on a random, ordered structure, the material would not be crystalline. It would be amorphous. The pattern these particles form is called the crystal lattice. The crystal lattice of a particular material results in the particular shape of the crystal. The manner in which the crystals of a material are packed together govern many of the properties of that material. Examples of these properties are malleability and ductility in metals.

Crystals can be formed in nature or in the lab in several different ways. For example, a crystal may be formed by evaporating a saturated solution, a chemical reaction, or cooling a molten substance to a solid. This can be seen in the formation of salt (sodium chloride) via the evaporation of a solution, i.e., oceans or salt lakes, and during the cooling of a molten iron which results in the formation of a crystalline metal.

In many cases, observing crystal formation is difficult. Crystals form at varying rates. As a result, the time required may be too fast or too slow for normal observation under a microscope. Temperature also affects crystal growth. An environment that is too hot or too cold for standard laboratory observations can not be safely duplicated in a laboratory environment.

This experiment will allow students to observe crystals while they are growing. Two different methods of crystal growth will be observed: a melt process using phenyl salicylate and a heat source; and a chemical reaction process using copper wire and silver nitrate.

Procedure:

Crystal Growth by Melt

1. Obtain a clean microscope slide.
2. Place a small amount of phenyl salicylate on the center of the slide.
3. Carefully heat the slide to just melt the phenyl salicylate.
4. Allow to cool while placing the slide onto the microscope. Adjust the microscope to observe the melted phenyl salicylate.
5. Use the forceps to add a single grain of phenyl salicylate to the melt. The crystal should immediately start to grow. If the grain melts allow the melt to cool and repeat the process.
6. Observe the crystal's growth noting the shape of the crystals and what happens when separate crystals interact. When observations are completed replace this slide with a clean slide.

Crystal Growth by Chemical Process

1. Place a small piece of copper wire on the clean slide and adjust the microscope.
2. Place one or two drops of silver nitrate solution onto the copper wire. Crystals should start to grow immediately. Once again observe the shape of these crystals and how they interact.
3. Wipe both slides with a paper towel and dispose of the paper towel in the solid waste container.

Summary:

This experiment has demonstrated two different methods by which crystals may be formed: the chemical reaction process and the melting process. The melt crystal formed when a heated solution cooled and was seeded with a grain of solid. The result was the rapid formation of crystals. These crystals had shapes that were similar to each other in individual shape but formed different surfaces when they interacted with each other. The chemical reaction resulted in crystal growth when silver nitrate was added to a piece of copper wire. The silver crystals grew as a result of a single replacement reaction. The copper was more reactive than the silver. The copper atoms therefore gave their electrons to the silver ions from the silver nitrate. The silver and copper switched places. Silver crystals were formed and copper went into the solution to form a copper nitrate solution.

Comments:

This experiment is one of 28 demonstrations and 66 experiments that are part of the Energy Concepts Incorporated Material Science Technology course. "Material Science Technology" is a complete turn-key learning system including curriculum, lab equipment, and supplies. This course is appropriate for implementation at secondary schools, community colleges, or institutions intending to offer a program that builds a foundation in Material Education. For information, contact Energy Concepts Inc., 595 Bond Street, Lincolnshire, Illinois, 60069.

References:

1. Jacobs, J.A., and Kidduff, T.F., *Engineering Material Science Technology, Third Edition*, Prentice Hall, 1997, pp 93.
2. Booth, Len, *Material Science Technology, Solids*, Energy Concepts, Inc., 1996, pp 3-7.

Acknowledgments:

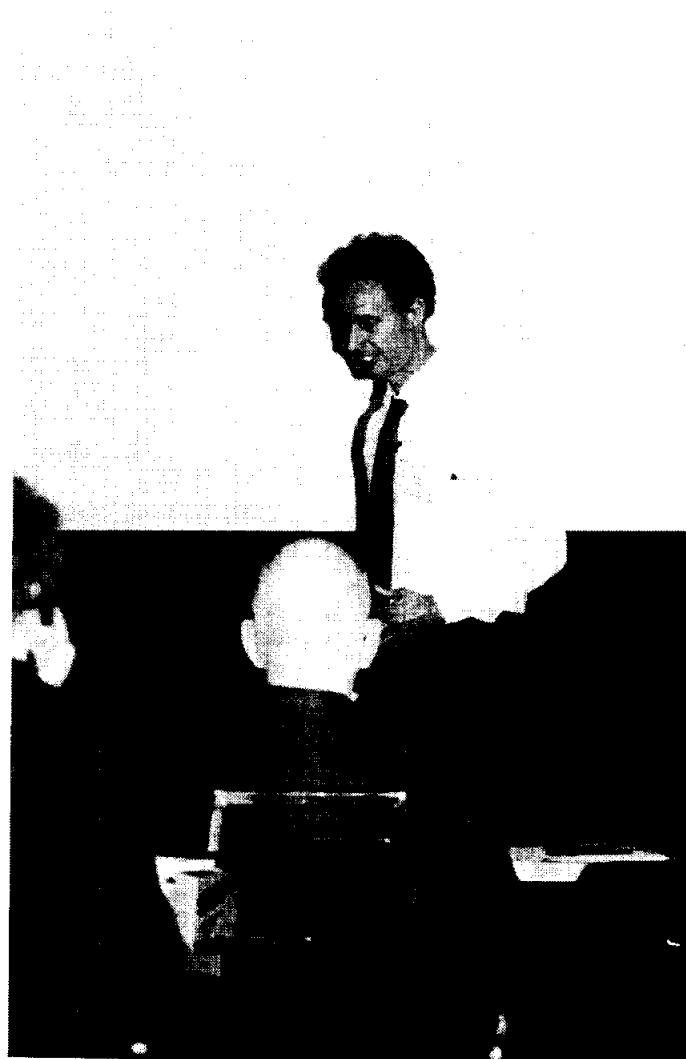
The author received assistance from Len Booth, author of Material Science Technology, James A. Jacobs, author of Engineering Material Science Technology, and Amalia D. Parthenios, Editor at Energy Concepts, Inc.

SIMULATING OPTICAL CORRELATION ON A PC

B. F. Draayer

Physics Department
Southeast Missouri State University
One University Plaza
MS 6600
Cape Girardeau, Missouri 63701

Telephone: 573-651-2391
e-mail draayer@physics.semo.edu



B. F. Draayer

Simulating Optical Correlation on a PC

By Bret Draayer
Physics Dept., Southeast Missouri State University
One University Plaza; Cape Girardeau, MO 63701

KEY WORDS

Correlation, Spatial light modulator, Composite filter, True class, False class

OBJECTIVES

1. Describe optical correlation and explain its relevance to material science.
2. Show how to simulate correlation on a PC and present simulation results.
3. Advocate correlation as a good subject for undergraduate research.

ABSTRACT

Mathematical correlation is often a useful tool to exploit in pattern recognition applications. Correlators have many desirable features that make them well suited for recognition systems; however, it is sometimes difficult to elicit reliable performance from correlation systems because slight changes in an object's orientation can significantly degrade correlation peaks. To overcome this problem, filters that represent multiple views of one or more objects, so called composite filters, have been designed for use in correlation systems. In this paper, the author explains how to use cheap, commercially available equipment to simulate optical correlation on a computer. Furthermore, this paper discusses how to design and construct a specific composite filter known as the the equal correlation peak synthetic discriminant function. Using simulations, the author discusses the characteristics of this composite filter, as well as its ability to provide rotationally invariant responses in a coherent optical correlator. Finally, plans for building other types of filters are presented, as is an endorsement about why correlation represents a good avenue for undergraduate research.

BACKGROUND

Figure 1 depicts the overall operation of a correlation-based recognition system. The basic idea is that a scene, which may or may not contain an object of interest, is correlated against a filter and the resulting correlation pattern is observed or captured for computer analysis. When an object in the input scene and the object(s) represented by the filter match, we should get a bright peak in the correlation pattern. When a weak peak

observed, we can infer that no object in the input scene matches the object(s) represented by the filter. A big part of the correlation-based recognition game then is deciding how strong a peak should be to count as a match. Figure 1 shows the classical 4f correlator in which the four essential elements of the correlator are all separated by one focal length; however, many other architectures exist [1].

To encode information in optical form, a scene is imprinted onto a laser beam by passing it through a computer controlled spatial light modulator (SLM) such as a liquid crystal TV. Spatial light modulators can be complex devices, but their operation in a correlator is fairly simple. Essentially, they function as a regular rectangular grid of electronically addressable pixels, with each pixel being capable of adjusting the plane of polarization of input light. Thus, when used in conjunction with a polarizer, they can pass, block, or partially attenuate input light, depending on how the transmission axis of the polarizer is aligned. As shown in Figure 2, the projection of the plane of polarization onto the transmission axis of the polarizer determines the degree of attenuation of input light.

Understanding how a correlator works is made simpler if one considers their operation in the spatial frequency domain. A lens takes a 2-d Fourier Transform of the input scene, which, in the classical 4f correlator, appears a distance of one focal length away from the lens. At the plane of the Fourier Transform, a second SLM filters the spatial frequency components of the imprinted scene by exploiting the relationship that correlation in the spatial domain is equivalent to multiplication in the frequency domain. A second lens then takes an inverse Fourier Transform of the Fourier Transformed scene multiplied by the transfer function written to the Fourier SLM, and the final correlation pattern appears a distance of one focal length away from the second lens.

If the filter represents a single view of a single object that is present in the input scene, as is the case in the matched filter [2] for example, then the correlation peak is very bright and is easily distinguishable from non-matching peaks. Physically what is happening in the case of a match is that the Fourier SLM takes a complicated wavefront, the Fourier Transform of the input scene, and rotates the plane of polarization at each pixel such that the exiting wavefront is planar. The final lens then focuses this plane wave to a bright point a focal length distance away. When a composite filter is used instead of a matched filter, the exiting wavefront is made nearly planar, and the sharpness of the resulting correlation peak is an indication of how closely the exiting wavefront resembles a plane wave, and, consequently, how well an object in the input scene matches the object represented by the filter.

COMPOSITE FILTERS

As noted earlier, a correlator will usually produce bright peaks when a filter is simple; i.e., when it represents a single view of an object. Unfortunately, when the object that a simple filter represents is subjected to small geometric distortions, correlation peaks tend to degrade. For example, a 2° difference in in-plane rotation between a simple filter and the object it represents can cause the correlation peak to decrease by as much as 50% [3]. Variations in size and viewing angle also cause similar decreases in correlation peaks.

Such sensitivity to geometric distortions is no problem if objects of interest are always viewed from the same perspective, with very little variation in size and shape. Indeed, it is often desirable. For example, when evaluating whether or not the size of parts fall within acceptable tolerances, we can correlate the image of a potentially defective part against the image of a standard-sized part and use the resulting correlation peak as a measure of how much the two parts differ in size. However, we likely do not care about the orientation of either part in this type of scenario. Thus, the sensitivity of simple filters to in-plane rotation could present a problem. To overcome this problem, we have two choices. One choice is to correlate the image of the part under test against several filters, each one representing a slightly different orientation of the object of interest, and assume that the brightest peak produced corresponds to when the filter and object are in the same alignment so that the degradation in peak value is due solely to size discrepancies. A negative side effect of this procedure is that it slows the system down in direct proportion to the number of filters used to represent an object. Our other choice is to use composite filters which represent multiple views of a single object, or even multiple views of multiple objects.

One of the simplest composite filters to build is called the synthetic discriminant function equal correlation peak filter, or ECP SDF filter. Historically, filters were designed to differentiate one class of objects, called the true class, from another class of objects called the false class; consequently, the ECP SDF design procedure will be presented in this context. All filter design processes start with a set of training images (TIs) that must be representative of the distortions in images that the filter is likely to encounter. For example, imagine we were trying to identify the class of an object placed on a table and viewed by a camera directly overhead. In this scenario, changes in scale and perspective would be negligible, and the system would only have to contend with variations in in-plane rotation. Ideally, images of true-class objects should trigger a recognition response from the system, whereas images of false-class objects should not trigger a response even though the false-class object may closely resemble the true-class object. In a scenario involving two or more target classes, it is important to include false-class training images in the filter design process to lower the filter's susceptibility to producing false alarms; i.e., indicating the presence of a true-class object in an input scene when a false-class object is actually present.

It should be noted that it is customary to place the center of mass of TI objects at the center of the image, or *origin* of the image. We do this because correlators are naturally shift-invariant linear systems; i.e., correlation patterns shift in direct proportion to shifts in the location of input objects. Thus, if we correlate a simple filter against a matching object that has been shifted away from the origin, we will find that the correlation peak shifts away from the origin of the correlation plane by a corresponding amount. If we do not center the TI objects, the peaks will still shift with shifts in input, but the shift will not be relative to the image center, which is usually inconvenient. Moreover, for some popular types of filters, non-centered TI objects cause two correlation peaks to appear in the correlation pattern [4]. Finding the center of mass of TI objects is generally easy because the objects are typically imaged against a dark background (or light background in the case of dark objects), and are easy to segment.

MATHEMATICAL DEVELOPMENT OF THE ECP SDF

In most applications, each TI is a digital image composed of $m \times n$ pixels; thus, each TI can be represented as a 2-dimensional array. Assume an integer number of TIs, say N , are chosen to comprise the TI set, and let the i th TI be denoted as $t_i(m, n)$, where m and n are row and column indices, respectively. In the ECP SDF formulation, a filter is assumed to be a linear combination of TIs. In other words, if $h(m, n)$ represents a filter, we may write:

$$h(m, n) = \sum_{i=1}^N a_i \times t_i(m, n), \quad (1)$$

where a_i is a possibly complex-valued constant. It is convenient to express Equation (1) in vector form. To do this, we lexicographically reorder $h(m, n)$ by stacking successive columns to create a vector, \mathbf{h} , with $m \times n$ entries. We also lexicographically reorder the TIs and define \mathbf{S} as the $(m \times n) \times N$ matrix whose i th column is the i th TI. Using this notation, Equation (1) becomes:

$$\mathbf{h} = \mathbf{S}\mathbf{a}, \quad (2)$$

where \mathbf{a} is a N -element vector whose i th value is a_i . Now we exploit a useful property; namely, that the origin value in the correlation plane is equal to the inner product of two vectors. One vector is the lexicographically rearranged input scene and the other is the filter vector. To come up with an expression for the filter function, the designer specifies the correlation value at the origin for each TI. In vector form, this is done via the equation:

$$\mathbf{S}^T \mathbf{h} = \mathbf{c}, \quad (3)$$

where \mathbf{c} is an N -element vector whose i th value is the designer-specified correlation origin value when the i th TI is correlated against the filter \mathbf{h} . We now substitute Equation (2) into Equation (3) with the result:

$$\mathbf{S}^T \mathbf{S}\mathbf{a} = \mathbf{R}\mathbf{a} = \mathbf{c}, \quad (4)$$

where \mathbf{R} is the $N \times N$ correlation matrix whose i th, j th value equals the origin value in the correlation plane when the i th TI is correlated against the j th TI. Thus, it is also equal to the inner product between the i th TI and the j th TI when each one is represented as a vector. Note that \mathbf{R} is a symmetric matrix. Solving for \mathbf{a} , we finally end up with the solution:

$$\mathbf{a} = \mathbf{R}^{-1} \mathbf{c}. \quad (5)$$

Generally, the designer chooses large correlation values for the true-class object and low correlation values for the false-class object with the hope that non-TI images of true-class objects will yield high enough peaks when correlated against the filter to distinguish them from peaks produced by non-TI images of false-class objects. One shortcoming of the procedure is that only the origin correlation value is controlled in the design process so it is not uncommon to produce peaks elsewhere in the correlation plane that exceed the

origin value, making it difficult to differentiate between true-class and false-class peaks with a crisp threshold. Another problem with composite filters is that they have a tendency to lose specificity as they become more composite. In other words, it is more difficult to maintain a significant difference between true-class peaks and false-class peaks as the range of distortions represented by the filter increases. As noted earlier, the ECP SDF is only one type of filter that has been designed for use in optical correlators, and many superior filter types exist [5]; however, this paper will not address these more complex filter designs.

SIMULATING OPTICAL CORRELATION ON A PC

For people who want to experiment with correlation but do not have the funds, time, or wherewithal to build an optical system, it is fortunate that a host of companies now produce frame grabbing/image processing boards that make simulating optical correlation easy. Companies such as EPIX, DIPIX, and Matrox, among others, build affordable boards that are designed to reside in a PC. A good board for simulating correlation should come with software that performs 2-dimensional Fourier Transforms, image addition, image rotation, convolution, and multiplication of complex images. Several boards are capable of performing correlation as it is mathematically defined, but it is still essential to have the previously listed features for designing filters even with correlation capable boards. Finally, the software accompanying the boards should be able to save images in different formats, such as text, TIFF, PCX, etc., since the processing for some of the more complicated filters is probably best done using a sophisticated program such as *MATLAB* [6], and having the ability to save images in different formats makes it easy to exchange data between different programs.

To produce simulations for this paper, an EPIX board called the 4MEG12 [7] was used to grab images, perform 2-d FFTs, and scale gray level values in images by a constant; furthermore, students programmed the board to automate the data collection and filter synthesis process. To design ECP SDF filters, we selected 9 images from a true class and 9 images from a false class. Figure 3 shows the reference true-class image on the left and the reference false-class image on the right. We generated TIs by rotating the reference image for each target class in 5° increments over a 40° span. An ECP SDF was designed by computing the correlation matrix defined in Equation (4), finding its inverse, and multiplying the inverse by the vector of designer specified constants. For true-class images, we chose an origin correlation value of 100, and for the false-class images, the origin value was chosen as 20.

In the frequency domain, the filter represents a transfer function. In the spatial domain then, the filter represents an impulse response. Once we have determined vector \mathbf{a} of Equation 2, we can find the impulse response by forming the sum in Equation 1. Figure 4 shows the resulting impulse response. As can be seen, several rotated versions of the two reference objects are clearly present. To produce simulation results, we take the Fourier Transform of the impulse response to get a transfer function. We then multiply the Fourier Transform of an input scene by the transfer function represented by

the filter and take an inverse Fourier Transform of the product to generate a correlation pattern. We could repeatedly perform the shift, multiply, and add operations that define correlation, but this is usually a much slower method to use on digital computers.

To test the filter, we first correlated it against TIs to check the agreement between experiment and theory; i.e., we checked how closely actual correlation values matched the designer specified values held in vector c . These tests revealed expected results—peak values for the true-class objects and center-of-mass correlation values for the false-class objects were almost always within 90% of the specified values. Also as expected, it was found that peak correlation values for false-class objects often did not coincide with the center-of-mass of input objects, but were still low enough to permit one to identify the object class by thresholding the peak value. For non-TI images, correlation peaks for true-class objects varied according to how much the rotational offset of the image differed from the rotation angle of the most closely aligned TI. Figure 5 is a plot of peak value versus object rotation from zero to 45° , with the top plot showing the response of true-class objects and the bottom plot showing the response of false-class objects. Note the fluctuations in the top plot have a period equal to the separation in rotation angle between successive TIs. Also note that distinguishing true-class objects from false-class objects could easily be accomplished by simply thresholding the peak value.

CONCLUSIONS

Correlation is a useful mathematical operation that can be exploited to solve problems in diverse situations. It has been successfully applied to problems involving target recognition systems, but it may also be of value to the field of material science, even though not much work has been done in this area to date. It represents a good research area for undergraduate students because it nicely illustrates the fundamentals of system design, optics, and image analysis, yet it doesn't require expensive equipment. Furthermore, students can come to speed on the subject fairly quickly. It does not take an inordinate amount of time for students to get to the point where they can perform some non-trivial experiments, which is important in undergraduate research. It is disappointing to get students to a position where they can contribute to a research project, only to have them graduate. Finally, correlation represents a research area in which students can build upon the work of earlier students. For example, students have written routines to build ECP SDFs, to correlate filters against input scenes, and to evaluate filter performance by collecting and analyzing data in an automated sequence for the EPIX board mentioned earlier. Future students may write routines to construct other varieties of filter functions, but they can still use the correlation and testing procedures written by the students that came before them. The filter design processes are often modular in nature, so that one student can work on a small part of the overall process and then combine it with the work of other students to complete a larger project. Thus, using correlation, an investigator can generate plenty of good research projects with a modest investment in equipment.

Although the ECP SDF was perfectly capable of distinguishing between true-class objects and false-class objects in the simplistic scenario given, it should be kept in mind that automated recognition systems often must contend with more challenging scenarios, and hence require more sophisticated filtering techniques. Future undergraduate students will work on developing circular harmonic filter routines, minimum average correlation energy filter routines, and others. Furthermore, applications for material science may require novel filtering techniques since the difference in objectives between material science and pattern recognition is fairly broad; however, some important investigations must be completed before such a conclusion is reached.

REFERENCES

1. Brett D. Bock, Thomas A. Crow, and Michael K. Giles, "Design considerations for miniature optical correlation systems that use pixelated input and filter transducers," SPIE Proc., Vol. **1347**, pp. 297-309, 1990.
2. Jack Gaskill, "Linear Systems, Fourier Transforms, and Optics," John Wiley and Sons, New York, pg. 261, 1978.
3. Gary W. Carhart, Bret F. Draayer, and Michael K. Giles, "Empirical Performance of Binary Phase-Only Synthetic Discriminant Functions," SPIE Proc., Vol. **1564**, pp. 348-362, July 1991.
4. Fred M. Dickey, K. Terry Stalker, and J. Jeff Mason, "Bandwidth considerations for binary phase-only filters," *Appl. Opt.*, Vol. **27**, No. 18, 1988.
5. B. V. K. Vijaya Kumar, "Tutorial survey of composite filter designs for optical correlators," *Appl. Opt.* **31**, No. 23, 1992.
6. *MATLAB*, student ed., Prentice Hall, Englewood Cliffs, NJ, 1997.
7. EPIX Inc., 381 Lexington Drive, Buffalo Grove, IL 60089, Tel: (847) 465-1818, email: epix@epixinc.com.

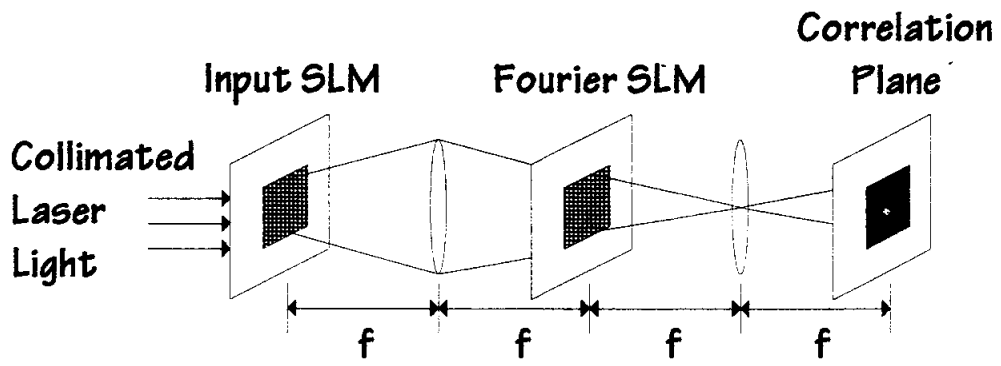


Figure 1: Classical 4f correlator.

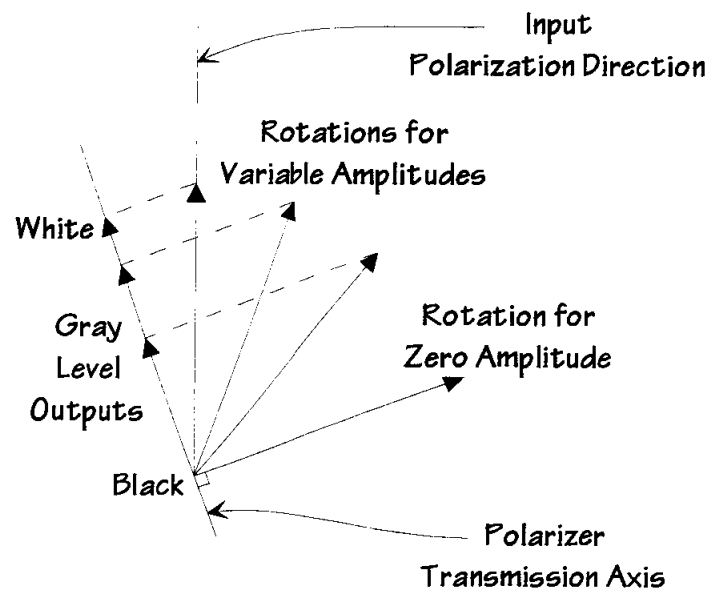
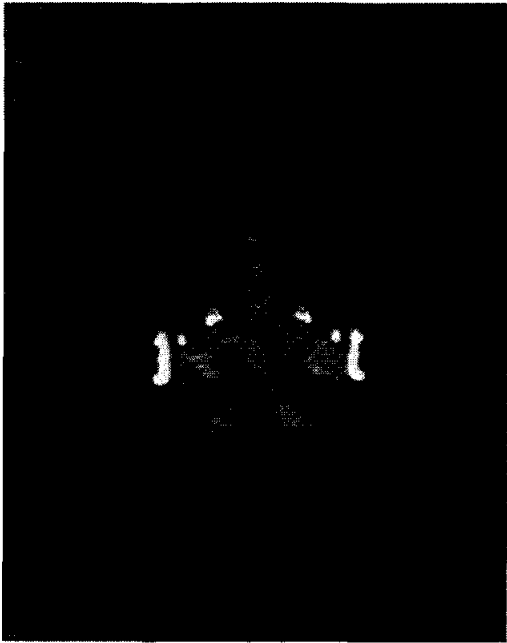


Figure 2: Intensity modulation using a SLM and a polarizer.



(a)



(b)

Figure 3: (a) True-class reference object, & (b) False-class reference object.



Figure 4: ECP SDF filter.

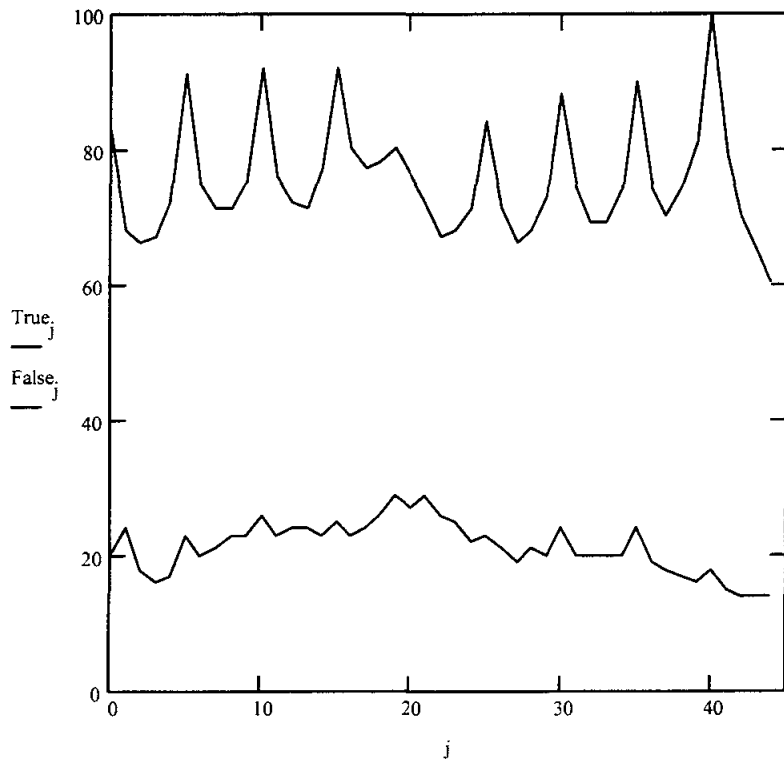


Figure 5: Peak correlation value versus rotation angle for true-class (top) and false-class (bottom) objects.

Bio:

Bret Draayer attended New Mexico State University where he received a Ph.D. in electrical engineering in 1993. He worked in industry for three years on projects involving image processing, telescope optics, and signal analysis. He is currently a professor in the Physics Department at Southeast Missouri State University, where he teaches courses in physics, circuit analysis, digital electronics, and capstone design.

TRENDS FOR AUTOMOTIVE MATERIALS

John E. Fillion

Senior Manager
Body Materials Engineering
DaimlerChrysler Corporation
800 Chrysler Drive
Auburn Hills, Michigan 48326-2757

Telephone: 248-576-7472
e-mail jef2@chrysler.com



John E. Fillion

Trends For Automotive Materials

John Fillion

Senior Manager

Body Materials Engineering

DaimlerChrysler AG

Presented November 4, 1998

National Educators Workshop

Brookhaven National Lab

Drivers for Materials Selection

- Lower total vehicle cost
- Meet new performance requirements
 - Customer driven
 - Government driven

Lower Total Vehicle Cost

- Lower component/system cost
 - Parts consolidation
 - Easier assembly
 - Faster production rate

Lower Vehicle Cost

- Lower Investment Cost
 - Parts consolidation
 - Ease of making complex shapes
 - Faster production rates
 - Use less capital intensive process

Lower Vehicle Cost

- Lower development cost
 - Less engineering time
 - Computer aided design
 - Rapid prototyping
 - Computer performance validation

Meet New Performance Requirements

- Customer demands
 - Increased quality
 - Increased durability
 - New features
 - Improved fuel economy
 - Increased safety
 - Environmentally friendly vehicles

Meet new performance Requirements

- Government demands
 - Increased safety
 - Lower vehicle emissions
 - Less environmental impact (i.e. recycling)
 - Improved fuel economy

Key Point #1

Materials are selected to optimize the balance between performance and total cost to Chrysler.

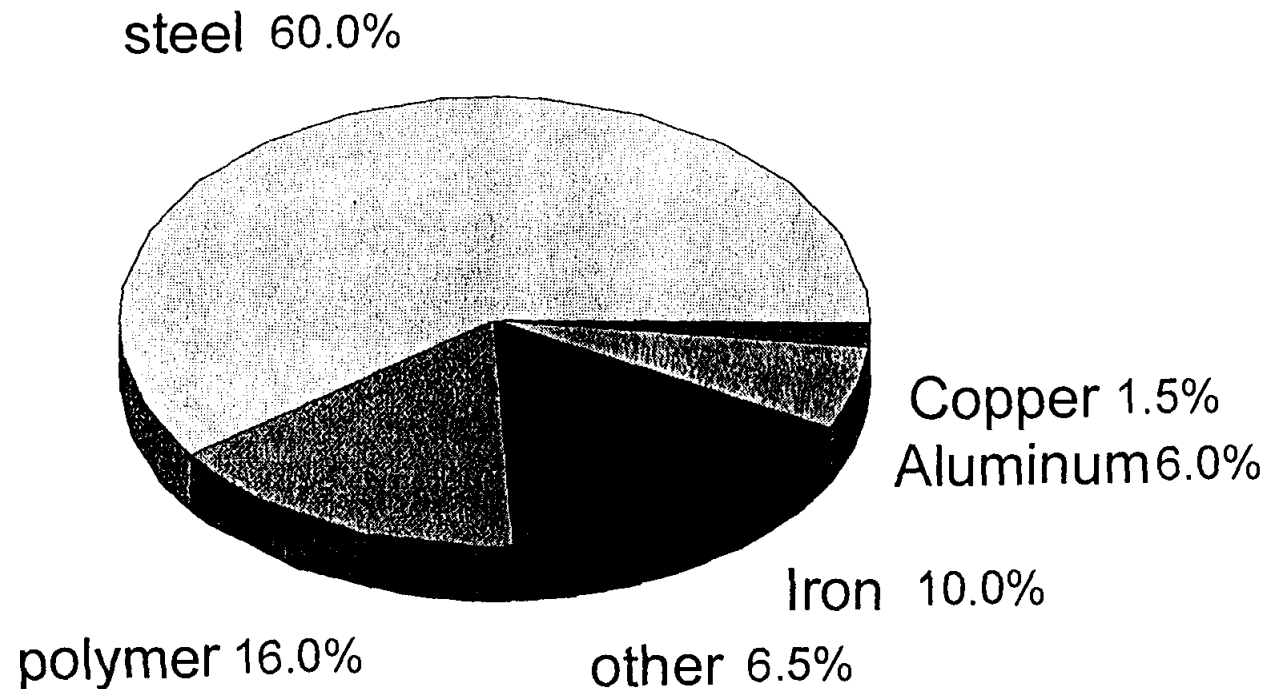
Key Point #2

Weight reduction is usually a form of cost avoidance

Key Point #3

There is only one Key Point -
Materials are selected to optimize
the balance between performance
and total costs to Chrysler

Composition of a Car 1997 By Weight



Automotive Materials Consumption of US Production

Steel	14%	Lead	68%
Cast Iron	60%	Platinum	34%
Aluminum	16%	Elastomers	50%
Copper	10%	Textiles	6%
Zinc	23%	Plastics	4%

The Amount of Steel Per Vehicle Has Steadily Decreased

- Downsizing of vehicles
- Gage reduction through new alloys
- Replaced by other materials

Government pressures to improve fuel economy and air emissions will continue the trend of substitution of steel by plastics ,aluminum, and magnesium.

Rank of Materials By Density (g/cm³)

Air	0.001	Aluminum	2.7
Water	1.0	Titanium	4.5
Plastics	1.1	Zinc	7.1
Carbon fiber composite	1.3	Iron	7.2
Glass fiber composite	1.8	Steel	7.6
Carbon fiber	1.8	Nickel	8.8
Magnesium	1.8	Copper	11.3
Glass fiber	2.5	Lead	11.3

Rank of Materials by \$/lb.

Steel	0.4
Iron	0.5
Aluminum	0.9
Plastics	1.0
Glass fiber composite	1.2
Magnesium	1.5
Carbon fiber composite	6.0
Titanium	10

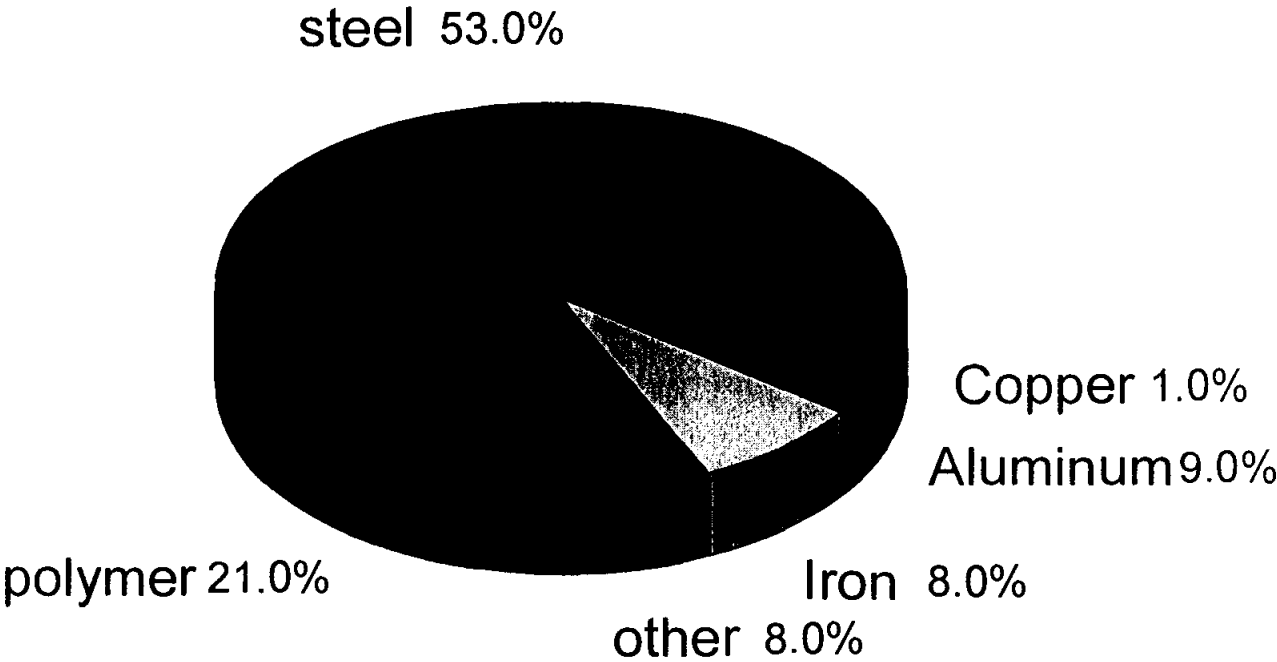
Weight Facts

- 100 lb. of weight savings = 1 MPG savings
- 1 lb of weight savings generates 0.75 lbs of secondary weight savings
- Aluminum can save 50% weight
- Magnesium can save 60% weight
- Glass composites can save 25% weight and carbon composite 60%

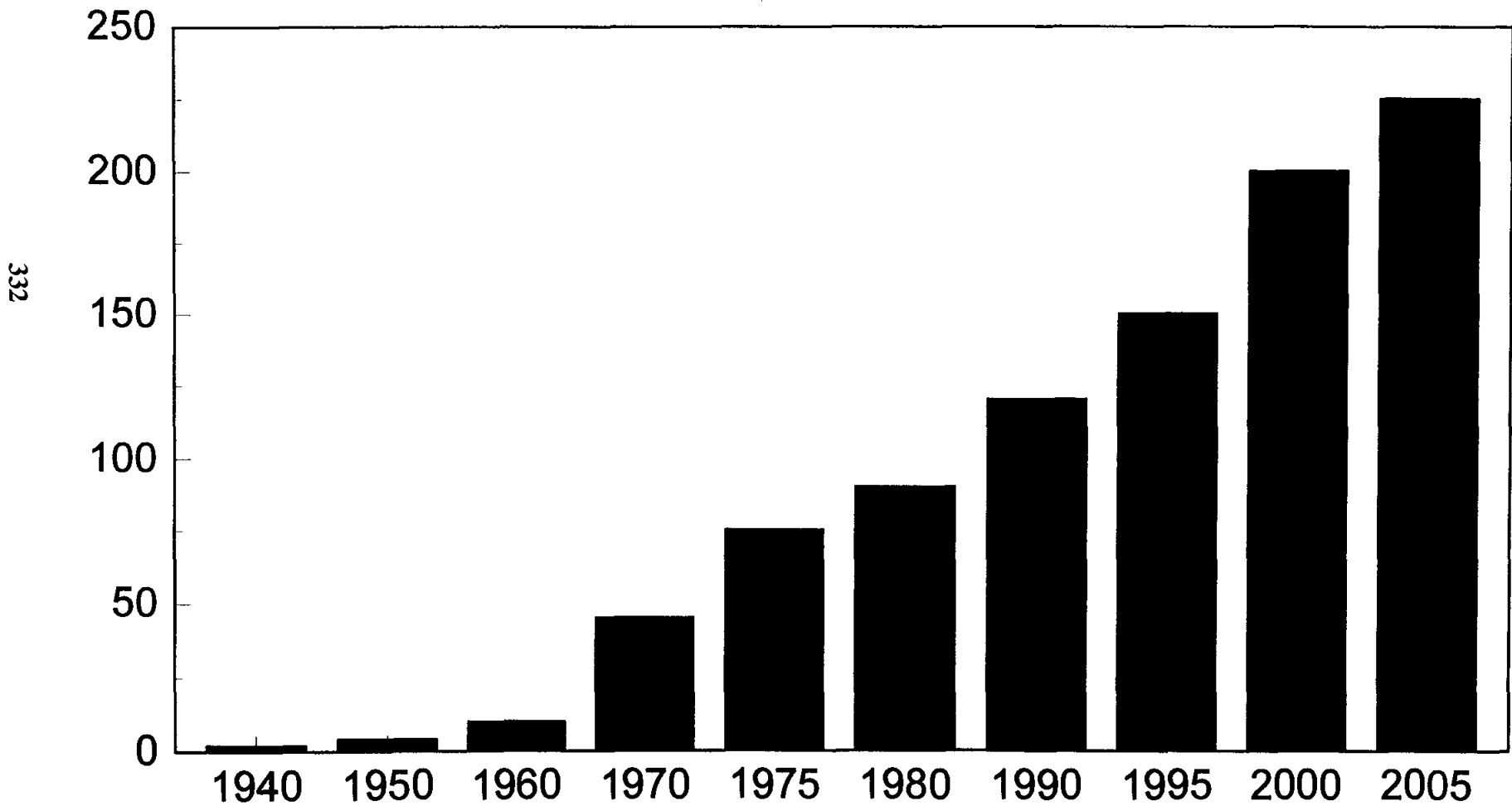
Weight Facts

- The weight breakdown of a vehicle is 35% body, 34% chassis, 27% powertrain, and 4% other
- The typical weight of a truck is 4000 lbs.
- The typical weight of a passenger car is 3200 lbs.
- By 2005 vehicle weight will be 5% less

Composition of a Car 2005 By Weight



Kg of Polymers per Vehicle



Trends for Plastics

- Intake manifolds
- Fuel rails
- Gas tanks
- Front end and bumper system
- Instrument panel structure
- Seat support and structure
- Closure panels

Trends For Aluminum

Cylinder Heads Body Panels

Cylinder Blocks Wheels

Intake Manifolds Control Arms

Oil Coolers Brake Drums

Heater Cores Radiators

Trends for Magnesium

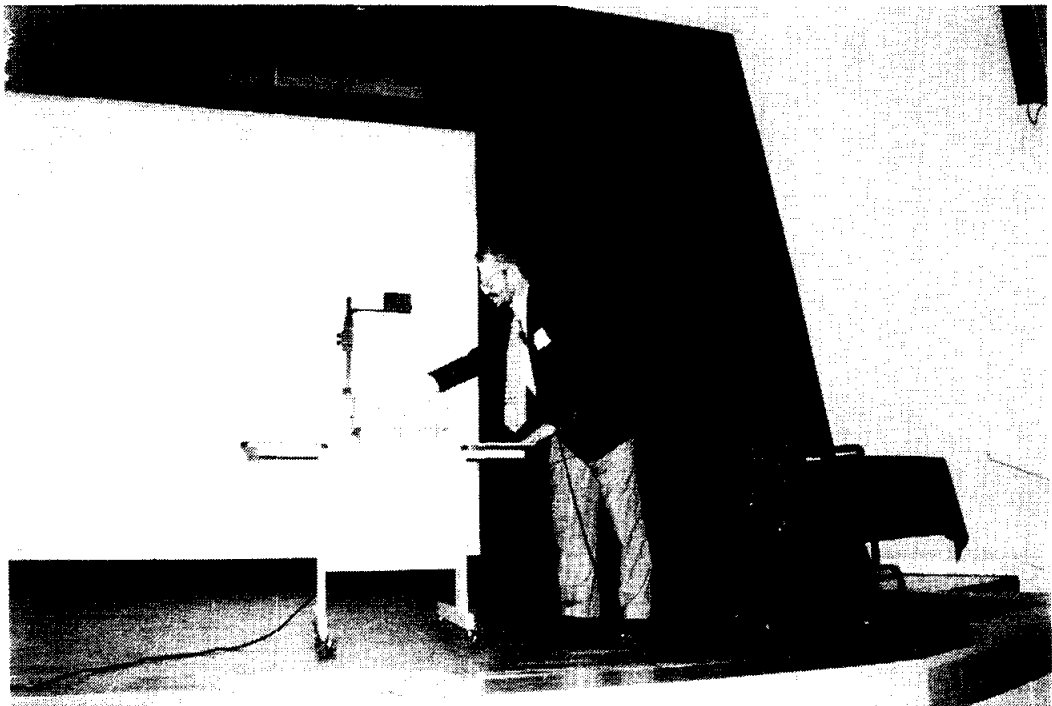
- Instrument panel structure
- Seat supports
- Steering wheel rims
- Support brackets
- Steering column supports

DENDRITIC POLYMER PROPERTIES AND MACROMOLECULAR ARCHITECTURE

Donald A. Tomalia

Michigan Molecular Institute in Midland
1910 West Saint Andrews Road
Midland, Michigan 48640

Telephone: 517-832-5555 ext. 601
e-mail tomalia@mmi.org



Donald A. Tomalia

DENDRITIC POLYMER PROPERTIES AND MACROMOLECULAR ARCHITECTURE

Donald A. Tomalia

University of Michigan
Center for Biologic Nanotechnology
Ann Arbor, MI 48109-0533

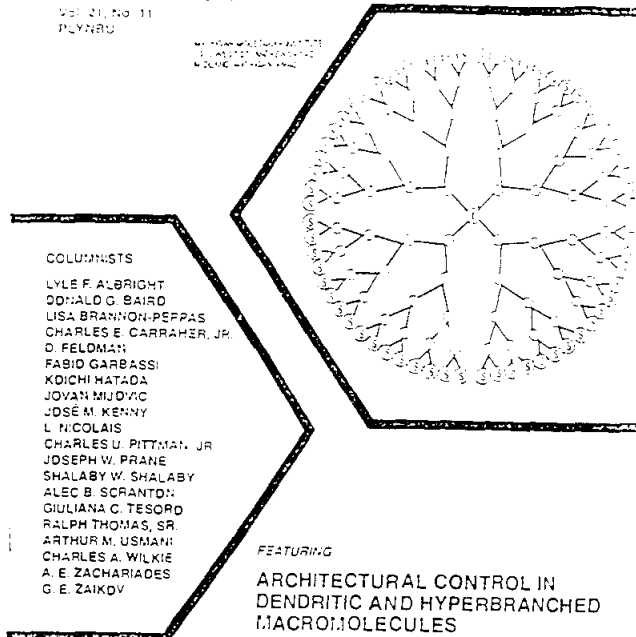
Michigan Molecular Institute
Midland, MI 48640

POLYMERNEWS

NOVEMBER 1996

Vol. 21, No. 11
POLYNU

WILEY-INTERSCIENCE
A JOHN WILEY & SONS, INC. PUBLICATION

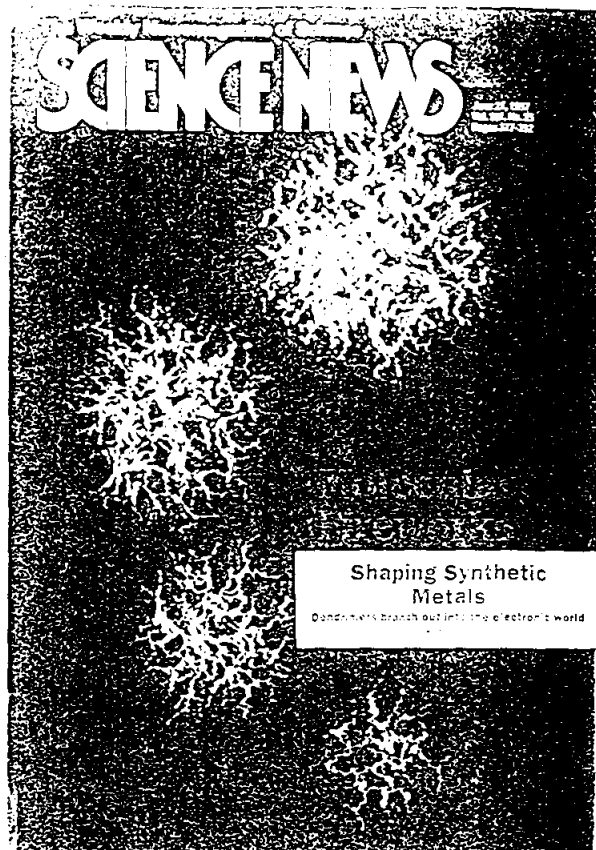


COLUMNISTS

LYLE F. ALBRIGHT
DONALD G. SAIRO
LISA BRANNON-PEPPAS
CHARLES E. CARRAHER, JR.
D. FELDMAN
FABIO GARBASSI
KIOCHI MATADA
JOVAN MIJODIĆ
JOSE M. KENNY
L. NICOLAIS
CHARLES U. PITTMAN, JR.
JOSEPH W. PRANE
SHALABY W. SHALABY
ALEC B. SCRANTON
GIULIANA C. TESORO
RALPH THOMAS, SR.
ARTHUR M. USMANI
CHARLES A. WILKIE
A. E. ZACHARIADES
G. E. ZAIKOV

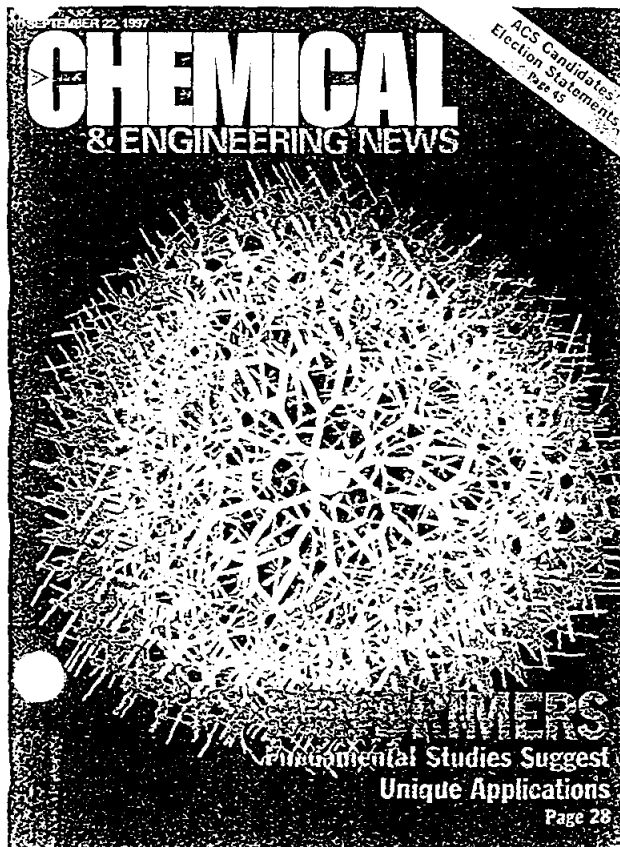
FEATURING

ARCHITECTURAL CONTROL IN
DENDRITIC AND HYPERBRANCHED
MACROMOLECULES



Shaping Synthetic Metals

Dendritic structures branch out into the electronic world

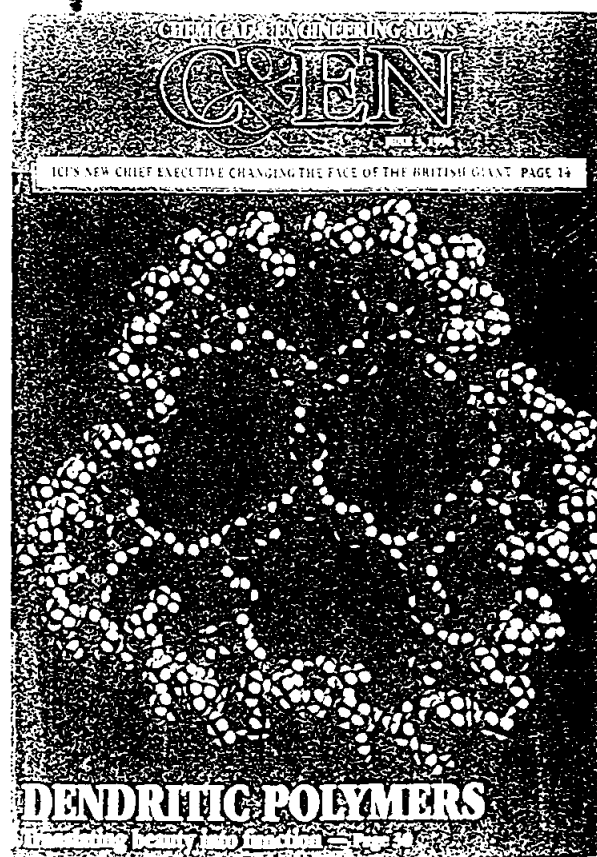


NOVEMBER 22, 1997

CHEMICAL & ENGINEERING NEWS

ACS Candidates:
Election Statements
Page 45

POLYMERS
Fundamental Studies Suggest
Unique Applications
Page 28



CHEMICAL ENGINEERING NEWS

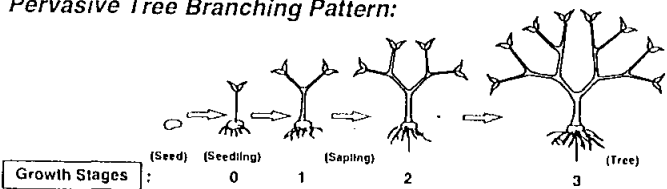
C&EN

NOVEMBER 2, 1996

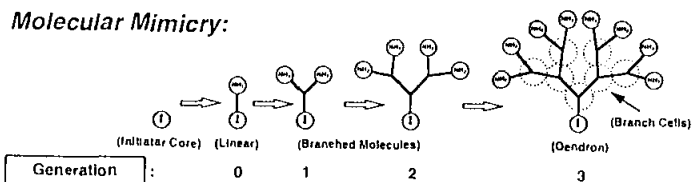
ICI'S NEW CHIEF EXECUTIVE CHANGING THE FACE OF THE BRITISH GIANT PAGE 14

DENDRITIC POLYMERS
Illustrating beauty and function Page 4

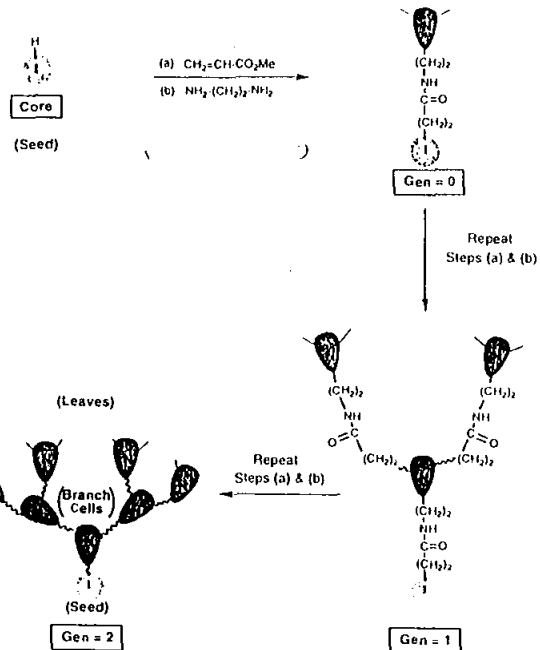
Pervasive Tree Branching Pattern:



Molecular Mimicry:



Ref: D. A. Tomalia *Scientific Amer.*, 272, 62 (May 5, 1995)



Abiotic Strategy

(Flask) \rightarrow Molecular Information Secrets \rightarrow Feed Stock Monomers (Acrylate Esters, Amines, etc.)

I. (Radial - Transcription / Translation) G=0, 1, 2, 3, 4

II. (Abiotic - Template Polymerization) G=0, 1, 2, 3, 4

III. (Radial - Iterative Sequencing Steps; G) G=0, 1, 2, 3, 4

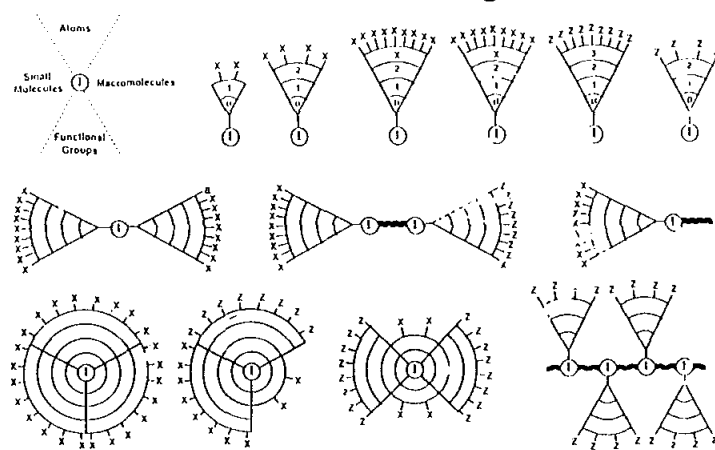
Size Control: Diameters increase by About 1 nm from Generation to Generation

Shape Control: From Spheres to Ellipsoids to Rods

Monomeric, Dimeric and Oligomeric Dendrimers

Chemical Structure Control: Ideal and Modified Dendrimers

Dendron / Dendrimer Lego® Set

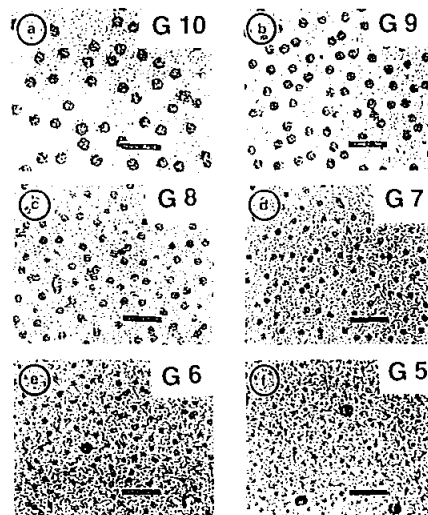


Starburst Poly(amidoamine) Dendrimers

	①	G=0 (Core)	G=1.0	G=2.0	G=3.0
M Wt.	17	359	1,043	2,411	5,147
D.P.	—	3	9	21	45
# of terminal groups (z)	—	3	6	12	24
M Wt.	10,632	21,583	49,451	87,227	
D.P.	93	189	381	765	
# of terminal groups (z)	48	96	192	384	

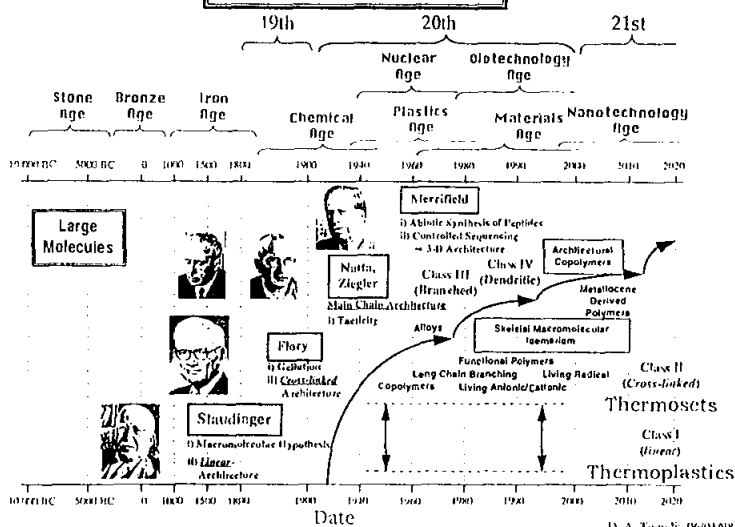
Visualization of Dendritic Molecules by Transmission Electron Microscopy (TEM): Staining Methods and Cryo-TEM of Vitrified Solutions

Catherine L. Jackson, Heidi D. Caskey, Frank P. Booy, Bartholomew J. Drake, David A. Tomalia, Barry J. Bauer, and Eric J. Amis
 Polymers Division, National Institute of Standards and Technology, Gaithersburg, Maryland 20899

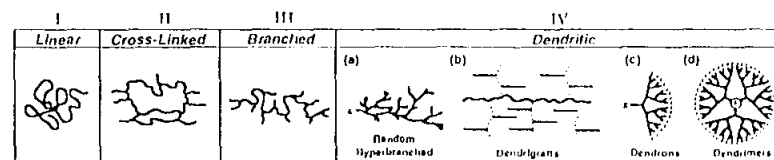


Macromolecules

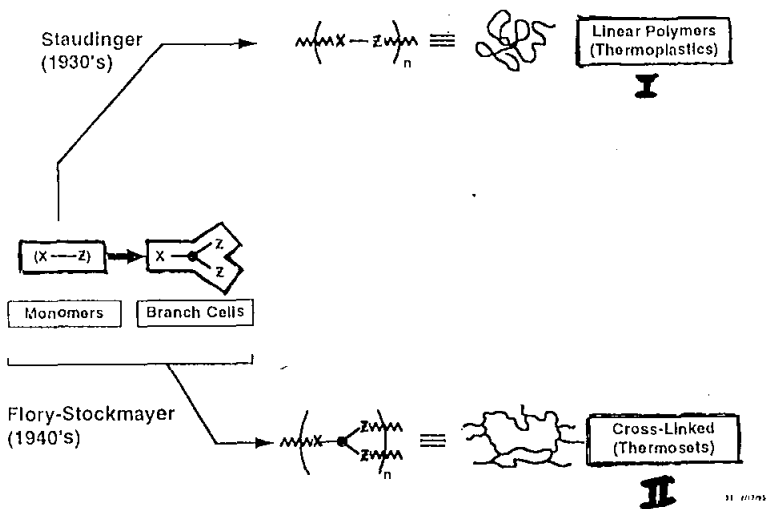
Technology Periods



Major Macromolecular Architectures



- | | | | |
|--------------------------------|-------------------------------|---------------------------------------|---|
| 1930's
Plexiglass,
Nylon | 1940's
Rubbers,
Epoxies | 1960's
Low Density
Polyethylene | Present |
| | | | Coatings - fast cure, low viscosities |
| | | | Biomedical - gene expression
- immuno diagnostics
- controlled delivery |
| | | | Electronics - 3-D conductivity
- quantum dots |
| | | | Sensors - chemical
- biological |

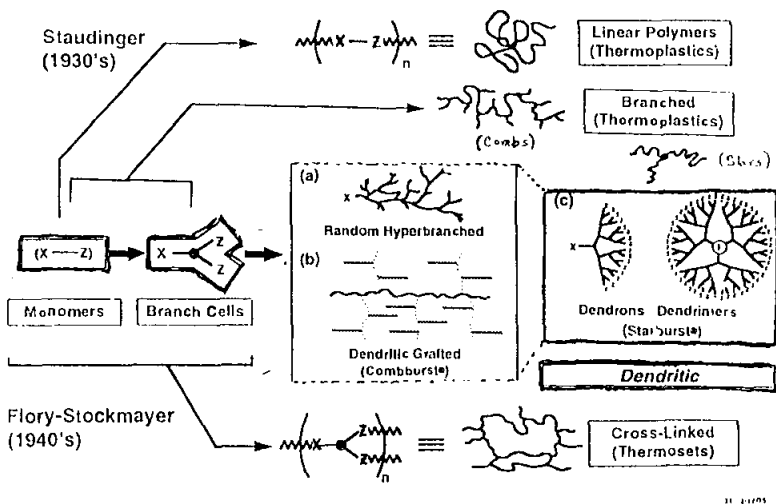


Commercial Synthetic Polymers

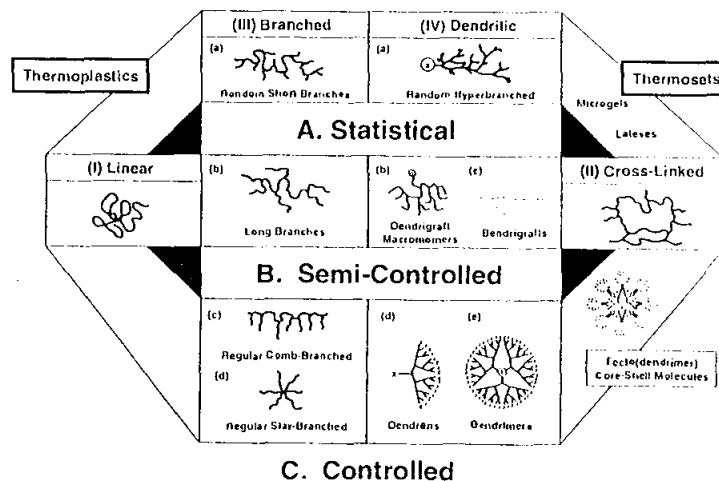
Thermoplastics Class I (Linear)				Thermosets Class II (Cross-Linked)			
Polymer Types	Discovery	Production	Main Applications	Polymer Types	Discovery	Production	Main Applications
Poly(methyl methacrylate)	1860	1928	Plastics (Plexiglass®)	Phenolic resins	1907	1910	Thermosets (Electrical Insulators)
Poly(vinyl acetate)	1912	1930	Adhesive, poly(vinyl alcohol)	Ethyl cellulose	1912	1915	Elastomers (Electrical Insulators)
Poly(ethylene)	1839	1930	Thermoplastic, foams	Acrylonitrile	1847	1926	Elastomers (Footwear)
Poly(bisphenol A)	1839	1931	Thermoplastic (synthetic fiber)	Ammoniacal	1915	1928	Thermosets
Poly(methylene acrylate)	—	1931	Thackery, sizes	Poly(methylol urea)	1917	1919	Elastomers (Number 1000s)
Poly(vinyl alcohol)	1928	1938	Adhesives, plasticizer	Poly(urea-formaldehyde)	1917	1927	Elastomers
Poly(oxaniline adipamide)	1926	1936	Fibers, thermoplastic	Unsaturated polyester	1930	1936	Thermosets
Poly(vinylidene chloride)	1928	1939	Thermoplastic (packaging films)	Poly(methylol siloxane)	—	1937	Elastomers
Poly(methyl acrylate)	—	1939	Blood plasma expander, binders	Styrene-butadiene	1928	1937	Elastomers (Motor Tires)
Poly(styrene), low density	1923	1938	Thermoplastic	Ethylene oxide	1903	1947	Fluids (seals, elastomers)
Poly(ε-caprolactone)	1928	1939	Fibers, thermoplastic	Cyclohexane	1938	1946	Adhesives
Polyacrylonitrile	1937	1940	Fibers, plastics, elastomers, foams	Epoxy resins	1938	1946	Adhesives
Poly(acrylonitrile)	1916	1933	Fibers	Poly(butadiene), etc. 1,4	—	1938	Elastomers
Poly(ethylene terephthalate)	1928	1950	Plastics, fibers				
Poly(ethylene terephthalate)	1941	1953	Fibers, foams				
Bisphenol A polycarbonate	1930	1953	Thermoplastics				
Poly(methyl methacrylate)	1939	1956	Thermoplastics, foams				
Poly(propylene), isotactic	1956	1957	Thermoplastics, fibers				
Poly(ethylene glycol)	1825	1959	Thermoplastics				
Aromatic polyamide	—	1961	High modulus fibers				
Styrene-butadiene styrene block copolymer	—	1965	Elastoplastic elastomers				

Properties Based On:

- (a) Elemental chemical compositions (e.g. monomers)
- (b) Copolymer compositions
- (c) Molecular weights/distributions
- (d) Cross-link densities



Evolution of Skeletal Macromolecular Architecture



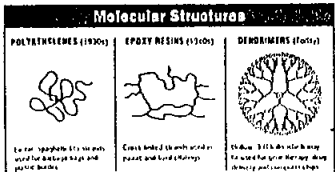
IN THE LAB

Persistent Inventor Markets a Molecule

By David Kirschner
 Staff Reporter of The Wall Street Journal

Over three times this century, chemists have developed a new type molecule that has launched whole industries. Nylon, polyethylene and Teflon. Now scientist Donald Tomalia thinks he has the answer.

In Tomalia's opinion, the next three molecular revolutions will be moderate, rather than explosive. His unique strategy is to keep the new polymer as soft and pliable as the old ones, rather than making it stiffer and more rigid. He says the new molecules will be used in a wide range of applications, from the softest to the stiffest. He says the new molecules will be used in a wide range of applications, from the softest to the stiffest.

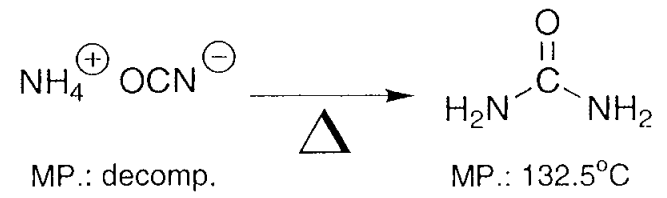


Persistent Inventor Markets a Molecule To Many Industries



has funded \$10 million in research fees from companies experimenting in Dallas to develop polyethylene, epoxy resins and other materials. A French chemist, Pierre Teyssie, has been studying the structure of dendrimers in his laboratory in France. He says the new molecules will be used in a wide range of applications, from the softest to the stiffest.

Wöhler Chemistry (1828)



A simple rearrangement of atoms in space can dramatically alter the physical as well as the chemical properties of a molecular composition.

J. Berzelius (1832)

(Isomeric State)

“Substances of identical compositions but different architecture - isomers - will differ in one or more properties.”

Ref: J. J. Berzelius, J. Phys. Wissench. (1832), 11, 44



J.J. Berzelius, 1779-1848

ISOMERISM (1832)

Berzelius refers to Isomeric Compounds (*isomorph*, composed of equal parts), which he defines as compounds having the same chemical composition "and the same capacity of saturation", but with different properties. As examples he quotes the phosphoric acids, fulminic acid and cyanic acid, the two kinds of stannic acid, and the two tartaric acids (tartaric and racemic). The case of fulminic and cyanic acids led to the recognition of isomerism by Berzelius.

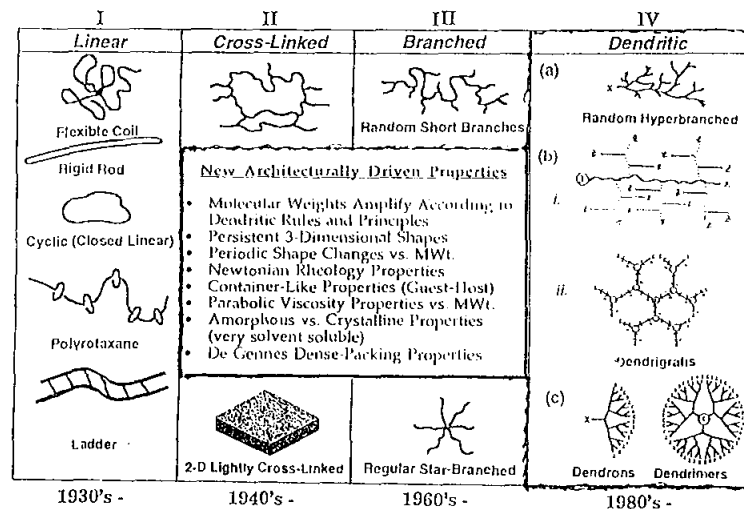
Skeletal Macromolecular Isomerism

“Macromolecular substances having the same structural building blocks in the same proportions but in different architectural configurations may be expected to exhibit different chemical and macroscopic property behavior.”

P. R. Dvornic and D. A. Tomalia
Science Spectra, 5, 36 (1996)

D. A. Tomalia 9/1/97

Major Macromolecular Architectures

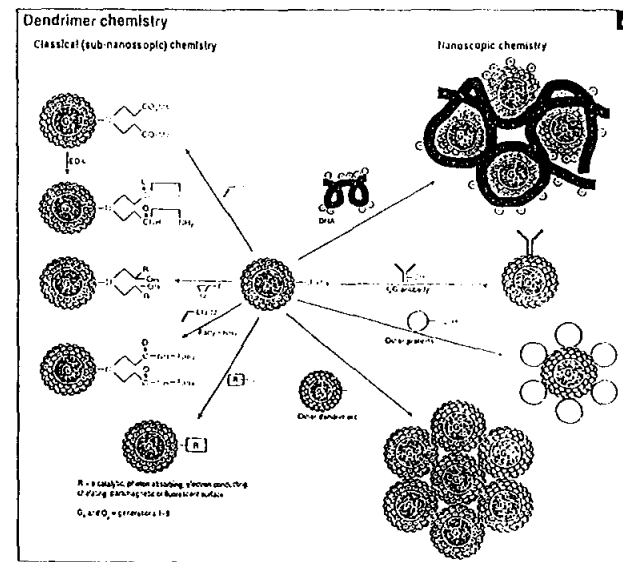


D. A. Tomalia 6/1/98

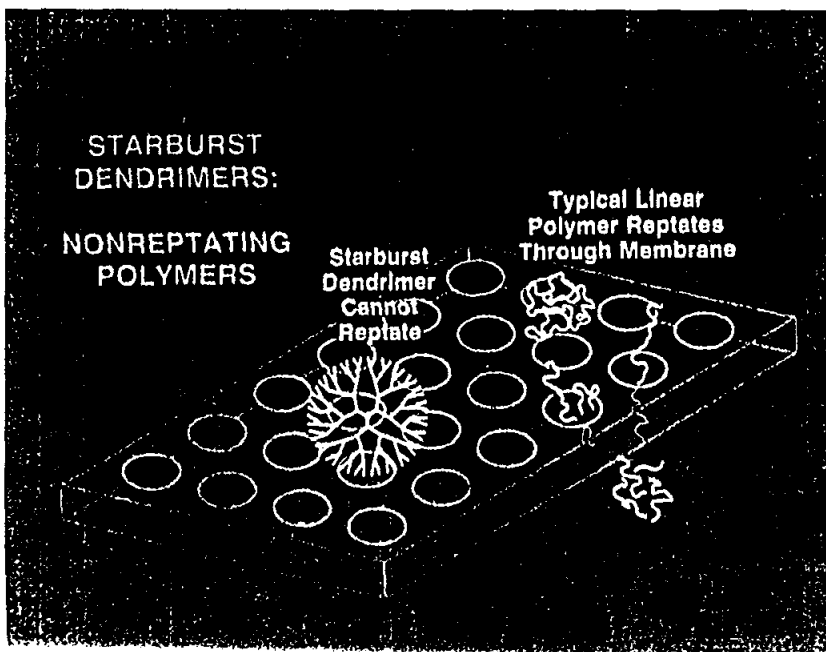
Dendrons, dendrimers and dendrigrafts

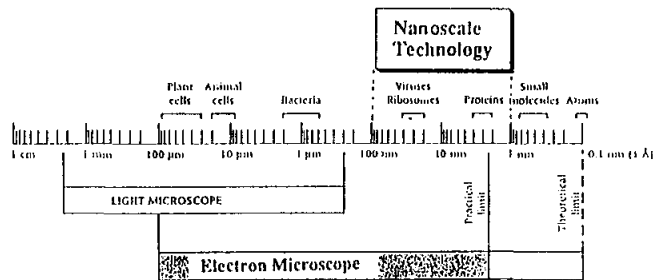
DONALD A. TOMALIA & ROSALITA ESPINOSA

The search for structural control at a nanoscopic level may well be, over the next few years, carefully orchestrated into a variety of new shapes



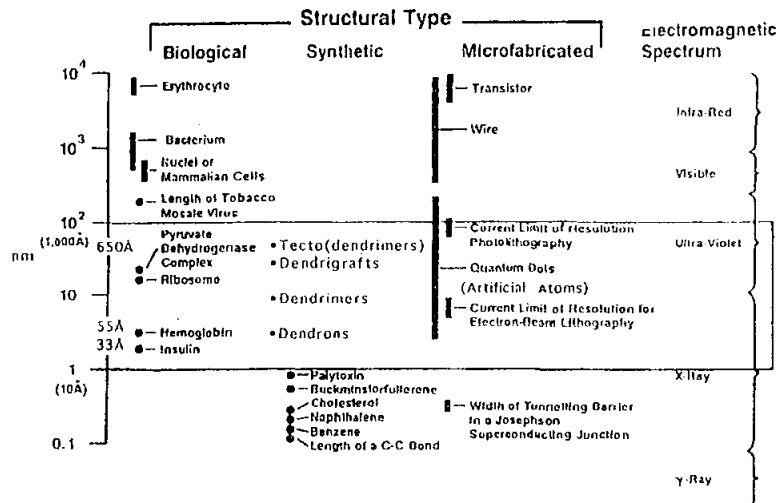
Chemistry & Industry, 2 June 1997





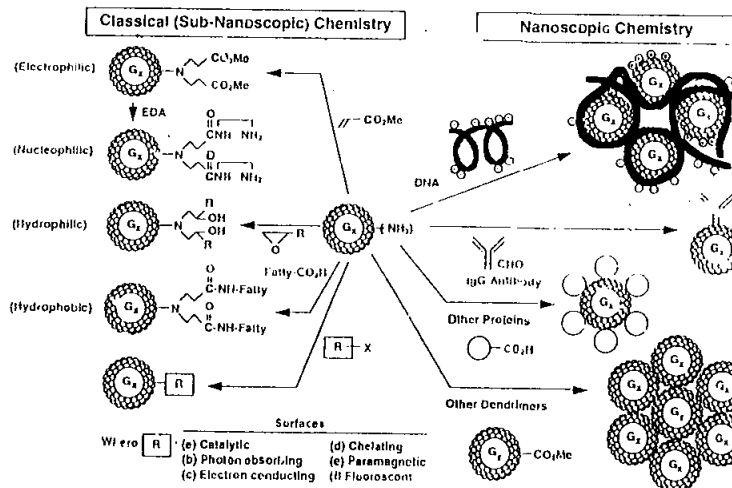
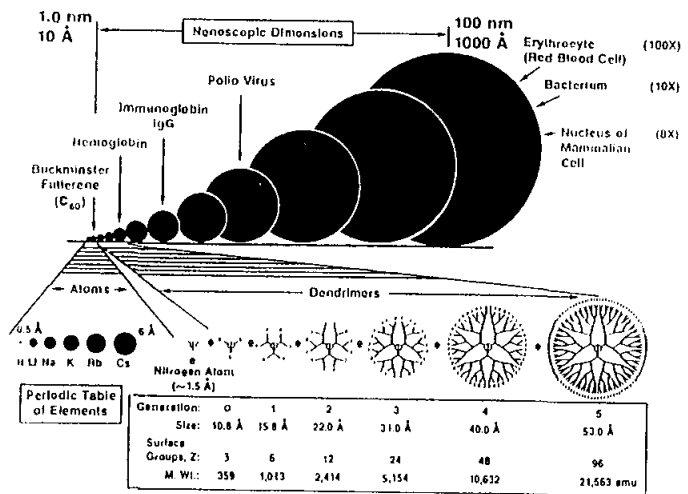
A logarithmic scale is used to compare the sizes of animal and plant cells, bacteria, viruses, proteins, molecules, and atoms. The light microscope can resolve objects of 0.2 micron. The electron microscope has a theoretical capacity of 1 to 2 angstroms, but its practical capacity is 2 to 3 nanometers. A micron or micrometer (μm) is 0.000001 (10^{-6}) meter. A nanometer (nm) is 0.000000001 (10^{-9}) meter. An angstrom is 0.0000000001 (10^{-10}) meter.

NANOSCOPIC TECHNOLOGY



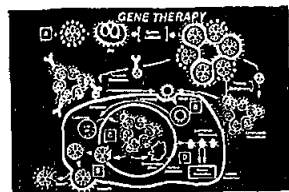
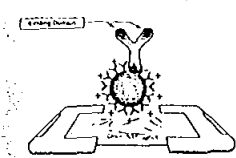
d379.032

Tomalia/7-94

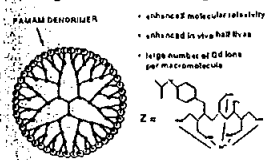


Some Current Nanobiological Devices Utilizing Dendritic Polymers

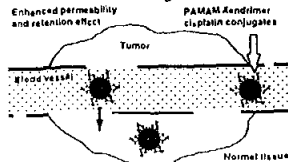
Dendrimer-Linked Antibody Assays



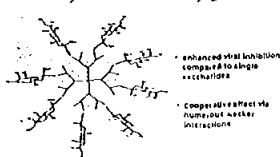
Magnetic Resonance Imaging



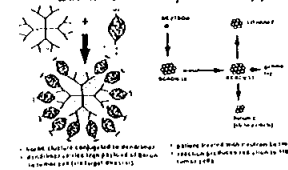
Anticancer Agents



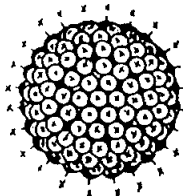
Glyco-Dendrimer Conjugates



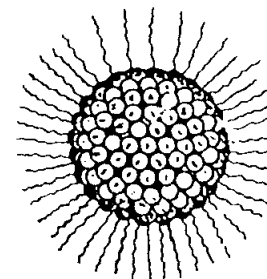
Neutron Capture Therapy



Covalently Fixed Regular Micelles



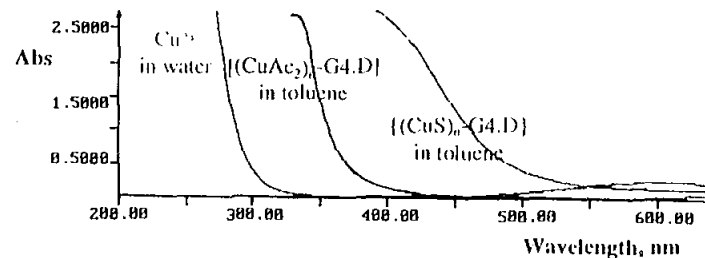
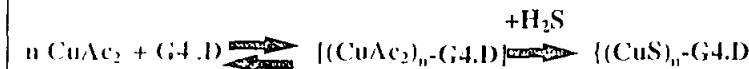
Covalently Fixed Inverse Micelles



347



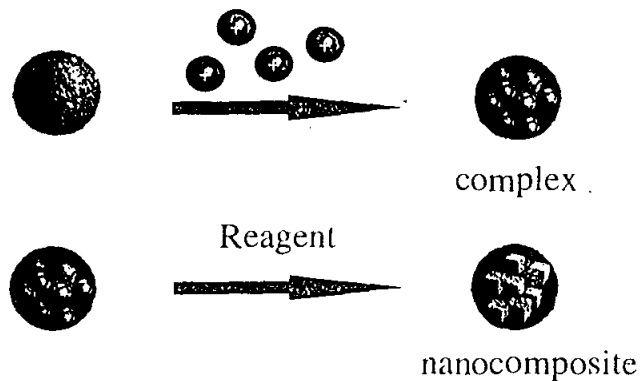
“Brown toluene” from “blue toluene”



Cu²⁺ in this inverted micelle must be inside and cannot be on the surface or in the toluene solvent



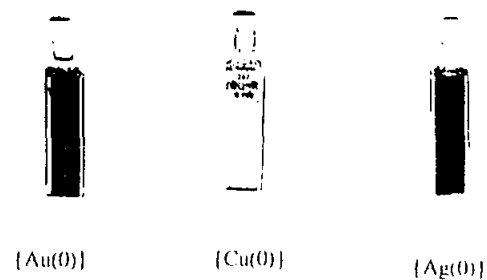
Formation of dendrimer nanocomposites



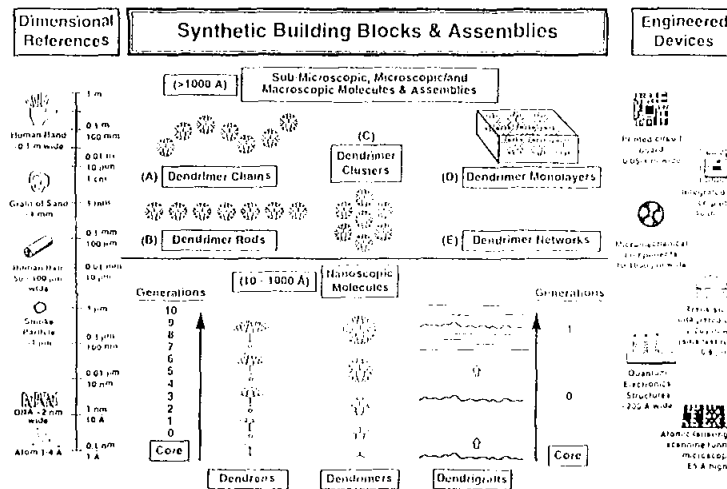
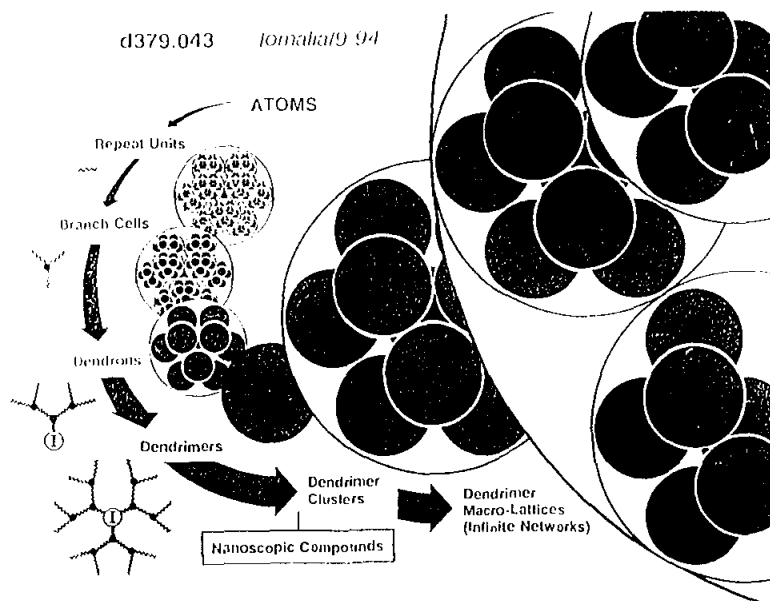
L. Balogh, 08/17/97

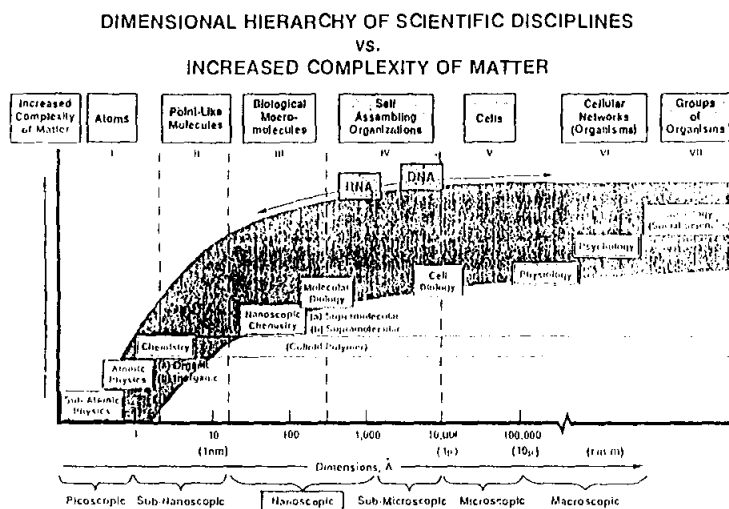


Metal-Dendrimer Nanocomposite solutions



L. Balogh, 01/15/98





Michigan Molecular Institute – University of Michigan
Nanoscopic Chemistry Group



U.S. Army Research Laboratory

Acknowledgements



Michigan Molecular Institute

Nanoscopic Chemistry & Architecture Group

Alicia Asadorian	David Hedstrand	Dujie Qin
Lajos Balogh	Agnes Jallouli	Ralph Spindler
Herb Brothers II	Steve Keinath	Teruyo Sugiura
Peter Carver	June Klimash	Doug Swanson
Roberta Cheng	Marc Mansfield	Srinivas Uppuluri
Petar Dvornic	Linda Nixon	Bing Wang
Roseita Esfand	Lars Piehler	Rui Yin
		Yucheng Zhu

Dendritech, Inc.
The U.S. Army Research Laboratory (ARL)
The U.S. Army Edgewood Research, Development and
Engineering Center (ERDEC)
The U.S. Army Research Office (ARO)
Defense Advanced Research Project Agency (DARPA)

**TUTORIALS
for
INTRODUCTION TO MATERIALS ENGINEERING**

Charles J. McMahon, Jr.

University of Pennsylvania
Department of Materials Science and Engineering
3231 Walnut Street
Philadelphia, Pennsylvania 19104

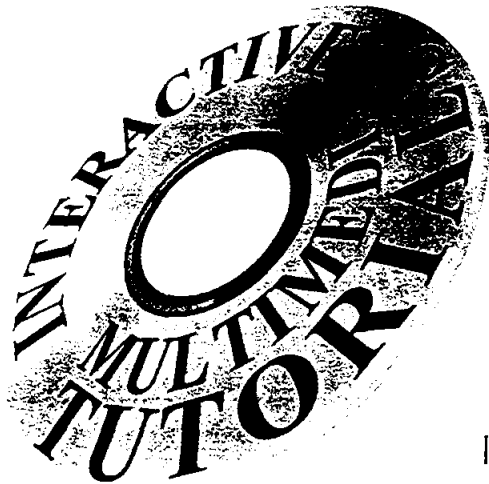
Telephone: 215-898-7979
e-mail: cmcmahon@lrsn.upenn.edu

Tutorials

for

Introduction to Materials Engineering

Charles J. McMahon Jr.



Dislocations and
Crystal Plasticity

Phase Diagrams

Magnetic Materials

Electronic Materials

Interactive Glossary

Animation Viewer

Illustrated Review Booklet

**MERION
MEDIA**



Order from:
Merion Books
Whitman Distribution Center
10 Water Street
Lebanon NH 03766
FAX 603 448 2576 Phone 800 353 3730
Student price: \$18.75

Acknowledgments

This work was supported mainly by the National Science Foundation under grant no. DUE-94-55333. Videos were contributed by Professor Ian Robertson of the University of Illinois, Professor K. A. Jackson of the University of Arizona, Dr. Howard Lieberman of the Allied-Signal Corporation, and by Texas Instrument Corporation. Clips from the Bragg and Nye bubble movie were also used.

This booklet was created by Asha Maliakal and Seamus Woods

Inside the Tutorials

Dislocations and Crystal Plasticity

- Slip in FCC Crystals
- Types of Dislocations
- Observation of Dislocations
- Crystal Plasticity
- Stress Fields of Dislocations
- Energy of Dislocations
- Mechanism of Strain Hardening

Phase Diagrams

- Brazing, Soldering, and Wetting
- Lowering the Melting Temperature
- A Simple-Eutectic Phase Diagram - The Lever Rule
- A Simple-Eutectic Phase Diagram - Microstructures
- The Phase Rule
- Brazing of Bikes

Magnetic Materials

- Recording and Magnetism
- Types of Magnetic Behavior
- Domain Wall Motion
- The Tape Head
- Recording Tape
- Motors and Headphones

Electronic Materials

- Introduction
- Electrical Conductivity
- Semiconductors
- Purification and Crystal Growth
- Silicon-Based Devices and ICs
- Other Materials and Devices

Animation Viewer

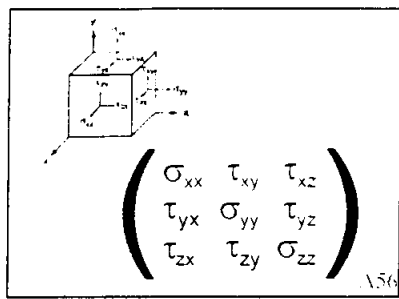
An index of animations for classroom use by instructors.

The Glossary

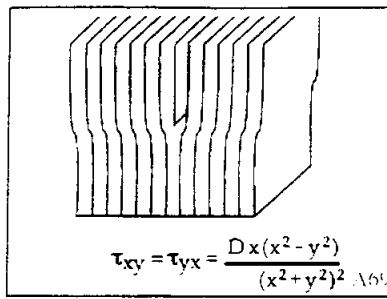
Interactive, hyper-linked, illustrated glossary for students.

Dislocations and Plastic Flow

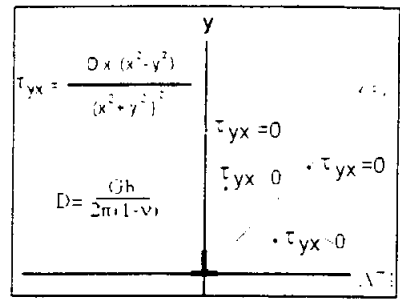
Tensile Test	Tension Causes Plastic Shear	Shear on the Atomic Scale
Slip Planes & Directions in FCC	Shear by Dislocation Glide	Edge Dislocation
Edge Dislocation in 3D	Screw Dislocation	Screw Dislocation & Burgers Vector
Cross Slip of Screw Dislocation	Mixed Dislocation	Dislocation Loop
Strain Around Screw Dislocation	Stress from a Screw Dislocation	Point in a Stress Field



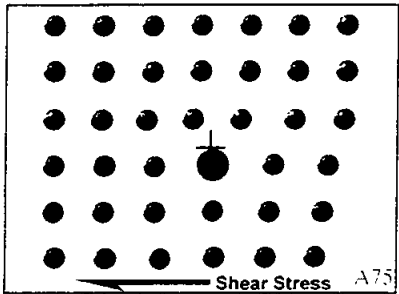
Stress Components



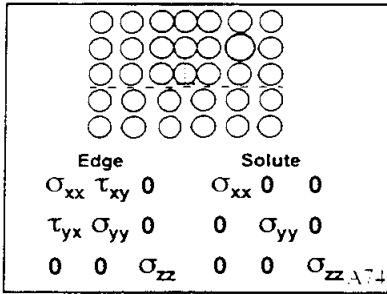
Shear Stress - Edge Dislocation



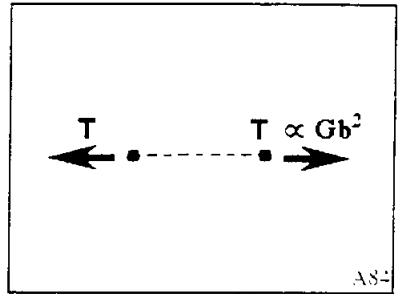
$\tau_{xy} = f(x, y)$



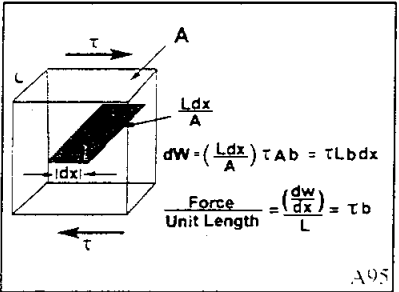
Edge vs. Solute - Attraction



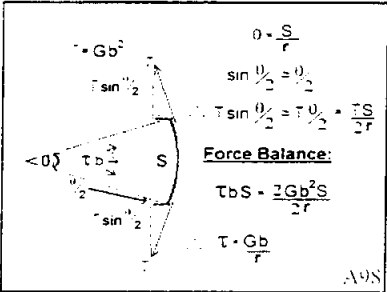
Edge vs. Solute - Repulsion



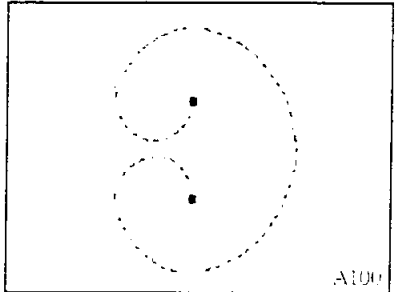
Line Tension



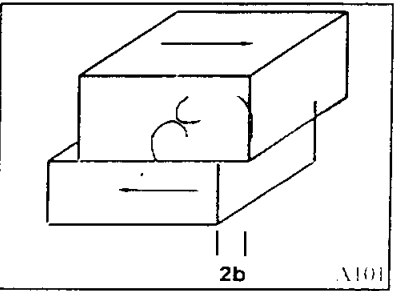
Force on a Dislocation



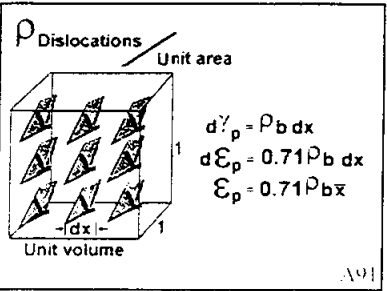
Bowing Dislocation Loop



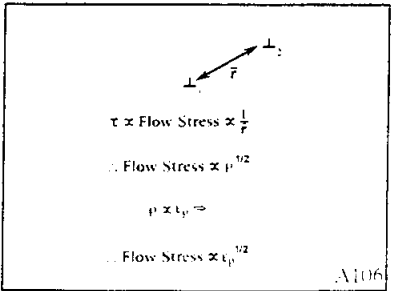
Frank-Read Source



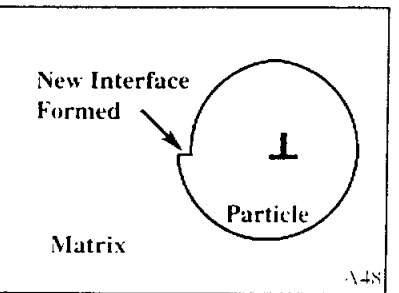
Shear by Frank-Read Source



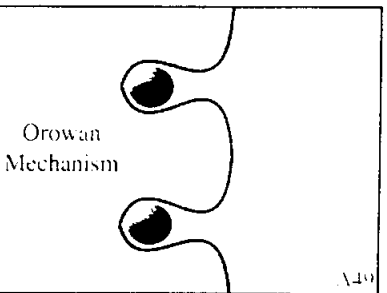
Plastic Strain



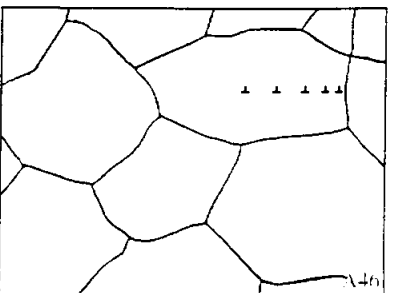
Strain Hardening



Cutting a ppt. Particle

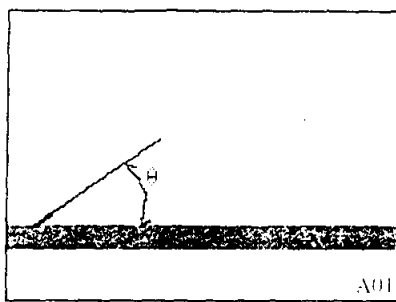


By-Passing ppt. Particles

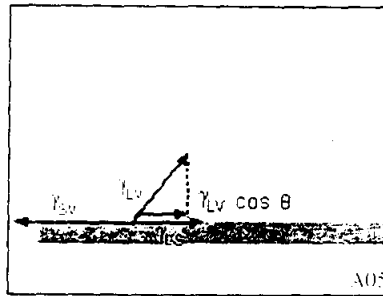


Dislocation Pile-up at Grain Boundary

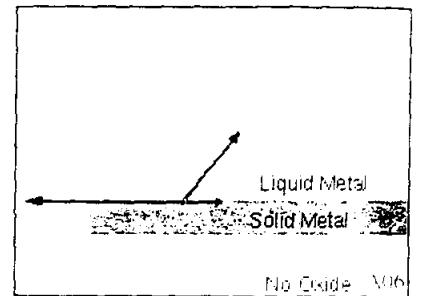
Phase Diagrams



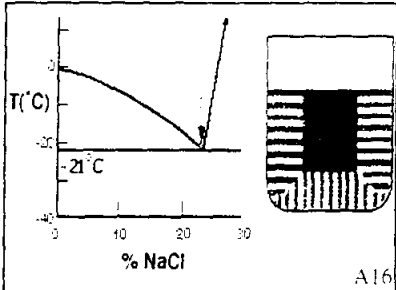
Wetting Angle



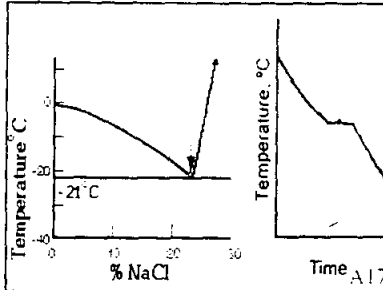
Surface Tension Equilibrium



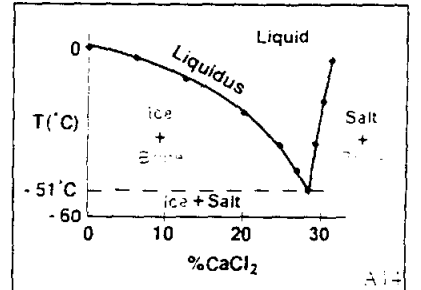
Cleaning Allows Wetting



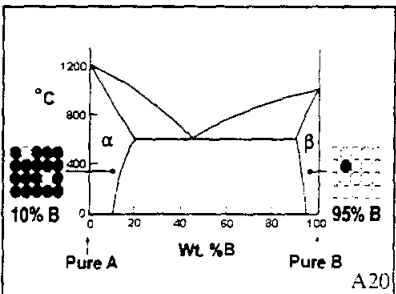
Eutectic NaCl in H₂O



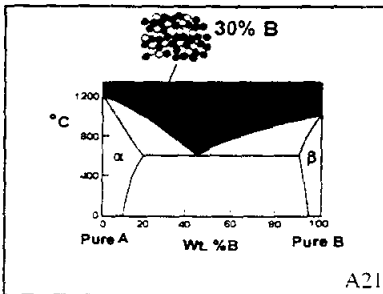
Isothermal Freezing - Eutectic



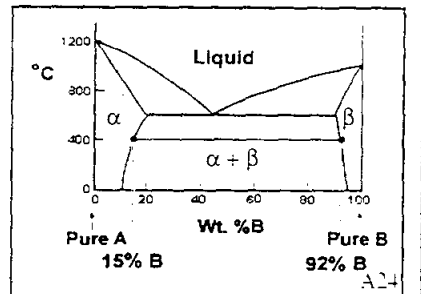
Phase Diagram, CaCl₂ in H₂O



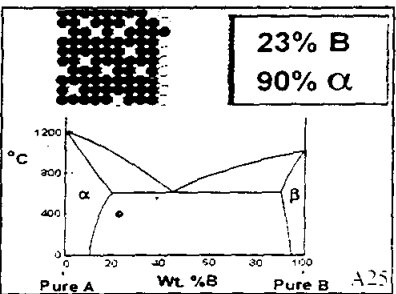
α & β Solid Solutions



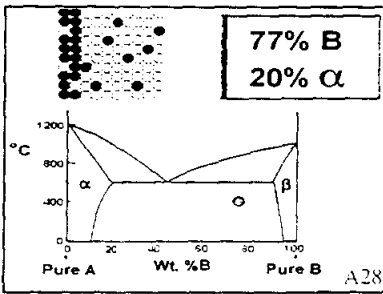
A-B Liquid Solution



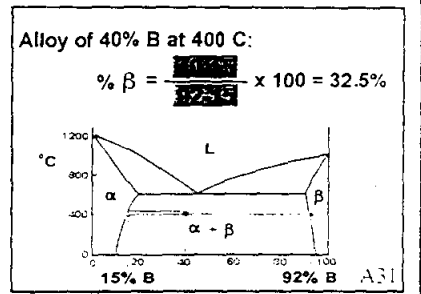
Tie Line in α + β



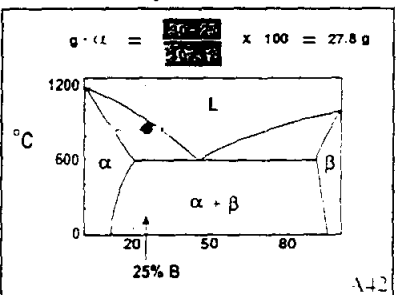
Major Phase α



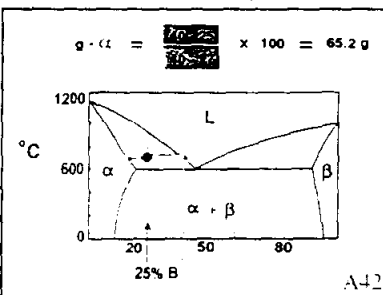
Major Phase β



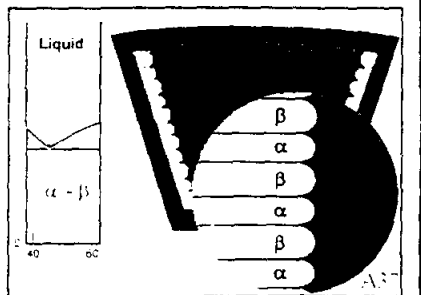
Lever Rule



A-25% B, Early Freezing

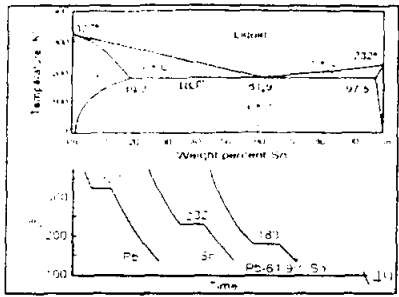


A-25% B, Later Freezing

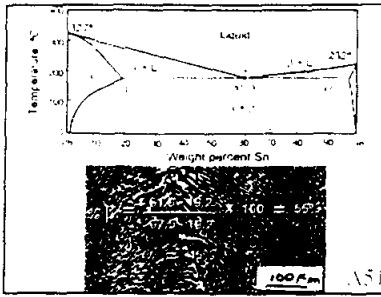


Eutectic Solidification

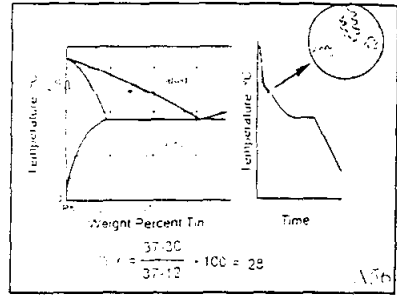
Phase Diagrams



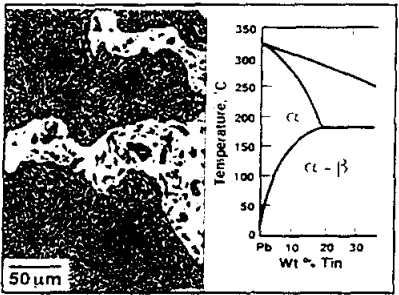
Pb-Sn Cooling Curve



Pb-Sn Eutectic



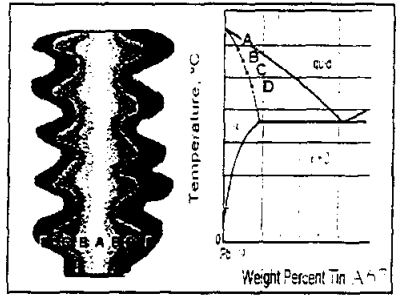
Pb-30%Sn Solidification



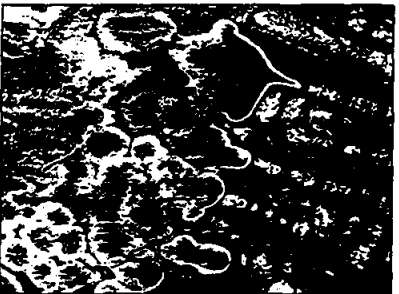
Pb-Sn Microstructure



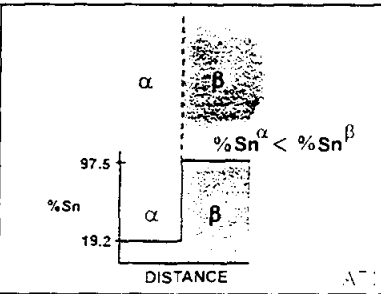
Dendrite Formation



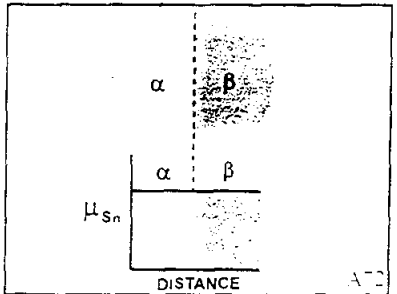
Coring of Dendrites



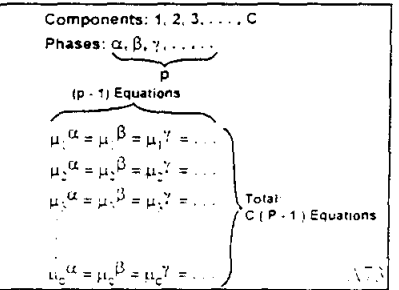
Cored Dendrites in Cu-Sn



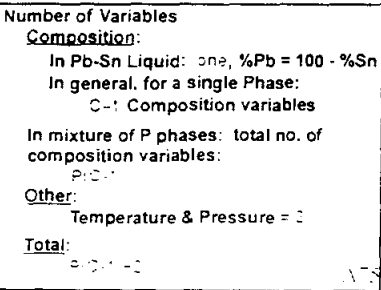
α - β Composition Gradient



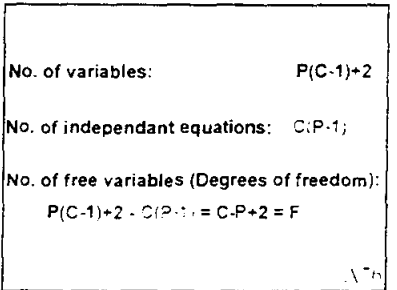
α - β 2-Phase Equilibrium



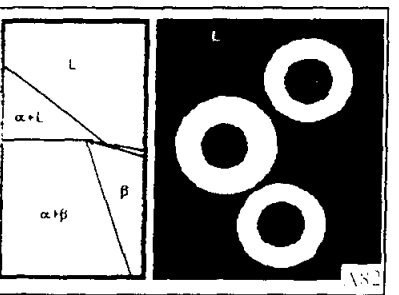
Equilibrium Equations



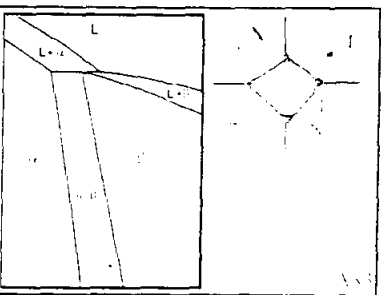
Thermodynamic Variables



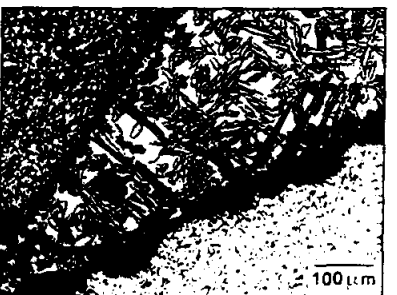
Phase Rule



Peritectic Freezing

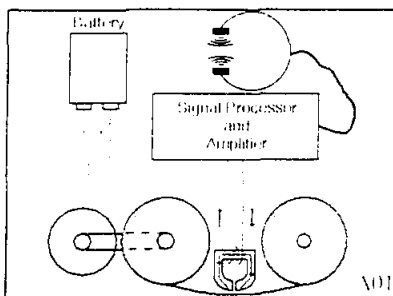


Cu-40%Zn Brazing Alloy

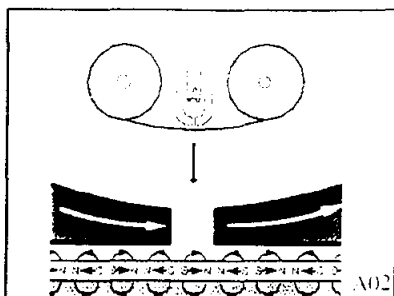


Cu-40%Zn Braze

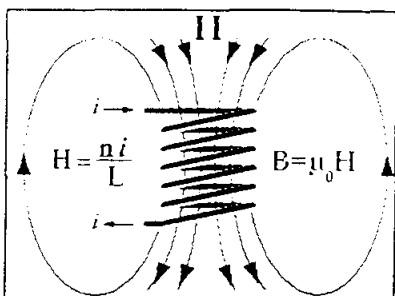
Magnetic Materials



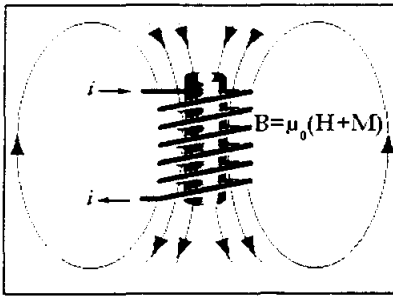
Walkman



Tapehead



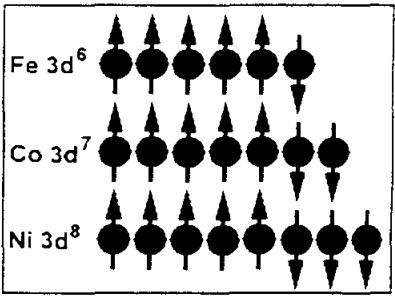
Solenoid



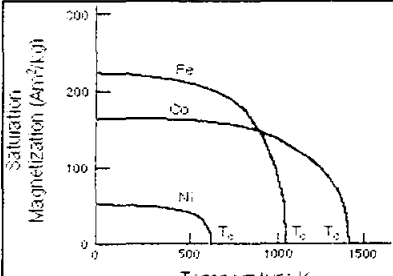
Magnetization

VIIB		VIII		IB		IIB	
25	26	27	28	29	30		
Mn	Fe	Co	Ni	Cu	Zn		
54.94	55.85	58.93	58.71	63.54	65.37		
43	44	45	46	47	48		
Tc	Ru	Rh	Pd	Ag	Cd		
(98)	101.07	102.91	106.4	107.87	112.40		
75	76	77	78	79	80		
Re	Os	Ir	Pt	Au	Hg		
186.2	190.2	192.2	195.09	196.97	200.59		

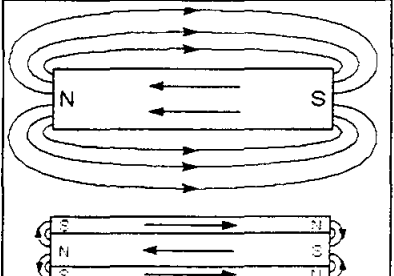
Ferromagnetic Materials



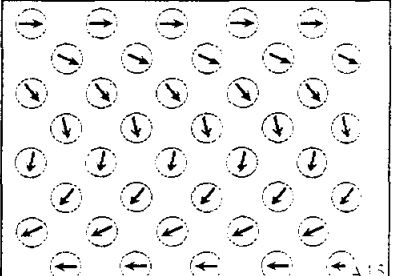
Unpaired Spins



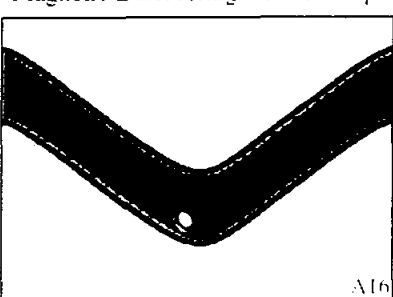
Magnetic Disordering - Curie Temp.



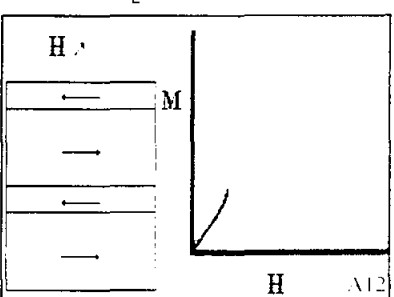
Magnetic Domains



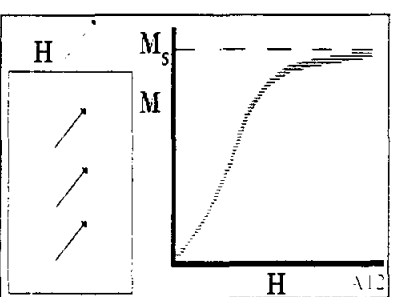
Domain Wall



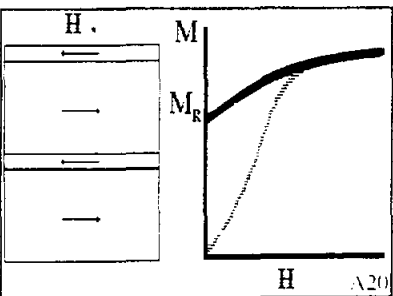
Pinned Domain Wall



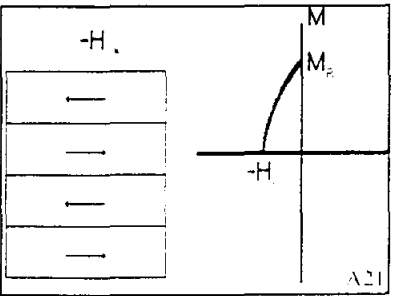
Magnetization Curve



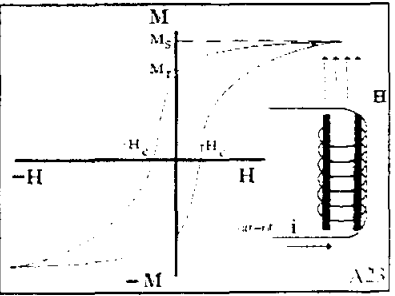
Saturation Magnetization, M_s



Remanent Magnetization, M_R



Coercive Field



Hysteresis Loop

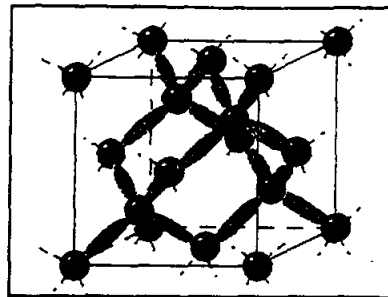
Magnetic Materials

<p>Laminated Tape Head</p> <p>A28</p>	<p>Fe₃O₄</p> <p>Copper ions in FCC lattice sites</p>	<p>Tape Particles</p> <p>100 nm X40,000</p>
<p>Eddy Currents</p> <p>A32</p>	<p>Single Domain Particle</p> <p>Domain Wall ~200 Å Tape Particle ~1000 Å ~1000 Å</p> <p>A33</p>	<p>Recording Head</p> <p>Head: Soft Magnetic Material</p> <p>S N</p> <p>A34</p>
<p>Aligning Tape Particles</p> <p>A32</p>	<p>Varying Sound Intensity</p> <p>A35</p>	<p>Headphones</p> <p>Magnet</p> <p>A37</p>
<p>Motor</p> <p>Permanent Magnet</p> <p>Soft Iron Rotor</p> <p>A40</p>	<p>Permanent Magnet</p> <p>M, M_R, H_c, H</p> <p>A38</p>	<p>Motor Operation</p> <p>soft iron rotor, permanent magnet</p> <p>A38</p>
<p>Single Domain Particles</p> <p>Permanent Magnet: Motor, Headphones</p> <p>A40</p>	<p>Permanent Magnet Materials</p> <p>Nd₂Fe₁₄B, SmCo₅, Alnico α, Ferrite</p> <p>M (Tesla), H (KA/m)</p>	<p>Alnico Heat Treatment</p> <p>T (°C), Alloy %B</p> <p>α, α + β, Aging to Precipitate β in a Magnetic Field</p> <p>A41</p>

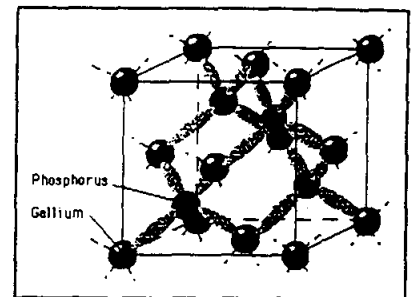
Electronic Materials

		III	IV	V	VI
	B	C	N	O	
	10.81	12.01	14.01	16.00	
II	Al		Si		
	26.98		28.09		
	Ga		As		
	69.72		74.92		
	In		Sb		
	114.82		121.75		
	Tl		Pb		
	204.37		207.19		
	Hg		Bi		
	200.59		208.98		
			Po		
			(210)		

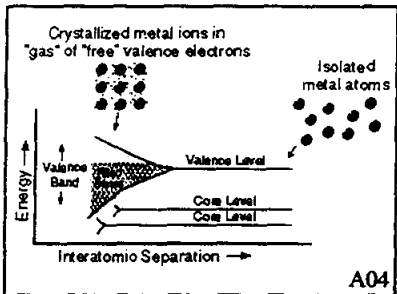
Semiconductor Materials



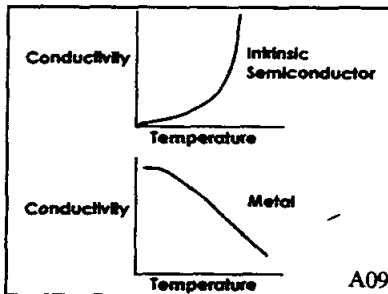
Structure of Si, Ge



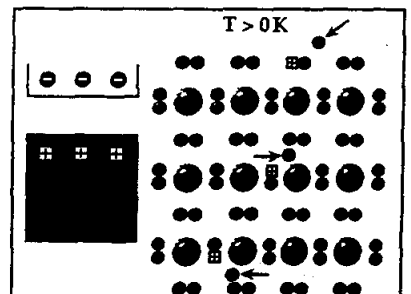
GaP



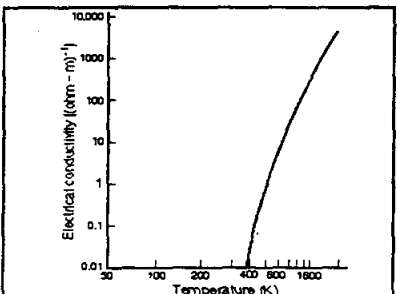
Energy Band Formation



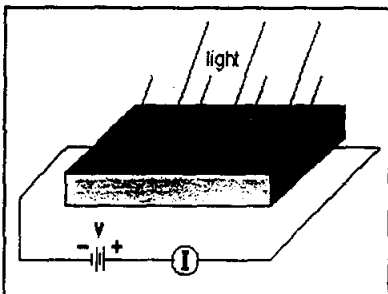
Metals vs. Semiconductors



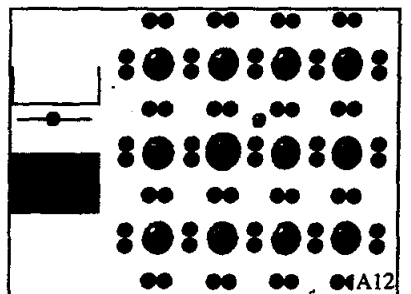
Intrinsic Si, e-h Pairs



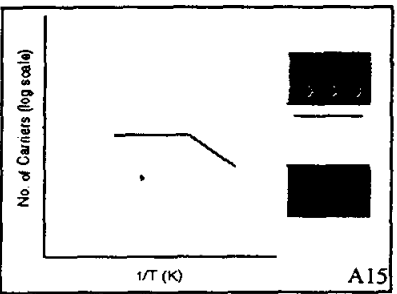
Intrinsic Si, Conductivity vs. Temp.



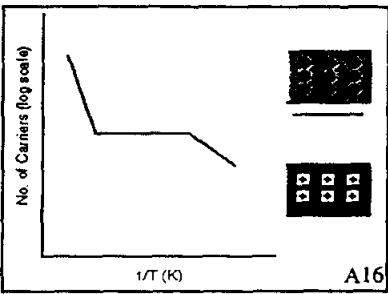
Photocell



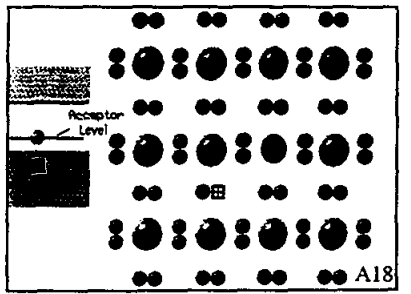
P-Doped Si



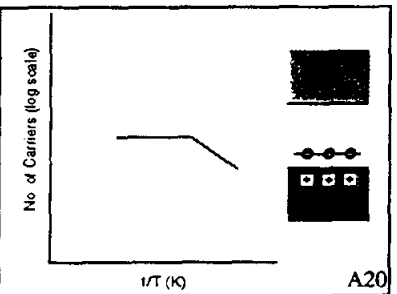
Donor Exhaustion



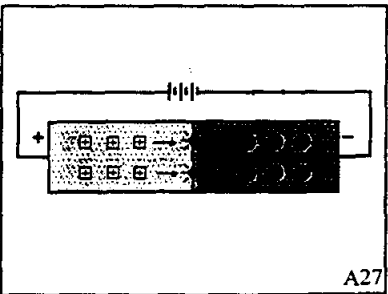
Extrinsic → Intrinsic



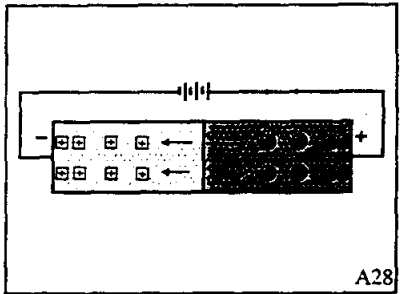
B-Doped Si



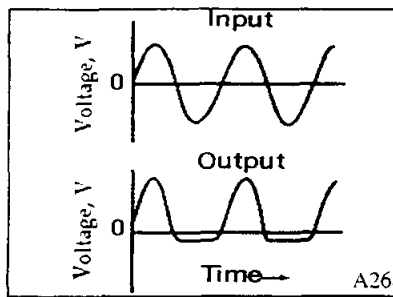
Acceptor Saturation



P-N Junction, Forward Bias

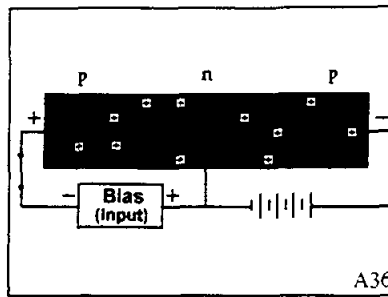


P-N Junction, Reverse Bias



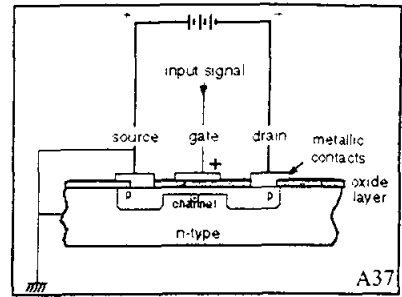
Rectification

A26



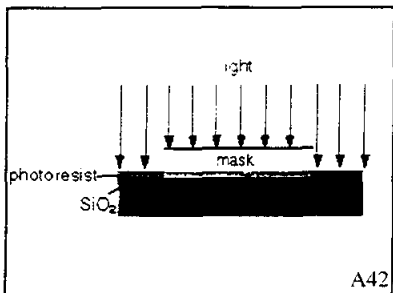
Junction Transistor

A36



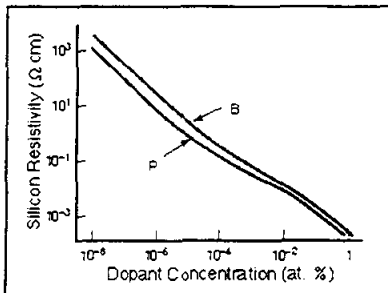
FET

A37



IC Fabrication

A42

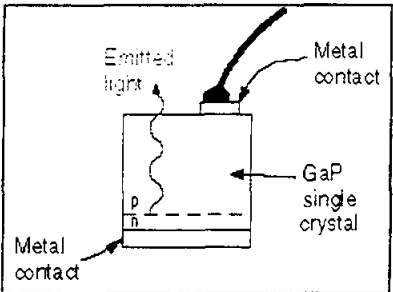


Conductivity, Extrinsic Si

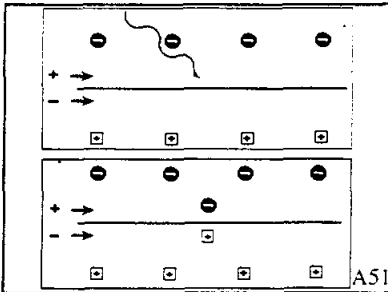
Material	Band Gap (eV)	Mobility of Electrons ($\text{m}^2/\text{V}\cdot\text{sec}$)	Mobility of Holes ($\text{m}^2/\text{V}\cdot\text{sec}$)	Electrical Conductivity ($\text{ohm}\cdot\text{m}^{-1}$)
Elemental				
Si	1.11	0.14	0.05	4×10^{-4}
Ge	0.67	0.38	0.18	2.2
III-V Compounds				
GaP	2.25	0.05	0.002	
GaAs	1.35	0.85	0.45	10^{-5}
InSb	0.17	7.7	0.07	2×10^{-4}
II-VI Compounds				
CdS	2.40	0.03		
ZnTe	2.26	0.03	0.01	

Semiconductor Properties

A47

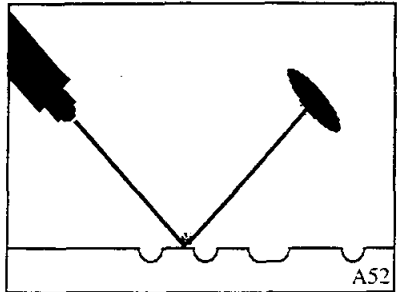


LED



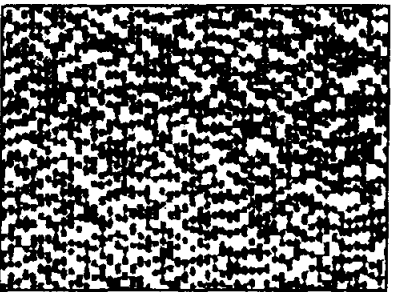
Solar Cell

A51

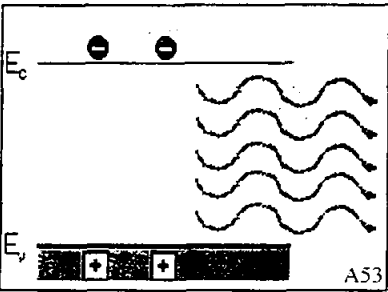


Laser Reading a CD

A52

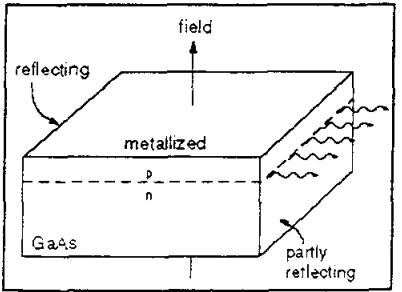


Pits on a CD

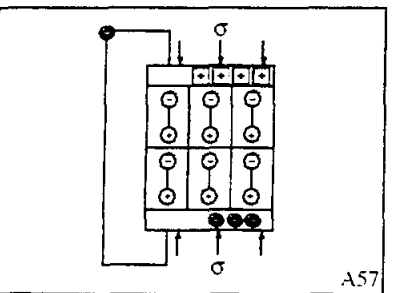


Pumped Laser

A53

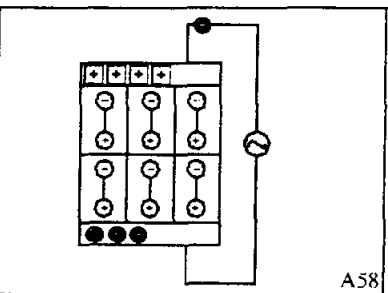


GaAs Laser



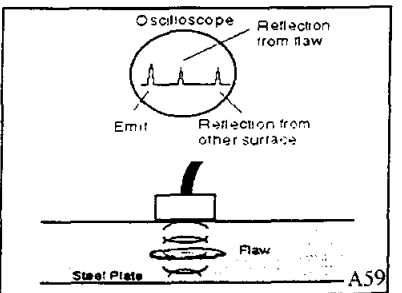
Piezoelectric - Stress Effect

A57



Piezoelectric - Voltage Effect

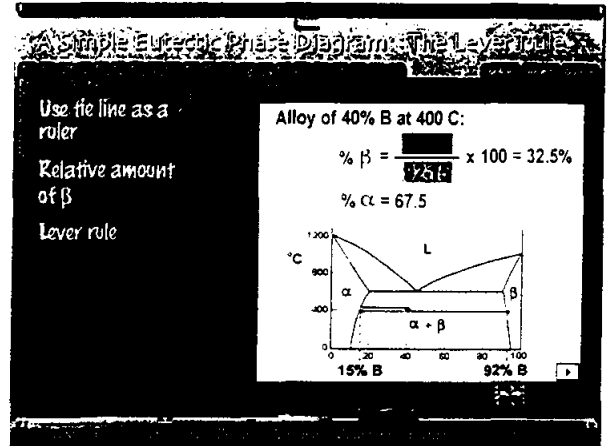
A58



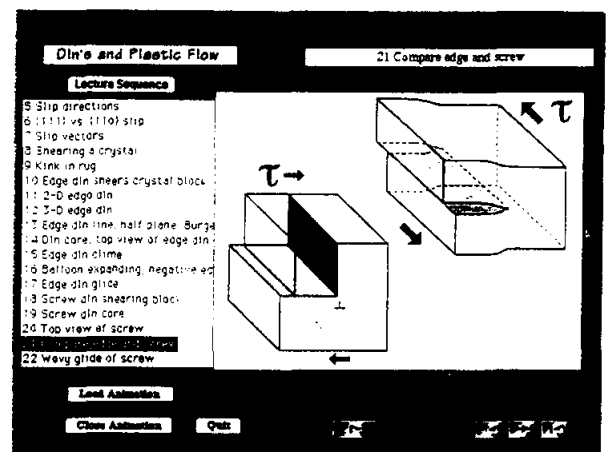
NDE with Piezo Crystal

A59

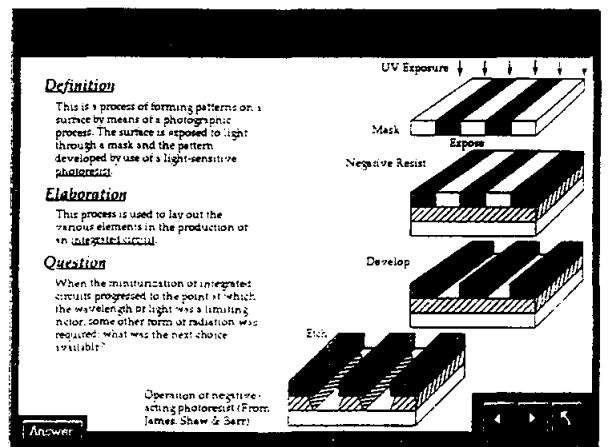
The tutorials have an interface that looks like a chalk board. Each is divided into sections, and then into "pages," and the latter are accessed by tabs at the top. The navigation controls are at the bottom, and each page contains synchronized board items, animations, videos, photos, drawings, derivations, etc. Here's one showing the definition and use of the lever rule.



The animation viewer can be used in the classroom by an instructor to teach concepts that involve motion and that are difficult to visualize for beginning students.



The interactive glossary is illustrated and hyper-linked to other terms. It is primarily for use by students with the tutorials and for review afterwards.



System Requirements

Windows® CD-ROM

Windows 95 or NT 4.0 required
100MHz Pentium® or faster
16MB RAM
4X CD-ROM or faster
640 x 480 display, 256 colors
Windows compatible sound device

Macintosh® CD-ROM

Mac™ OS System 7.5 or higher
90MHz PowerPC™ or faster
9MB RAM free
4X CD-ROM or faster
640 x 480 display, 256 colors

*In order to run properly, the included copy of Quicktime 3.0 must be installed. On slower machines the contents of the CD (460MB) may need to be copied to the hard drive for adequate performance



ISBN 0-9646598-2-4

ROOM TEMPERATURE CREEP OF SOLDER

Robert G. Stang

Department of Materials Science and Engineering
Box 352120
University of Washington
Seattle, Washington 98195-2120

Telephone: 206-543-2623
e-mail stang@u.washington.edu



Robert G. Stang

ROOM TEMPERATURE CREEP OF SOLDER

Robert G. Stang
Department of Materials Science and Engineering
Box 352120
University of Washington
Seattle WA, 98195-2120

ABSTRACT

Soft solder material, deformed under constant stress or load at room temperature, is actually being deformed at a homologous temperature greater than 0.6 of the melting temperature, where temperatures are expressed in degrees Kelvin. Deformation under these conditions, at constant stress or load, is time dependent and is usually called creep. The use of solder materials, in an undergraduate laboratory experiment, provides an inexpensive, simple, safe and convenient method to introduce students to high temperature creep behavior without the need for high temperature creep machines and the associated hardware. The materials used, the data collected and the analysis of this data from a series of creep experiments conducted at room temperature is discussed. The goal is to introduce the subject of high temperature creep and present methods used to identify the microscopic mechanisms controlling high temperature deformation.

ROOM TEMPERATURE CREEP OF SOLDER

Robert G. Stang
Department of Materials Science and Engineering
Box 352120
University of Washington
Seattle WA, 98195-2120

Keywords:

High Temperature Mechanical Behavior, Time Dependent Plasticity, Creep, Solder.

Prerequisite Knowledge:

The student should know or have general knowledge of the following:

1. How to calculate stress.
2. How to measure strain.
3. Know how to use binary phase or equilibrium diagrams.

Objective:

The objective of this experiment is to demonstrate high temperature behavior in metallic materials without the need for sophisticated measuring equipment and furnaces, with the associated safety problems involved with the use of high temperatures. The student will learn how to plot creep curves, use these curves to obtain strain rate, fit strain rate vs stress data to a power law equation and use the resulting parameters to identify the rate controlling creep mechanism.

Equipment and Supplies:

1. Laboratory space in which the temperature is reasonably constant for the duration of the experiment.
2. Thermometer.
3. Soft Solder material, Pb-Sn, or Bi-Sn.
4. 5 Minute Epoxy Cement.
5. Weights: lead or steel shot, scrap metal, etc.
6. Container to hold weight.
7. Balance to measure load on sample.
8. Measuring Device: Meter stick or cathetometer.
9. Timer: Clock or watch.
10. Micrometer: To measure sample diameter.
11. Computer with spread sheet program to analyze data obtained.

Introduction and Background:

The low eutectic temperatures for Bi-Sn (138.5.C) and Pb-Sn(183.C) and the availability of these soft solder materials in local markets make them ideal for use in room temperature creep experiments in undergraduate laboratories. These materials can often be purchased in the coiled round solid form, free of flux, from local hardware or electronic suppliers for use in plumbing applications (Bi-Sn) or electronic and stained glass work (Pb-Sn). In creep studies it is common to express temperatures as homologous temperatures in which test temperatures are expressed as a fraction of the melting temperature, where all temperatures are expressed in degrees Kelvin. When this is done eutectic Bi-Sn samples deformed at room temperature are undergoing deformation at $0.71T_m$ and eutectic Pb-Sn samples deformed under the same conditions are at $0.64T_m$. Metallic materials deformed under these conditions exhibit time dependent plasticity or creep. Virtually any soft solder material can be used to demonstrate creep behavior at room temperature without the need for a furnace and the associated equipment for strain measurement. Experiments have been conducted in this laboratory using Pb-Sn solders of various compositions between 95% Pb-5%Sn to 40% Pb-60% Sn and 50%Bi-50%Sn, where compositions are expressed in weight percent. Strain measurements can be simply made using a ruler or meter stick or if more precision is desired a cathetometer can be used.

The theoretical and experimental aspects of the study of time dependent plasticity can be found in references (1-8). Time dependent plasticity studies begin by collecting a number of creep or strain-time curves for a series of samples deformed under constant load or constant stress conditions. Constant load tests are easier to conduct because the initial load can be left on the sample for the duration of the test. During a constant stress test the load must be changed as a function of strain because the cross sectional area of the sample changes during the experiment making this type of test more difficult to conduct. In either case, the resulting strain-time data is plotted in a linear plot creating a creep curve. The strain rate, defined by the slope of the strain-time curve, given by equation 1, goes through a minimum during the test. Note: The terms used in all equations used in this paper are defined in table I.

$$\dot{\varepsilon} = \frac{\Delta\varepsilon}{\Delta t} \quad \text{Equation 1}$$

A schematic strain-time curve or creep curve for a well behaved annealed metallic material is shown in figure 1(1). This creep curve can be divided into three stages, a primary stage, the secondary or steady state stage and a tertiary stage as shown. The strain-time behavior in the primary region is characterized by an initial elastic strain on loading followed by a region in which the strain rate as measured by the slope of the strain time curve is very high. The initial strain rate in the primary region is high because the annealed material has a low dislocation content. As this annealed material work hardens the strain rate decreases with time or strain until the secondary or steady state region is reached. Strain rate behavior in the secondary or steady state region goes through a minimum in a constant stress test or exhibits a constant minimum strain rate in a constant stress test until the third or tertiary stage is reached. In the secondary region

the strain rate is a constant because a balance exists between work hardening and recovery. The strain rate in the tertiary stage increases because void nucleation and coalescence and necking reduce the cross sectional area of the sample and eventually the strain rate increases locally until failure.

The primary creep region is strongly influenced by sample material and its prior thermo-mechanical history. This region can be difficult to model. The secondary region on the other hand is well understood and several models resulting from theoretical and empirical studies fit the data very well. These models generally yield equations for the steady state strain rate which have the form suggested by Sherby and Burke (1) in equation 2 below or by Bird, Mukherjee and Dorn (2) in equation 3 below.

Sherby-Burke (1)

$$\dot{\epsilon}_s = AD_{sb} G \left(\frac{\sigma}{G} \right)^n \quad \text{Equation 2}$$

Bird-Mukherjee-Dorn (2)

$$\dot{\epsilon}_s = \frac{AD_{sb} G}{kT} \left(\frac{b}{d} \right)^p \left(\frac{\sigma}{G} \right)^n \quad \text{Equation 3}$$

At constant temperature and structure both equations reduce to a simple power law equation in stress as shown in equation 4.

$$\dot{\epsilon}_s = A(\sigma)^n \quad \text{Equation 4}$$

The parameters in equation 4 can be evaluated by fitting experimental data to the equation using a log-log plot of strain rate vs stress. These parameters after evaluation can be used to extrapolate steady state strain rates, at the temperature under consideration, for different stresses. The stress exponent, “n”, in equation 4 can be used to identify the microscopic mechanism controlling the creep process by a study of table II, which lists stress exponents and the corresponding microscopic rate controlling creep mechanism. These “n” values result from theoretical microscopic models which describe the creep process. Detailed information concerning these models can be found in the references.

Experimental Procedure:

A 10 inch length of 0.125 inch diameter solid uncoiled solder is uncoiled from the spool, carefully straightened to avoid work hardening or damage and cut. The sample is gripped by gluing each end in a separate 1 inch long round right circular cylinder made from 1/2 inch diameter aluminum rod. One end of this aluminum rod is drilled and tapped to accept a screw eye and the other end is drilled to clear the outside diameter of the solder. Epoxy cement is used to form the joint. Approximately 1/2 inch is jammed into the aluminum grip fixture filled with epoxy cement in the liquid state. It is important to weigh the grip-screw eye assembly before gluing the solder to the grip. After the epoxy cement has hardened, the assembly is transferred to a ring stand and supported vertically under a minimum load, below the lowest stress used for up to a week, to straighten the solder. The straightened sample is then ready for testing.

The sample gage length is established by marking each end of the sample, approximately 1/2 inch from the aluminum grip, with a black permanent marking pen used for metal layout. The sample is loaded and timer started for the test. Sample elongation can be determined by measuring the distance between these fiducial marks using a ruler or a cathetometer. Stress is determined and the creep curve plotted.

Results and Discussion:

The data presented here is for 50% Pb-50% Sn solder, although other solders could be used for this experiment as discussed in the introduction. A typical creep curve is shown in figure 2 for this solder. This material exhibits limited primary deformation because of its thermomechanical history. After an abbreviated primary region the sample enters the steady state region. The strain rate in the steady state region can be determined after the sample fails or when one is certain the deformation process has reached the tertiary creep stage. A series of tests can be conducted at constant temperature, in this case room temperature, at different stress levels and a log-log plot of strain rate vs stress constructed. Such a plot for the 50-50 Pb-Sn solder used in this study is shown in figure 3. Curve fitting techniques coupled with data analysis packages which accompany most spreadsheet software can be used to determine the stress exponent and the equation for the best fit line which the experimental data describe. The slope of the log-log plot for the set of data collected in this set of experiments is very close to 2. Study of table II suggests that grain boundary sliding and accommodation is the rate controlling creep process. The resulting data and equation can be used in exercises to extrapolate strain rates for stresses outside the range of the test or to predict stress-strain rate behavior within the range of stresses studied.

Comments:

This experiment provides a simple way to introduce the concepts used in high temperature time dependent plasticity studies to undergraduate students. The lab group gains experience in constructing creep curves, plotting data and fitting that data to a power law expression.

Acknowledgments:

The author wishes to acknowledge the help of Han Kim, Hao Pham, Corey Nianekeo, Richard Chou, Linda Hoke, Mike Heit and Dan Williams, all former undergraduate students in The Department of Materials Science and Engineering at The University of Washington.

References:

1. Sherby, Oleg D. and Peter M. Burke, Mechanical Behavior of Crystalline Solids at Elevated temperatures, Progress in Materials Science, Edited by Bruce Chalmers and W. Hume-Rothery, Pergamon Press, Volume 13, Number 7, p. 326. 1968.
2. Bird, James E., Amaiya K. Mukherjee, and John E. Dorn, Correlations Between High-Temperature Creep Behavior and Structure, Proceedings of an International Conference on The Quantitative Relation Between Properties and Microstructure, Haifa Israel, Edited by D. G. Brandon and A. Rosen, p. 255, 1969.
3. Ashby, Michael F. and David R. H. Jones, Engineering Materials: An Introduction to their Properties and Applications, pp. 157-190, Pergamon Press, New York, 1980.
4. Dieter, George E., Mechanical Metallurgy Third Edition, pp. 432-470, McGraw-Hill, New York, NY, 1986.
5. Meyers, Marc A. and Krishan K. Chawla, Mechanical Behavior of Materials, pp. 540-591, Prentice Hall, Upper Saddle River, NJ, 1999.
6. Courtney, Thomas H., Mechanical Behavior of Materials, pp263-324, McGraw-Hill, New York, NY, 1990.
7. Poirier, Jean-Paul, Creep of Crystals: High-Temperature Deformation Processes in Metals, Ceramics and Minerals, Cambridge University Press, Cambridge, 1985.
8. Wilshire, Brian and R. W. Evans, Introduction to Creep, Institute of Materials, London, 1993.

Robert G. Stang

Associate Professor
Department of Materials Science and Engineering
University of Washington
Seattle, WA 98195-2120

B.S. 1961	Long Beach State College	Engineering-M.E. Option
M.S. 1965	UCLA	Materials
Ph.D. 1972	Stanford University	Mat. Sci. & Engineering

After earning a Ph.D. in Materials Science and Engineering at Stanford University in 1972 Robert Stang accepted a temporary teaching position at Instituto Militar de Engenharia in Rio de Janeiro, Brazil. In September 1972 he returned to Stanford University as a research associate remaining until December 1973 when he accepted an Assistant Professorship at the University of Washington, Seattle. He received a Senior Fulbright-Hayes Fellowship to teach and conduct research at Montanuniversitat in Leoben, Austria in 1980-81. During the 1984 and 1985 academic years Professor Stang served as a Program Director with National Science Foundation in Washington, D.C., in the Division of Materials Research. He is a member of several professional societies and has been active in ASM International at local and national levels.

Research Interests:

Professor Stang's interests lie in the area of mechanical behavior of materials. In particular the relation between structure, processing and properties of materials. Much of this work has focused on model systems for high temperature applications.

Current research programs focus on the study of creep in solder materials used in the electronics industry. The creep work is attempting to develop techniques to speed the acquisition to data which can be used to model creep behavior in and to study the effects of hydrostatic pressure on the creep behavior of solder materials. Another study is examining the effect of microstructure on porosity formation during plastic deformation in two-phase alloy systems. In this study steels with various microstructures are studied.

Table I: Terms Used in Equations

ϵ = Strain

$\dot{\epsilon}$ = Strain Rate

$\dot{\epsilon}_s$ = Steady State Strain Rate

t = Time

A = A Material Constant

D_{SD} = Self Diffusion Coefficient

G = Shear Modulus

σ = Stress

n = A Constant which Depends on the Deformation Mechanism

k = Boltzmann's Constant

T = Temperature in Degrees Kelvin

b = Magnitude of the Burgers Vector

d = Grain Size

TABLE II

Stress Exponent-Microscopic Mechanism

n	Microscopic Mechanism
1	Stress Vacancy Diffusion Controlled Creep Nabarro-Herring Mechanism Coble Mechanism
2	Grain Boundary Sliding and Accommodation
3	Diffusion Controlled Viscous Glide Dislocation Motion
4.5	Diffusion Controlled Climb Motion of Dislocations

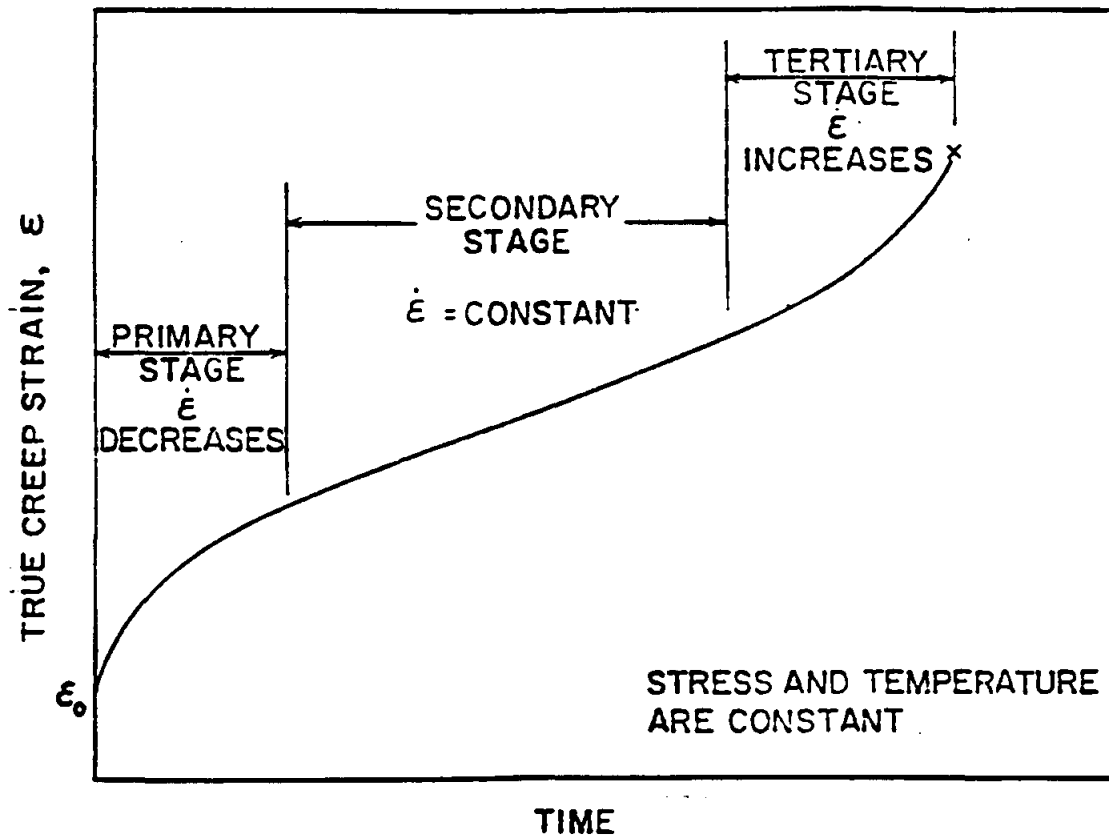


Figure 1: Schematic strain-time or creep curve showing the primary, secondary and tertiary stages of creep (1).

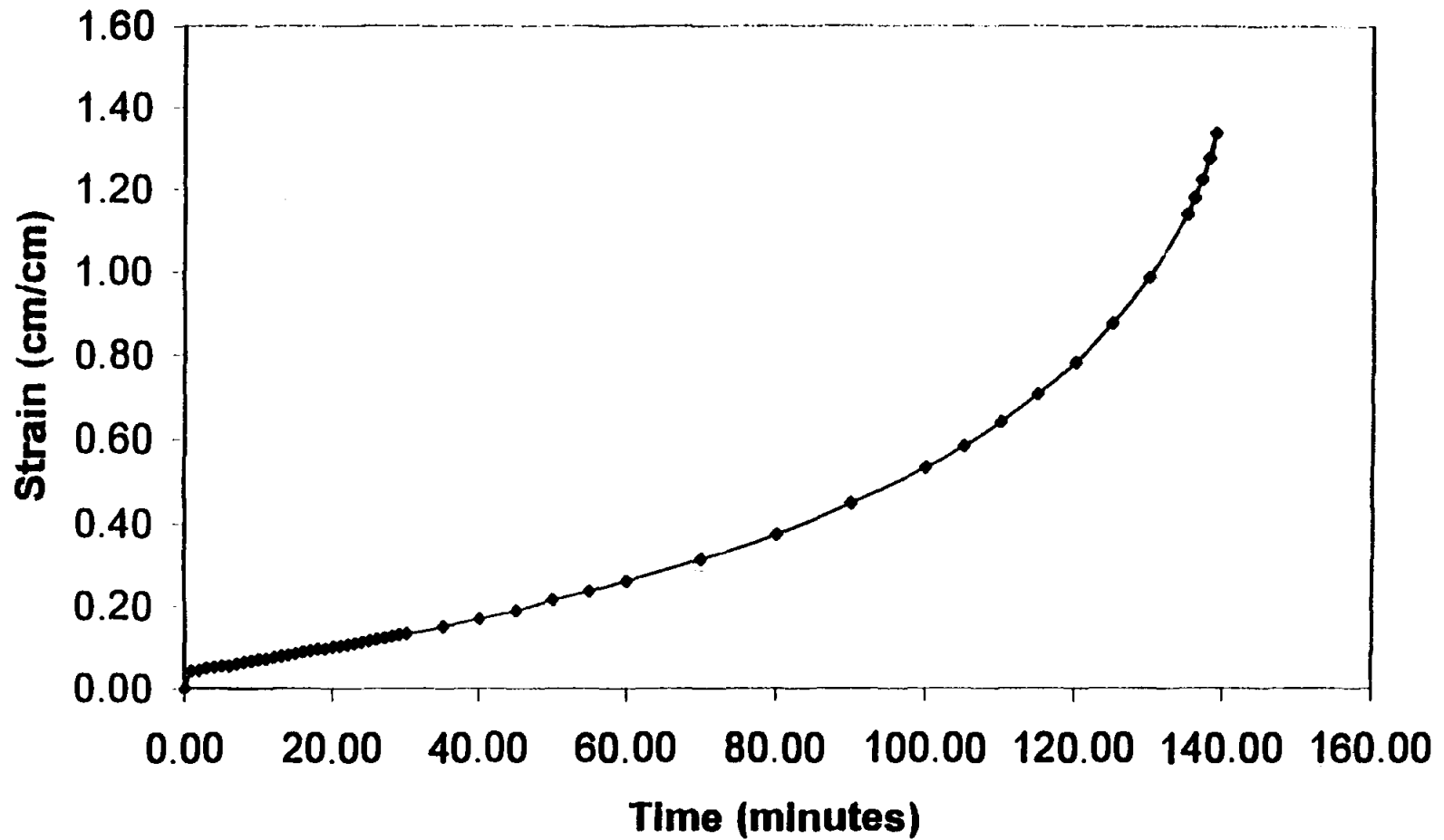


Figure 2: Strain-Time Curve for 50Pb-50Sn deformed at 1278.8 psi at room temperature. The minimum strain at this stress was determined by considering data points between 10 and 100 minutes when the strains were 0.07 and 0.27 respectively. This yields a strain rate of 0.00333 min^{-1} which is plotted in figure 3 for a stress of 1278.8 psi.

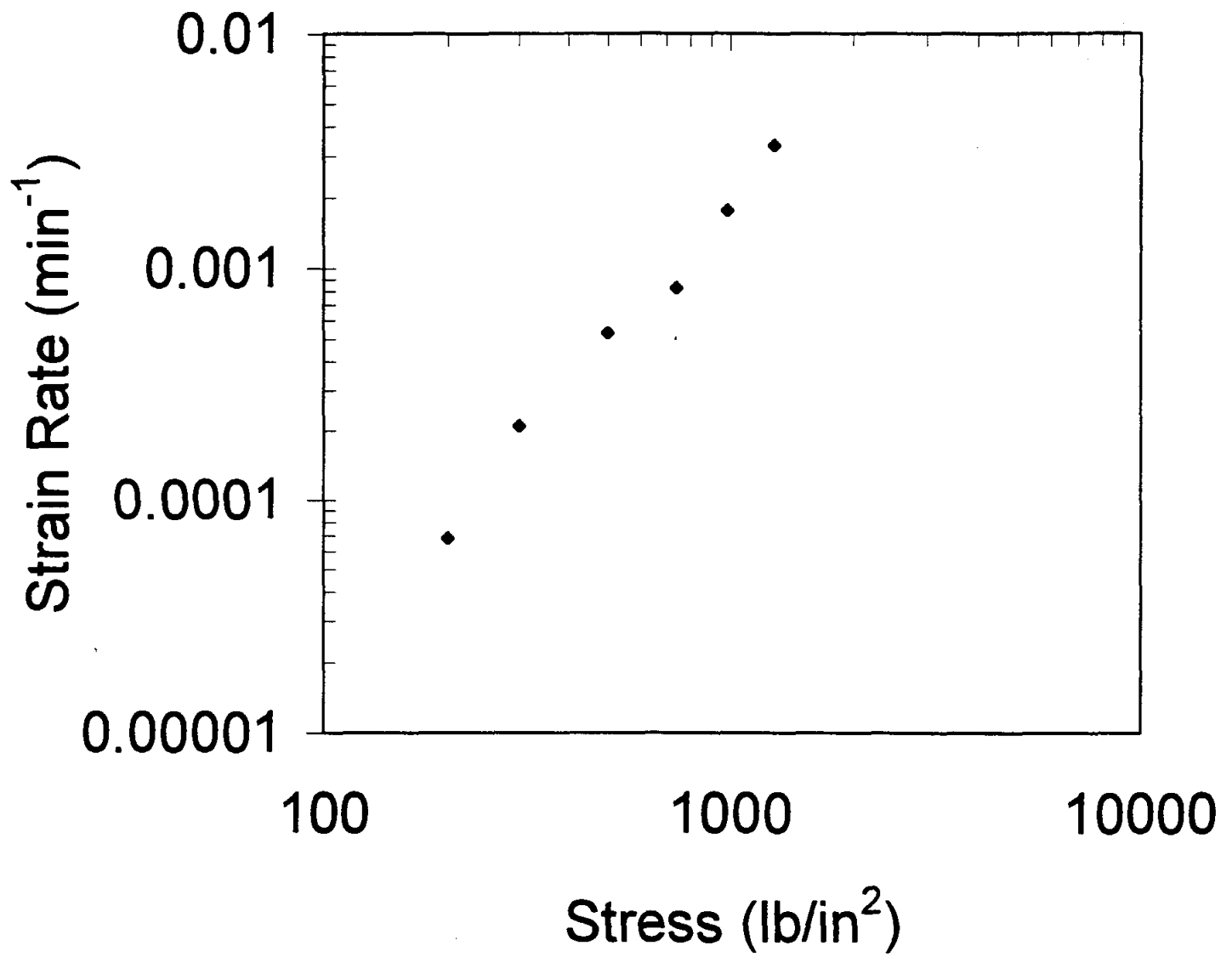


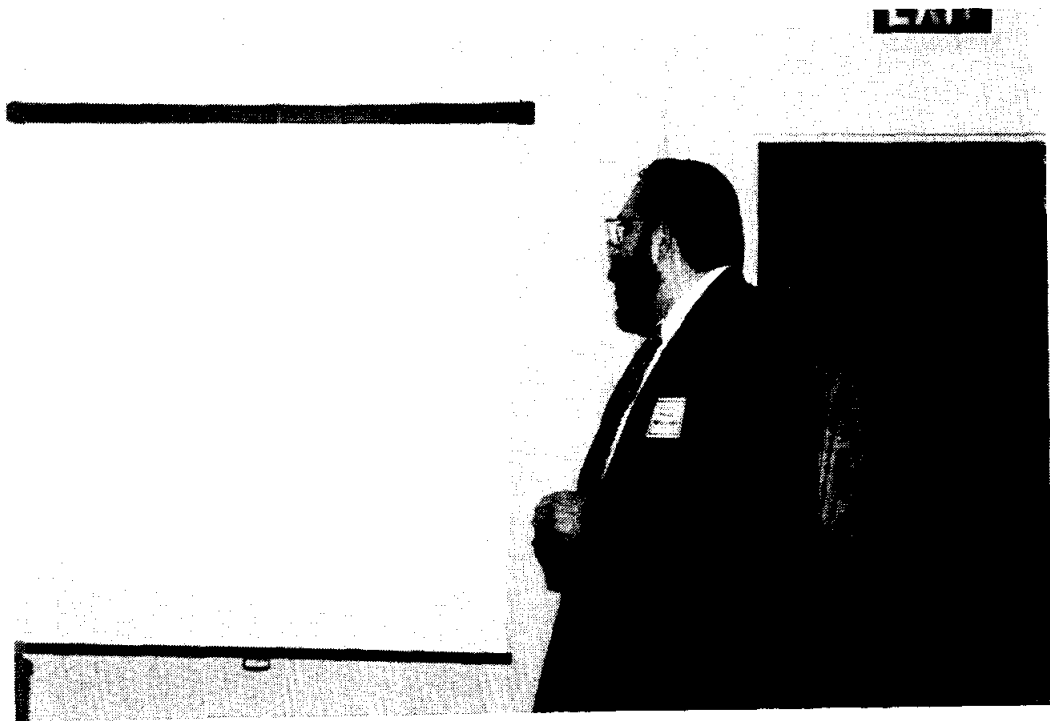
Figure 3: Log stress vs Log strain rate curve for the data collected for this study.

USE OF PIEZOELECTRIC CRYSTALS FOR VOICE RECOGNITION

Harvey Abramowitz

Department of Engineering
Purdue University - Calumet
2200 169th Street
Hammond, Indiana 46323

Telephone: 219-989-2473
e-mail harveya@calumet.purdue.edu



Harvey Abramowitz

Use of Piezoelectric Crystals for Voice Recognition

Harvey Abramowitz
Purdue University Calumet
Hammond, IN

Keywords:

Piezoelectric Effect, Electrostriction, Reverse Piezoelectric Effect, Voice Recognition

Prerequisite Knowledge:

The student

1. should be familiar with the concepts of the piezoelectric effect and electrostriction or the reverse piezoelectric effect,
2. should be familiar with frequency generators and oscilloscopes,
3. should be familiar with PC's operating with MS Windows 95, and
4. should be familiar with a spectrum analysis software.

Objectives:

1. To demonstrate to students in a first materials science course the two modes in which a piezoelectric crystal can be used, utilizing either the piezoelectric effect or the electrostriction/reverse piezoelectric effect.^{1,2}
2. To show the potential for using a piezoelectric crystal for voice recognition.

Equipment and Supplies:

1. 1" Piezo Discs, such as those supplied by Edmund Scientific Company, Barrington, NJ
2. Oscilloscope
3. Function Generator
4. BNC to Alligator Leads
5. 10x Oscilloscope Probe
6. Microphone
7. 2 PC's with MS Windows 95, software for capturing oscilloscope images, and data

acquisition/spectrum analysis software

8. Workstation (optional)

Demonstration of Electrostriction/Reverse Piezoelectric Effect

Procedure

Connect the piezo disc to the Function Generator using the BNC to Alligator leads. The disc should have two leads - the positive, red lead, soldered directly to the crystal and the negative, black lead, attached to the brass plate to which the opposite side of the crystal is attached. Adjust the frequency until an audible sound is heard. Find the audible frequency range of the crystal. To amplify the sound, place the metal side of the crystal on another piece of metal, sheet or plate.

Result

A frequency range of 800 Hz to 17 kHz should be obtained.

Demonstration of Piezoelectric Effect

Procedure

Connect the crystal to an oscilloscope. Set the sweep rate to 5 or 10 ms/div (X axis), and the voltage scale to 50 or 100 mV/div (Y axis). Put the crystal on the table, crystal side up, and press the crystal with a finger for an instant. Alternatively, press the crystal by holding it between the thumb and forefinger, also for a short time.

Result

As the pressure on the crystal is increased, a higher voltage spike is generated. If the pressure is too high, the spike will go off screen. In such a case, change the voltage scale as needed.

Use of Piezoelectric Crystals for Voice Recognition

Oscilloscope Patterns

Procedure

Set the sweep rate to 5 ms/div and the voltage range to 100 mV/div. Place the crystal on the larynx and hold one particular sound for a few seconds. A distinctive pattern for

each individual should be seen. Suggested sounds to begin this exercise are a, b, la, da, and ma. Try the same sounds with both a male and female student.

Results

Figures 1-4 show the results for two speakers - male1 and female1 - continuously saying the letters a and b. As expected, the female voice has a higher frequency and the pattern repeats approximately every 5 ms for the letter a and 4 ms for b. The pattern of the male voice repeats every 9 ms for a and b.

Discussion

These plots indicate the possibility of using the crystal to identify individuals, and perhaps establish a voice recognition system based on a single crystal. Usually, such a system relies on a comparison of a full frequency spectrum analysis of the voice in question with a filed spectral analysis of that individual. In most of these systems, a microphone is used. Also, a normal speech pattern is employed, where letters, words and sentences are spoken at a normal rate, instead of holding a single continuous sound. Therefore, the next step of the demonstration is to see if a microphone can be replaced by the crystal.

Comparison of Piezoelectric Crystal with Microphone

Time Domain Plots

Procedure

Connect the crystal to the audio input of one PC and a mic to the audio input of another PC. Open the Sound Recorder software available in MS Windows 95 and record predetermined sounds on each PC by pressing the record buttons of both PC's at the same time. Stop the recording in a similar fashion. The start to finish time of recording should thus be approximately the same. By recording simultaneously, the inputs to the transducers are from the same speaker. The wave files produced are imported into analysis software, such as MATLAB. Time domain plots can thereby be obtained.

Results

Typical time domain plots are shown in Figs.5-8. These plots were made by two speakers (male2 and female1) pronouncing the letters a, b, and c into the mic and

crystal at the same time. The graphs plot voltage versus the sample number or index. Sampling takes place every 45 μ s. Total sampling time ranges from 4-5 seconds.

Discussion

The major difference between the plots for the mic (Figs.5 and 7) and the crystal (Figs.6 and 8) is that the crystal plots show saturation. This is due to the fact that the piezoelectric crystal disc was placed near the throat cavity/voicebox and breathing causes vibrations in addition to those produced by speaking. In terms of signal to noise ratios, the ratio for the crystal is much higher than that for the mic. The reason for this difference is that the mic picks up ambient noise from the environment, while the crystal signal is independent of the environment and is a function of the speaker's throat cavity/voicebox movements. How high the crystal signal to noise ratio can go is still unknown and will be investigated.

Comparison of Vocal Tract Spectra

Procedure

Find the vocal tract spectra by manipulation of the time domain data via fourier transforms. This can be accomplished, for example, by using the X waves package from Entropic Research Lab, Inc. on a Sun workstation. A comparison of the formant (key) frequencies will give an idea as to whether or not the crystal can replace the mic.

Results

The vocal tract spectra plots comparing the mic with the crystal for the 'a' vowel sound spoken by male speaker 2 are shown in Figs.9 and 10. The first four formant (key) frequencies are listed in Table 1.

Discussion

The comparison listed in Table 1 indicates that the spectra are similar, although not exact. It appears that the possibility exists for using the crystal for voice recognition. Further work is underway to refine this usage for very inexpensive crystals.

Conclusions

1. The electrostriction and piezoelectric effects can be demonstrated using crystal discs.
2. The possibility of using these discs as the transducer for a voice recognition system has also been shown.

Acknowledgements

The author would like to thank Prof. G. Gopalan, Jack Woods, and Leticia Soto Jones for their help.

References

- 1 . Askeland, D.R., *The Science and Engineering of Materials, 3rd ed.*, PWS Publishing Company, Boston, MA, 1994, pp.636-638.
- 2 . Shackelford, J.F., *Introduction to Materials Science for Engineers*, Prentice Hall, Inc., 4th ed., Upper Saddle River, NJ, 1996, pp.454-455.

Table 1

**Formant (F) Frequencies for Male2 Speaker, 'a' Vowel Sound,
Using Mic and Piezoelectric Crystal**

Transducer	Formant Frequencies (Hz)			
	F1	F2	F3	F4
Mic	394	1856	2306	3150
Piezoelectric Crystal	366	1462	2306	2900

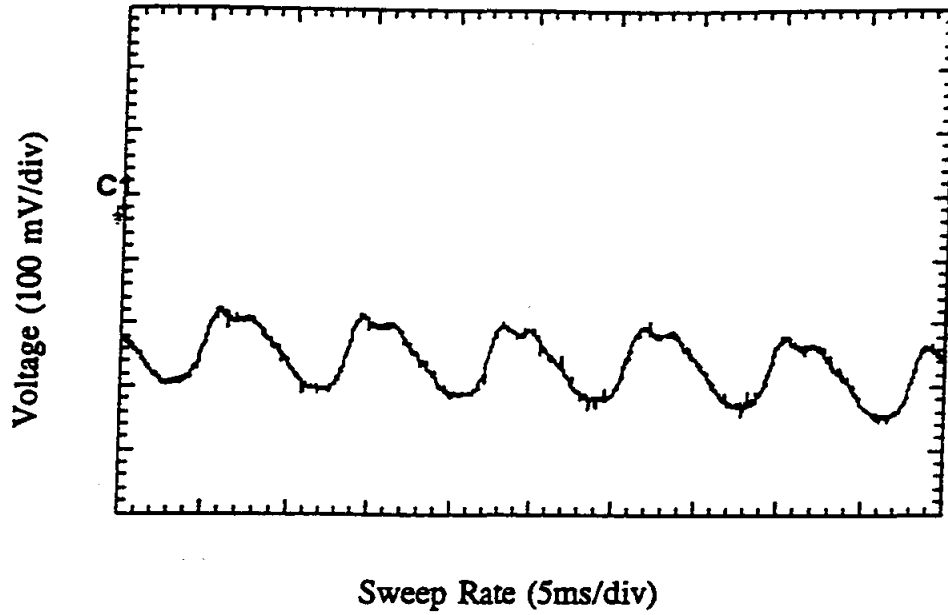


Figure 1: Oscilloscope Pattern for Male1 Speaker, 'a' Sound

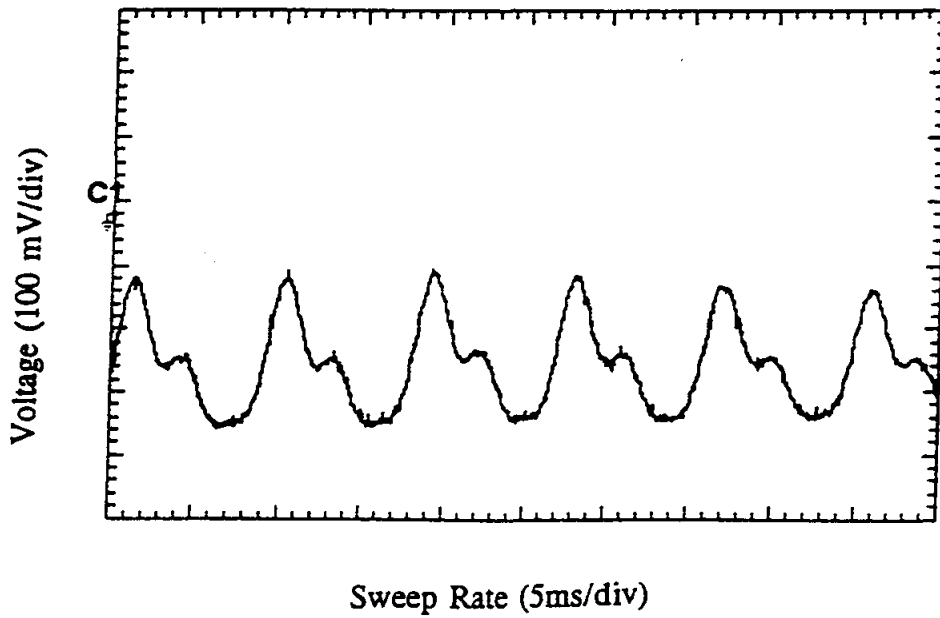


Figure 2: Oscilloscope Pattern for Male1 Speaker, 'b' Sound

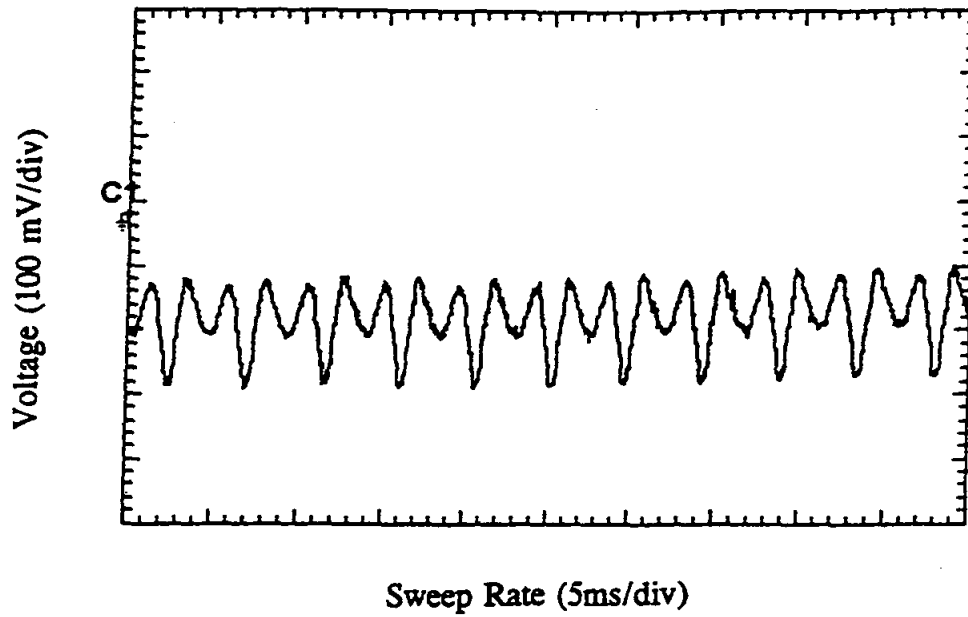


Figure 3: Oscilloscope Pattern for Female1 Speaker, 'a' Sound

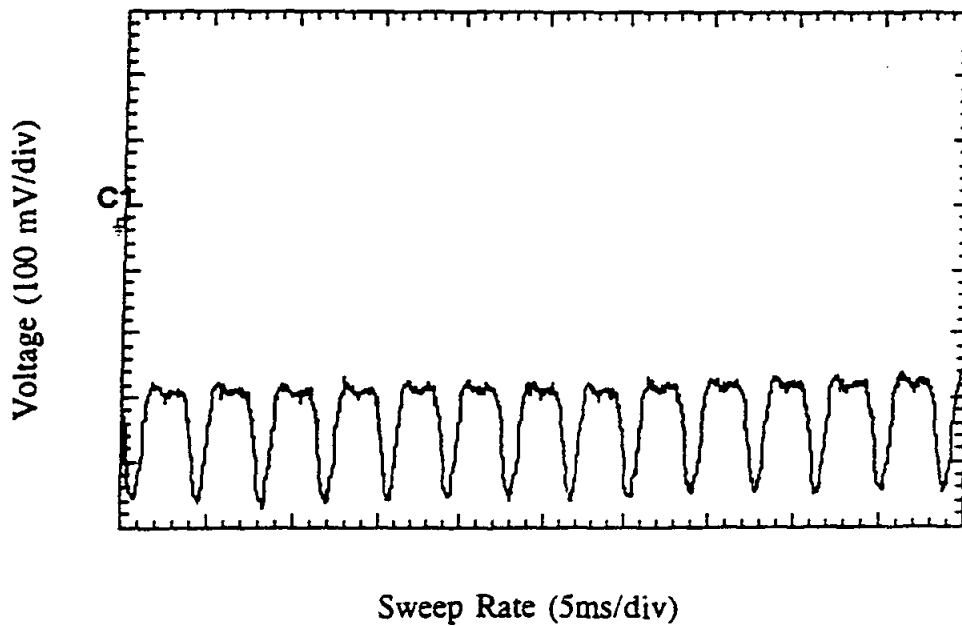


Figure 4: Oscilloscope Pattern for Female1 Speaker, 'b' Sound

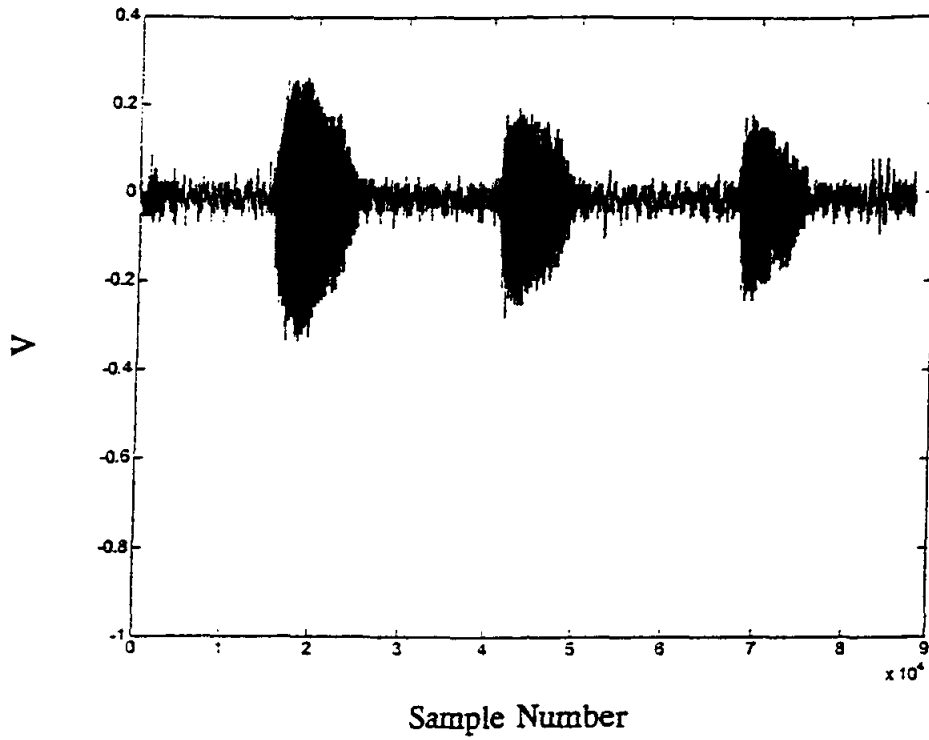


Figure 5: Time Domain Plot for Male2 Speaker, 'a', 'b', and 'c' Sounds, Mic

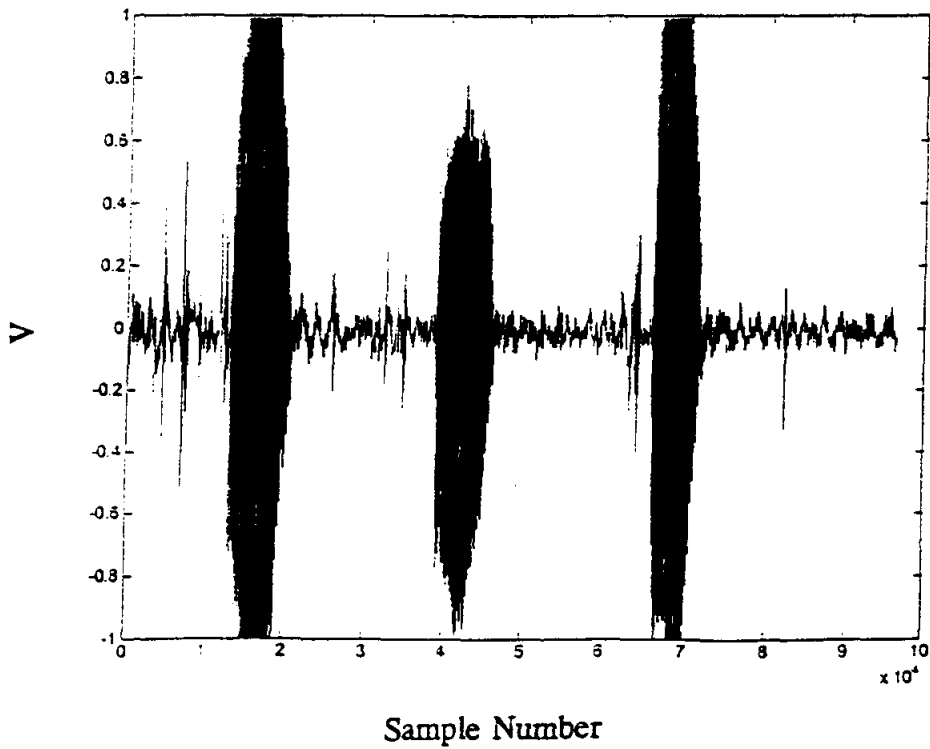


Figure 6: Time Domain Plot for Male2 Speaker, 'a', 'b', and 'c' Sounds, Crystal

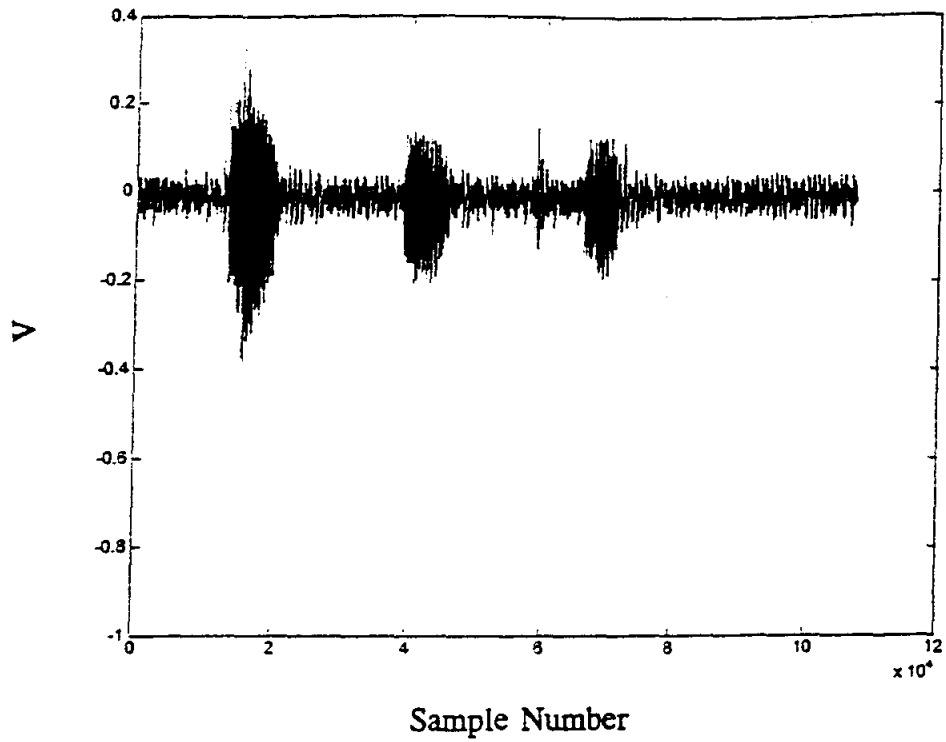


Figure 7: Time Domain Plot for Female1 Speaker, 'a', 'b', and 'c' Sounds, Mic

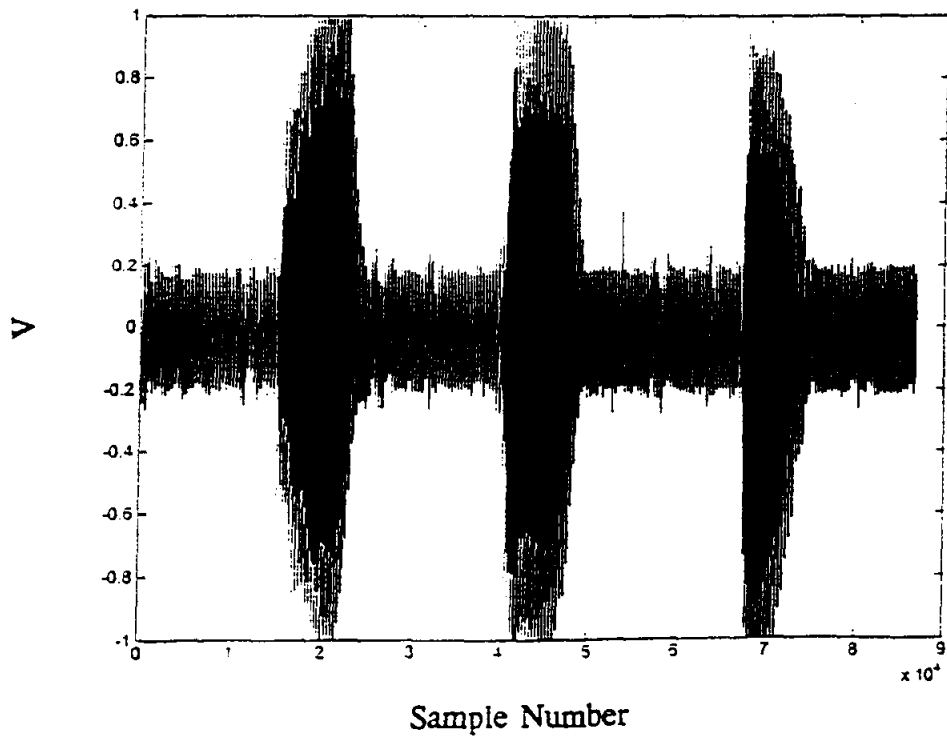


Figure 8: Time Domain Plot for Female1 Speaker, 'a', 'b', and 'c' Sounds, Crystal

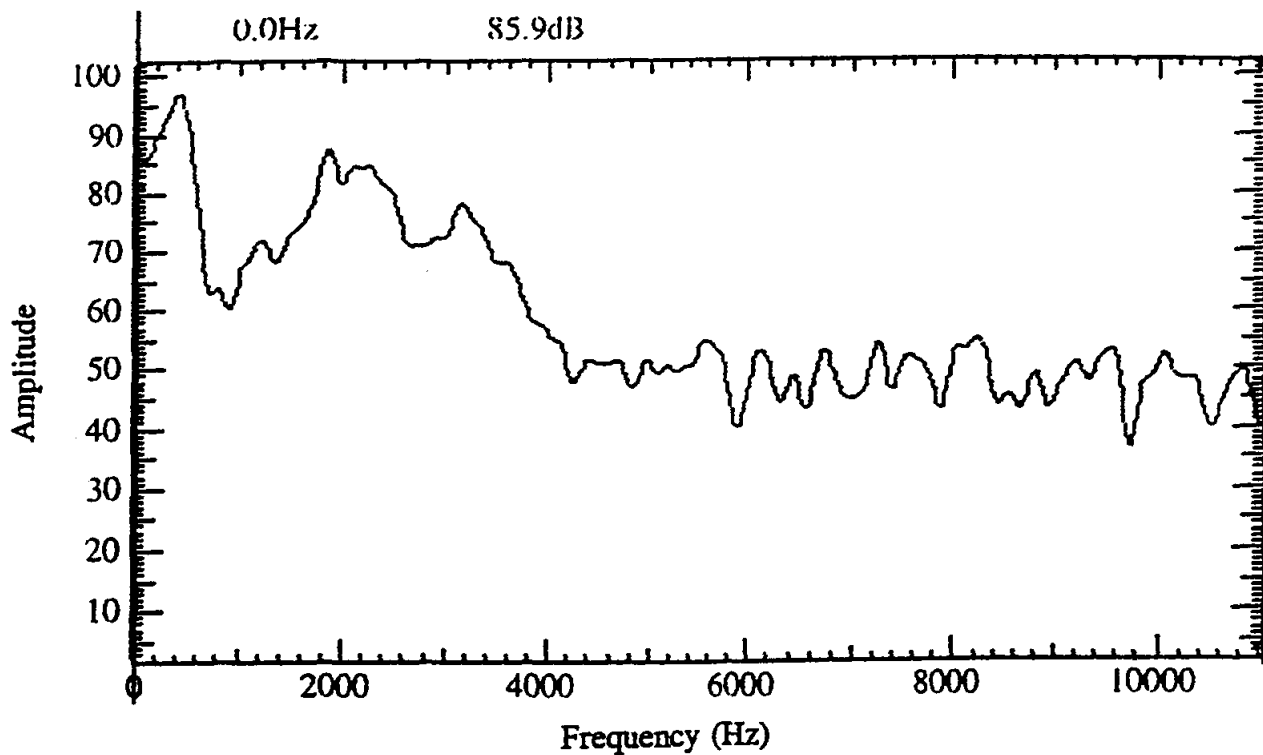


Figure 9: Vocal Tract Spectrum for Male2 Speaker, 'a' Sound from Figure 5, Mic

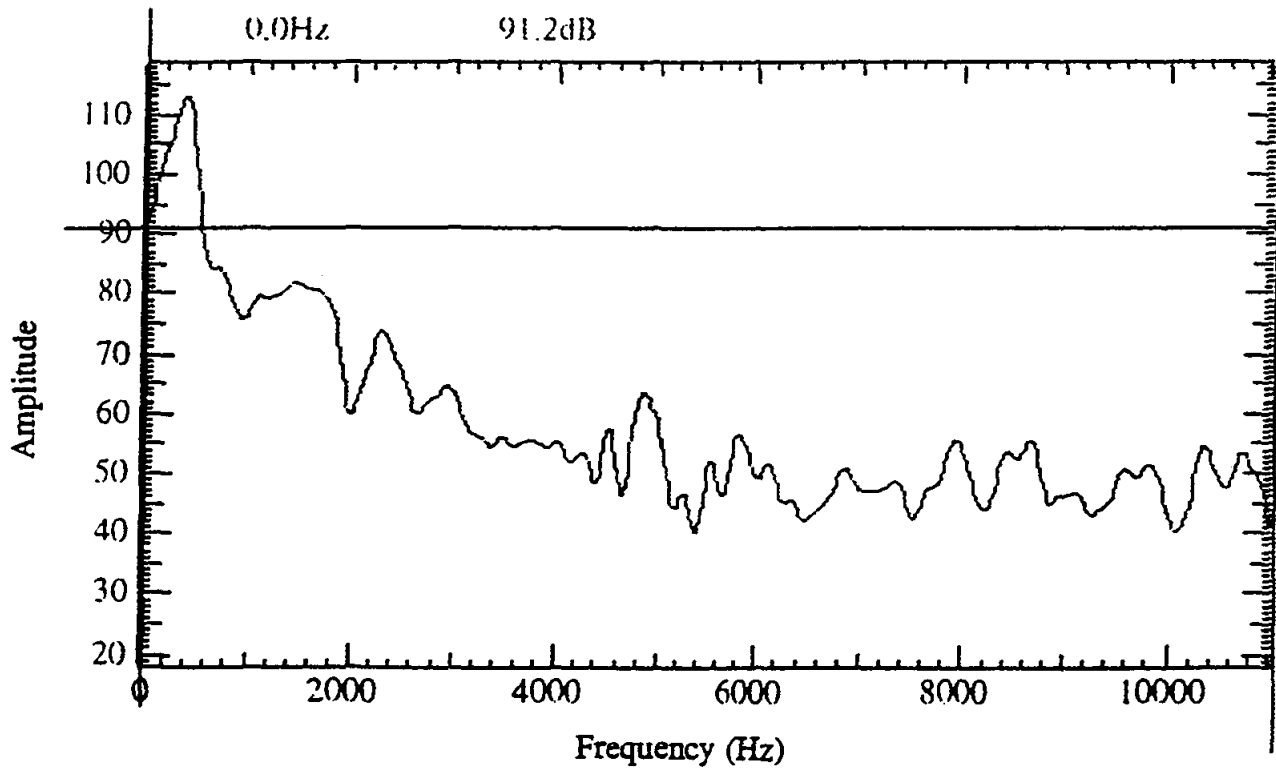


Figure 10: Vocal Tract Spectrum for Male2 Speaker, 'a' Sound from Figure 6, Crystal

Biographical Information

Harvey Abramowitz received a B.S. in Materials Science from the Henry Krumb School of Mines, School of Engineering and Applied Science, Columbia University. He completed M.S. and D.Eng.Sc. degrees from the same school in extractive metallurgy/mineral engineering. Prior to coming to Purdue University Calumet, he was a Research Engineer at Inland Steel Research Laboratories and a Visiting Professor at the University of Missouri, Rolla. He is currently an Associate Professor of Mechanical Engineering and is responsible for the materials courses. Major areas of research are the treatment of waste streams for metal recovery, and the cryogenic treatment of steels.

CONCURRENT ENGINEERING: EXPERIMENT 1 PRODUCT ANALYSIS AND PROTOTYPING

James B. Higley

Yulian B. Kin

Bernard W. Parsons II

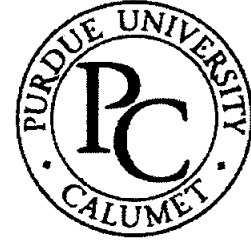
and

Christopher M. Prochnow

Purdue University Calumet
METS Department
Hammond, Indiana 46323

Telephone 219-989-2584
e-mail higley@calumet.purdue.edu

This project was supported, in part,
by the
National Science Foundation
Opinions expressed are those of the authors
and not necessarily those of the Foundation



Concurrent Engineering: Experiment 1 Product Analysis and Prototyping

James B. Higley
Yulian B. Kin
Bernard W. Parsons II
Christopher M. Prochnow

Purdue University Calumet
Hammond, IN 46323

Key Words: finite element analysis (FEA), laminated object manufacture (LOM), rapid prototyping (RP)

Prerequisite Knowledge: Knowledge of three dimensional solid modeling software and basic strength of materials are required to complete this experiment.

Objective: This experiment explores two areas of product engineering: finite element analysis and rapid prototyping.

Equipment:

1. Personal computer workstation with Mechanical Desktop™, Design Space™, Silverscreen™, and JP5™ software.
2. JP5 rapid prototyping system with Roland PNC-910 sign maker plotter, cutting board, registration board, registration pins, pressing board, spray adhesive, X-Acto Knife, prototype material, masking tape, and Elmer's glue.

Introduction

The technical portion of a product's life cycle includes design, analysis, prototyping, testing, manufacture, and reclamation. When all these activities are done in parallel and combined with non-technical activities such as marketing, the whole process is frequently referred to as concurrent engineering (CE). The use of computerized three dimensional solid modeling techniques has made great advances in CE possible. The key to CE is a single, solid model database for each part used in a product. Engineers use this file, created during the design phase, to analyze the part, build prototypes, and manufacture

the part. Changes are then quickly made available to all people working on the part because everyone works off the same database.¹

Along with three-dimensional solid modeling, other powerful tools are available to speed the design, analysis, and prototype portion of a product's life cycle. These tools include finite element analysis to check stresses, rapid prototyping to quickly build part models, and graphical computer numerical control programming. The first two of these tools will be examined in this experiment; the third is covered in the next experiment.

Finite element analysis (FEA) is an old technique using numerical approximations to estimate stress and deformation of solid parts.² This is done by breaking the part down into many small volumes, analyzing each volume individually, and then summing them together for the final result. Like most numerical approximations, powerful computers are necessary for effective use. Now, FEA tools are available which can perform complicated analysis on the 3-D data the designer creates. Part 1 of this experiment illustrates this.

The term rapid prototyping (RP) is a relatively new expression for the generation of three-dimensional models manufactured directly from the three dimensional solid model without the need for machining or tooling.³ This process, which was first introduced by NASA in 1988, adds material layer by layer until the desired shape is achieved. A number of different processes and materials may be used for RP, but all follow roughly the same steps. RP machines operate by slicing the 3-D CAD data into thin slices (roughly the thickness of paper) and then creating the thin slices from solid material and joining the slices together. The result is a reasonably accurate physical part that can be handled and, depending on the material, actually used.

In the second part of this experiment, you will use a method called Laminate Object Manufacture; perhaps the simplest RP method available. The slicing software drives an X-Y sign cutter which cuts out pieces of paper to the desired shape. The paper slices are then manually glued together to create the finished part. This process has the advantages of simplicity and low cost, but errors in assembly are possible.

Procedure Part 1 – Finite Element Analysis

Design Space™ is a powerful software program that computes many common engineering calculations very quickly and very precise. Follow the steps outlined below to graphically analyze a sample part from its solid model.

STEP 1: Drawing an AutoCad™ drawing.

1. Before analyzing a part, you must create a three dimensional solid model of the part using software like Mechanical Desktop™. For this experiment, a model has already been created for you to use.

STEP 2: Opening Design Space.

1. In Window's, click the Mechanical Desktop icon. Design Space automatically loads with Mechanical Desktop.

STEP 3: Opening and preparing an AutoCad drawing.

1. The sample file, **Experiment#1.dwg**, is on the network. Choose the open icon and follow the links to Find File, Network, Netware Services, Intranetware Servers, Lab, Dept, L_mets, MET305. Locate the file in this directory, click on it, and click OK. The part looks like Figure 1 below. Note, once this link has been made, Windows will assign a drive letter to the final directory. Hence, once the drive letter has been assigned, the directory may be referenced using the letter instead of the long link. Once the user logs off or reboots the computers, the link will have to be performed again.

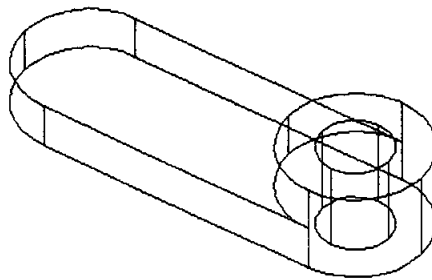


Figure 1. Sample Part

2. Highlight the isometric view of the part, top right quadrant, and type '1' and press **ENTER**. This will zoom in to show only the isometric view.

STEP 4: Entering Design Space.

1. Click on **Design Space-Stress Wizard**. This will take you to a wizard. Wizards are used to make complicated tasks much easier. This is done by breaking the tasks down to simpler steps, and pressing Next as each task is completed.

STEP 5: Working with the Wizard.

1. The introduction page of the wizard will give you an idea of what will be happening. Read this screen and press **NEXT** when ready to begin.
2. Verify that the **Potential Stress Failure Units** are in 'U.S. Customary (in, lbm, psi,s)'. Also, check to see that 'Inches' are marked in the box which reads 'What units is your drawing in?' Click on **NEXT** when completed.
3. Be sure the 'What material is the part made of?' is set to **STRUCTURAL STEEL** and **DUCTILE** is set in the 'How does this material behave' box. Click **NEXT** when this task is complete. Other materials are available, and the list can be customized with additional materials.

4. A box will appear on the screen reading '**You must now pick the part box!**' Click on **OK** and the screen will switch to the familiar Mechanical Desktop. Pick the part as the prototype to be worked with.
5. The program will revert back to the Design Space screen where the wizard will be reading **LOADING** and **SUPPORT**. You will now want to click onto the **ADD...** button in the **LOADING** section to add a simple loading to the part.
6. Click on the **FORCE** tab and be sure the '**Full Surface**' is highlighted. Click on **NEW** to place the location of the loading. Click on the face where you will want to place the load. This face will become highlighted with a dashed-line. You may choose **N (Next)** or **ENTER** to accept.
7. After accepting the face, you will need to enter the loading value using the World UCS as the guide. *Remember to keep in mind if you are representing a positive force or a negative force according to the UCS.* After entering the value of the force (in pounds), click on **CLOSE**. You will return to the **LOADING** and **SUPPORT** screen again.
8. Continue to add loadings as is necessary for the application of the prototype. If a mistake is made, click on the loading line and **DELETE** to remove the loading from the part.
9. When all loadings are entered and complete, there is a need for at least one support hold or guide for the part. To do this, click on **ADD...** in the **SUPPORT** section.
10. Again, select the surface that is the actual support or guide which the part will follow. Press **N (Next)** if you need to shuffle through the faces and **ENTER** to accept. However, with support, no value is needed.
11. Continue to add support to the part if it is required in your application. Choose **CLOSE** when the task is complete.
12. You will return to the wizard which will give you the status and press **NEXT**. Read the next page to the wizard and click on **FINISH** to finally complete the process. Design Space will now compute the stresses, deformation, and factor of safety using the applied forces. This may take a few moments to complete.
13. Upon completion, Design Space will post the Minimum and Maximum Stress, and the Minimum and Maximum Deformation. Factor of Safety is found by right-clicking on the **MAX EQUIVALENT SAFETY TOOL** and then clicking on **RUN TOOL**. By clicking on the **CONCLUSIONS** tab, the Factor of Safety will be displayed. Click on close to escape.

STEP 6: Data pictorials.

1. To pictorially represent the stresses, right click on the **EQUIVALENT STRESS** line and click on **DRAW**. The Mechanical Desktop window will

reappear and you will be prompted to pick a point to insert the drawing. Pick a point which is well away from the rest of the drawing.

2. Repeat the same procedure if you desire to display a picture of the deformation.

STEP 7: View the pictures.

1. In order to view the pictures, you need to return to Mechanical Desktop. To do this, click on the minimize button in the top right corner of the screen. This will automatically take you to Mechanical Desktop.

STEP 8: Plotting pictures.

1. These pictures may be plotted as a regular AutoCad file is plotted or you can CUT and PASTE them into a word processing or paint brush application.
2. Close out Design Space once complete.

Procedure Part 2 – Rapid Prototyping

This Laminated Object Manufacture (LOM) machine uses SilverScreen / JP-5 System in combination with the Roland PNC-910 plotter. Follow the steps listed below to complete a prototype of the sample part.

When completing a LOM prototype, there are eight (8) simple steps. They include:

1. Draw a 3-D solid model.
2. Convert the model to a .STL file.
3. Open the .STL file.
4. Orientate the .STL file.
5. Slice the .STL file.
6. Load plotter with material.
7. Plot the .STL file.
8. Assemble the prototype.

KEYPOINT: *The key thing to remember when orienting and slicing the object is that the slice acts like a knife cutting along the x-axis and works its way up the y-axis. In addition, the final assembly of a prototype is much easier when the base (larger end) is on the upper region of the part. This will reduce much of the difficulty when it comes time to put the prototype together.*

STEP 1: Drawing an AutoCad drawing.

1. Open file **Experiment#1.dwg** following the same steps from Part 1, Step 3 above. Note, if you already made the link in this login session, you do not have to relink the directory. Choose open and find the drive Windows assigned to the MET305 directory.

STEP 2: Converting an AutoCad file (.dwg) to .stl.

1. In Mechanical Desktop, verify part is in the positive x, y, and z octant. To do this, check all extremes of the part and keep close attention to the coordinates located at the bottom of the screen. In order to complete this step, all

coordinates must be positive. Change **UCS (UU)** if needed in different views to verify. If part needs to be moved, use the **MOVE** command.

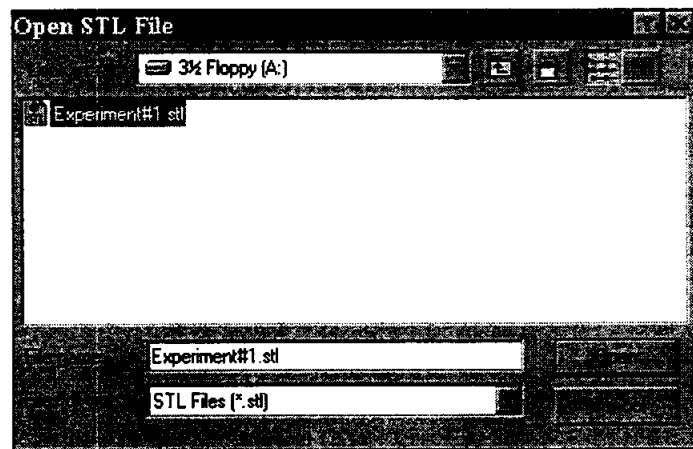
2. Type **EXPLODE**, click on the part, and press **ENTER**. This changes the part from a Mechanical Desktop parametric part to a simple AutoCAD solid. This operation destroys the ability to edit the part, so do not save the file after performing this operation.
3. Type in **STLOUT** and press **ENTER**. Click on the part and press **ENTER**. Type in **Experiment#1** when prompted and press **OK**. Enter “N” when prompted to **create a binary stl file**. Save the file in your directory, in the temporary directory, or on a floppy disk. This is the sliced file required as input to the RP system.
4. Close Mechanical Desktop.

STEP 3: Opening an .STL file.

1. To start SilverScreen / JP-5 System, double click the shortcut icon on the Window's desktop.



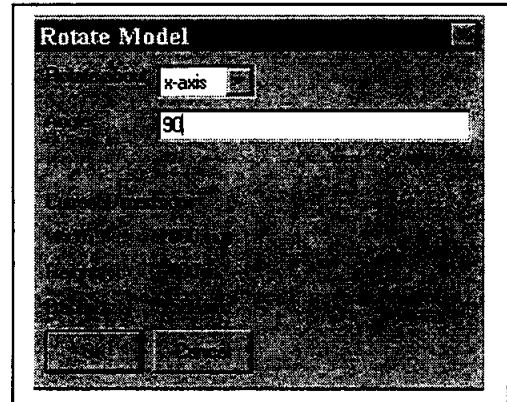
2. Click on **TOOLS – EXECUTE** and pick “**sys5.ex**” and click on **OK** button. Moment's later, JP-5 System will load. Note the background will turn to a white screen and JP System 5 will read at the top left corner of the screen.
3. Click on **FILE-OPEN STL FILE** and change **Look in Box** to to where you saved the .stl file.
4. Choose “**Experiment #1.STL**” file and click the **OPEN** button. This may take a few moments for the file to load.



5. The file viewed in Mechanical Desktop will appear as a white solid model in the JP-5 System.

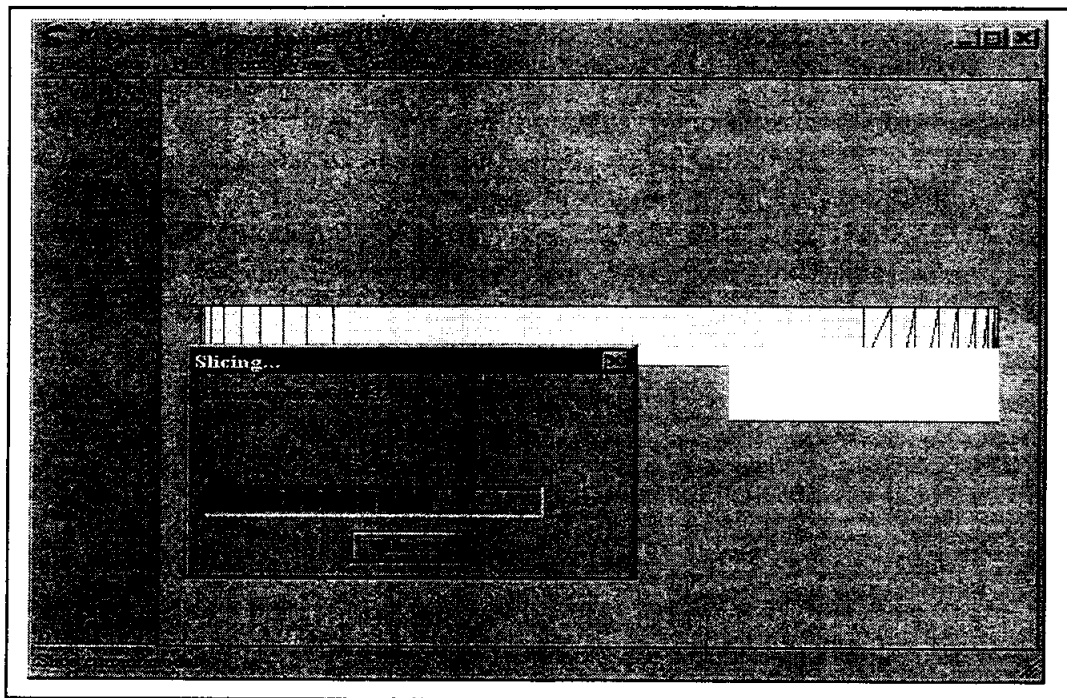
STEP 4: Orientate the .STL file.

1. Click on the **SETUP-ROTATE** and choose the **x-axis** in the “**Rotate about**” box. Next, enter **90** in the box for which to rotate the part. Click on **OK** when complete. JP System 5 will then inform you of the new dimensions and click **OK** to continue. Refer to the above *KEYPOINT* for clarification on why and when rotation is necessary.



STEP 5: Slicing an .STL file.

1. Click on **SETUP-SLICE** and be sure that the **Slice Extent** is set to **Full** and the **Material** chosen is **Standard**. Click on **OK** to continue. Click on the **YES** button when you are prompted to continue. This process of slicing the object may take several moments to complete depending on the speed of your computer. When slicing is complete, object will turn brown in color and Slice Current Model will be displayed in the lower right corner of the screen.



2. You may wish to view the sheets before plotting. To do this, click on **VIEW-SHEETS** and you may need to wait for a few moments for the preview of the sheets will be displayed. You then may scroll through the

pages to be printed by pressing the arrow keys located on the left side of the screen. This step is not completely necessary but convenient to identify what will be plotted.

STEP 6: Loading the plotter.

1. This system utilizes the **Roland PNC-910 Sign Maker** to cut out patterns for assembly. Locate the lever on left side of machine. This lever is used to lower and raise the rollers on the machine. When the rollers are in the up position, they are open and ready to insert material. When lowered, the material is secure.
2. Turn power switch on left side to **ON**. Notice the cutter head moves to right side.

BE CAREFUL NOT TO HAVE YOUR HANDS OR OTHER OBJECTS NEAR THE TOOL CARRIAGE OF THE PLOTTER TO AVOID DAMAGE OR INJURY.

3. Press the **SETUP** button until the cutting head moves to the right side of the machine. Push roller levers to the up position. You are now ready to load material.
4. Slip material under rollers and push through until the front edge of the material lines up with the front of the blue cutting surface using pencil mark as guide for left edge of material. *The first two sheets (MASK and Sheet #1) are loaded with the off-white side of the material facing upward. The following sheets are placed with the bright white side of the material facing upward as shown in Figure 2.*

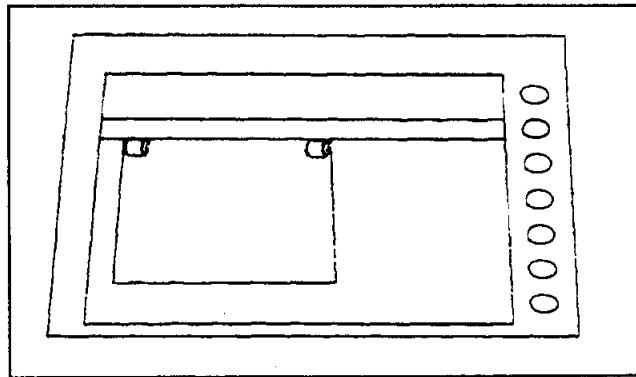


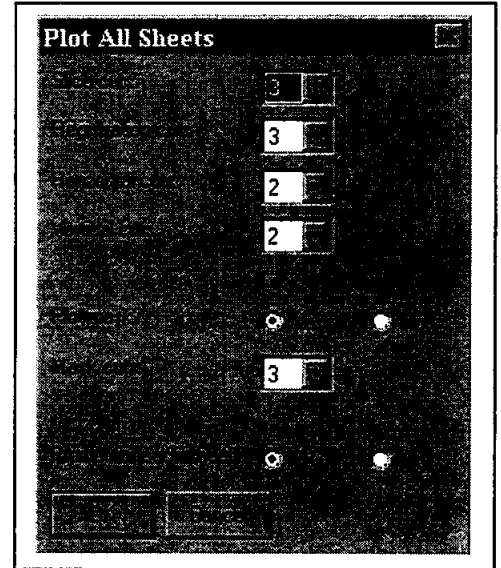
Figure 2. Sheet Placement on Plotter.*

5. Once aligned, push lever down to lock the material into position. Press **SETUP** button once again keeping hands and objects away from the cutter head. Once head reaches left side of machine, press **ORIGIN SET** button. The machine is now prepared to cut material for assembly.

- To remove material in the future, press **SETUP** button, push lever to up position, remove material, insert new material align, push lever to down position, press **SETUP** button again. You are now ready to cut another sheet.

STEP 7: Plotting an .STL file.

- Click on **PLOT-CUT SHEETS** and click on the “**ALL**” button at the top left corner of the screen and choose **OK**. This will print all sheets along with a **MASK**. Change the cutting data, if needed, to read as the dialogue box appears to the right:
- Remove material plotted upon and re-load the material in the correct fashion as indicated in Step #20. Click on **OK** to plot the next page. Repeat this step until all pages are plotted.



STEP 8: Assembling the prototype.

- Insert registration posts into registration holes located in the near middle of the board. These holes are approximately 8.0 inches apart from each other.
- On all sheets, be sure all the registration holes are completely cut out and the material is removed from the holes.
- Remove any non-sliced interior void areas from **Sheet #1** as shown in Figure 3.

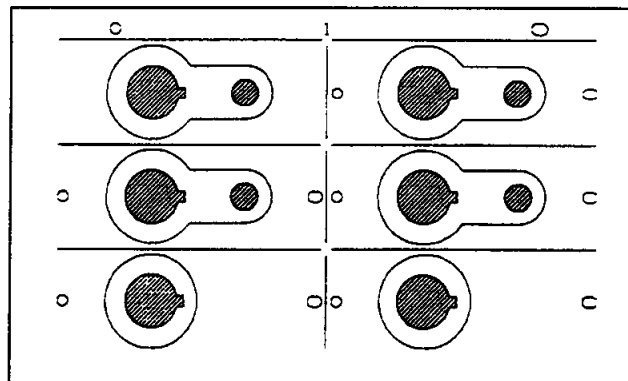


Figure 3. Removal of Non-sliced Areas.*

- Layout **Sheet #1** onto the major registration posts with the circular hole over the left pin and the slot over the right.

5. Tape this first sheet down to registration board as shown in Figure 4.

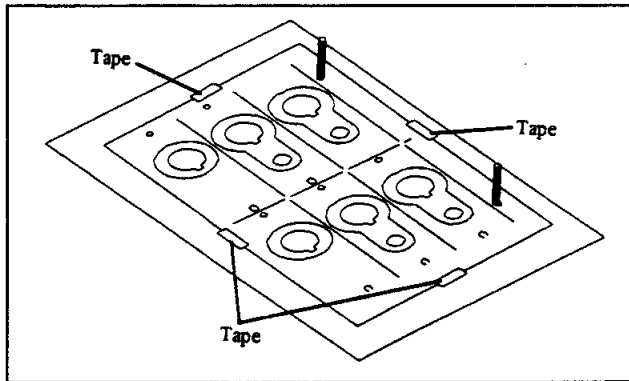


Figure 4. Paper orientation on registration board.*

6. Using the cutting board and the X-acto knife, cut out the partially cut openings of the sheet labeled **MASK**.
7. Cover **Sheet #1** with the **MASK** with round hole again on left side.
8. Spray adhesive evenly through openings on **MASK**. *Adhesive will only be sprayed onto **Sheet #1*** as shown in Figure 5.

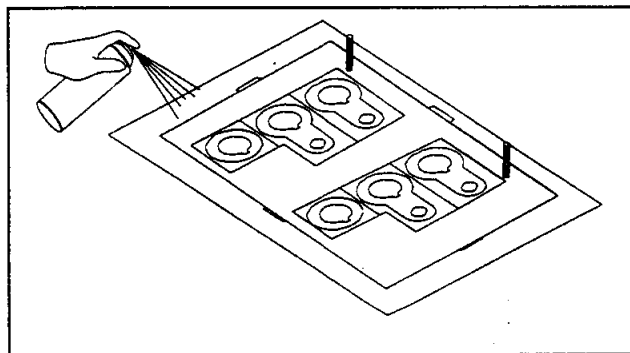


Figure 5. Spray adhesive through mask.*

9. Remove **MASK** when the spraying task is complete.
10. Remove any non-sliced interior and exterior voided areas from **Sheet #2 and Sheet #3 only** leaving only the cut-out design.
11. Place **Sheet #2** with the side with the enclosures removed facing down onto **Sheet #1**. The circular hole still on left pin. Be careful because **Sheet #1** will be very tacky from the spray adhesive.

- Using the application board, press the material firmly being careful not to shift the material being sandwiched as shown in Figure 6.

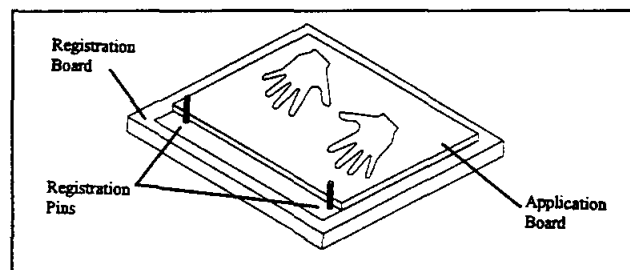


Figure 6. Joining Sheets.*

- Once the pressing is complete, remove the support base (backing of the sticker) leaving the cutout portion of the material behind as shown in Figure 7. Be very cautious when removing material to see that the cutout did actually fasten to the previous sheet. Attempt to remove backing at a 90° angle when possible.

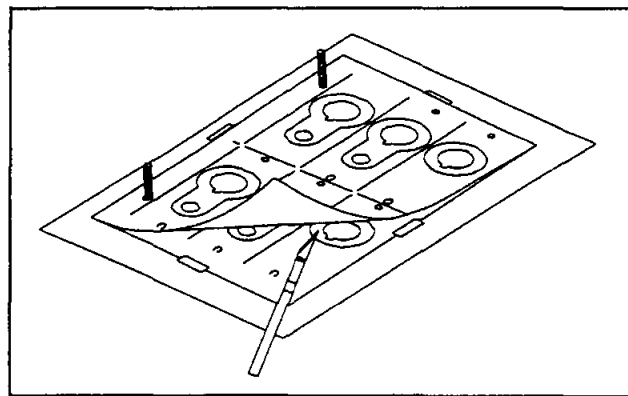


Figure 7. Peel Off Unused Paper.*

- Repeat Steps 33 – 35 for all sheets *except for the final sheet*.
- Place the final sheet onto the sandwich of sheets and press.
- Again, remove the backing from all sections with exception to the section marked as A-A, top left section.
- Cut section A-A out using the x-acto knife.
- Remove the sandwiched set of sheets from the board. Reposition the registration pins into the holes approximately 4 ½ inches apart.

19. With a pencil or pen, mark each section of the last sheet with an identifier starting in the upper left hand corner, as follows:

A	B
C	D
E	F
G	H
I	J
K	L

20. Cut all sections out at the horizontal and vertical separator lines. Once cut, turn these sections over starting with A and place onto the minor registration holes. Section A should contain the cutout for the registration holes.
21. Press the stack and remove the support base backing and repeat placing the next section onto the registration posts and pressing firmly. Repeat until all sheets have been attached. Remove the entire assembly from the minor registration posts and bottom support base. Care should be taken since stick adhesive will be present on the outside of the prototype. Coat the assembly with Elmer's Glue. Give the assembly a second coat once the first is completely dried.

Cutter and Plotter Reference Settings

Left roller distance from left side of machine = 2 inches

Right roller distance from left side of machine = 10 inches

Plotter width = 10 inches

Plotter length = 7.50 inches

Rotation – Off (Portrait setting)

Major Registration = 8 inches

Minor Registration = 4.5 inches

Project Report

Search the internet to find another method of rapid prototyping and search the library for a third. Write a short report comparing the LOM method with the two methods you found.

References

1. Chipley, K.; Viswanathan, S.; Cooper, RH.: Concurrent Engineering and Rapid Prototyping for Die Casting. *Die Casting Engineer*, vol. 40, no. 2, Mar-Apr, 1996.
2. Roensch & Associates, <http://eee.execpc.com/!sroensch/fea.html>.
3. Studt, Tim. Rapid Prototyping Key to Fast Development. *R&D Magazine*, May, 1994, pp. 55-56.

Credits

* Drawings marked with an asterisk (*) used with permission of Schroff Development Corporation.

CONCURRENT ENGINEERING: EXPERIMENT 2 DESIGN THROUGH PROTOTYPING

James B. Higley

Yulian B. Kin

Bernard W. Parsons II

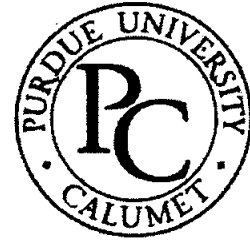
and

Christopher M. Prochnow

Purdue University Calumet
METS Department
Hammond, Indiana 46323

Telephone 219-989-2584
e-mail higley@calumet.purdue.edu

This project was supported, in part,
by the
National Science Foundation
Opinions expressed are those of the authors
and not necessarily those of the Foundation



Concurrent Engineering: Experiment 2 Design Through Prototyping

James B. Higley
Yulian B. Kin
Bernard W. Parsons II
Christopher M. Prochnow

Purdue University Calumet
Hammond, IN 46323

Key Words: finite element analysis (FEA), multi-jet modeling (MJM), rapid prototyping (RP), computer numerical control (CNC) machining

Prerequisite Knowledge: Knowledge of three dimensional solid modeling software and basic strength of materials are required to complete this experiment. Completion of Experiment 1 in this series is also required.

Objective: This experiment explores the design, analysis, prototype, and manufacture of a simple part.

Equipment:

1. Personal computer workstation with Mechanical Desktop™, Design Space™, Allegro™, and EdgeCam™ software.
2. Actua 2100 rapid prototyping machine.
3. Bridgeport Series I CNC milling machine with fixtures, end mill holder, and ½" diameter two flute endmill.

Introduction

The key element of Concurrent Engineering is the three dimensional solid model drawn in a CAD system. This central item is used, in varying formats, as inputs to FEA software, Rapid Prototyping (RP) machines, and Computer Numerical Control (CNC) machines among others.

In this experiment, you will create a part with a 3D solid modeler, analyze the part with a graphical FEA package, prototype the part with an MJM RP machine, write the CNC

program, and machine the real part. These are all the steps needed to successfully design and build a useful part.

Problem Statement

Design a connective member from aluminum alloy 6061-T6. The blank measures a nominal 2" by 4". The member will experience tensile forces totaling 13.75 kips from a pair of pins 0.6875" in diameter spaced 2.2500" apart. The part will be machined with a 1/2" diameter endmill, so all internal features must accommodate the cutter. Internal features will be machined first, and then the part will be clamped with 1.5" diameter washers over the pins to machine the exterior. Be sure the part clears these washers.

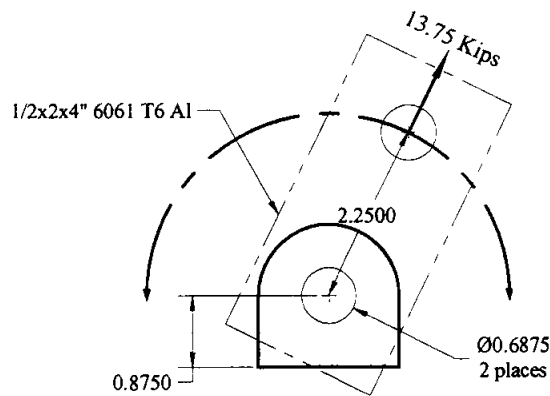


Figure 1. Layout

Procedure Part 1 – Design and Analysis

1. Load Mechanical Desktop. EdgeCAM and Design Space both load with Mechanical desktop.
2. Draw your fully constrained part and orient it as shown in Figure 2 using the left front isometric view. Be sure your XY axes point as shown in Figure 2, and move the origin (use the UCS command) so the part lies entirely in the positive XYZ quadrant.

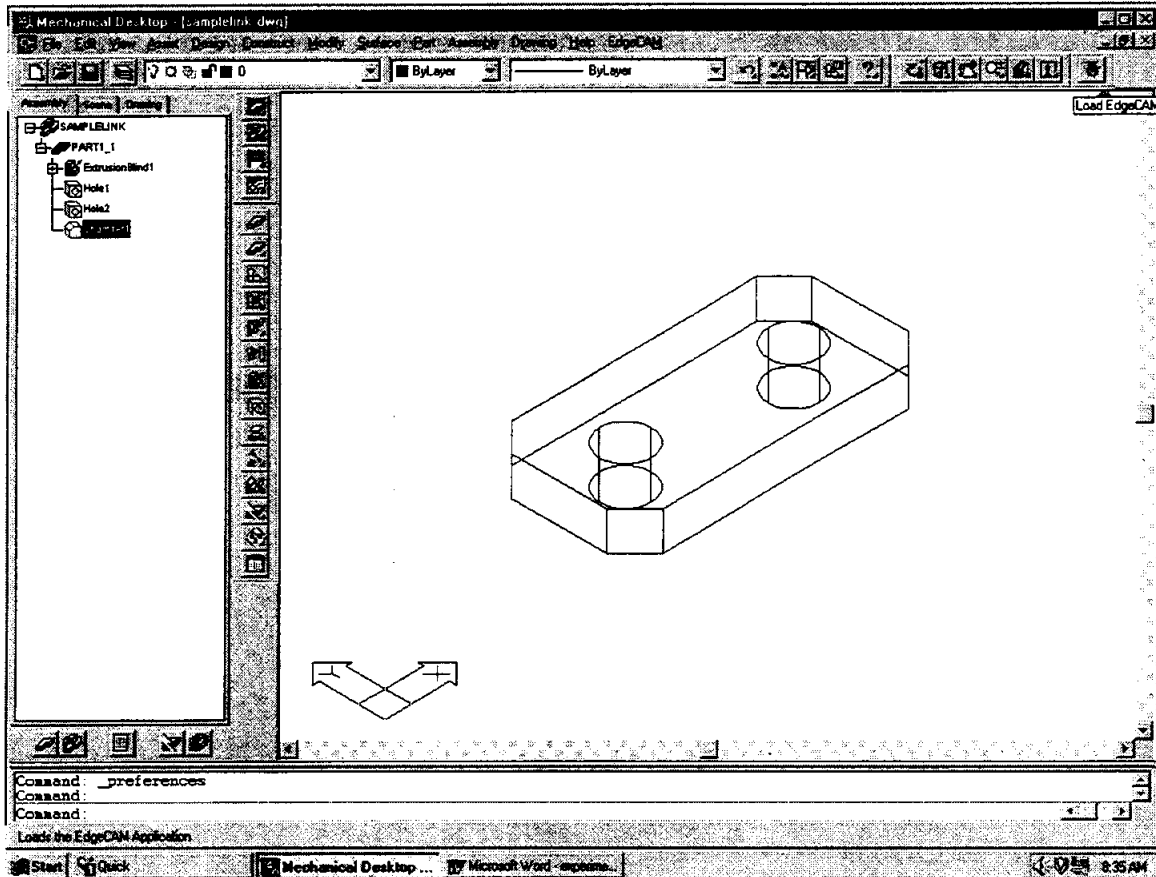
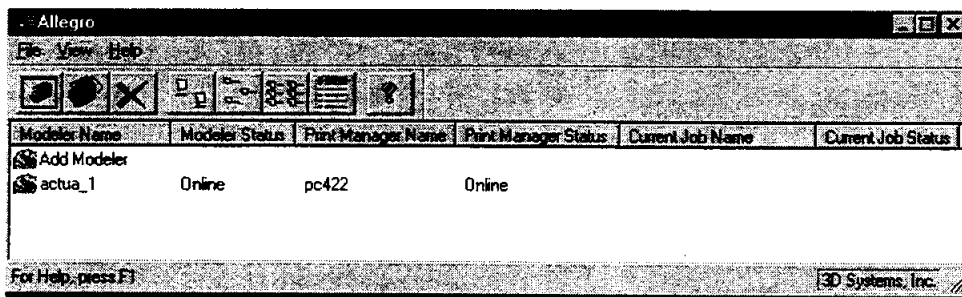


Figure 2. Layout

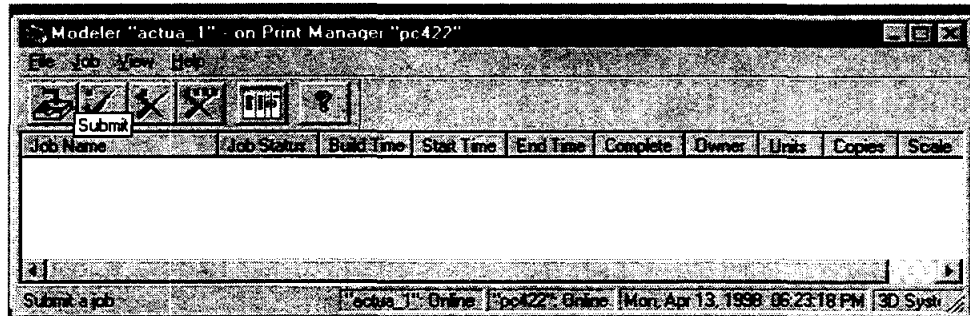
3. Use DesignSpace to verify and improve your design. (Specific instructions are contained in laboratory experiment #1.) The part should be as light as possible while still maintaining an acceptable stress level in the chosen material.

Procedure Part 2 – Prototyping

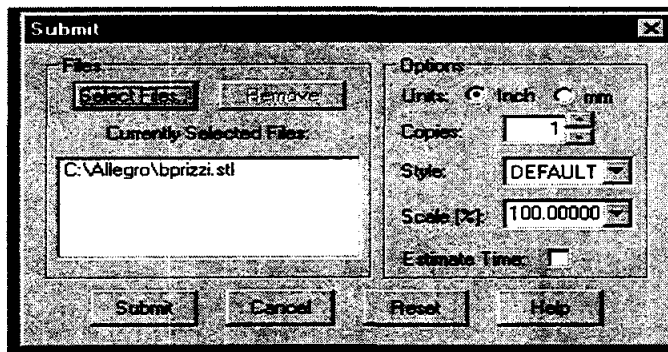
1. From the browser, make a copy of your part. Explode the copy and then use STLOUT to create a .STL file from the exploded copy.
2. From START menu on your desktop select PROGRAMS and ALLEGRO, and the Allegro dialog box appears.
3. Select Actua_1 in the Allegro window by double clicking on it.



4. The Print Manager dialog box will then appear.



5. To submit a job, click on submit icon, and the Submit dialog box appears. As



6. files are selected, they will appear in the Currently Selected Files window. Click the Select Files button to see the Select Files dialog box.
7. Navigate normally to locate your .STL file. Click on Open when located to place the file in the Currently selected Files area of the Submit dialog box.
8. Verify Options are correct and click Submit.
9. The Print Manager dialog box now contains submitted request and will show job status until finished at which time a pop-up message will direct the operator to remove the finished model.
10. After the MJM modeler creates the part model, clean up the model and examine it for fit and function. If any changes are needed, go back to Part 1, Step 1, and make the changes.

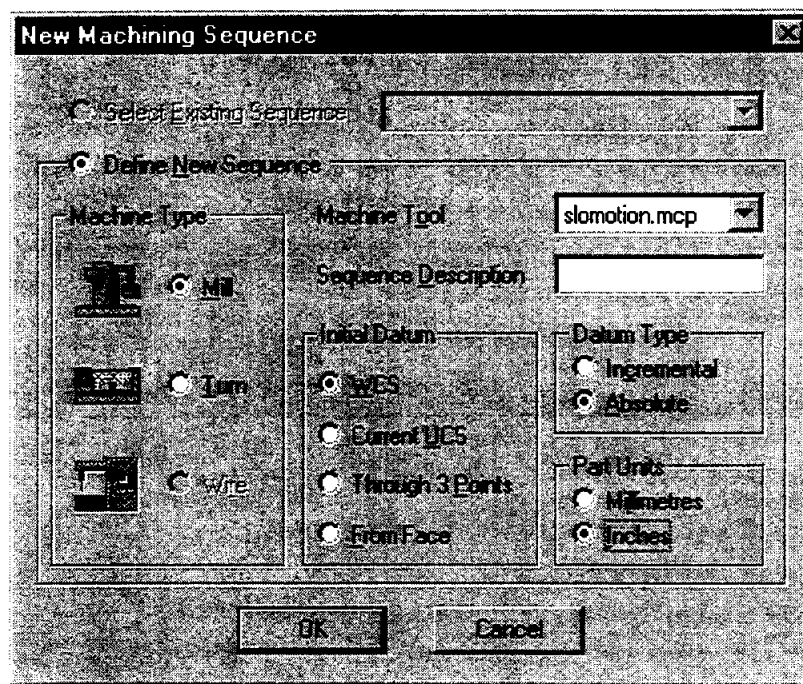
Procedure Part 3 – Manufacturing

1. Once satisfied with the part, load the drawing in Mechanical Desktop, orient the part as shown in Figure 2 being sure the XY axes are oriented as shown. Then, click on the EdgeCAM icon as shown in the upper right corner of Figure 2. This links EdgeCAM with Mechanical Desktop allowing you to write CNC machining instructions from within Mechanical Desktop. Any changes made to the model automatically change the CNC code.

EdgeCAM brings up its Operations toolbar as shown below. Dock it in an open border area.

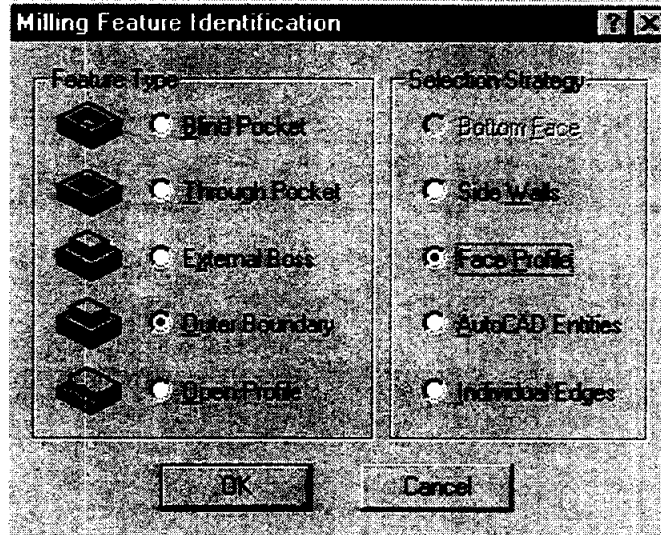


- Click on the Identify Mill Feature icon, the left hand one in the Operations tool bar. When choosing the first manufacturing operation, we must supply some information about the machine tool, so EdgeCAM presents the following dialog box which is not part of Identify Mill Feature. You'll only need to fill it out once as shown below:



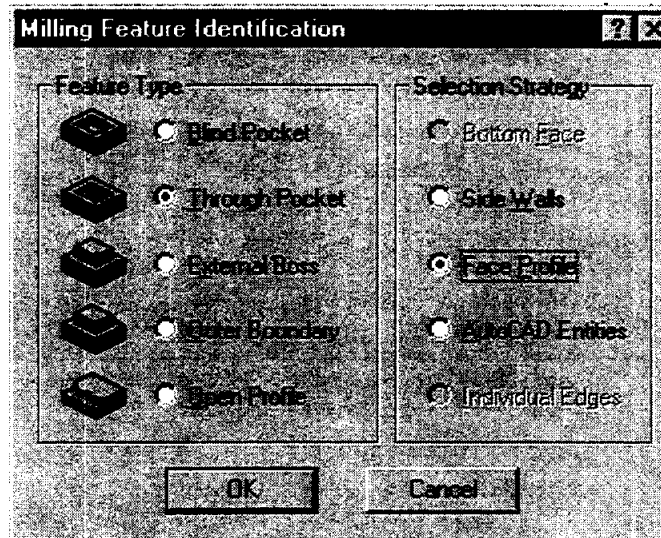
Pick O for origin and specify the origin as the center of the top left hole. Use the CENTER OSNAP to choose it.

- We must now define the outer profile. Fill out the next dialog box as shown below:



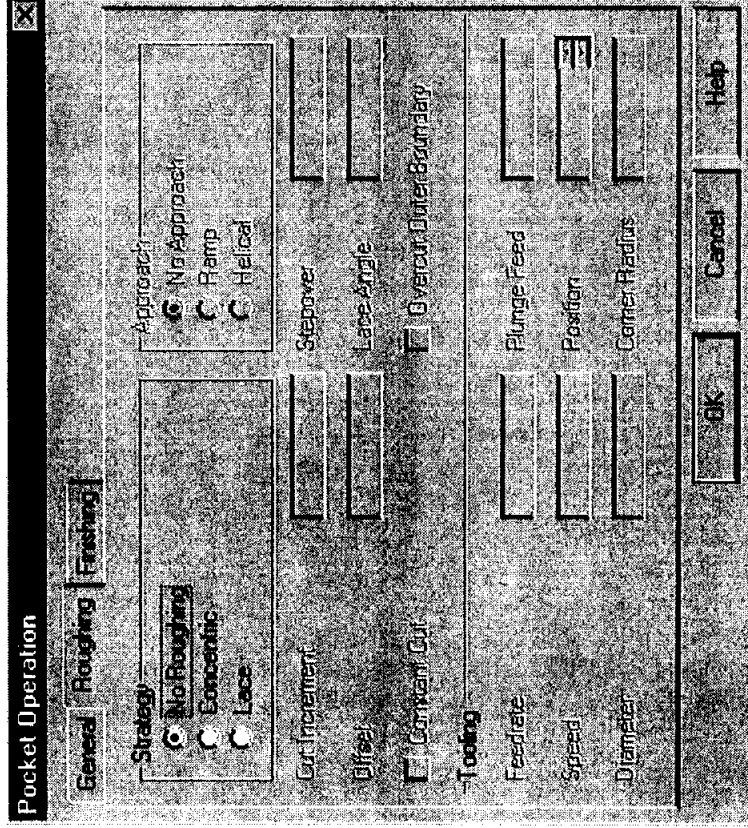
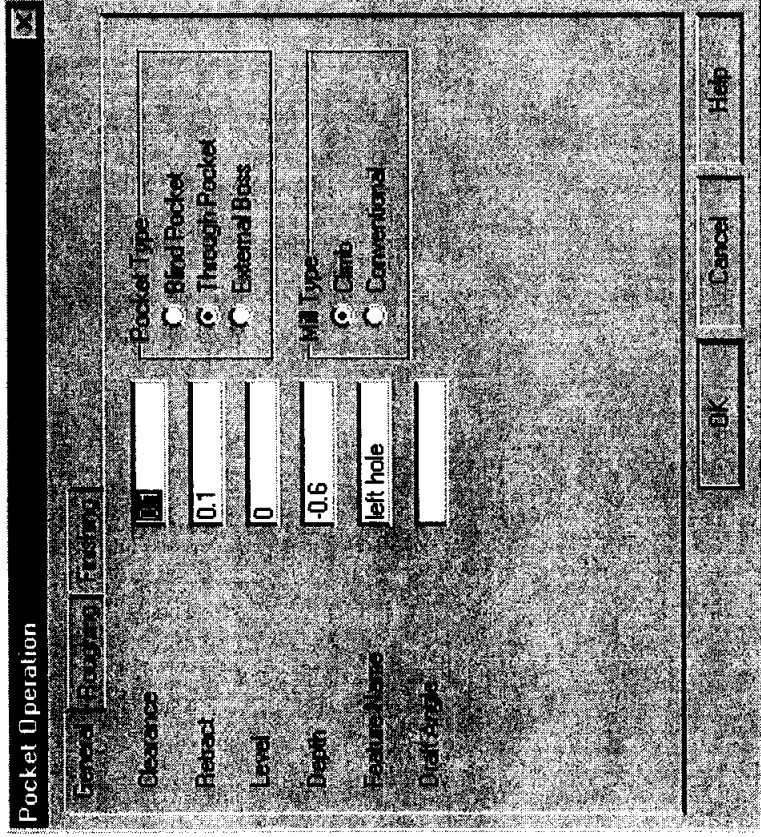
Pick an edge on the upper profile, accept it, and press enter until the command prompt appears again. The edges on the upper surface are now green signifying that they have been defined.

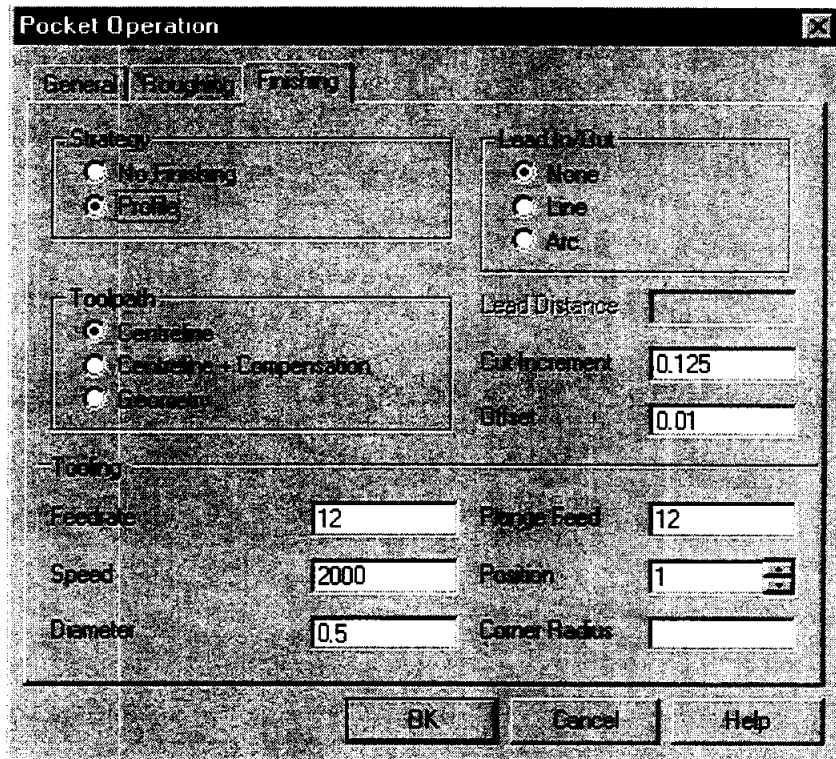
4. Click on the Identify Milling Feature icon, and fill out the dialog box as shown below:






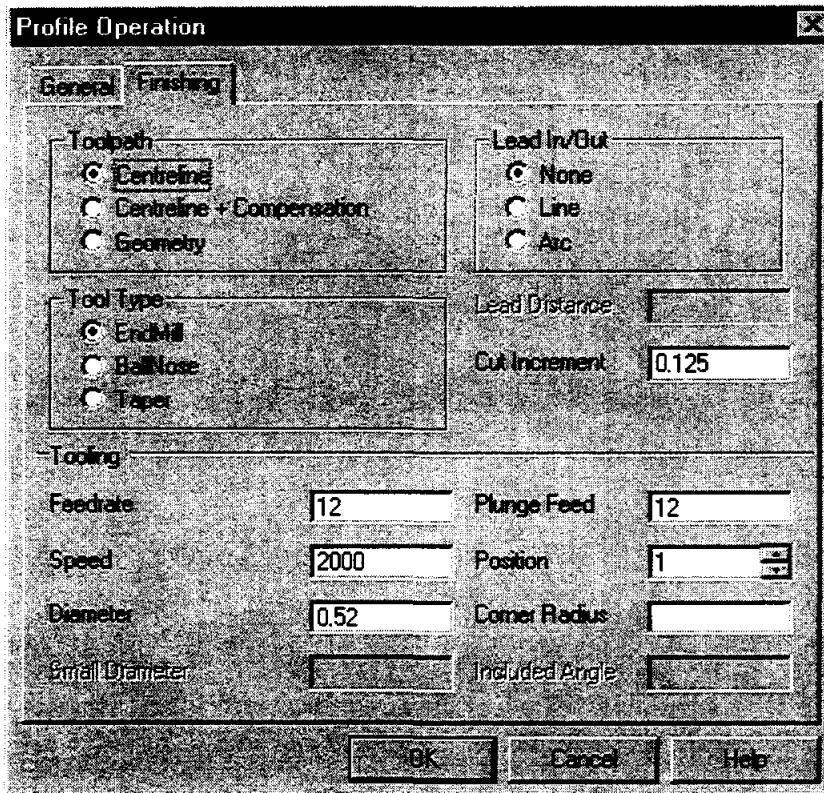
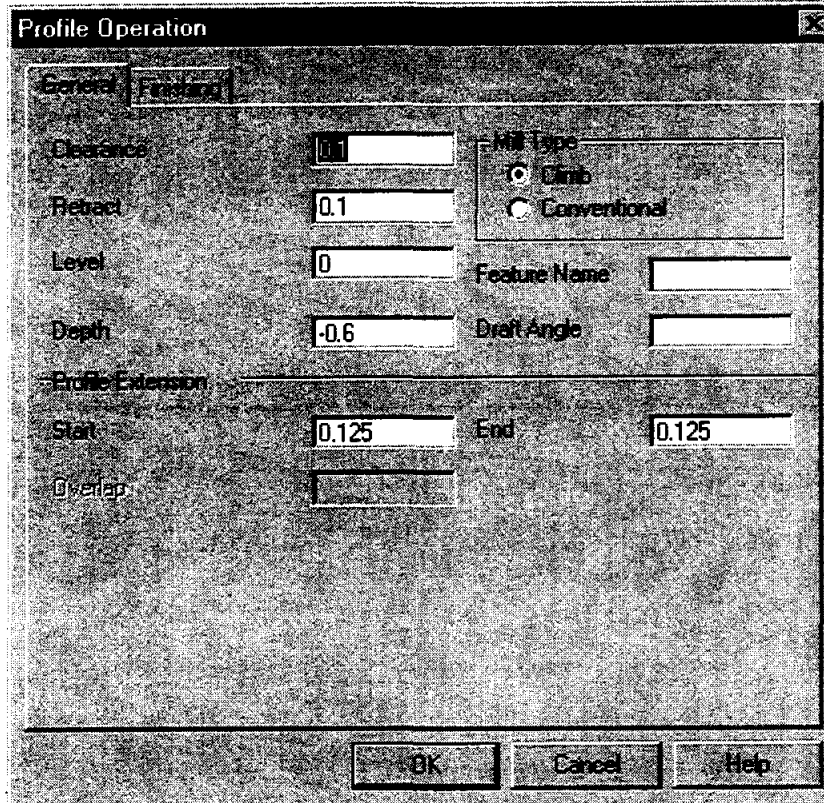
Choose any internal features you may have such as holes or slots and accept the default heights.

5. Select the Pocket Operation from the Operations toolbar and choose the left hand hole. You may have to use a window to pick the hole. Click each of the three tabs in turn and fill them out as shown below:

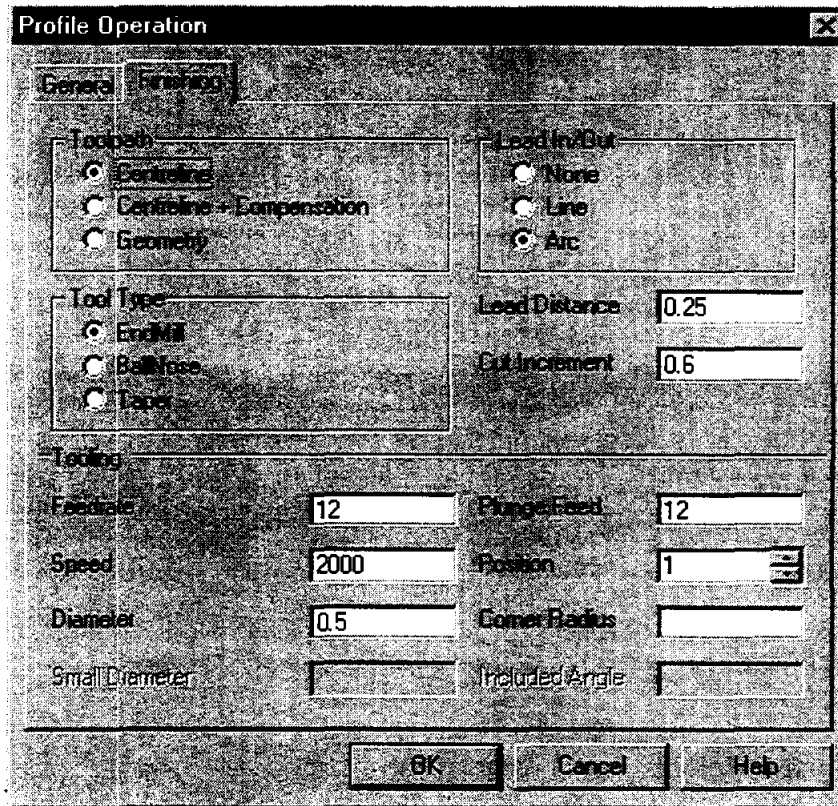






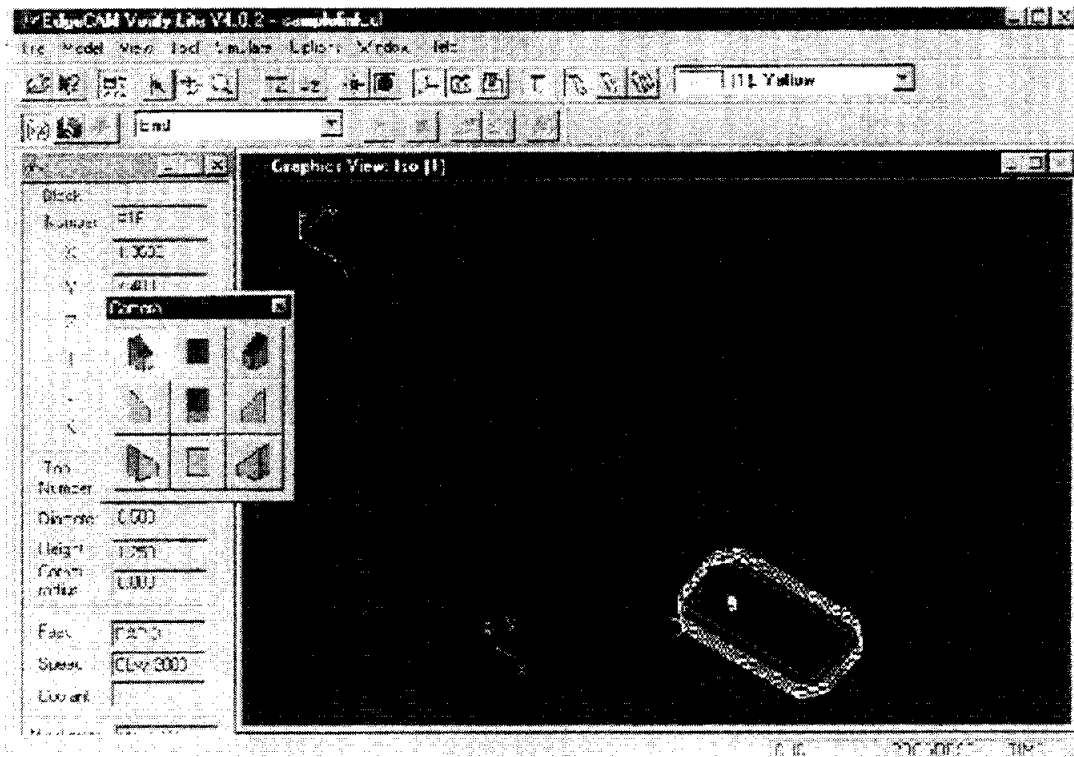
6. Repeat Step 5 for the same hole and change the Offset to 0 and the Cut Increment to 0.3 in the Finishing dialog box.
7. Repeat Steps 5 and 6 for the remaining hole.
8. Click on the EdgeCAM icon . EdgeCAM will now load.
9. Click on the Rapid To Toolchange icon. 
10. Click on the Mechanical Desktop icon  to return the Mechanical Desktop.
11. Click on the Profile Operation from the Operations toolbar. Fill out both dialog boxes as shown below:






12. Repeat Step 11 with the same General data, but change the Finishing dialog box as shown below:



13. We can now simulate the machining operations to look for errors. Click on the Define Stock icon . Choose box and -0.5 for the depth. Type in -0.875,-1 for the first corner and 3.125,1 for the second corner.
14. Click on the EdgeCAM Verify icon . This loads a separate program to simulate machining. Once the program loads, click once to remove the title, and the screen appears like this:



15. Now, click on the Simulate Mode icon  and then the start icon . Watch for gouges in your part. If the part looks as you intend, close out of Verify which then returns you to Mechanical Desktop.
16. The program is now complete, but the instructions must be converted to a language the CNC machine can understand. Click on the Generate CNC Code icon  and place the file in your directory. Save all files and leave Mechanical Desktop.
17. Change the program file's extension from .NC to .AGC and copy the file onto a floppy disk. Your instructor will help you set up and run the milling machine.

Project Report

Prepare a professional looking folder with an orthographic drawing of your part, a printout of the FEA analysis including stress gradient and distortion profile, and a printout of the CNC code to machine your part. Briefly explain your rationale for the shape of your part. Prepare a short presentation to share your design with the class.

CONCURRENT ENGINEERING: EXPERIMENT 3 DESIGN PROJECT

James B. Higley

Yulian B. Kin

Bernard W. Parsons II

and

Christopher M. Prochnow

Purdue University Calumet
METS Department
Hammond, Indiana 46323

Telephone 219-989-2584
e-mail higley@calumet.purdue.edu

This project was supported, in part,
by the
National Science Foundation
Questions regarding use of the software
and not necessarily those of the Foundation



Concurrent Engineering: Experiment 3 Design Project

James B. Higley
Yulian B. Kin
Bernard W. Parsons II
Christopher M. Prochnow

Purdue University Calumet
Hammond, IN 46323

Key Words: finite element analysis (FEA), multi-jet modeling (MJM), rapid prototyping (RP)

Prerequisite Knowledge: Knowledge of three dimensional solid modeling software and basic strength of materials are required to complete this experiment. Completion of the first two experiments in this series is also required.

Objective: This experiment presents a comprehensive project that covers design, analysis, prototype, and reclamation of a product.

Equipment:

1. Personal computer workstation with Mechanical Desktop™, Design Space™, and Allegro™ software.
2. Actua™ 2100 rapid prototyping machine.

Problem Statement

Design a tool to remove two gears on an industrial conveyor system, Figure 1.

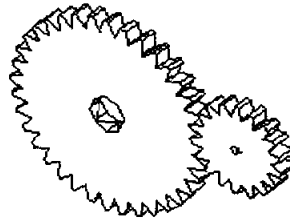


Figure 1. Gear System

This conveyor uses a ten (10) horsepower, 1800 RPM motor with a spur gear system. Both gears, as shown in Figure 1, are made of a case hardened nickel-molybdenum 4620 steel with a surface hardness of approximately Rc 60 and a core hardness of approximately 200 Hb. One gear has 30 teeth with a diametric pitch of 5.0 inches and an inner diameter of 0.75 inches. The second gear has 21 teeth with 1.5 inch diametric pitch and an inner diameter of 0.50 inch. The gears are press fit on their shafts and may take as much as 3000 pounds of force to remove.

Design and assemble your tool using Mechanical Desktop. Analyze each part with Design Space. A factor of safety is not given because Design Space will be used to compute this for your proposed tool. Finally, prototype the tool with the Actua 2100 MJM modeler. When designing your tool, consider how to reclaim materials once the tool wears out or breaks.

Due to material costs, only two (2) prototypes of the proposed tool will be allowed on the Actua 2100. ***In addition, only one (1) plate will be allowed for plotting of each prototype, so orientation of the multiple parts of this tool is critical.***

With regards to the hardware, you are instructed to use nominal size bolts, nuts, and washers. Such sizes include diameters in 1/16" increments between 1/4" and 1/2" and lengths in 1/4" increments between 1/4" to 2 inches.

Project Report

Prepare a professional looking folder with an abstract of the project, a discussion of your design, a reclamation plan, a complete set of drawings with a bill of materials, the Design Space analysis, and disks with copies of all files. Prepare a short presentation with visual aids including your two assembled prototypes.

Biographies

James B. Higley holds the rank of Professor of Manufacturing Engineering Technology. He is responsible for coordinating the Manufacturing Engineering Technology (MFET) program, as well as advising all MFET students. He holds a Bachelor of Science Degree in Mechanical Engineering from Purdue University Calumet and a Master of Science Degree in Mechanical Engineering from Purdue University. He teaches courses in manufacturing, CNC machining, automation, quality control, strength of materials, and simulation. Professor Higley frequently consults in the area of parametric design, manufacturing processes, and industrial training.

Yulian B. Kin holds the rank of Professor of Mechanical Engineering with a PhD from the Petrochemical and Gas Institute in Moscow. He is responsible for the Mechanical Engineering Design Laboratory. Professor Kin teaches courses in machine design, mechanics, fatigue analysis, and reliability and fracture mechanics. His research interests include stress analysis and fatigue fracture mechanics.

Bernard W. Parsons II holds a Bachelor of Science Degree in Mechanical Engineering from Purdue University Calumet and holds the title of Technical Supervisor for the Mechanical Engineering Labs. He is responsible for installing and maintaining all the equipment used in the Mechanical Engineering Laboratories.

Christopher M. Prochnow holds a Bachelor of Science Degree in Mechanical Engineering Technology from Purdue University Calumet. A 1998 graduate, he now is employed as a design engineer by Union Tank Car Company, East Chicago, Indiana.

STRETCHY "ELASTIC" BANDS II

Alan K. Karplus

Department of Mechanical Engineering
Western New England College
1215 Wilbraham Road
Springfield, Massachusetts 01119-2684

Telephone 413-782-1220
e-mail akarplus@wnec.edu



Alan K. Karplus

Stretchy “Elastic” Bands II

Alan K. Karplus
Department of Mechanical Engineering
Western New England College
Springfield, MA 01119-2684

Key Words: Elastics, Tension Tests

Prerequisite Knowledge: Have an idea about changes in the load an elastic loop holds as it is stretched and unloaded.

Objective: To work as a team member in the collection of data, to make plots for near constant rate loading and unloading of fabricated rubber loops, and to show features which are unique to these elastic products.

Equipment:

1. Collect fifteen three and one half inch long rubber “elastic” bands of 1/8 inch width, 0.034 inches thickness, and referred to as 33 rubber bands. These fifteen bands are required to build four group members: A) two bands each cut and tied with square knots at the cut ends to create a single 4 inch loop (this is equivalent to an uncut band in starting length), B) two bands each cut and tied with square knots at the cut ends to create a single 6 inch loop, C) four bands each cut and tied with square knots at the cut ends to create a single 12 inch loop, and D) six bands each cut and tied with square knots at the cut ends to create a single 18 inch loop. Then clearly designate the group as **Group 33**. Without the designator of elastic band size, “group” refers to the four members alone: loop size A, loop size B, loop size C, and loop size D. Most office supply houses have number 33 size elastic bands.
2. Fifteen foot long Tape measure.
3. Mounting board (2 in. by 1 in. by 30 inch) with a six penny nail inserted one inch from one end on the 2 inch by 30 inch face, and to which the twenty foot long scale can be attached. The 30 inch long board should be clamped to a table that is 15 feet long parallel to the long length. C-clamps can be used to secure the board and the tape measure once the tape measure has been wrapped with a protective material. The zero of the measure should be at the nail.
4. Safety Goggles
5. Heavy work gloves
6. Load scale for loads to 15 pounds or 7.5 kg. A scale with a capacity to 10 pounds or 5 kg. may be helpful, if available.
7. Micrometer or vernier caliper.
8. Data page with 25 lines and nine columns for each loop to be tested. For the loop size A the measurements are taken at one inch increments starting at a value of four inches and are to be listed in the first column. The next two columns are used in pairs to record load and unload for each elastic. Be sure to label columns and include units of measure selected. For the remaining group members, B, C, and D, the starting length and increment size change as follows: at one and one-half inch increments starting at a value of six inches listed in the first column for group member B, at three

inch increments starting at a value of twelve inches listed in the first column for group member C, and at 4.5 inch increments starting at a value of 18 inches listed in the first column for group member D, respectively.

9. A Spreadsheet such as EXCEL™ is recommended. However, all work performed on the spreadsheet can be done by hand.
10. When the computations are to be done by hand, computation paper and several pieces of linear graph paper with 20 divisions to the inch are needed.

Introduction:

The approach is to stretch each rubber loop (LOADING LINE) at a near constant rate and to unstretch (UNLOADING LINE) it at the same near constant rate while recording the load present at each stretch point. One team member should do the loading and read the load at each position while the second team member should record the data. Try to load and unload the elastic at a constant rate, and about the same rate for each loop so that meaningful comparisons between loops can be made. Both team members should work on the data analysis, make observations from the computations and plots, and formulate conclusions.

In each group there are four members which are: A) two bands cut and tied in series with square knots to represent an original length rubber band (do not use an original rubber band because the force to stretch the band is excessive in relation to the loads needed to stretch the fabricated loops), B) two bands cut and tied in series to create a six inch long loop, C) four bands cut and tied in series to create a twelve inch long loop, and D) six bands cut and tied in series to create an eighteen inch long loop. Each elastic band is initially three and one-half inches long and when cut, is seven inches long. When two cut bands are tied end-to-end, the effective length of each elastic is six inches, and can be less when tied to make a four inch loop. The selected loop lengths given earlier are based on an average loop length and experience. For this experiment each loop is stretched to six times the initial loop length to obtain a strain of 500 percent which is defined as final length minus initial length divided by the initial length.

To efficiently record the data, to process the data that has been collected, and when a spreadsheet is used consider making a column of deformation that starts at four inches and ends at 24 inches (LOADING LINE) and returns to four inches (UNLOADING LINE), or starts at six inches and ends at 36 inches (LOADING LINE) and returns to six inches (UNLOADING LINE), or starts at twelve inches and ends at 72 inches (LOADING LINE) and returns to twelve inches (UNLOADING LINE), and or starts at eighteen inches and ends at 108 inches and returns to eighteen inches for group members A, B, C, and D, respectively. Enter the collected data into the spreadsheet and the make a plot for the entered deformation - load data. In all cases there are 21 deformation entries in the data sheet. The A member has loads recorded at of 4.0, 5.0, 6.0 inches, etc. while the B member has loads recorded at 6.0, 7.5, 9.0, 10.5 inches etc. with member C loads values recorded at 12.0, 15.0, 18.0, 21.0 inches, etc. and member D has loads recorded at 18.0, 22.5, 27.0, 31.5, 36.0 inches, etc.

At each deformation position a computation for engineering strain and engineering stress can be made. Engineering strain is the length (L) at any displacement minus a reference displacement (R) divided by the reference displacement (R) or $(L-R)/R$. For the A loop, four (4) inches is chosen as the reference dimension (R) for this experiment. Engineering stress or (P/A) is the load (P) divided by the cross section area (A) of the loop. Note that the loop has two strands carrying load. Compute the strain and stress for the collected data. Make a second plot for the stress and strain found. As presented above, the increments used provide a strain of 500 percent.

Increments for the area under the LOADING LINE are computed separately from the UNLOADING LINE. The totaled incremental areas each represent the energy used to stretch and unstretch the loop,

respectively. Now compute the area under the curves with trapezoidal increments. First the upload curve and then the down load curve. A spreadsheet cell should be used to store each trapezoidal area increment. The trapezoidal increment is computed by forming the average of two stresses and multiplying by the change in strain. The total area under a curve can be found by adding the incremental areas in a column, and is the energy related to each curve. The difference between column totals found is the hysteresis. A ratio between the difference and the upload curve area when shown in percent finds the portion of energy lost to internal friction or hysteresis. Be sure to check UNITS.

An informative comparison for the group of four rubber loops tested can be made by plotting and clearly labeling first the load deflection data for all elastic loops on one set of axes and secondly the stress - strain data for all elastic loops on another set of axes. Note how the stress-strain plot curves compare favorably, and the percentage of energy allocated to hysteresis is seen to be similar while the load - deflection plot clearly shows the change in length and very similar loads for each elastic loop.

Preparation:

Prepare the Mounting Board by placing a six penny nail into the 2 inch by 30 inch surface of the board one inch from the three surfaces at one end. Place, and then clamp the board onto a table parallel to a 15 foot long edge. Secure the 'zero end' of the tape measure at the nail and attach to the board after wrapping the tape measure so it is protected and not covered so that the scale can be seen. Similarly, secure the other end of the tape measure at the 15 foot mark. The experimenter should now be able to place an elastic loop over the nail and extend a long loop elastic up to 15 feet.

In each group there are four members which are A) two bands cut and tied with square knots to represent an original length rubber band, B) two bands cut and tied in series to create a six inch long loop, C) four bands cut and tied in series to create a twelve inch long loop, and D) six bands cut and tied in series to create a eighteen inch long loop. Each cut elastic band is initially three and one-half inches long and when cut, is seven inches long. When two cut bands are tied end-to-end, the **effective** length of each elastic is often six inches. However, shorter effective lengths can be used depending on the location of the square knot in relation to the end of the cut band and the chosen loop size. Fifteen number 33 elastic bands are required to build **four Group 33 members**: A) two bands each cut and tied with square knots¹ at the cut ends to create a single 4 inch loop, B) two bands each cut and tied with square knot at the cut ends to create a single 6 inch loop, C) four bands each cut and tied with square knots at the cut ends to create a single 12 inch loop, and D) six bands each cut and tied with square knots at the cut ends to create a single 18 inch loop.

Secure several rubber loops of each length for a group to be tested (if one breaks, a replacement is readily available!). Measure the length, thickness and width of the loop and record the results. Group 33 elastics are approximately 0.034 inches thick, 1/8 inch wide. Remember there are two strands of each loop carrying load. Now compute the cross sectional area.

Prepare the data sheet with 25 lines and nine columns. Make a column of deformation with 21 data entries that starts at four inches, has 1 inch increments, ends at 24 inches (LOADING LINE) and returns to four inches (UNLOADING LINE), or starts at six inches, has one and one-half inch increments, ends at 36 inches (LOADING LINE) and returns to six inches (UNLOADING LINE), or starts at twelve inches, has three inch increments, ends at 72 inches (LOADING LINE) and returns to twelve inches (UNLOADING LINE), and or starts at eighteen inches, has four and one-half inch increments, ends at 108 inches and returns to eighteen inches for group members A, B, C, and D, respectively. Enter the

¹ Be sure to use the SQUARE KNOT as its cousin, the "Granny Knot" will creep along the elastic when the loop is pulled and destroy the experiment.

collected data into the spreadsheet and then make a plot for the entered deformation - load data. In all cases there are 21 deformation entries in the data sheet. The A member has loads recorded at of 4.0, 5.0, 6.0 inches, etc. while the B member has loads recorded at 6.0, 7.5, 9.0, 10.5 inches, etc. with member C loads values recorded at 12.0, 15.0, 18.0, 21.0 inches, etc. and member D has loads recorded at 18.0, 22.5, 27.0, 31.5, 36.0 inches, etc.

In the case of the loop A, measurements are to be taken at one inch increments starting at a value of four inches listed in the first column and end at the 24 inch position. The remaining columns are used in pairs to record load and unload for each elastic size. Be sure to label the load columns in pairs (LOADING and UNLOADING) and include units of measure selected. The first LOADING value is made at the four inch position. A position is designated where the hook of the load scale attaches to the rubber loop and is sited on the tape measure. The last LOADING value at 24 inches should be the FIRST UNLOADING value at 24 inches because the UNLOADING values are recorded for decreasing positions.

In the case of the loop A when the extension exceeds 20 inches you must make a *concentrated* effort to keep the current loop under load. DO NOT UNLOAD or LOOSE LOAD on the scale on the upload because the loop will be unloaded and the upload data will not be represent near constant rate loading. This becomes an increasing challenge as the loops become longer. With the longer loops unloading needs to continue carefully so that meaningful data is collected. Remember elastic bands creep and hesitation in the loading and unloading process can impact findings. A steady rate of loading and unloading is important. In case a loop breaks when under test, COMPLETELY redo the test. Special efforts are needed to record load values for the loops B, C, and D.

In preparation for a test run place a designated rubber loop over the nail and through the hook of the load scale. Check that a load measurement can be made at the four inch mark on the tape measure. Be sure the operator of the load scale has safety glasses on and is wearing the heavy gloves. These safety devices will protect the operator if the elastic loop breaks and the spring scale unloads and the elastic loop flies around.

Procedure:

1. Tensile load - deflection tests are to be performed on **Group 33**, a group of four member rubber loops with each loop prepared from three and one half inch long rubber bands of 1/8 inch width (number 33) rubber bands. **Place safety glasses and gloves on the spring scale operator, and prepare the recorded for writing the data on the data sheet.** The approach is to stretch a loop, and as this is done at a near constant rate, record the load to stretch the rubber loop at each added inch. For the loop A start at four inches. Continue with one inch increments until the length of the loop is 24 inches. Next, unload the loop at the same rate as was used to load the loop taking load measurements at each inch of reduced length. Remember the load value at the 24 inch position is the same for the last LOADING position and the end of UNLOADING column on the data sheet. As the loop is unloaded fill the UNLOADING column backwards, i.e. from 24 to 23 to 22 inches, etc. The recorded data is defined as "raw data" for elastic loop A of Group 33 which is the first elastic loop tested. Be sure to label the length of the rubber loop tested, and measure and record its thickness and width.

2. The first comparison to be made is for the shape of loading and unloading paths for load/deflection data. Repeat step one, above, for loops B, C, and D. Start at 6 inches, use 1.5 inch increments, end at 36 inches, and return to 6 inches for loop B, start at 12 inches, use 3 inch increments, end at 72 inches, and return to 12 inches for loop C, and start at eighteen inches, use 4.5 inch increments, end at 108 inches,

and return to 18 inches for loop D. At each deformation level, enter the load. Make an XY^2 or **Scatter Plot** of the data. The horizontal axis should be Deformation in inches while the vertical axis is Load in pounds. Label the Load - deflection line as **Loop A - Group 33**. The approach to use with EXCEL™ is to make the Loop D plot first and place axes labels and a Plot Title “Elastic 33 Load - Deflection Group Comparison”. Remember the loop D has the greatest length, check the 108 inches, while the other loops have less. Next INSERT the C data by selecting the data and dragging it onto the plot. The data will be plotted to the appropriate scale and the series labeled. Repeat for the process for B and A data.

The applied load - deflection plots on the same graph show magnitude changes. The largest load carried by each loop should be clearly evident on the right hand end of the loop deflection axis when the Load axis value is read. Note if a trend appears which shows that, in general, the longer loops carry the same load.

3. The second comparison is dependent on two modifications made to the raw data. The first modification is to define the engineering strain as the ratio computed by taking the measured loop length minus the starting length and dividing this quantity by the initial length. For all loop A use four inches as the initial length, and for loops B, C, and D, six, twelve, and eighteen inches, respectively. This means that the first value of strain is zero with UNITS of inches/inch and strain units of 0.25 in./in. are used. The strain is to be plotted on the horizontal axis and should start with zero and end at five.

The second data modification is to divide the load by the cross-sectional area of the original rubber loop. For Elastic 33, the area is 0.0625 in. by 0.125 in. times 2 (number of strands holding load). This computes the engineering stress in the loop which has UNITS of pounds per square inch in the English system and is to be plotted on the vertical axis. Again prepare an XY or **Scatter Plot** with the modified data. This will be a stress-strain plot for the elastic or rubber loop. Label the line on the plot as **Loop A - Group 33**.

Repeat the strain and stress calculations for loop B, C, and D, and make separate stress-strain plots for each elastic. Then add this data to the same stress-strain plot as for Loop A and label each line. Remember in EXCEL™ to prepare on plot and then select and drag onto the plot the other sets of data. Note the similarities between these curves on the composite plot for the Number 33 Elastic Loops. If the effect of initial elastic length and original cross sectional area are considered, the stain range of 5 times or 500 percent is the same for each rubber loop and the stress ranges are comparable. How closely do the four stress – strain plots resemble one another?

4. Areas under each of the stress/strain curves are to be found by approximation. An approach is to represent the area between strain values as a trapezoid and to sum the areas of all the trapezoids to obtain the area under the LOADING line. The summing of trapezoids is repeated for the UNLOADING line. Note that the trapezoid has a ‘height’ in stress units of pounds per square inch and that the ‘width’ of the trapezoid has strain units of inches per inch. The product of stress times strain becomes inch-pounds per cubic inch. In summary, the difference between these sums is the residual often referred to as hysteresis. The hysteresis represents the energy consumed in the deformation process. Compute the portion of the UNLOADING LINE energy is of the LOADING LINE energy. Then subtract this value from 100 percent to find the percentage of energy lost to hysteresis.

What can be presented about the energy differences between the loops A, B, C, and D? A rapid visual comparison is found when the stress/strain plots are super-imposed on one another. This shows the common features such as the LOADING lines as well as differences such as for the UNLOADING lines

² Be sure to make a plot of two variables and NOT a line chart as is the usual default setting on a spreadsheet.

between the four rubber loops from zero to 500 percent strain. Note that the area term represents ENERGY. When English units are used, the product of pounds per square inch times inches per inch becomes inch-pounds per cubic inch.

What relationship can be found between LOADING energy, UNLOADING energy, and hysteresis? A table of rubber loop size with columns of LOADING, UNLOADING, and hysteresis can show that about half the energy is assigned to hysteresis.

Comments:

1. To aid the instructor in the execution of this experiment, a sample for loop A of Group 33 is shown below. Figure 1 presents the data. Note the starting position for deformation at 4 inches and the load values at 24 inches. In Figure 2 the upload and download curves are seen. Figure 3 is presents the stress – strain plot for the data seen in Figure 1. Deformation and load values have been presented as strain values in column four, upload stress, download stress in columns five and six and the trapezoidal areas between strain increments in columns seven and eight with total work done in nine and ten.

To make a hand calculation for the 6 inch displacement: A. strain $[(L-R)/R]$ is $(6-4)/4 = 0.5$ and B. the upload stress (P/A) is $0.25 \text{ pounds} / (2 * 0.034 * 1 / 8) \text{ in. sq.}$ or 29.41 psi. as seen in Figure 3, column five. In column seven of Figure 1 is C. the area under a part of the upload curve as 3.68 in.-lb. per cubic inch which is found by averaging 0 and 29.41 $= (29.41 / 2 = 14.71) \text{ psi.}$ and multiplying by 0.25 in./in. which is the change in strain increment. For the incremental download the energy computed is 1.84 in.-lb./cubic inch found by averaging 14.71 and 0.0 and multiplying by 0.25.

The sum of the incremental work is found in columns nine and ten. A comparison of the total download energy of 367.65 in.-lb./cubic inches (found by adding all the incremental energies) to the upload value of 794.12 in.-lb./ cubic inch shows a ratio of 0.463 or 46.3 percent. The hysteresis value is likewise 100 - 46.3 or 53.7 percent which represents the energy consumed.

2. Figures 4 and 5 show a comparison of the four Group 33 Cut Band Loops for the Load - Deflection and Stress - Strain presentations, respectively. Note the differences in load for the four loops. Remember the loops were manufactured and the loaded length of each elastic may be different length.
3. To provide added perspective the lengths of the loops prepared which number 33 elastic bands can be changed. One requirement for a rapid comparison is to keep the strain increments at 0.25 and the total strain at 500 percent. Loops of 4 inches, 8 inches, 16 inches and 32 inches provide stress -- strain plots that superpose readily on the Group 33 length selections used in this experiment.
4. Another approach is to change the elastic size. Two sizes have been considered: 1) A 1/16 inch wide or number 19 rubber band can be tried. The number 19 adds a valuable perspective to the data base and can enhance the experiment. However, be aware that the loads will be less and a different capacity scale with different increments should be considered. 2) Elastic band size 54 can be used, too. In this case three significant observations are noted. The first observation is that when the size 54 bands which are ¼ inches in width were cut and tied - and pulled - in the tying process that the material in the vicinity of the knot was severely distorted, so much so that the elastic material changed color from brownish to a whitish hue. This coloration showed that the structure of the rubber in the bands had changed. Note this occurs with the number 33 and 19 bands, also, but the visual impact is not as strikingly evident!. The second observation is that sometimes the knots crept along the distorted band ends and the loop separated, especially under loads approaching five

pounds. The third observation is that the change in cross section at the knot location and five to ten knots lengths to either side of the knot creates a “jog” in the loop so that the loop becomes noticeably altered which destroys the idea of a uniform cross section loop.

5. The author was able to obtain solid rubber band material to construct “homogeneous” style loops with a single knot. This elastic is used for rubber band model aircraft when the builder/pilot selects his/her own rubber band length. The band often is available from a hobby store as a 96 inch long rubber thread, 3/16 inch by 0.034 inches in cross-section. Test results are similar. However, the model aircraft rubber band (rubber thread) exhibited a strain limit of 350 percent in contrast to the 500 percent for loops.
6. Reference to Stretchy “Elastic” Bands from New’97 can lend added understanding to how not only the impact of changing elastic size effects the stress stress-strain findings for elastics 33, 54, and 84, but how the work in this experiment shows very similar stress-strain plots for strains to 500 percent. However, the New’97 experiment used bands in the “as received” condition. A comparison of the Number 33 band from Stretchy “Elastic” Bands shows that the maximum load at 24 inches elongation is 5.5 pounds in contrast to 3.5 pounds for the manufactured loop! This leaves the manufacturing process as an investigation challenge. Hint: Most elastics are cut to width perpendicular to the axis from extruded “elastic band” cylinders.

Acknowledgments:

The author is appreciative of the assistance provided by Mr. Richard DeCelle, Mechanical Laboratory Technician, Mr. Peter Bennett, Mechanical Laboratory Machinist, and by Jason Misiasek in the recording of data.

Cut Bands used to make loops Band cross section
 0.034 in. by 1/8 times 2 tendons

A two unit loop

displacement in	loading		strain	stress		Inc work		Total Work	
	upload lb	download lb		upload psi	download psi	up in-lb/in ³	down in-lb/in ³	Upload in-lb/in ³	Download in-lb/in ³
4	0.00	0.00	0.00	0.00	0.00	0.00	0.00	0.00	0.00
5	0.00	0.00	0.25	0.00	0.00	0.00	0.00	0.00	0.00
6	0.25	0.13	0.50	29.41	14.71	3.68	1.84	3.68	1.84
7	0.50	0.25	0.75	58.82	29.41	11.03	5.51	14.71	7.35
8	0.50	0.25	1.00	58.82	29.41	14.71	7.35	29.41	14.71
9	0.63	0.25	1.25	73.53	29.41	16.54	7.35	45.96	22.06
10	0.75	0.38	1.50	88.24	44.12	20.22	9.19	66.18	31.25
11	0.88	0.38	1.75	102.94	44.12	23.90	11.03	90.07	42.28
12	1.00	0.38	2.00	117.65	44.12	27.57	11.03	117.65	53.31
13	1.13	0.38	2.25	132.35	44.12	31.25	11.03	148.90	64.34
14	1.25	0.50	2.50	147.06	58.82	34.93	12.87	183.82	77.21
15	1.25	0.50	2.75	147.06	58.82	36.76	14.71	220.59	91.91
16	1.50	0.50	3.00	176.47	58.82	40.44	14.71	261.03	106.62
17	1.63	0.50	3.25	191.18	58.82	45.96	14.71	306.99	121.32
18	1.75	0.63	3.50	205.88	73.53	49.63	16.54	356.62	137.87
19	2.00	0.75	3.75	235.29	88.24	55.15	20.22	411.76	158.09
20	2.13	0.75	4.00	250.00	88.24	60.66	22.06	472.43	180.15
21	2.38	1.00	4.25	279.41	117.65	66.18	25.74	538.60	205.88
22	2.75	1.25	4.50	323.53	147.06	75.37	33.09	613.97	238.97
23	3.00	2.00	4.75	352.94	235.29	84.56	47.79	698.53	286.76
24	3.50	3.50	5.00	411.76	411.76	95.59	80.88	794.12	367.65

Down load % of Upload 46.30

Figure 1. Elastic 33 Cut Band Loop A Data

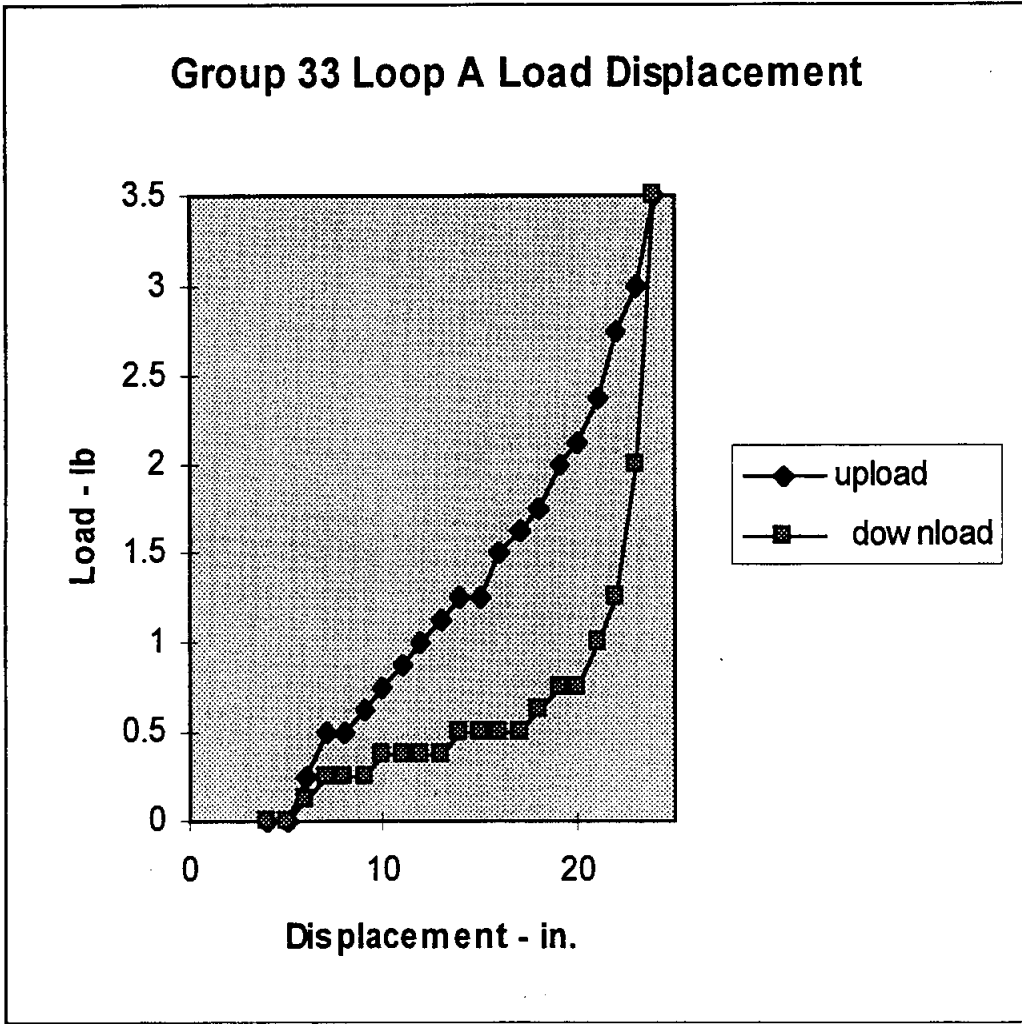


Figure 2. Elastic 33 Cut Band Loop A Load Deflection Plot

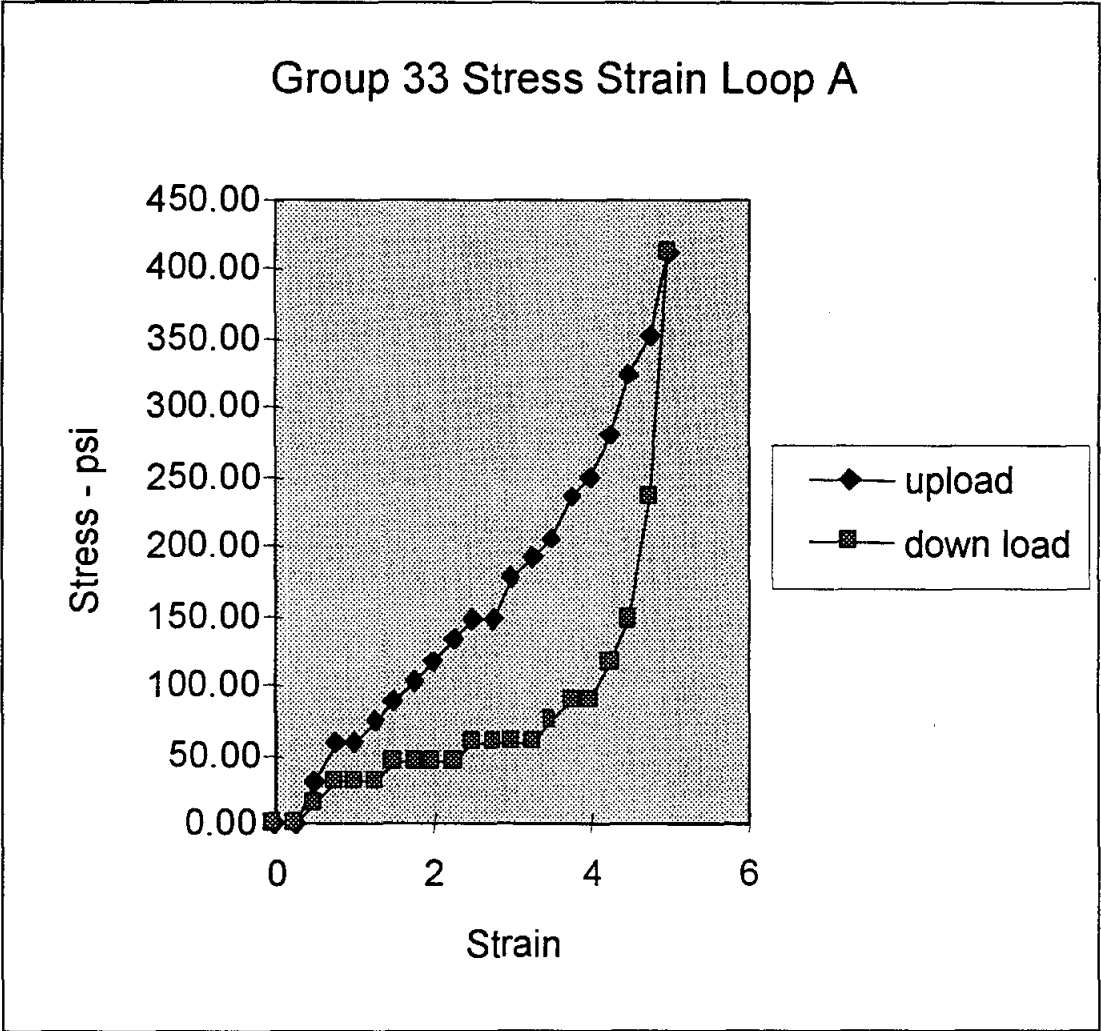


Figure 3. Elastic 33 Cut Band Loop A Stress -- Strain Plot

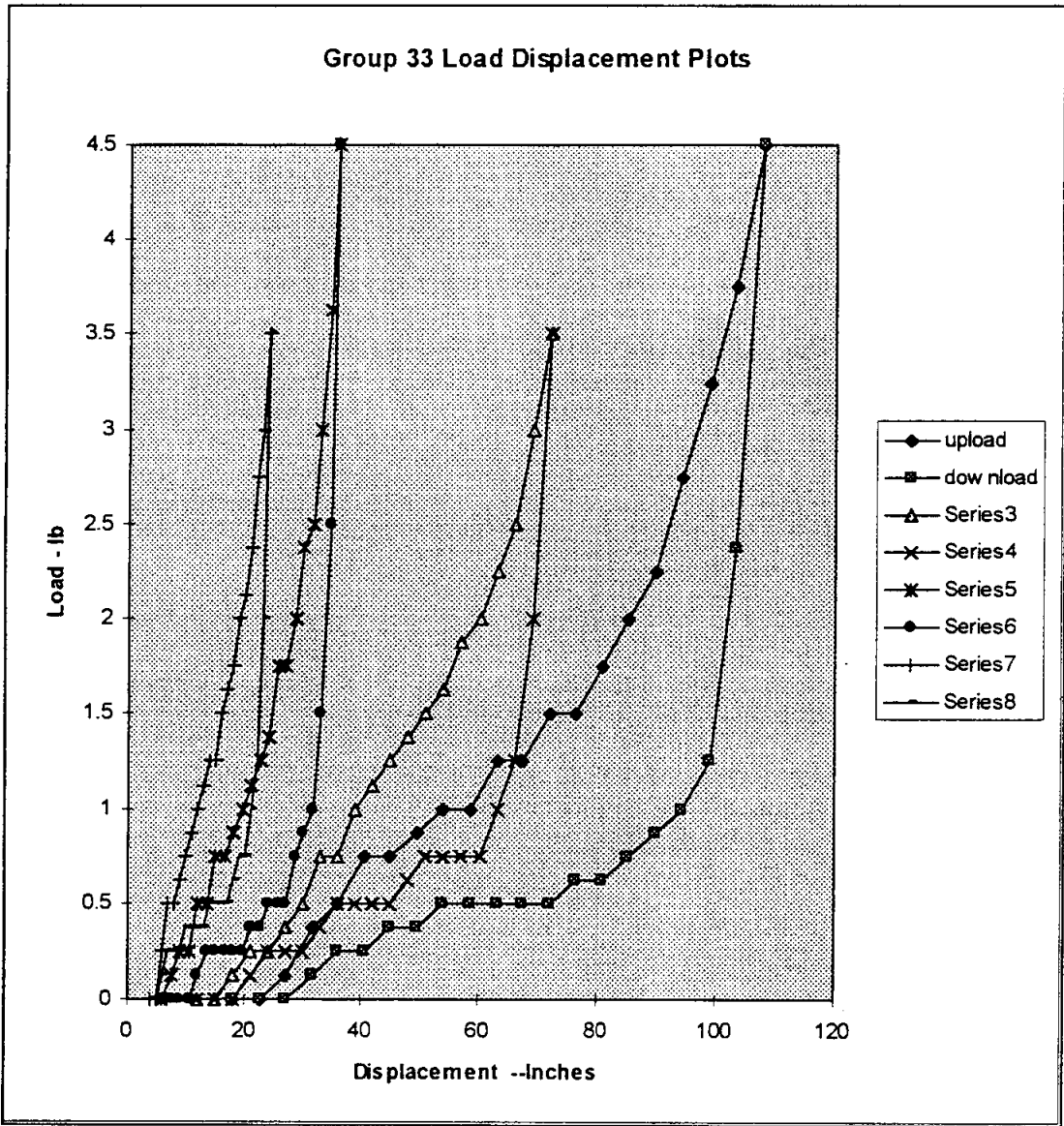


Figure 4. Elastic 33 Cut Bands Load - Deflection Plot Comparison
 Series 7 and 8 Loop A, Series 5 and 6 Loop B
 Series 3 and 4 Loop C, Upload and Download Loop D

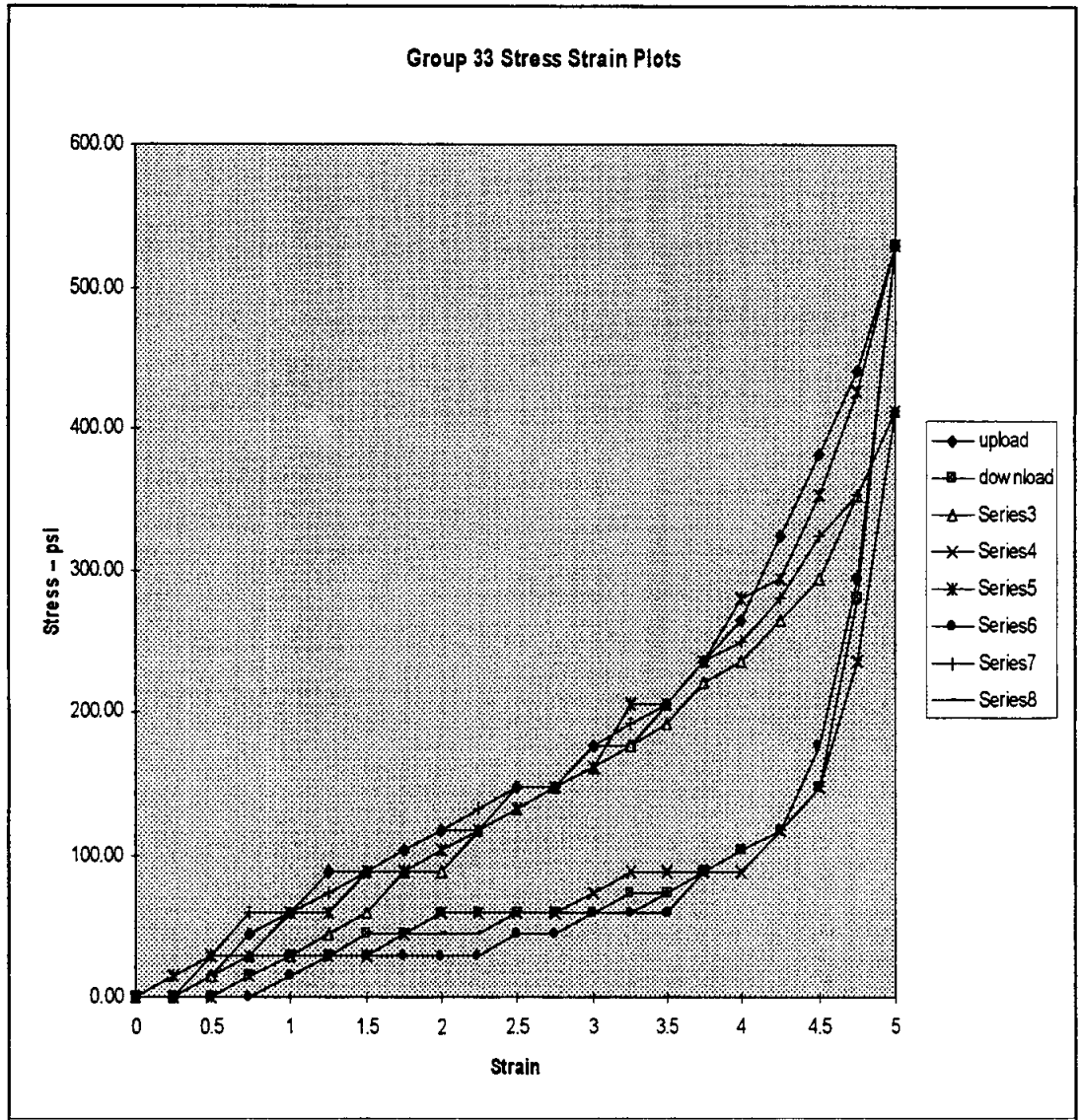


Figure 5. Elastic 33 Cut Bands Stress -- Strain Plot Comparison
 Series 7 and 8 Loop A, Series 5 and 6 Loop B
 Series 3 and 4 Loop C, Upload and Download Loop D

ALAN K. KARPLUS

Alan K. Karplus is Professor of Mechanical Engineering at Western New England College, Springfield, Massachusetts. He has a Bachelor's degree from Tufts College, a Master's degree from Iowa State University and a Ph.D. from Colorado State University. He has been involved with the freshman engineering program, coordinates the senior mechanical engineering laboratory program, teaches Materials Science and supervises M.E. Senior Projects. His interests include materials and design. He is a member of ASME and ASEE. He has contributed to the National Educators' Workshop and ASEE Annual Conference for several years.

**PRODUCING PDF FILES USING
ADOBE ACROBAT CAPTURE V2.01**

Alfred E. McKenney

516 Fairfax Way
Williamsburg, Virginia 23185

Telephone: 757-221-0476
e-mail HDJC41A@prodigy.com



Alfred E. McKenney

EMSET CD-ROM

Experiments in Material Science

James A. Jacobs

ISBN: 0-13-648486-7

Containing over 300 peer-tested experiments and demonstrations that have been presented at *National Educators' Workshops* over the last decade. Sponsored by NASA, NIST, the Department of Energy and Norfolk State University, the NEW: Update conferences and the cooperative efforts of over 1000 educators, engineers and scientists made this CD-ROM possible.

- ξ Laboratory experiments and classroom demonstrations that you can modify to suit your teaching objectives, environment, and students' needs.
- ξ Access to instructional aids developed by hundreds of materials educators and industry specialists.
- ξ Provides students with "hands-on" activities that cover the full range of materials science and technology—topics such as woods, metals, and emerging technologies including processing and structures of advanced composites and sol-gel ceramics.
- ξ Flexibility—emphasis is placed on low-cost, multi-concept exercises in recognition of the many settings in which materials education occurs.
- ξ Allows you to read, navigate, search for other experiments and documents, print and edit.
- ξ This CD-ROM has captured both classical and new and innovative experiments and demonstrations.

To reserve your desk copy, please contact your local Prentice Hall Sales Representative, or call Faculty Services at 1-800-526-0485.



www.prenhall.com

Producing PDF Files Using Acrobat Capture V2.01

(capture processv2.wpd)

Original prepared in 1996 by Alfred E McKenney for NEW:Update Lab Experiment Project
Rev: January 27, 1999

Overview

The PDF files will be produced using *Acrobat Capture* to scan and process the hard copy proceedings. The sizes of the output files are dependent on the number of pages and the number and size of the graphics contained in the paper. Each formula, table and illustration is a separate graphic.

The first part of the *Capture* process involves scanning clearly-printed* hard copy documents to produce an intermediate graphics file. Usually this is a TIF format. This can be done at less than a minute a page, using a scanner the speed of the UMAX Vista S-12. The intermediate graphics pages can be stored for final processing later, unattended.

After processing through the second and final step of *Capture*, which involves optical character recognition (OCR) and page formatting, an ACD file is produced. Although a preliminary PDF file can also be produced at this time, there are usually questions raised in the OCR process. The documents should, therefore, be proofed in a third step, using *Capture Reviewer*. *Capture* has previously marked the suspects to make the job easier. This review may take four or five times as long as the scanning process, depending on the complexity of the paper and the subject knowledge of the reviewer, that is, someone familiar with the terminology and conventions of technology. A five page paper, clearly printed, containing only text might be proofed in about five minutes. Once the review is complete, the ACD is finally saved as a PDF. These PDFs should be checked by using *Acrobat Reader* and sampled by printout to ensure the validity of the *Capture* and *Review* process.

* Clearly-printed means a paper submitted using:

A laser printer. A good ink jet printer is acceptable, but not dot matrix printing.

Body type size, 11 to 12 pt.

Clear type, preferably a serif (Roman) face. Sans-serif is acceptable.

No underscores. Use italics, if possible.

It should be noted that if the paper were available in digital form, the *Acrobat PDF Writer* program could be used to quickly and accurately produce the PDF file directly, without need for the *Capture* program. However, this means that the formulas, tables and graphics would have had to be created within the word processor, as well as the text, so it is unlikely that many papers will be produced this way. Thus, there is little need for submission by diskette when clear hard copy is available.

Note: The following procedure describes the use of a UMAX Vista S-12 scanner, utilizing a Twain driver. Adobe recommends the use of an ISIS driver for full functionality, if possible. The procedure may differ slightly for other scanners or when using an ISIS driver.

The Procedure

Start Up

Start the PC, and Windows, making sure that the UMAX scanner is ON and that the middle green pilot light is on steady (not flashing) upon completion of boot up. Start Acrobat *Capture V2*

If Capture does not recognize a valid scanner, it will be necessary to set it up. Go to Input/Setup Scanning Device. The Device field may be grayed out. If so, hit the button to the right with the three dots. This will allow the correct driver to be selected. Even after selecting OK, the field may still be grayed out, but the scanner will be recognized as indicated by the green Scan arrow.

Select the papers to be Acaptured.≡ If there are any Afull text≡ papers, without graphics, tables or formulas, check to see if there is a diskette for these papers which can be processed directly with *PDF Writer*. The balance (most of the papers) will be processed with *Capture*.

Scan

Verify that AUMAX/VistaScan≡ (the Twain driver) is selected for the input device.

In the Input/Setup Input Folder drop down menu, make sure that the box, ACollate files by common prefix≡ is checked. This will collate each page of a paper into a common ACD file during the Process operation. Collation uses the first four characters of the paper name, the prefix, to do this. This means that the name of each individual paper must have a unique Aprefix≡ as defined by this collation logic. If this box is not checked, each page scanned will be Processed independently into a separate ACD file and will require the use of *Acrobat Exchange* to merge the resulting PDFs later, when required.

Select the AEMSET In≡ folder (or the appropriate folder) to receive the scanned TIF images.

Make sure the scanner glass is clean.

Insert the first page of the first paper into the scanner, face down.

The top edge goes to the back, flush with the top (far) edge of the scanner glass. The long edge of the page goes flush with the right edge of the bed.

>>> The accuracy of the results is highly dependent on the text being horizontal. If the page has been reproduced slightly askew, compensate by turning it on the bed slightly. Check this later in the preview process.<<<

Select AScan≡

Enter the paper name or number in the Document Name box. (See above for naming requirement). Make sure the starting page number assigned is 0001. (If you need to rescan a page, use that page=s number.) File format default is TIF.

Select AStart≡

Make sure the settings on the VistaScan32 screen are:

Line art or B/W Document
Reflective
300dpi
100%

Select APreview≡ to set the frame size. Leave the original page margins. Make sure there is a normal margin around all text, and graphics, including titles. Make sure the text is horizontal.

Note: When using an ISIS driver, the Twain setup screen will not appear. It is necessary to enter these settings ahead of time in the ISIS setup box.

Do not adjust the page size for partial pages, such as the last page of a paper, as this causes the text to be centered vertically. Determine whether or not it is desired to exclude the original page numbers if this paper is from a larger document.

Except for spot checks, it is not necessary to preview again unless the page layout changes or it is necessary to check for horizontal text.

Select AScan≡ when the Preview is OK.

When the scan of the current page is complete and there are additional pages remaining to be scanned in this paper, select AScan Next Page≡ in the Scan Document window. The present page can be removed and the next page can be inserted as soon as the scan is finished. It is not necessary to wait for this box to appear.

Start at the beginning of the Scanning process with the next paper, until all papers in the batch are scanned satisfactorily

>>> It is important that the pages in a paper be scanned sequentially. If a page has been scanned out of order, it is important to note this in the Log, so the error can be corrected. Except for a long document, it will usually be easier to begin scanning of the document again.<<<

When the last page of the current paper has been scanned, select ADocument Finished.≡

>>> It is important to check that the number of TIF files is equal to the number of pages in each document. <<<

Process

Select the TIF files to be converted to PDF and ACD files from the AEMSET In≡ folder. First, clear the selection by selecting any file. Then select the papers desired by holding down the Shift key while selecting. Be sure to select all the TIF images (all the pages) in each paper to be processed.

Select the AEMSET Out≡ folder in the output area. Make sure that the folder is set to AAcrobat Capture ACD.≡

Select AProcess≡ and wait for the files to be processed.

>>> This processing can be done over a lunch period or overnight as it is completely automatic and takes some time to complete. Therefore, it is best to Scan as many papers as possible while in attendance at the PC, leaving Process for later.<<<

Review of Capture Process Results

Look for any error messages. Make sure that the job went to completion and that there is an ACD file for each paper. There may also be a number of ACI files which contain the graphics for each paper. The ACI files will not be visible in the folder, but they are there.

The next step is to EDIT, or Areview≡ and correct, the ACD files in the *Capture Reviewer* program to correct any scanning or process errors.

Reviewing and Correcting PDF Files Using Acrobat Reviewer

(See the Overview section)

To begin the Review process, either start *Capture Reviewer* from Windows or double click on the ACD file which you wish to edit. By double-clicking on the ACD file, you will automatically start *Capture Reviewer* and open the selected file. If you start from Windows, you will need to Open and locate the ACD file in question.

Minimize the *Capture* program if necessary.

Once the file is open, you will see yellow and blue text and graphics blocks marking Asuspects≡ the process program has identified. Included are words with less than the specified confidence level. For this project we will normally preset a 95% confidence level. Recognition suspects are highlighted in yellow. Spelling, font and alphameric suspects are highlighted in blue.

Press TAB to move the cursor to the first suspect. The corresponding graphical representation of that block appears in enlarged format at the top of the screen.

If the word is correct, press Ctl-Tab to accept it and move to the next suspect. If this is a technical term and you know the spelling is correct, it can be entered in the Custom

Dictionary. This will prevent it from being highlighted in future processes. To do this, select *Suspect* and *Add Word to Custom Dictionary*.

If the word needs to be corrected, double click to select the whole word or move the cursor to the letter(s) needing correction and delete and add as required until the word is spelled correctly. The case or font may need to be corrected. If so correct them.

In some cases, it will be necessary to substitute the graphic representation for the letters recognized by the *Capture* OCR process. This will normally be the case for formulae, graphics and handwriting. To do this, select *Edit*, then either *Convert Text Block to Image* (Ctl-Sh-G) or *Convert Text Line to Image* (Ctl-G). It is preferable to convert only the line if the rest of the block is fairly accurate. Converting to Image means that the text is no longer text and is not searchable. **Do not substitute a graphic image** for paper titles, authors or key words as this will prevent proper indexing of papers.

Experience will show when it is best to use *Convert Text Block to Image* or *Convert Text Line to Image*. **The objective is to minimize the amount of text converted to graphics.** However, the best representation of some text may actually be the graphic line or block, such as for formulae or mathematical and scientific symbols. See the new facility for inserting symbol characters. This should save considerable text editing effort or replacing an otherwise valid text line with a graphics image.

When the ANo further suspects≡ message is seen, go back to page 1 and Tab to be sure that all suspects have been handled.

>>> If any page has numerous errors or is unreadable in part, that page can be re-Scanned by placing the corresponding paper file name and page number in the Scan box. This will replace the corresponding TIF file. The paper can then be re-Processed. Alternatively, to avoid reprocessing, the page can be rescanned with a unique name. Then use *Acrobat Exchange* to delete the offending page and insert the new page. (See Rescanning... below)

When rescanning, using the original document name, it is necessary to delete the original ACD file, otherwise the collate process will add this later scan to the original file.

Saving the Revised Files

Once the entire paper has been corrected and the *Reviewer* prompt indicates, ANo more suspects,≡ the revised ACD and the new PDF need to be saved. From the *File* menu, chose *Save as ACD*. After the ACD is saved, chose *Save As* from the *File* menu. (*Save As* minimizes the pdf file size.) Make sure the default file type is Acrobat PDF/Normal and the default (file name) and PDF extension are correct. Close the *Reviewer*.

Selected PDFs, particularly graphics intensive papers, should be reviewed in the *Acrobat Reader* and also printed in part to check the accuracy of the PDF generation. Corrections can be made by opening the ACD again.

Check for correct page sequence.

Rescanning and Correcting Part of a Document

Changes to PDF files can be made using the *Capture Reviewer* or *Exchange* programs. However, it may be necessary to rescan a page or pages of a multiple page document to achieve the desired result. If this is the case, there are two methods which can be employed:

- X The desired page(s) can be rescanned using the correct page number in the Scan menu. Note that if pages have been added or deleted in *Exchange*, the new page number must be used.

- X A new document can be prepared by rescanning the desired page(s). For convenience, use as a document number, the original document name or number with the prefix A9". Eg: Document 123a becomes 9123a.

The second method is recommended for ease of control. Assuming this Anew≡ document method is used, *Acrobat Exchange* can be used to update the original document.

First, open the original document in *Exchange*.

Then select Insert Pages from the Document menu.

Insert the Anew≡ document at the desired place in the original document.

If only one page has been rescanned or if more than one page has been rescanned and they are contiguous, select Delete Pages from the Document menu and delete the Aold≡ (replaced) page(s).

If more than one page has been rescanned and they are not contiguous, proceed as above. Then Delete the new pages which are not in the correct sequence. Next, proceed to Insert the Anew≡ document in the correct page location for the next new page. Proceed as above to Insert and Delete until all the new pages have been added at the correct locations and all the Aold≡ pages have been deleted.

Recheck the document for correct page sequence.

Always *Save As* before exiting. This minimizes the size of the PDF.

END



**CAST IRON, WROUGHT IRON & STEEL
(HISTORICAL PERSPECTIVE OF PROPERTIES
OF FERROUS MATERIAL)**

Archie M. Cooke

Retired Metallurgist
96 Arrowhead Drive
Carson City, Nevada 89706

Telephone: 702-885-8854

CAST IRON, WROUGHT IRON & STEEL
(HISTORICAL PERSPECTIVE OF PROPERTIES OF FERROUS MATERIAL)

Archie M. Cooke
Retired Metallurgist
Carson City, Nevada

Keywords:

Cast-iron, Wrought-iron, Steel, Rockwell Hardness

Prerequisite Knowledge:

The Student

1. Should have observed objects made of cast-iron, and observed its brittle character. (Stove parts, auto engines, etc.)
2. Should have observed ornamental fences, gates, etc. made of what is called wrought-iron.
3. Should have been subjected to sales talk of the strength advantages of some heat treated steel object. (Golf clubs, knives, gears, etc)

Objective:

The objective of this exercise is to compare the properties of cast-iron, wrought-iron, and steel in a background of historical development.

Equipment and supplies:

1. Two pieces of $\frac{1}{4}$ "X $\frac{1}{2}$ "X72" wrought-iron bar. (Annealed low carbon steel would be a suitable substitute.)
2. One piece of $\frac{1}{4}$ "X $\frac{1}{2}$ " X30" low alloy carbon steel heat treated to Rockwell C50.
3. One piece of $\frac{1}{4}$ "X $\frac{1}{2}$ "X30" cast-iron. (Machine from any casting)
4. One five gallon bucket with a bail handle
5. Fifty pounds of lead shot.
- 6 One hack saw
7. One strong bench with a metal vise.
8. One two handed wrench or hand wheel.

Procedure:

Overview:

For the bend tests the $\frac{1}{4}$ "X $\frac{1}{2}$ " bars should be cut to the lengths specified. One end should be clamped in the vise, and at 20 inches from the vise face, adhesive tape should be wrapped around the bar. The bucket should be hung on the bar with the bail in such a position that the tape keeps the bucket from sliding away from the 20 inch position.

Bend Testing the Wrought-iron Bar.

Place a 30 inch long wrought-iron bar in the set-up described and slowly pour lead shot into the bucket until the bar bends to a 45 degree angle. Remove the bar and observe the permanent set.

Bend Testing the Steel Bar:

Place a 30 inch long steel bar in the set-up described, and hang the bucket containing the shot from the wrought-iron bend test at the 20 inch position. Observe the different action from that of the wrought-iron bar. Continue adding lead shot until the bar either breaks or the bucket becomes full of shot.

Bend Testing the Cast-iron Bar:

Place the 30 inch long cast-iron bar in the test set-up described with an empty bucket hanging at the 20 inch position; then, slowly add lead shot to the bucket until the bar breaks. Observe the fracture faces.

Demonstration of Work Hardening:

Place a piece of the wrought-iron bar in the vise projecting out about 18 inches; then, bend the bar back and forth about ten degrees until it breaks. Observe that as the process proceeded it became progressively difficult to bend until a crack formed and grew until failure. Obviously the bar became stronger by this cold work. Did we strengthen it just to break it? What other property did the bar obtain during the process? Do not say fatigue; such a description is an old wives tale cautioned against by elementary metallurgy text books. Consider the fact that the beam bending formulas in handbooks consider all materials equal. i.e. The ratio of extreme fiber stress to bending moment equals the section modulus for all materials.

Demonstration of Strengthening by Twisting:

Place a 72 inch long bar of $\frac{1}{4}$ " X $\frac{1}{4}$ " wrought-iron on a table with one end held by the vise and the other end attached to a hand wheel or two handled wrench. Twist the bar until uniform nodes of about one inch spacing occurs. Remove the bar and compare the stiffness with that of the untwisted bar. If the bar was crooked before twisting observe the straightening effect of the twist.

Results Review:

Note the dates of discovery of the various ferrous products as shown on Figure . Apparently Wrought-iron was the only ferrous material known to mankind at the age of King Arthur's saga. The student might suggest a correction to the story of extraordinary properties of his sword named Excalibur. Consider an extraction from an old Norse saga by Davidson (1) which reads:--"SteinThor-----hewed with both hands, but the elaborate sword was of little use when it came against a shield, and he often had to straighten it under his foot"

Apparently straightening the sword blade under the foot was a common occurrence in these battles because some blades were soft. Some have suggested that the sword blades which were stiff like King Arthur's instead of soft like Steinthor's was due to absorption of carbon and inadvertent heat treatment strengthening; however, laboratory tests of some of these old sword blades have failed to find any evidence of carbon absorption.

These blades have been found to be made of thin strips of wrought-iron hammered together and then twisted. This twisting, like that in the above demonstration might have strengthened the blade by cold work. The loss of this cold work strengthening by inadvertent heating above a recrystallization temperature might explain why some blades were soft.

Historical Perspective:

Figure shows that wrought-iron production began in antiquity and ended in the 1930's when the Aston-Byers process could no longer command a premium price over low carbon steel. Having been the primary ferrous product for over 3500 years, it is worth noting that Bessemer invented his steel to be cheaper (not better) than wrought-iron. Cast-iron got its big development by the ability to be poured in liquid form into molds for muzzle loading cannons. It has subsequently become the main material for other items that can take advantage of its superior fabrication properties. The puzzle is that it took so long for the discovery of heat treated steel.

We do not know when it was discovered that control of carbon content could be utilized to strengthen iron. There is some thought that carbon in a suitable range could be obtained in wrought-iron by prolonged exposure to carbon at elevated temperature. We know that such treatment will not get carbon to diffuse more than a few millimeters into the surface of solid iron, and that melting is necessary to get the carbon to distribute uniformly through the iron. Figure shows that this could not have been obtained until the crucible process was introduced about 1700AD. The development of the art of strengthening steel by heat treatment originated in the tool-steel industry's use of various alloy additions in the crucible melting process. The other steel uses were slow to adopt these procedures. For general structural applications the trade-offs between cost of extra size of structural members vs cost of extra heat treatments and alloy elements usually falls on the side of larger structural members.

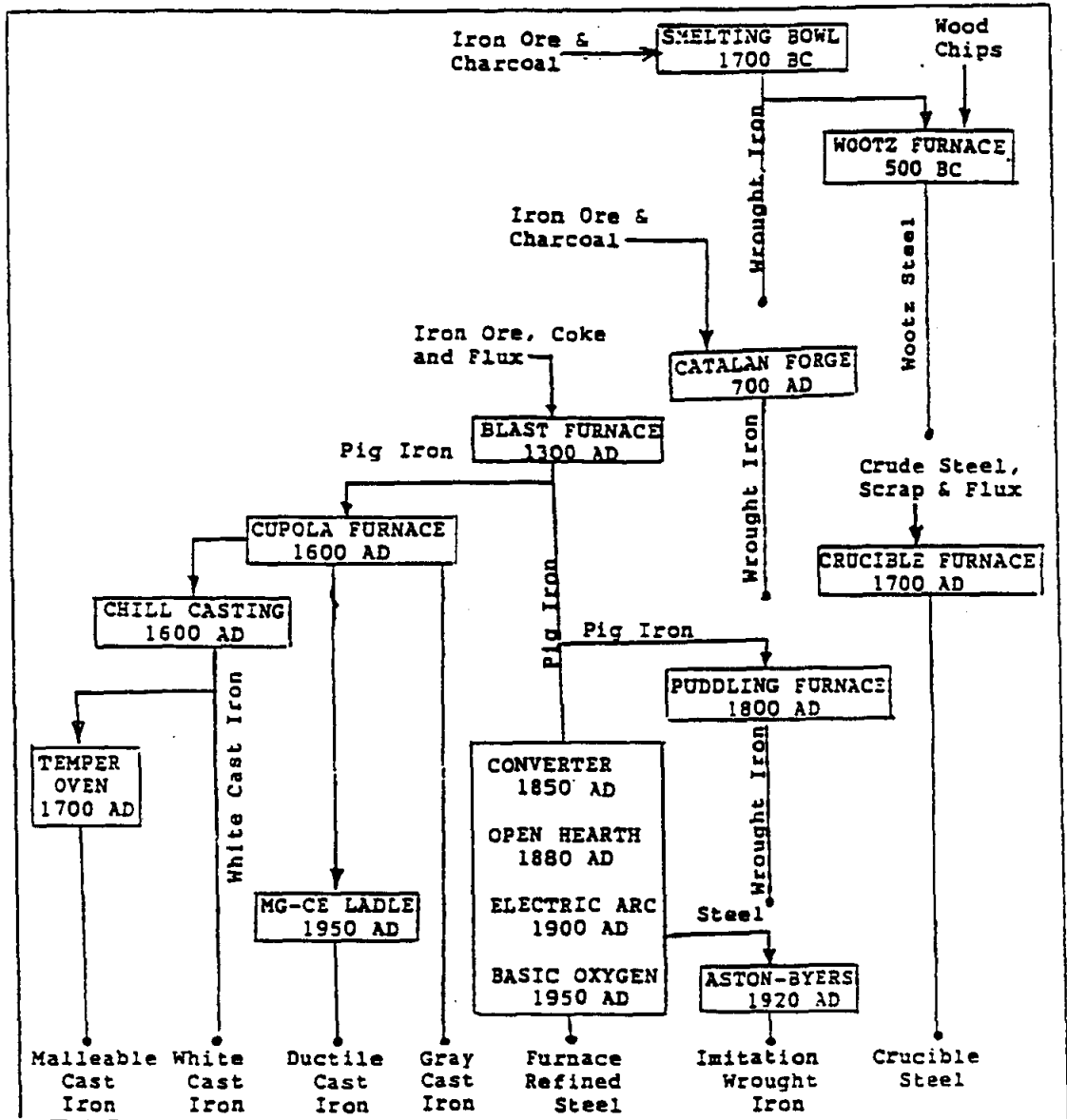


Figure History Flow Chart
-Iron 2000 BC to 2000 AD

Effect of Chemistry of Iron on its History

The convoluted history of iron and steel has through the centuries been guided by luck intertwined with the chemical properties of the metal iron in relation to carbon and oxygen. This is the story of how the chemistry of iron and lack of knowledge thereof effected the history of use of iron and steel. These effects are:-

- (1) Lack of knowledge by prehistoric man of how to produce a temperature above 2000 degrees.
- (2) The fact that solid iron ore can be reduced to solid metallic iron by the action of carbon monoxide gas at a temperature far below the melting point of iron, the product being essentially pure iron.
- (3) The fact that solid iron when free of carbon is a very malleable metal.
- (4) The fact that iron will absorb carbon when heated above 2400F degrees in the presence of carbonaceous material and that the melting point of iron is reduced by absorption of carbon to about 2100F degrees at 4 percent carbon.
- (5) The fact that if iron in the liquid state contains between 2 percent and 4 percent carbon it will upon solidifying by slow cooling precipitate out most of the carbon in the form of graphite flakes.
- (6) The fact that graphite precipitation can be prevented by rapid cooling causing the carbon to combine with iron as iron carbide resulting in a very hard and brittle material called white cast iron.
- (7) The fact that white cast iron upon prolonged heating at about 1600F degrees will become malleable through a graphite precipitation mechanism which concentrates the graphite as compacted aggregates instead of graphite flakes.
- (8) The fact that iron with dissolved carbon between $\frac{1}{2}$ and 1 percent can be strengthened by a heat, quench, and temper cycle.

Discovery of Iron

The first three effects listed above can be linked to explain the first production of iron by man. We see that after about 1000 years of

bronze smelting, prehistoric man probably discovered iron by accidentally mixing iron ore (iron oxide) with tin ore (tin oxide) during the reduction of tin ore with charcoal to make bronze, an alloy of tin and copper. The result probably left a lump of red hot, more or less pure iron, mixed with iron oxide and slag at the bottom of the reduction pot. Prehistoric man might have treated this lump the same as he would bronze; i.e. hammer it into shape. This might have given him the idea that this new material would be an ideal substitute for bronze; which by this time was getting scarce due to depletion of the easily mined copper deposits.

Luck

Fourth and fifth effects listed above bring luck into the equation. Luckily prehistoric man could not produce a temperature high enough in his reduction pot to cause the iron to absorb carbon from the charcoal fuel. If he had, the iron would have melted and solidified as flake graphite cast iron which he would have been unable to shape by hammering. Luckily, the metal he produced was a malleable metal that later became known as wrought iron.

Wrought Iron

The first recorded use of iron places the discovery at about 1700 BC. The early iron smelting furnace probably was a bowl shaped hole in the ground, lined with clay, and charged with a mixture of charcoal and iron ore. It is assumed that temperature was maintained by burning the charcoal with air forced in through clay pipes fed by crude bellows. Figure is a diagram of the subsequent progressive developments in iron smelting from this primitive furnace producing wrought iron to the present day products of steel, malleable iron, white cast iron, nodular cast iron, and flake graphite cast iron. In Figure , following the direct line of descendants of the bowl furnace, we have the Catalan forge replacing it about 700 AD. The Catalan forge produced wrought iron using essentially the same process as the bowl furnace. The Catalan forge was obsoleted about 1800 AD by the puddling furnace which made wrought iron from blast furnace products by

burning out the carbon with iron oxide. The puddling furnace was subsequently replaced about 1920 AD by the Aston-Byers process of making wrought iron from steel.

Crucible Steel

In Figure follow the side descendant of the bowl furnace wherein steel is made from wrought iron, first in the Wootz furnace and subsequently in the crucible furnace. These furnaces utilized the chemical property of iron exemplified by effect number 8 of the introductory list, namely, that although a large amount of absorbed carbon in iron produces a very brittle solid, a small amount produces a product which can be strengthened by heat treatment. For instance, the Wootz process consisted of placing pieces of wrought iron in a clay pot along with a carbonaceous material such as wood chips; sealing the pot; and then heating it in a separate furnace for several days. Upon removal from the furnace the clay pot was broken away leaving a lump of steel. In a similar manner, in the crucible process, developed about 1700 AD a pot called a crucible is loaded with wrought iron plus the amount of carbon and alloying elements desired in the finished steel. The loaded crucible is then placed in a furnace with a temperature high enough to melt the charge. The melted steel is poured from the crucible and the crucible is reused.

Gray Iron

Balance of Figure shows the inter-relationships of blast furnace products. It is postulated that as the size of the Catalan forge increased to meet larger demands for wrought iron the ability to heat the charge to higher temperatures occurred by accident. Then, lack of temperature control allowed some of the iron to absorb sufficient carbon to melt and flow out of the furnace where solidification as flake graphite cast iron occurred. Such iron was useless to the smelter who wanted carbon free wrought iron capable of being shaped by hammering. This unwelcome molten high carbon iron running from the furnace eventually was found to be castable into useable items where brittleness would not be a problem. To satisfy this market, the blast furnace was developed about 1300 AD. This was followed about 1600 AD by the cupola furnace used to remelt the blast

furnace product. For many years thereafter cast iron from the blast furnace or cupola furnace dominated the iron industry. By 1800 AD the blast furnace had proven to be such an economical way to smelt iron ore that its product became the starting material for nearly all iron and steel products.

Malleable Iron

Figure shows a gap of many years between introduction of the blast furnace and the introduction of white cast iron and malleable cast iron. During this time the medieval metallurgist probably learned how cast iron properties are dependent upon the method of doping and casting. They must have learned how the properties of flake graphite cast iron varied with the size and distribution of graphite, and eventually learned that doping with iron oxide and rapid cooling completely prevented the precipitation of graphite. Finally, they must have discovered the process for the production of malleable cast iron

As described in a French publication in 1722 AD and still in use today malleable iron is made in two steps. First, the blast furnace product composition is adjusted so that rapid cooling produces white cast iron in which the carbon remains in solution in the solid metal. Second, this white cast iron is held at a temperature of about 1600F degrees for several days during which time the carbon precipitates as compacted aggregates; now called temper carbon. The matrix being more or less depleted of carbon becomes essentially low carbon steel; hence, malleable.

Ductile Iron

The latest development in the field of cast iron was the introduction of nodular cast iron at about the end of world war two. This followed the discovery that addition of magnesium and/or cerium to the ladle during pouring of a cast iron which would otherwise have been flake graphite cast iron causes the graphite to collect as tiny balls rather than flakes. As in the case of malleable cast iron this depletes the matrix of most of the carbon resulting in a malleable product. This product, advertised as "ductile cast iron" has the advantage over malleable iron of elimination of the white cast iron middle production step.

References

1. Davidson, H.E., *The Sword in Anglo-Saxon England*, The Boydell Press, Woodbridge, Suffolk, U.K.

REPORT DOCUMENTATION PAGE			Form Approved OMB No. 07704-0188	
Public reporting burden for this collection of information is estimated to average 1 hour per response, including the time for reviewing instructions, searching existing data sources, gathering and maintaining the data needed, and completing and reviewing the collection of information. Send comments regarding this burden estimate or any other aspect of this collection of information, including suggestions for reducing this burden, to Washington Headquarters Services, Directorate for Information Operations and Reports, 1215 Jefferson Davis Highway, Suite 1204, Arlington, VA 22202-4302, and to the Office of Management and Budget, Paperwork Reduction Project (0704-0188), Washington, DC 20503.				
1. AGENCY USE ONLY (Leave blank)	2. REPORT DATE October 1999	3. REPORT TYPE AND DATES COVERED Conference Publication		
4. TITLE AND SUBTITLE National Educators' Workshop: Update 98 <i>Standard Experiments in Engineering, Materials Science, and Technology</i>			5. FUNDING NUMBERS 251-10-01-01	
6. AUTHOR(S) Compiled by Ginger L. F. Arrington, James E. Gardner, James A. Jacobs, Karl J. Swyler, and Leonard W. Fine				
7. PERFORMING ORGANIZATION NAME(S) AND ADDRESS(ES) NASA Langley Research Center Hampton, VA 23681-2199			8. PERFORMING ORGANIZATION REPORT NUMBER L-17898	
9. SPONSORING/MONITORING AGENCY NAME(S) AND ADDRESS(ES) National Aeronautics and Space Administration, Washington, DC 20546-0001; Norfolk State University, Norfolk, VA 23504; National Institute of Standards and Technology, Gaithersburg, MD 20899; Brookhaven National Laboratory, Upton, NY 11973; International Council for Materials Education, Columbia University, New York, NY 10027; and Gateway Coalition, State University of New York at Stony Brook, NY 11794			10. SPONSORING/MONITORING AGENCY REPORT NUMBER NASA/CP-1999-209549	
11. SUPPLEMENTARY NOTES Arrington and Gardner: Langley Research Center, Hampton, VA; Jacobs: Norfolk State University, Norfolk, VA; Swyler: Brookhaven National Laboratory, Upton, New York; and Fine: Columbia University, New York, NY				
12a. DISTRIBUTION/AVAILABILITY STATEMENT Unclassified—Unlimited Subject Category 23 Distribution: Standard Availability: NASA CASI (301) 621-0390			12b. DISTRIBUTION CODE	
13. ABSTRACT (Maximum 200 words) This document contains a collection of experiments presented and demonstrated at the National Educators' Workshop: Update 98, held at Brookhaven National Laboratory, Upton, New York on November 1–4, 1998.				
14. SUBJECT TERMS Materials; Experiments; Education			15. NUMBER OF PAGES 486	
			16. PRICE CODE A21	
17. SECURITY CLASSIFICATION OF REPORT Unclassified	18. SECURITY CLASSIFICATION OF THIS PAGE Unclassified	19. SECURITY CLASSIFICATION OF ABSTRACT Unclassified	20. LIMITATION OF ABSTRACT UL	
